DREA SR/97/002

National Defence
Research and
Development Branch

Défense nationale
Bureau de recherche
et développement

ABSTRACTS and SUMMARIES

of

3rd (7th) CF/CRAD MEETING on NAVAL APPLICATIONS of MATERIALS TECHNOLOGY

and

INTER NAVAL CORROSION CONFERENCE

held at Halifax, Nova Scotia, Canada

22 - 24 April 1997

Compiled by J.R. Matthews

Defence
Research
Establishment
Atlantic

Centre de
Recherches pour la
Défense
Atlantique

Canada

3rd (7th) CF/CRAD Meeting on
Naval Applications of Materials Technology
and
Internaval Corrosion Conference

ABSTRACT

This was the seventh naval materials CF/CRAD (Canadian Forces/Chief Research and Development) meeting. These meetings have been held every two years since 1985. The first four meetings were devoted to fabrication and inspection of submarine pressure hulls with sessions on welding, inspection and fracture. The last three have expanded to include all aspects of naval materials.

The purpose of these meetings has been to bring together industrial research contractors, university contractors, defence scientists, and NDHQ (National Defence Headquarters) design authorities from the naval materials technology area and invited scientists and engineers from other countries to share advances in naval materials technology in a conference like setting. In 1997 the meeting was held in conjunction with the Inter Naval Corrosion Conference.

The combined program includes welding and laser surface modification, fracture and fatigue, Non-Destructive Evaluation, firesafe materials, organic materials (polymers), vibration and damping materials, and of course, corrosion and coatings.

Troisième (Septième) Réunion Du CR Dev/Dés FC
Sur Les Applications De La Technologie
Des Matériaux Au Domain Naval
Et
Conférence Intermarine Sur La Corrosion

RÉSUMÉ

Le CR Dév/FC a tenu sa septième réunion sur les applications de la technologie des matériaux au domaine naval. Ces réunions ont lieu tous les deux ans depuis 1985. Les quatre premières rencontres ont porté sur la fabrication et l'inspection des coques épaisses de sous-marins. Elles comprenaient des ateliers sur la soudure, l'inspection et la rupture. Les thèmes des trois plus récentes réunions couvraient tous les aspects des matériaux appliqués au domaine naval.

Ces réunions ont pour objet de rassembler des entrepreneurs spécialisés en recherche industrielle ou provenant du secteur universitaire, des scientifiques de la défense représentants du QGDN responsables de projets de conception dans le domaine de la technologie des matériaux appliqués au secteur naval ainsi que des scientifiques et des ingénieurs invités venus de l'étranger afin de leur permettre de partager leur savoir sur les progrès de la technologie des matériaux dans le cadre de rencontres de type conférence. En 1997, la réunion a eu lieu de concert avec la Conférence intermarine sur la corrosion.

Les thèmes abordés au cours de la réunion portaient entre autres sur la soudure et la modification d'une surface au laser, la rupture et la fatigue, l'évaluation non destructive, les matériaux assurant une protection contre l'incendie, les matériaux organiques (polymères), les matériaux antivibrants et la vibration ainsi sur la corrosion et les revêtements.

3rd (7th) CF/CRAD MEETING
on
NAVAL APPLICATIONS OF MATERIALS TECHNOLOGY
and
INTER NAVAL CORROSION CONFERENCE

8th floor
Hotel Halifax
22nd, 23rd and 24th April 1997

Welcome: Commodore D.G. Faulkner
Chief of Staff, Maritime Command HeadQuarters

SESSION I:
Chairman: Dr. J. R. Matthews, DREA
page

1. Introduction to 3rd CF/CRAD Meeting, J.R. Matthews 1

2. Advanced Materials for Submarine Construction, Dr. R.L. Jones Defence Research Agency Farnborough, U.K. 2

3. Factors Affecting the Fracture Toughness of High Strength Steel Weldments, J.A. Gianetto, J.T. Bowker, J.E.M. Braid and W.R. Tyson, NRCan, Ottawa 29

4. GMAW Power Sources for the Joining of High Strength Steels, Mr. C.J. Nicholson, and Dr. L. Malik, Fleet Technology Limited, Kanata, and Dr. J.R. Matthews, DREA 60

5. Investigation Of Fumes Generated In Welding and Cutting Of Navy Materials, by Gene L. Franke, Raymond H. Juers and Reynold T. Brenna, Naval Surface Warfare Center, West Bethesda, MD 74

Session II:
Chairman: Dr.R.S.Hollingshead, DREA/Head Dockyard Lab (Atlantic)

6. Introduction to Inter Naval Corrosion Conference, R.S.Hollingshead

7. Coatings With Selected Infrared Properties For Use On CF Ships, Dr.Terry Foster, Esquimalt Defence Research Detachment, and David Hacker and Bill Abel, Ortech 98

SESSION III:
Chairman: Dr. Richard Morchat, NDHQ/CRAD/DSAM-4

8. Host Structure and Active Material Interactions: Implications for Design of Smart Materials, Virginia DeGiorgi, Naval Research Laboratory, Washington, D.C. 142

9. Designing with Glass Reinforced Engineering Thermoplastics, Dr. P.J. Bates and Dr.V.T. Bui, Royal Military College of Canada 170

10. Applications of Composites for C5 Sonar Dome Components, T.S. Koko, Martec Ltd., M.J. Connor, Composites Atlantic Ltd., and G.V. Corbett, NDHQ 186

11. Impact Properties of Composite Sonar Dome Materials, J.P. Szabo, A.J. Russell, and J.A. Hiltz, DREA 187

12. APHIUS III Work Station, Dr. Bob Hay and Dr. Emmanuel Bissé, Tektrend International Inc.

13. An Introduction to Fiber Optic Strain Sensing for Composite Materials, Doug MacDonald, InNova Corp 222

SESSION IV:
Chairman: Stéphane Garneau, NDHQ/DMSS 2-4-3

14. A Reference Electrode Data Acquisition System for Cathodic Protection Studies, Dr. Derek Lenard, Esquimalt Defence Research Detachment, DREA 224

15. Corrosion Sensors for Field Applications, M. Tullmin and P.R. Roberge, Royal Military College, Kingston Ontario 248

16. A Laboratory Simulation of the Galvanic Corrosion of Ship Hull Plate by Shaft Grounding Systems, Dr. Trisha Huber, Esquimalt Defence Research Detachment, Victoria, B.C. 260

17. Corrosion and Coatings in the RAN, Mike Sim, Australia 276

SESSION V:
Chairman: Dr. Calvin Hyatt, DREA

18. Development of an Optimum Consumable Alloy for Low Heat Input Welding of Nickel Aluminum Bronzes, Dr. Calvin Hyatt, DREA, J.C. Bennet, Acadia, G. Pelletier, DREA, K. KarisAllen, Facts, J.Hewett, Kova Engr Ltd., T. Betancourt (retired), and J. Gianetto, NRCan 280

19. Laser Processing of Nickel Aluminum Bronze for Use in Propeller Fabrication and Repair, Dr T.A. Marsico, Applied Research Laboratory, The Pennsylvania State University 299

20. Microstructural Characterization of Laser-Clad Nickel Aluminum Bronze Alloys by TEM, J.C Bennett, Acadia University and C.V. Hyatt, DREA 321

21. Variable Polarity Plasma Arc Welding of Aluminum Alloys by Robert J. Pistor, G. R. Labbe, and W.H. Tuttle, Liburdi Engineering Ltd 340

22. Laser Welding in Ship Construction, J. Bird, MOD UK, and A. Furio, NSWC 350

23. Tail Shaft Struts on an Aluminum Planing Craft: Problems and Repairs, J.C. Thornley, K.G. Sedman and J.W. Carter, RPC, New Brunswick 370

Session VI:
Chairman: Dr. J.A. Hiltz, DREA

24. Inorganic Intumescent Coatings for Improved Fire Protection of GRP, K. B. Langille, D. T. Nguyen and J.O. Bernt, J.O. Bernt and Assoc, and D.E. Veinot, DREA 371

25. Development of Novel High-Performance Protective Coatings for Applications in Severe Environments, Dr. Samir Aouadi and Dr. Kam L. Yan, Cametoid Advanced Technologies Inc. 383

26. Overview of Waterjetting on U.S. Navy Vessels as Alternative to Dry Abrasive Blasting, Dr. Brenda S. Holmes, Naval Sea Systems Command, and John Tanner, Ameron International 396

SESSION VII:
Chairman: Dr. Jack Morrison, DREA/EDRD

27. Ship Fracture, Dr. James R. Matthews, DREA 409

28. Fracture Resistance of Canadian Patrol Frigate Hull Steels, Dr.Jack Morrison, DREA Dockyard Laboratory (Esquimalt), and Stephane Garneau, NDHQ 430

29. Effect of Notch Acuity on Fracture, M.N. Bassim, University of Manitoba 473

30. Crack Arrest Toughness of a Ship Structural Steel, L.N. Pussegoda and L. Malik, Fleet Technology Centre, J. Morrison, EDRD and S. Garneau, NDHQ 483

31. JId Testing of an HY 80 Steel Weldment, Ken D. MacKay, Martec Ltd. and J.R. Matthews, DREA 499

SESSION VIII:
Chairman: Dr. Derek Lenard, DREA/EDRD

32. Delivering Corrosion Courseware: The Evolution of the RMC Corrosion Short Course, P.R. Roberge, Royal Military College, Kingston Ontario 512

33. Forged Copper-Nickel-Chromium Alloy for Seawater System Components, John Galsworthy and D. Baxter, Defence Research Agency, Holton Heath, UK 522

34. Development With and Corrosion Performance of Copper Nickel Chrome Castings, J. Bird, Dir of NA, MOD UK, Bristol 535

35. Self Reliance by Commercialisation - A Revolution in Naval Engineering Management, Mr. P.C. Conor, NZ Defence Force 542

36. US Navy Corrosion Presentation, Paul Holsberg, Naval Surface Warfare Center 548

Wednesday EVENING, 23rd April
RECEPTION and BANQUET
Hotel Halifax
Bluenose Room 8th Floor

SESSION IX:
Chairman: Dr. John Hiltz, DREA

37. Underwater Acoustic Radiation Of An Elastic Plate Covered By A Decoupling Coating, O. Foin and Alain Berry, Université de Sherbrooke, and J. Szabo, DREA 566

38. Vibration Isolation Research for Naval Ships at the Australian Defence Force Academy, Dr. Hugh Williamson, Australian Defence Force Academy 584

39. Minimization of Vibration Transmission Through Engine Isolation Mounts, S.G. Hutton, A. Muravyov and G. Chen, University of British Columbia, and J. Szabo and D. Stredulinski, DREA 597

40. Modeling and Analysis of Active Vibration Control of Naval Structural Components, T.S. Koko, I.R. Orisamolu, M.J. Smith and U.O. Akpan, Martec Ltd. 611

Session X:
Chairman: John Porter, DREA

41. Inspection Of Round Robin Test Plates Using APHIUS, Mr. R. Bergeron, Tektrend International Inc.

42. Residual Stress Determination by Non-Destructive Methods, Sensors: Numerical Modeling and Construction, Dr. George Roy, CANMET/Materials Technology Laboratory 612

43. Measurement of Residual Stress, Plasticity and Fatigue in 350WT Steels by Neutron Diffraction, T.M. Holden and J.H. Fox, Chalk River, J. Pang and T.E. Mason, U of T 620

44. An Overview of Some Current Research on Welding Residual Stresses and Distortion in the U.S. Navy, Joe Blackburn et al (presented by Paul Holsberg) Naval Surface Warfare Center, West Bethesda, MD 632

SESSION XI:
Chairman: Mr. John Porter, DREA

45. Modeling the Initiation and Propagation of Fatigue Cracks in Welded Steel Structures, S. B. Lambert and G. Glinka, University of Waterloo, and R. D. Yee, Fleet Technology Ltd. 655

46. An Overview of the CRAD Major Development Project ISSMM (Improved Ship Structural Maintenance Management), Steve Gibson, DMSS, J. Porter and Neil Pegg, DREA 675

47. Fatigue Crack Growth of Naval Platform Materials Under Spectrum Loading, J. Porter, DREA, Richard Yee, Fleet, and Mike Chernuka, Martec 676

48. A Summary of Experimental Strain Measurements on Canadian Patrol Frigates, Mr. John Porter, DREA, Mr. Mike Brauss, Proto Manufacturing, Mr. Rod Kennett and Bruce Paterson, NETE, and Richard Yee, Fleet 677

SESSION XII:
Chairman: Dr. Roger Hollingshead, DREA

49. Research and Development Activities Within the CRAD Aircraft Structures and Materials Program, Ken McRae, Major B.J. Miller and Capt. B.A. Lepine 678

50. Open Discussion on Corrosion/Coating, panel

Introduction to 3rd (7th) CF/CRAD Meeting

by

J.R. Matthews
DREA

This is the seventh naval materials CF/CRAD meeting. These meetings have been held every two years since 1985. The first four meetings were devoted to fabrication and inspection of submarine pressure hulls with sessions on welding, inspection and fracture. The last three have expanded to include all aspects of naval materials.

The purpose of these meetings has been to bring together industrial research contractors, university contractors, defence scientists, and NDHQ design authorities from the naval materials technology area and invited scientists and engineers from other countries to share advances in naval materials technology in a conference like setting. In 1997 the meeting is being held in conjunction with the Inter Naval Corrosion Conference.

The combined program includes welding and laser surface modification, fracture and fatigue, Non-Destructive Evaluation, firesafe materials, organic materials (polymers), vibration and damping materials, and of course, corrosion and coatings.

#507204 ①

102-03465/

Advanced Materials for Submarine Construction

by

Dr. R.L. Jones
Defence Research Agency Farnborough, U.K.

Advanced Materials for Submarine Construction

As a class of vessel, submarines are used in a wide variety of applications. The most familiar roles include:

- covert attack of enemy shipping using torpedoes to isolate or blockade a given area.
- a platform for strategic nuclear weapons.
- hunter/killer of enemy submarines.
- a platform for delivery of personnel and/or equipment into enemy territory to conduct covert operations.
- seeking and destroying undersea explosive mines.

These applications can be categorised into a number of distinct groups by means of size of vessel, whether manned or unmanned, by required operating depth and by mission profile (e.g. speed, manoeuvrability, payload, rate of dive/surfacing, fatigue life expectation).

A platform for strategic nuclear weapons. These are large (in excess of 15,000 tons) and manned (a crew complement in excess of 100. A typical mission profile is to have the ability to cruise at relatively high speed then to remain stealthy by being submerged for long periods (months), at depth.

An oceanographic research vessel. This may be small (around 1 ton), unmanned, and with a deep diving (in excess of 4000 metres) capability. A typical mission profile might be to survey areas of the ocean floor (perhaps 10 km by 10 km) at very low speed whilst in an autonomous mode from the supply vessel for, perhaps, 20 hours.

Pressure Hull Materials

From a hull design viewpoint, these represent two quite different situations. In the former, minimising the internal volume is not the principal driver and that, coupled with the depth/mission requirements, leads to a hull design dictated by **buckling resistance**. In the latter example, the relationship between internal volume, payload mass, power supply mass/volume and vessel cross section (ie drag resistance) is critical, as it dictates the length of mission which can be achieved. This can lead to a hull design which is dictated by **crushing resistance.**

Materials Selection.

The design requirements of high buckling resistance and/or high crush resistance translate to key material requirements of **high Young's modulus** and **high compressive strength.** Based on availability, ease of fabrication, low cost and its historical usage in ship building, steel is the baseline material for submarine hull construction. A comparison of the specific Young's moduli of a range of engineering materials shows that most materials (including steels) have a similar value whereas aramid reinforced plastic and carbon fibre reinforced plastic materials offer significant improvements (more than a factor of five). A comparison of the specific compressive strength values for the same materials shows that most materials (including steels) have a similar value with the exception of Titanium alloy, glass fibre reinforced plastic and carbon fibre reinforced plastic materials, which all offer significant improvements. It should be noted that aramid reinforced plastics exhibit modest levels of compressive strength, discounting them from further consideration.
Thus, contending materials for submarine hulls are:

- steel
- Titanium alloy
- glass fibre reinforced plastics
- carbon fibre reinforced plastics

These are now considered in more detail below.

Steel

Steel has been the principal material used to date for submarine hull construction, based on availability, ease of fabrication, low cost and its historical usage in the general ship building industry. In the west, all large military submarines have utilised a ring stiffened, cylindrical, pressure hull configuration --both the rings and cylinder being fabricated from steel.

Advantages:

- readily available, cheap raw materials.
- well developed, reliable, fabrication process.
- steel has good fracture toughness which translates into good shock/blast resistance.

Disadvantages:

- ferromagnetic (hence raising the possibility of detection via magnetic signature).
- prone to corrosion.

There has been a major research effort to date investigating HSLA steels as a cost reduction exercise to replace the presently employed Q1N steels for submarine hull construction. These steels offer the potential of reduced material and fabrication costs through lower alloy element content and improved weldability requiring no weld preheat. Savings of the order of 10% of hull construction costs have been estimated, although these must be regarded as low since these costs relate to preheat only and no additional cost savings resulting in a more efficient process were not included.

Two generic types of HSLA steel are currently under evaluation. They derive their combinations of strength and toughness via two radically different alloying philosophies involving either the addition of Cu (HSLA100) or the addition of B (BIS812EMA). There has been a detailed programme to investigate the mechanical properties of these steels and their weldments. Work is now in hand to determine the stress corrosion susceptibility and low frequency corrosion fatigue crack growth behaviour.

Work on HSLA100 has shown that this steel is not susceptible to SSC at load levels close to or approaching the limit load under applied electrochemical potentials (AEP) ranging from -700 to -1100 mV SCE over the test duration of 1000 hours. Tests on samples at an AEP of -500 and -600 mV SCE (i.e. an AEP above the free corrosion potential) caused general anodic dissolution of the steel and although time dependent failure was observed this was attributed to general corrosion wastage of the bulk material.

However tests at -1200 mV SCE did show evidence of time dependent cracking at normalised load ratios Pa/PL in excess of 0.9.

A general summary of the corrosion fatigue performance is that at R=0 HSLA100 steel exhibit slightly faster fatigue crack growth rates than Q2N at the free corrosion potential.

Titanium Alloy

Titanium alloy has been considered by many military submarine designers, but has only been used for the purpose, in earnest, within the Former Soviet Union.

Advantages:

- better specific strength than steel.
- non-ferromagnetic (hence reducing the possibility of detection via magnetic signature).
- good corrosion resistance.

Disadvantages:

- hull fabrication is perceived to be difficult, due to complexities in welding Ti alloy.
- Ti alloy is relatively expensive (20 times that of steel), due relative scarcity (except in the Former Soviet Union).

Titanium alloys have been used in the construction of a number of smaller, specialist, submarines, where the performance advantages over steel are considered to be essential and justify the cost penalty.

Glass and Carbon Fibre Reinforced Plastics

Advantages:

- better specific strength (GRP, CFRP) and stiffness (CFRP) than steel.
- non-ferromagnetic (hence reducing the possibility of detection via magnetic signature).
- good corrosion resistance.
- potentially lower maintenance costs.
- stealth capability can be incorporated into the FRP during fabrication.

Disadvantages:

- a revolutionary hull fabrication route needs to be developed, well beyond current capabilities.
- basic materials costs for GRP are broadly equivalent to steel whilst CFRP is 15 times as expensive. Thus, overall fabrication costs, life cycle costs and improved operational envelope must be attractive drivers.

Glass fibre reinforced plastic materials are already well established in the marine sector. They are used in the fabrication of hulls and superstructures for a wide variety of vessels, from sailing yachts and passenger ferries, through to 80 metre long minehunters. The range of sea states likely to be encountered in service dictate that a surface ship hull must be designed to withstand a wide variety of in-plane and out of plane bending loads - a material with near -isotropic in-plane strength distribution is called for. At the bottom end of the market, this is achieved by applying the glass reinforcement and the resin, in a random distribution from a spray gun, in the form of short, chopped fibres. At the top end of the market, the reinforcement is applied in the form of a woven cloth (typically a coarse weave 0/90 arrangement) which is cut to fit the mould contours. Resin impregnation methods range from "bucket and brush" to the more sophisticated "SCRIMP" (Siemens Composite Resin Injection Moulding Process - a variant of resin transfer moulding using single-sided, low cost tooling which is suited to large, fairly flat geometry's). Low resin viscosity (to aid resin flow into the cloth) and long pot life (to avoid occurrence of cure before having the time to complete the impregnation) are essential attributes of the resin system. Due to the size of the parts, cold-cure thermosetting resin systems are used (either polyester, epoxy or vinyl-ester), to avoid the need for large post-cure ovens.

This level of technology will typically result in laminates with a near-isotropic in-plane Young's Modulus of 20-28 GPa and strength levels of 200-300 MPa. These values are sufficient for boat hulls, but they are rather uncompetitive for submersible hulls. However, the design of a submarine hull is driven by one principle load case -- withstanding the external hydrostatic pressure whilst at maximum dive depth. Since a submarine hull is essentially a closed ended cylinder, the external hydrostatic pressure results in an in-plane -2(hoop) : -1(axial) biaxial stress state acting in the hull wall. There is no need for a near-isotropic fibre arrangement and optimisation of the fibre placement geometry is therefore possible, making a more efficient use of the inherent fibre properties. This opens the door to both glass and carbon fibre materials.

Filament winding is ideally suited to this application, a technology used in the military/commercial sector for the fabrication of rocket launch tubes, rocket motors, chemical pipelines and a variety of pressure vessels, though a new departure for the marine industry. A winding machine is used to place a continuous unidirectional fibre tape onto a mandrel under precise geometric control. Prior to placement on the mandrel, the fibre tape may pass through a resin impregnation bath which is mounted on the winding machine (wet winding) or, alternately, the tape is impregnated in a separate operation prior to the winding process (pre-preg winding). Resin cure is normally effected by post curing the mandrel plus windings in an oven. Cold cure systems are sometimes used but these are in the minority because they cannot be pre-impregnated (a lack of shelf life) and they have a pot life which is rather short, placing severe restrictions on the maximum allowable winding time (hence size of component). Once curing is complete, the mandrel must be removed. There are a number of schemes for this, including soluble mandrels, collapsible mandrels and using a thin former as a sacrificial mandrel which is retained as part of the final structure.

There has been considerable research, both in the West and in the Former Soviet Union, into the feasibility of filament winding a submarine pressure hull using glass or carbon reinforcement. Among the topics investigated are:

Development of a reliable analytical method to predict the buckling/crushing performance of FRP hulls.

Given that buckling theories for simple metallic (i.e. isotropic) cylinders are somewhat inexact, the status of buckling theories for fibre reinforced (i.e. anisotropy) cylinders are even less mature. Studies have been conducted by a number of organisations, including DARPA and ONR in the USA, IFREMER in France, DERA in the UK and labs in the FSU. Though useful experimental data and a better understanding has been gained, the ability to predict with accuracy the limit strength of a filament cylinder in the general case (ie as a function of wall thickness, fibre lay-up and material type), is still beyond current capabilities.

What has emerged is the ability to predict the response of a strictly limited range of cylinders, given some test results on "representative" small scale versions.

Development of optimal pressure hull geometry's.

Putting material type and lay-up geometry to one side for the moment, there are many possible permutations of hull configuration ranging from a thick-walled monocoque to a thin walled, closely spaced, integral rib stiffened arrangement. The principal research work in this area has been conducted in the FSU and in the USA. Design rules have been derived empirically, though it is not known how widely applicable these are.

Optimising the fibre lay-up configuration.

Having previously established that the principal hull loading is a -2(hoop):-1(axial) stress ratio, there are a number of possible winding configurations, ranging from 2 hoop layers /1 axial layer (referred to as a 0(2)/90(1) to mirror the biaxial load arrangement) through a +-55 degree angle ply (to coincide with the biaxial load vector) to a compound arrangement of two or more angle ply configurations. This has been the topic of research in the USA (Cardaroc and Oak Ridge), in the UK (DERA, UMIST, Imperial College), in France (DFN) and in the FSU.

Developing the fabrication route.

The filament winding process can accommodate components of the order 1 metre diameter x 10 metres long x 15 mm wall thickness in GRP on a fairly routine basis. Somewhat thinner (5 mm) components in CFRP are not uncommon. Certain small submersibles fit into this envelope and indeed a limited number of research craft have been successfully designed and built in this way. However the majority of submarine hulls are far bigger than this, perhaps 10 metres diameter, 50 metres in length and requiring a wall thickness in FRP of the order 200 mm.

This is clearly beyond current filament winding practise and has in turn led to a number of issues:

- Building the hull in modules, which can be joined together.
- Co-cured integral rib/hull fabrication versus separately cured then assembled rib/hull fabrication.
- How to cure a thick section composite and avoid damage.
- How to design intrusions into the hull (entry and exit features) and avoid stress concentrations.
- Making a robust FRP hull (i.e. which can survive handling and impact damage)

Seawater System Materials

A submarine platform uses seawater within a number of different systems. The primary use is for cooling the main condensers and the combined heat exchangers of the fresh water cooling systems. Simplistically these systems comprise hull valves, pipe work, valves, pumps, together with the condensers and heat exchangers.

Nickel aluminium bronze castings were selected as the material of choice for the seawater system of nuclear submarines in the 1960,s. The material exhibited a good combination of strength and toughness and shock loading resistance and good general corrosion performance. However after a number of years in service components cast in this alloy were found to be susceptible to severe selective phase corrosion attack. The corrosion was particularly severe in crevices and in weld heat affected zones, especially when associated with low flow conditions or galvanic coupling. Selective phase corrosion rates of the lamella kappa phase as high as 1.1 mm/year were measured. Although there was an extensive programme to look at compositional modifications and heat treatments to try and reduce the corrosion susceptibility these met with only limited success. In part the problem lay with the observed incubation period for the corrosion to commence, the kappa phase appearing to be initially cathodic to the surrounding alpha., and hence the difficulty in determining as to whether any proposed treatment was having a beneficial effect. Although the composition of the alloy is now tightly controlled and welding not permitted on or close to the seawater wetted face corrosion damage of NAB components is the life limiting criteria of the systems of which they are part. The systems need a management system to ensure safe life, with revalidation and replacement of selected safety critical castings at refit intervals. The major contributions to through life costs of these seawater systems are associated with these revalidation costs. At present the candidate replacement for NAB castings is a high strength cupro nickel chromium alloy, however this alloy itself has had casting and welding problems.

For future platforms alternative materials including super duplex stainless steels, super austenitic stainless steels, Inconel Alloy 625 and titanium alloys are being investigated which would give a fit and forget installation, hence giving significant through life cost reductions.

In addition to a replacement for NAB castings titanium has been considered for use in condenser tubes which would allow a U tube design eliminating the need for a return end header. Such a design gives a significant reduction both in size and weight of the condenser and would give opportunities for increased payload. The conventional condenser tube material, cupro nickel has adequate corrosion resistance for a straight through design although it can suffer from hot spot corrosion and sulphide attack. However, the U tube design using cupro nickel tubes would necessitate a reduction in water velocity to prevent erosion occurring in tubes. Such a reduction in water velocity would then reduce the heat transfer performance of the condenser. Titanium in comparison, has a much improved erosion resistance, in fact the water speed could be as high as 30m/s compared to the limit of 3m/s for cupronickel.

In any application fitness for purpose is of importance and an understanding of the fracture degradation processes is crucial. During the early studies on CP titanium it was shown that continuous crack extension could occur at stress intensities below the maximum load toughness. This cracking mechanism has subsequently been referred to as sustained load cracking. The implications of this failure mechanism on service performance on service performance are presently being studied to elucidate the boundary conditions controlling this mechanism. The rate effects observed of increasing yield stress with increasing strain rate were shown to agree with computed curves modeled using a constitutive equation proposed by Cernocky and Kremple. The yield stress of CP titanium is a linear function of the logarithm of strain rate showing an enhancement with increasing rate from 238 MPa to 488 MPa. Under conditions of fixed loading the yield stress will be lower than that measured from a conventional tensile test undertaken at a strain rate of 10-4/s, however, under dynamic or shock loading the yield stress will be higher.

The influence of rate dependent deformation behaviour needs to be considered when assessing the structural integrity of components manufactured from titanium. Work is underway to study rate effects on J R curves and on a broader front to develop a "local approach" to our understanding of fracture.

The local approach is an attempt to use macroscopic constitutive modeling in the understanding of deformation and fracture.

Vibroacoustic Materials

To date all UK submarines have an extensive covering of purpose designed rubber like tiles to provide the required acoustic signature, radiated and self noise signatures. These tiles are labour intensive and costly to apply. The major thrust of our research is therefor directed to reduced UPC and where possible improved performance.

The way head however, is seen to be intrinsically stealthy, structural composites. These will obviate the need for add on parasitic coatings and would replace the steel presently used for fabrication of submarine free flood structure (Casings, fins, rudders, stabilisers hydroplanes etc.). They will thus provide lower UPC when compared to clad steel structures (~20% reduction), will reduce the weight of say a fin by ~40% and it is anticipated that LCC will also be much reduced. The technology is being developed in the submarine composite rudder technical demonstrator programme. To date a 3 dimensional composite structure has been manufactured which is fabricated in such a way as to allow the required through direction compliance necessary for acoustic performance but at the same time has a bending stiffness equivalent to 12 mm of steel. It has a low acoustic reflectivity, low noise radiation characteristics and high intrinsic damping. Ongoing programmes are aimed at providing both Acoustic and Electromagnetic stealth while a further programme is aimed at additionally providing low magnetic stealth features.

As stated earlier traditionally, passive viscoelastic materials are used to reduce the acoustic signature of submarines. However, these treatments presently suffer from a number of limitations, namely:

- Performance varies with depth (pressure)
- Layers are compressible, leading to boat instability
- Performance varies with temperature
- Low frequency performance is poor unless the materials are thick (impractical)

In response to these limitations the SMC have been developing a "smart" active noise control alternative to passive vibroacoustic materials. The active system consists of a sensing layer, an actuating layer and an electronic controller to couple the two together. The principle is as follows:

1. The acoustic sensor (piezoelectric 0-3 composite material) detects an incoming pressure wave and converts this pressure into an electrical signal.

2. The electrical signal is fed to an electronic controller which provides gain and phase control.

3. The modified electrical signal is then fed to the actuator (typically a 0-3 or 1-3 piezoelectric composite material) which results in a movement of the actuator front face. An active compliant surface is created which, with an appropriate control algorithm can absorb the incident sound.

4. The acoustic pressure that is reflected (and transmitted) is monitored and the active control is modified to optimise performance levels.

The advantages of active noise control for underwater signature reduction include:

- layers are incompressible
- performance is not sensitive to pressure or temperature changes
- low frequency performance is good and can be achieved with a thin layer.
- performance levels can be modified to suit particular operational and environment conditions
- stealth capability can be hidden (downgraded) during routine operations (by switching the active system off)

SMC have successfully demonstrated that this technology is feasible, and are now looking to further refine the structures. The construction of a technology demonstrator is being considered.

It is envisaged that these low frequency active systems would be used to compliment existing passive treatments (which perform better at higher frequencies), concentrating on specific problematic areas.

Transducer Materials Research

The transducer materials research covers all aspects of active and passive materials utilised in Sonar systems. One of our main areas of work is characterisation of active materials for Low Frequency Active Sonar's (LFAS). These materials are used in towed array systems for Anti-Submarine Warfare. Under operation, the ceramic material which produces the acoustic energy is subjected to extremely high stresses and voltages. The materials parameters change under these conditions, and at high drive levels the acoustic output can degrade and become very non-linear. Accurate characterisation can reveal the maximum drive levels for the ceramic before this non linear region is attained and also how the ceramic properties change under these drive levels. From this work, a new ceramic material with a lower loss coefficient has recently been recommended for use in high power LFAS systems. The lower loss means the material can be driven at significantly higher power levels before non linearity occurs, thus increasing search range of the Sonar.

Newer types of active material are being examined for use in LFAS systems. Electrostrictive ceramics are of particular interest. These have a superior strain in comparison to the conventional piezoelectric ceramics, but several problems do exist. Primarily a very strong temperature dependence which means the large strain coefficient can be vastly reduced with a small change in temperature, and also the material is very prone to microcracking. New compositions of electrostrictive materials are being investigated in order to reduce these effects and allow the large strain coefficient to be used in an LFAS system

Also within the group, new types of hydrophone materials for submarine flank array applications are being tested. Composite materials are now available with an order of magnitude sensitivity increase. Two specific composites are under development within the research team. These are 0-3 and 1-3 composites. The first number refers to the dimensional connectivity of a passive filler. Hence 0-3's are particles of ceramic in a polymer material, and 1-3's are aligned rods of ceramic again in a polymer material. These composites have several benefits beside increased sensitivity. They are lighter than conventional hydrophones, have a significantly better acoustic impedance match to water, and can be fabricated into arrays. However they are expensive to make and efforts are being made in order to reduce the cost of manufacture.

Even through these materials are expensive to fabricate, smaller 1-3 composite panels are ideal for use in array systems and an international collaboration involving the UK, US and Canadian defence research organisations has been exploring the use of 1-3 composites for mine hunting systems. A 500 kHz prototype imaging system is currently under production and will be trailed in March of this year. This has the benefits of high resolution and wide receive angle.

ADVANCED MATERIALS FOR SUBMARINE CONSTRUCTION

R L JONES
CHIEF SCIENTIST SEA
SMC

DERA

PRESSURE HULL MATERIALS

- DEPENDENT ON PLATFORM ROLE, DESIGN REQUIRES HIGH BUCKLING RESISTANCE OR HIGH CRUSHING RESISTANCE

- KEY MATERIAL PROPERTIES
  - HIGH YOUNGS MODULUS
  - HIGH COMPRESSIVE STRENGTH

- CONTENDER MATERIALS
  - STEEL
  - TITANIUM
  - GRP
  - CRP

DERA

SUBMARINE PRESSURE HULL MATERIALS

- STEEL
  - ADVANTAGES
    - READILY AVAILABLE
    - RELATIVELY CHEAP
    - WELL DEVELOPED RELIABLE FABRICATION PROCESS
    - GOOD FRACTURE TOUGHNESS/SHOCK RESISTANCE
  - DISADVANTAGES
    - FERROMAGNETIC , PRONE TO CORROSION
    - DETECTION ISSUES

DERA

SUBMARINE PRESSURE HULL MATERIALS

- **HSLA STEEL**
  - REDUCED MATERIAL AND FABRICATION COSTS
  - LOWER ALLOY CONTENT
  - NO WELD PRE HEAT
  - SAVINGS of 10% of HULL CONSTRUCTION COSTS

- **TWO GENERIC TYPES BEING STUDIED**
  - Cu HARDENED HSLA100
  - B HARDENED BIS812EMA

DERA

HSLA STEELS

- **EVALUATION PROGRAMME**
  - METALLOGRAPHIC EXAMINATION
  - TENSILE
    - STAR FRACTURE
  - IMPACT
  - FRACTURE TOUGHNESS
  - EXPLOSION BULGE
  - STRESS CORROSION RESISTANCE
  - CORROSION FATIGUE

DERA

6

SUBMARINE PRESSURE HULL MATERIALS

- TITANIUM
  - ADVANTAGES
    - BETTER SPECIFIC STRENGTH THAN STEEL
    - NON FERRO MAGNETIC
    - GOOD CORROSION RESISTANCE
  - DISADVANTAGES
    - COST 20X THAT OF STEEL

SUBMARINE PRESSURE HULL MATERIALS

- GRP
  - ADVANTAGES
    - BETTER SPECIFIC STRENGTH AND STIFFNESS THAN STEEL
    - NON FERROMAGNETIC
    - GOOD CORROSION RESISTANCE
  - DISADVANTAGES
    - REVOLUTIONARY FABRICATION
    - COST 15X THAT OF STEEL

DERA

CRP/GRP HULLS

- DEVELOPMENT OF ANALYTICAL METHOD TO PREDICT BUCKLING/CRUSHING
- OPTIMISING FIBRE LAY UP CONFIGURATION
- DEVELOPING FABRICATION ROUTE
  - FILIMENT WINDING 1M DIA, 15MM WALL, 10M LONG
  - BUILDING IN MODULES
  - CO CURED INTEGRAL RIB/HULL?
  - CURING THICK SECTIONS WITHOUT DAMAGE

DERA

SEAWATER SYSTEM MATERIALS

- **NAB MATERIAL OF CHOICE IN 1960'S**
  - GOOD STRENGTH, TOUGHNESS AND GENERAL CORROSION RESISTANCE
- **IN 1970'S SELECTIVE PHASE CORROSION OBSERVED**
  - 1.1MM/YEAR IN CREVICES AND HAZ OF WELDS
- **COMPOSITIONAL MODIFICATIONS AND HEAT TREATMENTS ASSESSED**
- **REVALIDATION AND REPLACEMENT AT REFIT ARE MAJOR CONTRIBUTION TO THROUGH LIFE COSTS**

DERA

SUBMARINE SEAWATER MATERIALS

- NAB ALTERNATIVES
  - HS CUPRO NICKEL CHROMIUM ALLOY
    - CASTING PROBLEMS
    - WELDING PROBLEMS
  - SUPER DUPLEX STAINLESS STEELS
  - SUPER AUSTENITIC STAINLESS STEELS
  - INCONEL ALLOY 625
  - TITANIUM ALLOYS

Ti CONDENSER TUBES

- U TUBE DESIGN
  - ELIMINATES NEED FOR RETURN END HEADER
  - REDUCTION IN SIZE AND WEIGHT

- BUT INCREASED EROSION
- CuNi 3m/s EROSION LIMIT
- TI 30m/s EROSION RESISTANCE

DERA

SUSTAINED LOAD CRACKING

- CONTINUOUS CRACK EXTENSION BELOW MAXIMUM LOAD TOUGHNESS
- BOUNDARY CONDITIONS CONTROLLING MECHANISM BEING STUDIED
- INCREASING YIELD STRESS WITH INCREASING STRAIN RATE MODELED
  - RATE DEPENDENT DEFORMATION IS CONTROLLED BY DEVIATION FROM AN EQUILIBRIUM STRESS STRAIN CURVE

DERA

SUSTAINED LOAD CRACKING

- FURTHER WORK ON
  - RATE EFFECTS ON J-R CURVES
  - LOCAL APPROACH TO FRACTURE
    - BASED ON UNDERSTANDING OF THE MICROMECHANISMS OF DEFORMATION AND FRACTURE

VIBROACOUSTIC MATERIALS

- SUBMARINES COVERED BY RUBBER LIKE TILES
  - TO PROVIDE REQUIRED ACOUSTIC SIGNATURE, RADIATED AND SELF NOISE SIGNATURES

- CAST ANECHOIC
  - TO REDUCE LCC AND UPC

INTRINSICALLY STEALTHY STRUCTURAL COMPOSITES

- OBVIATE NEED FOR PARASITIC COATINGS
  - REPLACE STEEL IN FREE FLOOD STRUCTURES
  - CASINGS, FINS,RUDDERS, STABILISERS,HYDROPLANES
  - PROVIDE LOWER UPC 20% c/f CLAD STEEL
  - REDUCE WEIGHT BY 40% c/f CLAD STEEL
  - ANTICIPATED REDUCTION IN LCC

INTRINSICALLY STEALTHY STRUCTURAL COMPOSITES

- 3D COMPOSITE STRUCTURE
  - HAS REQUIRED THROUGH DIRECTION COMPLIANCE NECESSARY FOR ACOUSTIC PERFORMANCE
  - WITH BENDING STIFFNESS EQUIVALENT TO 12mm STEEL
  - HAS LOW ACOUSTIC REFLECTIVITY
  - LOW NOISE RADIATION CHARACTERISTICS
  - HIGH INTRINSIC DAMPING

DERA

ACTIVE NOISE CONTROL

- PASSIVE VISCOELASTIC MATERIALS LIMITED BY:-
  - PERFORMANCE VARIES WITH DEPTH
  - LAYERS ARE COMPRESSIBLE, BOAT INSTABILITY
  - PERFORMANCE VARIES WITH TEMPERATURE
  - LOW FREQUENCY RESPONSE POOR UNLESS MATERIALS THICK

DERA

ACTIVE NOISE CONTROL

- ADVANTAGES
  - LAYERS ARE INCOMPRESSIBLE
  - PERFORMANCE IS NOT SENSITIVE TO PRESSURE OR TEMPERATURE
  - LOW FREQUENCY RESPONSE GOOD (20dB FROM 2-6kHZ) DEMONSTRATED
  - STEALTH CAPABILITY CAN BE HIDDEN

#507205 ③

Factors Affecting the Fracture Toughness of High Strength Steel Weldments

by

J.A. Gianetto, J.T. Bowker, J.E.M. Braid and W.R. Tyson

Materials Technology Laboratory-CANMET
568 Booth Street
Ottawa, Ontario, Canada

ABSTRACT

Over the past decade considerable research and development efforts have been directed towards assessment of weld metal and heat-affected zone microstructures and their resultant mechanical properties. In this presentation an overview of several R&D investigations conducted at CANMET will be described. In studying the factors that affect the fracture behaviour of high strength steel weldments a primary goal has been optimizing welding consumables and procedures, as well as developing appropriate testing techniques for evaluation of weld metal and heat-affected zone regions of multipass weldments.

The influence of energy input, proportion of as-deposited to reheated, and the final weld metal microstructure and hardness are important factors to be considered in explaining the variations in weld metal toughness for welds produced in both HY and HSLA steels. For HAZ evaluations, the influences of base metal chemistry, welding thermal cycle, and effects of local brittle zone and strength mismatch are important in understanding and controlling the fracture toughness of the HAZ region.

Factors Affecting the Fracture Toughness of High Strength Steel Weldments

by

J. A. Gianetto, J.T. Bowker,
J.E.M. Braid and W.R. Tyson

Materials Technology Laboratory-CANMET,
Ottawa, Ontario

CANMET

Objective

To provide an overview of CANMET R&D on the factors affecting toughness of high-strength steel weld metal and heat-affected zone regions in single and multipass submerged-arc weldments.

CANMET

Factors Affecting Weld Metal Toughness

- » Weld metal composition
  - - electrode wire/flux combination
  - - dilution with respective base materials
- » Energy input and reheating
  - - single and multipass welds
- » Small-scale tests such as CVN and DT
- » Notch position
  - - conventional vee groove
  - - narrow gap

HY80 and HSLA80 Multipass Welds

HY80

% C = 0.09

% Mn = 0.9-1.3

% Ni = 2.0

% Cr = 0.4-0.8

% Mo = 0.26-0.38

% Cu = 0.03-0.04

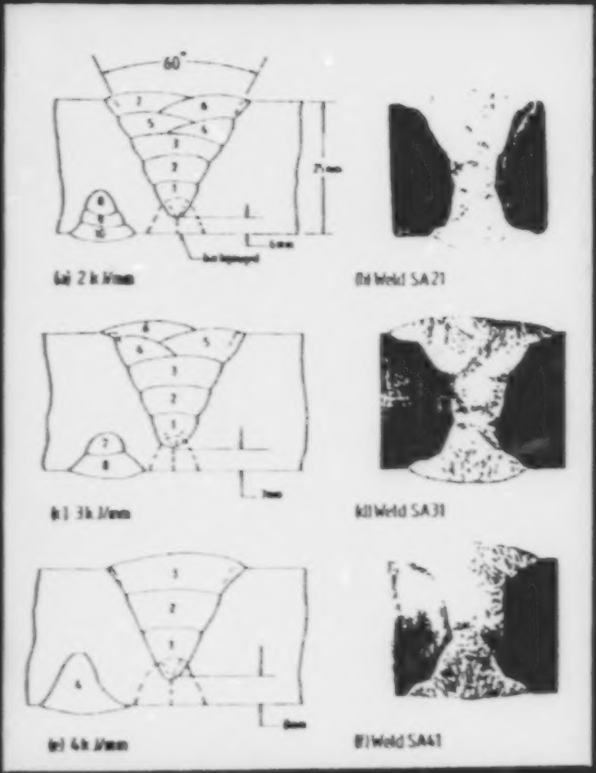
60°
7
6
5
4
3
2
1
8
9
10
25 mm
6 mm
(a) 2 kJ/mm
(b) Weld SA21
6
5
4
3
2
1
7
8
(b) 3kJ/mm
(d) Weld SA31
3
2
1
4
(c) 4kJ/mm
(f) Weld SA41

HSLA80

% C = 0.06

% Mn = 1.0-1.2

% Ni = 1.3-1.7

% Cr = 0.3-0.4

% Mo = 0.30

% Cu = 0.35-0.59

CANMET

Yield Strength of Multipass Welds

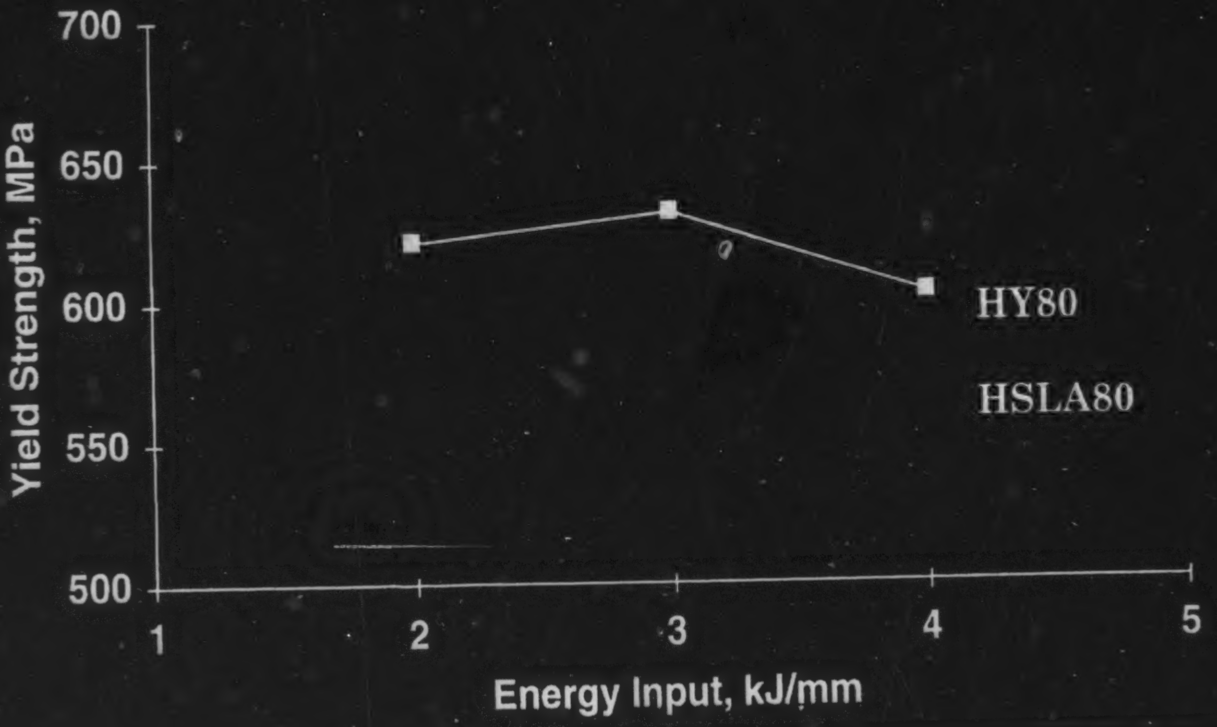

CANMET

CVN Toughness of Multipass Welds

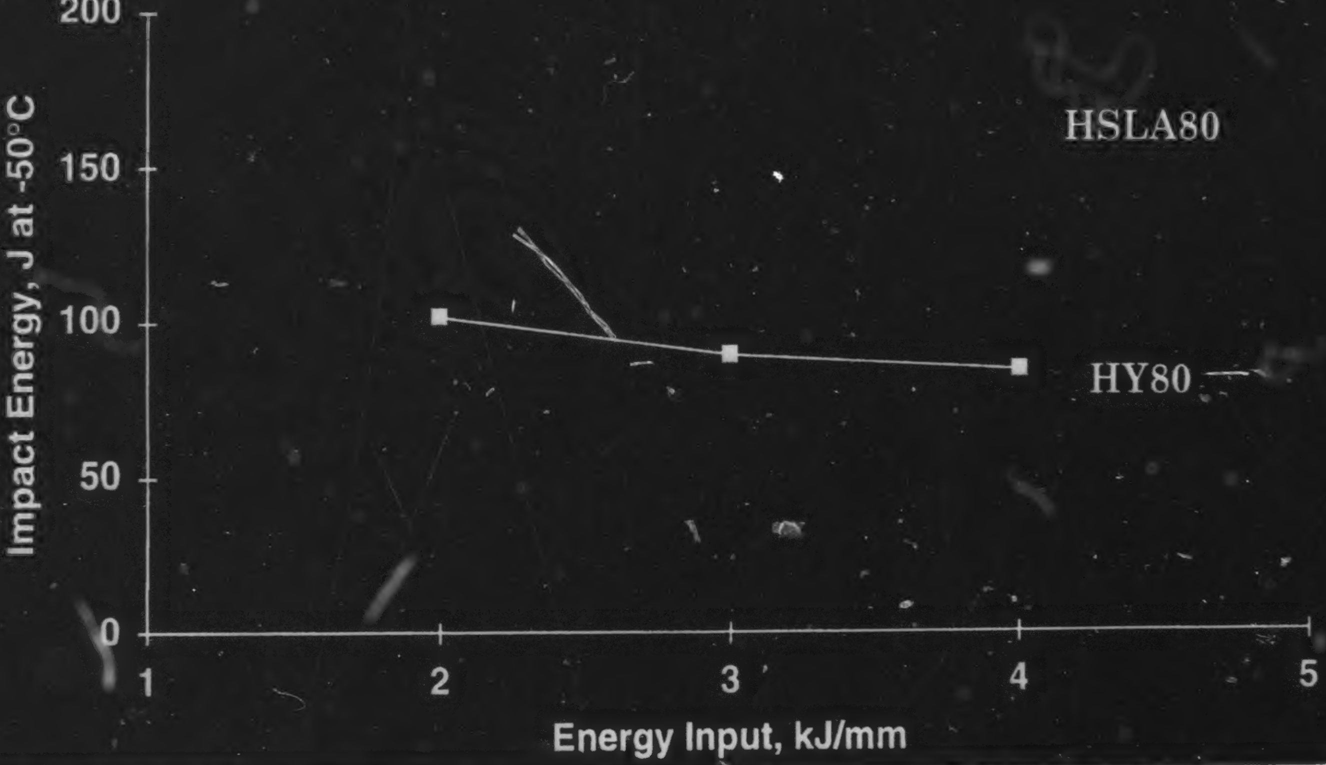

CANMET

Microstructure of HSLA80 SAW welds

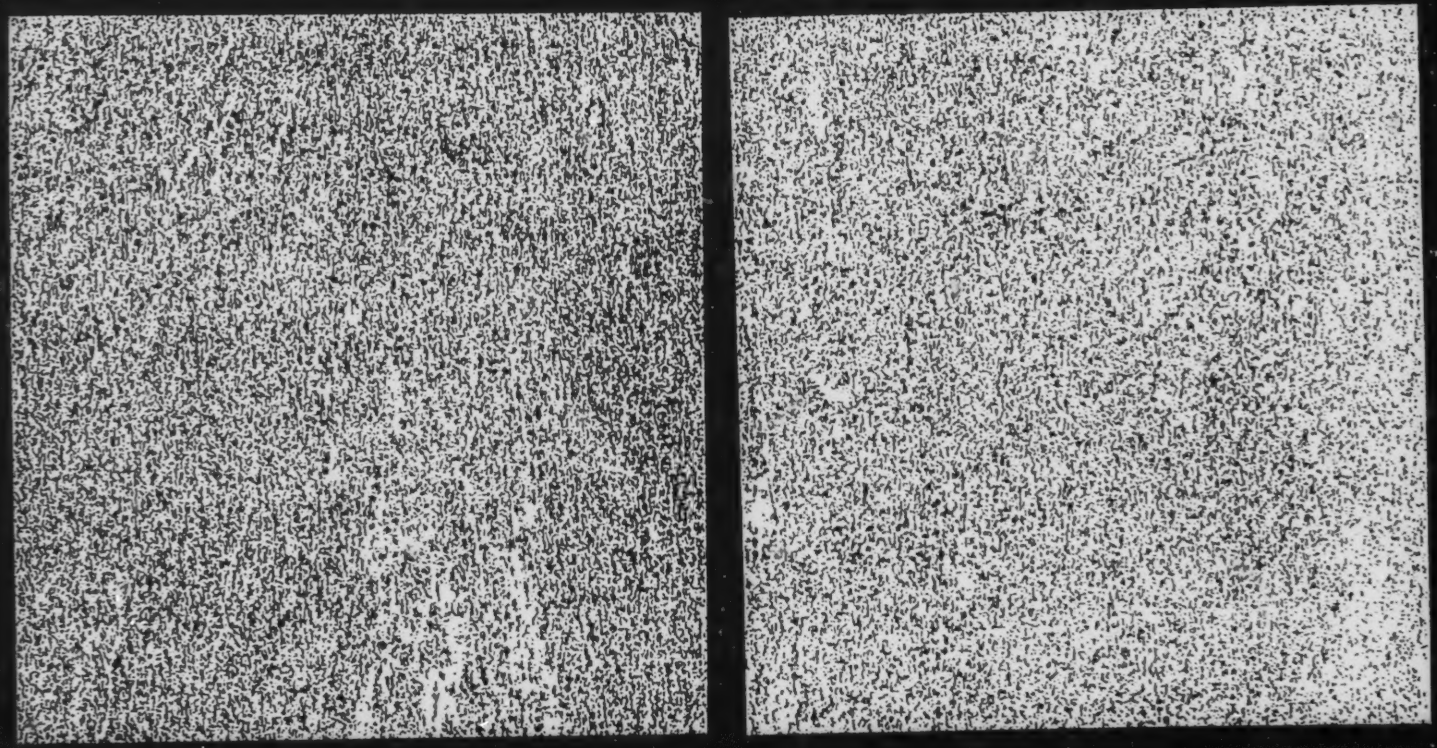

2 kJ/mm

4 kJ/mm

CANMET

Fracture Path Through As-Deposited Weld Metal

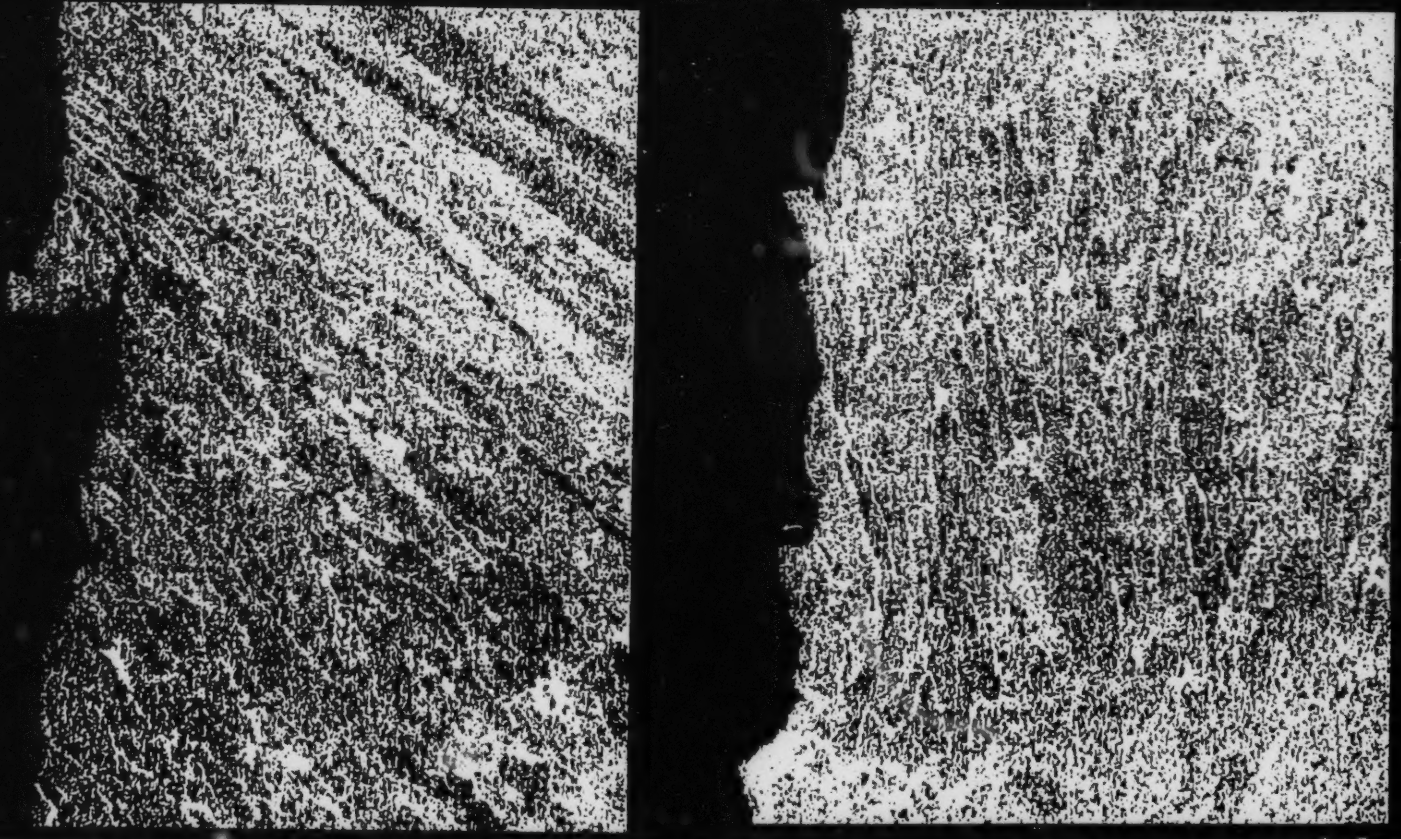

CANMET

HY80 & HSLA80 Bead-in Groove Welds

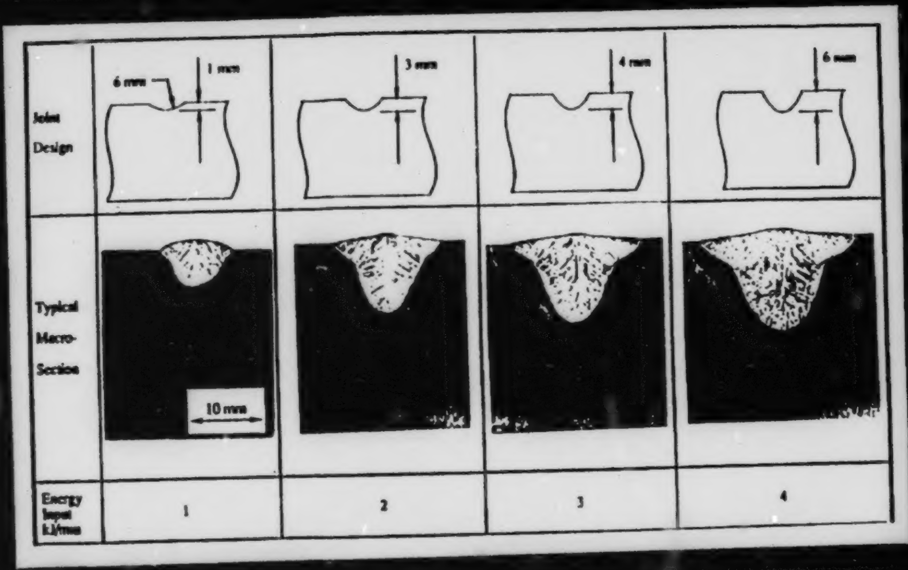
Joint Design
6 mm
1 mm
3 mm
4 mm
6 mm
Typical Macro-Section
10 mm
Energy Input kJ/mm
1
2
3
4

	Element wt%								
Weld No.	C	Mn	Ni	Cr	Mo	Cu	O	CE	Pcm
HY80-1	0.13	0.72	2.2	0.98	0.40	0.04	0.0330	0.67	0.29
HSLA80-1	0.06	0.86	1.1	0.48	0.27	0.68	0.0301	0.47	0.21

CANMET

Yield Strength of BIG Welds

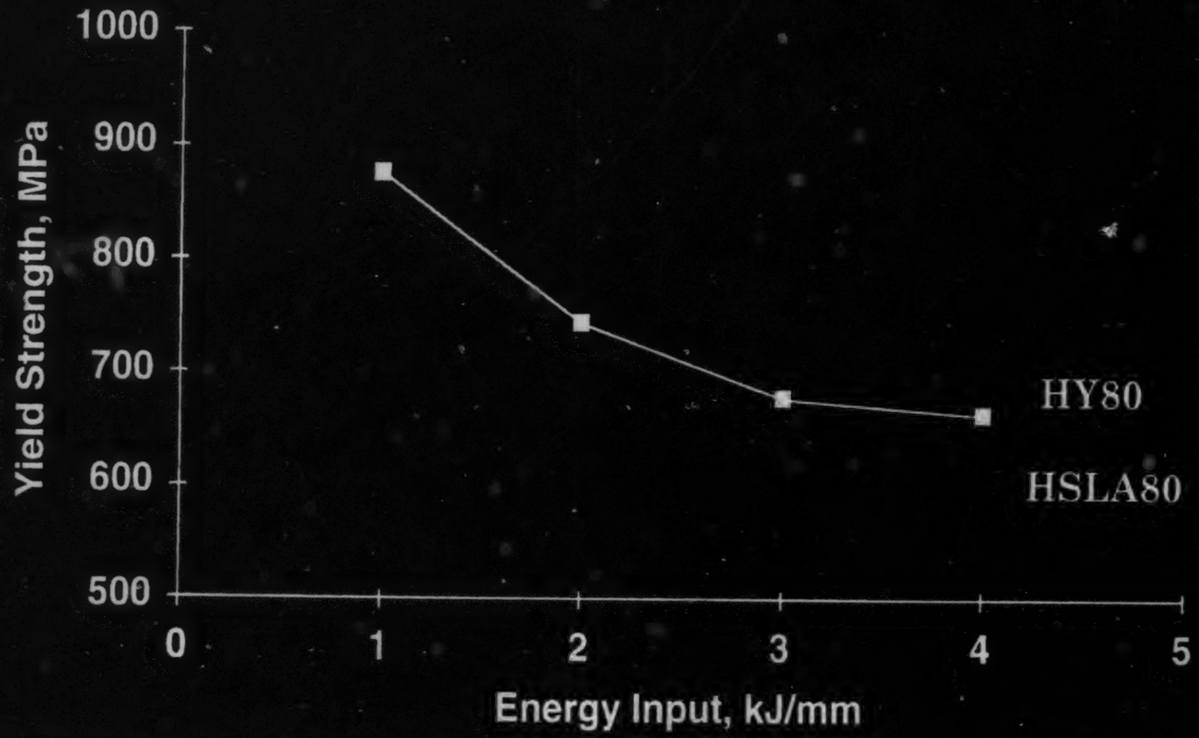

Sub-Charpy Notch Toughness

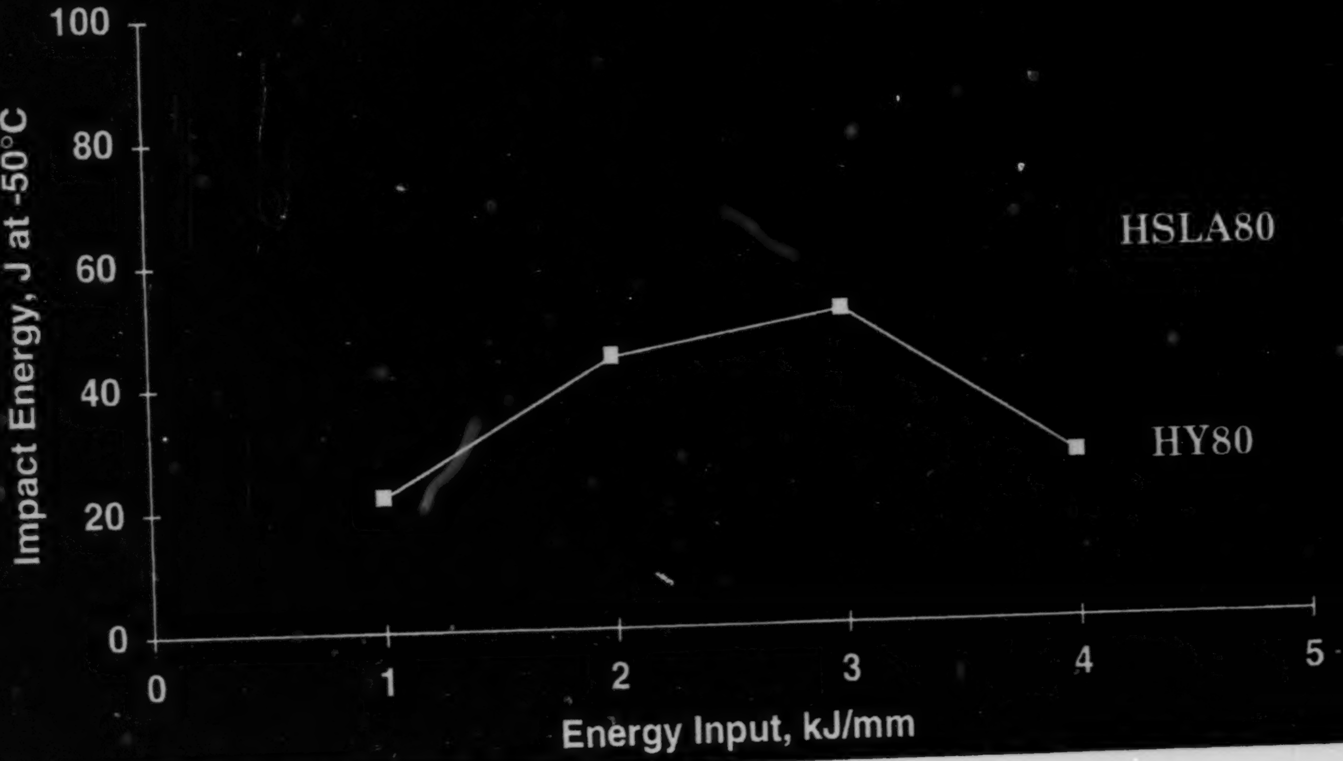

CANMET

Microstructure of Single Pass Welds

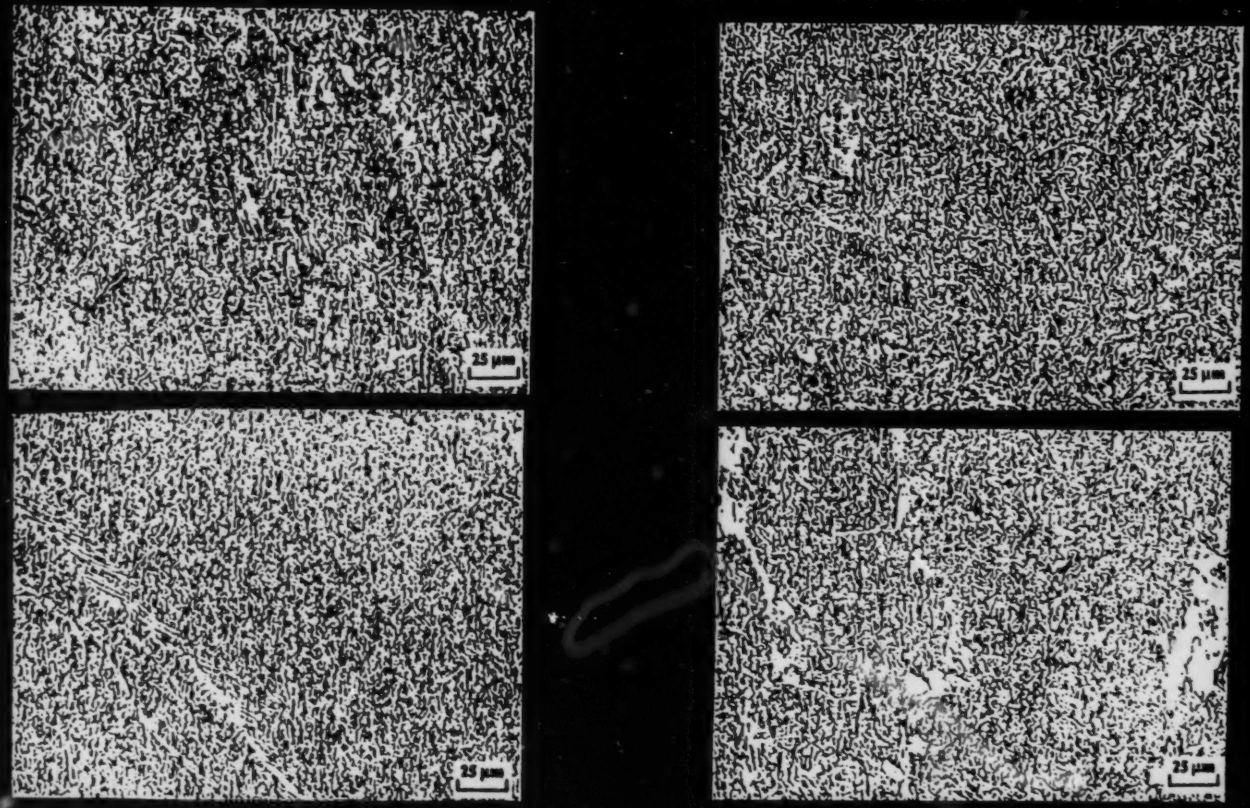
HY80
HSLA80
25 µm
25 µm
25 µm
25 µm
1 kJ/mm
4 kJ/mm

CANMET

CCT Diagrams for HY80 and HSLA80 Weld Metal

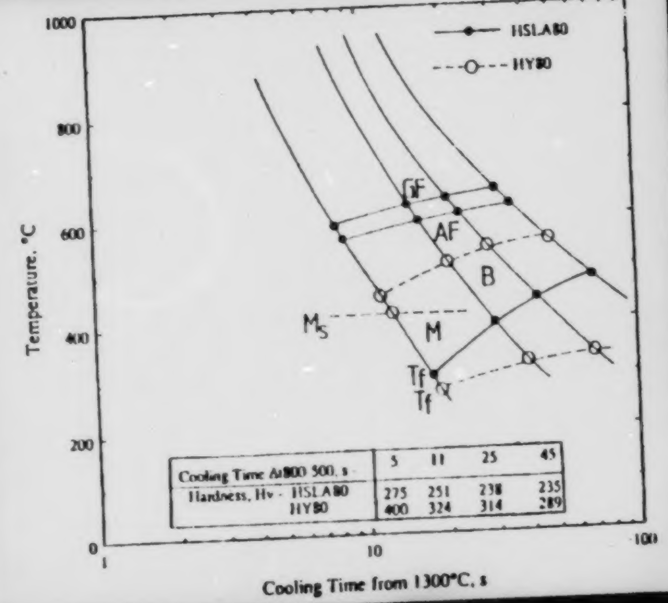

Cooling Time Δt800 500, s	5	11	25	45
Hardness, Hv - HSLA80	275	251	238	235
HY80	400	324	314	289

CANMET

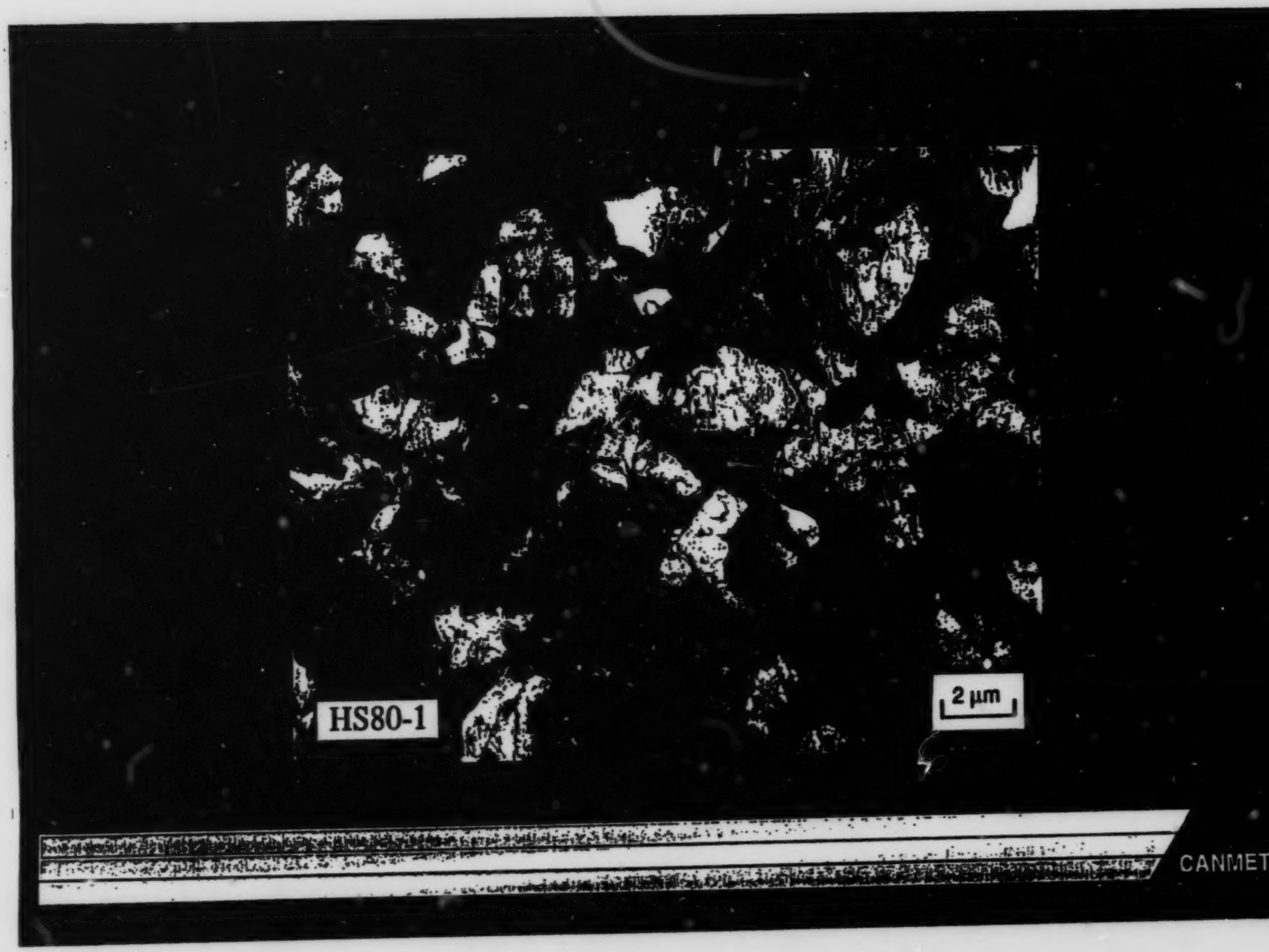

HS80-1
2 µm
CANMET

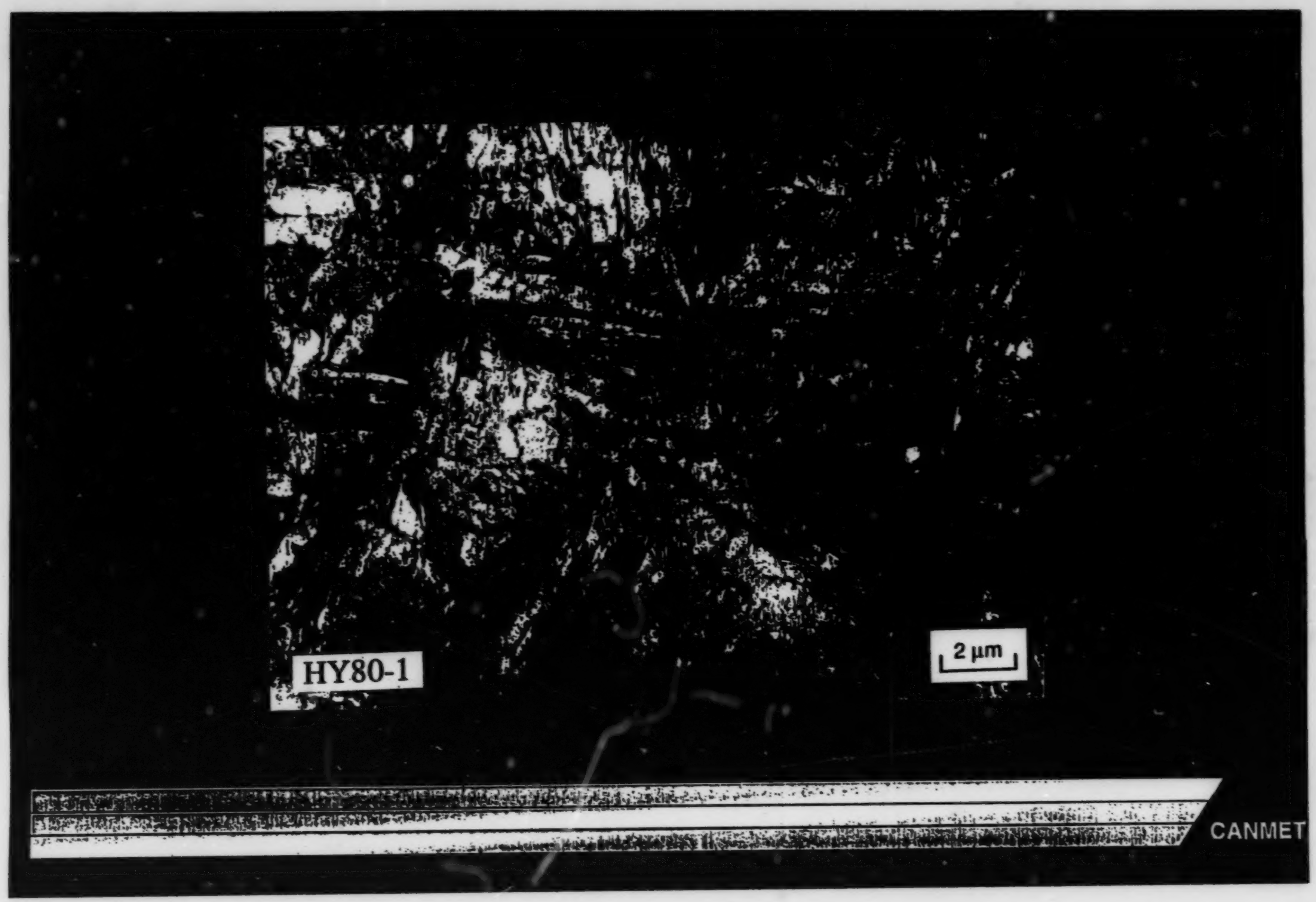
HY80-1
2 µm
CANMET

Weld Metal Summary

- Multipass Welds
  - increase in energy input produces a decrease in yield strength.
  - differences in the proportion of AD and RH weld metal.
  - evidence to suggest preferential crack propagation along prior austenite grain boundaries .
- Single Pass Welds
  - high dilution with respective base materials results in major differences in microstructure and resultant properties.

CANMET

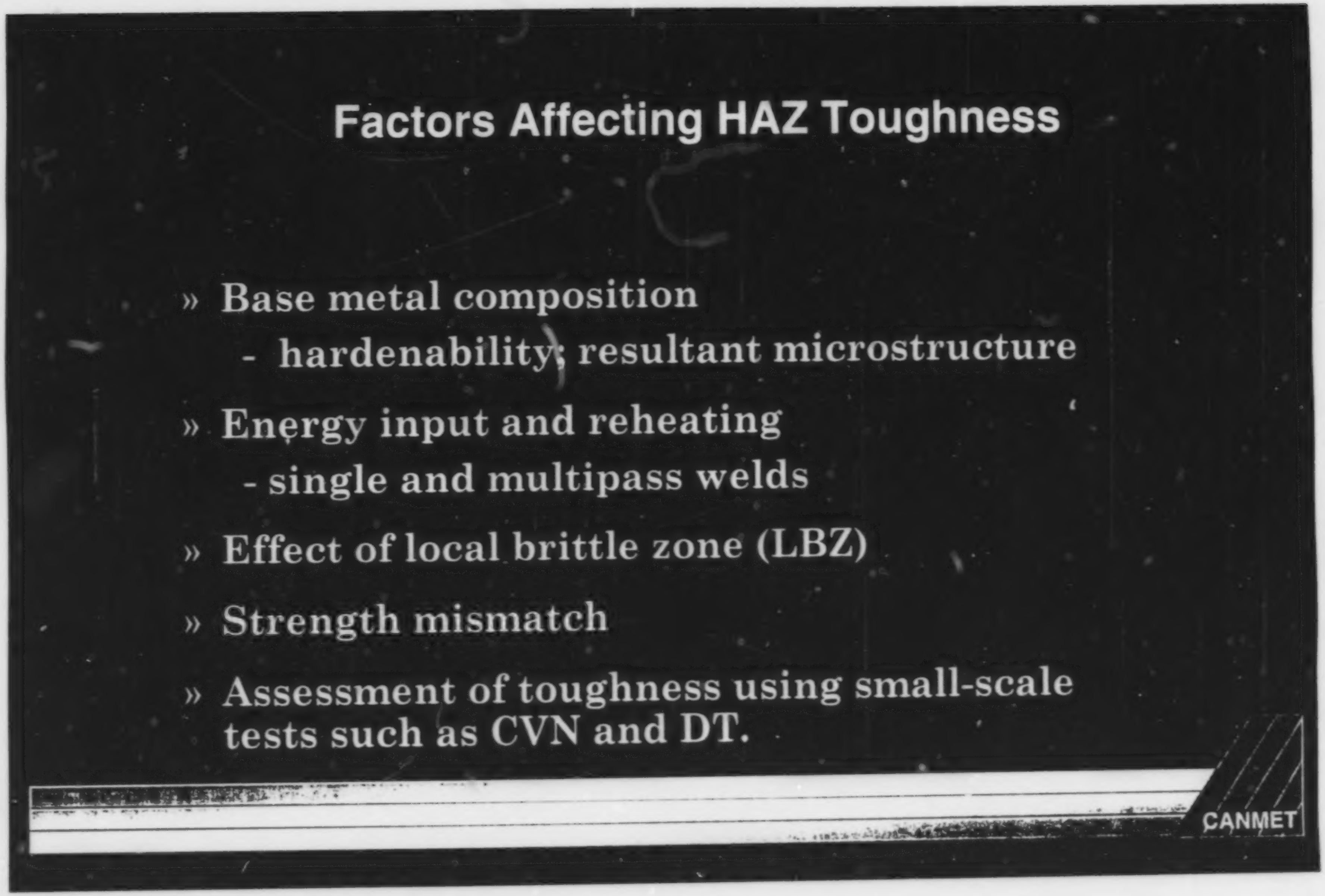

Factors Affecting HAZ Toughness

- » Base metal composition
  - hardenability; resultant microstructure
- » Energy input and reheating
  - single and multipass welds
- » Effect of local brittle zone (LBZ)
- » Strength mismatch
- » Assessment of toughness using small-scale tests such as CVN and DT.

CANMET

Intercritically Reheated GCHAZ

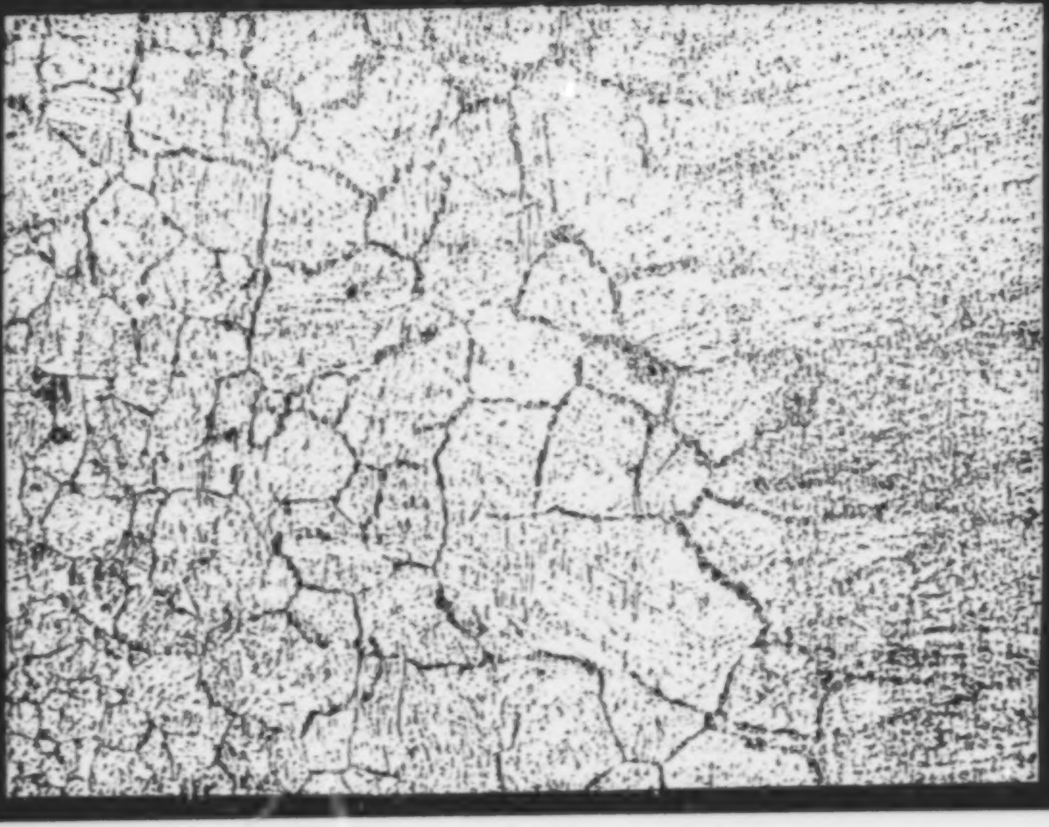

CANMET

Chemical Compositions

Steel	Element wt %										
	C	Mn	Si	S	P	Cr	Ni	Mo	Cu	Nb	CE
HSLA100	0.05	1.00	0.34	0.003	0.009	0.61	1.77	0.51	1.23	0.037	0.64
HY100	0.17	0.33	0.23	0.008	0.010	1.52	2.62	0.48	0.03	-	0.80

CANMET

CVN Toughness of Simulated GCHAZ
Tp = 1350°C and Cooling Time Δt8-5 = 11s

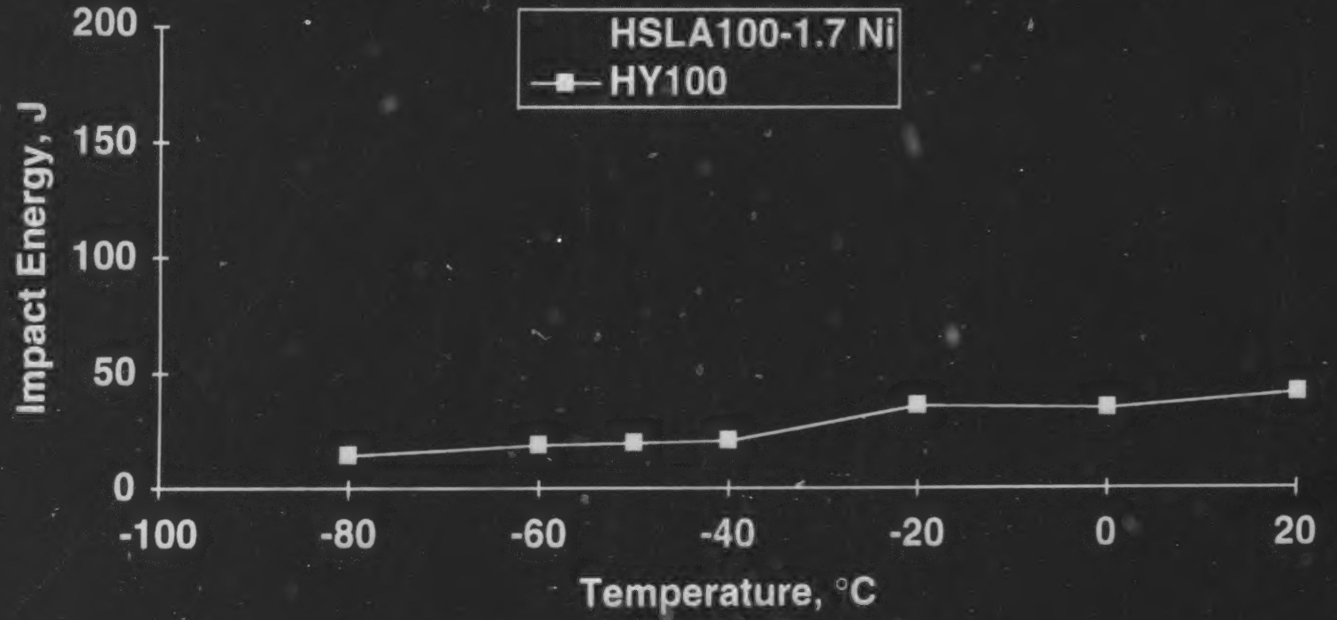

CANMET

Heat-Affected Zone

- Joint Design
  - Narrow-gap versus single-vee
- HAZ Microstructure
  - HSLA100 versus HY100

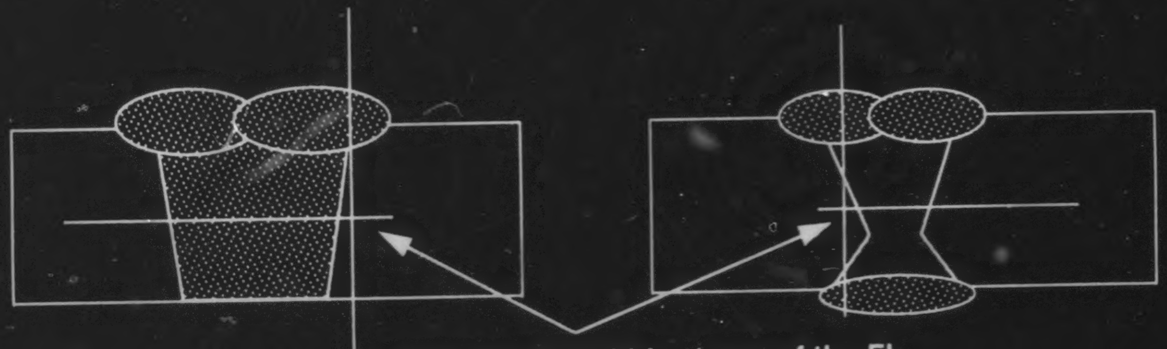

notch located within 1 mm of the FL

CANMET

DT transition curves for the HAZ region

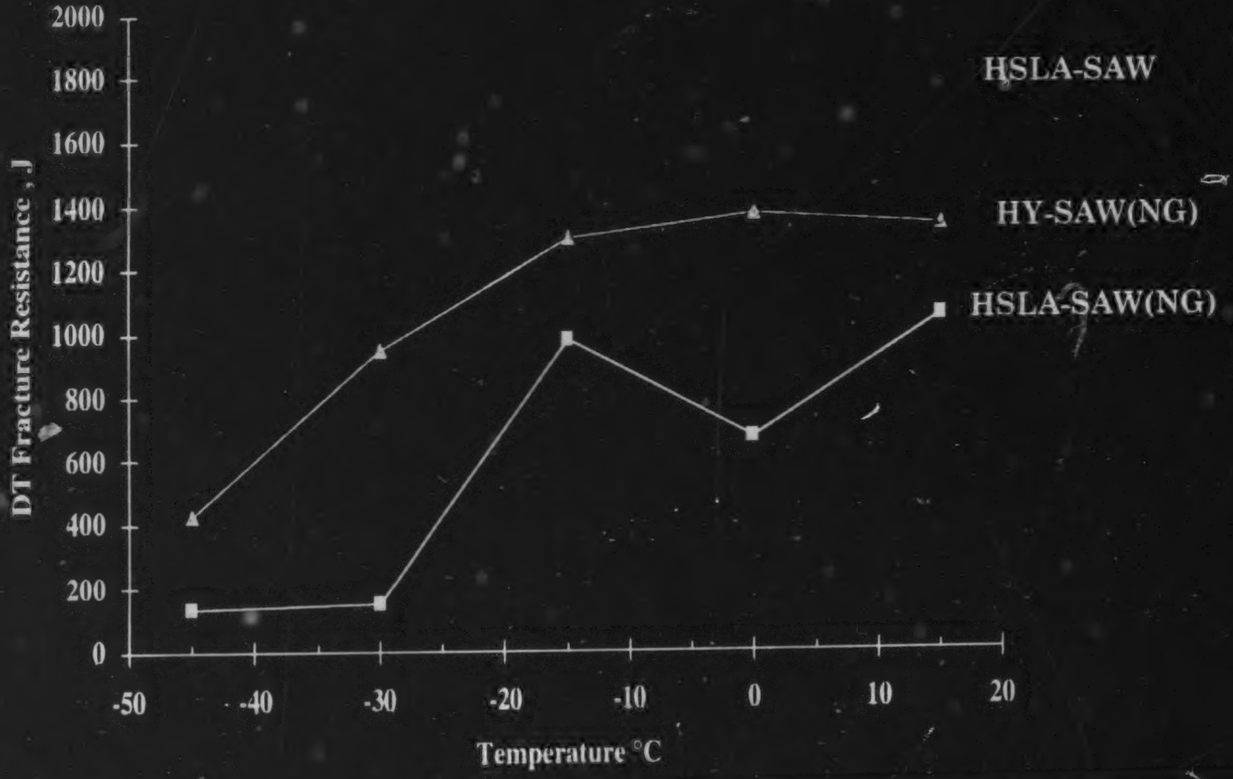

CANMET

Microhardness of HAZ regions

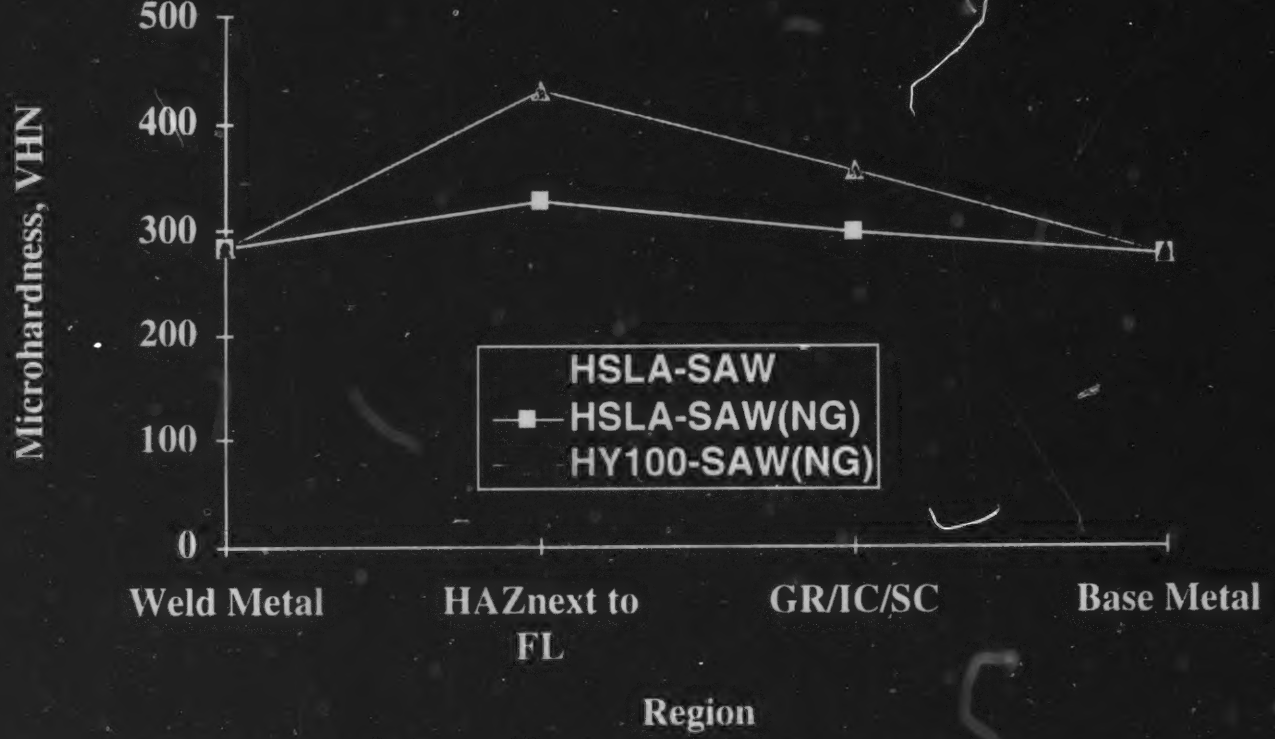

CANMET

HSLA100

GCHAZ

HY100

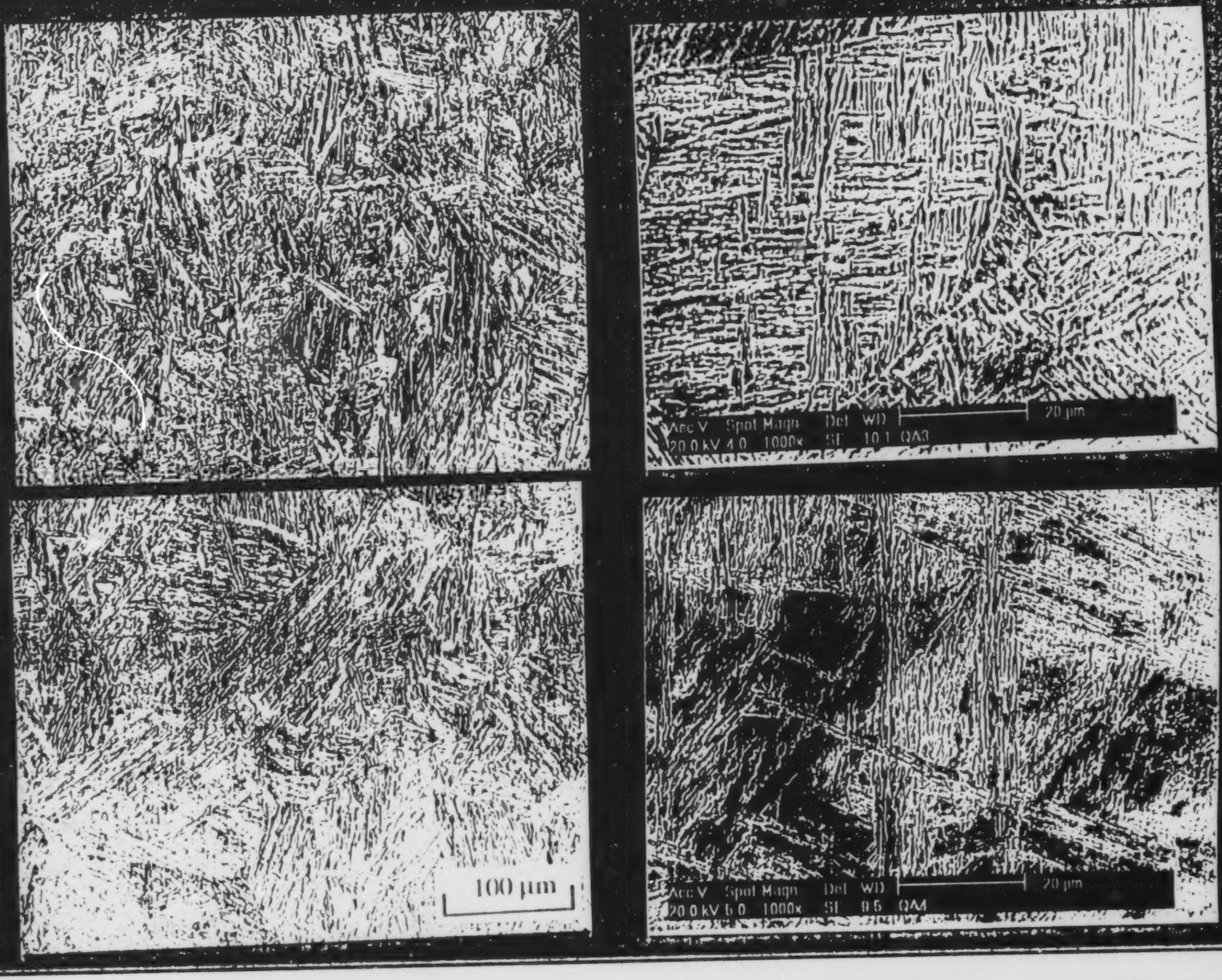
Acc.V Spot Magn Det WD 20 µm
20.0 kV 4.0 1000x SE 10.1 QA3
100 µm
Acc.V Spot Magn Det WD 20 µm
20.0 kV 6.0 1000x SE 9.5 QA4

CANMET

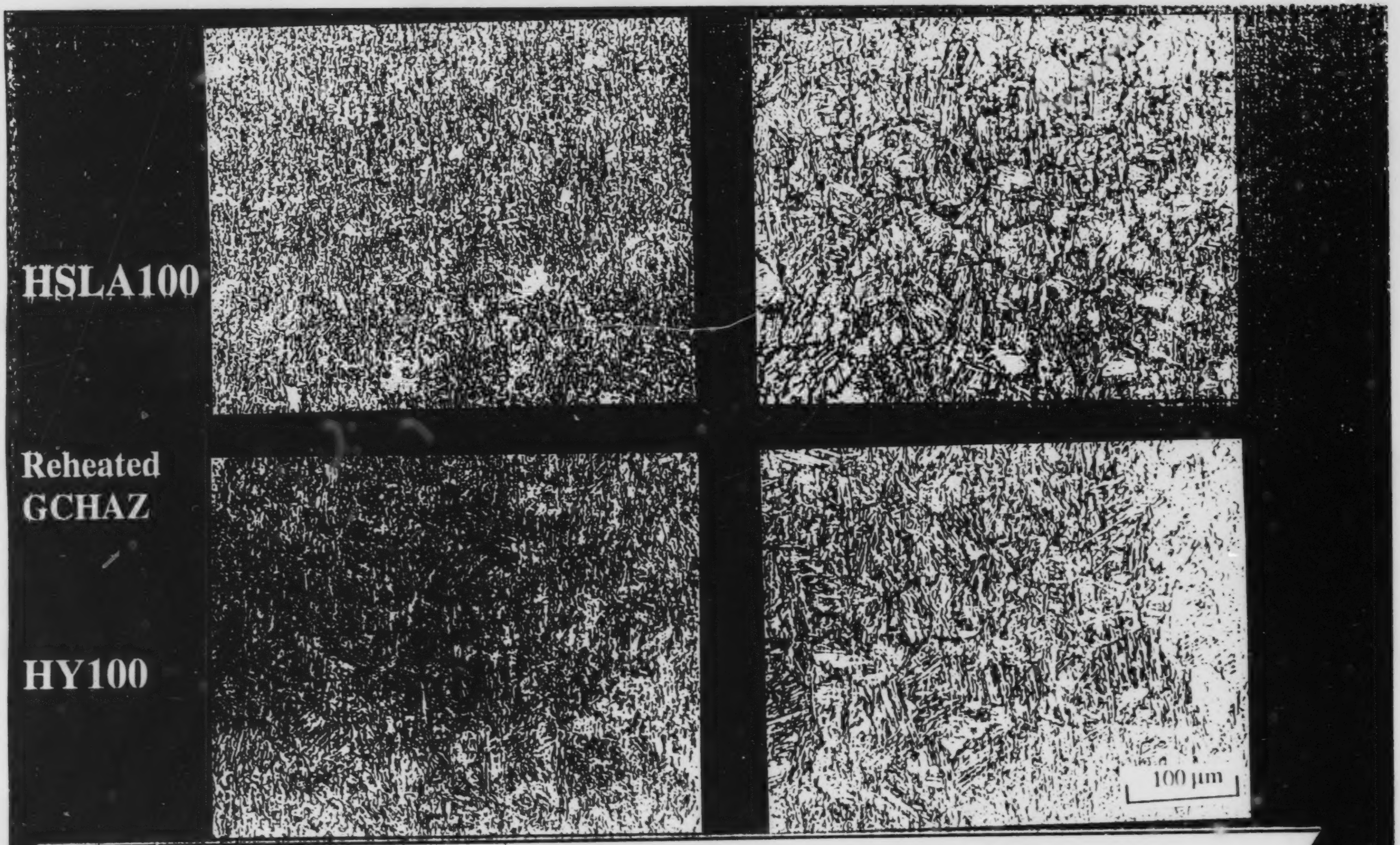
HSLA100
Reheated GCHAZ
HY100
100 µm

CANMET

Post-test Metallographic Sections

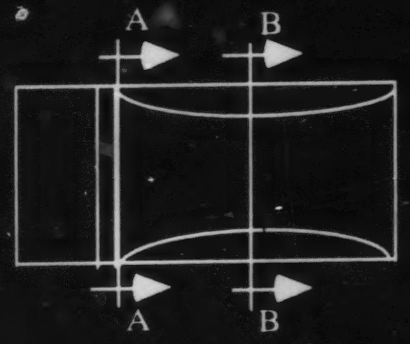

A-A just below the notch tip and B-B half-way along the fracture ligament.

HSLA-SAW(NG)
HAZ Fracture Paths

Notch Tip

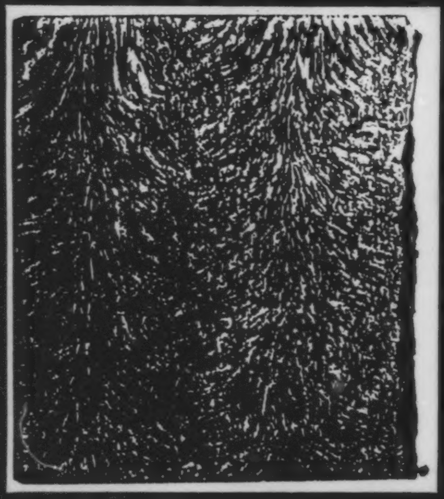

42% HAZ near FL

1/2 way along fracture path

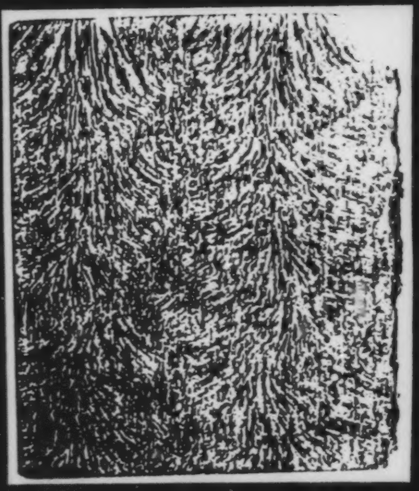

78% HAZ near FL

HY-SAW(NG)
HAZ Fracture Paths

Notch Tip

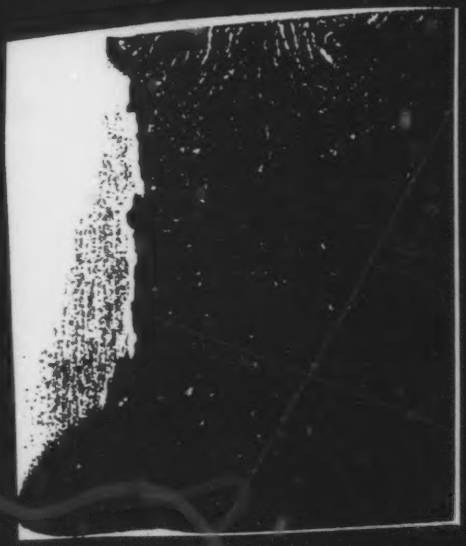

49% HAZ near FL

1/2 way along fracture path

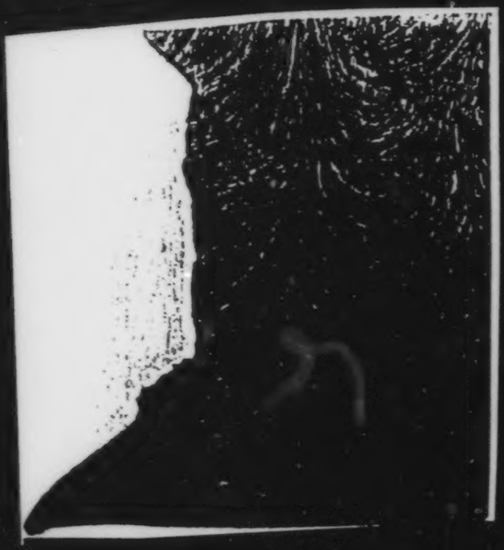

20% HAZ near FL

CANMET

Through-Thickness Fracture Path

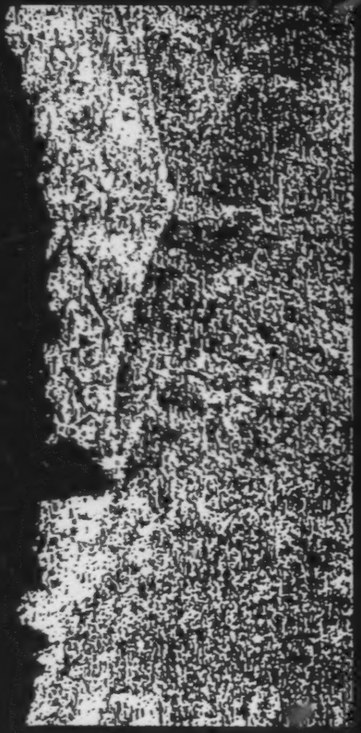

HSLA100

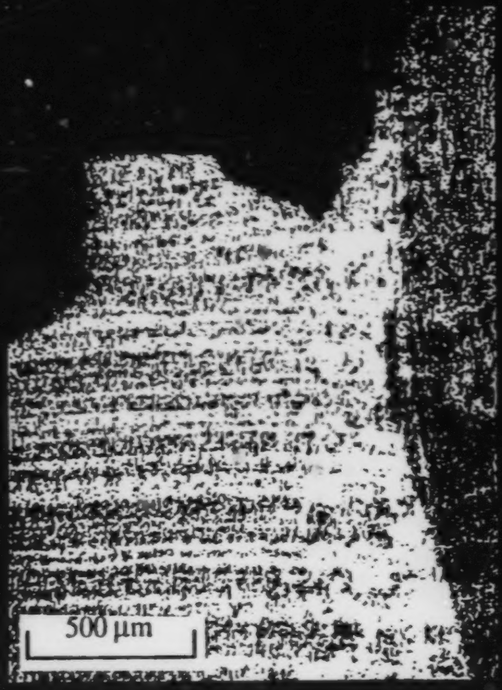

HY100

CANMET

HAZ Summary

- Considerable variation in DT fracture resistance
  - HY-SAW(NG) 949J at -30°C
  - HSLA-SAW(NG) 150J at -30°C
- Factors

- marked difference in HAZ microstructure and hardness,
- inhomogeneity of strength and toughness of the many HAZ regions sampled,
- influence of reheating on toughness,
- effect of strength mis-match on the deformation behaviour, particularly crack deviation towards softer material, and
- effect of both total amount and width of HAZ sampled by the notch tip.

#507206 ③

GMAW Power Sources for the Joining of High Strength Steels

by

Corby Nicholson and Lalit Malik
Fleet Technology Limited, Kanata

and

James R Matthews
Defence Research Establishment Atlantic

ABSTRACT

Commercially available Pulsed Gas Metal Arc Welding power sources were reviewed and evaluated, the main objective being to recommend the most applicable package for all position welding of high strength steels used in the construction of naval vessels.

Evaluation criteria included practical considerations such as size and usability, along with factors such as arc control methods and arc characteristics which relate directly to the suitability of any particular package for successful all position welding of high strength steels.

In addition, a literature review was conducted to determine if any new flux cored or metal cored arc welding consumables have recently been developed which provide adequate weld metal toughness in naval structural steel welds.

GMAW Power Sources For The Joining of High Strength Steels

by

- C. J. Nicholson(Fleet Technology Limited)
- Dr. L. Malik (Fleet Technology Limited)
- Dr. J. R. Matthews (DREA)

presented at

3rd CF/CRAD Meeting on Naval Applications of
Materials Technology
Halifax, N.S., April 22-24, 1997

FTL FLEET
TECHNOLOGY LTD.

Objective

- The main objective was to recommend one or more P-GMAW power sources for use in the Dockyard environment
- A secondary objective was to investigate recently developed flux cored and metal cored consumables for joining high strength naval steels

FTL FLEET TECHNOLOGY LTD.

Approach

- Determine Current Practices in Shipyards in the US, UK, and Australia
- Review Technical Literature for Candidate Flux or Metal Cored Consumables
- Review Technical Literature Available from Power Source Manufacturers
- Conduct Limited Hands-on Trials with Candidate Power Sources

FTL FLEET TECHNOLOGY LTD.

Determine Current Practices

- Simulated Trials have been Successfully Completed in the UK with FCAW
- FCAW Consumable has been Approved for use in Australia
- Pulsed-GMAW is being Successfully Employed in the U.S.

FTL FLEET TECHNOLOGY LTD.

Review of Consumables

- Lincoln Electric - Outershield E91T1-K2 reported as a replacement for the Murex Corofil B 65 used in UK trials
- ESAB/Alloy Rods - Dual Shield II series provides various FCAW consumables which may be suitable for the joining of QT-28, HY-80, and HY-100
- Lincoln Electric - MC 100 for MCAW
- GMAW Consumables Available from Lincoln, ESAB, and Soudor

Power Sources Reviewed

- **Review of Technical Literature from Manufacturers Identified the Following Packages for Further Evaluation:**
  - Hobart Arcmaster 501 w/2410 wire feeder
  - ESAB Digipulse 450 w/XRT feeder
  - ESAB SVI 450 w/4HD wire feeder
  - Miller Maxtron 450 w/64M wire feeder
  - Lincoln Powerwave 450 w/Synergic 7 wire feeder

Power Source Criteria

- **Primary Evaluation Criteria:**
  - Arc Control Methods
  - Arc Characteristics
- **Secondary Criteria:**
  - Ease of Use
  - Size and Portability

FTL FLEET TECHNOLOGY LTD.

Arc Control Methods

- **Adaptive**
- **Synergic**
- **Adaptive-Synergic**
  - In P-GMAW methods of arc control strongly influence how well any given machine can adjust to variations in electrical stickout (ESO). This ability is particularly important for all-position semi-automatic welding

FTL FLEET TECHNOLOGY LTD.

Arc Characteristics

Arc Characteristics are Generally Defined by:

- **Pulse Parameters**
- **Dynamic Response**

FLEET
TECHNOLOGY LTD.

Power Source Findings

- All Five Packages are Suitable from the Standpoint of Size, Portability, and Ease of Use
- Two Packages, the Miller Maxtron 450 and Lincoln Powerwave 450 Provide the Most Favorable Arc Characteristics
- The Lincoln Powerwave 450 is the Preferred Package as a Result of Advanced Arc Control Methods and Low Alloy Steel Pulse Programs that Perform Well for All Position Welding

Miller/BOC Canox

- Maxtron (BOC Invertron) 450 w/64M wire feeder:

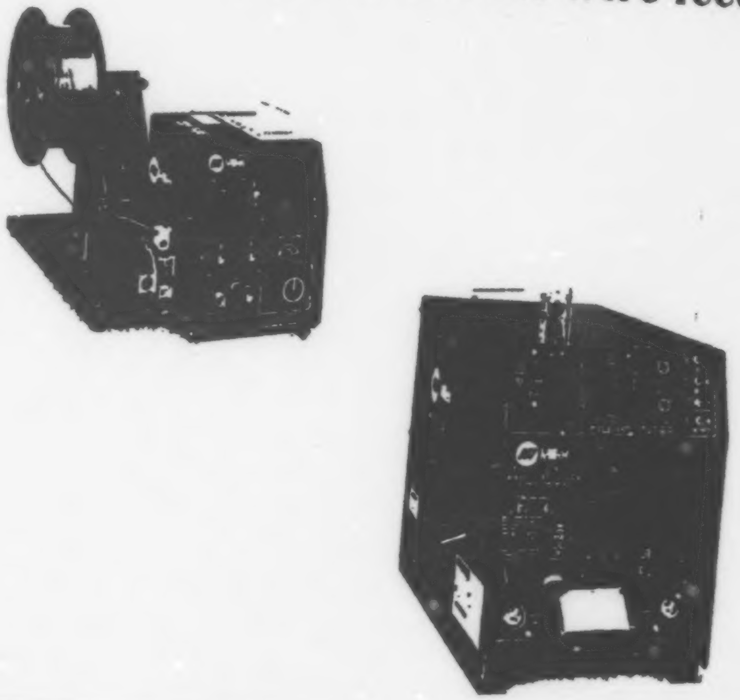

FTL FLEET TECHNOLOGY LTD.

Lincoln Electric

- Powerwave 450 w/Synergic 7 wire feeder

Conclusions

- **Developments in Power Source Technology and Consumable Formulation Present More Options Than Ever Before for the Joining of High Strength Steels Used in the Construction of Naval Vessels:**
  - The Lincoln Powerwave 450 has been judged to be the most suitable package for P-GMAW in the Dockyard application
  - FCAW and MCAW consumables now demonstrate some promise as an eventual alternative to P-GMAW

#30

Investigation of Fumes Generated in Welding and Cutting of Navy Materials

by Gene L. Franke, Raymond H. Juers and Reynold T. Brenna

Naval Surface Warfare Center, Carderock Division
9500 MacArthur Boulevard
West Bethesda, Maryland 20817-5700 USA

ABSTRACT

A Navy/Industry Task Group, coordinated by the Naval Sea Systems Command, is addressing the technical and economic impact of anticipated United States Occupational Safety and Health Administration (USOSHA) reductions in permissible worker exposure limits for hexavalent chromium (Cr(VI)). This change is expected to reduce the permissible exposure limit (PEL) from an existing ceiling level of 100 mg/m^3 to between 0.5 mg/m^3 and 5.0 mg/m^3. As a part of this effort, the Naval Surface Warfare Center, Carderock Division, is investigating methods that can be adopted to reduce worker exposure to Cr(VI) and other hazardous components (Mn, Ni) of airborne emissions from welding and other related operations.

The first step of this process has been to establish baseline data for several of the Navy's materials. A standardized approach was taken to facilitate comparisons of materials, operations, and fume test methods. The operations investigated were shielded metal arc welding (SMAW), gas metal arc welding (GMAW), flux cored arc welding (FCAW), and oxyacetylene cutting. Plate materials included mild steel; DH-36, A387-Grade 22, HSLA-65, HSLA-80, HSLA-100, HY-80, and HY-100. SMAW electrodes included 7018, 11018, 12018, 8018-B2L, 9018-B3L, 309-15, and 309-16. GMAW electrodes included 70S, 100S, 120S, and Alloy 625. FCAW consumables included 71T, 101T, and 309LT. Shielding gases included Ar - 2% O_2, Ar - 5% CO_2, Ar - 25% CO_2, and 100% CO_2. The laboratory space used for all operations met the Task Group definition of an open space (ceiling height greater than 16 feet). All operations were performed for a testing period of 150 minutes. Welding was performed at a 60% duty cycle, while cutting was continuous. Appropriate filters were placed on the welder's collar, and additional filters were placed approximately ten feet from the operation to collect personal as well as area fume samples. No local exhaust system was imposed to extract fumes from the work site. USOSHA draft Method 215 was used to determine Cr(VI),and inductively coupled plasma was used to determine thirteen additional elements in the fume samples.

Correlations are made between materials, operations, and fume results. Additional comparisons are discussed concerning the effects of shielding gas, SMAW electrode coating formulation, product formulation/chemistry, and plate material used. Results indicate that, without engineering controls, use of welding products for all materials investigated can result in fumes with Cr(VI) above action levels. Oxyacetylene cutting also requires engineering controls to reduce worker exposure to hazardous fume constituents. Certain operations and materials will also produce unacceptable levels of nickel and manganese in fume.

The next phase of this work will investigate the effectiveness of several types of engineering controls on reducing these airborne emissions to acceptable levels.

3rd CF/CRAD Meeting

Halifax, Nova Scotia

Investigation of Fumes Generated in Welding and Cutting of Navy Materials

G.L. Franke, R.H. Juers, and R.T. Brenna

Naval Surface Warfare Center
Carderock Division
West Bethesda, Maryland, USA

NSWCCD 615 - 0497CRAD

Cr(VI) Reduction in Navy Welding and Manufacturing Operations

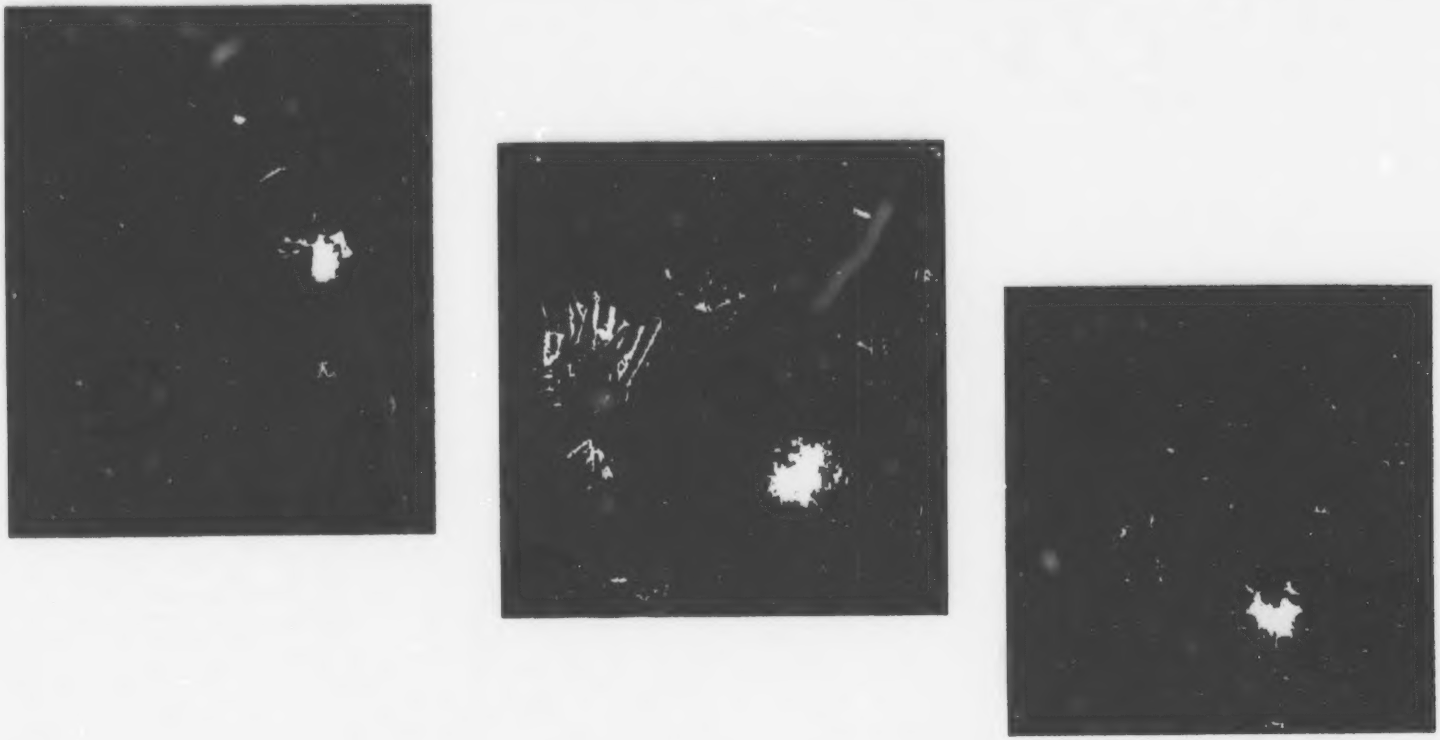

Proposed Exposure Limits Validation Criteria

	Current	Proposed
➢ Cr(VI)	100 (as chromates)	0.5
➢ Mn	1000	200
➢ Ni	1000	50

All values in ug/m^3

Manufacturing Operations Impact

- Construction, repair, and fabrication of Navy facilities
- Metal cleaning of chromate-coated materials
- Electroplating
- Painting/application of chromate paints and coatings
- Welding, thermal spraying, thermal cutting, and gouging

Economic Impact

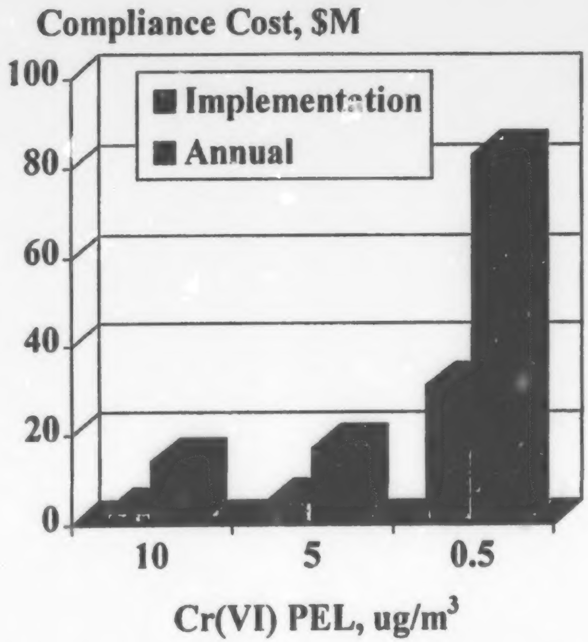

- Equipment purchase
- Implementing engineering controls
- Process/procedure modification
- Education
- Monitoring exposure levels

Potential Solutions

- *Engineering controls*
  - Commercially available, cost effective
- *Process modifications*
  - Can be developed, easy to implement
- *Materials modifications*
  - Major development and certification
- *Alternative practices (e.g., reduced work hours, training, monitoring)*
  - Expensive, cumbersome

Objective

- *Characterize airborne emissions of chromium, nickel, and manganese from welding and related operations in Navy fabrication and repair.*
- *Evaluate methods to minimize these emissions in order to comply with anticipated OSHA and EPA requirements.*

Baseline Fume Testing

- ***Operations, with duty cycle***

Oxy-Fuel Cutting (OFC)	100%
Shielded Metal Arc Welding (SMAW)	66%
Gas Metal Arc Welding (GMAW)	60%
Flux Cored Arc Welding (FCAW)	60%

- ***Conditions***
  - Open space (high ceiling)
  - 150 minute duration
  - No engineering controls

Baseline Fume Testing

- *Materials*
  - **Plate** - Mild steel, DH-36, ASTM A387-Gr.22, HSLA-65, HSLA-80, HSLA-100, HY-80, HY-100
  - **SMAW** - 7018, 11018, 12018, 8018-B2L, 9018-B3L, 309-15, 309-16
  - **GMAW** - 70S-6, 100S-1, 100S-2, 120S-1, 625
  - **FCAW** - 71T-1, 101TM, 309LT-1
  - **Gases** - Ar-2% O_2(M2), Ar-5% CO_2(C5), Ar-25% CO_2(C25), 100% CO_2

Baseline Fume Analysis

- *Sampling*
  - **Stressors, test methods**
    - Cr(VI), Method 215
    - Total fume, ICP scan for 13 elements
  - **Locations**
    - Personal (operator's collar)
    - Area (10-15 feet from operation)
- *Calculate 8-hr time weighted average (TWA)*

Filter Placement

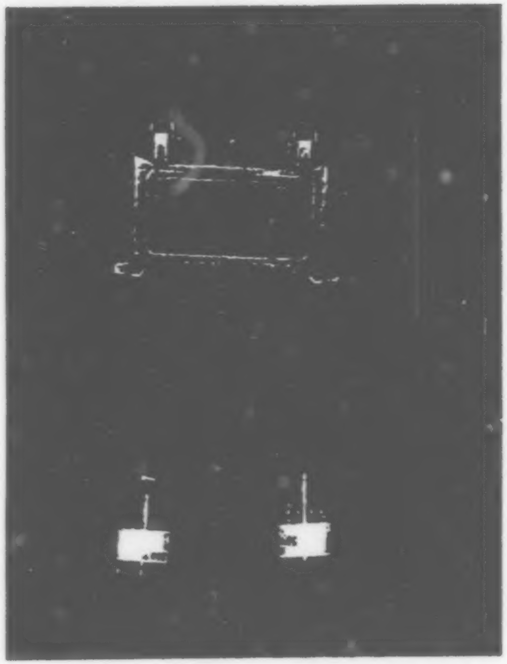

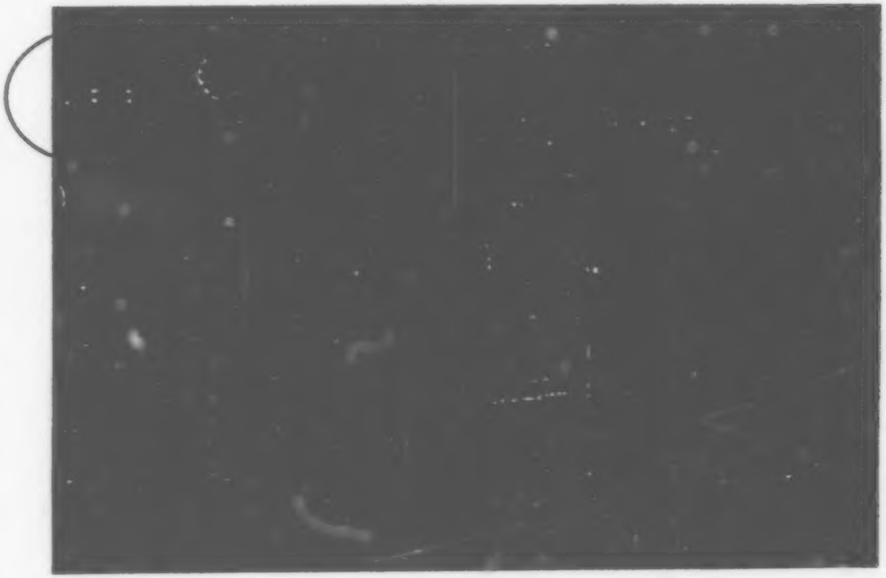

Personal Results Summary - Current Requirements

Action level
Exceeds reg't

% Cr	OFC	GMAW	SMAW	FCAW	
<0.50	0 - 2	0 - 0.4	0.3 - 0.7	0 - 0.4	Cr(VI) [100 ug/m3]
0.50 - 1.00	0.1 - 0.2	0.1 - 0.2	0.3 - 0.5	——	
1.00 - 2.50	0.2 - 3	——	3 - 8	——	
>20	——	5	[illegible]	?	
<0.50	19 - 156	78 - 609	81 - 125	253 - 534	Mn [1000 ug/m3]
0.50 - 1.00	8 - 29	59 - 75	100 - 159	——	
1.00 - 2.50	3 - 17	——	44 - 84	——	
>20	——	9	47 - 141	?	
<0.50	1 - 81	2 - 17	1 - 6	1 - 16	Ni [1000 ug/m3]
0.50 - 1.00	2 - 62	7 - 9	8 - 9	——	
1.00 - 2.50	106 - 450	——	1	——	
>20	——	540	8 - 62	?	

All fume values are 8-hr TWA in ug/m^3

NSWCCD 615 - 0497CRAD

Personal Results Summary - Proposed Requirements

Action level
[illegible]

% Cr	OFC	GMAW	SMAW	FCAW
<0.50	[illegible]	0 - 0.4	[illegible]	0 - 0.4
0.50 - 1.00	0.1 - 0.2	0.1 - 0.2	[illegible]	-----
1.00 - 2.50	[illegible]	-----	[illegible]	-----
>20	-----	[illegible]	[illegible]	?

Cr(VI)
[0.5 ug/m3]

<0.50	19 - 156	[illegible]	81 - 125	[illegible]
0.50 - 1.00	8 - 29	59 - 75	100 - 159	-----
1.00 - 2.50	3 - 17	-----	44 - 84	-----
>20	-----	9	47 - 141	?

Mn
[200 ug/m3]

<0.50		2 - 17	1 - 6	1 - 16
0.50 - 1.00		7 - 9	8 - 9	-----
1.00 - 2.50	[illegible]	-----	1	-----
>20	-----	[illegible]	[illegible]	?

Ni
[50 ug/m3]

All fume values are 8-hr TWA in ug/m³

Area Results Summary - Proposed Requirements

Action level
[illegible]

% Cr	OFC	GMAW	SMAW	FCAW	
<0.50	[illegible]	0 - 0.2	[illegible]	0 - 0.4	Cr(VI) [0.5 ug/m3]
0.50 - 1.00	0.1 - 0.2	0.1 - 0.2	0.3	-----	
1.00 - 2.50	[illegible]	-----	[illegible]	-----	
>20	-----	[illegible]	16 - 28	?	

<0.50	2 - 122	[illegible]	78 - 181	[illegible]	Mn [200 ug/m3]
0.50 - 1.00	5 - 40	62 - 75	78 - 128	-----	
1.00 - 2.50	2 - 16	-----	25 - 112	-----	
>20	-----	7	53 - 88	?	

<0.50	[illegible]	1 - 13	1 - 5	1 - 16	Ni [50 ug/m3]
0.50 - 1.00	3 - 38	6 - 8	3 - 5	-----	
1.00 - 2.50	169 - 625	-----	1	-----	
>20	-----	[illegible]	5 - 38	?	

All fume values are 8-hr TWA in ug/m^3

Personal Results Summary - Cr(VI) Requirements

Action level
[illegible]

% Cr	OFC	GMAW	SMAW	FCAW	
<0.50	0 - 2	0 - 0.4	0.3 - 0.7	0 - 0.4	Cr(VI) [100 ug/m3]
0.50 - 1.00	0.1 - 0.2	0.1 - 0.2	0.3 - 0.5	-----	
1.00 - 2.50	0.2 - 3	-----	3 - 8	-----	
>20	-----	5	[illegible]	?	
<0.50	0 - 2	0 - 0.4	0.3 - 0.7	0 - 0.4	Cr(VI) [5 ug/m3]
0.50 - 1.00	0.1 - 0.2	0.1 - 0.2	0.3 - 0.5	-----	
1.00 - 2.50	0.2 - 3	-----	[illegible]	-----	
>20	-----	[illegible]	[illegible]	?	
<0.50	[illegible]	0 - 0.4	[illegible]	0 - 0.4	Cr(VI) [0.5 ug/m3]
0.50 - 1.00	0.1 - 0.2	0.1 - 0.2	[illegible]	-----	
1.00 - 2.50	[illegible]	-----	[illegible]	-----	
>20	-----	[illegible]	[illegible]	?	

All fume values are 8-hr TWA in ug/m^3

Personal Results Summary - Mn

Action level
■

% Cr	OFC	GMAW	SMAW	FCAW
<0.50	19 - 156	78 - 609	81 - 125	253 - 534
0.50 - 1.00	8 - 29	59 - 75	100 - 159	-----
1.00 - 2.50	3 - 17	-----	44 - 84	-----
>20	-----	9	47 - 141	?

Mn
[1000 ug/m3]

<0.50	19 - 156	78 - 609	81 - 125	253 - 534
0.50 - 1.00	8 - 29	59 - 75	100 - 159	-----
1.00 - 2.50	3 - 17	-----	44 - 84	-----
>20	-----	9	47 - 141	?

Mn
[200 ug/m3]

All fume values are 8-hr TWA in ug/m^3

Personal Results Summary - Ni

Action level
[illegible]

% Cr	OFC	GMAW	SMAW	FCAW
<0.50	1 - 81	2 - 17	1 - 6	1 - 16
0.50 - 1.00	2 - 62	7 - 9	8 - 9	-----
1.00 - 2.50	106 - 450	-----	1	-----
>20	-----	540	8 - 62	?

Ni
[1000 ug/m3]

<0.50	1 - 81	2 - 17	1 - 6	1 - 16
0.50 - 1.00	2 - 62	7 - 9	8 - 9	-----
1.00 - 2.50	[illegible]	-----	1	-----
>20	-----	[illegible]	8 - 62	?

Ni
[100 ug/m3]

<0.50	[illegible]	2 - 17	1 - 6	1 - 16
0.50 - 1.00	[illegible]	7 - 9	8 - 9	-----
1.00 - 2.50	106 - 450	-----	1	-----
>20	-----	[illegible]	[illegible]	?

Ni
[50 ug/m3]

All fume values are 8-hr TWA in ug/m^3

Results - OFC

Action level
■

Material	% Cr	Cr(VI)	Mn	Ni
DH-36	<0.50	0.10	21	1
HSLA-65	<0.50	[illegible]	26	[illegible]
HSLA-80	0.50 - 1.00	0.10	29	2
HSLA-100	0.50 - 1.00	0.16	8	[illegible]
HY-100	1.00 - 2.50	0.20	3	[illegible]
		[illegible]	7	
			13	
		1.75	17	450

All fume values are 8-hr TWA in ug/m^3

Results - SMAW

Action level
[redacted]

Material	% Cr	Cr(VI)	Mn	Ni
11018 (Mfr A)	<0.50	[redacted]	122	6
11018 (Mfr B)	<0.50	0.38	125	5
12018 (Mfr C)	0.50 - 1.00	0.47	159	9
12018 (Mfr D)	0.50 - 1.00	0.30	100	8

Material	% Cr	Cr(VI)	Mn	Ni
309-15 (Old)	>20	[redacted]	141	23
309-15 (New)	>20	[redacted]	106	18
309-16 (Old)	>20	[redacted]	116	[redacted]
309-16 (New)	>20	[redacted]	47	8

All fume values are 8-hr TWA in ug/m^3

NSWCCD 615 - 0497CRAD

Results - GMAW

Action level
[illegible]

Material	Shielding	% Cr	Cr(VI)	Mn	Ni
100S-1	C5	<0.50	0.38	100	8
100S-1	M2	<0.50	0.29	106	12
100S-2	C5	<0.50	0.05	[illegible]	17
100S-2	C5	<0.50	0.05		16
120S-1	C5	0.50 - 1.00	0.14	75	9
120S-1	M2	0.50 - 1.00	0.17	59	7

All fume values are 8-hr TWA in ug/m^3

Results - Lower Strength Steels

Process	Material	Shielding	% Cr	Cr(VI)	Mn	Ni
SMAW	7018	---	<0.50	0.34	81	1
SMAW	7018	---	<0.50	[illegible]	109	1
GMAW	70S-6	C5	<0.50	0.05	122	2
FCAW	71T-1	CO2	<0.50	0.38	[illegible]	1
FCAW	71T-1	C25	<0.50	0.29		1

Action level
[illegible]

All fume values are 8-hr TWA in ug/m^3

Conclusions

- *The potential exists, with the materials and operations investigated, to exceed the lower anticipated ceilings for Cr(VI), Mn, and Ni for both operators and personnel in the immediate area surrounding the operation.*
- *The PEL finally adopted by OSHA will dictate the extent of this problem, and, therefore, the cost of the solution.*

Conclusions (continued)

- *Of the identified solutions, application of engineering controls appears to be the most appropriate for successful reduction of airborne emissions.*
- *Variability observed in the results may be inherent to the operations and measurement techniques. A broader data base is required to resolve issues and establish the statistical significance of the data.*

#507208 ⑤

Coatings with Selected Infrared Properties For Use On CF Ships

by

Dr. Terry Foster
Head, Dockyard Laboratory Esquimalt, Esquimalt Defence Research Detachment
P.O. Box 17000 STN FORCES
Victoria BC V9A 7N2

and

David Hacker and Bill Abel
ORTECH Corporation
2395 Speakman Drive, Mississauga, ON L5K 1B3

ABSTRACT

Infrared properties of coatings used on naval vessels are important in maintaining ship habitability, i.e. reducing heat build-up in compartments and protecting equipment from excessive temperatures. Coatings can also be used to control the infrared signature of a ship.

In this presentation, a brief overview of the various properties of infrared radiation (solar, near and thermal infrared) and the significance of infrared radiation for naval vessels will be given. Various ways of changing the solar infrared, near infrared and thermal infrared properties of coatings such as choice of pigment content, resin type and surface property will be presented along with the effects these changes can have on the temperature and IR reflectivity of the coated surface.

Finally, the development of new solar reflective coatings for naval vessels will be presented. These new coatings reflect up to 80% of the incident solar infrared radiation, as compared to 30% for the currently used coatings. These coatings will significantly affect the surface temperature of the ship sides and decks and contribute to a reduction in the IR signature of the ship.

COATINGS WITH SELECTED INFRARED PROPERTIES

Dr. Terry Foster,
Head Dockyard Laboratory Esquimalt,
EDRD

Mr. David Hacker

Manager Coatings and Adhesives

ORTECH

Coating Properties of Interest

- ➢ Visual Camouflage
- ➢ Ice Release Properties
- ➢ Non-Skid Properties
- ➢ Ease of Application
- ➢ Maintainability
- ➢ Cosmetic Appearance
- ➢ Corrosion Resistance
- ➢ Durability
- ➢ Cleanability
- ➢ Toxicity or Hazardous Components

Cosmetic

- CHOICE OF COLOUR
- CHOICE OF GLOSS OR REFLECTIVITY
- EASE OF CLEANING AND MAINTENANCE
- CORROSION PROTECTION USUALLY THE FUNCTION OF THE PRIMER
    - INORGANIC ZINC OR ZINC RICH EPOXY

Coating to Control Radiation

- Reduce excessive heating of equipment due to absorption of solar radiation
- Reduce signature (IR, NIR and VIS) by decreasing emission of radiation in the IR and visual regions
- Absorb solar radiation for solar heating systems
- Transmit visible light while filtering out IR wavelengths (architectural glass)

Coating Requirements to Control Emission

- Coatings Which Act by Controlling Reflectance of Incident Solar Radiation, Predominantly Visible and NIR
- Coatings Can Control Emissions Resulting From a Combination of Reflected Incident Solar Radiation and Thermal Self Emitted Radiation Which Is a Function of the Emisivity and Temperature of the Radiating Surface. These Coating Operate in the Visible, NIR, Mid -IR and Far - IR

Signature and Vis/IR Frequencies

- Visible
  - 400 - 720 nm (0.4 - 0.72 um)
- Near Infrared (NIR)
  - 700 - 2300 nm (0.7 - 2.3 um)
- Thermal Infrared (TIR)
  - 2.5 - 15 um
  - 3-5 um and 8-14 um are the bands of interest for thermal missile and surveillance
- Distribution of Solar Energy
  - 5% ultra-violet (less than 400 nm)
  - 45% in the visible region
  - 50% in the solar infrared region.

Visible and IR Radiation of Coatings

- The solar radiation striking a coated surface is either reflected, absorbed or transmitted at each interface
  - coating surface / air
  - internal coating - pigment and resin
  - substrate
- The reflected radiation can be either specular (mirror-like) or diffuse (scattered) and is dependent on the pigments used in the coating or the texture of the surface.
- Radiation not reflected from the film is converted into heat or chemical energy

Infrared Radiation

- Objects having temperatures of 300°K are strong sources of thermal infrared radiation and emit 98% of their total radiation in the 3-30 um region
- Overlap between reflected solar and emitted is in the 3-5 um region
- Therefore "at room temperature, the power emitted at 5 um by an efficient radiator is as great as the power from sunlight falling on the same area" (black body energy in 3 - 5 um = 4 x 10^{-2} W/m^2)
- In the 8-13 um region reflected solar radiation is not very important (black body energy in 8 -13 um = 1 x 10^{-4} W/m^2)

Reflection and Absorption

- The radiation reflected has not been absorbed and thus has not affected the thermal properties of the coating and substrate.
- It is the absorbed radiation that affects the thermal energy of the substrate and the transmitted radiation that contributes to the thermal or IR signature.
- For optimum camouflage the reflective properties of a coating in the visible and infrared regions must be similar to its surrounding in either natural or artificial light such that the coated object is indistinguishable from its surroundings.

Reflectivity / Emissivity

Reflectivity/Emissivity of Materials

	Emissivity	Reflectivity
Blackbody	1	0
Glass	0.94	.04
Rubber	0.8	0.2
Steel	0.6	0.4
Stainless Steel	0.09	0.91
Aluminum	0.08	0.92
Silvered Mirror	0.02	0.98
Ocean (SS4)	~0.8	~0.2

Resins and IR Coatings

- Resins must transparent in the IR region of interest as well has have the properties required to make a good paint film
- Resins generally do not absorb in the NIR region and most can be used in this region
- In the thermal IR region organic resins have absorption bands at 3.3 um (C-H stretch), 5.7 um (C-H bending) and 8.0 um (C=O stretch)
- Absorption by resins can also be reduced by the selection of pigments that scatter light in the region of concern

Pigments and IR Coatings

- Pigments form the major contribution to the IR properties of coatings
- The combination of diffuse and specular reflectance, absorption and transperance properties of a pigment in the IR define its IR properties
- Particle size will also affect diffuse reflectance properties due to light scattering
- Brady (US) and Wake (AS) have measured the IR properties of pigments in a standard paint film over the spectral range 400nm to 2300 nm using diffuse reflectance techniques
- Pigments were then classified into six categories

Pigment Classification

- Transparent
  - Amorphous Silica
- Reflective
  - Titanium Dioxide (10 um)
- Highly Reflective
  - Titanium Dioxide (2 um)
- Absorbent-Transparent
  - Palogen Black
- Reflective-Transparent
  - Chromium Oxide
- Highly Absorbent
  - Black Iron Oxide

Scattering Power

- Scattering of radiation is a function of the difference between the refractive index of the pigment and the resin
- Refractive index of commercial pigments varies between 1.4 and 2.8
- The scattering power (*m*) the ratio of the refractive index of the pigment to the resin
- Hiding pigments have m above 1 (TiO_2, red iron oxide *m*=1.9) - hide the substrate by modifying the reflectance curve of the substrate
- Extender pigments have values of *m* at or below 1.1 - talc (1.07) or silica (0.97- 1.05)

Particle Size

- From scattering power measurements, refractive index and particle size the wavelength for most efficient scattering can be determined
  - e.g. TiO_2 particle size 200 nm wavelength of 500nm
  - TiO_2 and Red Iron Oxide 1 um particle sizes would be required to scatter NIR at 2.3 um
  - For NIR particles sizes of the order of mm would be required

Objectives

- Evaluate the current infrared properties of the topside alkyd and non-skid deck coatings
- Reformulate these coatings to enhance the reflectivity in the 700-1000 nm region and maintain the colour requirements for visual camouflage
- Evaluate by thermography the thermal properties of the reformulated coatings

Coating Preparation - 1

- Pigment pastes were made from a variety of combinations of pigments as suggested by the pigment manufacturers
- Pigment pastes where then dispersed in an alkyd resin and ground to a Hegman fineness of 6.5-8 using a ball mill
- Tints for the urethane coatings were dispersed in an acrylic resin
- These tints and pastes were then used to formulate urethane and alkyd coatings

Coating Preparation - 2

- Colour matching was carried out using a daylight source as many of the formulations were metameric
- Metameric - appears to be the same colour but colour will differ under different lighting conditions
- Final formulations were tested for resistance to salt spray, accelerated weathering and adhesion to substrate and primer
- Thermography was carried to determine the heat reflective effect of each coating

Pigments and Suppliers

Manufacturer	Pigment	Type	Price ($/kg)
BASF	Paliogen Black L0084	Perylene	$210.00
	Paliogen Black L0086	Perylene	$210.00
Bayer	Red Oxide 130M	Iron oxide	$3.31
	Yellow Oxide 3910	Iron oxide	$3.42
Ciba-Geigy	IRGACOLOR Black 10333	Chrome iron nickel black spinel	$20.00
	IRGACOLOR Buff 10406	Chrome antimony titanium rutile	$11.00
	IRGACOLOR Green 10405	Cobalt chromite green spinel	$26.30
	IRGACOLOR Green 10342	Cobalt titanate green spinel	$41.15
	IRGALITE Green GLN	Polychloro-copper phthalocyanine	$30.50
	IRGAZIN Yellow 3RLTN	Isoindolinone	$93.10
Harshaw	9885 Meteor Plus High IR Black	Iron chromite brown spinel	$25.75

Pigments and Suppliers

Manufacturer	Pigment	Type	Price ($/kg)
Ferro Corp.	V-700 Black	Chromium green/black hematite	$18.06
	V-9238 Blue	Cobalt chromite blue/green spinel	$59.77
	V-11674 Green	Chromium (III) oxide	$9.59
	V-11692 Green	Chromium (III) oxide	$9.59
	V-12600 Green	Cobalt chromite green spinel	$25.05
Harcros Pigments, Inc. (Engelhard Corp.)	G 6099 Green	Chromium (III) oxide	$12.00
Shepherd Color Co.	Green 179	Cobalt chromite green spinel	$17.84
	Green 4	Cobalt titanate green spinel	$18.24
	Black 123	Chrome, iron oxides	$14.52
	Black 376	Chrome iron nickel black spinel	$18.15
	Yellow 195	Nickel antimony titanium yellow	$9.83
	Gray A8151	Mixed metal oxides	$0.75

Aklyd 501-109

- Six formulations of grey alkyd were prepared and the VIS/NIR reflectance were compared to a standard grey alkyd (General Paints)
- Reflectance at 900 nm varied from 42% for the standard to 51% to 81% for the new formulations
- Costs for formulation 7222-57 using perylene black are much higher than for 7222-68 using mixed metal oxides

GP-61, 501-109 Matches

Clear Base	Amt.	White Base	Amt.
Aroplaz 2502-ML-60	84.243	Aroplaz 2502-ML-60	58.353
Xylene	15.164	Kronos 2102	35.012
NeoCem 250	0.147	Xylene	6.224
Dri Rx	0.147	NeoCem 250	0.102
Nuxtra cobalt 12%	0.152	Dri Rx	0.102
Exkin #2	0.147	Nuxtra cobalt 12%	0.105
	100	Exkin #2	0.102
			100

7222-55	Amt.	7222-57	Amt.
Clear Base	27.79	Clear Base	26.24
White Base	63.31	White Base	69.36
Ferro V12600	3.59	Ferro V12600	2.08
Ferro V11674	2.78	Ferro V11674	0.92
Ferro V700	2.53	BASF L0086	1.39
	100		100

GP-61, 501-109 Matches

7222-62	Amt.	7222-82	Amt.
Clear Base	26.96	Clear Base	28.66
White Base	55.76	White Base	58.72
Shepherd A8151	9.46	Shepherd 4	4.36
Shepherd 195	1.35	Shepherd 179	3.62
Shepherd 179	6.47	Shepherd 376	2.01
	100	Shepherd 195	2.62
			100

7222-80	Amt.	7222-87	Amt.
Clear Base	24.51	Clear Base	26.53
White Base	64.73	White Base	70.76
Shepherd 179	3.27	Ciba 10405	2.39
Ferro V11674	5.25	Ciba 10406	0.21
Harshaw 9885	2.25	Bayer 130M	0.12
	100		100

Alkyd Topcoats

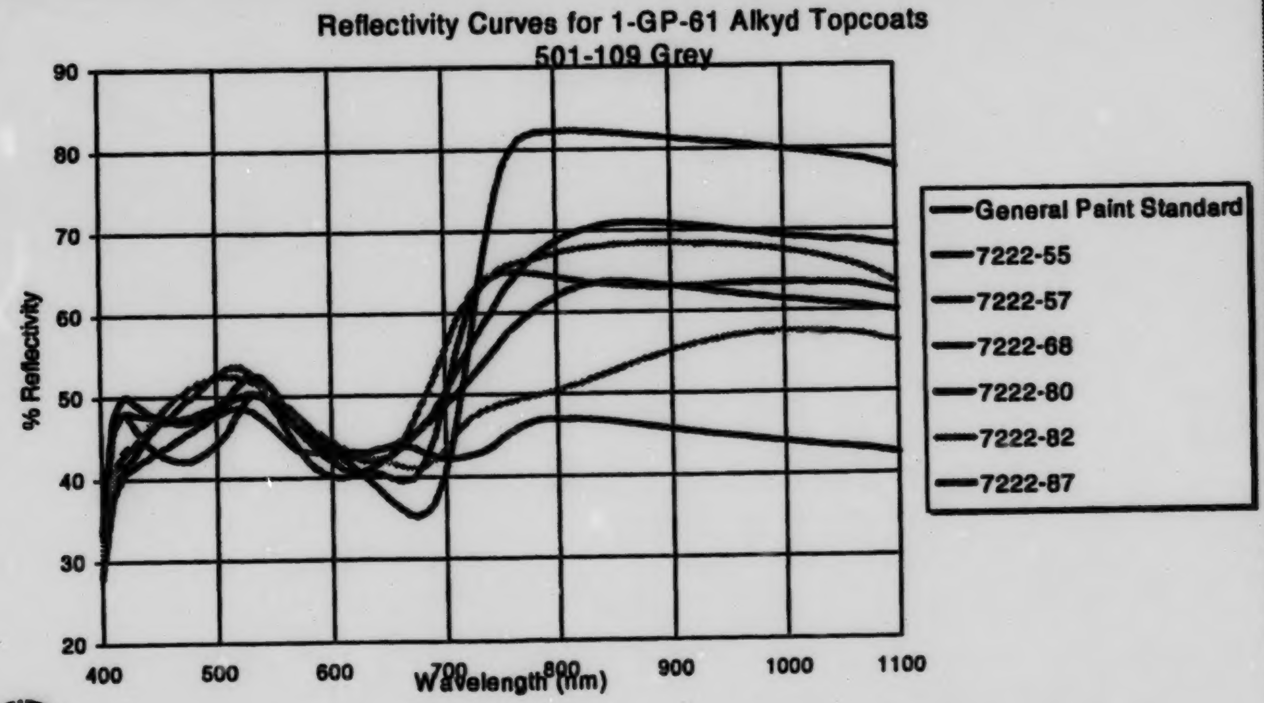

Reflectivity Curves for 1-GP-61 Alkyd Topcoats
501-109 Grey

Non-Skid - Dark Green, 503-305

- Four formulations of dark green non-skid were prepared and the VIS/NIR reflectance were compared to a standard green non-skid (Tibbetts)
- Reflectance at 900 nm varied from 6% for the standard to 20% to 50% for the new formulations
- The perylene black formulation gave the best performance but the matches using the Shepard and Ferro pigments matches gave similar performance at less cost

1-GP-200, 503-305 Matches

7222-125	
Clear Base	29.30
White Base	0.35
Ferro V12600	2.77
Ferro V11692Z	5.13
Ferro V9238	1.70
Ferro V700	0.87
Talc	43.93
PE Fibre	2.87
Desmodur E 3265	13.09
	100.00
Glass	58.30
	158.30

7222-127	Amt.
Clear Base	28.93
White Base	2.71
Ciba 3RLTN	0.61
Ciba 10342	3.58
Ciba 10333	1.76
Ciba GLN	1.81
Bayer 3910	0.10
Talc	43.91
PE Fibre	2.84
Desmodur E 3265	13.76
	100.00
Glass	58.30
	158.30

7222-122	Amt.
Clear Base	21.11
White Base	1.75
BASF L0084	4.19
Harcros 6098	8.26
Ferro V9238	3.00
Huls C844-2862	1.18
Talc	44.82
PE Fibre	2.83
Desmodur E 3265	13.00
	100.00
Glass	58.30
	158.30

7222-124	Amt.
Clear Base	27.81
White Base	0.92
Shepherd 179	8.25
Harcros 6098	2.66
Talc	44.55
PE Fibre	2.82
Desmodur E 3265	13.00
	100.00
Glass	58.30
	158.30

Green Polyurethane

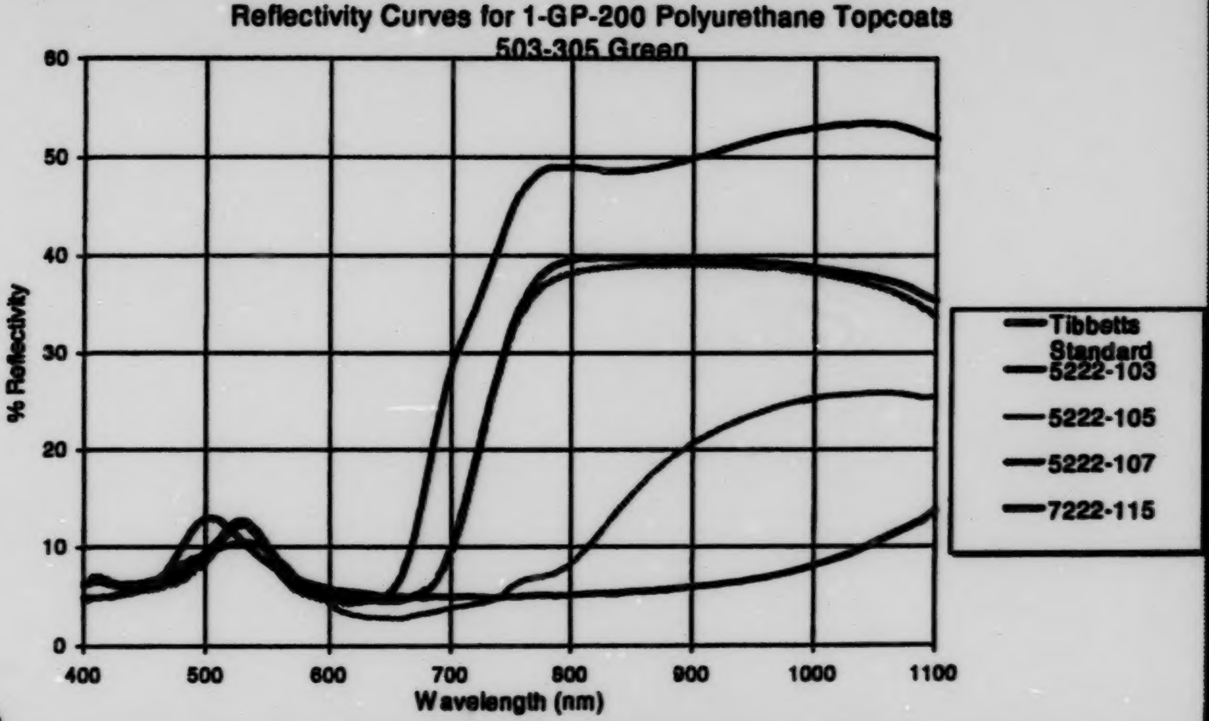

Reflectivity Curves for 1-GP-200 Polyurethane Topcoats 503-305 Green

Non-Skid - Dark Grey, 501-302

- Two formulations of grey non-skid were prepared and the VIS/NIR reflectance were compared to a standard grey non-skid (Tibbetts)
- Reflectance at 900 nm varied from 8% for the standard to 39% to 44% for the new formulations
- The formulation using perylene black gave the most improved reflectance but at a significantly higher pigment cost

GP-200, Base Formulation and 501-302 Matches

Clear Base	Amt.	White Base	Amt.
Desmophen A 160	85.967	Desmophen A 160	63.158
Xylene	14.033	Kronos 2102	26.316
	100.00	Xylene	10.526
			100.00

7222-126	Amt.	7222-82	Amt.
Clear Base	38.46	Clear Base	46.26
White Base	4.35	White Base	4.89
Ferro V700	8.64	BASF L0084	1.90
Ferro V9238	1.56	Shepherd 123	20.01
Talc	19.60	Talc	8.00
PE Fibre	1.40	PE Fibre	1.45
Desmodur E 3265	13.17	Desmodur E 3265	17.48
Xylene	12.82		100.00
	100.00	Glass	58.30
Glass	58.30		158.30
	158.30		

Grey Polyurethane

Reflectivity Curves for 1-GP-200 Polyurethane Topcoats
501-302 Grey

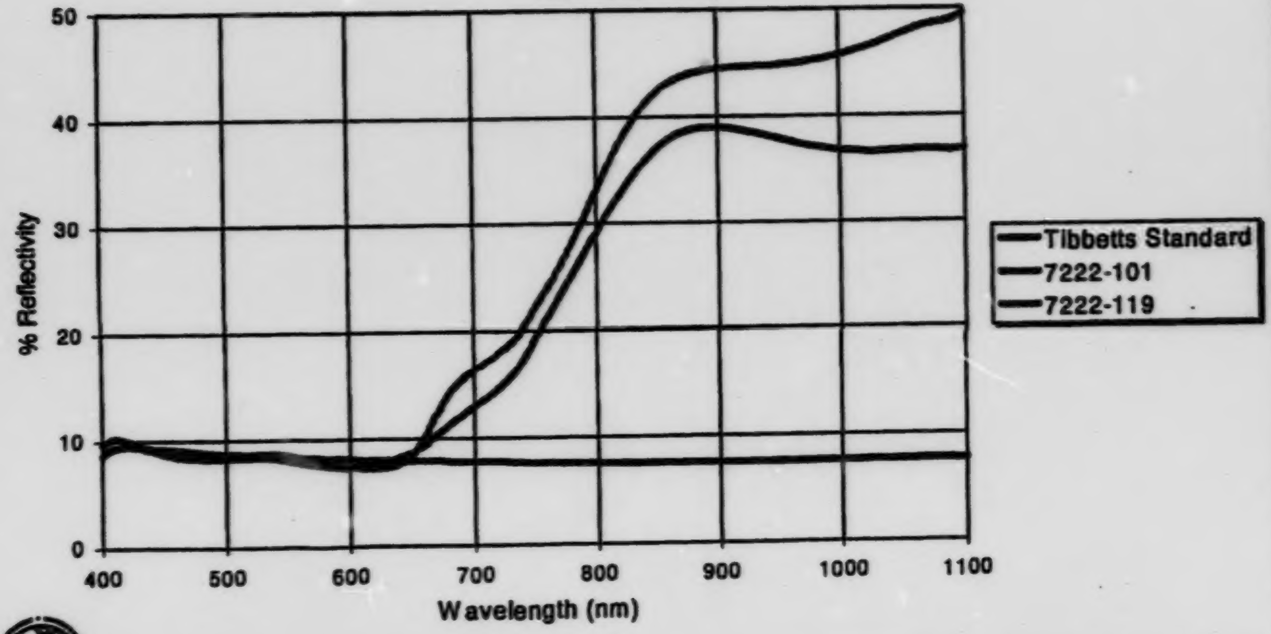

Test Methods

- Resistance to salt spray ASTM B 117-94 for 240 hours
  - Panels were not scribed and corrosion and blistering were monitored
- Accelerated weathering was carried out for 360 hours in a xenon arc weatherometer
  - Observations were made for colour and gloss changes on the alkyd system and colour changes on the polyurethane system
- Adhesion to substrate was carried out according to ASTM D 3359-93 (Cross-Cut Method)

Accelerated Weathering GP-61

Reference	Initial Colour	Final Colour	Difference	Initial Gloss (60°)	Final Gloss (60°)	Difference
General Marine 1-GP-61 501-109	L* 74.28 a* -6.11 b* 1.66	L* 74.79 a* -5.93 b* 0.64	ΔE 1.16 ΔC -0.37 ΔH 0.97	79.6	55.3	-24.3
7222-55	L* 73.03 a* -5.43 b* 0.21	L* 74.19 a* -5.52 b* -0.78	ΔE 1.52 ΔC 0.13 ΔH 0.98	81.5	68.3	-13.2
7222-57	L* 73.16 a* -6.22 b* 0.62	L* 73.32 a* -5.74 b* -0.72	ΔE 1.43 ΔC -0.46 ΔH 1.35	83.7	72.3	-11.4
7222-68	L* 73.32 a* -8.55 b* 2.40	L* 73.86 a* -8.38 b* 1.02	ΔE 1.49 ΔC -0.44 ΔH 1.32	82.5	43.5	-39.0
7222-87	L* 73.33 a* -6.84 b* 2.88	L* 74.23 a* -6.61 b* 2.45	ΔE 1.02 ΔC -0.37 ΔH 0.31	87.6	82.8	-4.8

Accelerated Weathering GP-200

Reference	Initial Colour		Final Colour		Difference	
Tibbetts 1-GP-200 501-302	L* a* b*	29.39 -0.22 -2.29	L* a* b*	28.33 -0.35 -2.02	ΔE ΔC ΔH	1.09 -0.24 -0.16
7222-123	L* a* b*	32.86 1.22 -0.08	L* a* b*	33.20 1.37 -0.04	ΔE ΔC ΔH	0.37 0.14 0.05
7222-126	L* a* b*	35.29 -0.28 -2.26	L* a* b*	35.66 -0.19 -2.13	ΔE ΔC ΔH	0.40 -0.13 0.07

Accelerated Weathering GP-200

Reference	Initial Colour	Final Colour	Difference
Tibbetts 1-GP-200 503-305	L* 28.79 a* -15.13 b* 3.92	L* 27.35 a* -13.84 b* 4.38	ΔE 1.99 ΔC -1.11 ΔH -0.80
7222-122	L* 33.21 a* -8.32 b* 3.81	L* 34.47 a* -8.69 b* 4.13	ΔE 1.35 ΔC 0.47 ΔH -0.13
7222-124	L* 36.46 a* -15.39 b* 5.11	L* 37.37 a* -15.45 b* 5.32	ΔE 0.94 ΔC 0.12 ΔH -0.18
7222-125	L* 32.72 a* -9.47 b* 2.89	L* 33.31 a* -9.43 b* 2.91	ΔE 0.60 ΔC -0.04 ΔH -0.02
7222-127	L* 34.43 a* -15.29 b* 2.67	L* 34.58 a* -15.17 b* 2.80	ΔE 0.23 ΔC -0.10 ΔH -0.15

Adhesion to Primer

Reference	Before Weathering	After Weathering
General Marine 1-GP-61 501-109	4A	4A
7222-55	3A	3A
7222-57	2A	2A
7222-68	2A	3A
7222-80	3A	N/A
7222-82	3A	N/A
7222-87	4A	4A
Tibbetts 1-GP-200 501-302	5A	5A
7222-123	5A	5A
7222-126	5A	5A
Tibbetts 1-GP-200 503-305	5A	5A
7222-122	5A	5A
7222-124	5A	5A
7222-125	5A	5A
7222-127	5A	5A

Results of Exposure

- None of the formulations showed any signs of corrosion or blistering
- None of the formulations showed any significant colour changes
- The gloss changes for GP-61 were less than that for the control
- Alkyd systems gave weak to acceptable adhesion results
- All urethane systems gave excellent adhesion results

Thermography

- Solar energy produced by Vortek^{tm} 150 kW Solar Simulator Lamp (MIl No. A06264)
- Distance panels to lamp 29 ft
- Light intensity at panels 970-980 W/m^2
- Panels mounted side by side 30° from vertical, incident light normal to surface
- Temperatures monitored with thermocouple soldered to back of panels
- Thermography carried out after panels reached equilibrium - 15 minutes for GP-61 and 20-30 minutes GP-200

Thermography

- Agema 470 Thermovision infrared camera - accuracy is either 2°C or 2%, which ever is less
- Warmer surfaces indicated by lighter colours (orange-red-white)
- Cooler surfaces indicated by darker colours (violet-blue-black)
- In each case the standard panels exhibited higher emissivity, formulated coatings were more reflective
- Emissivity values are relative and cannot be compared between sets

Thermography Results

Coating	Standard	Experimental	Difference
1-GP-61, 501-109 7222-57	52.8°C	44.0°C	8.8°C
1-GP-200, 501-302 7222-123	70.1°C	62.6°C	7.5°C
1-GP-200, 503-305 7222-122	69.3°C	60.9°C	8.4°C

Conclusions

- Six variants of grey alkyd, 501-109 have been formulated with good solar reflective properties
- Further work required to confirm IR reflectance properties in the 3-5 um region
- Two variants of grey and four variants of green polyurethane non-skid have been formulated with increased solar reflectance properties
- Currently investigating the development of a commercial formulation of the non-skid for future ship trial

1-GP-200, 501-302 Dark Grey Panels	
7222-123	Tibbets Standard
Reverse side panel temperature = 62.6°C	Reverse side panel temperature = 70.1°C
Assumed face panel temperature = 67.6°C	Assumed face panel temperature = 75.1°C
Calculated emissivity = 0.87	Calculated emissivity = 0.92

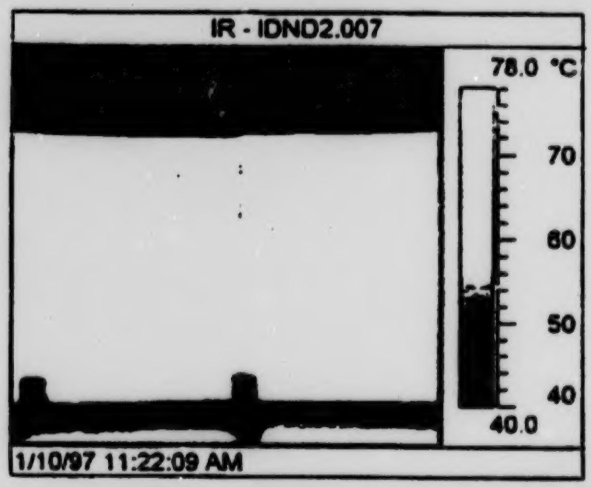

SCANNER DATA	
Level	471
Sens	6
Aperture	0
Filter	NOF
Lens	20
IMAGE OBJ. PAR.	
Emissivity	0.90
Amb. temp.	30.2 °C
Atm. temp.	27.0 °C
Object dist.	3.0 m
Transmission	0.97

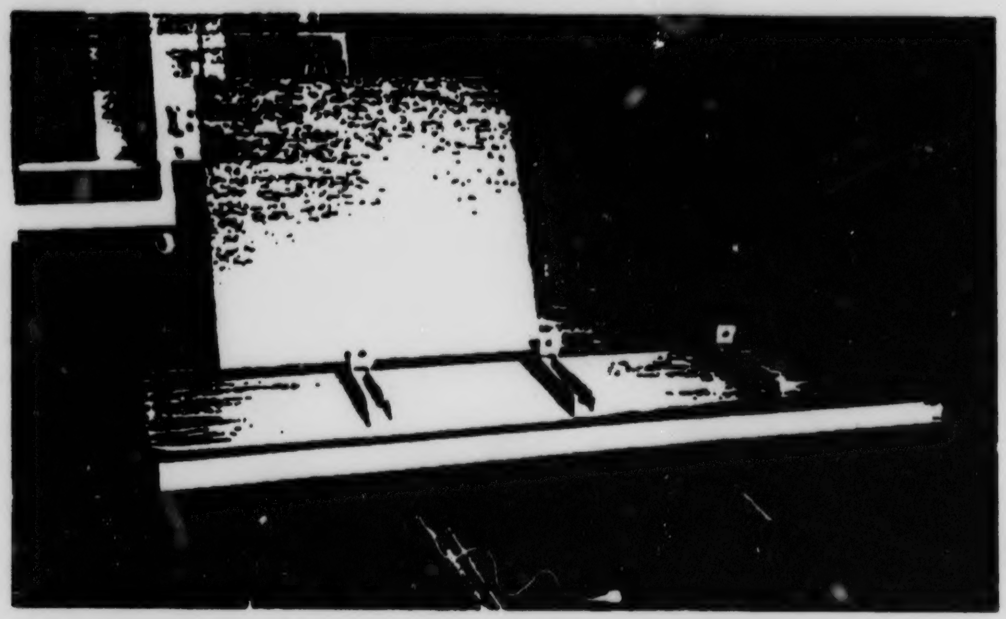

1-GP-61, 501-109 Light Grey Panels	
7222-57	General Paint Standard
Reverse side panel temperature = 44.0°C	Reverse side panel temperature = 52.8°C
Assumed face panel temperature = 49.0°C	Assumed face panel temperature = 57.8°C
Calculated emissivity = 0.95	Calculated emissivity = 1 00

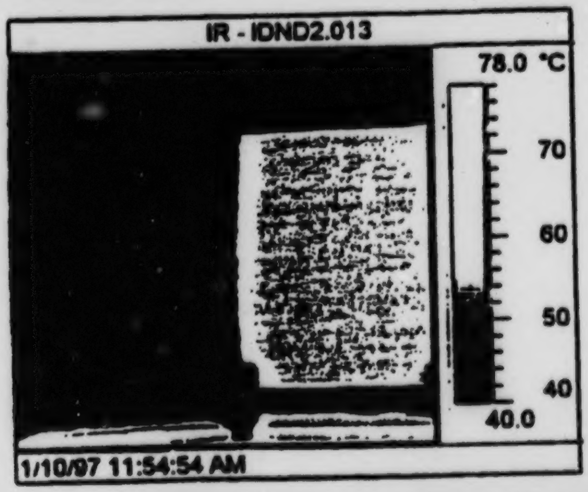

SCANNER DATA	
Level	913
Sens	7
Aperture	0
Filter	NOF
Lens	20
IMAGE OBJ. PAR	
Emissivity	0.97
Amb. temp	30 5 °C
Atm. temp	28 6 °C
Object dist.	3.0 m
Transmission	0.97

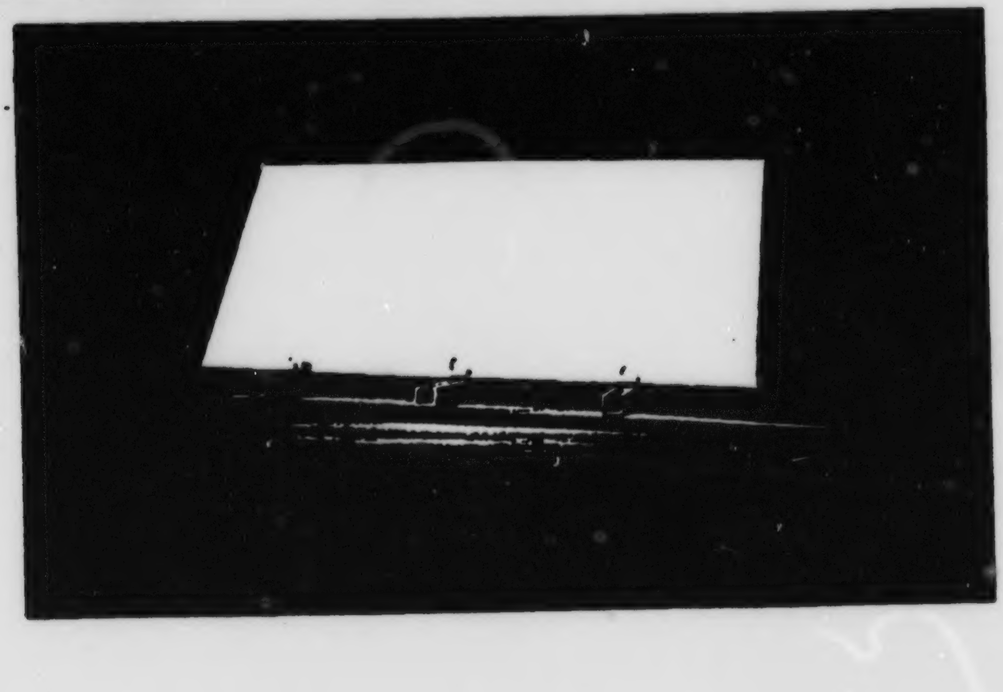

1-GP-200, 503-305 Dark Green Panels	
7222-122	Tibbets Standard
Reverse side panel temperature = 60.9°C	Reverse side panel temperature = 69.3°C
Assumed face panel temperature = 65.9°C	Assumed face panel temperature = 74.3°C
Calculated emissivity = 0.89	Calculated emissivity = 0.92

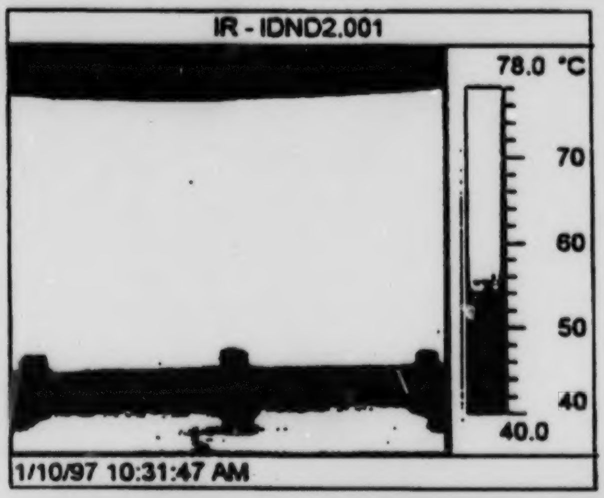

SCANNER DATA	
Level	471
Sens	6
Aperture	0
Filter	NOF
Lens	20
IMAGE OBJ. PAR	
Emissivity	0.91
Amb. temp.	29.2 °C
Atm. temp.	25.7 °C
Object dist.	3.0 m
Transmission	0.97

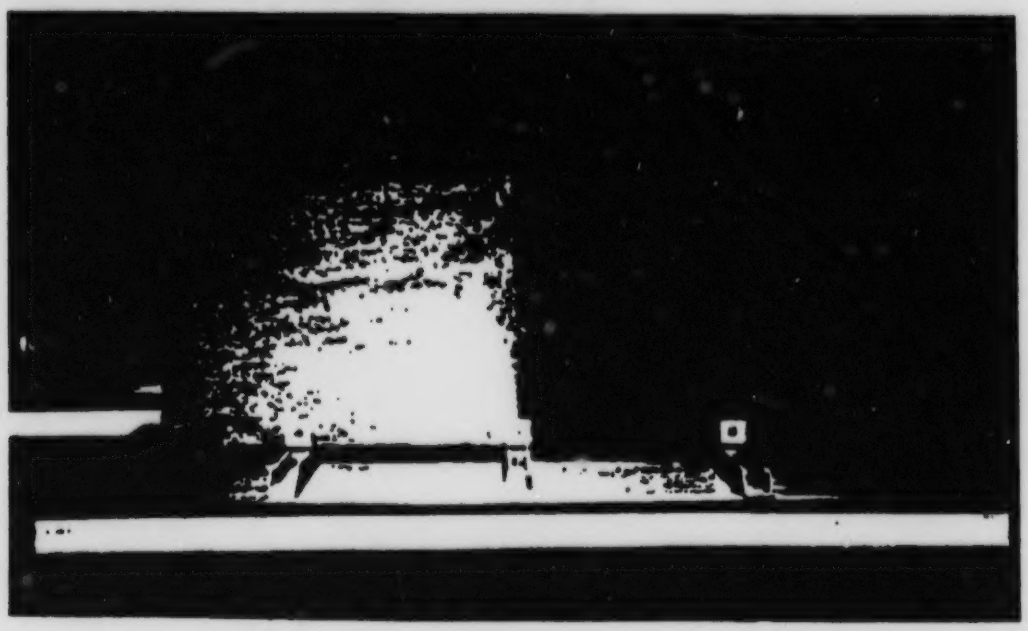

#507209 (6)

Host Structure and Active Material Interactions: Implications for Design of Smart Materials

V.G. DeGiorgi

Mechanics of Materials Branch, Naval Research Laboratory
Washington, D.C. 20375 U.S.A.

ABSTRACT

There is an increasing emphasis on incorporating smart materials into existing naval structures. Special purpose materials and devices which are a combination of active and passive materials are currently being designed for a wide variety of applications including space structures, control and noise reductions on helicopters, control and noise reduction system on conventional aircraft and quieting systems on submarines. Successful incorporation of active materials into structures requires an understanding of the performance characteristics of the modified structure in addition to an understanding of the performance characteristics of the un-incorporated active material. The latter does not provide sufficient information for the design of smart material. An understanding of the interactions between active and passive components is necessary for appropriate design of composite smart materials. This presentation will highlight issues which must be addressed in the design process.

The basic device examined is an active panel. Different configurations of actuator placement have been evaluated for different applications. In two of the design cases discussed, prototype panels have been built and tested. The primary active components are PMN actuators. Typical displacement requirements are in the micrometer range. Common issues which will be discussed are: loss of actuator authority resulting from interactions with the surrounding passive material, interaction stresses and strains at passive/active material junctions, mechanical coupling between individual active components and support structure influence on performance characteristics.

Host Structure and Active Material Interactions: Implications for Design of Smart Materials

V. G. DeGiorgi

Mechanics of Materials Branch
Code 6382
Naval Research Laboratory
Washington, DC 20375-5000
virginia@walkinghorse.nrl.navy.mil

CF/CRAD Meeting
April 22-24, 1997
Halifax, NS

Issues

Active - passive material interaction

Interfacial stresses

Compliance mismatch

Device softening

Reduction in actuator authority

↓

Performance Characteristics

Displacement response

Stress levels

Composite Smart Materials (CSM) for Defense and Dual Use Applications

A DARPA Funded Program

- Goal: Develop a smart composite material for acoustic quieting application. Major design goals include use of integrated actuators, sensors and electronics. Stand alone design will incorporate all required electronics and intelligence.

- Lockheed Martin
  - Program Management
  - Composite design, modeling and fabrication
  - Structural modeling
  - Controls
- AVX Corp.
  - Actuators and sensors
- VPI/VPT
  - Power supplies
  - Modeling
- AST
  - Acoustic design
  - Acoustic testing
- Signal Systems Corp.
  - Controls
- NRL
  - Structural modeling

CSM - Teaming or A Virtual Company

- Virtual Company concept
  - Reduce corporate protectiveness which hinders cooperative effort
  - Attitudes
  - Physical seperation
  - Communication technologies

- CSM Team utilizes
  - Phone/fax and other traditional means
  - Email/information and documents
  - Weekly tele-conferences
  - Special topic tele-conferences as needed
  - Video conferencing
  - Ad-hoc meetings scheduled in conjunction with other meetings or conferences
- Successfully developed team atmosphere on program

First Generation Design 4 Actuators per Piston, 4 x 4 array of Pistons per Unit Device

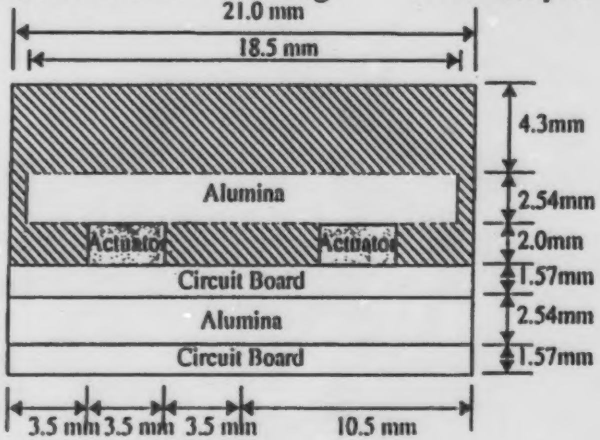
21.0 mm
18.5 mm
4.3mm
Alumina
2.54mm
Actuator
Actuator
2.0mm
Circuit Board
1.57mm
Alumina
2.54mm
Circuit Board
1.57mm
3.5 mm
3.5 mm
3.5 mm
10.5 mm

Basic 33 Chiplet Actuator

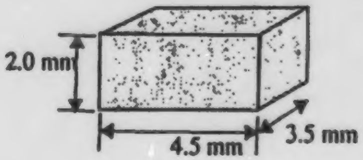
2.0 mm
4.5 mm
3.5 mm

Second Generation Design 36 Actuators per Piston in 6 x 6 array, 1 Piston per Unit Device

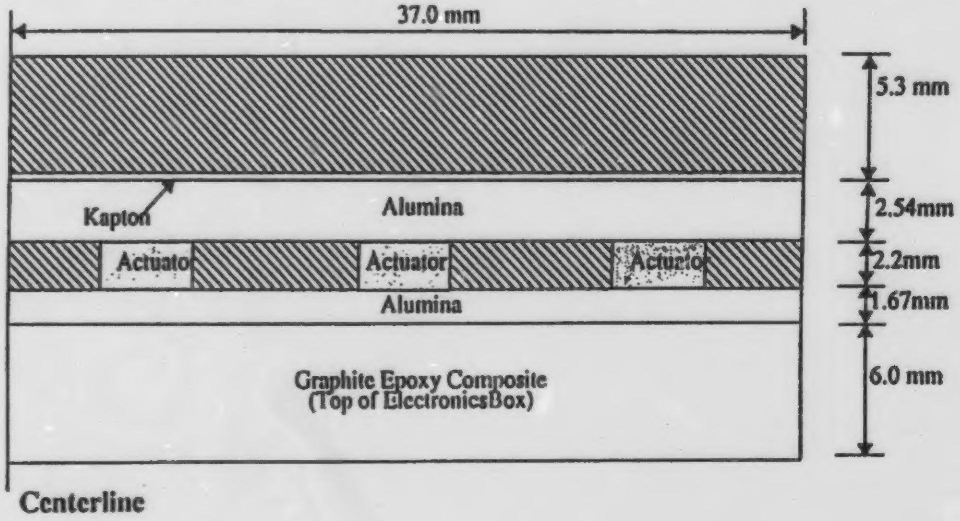
37.0 mm
5.3 mm
Kapton
Alumina
2.54mm
Actuato
Actuator
Actuato
2.2mm
Alumina
1.67mm
Graphite Epoxy Composite
(Top of ElectronicsBox)
6.0 mm
Centerline

Composite Smart Materials

Acoustic Tile

System Integration
Team Leader
Lockheed Martin

Actuators
AVX

Electronics
VPT / VA Tech

Control
SSC

Testing
AST

Modeling
NRL

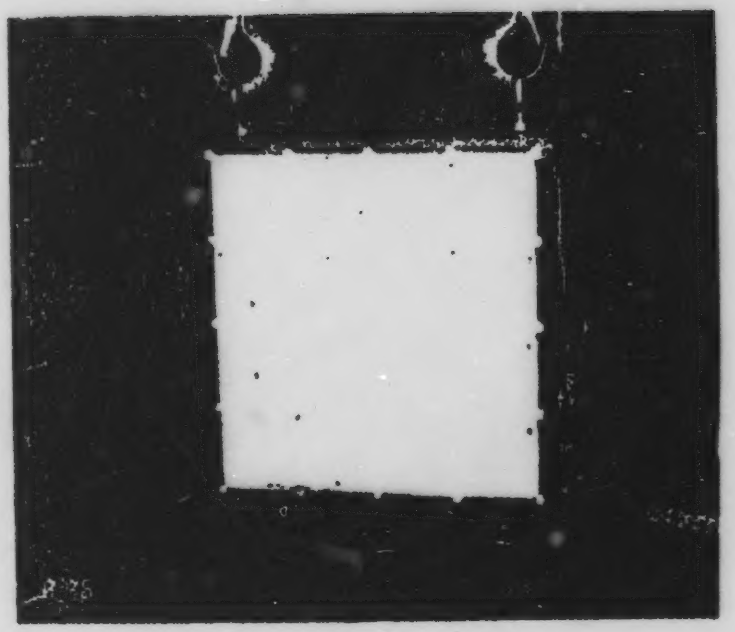

Acoustic Piston

System Integration
Team Leader
Lockheed Martin

Actuators
AVX

Electronics
VPT / VA Tech

Control
SSC

Testing
AST

Modeling
NRL

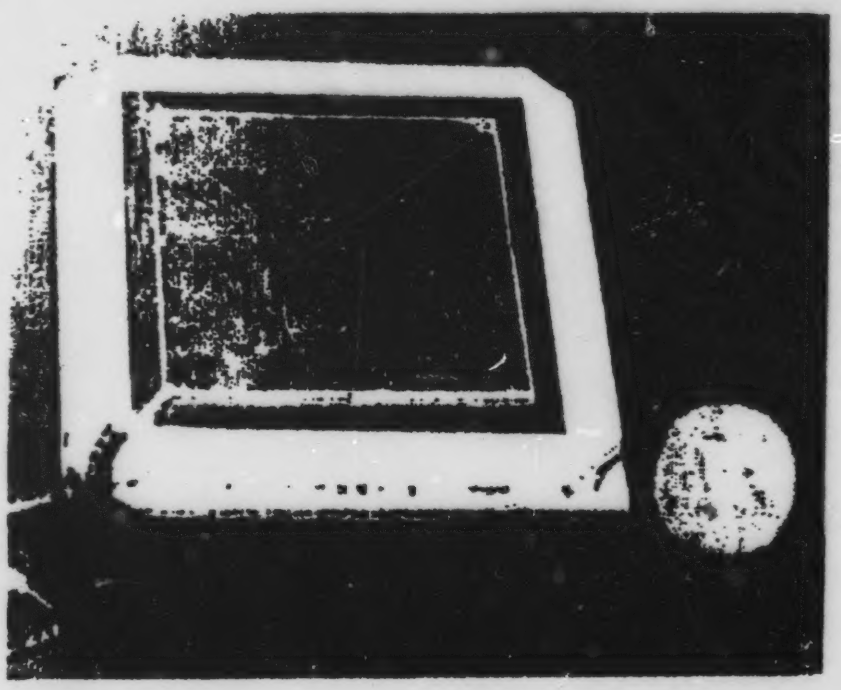

Composite Smart Materials

Acoustic Piston

System Integration
Team Leader
Lockheed Martin

Actuators
AVX

Electronics
VPT / VA Tech

Control
SSC

Testing
AST

Modeling
NRL

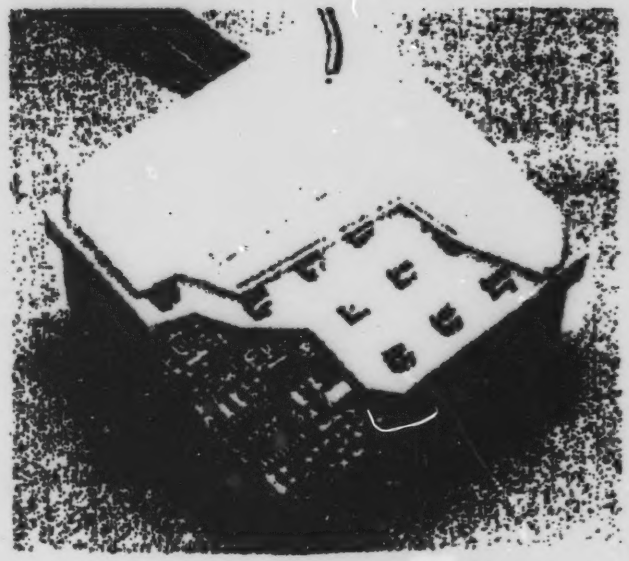

Cut Away View

Generation 1 and 2 Finite Element Analysis

Model

2D - 3 Actuator using symmetry - Static analysis - 2340 8-noded elements

Basics

ABAQUS

Piezoelectric material properties

All materials explicitly included in model

Fixed (Rigid) connection between baseplate and support box

2D - Plane Strain and Plane Stress conditions examined
    5^{o} and 20^{o}C
    Adhesive connection between actuator and base
    Rigid connection between actuator and base

Active Material

PMN chiplets

Similar to AVX 1418 actuators

Layered actuators

PMN

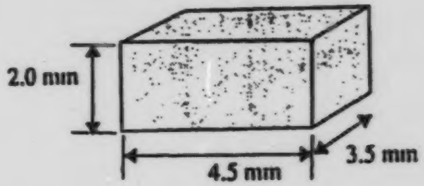

Basic 33 Chiplet Actuator

Modeling Simplifications

Piezoelectric - Linear approximation of PMN electrostrictive behavior

Monolithic - Approximate layered behavior

Piezoelectric Material Properties

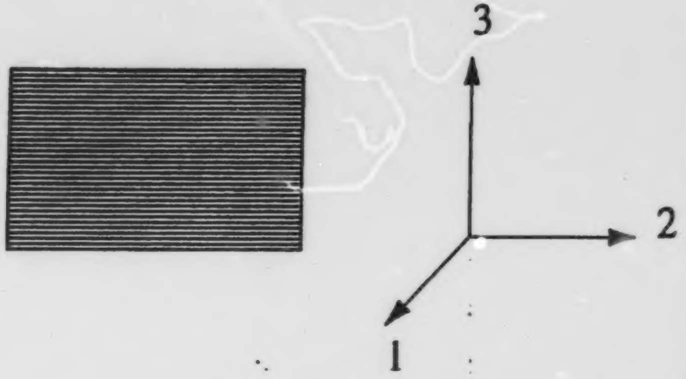

PMN Chiplets

	5°C	20°C
d_{33}	9.35×10^{-10}	8.30×10^{-10}
d_{31}	-4.68×10^{-10}	-4.15×10^{-10}
d_{32}	-4.68×10^{-10}	-4.15×10^{-10}

n=93 layers

Layered
    Increased displacement/voltage response
    Each layer acts as individual actuator
    More complex but standardized fabrication

Resulting displacement

$\Delta_{33}=\Sigma\delta_{33}$

Equivalent material properties

$d'_{33}=nd_{33}$

$d'_{31}=d_{31}$

$d'_{32}=d_{32}$

Verification of Simplified Piezoelectric Model

Analytical	1.85×10^{-6} m
FEM one actuator model	1.85×10^{-6} m
Electrical circuit model*	1.9×10^{-6} m

*D. T. Lindner, "An Integrated Model of a PWM Switching Amplifier and Electrostrictor Actuator," CSM Progress Report dated 12 April 1996, VPI, Blacksburg, VA.

Material Properties

Material	E (GPa)	Poisson's Ratio	Failure Stress (MPa)
Alumina	372.0	0.25	172.0
Polymer Filler	23.0	0.30	-
Kapton	3.1	0.30	-
Adhesive	3.1	0.30	-
Graphite composite	165.0	0.30	380.0
Ceramic actuator	80.0	0.30	6.9 (Tensile) 60-70 (Comp.)

Structural Evaluation

Stress levels in actuators greater than critical stress for all cases considered

Location of maximum stress is interface between active and passive materials

Rigid connections cause significant increase in stress levels at critical location

Location of maximum stress at corners of actuators

Actuators modeled with sharp corners, stress concentation

- Real actuators - rounded corners with finite radii
- Artifact of 2D modeling

Third Generation Design Options

- Actuator Type
  - 1418 vs. 1812
  - availablity, cost & performance
- Headmass Thickness
  - 0.025, 0.040, 0.060, 0.100 inch alumina
  - performance
- Baseplate Thickness and Material
  - 1.57 mm thick alumina (original)
  - 0.040 inch thick alumina
  - 0.065 inch thick fiberglass circuit board
  - availablity, cost & performance
- Support Box Configuration
  - impact on electronics
  - performance

Third Generation Design 18 Actuators per Piston in 3 x 6 array, 2 Piston per Unit Device

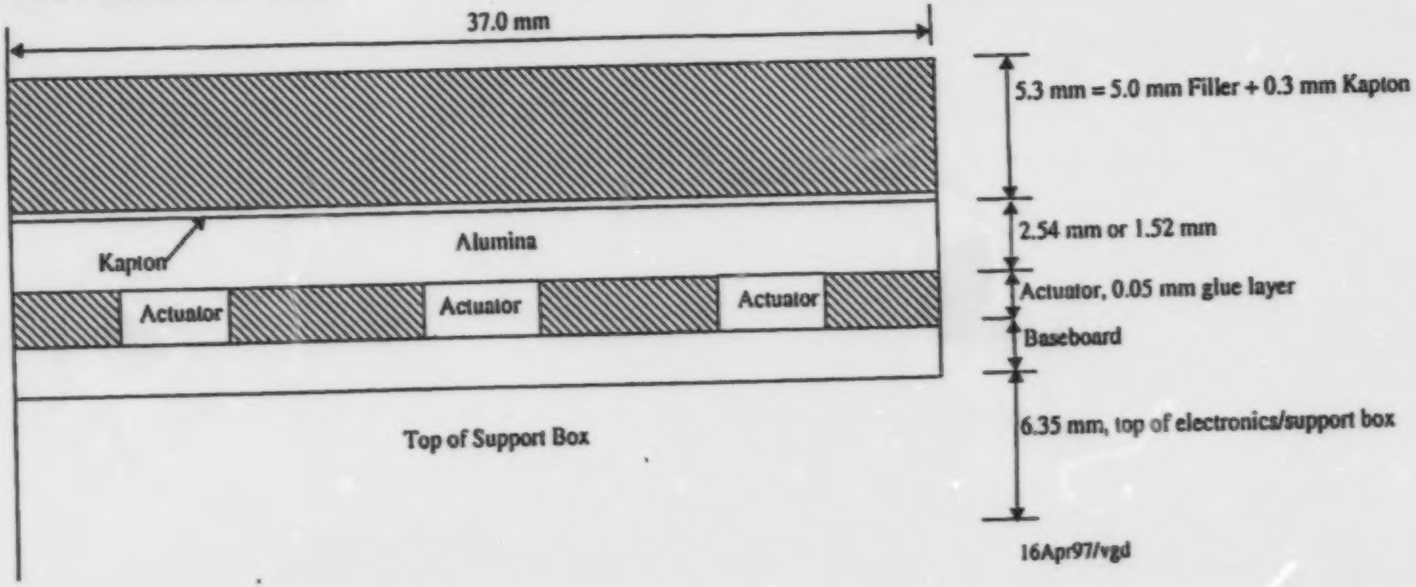
37.0 mm
Kapton
Alumina
Actuator
Actuator
Actuator
Top of Support Box
5.3 mm = 5.0 mm Filler + 0.3 mm Kapton
2.54 mm or 1.52 mm
Actuator, 0.05 mm glue layer
Baseboard
6.35 mm, top of electronics/support box

16Apr97/vgd

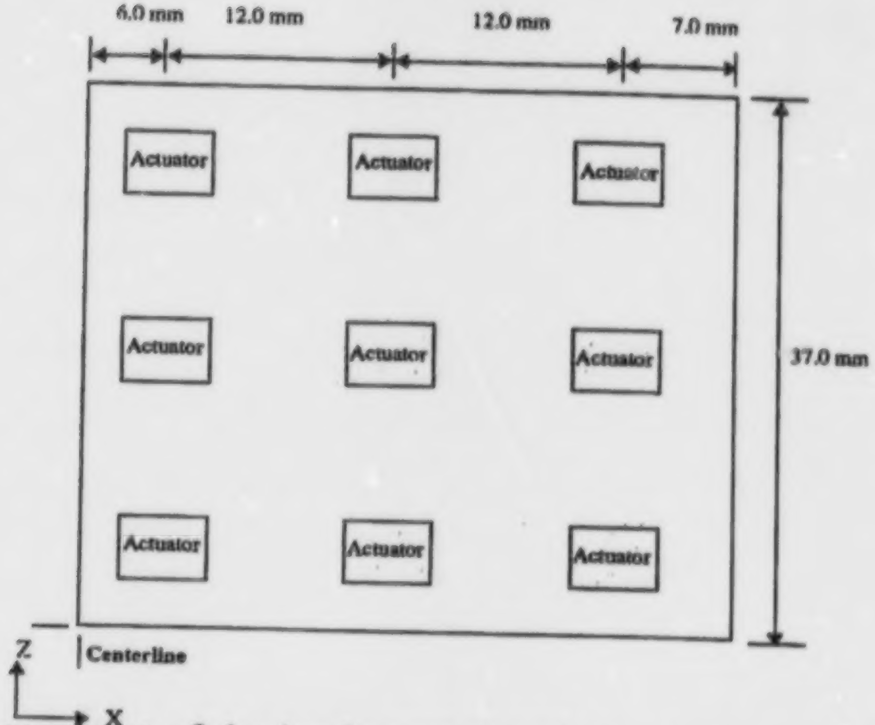
6.0 mm
12.0 mm
12.0 mm
7.0 mm
Actuator
Actuator
Actuator
Actuator
Actuator
Actuator
Actuator
Actuator
Actuator
37.0 mm
Z
Centerline
X

One quadrant of device layout showing actuator position

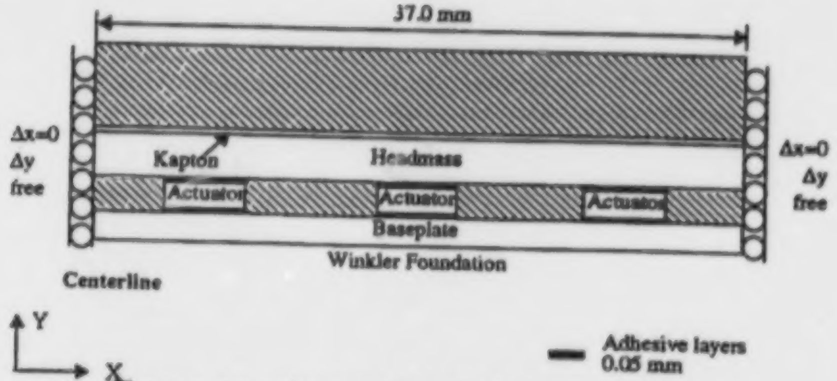
37.0 mm
Δx=0
Δy
free
Kapton
Headmass
Δx=0
Δy
free
Actuator
Actuator
Actuator
Baseplate
Winkler Foundation
Centerline
Y
X
Adhesive layers
0.05 mm

Cross section of quadrant modeled

Device Layout and Section Modeled of
76.2 x 76.2 mm piston

Device Design Conditions

ΔVoltage = 24 Volts

18 Actuators per piston
Piston dimensions ~1.5 inch x 3 inch

Multiple pistons per panel
Independent control/performance

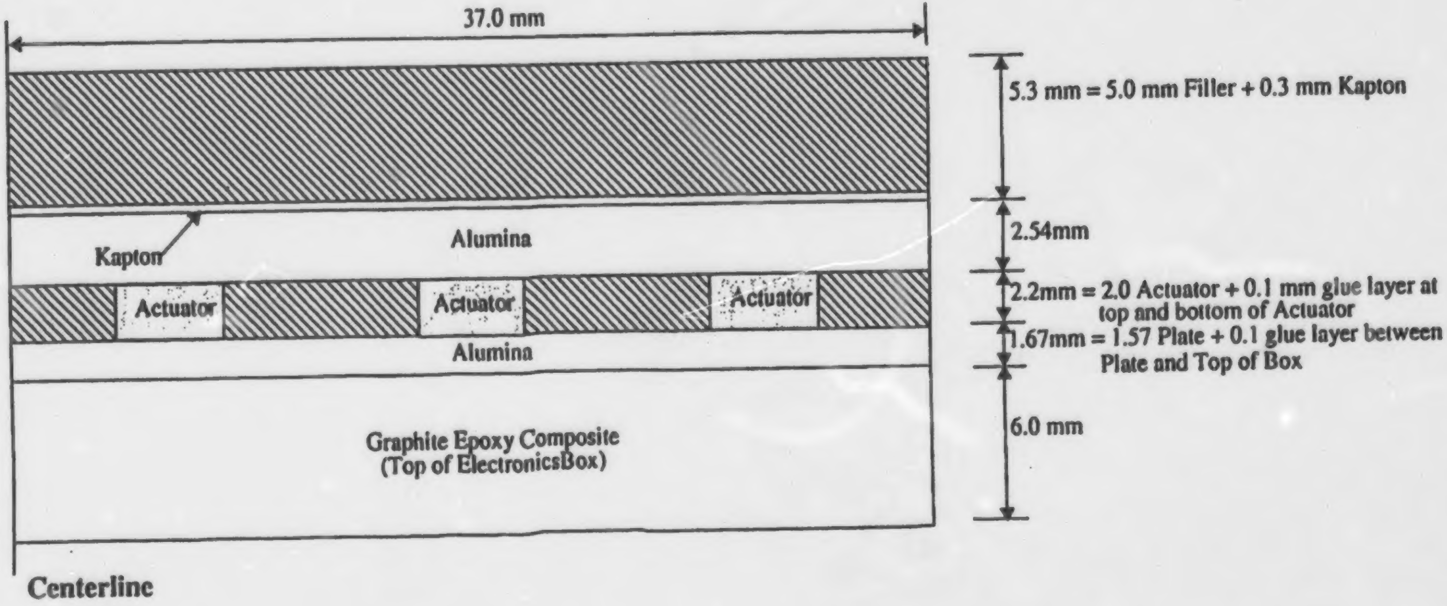
37.0 mm
5.3 mm = 5.0 mm Filler + 0.3 mm Kapton
2.54mm
Alumina
Kapton
Actuator
Actuator
Actuator
2.2mm = 2.0 Actuator + 0.1 mm glue layer at top and bottom of Actuator
1.67mm = 1.57 Plate + 0.1 glue layer between Plate and Top of Box
Alumina
6.0 mm
Graphite Epoxy Composite (Top of ElectronicsBox)
Centerline

Material Properties
(Textbook/Average vs. Measured)

Material	E (GPa)	Poisson's Ratio	Failure Stress (MPa)
Alumina	~~372.0~~ 360.0	0.25	172.0
Polymer Filler	~~23.0~~ 2.5	0.30	-
Kapton	3.1	0.30	-
Adhesive	3.1	0.30	-
Graphite composite	165.0	0.30	380.0
Ceramic actuator	~~80.0~~ 71.0	0.30	6.9 (Tensile) 60-70 (Comp.)

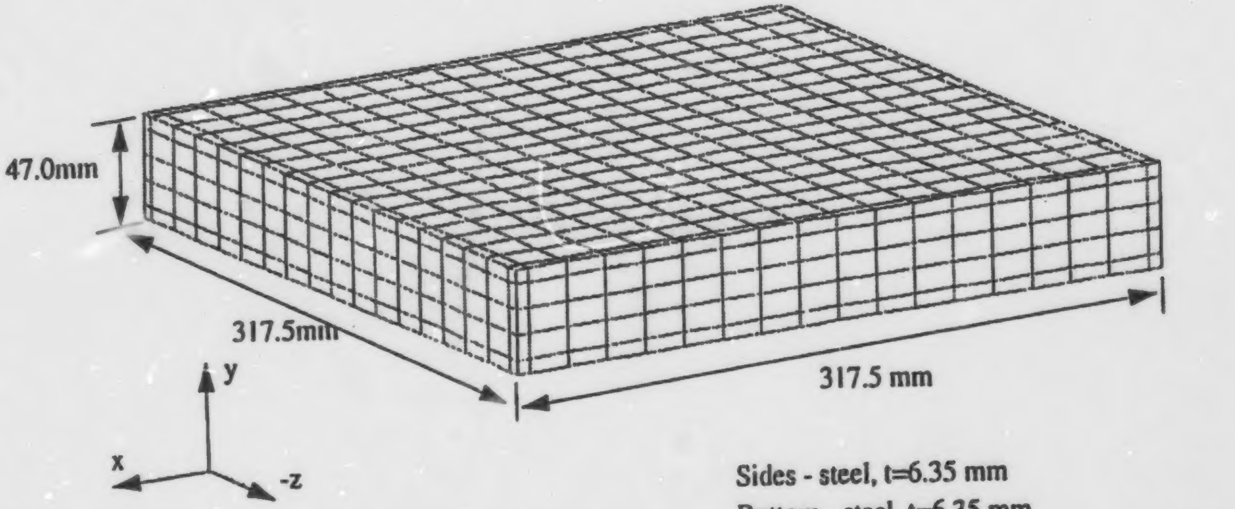

Sides - steel, t=6.35 mm
Bottom - steel, t=6.35 mm
Top - graphite epoxy composite, t=6.35 mm

Finite Element Model of Support Box

Used to Calculate Spring Stiffness for Winkler Foundation
Model Information
ABAQUS 1620 elements: 20 noded solid elements
Support box modeled as filled with polymer material

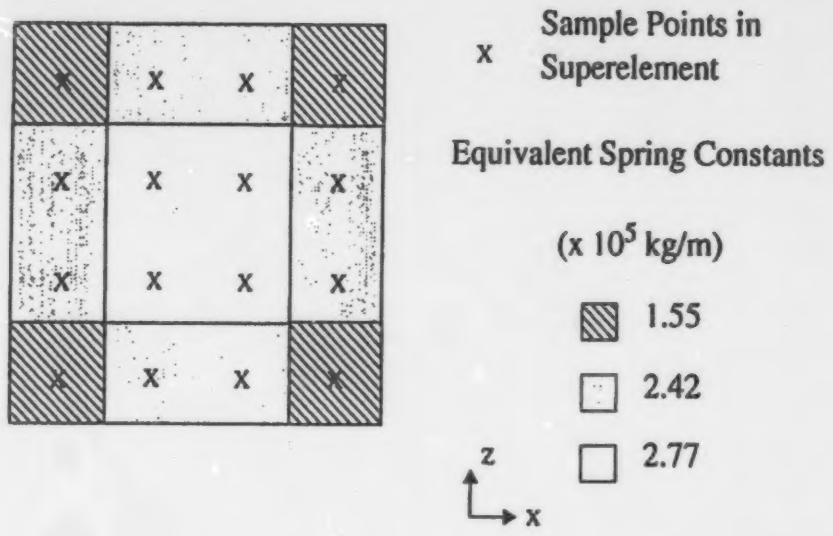

x
Sample Points in Superelement
Equivalent Spring Constants
(x 10⁵ kg/m)
▨ 1.55
□ 2.42
□ 2.77
z
x

Calculated Equivalent Spring Stiffness Values from Support Box Model

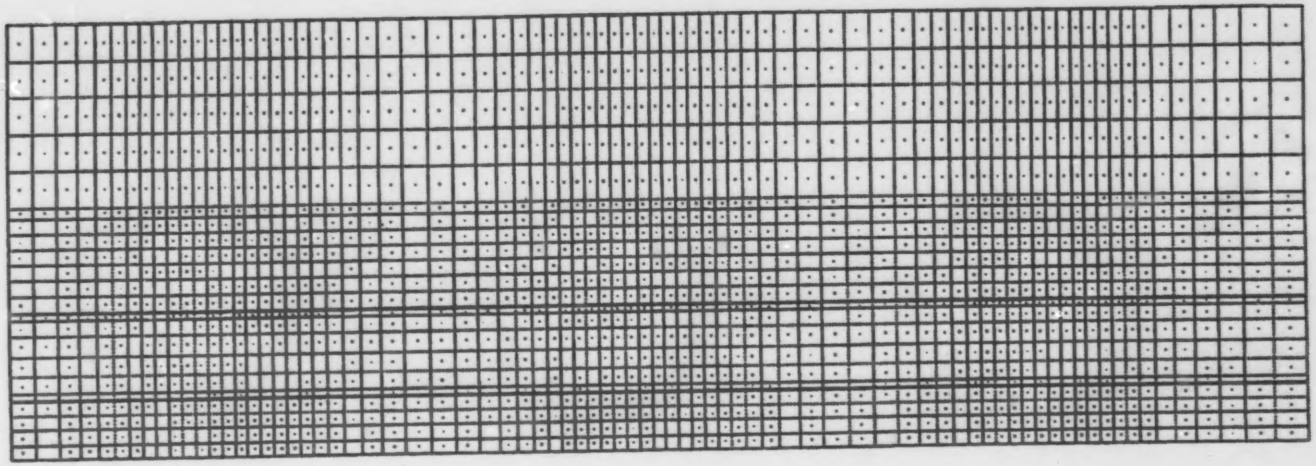

Finite Element Mesh of Composite Panel

ABAQUS 1872 elements: 8 noded 2D CPE8 and 8E elements
157 linear spring elements for Winkler Foundation

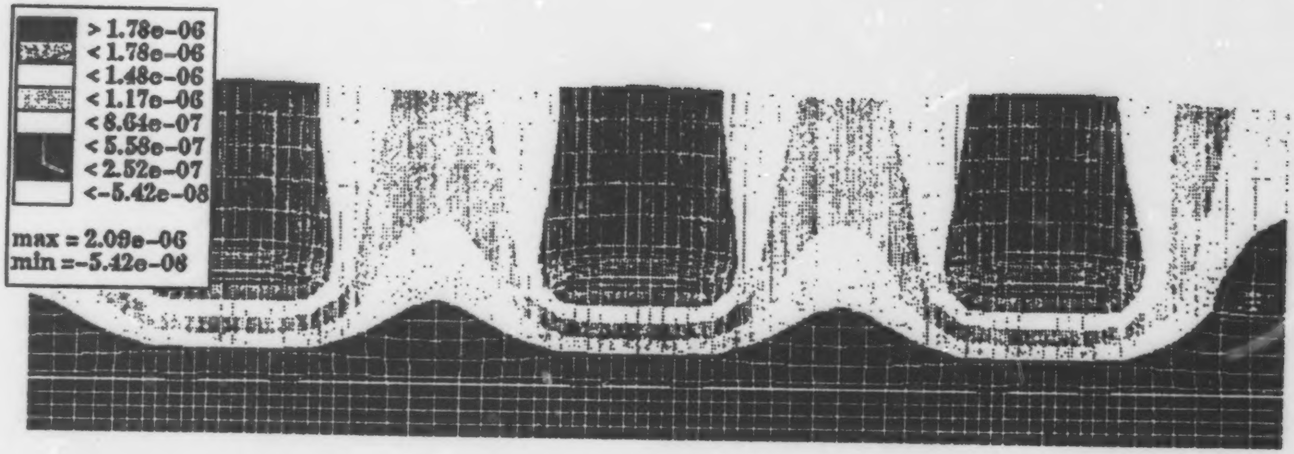

Vertical Displacement Contour Plot

1418 actuators, 1.57 mm alumina baseplate and 0.64 mm headmass
Displacement reported in meters.
Magnification factor of 5×10^5 for deformed shape.

Calculated Displacement

2D Structural FEM Model

2.54 mm headmass

Location	1418 Alumina Baseplate (micro-m)	1418 Fiberglass Baseplate (micro-m)	1812 Alumina Baseplate (micro-m)	1812 Fiberglass Baseplate (micro-m)
Bottom of Actuator	-0.10	-0.31	-0.10	-0.30
Top of Actuator	1.94	1.74	1.34	1.16
Top of Headmass	1.88	1.70	1.28	1.12
PVDF	1.87	1.69	1.27	1.11
Top of Device	1.80	1.64	1.20	1.06
Total Stroke	2.04	2.05	1.44	1.46

NRL, Code 6380

Calculated Displacement

2D Structural FEM Model

1418 actuators with alumina baseplate

Headmass Thickness (mm)	Displacement at Top of Headmass (mirco-m)	Displacement at Top of Device (above actuator) (micro-m)	Difference in displacement at Top of Device (above actuator & centerline between actuators) (micro-m)
0.64	2.07	1.64	0.5
1.02	2.03	1.69	0.34
1.52	1.95	1.75	0.17
2.54	1.88	1.80	0.05

NRL, Code 6380

Performance and Structural Evaluation

Actuator authority significantly effected by passive materials

- Wave-pattern in top surface displacement
- Wave-pattern in headmass
- Significant actuator back surface displacement
- Headmass thickness has a significant impact on flatness of device
- Passive materials have significant effect on device displacement authority
    - ~50% reduction at top surface
    - Must know for device design
- Stress levels fall to acceptable levels when actual material properties are used
- Compliant filler material required for acceptable stress levels

Final Thoughts

- Smart materials/devices are complex structures; limited simplification possible
- Interactions will drive system performance
- Device performance is objective, not isolated performance of smart component
- Support structure has direct affect on performance
- Need an understanding of system/device loss mechanisms for effective design
- Material variablity can greatly affect analysis results

#567210 ⑦

Designing with glass reinforced engineering thermoplastics

P.J. Bates, V.T. Bui
Department of Chemistry and Chemical Engineering
Royal Military College of Canada
P.O. Box 17000 STN Forces
Kingston, ON K7K 7B4
Canada

(Paper presented at the 3rd CF/CRAD Meeting on Naval Applications of Materials Technology and Inter Naval Corrosion Conference. Halifax NS, April 1997)

1. ABSTRACT

Glass reinforced thermoplastic materials are used in a wide variety of civilian and military applications. They are often chosen over metals and glass reinforced thermosetting materials for reasons of lower cost combined with equal or superior part performance. The higher production rates and part function integration capability associated with injection moulding, allow these thermoplastic based compounds to deliver a lower part cost than other often less expensive metallic or thermosetting materials. Prior to profiting from these cost advantages, the designer of glass reinforced injection moulded parts must first confront a number of issues : orientation of the glass fibre reinforcement causing anisotropy of all material properties, weldlines leading to areas of low mechanical strength, temperature limitations of engineering thermoplastics, as well as high equipment costs due to the high pressures required to manufacture large parts. Recently, a number of new glass reinforced engineering thermoplastic materials have been developed to address some of these problems. Semi-aromatic polyamides, long fibre reinforced compounds, and glass mat reinforced thermoplastic are several examples.

2. INTRODUCTION

The ability to produce a correctly functioning part using glass reinforced thermoplastics will depend largely on the nature of the thermoplastic polymer matrix, the form of the glass reinforcement and the processing technique used to manufacture the part. Each of these aspects is discussed in the following sections with emphasis on several developments within that particular area.

3. THERMOPLASTIC POLYMER

3.1 Thermoplastic Background

From their humble beginnings following the second World War, glass reinforced thermoplastics have grown into a 700 million pound market [1]. Although the total volume of glass reinforced thermoplastics is still smaller than that of glass reinforced thermosetting resins, the former present many unique advantages.

Thermoplastic polymers differ from thermosetting resins in that thermoplastics are processable in a relatively high temperature melt state and then will solidify without a chemical reaction upon cooling below a characteristic temperature. Versus thermosetting resins, this generally allows thermoplastic polymers to have :

- ***lower processing cycle time*** : The major component of most thermoset resin or thermoplastic polymer processing cycles is the time required for material solidification. The solidification of thermoplastic polymer is predominantly linked to the rate of cooling of the material which is measured in seconds. The solidification of thermoset resin is related to the rate of the cure or cross-linking reaction which is often measured in minutes.

- ***increased ductility*** : In general, thermoplastic polymers have a higher elongation at break than thermoset resins. This is often attributed to the absence of chemical cross-linking within the thermoplastic matrix.

- ***unlimited shelf life*** : The absence of chemical cross-linking in thermoplastic polymers allows these materials to be stored for very long periods of time without a change in molecular weight. The shelf life of uncured thermoset resins is limited.

- ***reprocessing of scrap*** : Although often of secondary importance, clean thermoplastic scrap, resulting from industrially rejected parts or trimming, can be reground and recycled in many processing operations. This is often performed at regrind levels of the order of 20 weight % without significant changes in mechanical or physical properties of the manufactured part [2]. Recycling of industrial thermoset scrap is more difficult due to the chemical cross-links which prevent the cured thermoset resin from flowing.

It is possible to reinforce most thermoplastic polymers. Semi-crystalline polymers have however achieved the most industrial success due, in large part, to their superior thermomechanical properties versus those of purely amorphous polymers.

Amorphous polymers exhibit one principal characteristic temperature called the glass transition temperature. The glass transition temperature is associated with movement of various segments of the polymer chain. Above the glass transition temperature, amorphous polymers display little mechanical strength and are, under these conditions, considered to be in the melt state. Semi-crystalline polymers exhibit both a glass transition temperature and a melting temperature. The latter is associated with the breakup of the ordered crystalline regions. Under certain short term loading, reinforced semi-crystalline polymers may be used at temperatures almost up to their crystalline melting point.

Two of the most common semi-crystalline thermoplastic polymers used industrially with reinforcements are polypropylenes and polyamides (nylons). Polypropylene is chosen for its low cost, high fluidity and chemical inertness. Nylon is used for good adhesion to the reinforcement and its relatively high glass transition and melting temperatures. It is impossible to cover the axes of development of these two common thermoplastic polymers in this short article. Instead, it is interesting to focus on recent developments in the polyamide family.

3.2 Polyamide - axes of development

Polyamide was discovered in the 1930's by Dupont. This family of polymers is characterized by a relatively high strength and stiffness which makes it well suited to many engineering applications [3]. This is mainly due to the hydrogen bonding that occurs between amide linkages on adjacent polymer chains. These amide linkages also improve the mechanical properties of reinforced polyamides by facilitating the chemical coupling of the polymer to the surface of the reinforcement.

Polyamide is polymerized by a condensation reaction between diacid and diamine monomer species. **Figure 1** shows the stepwise condensation of two polyamide chains resulting in water being liberated :

$$R_1\text{-}R_{acid}\text{-}CO\ OH\ +\ H_2N\text{-}R_{amine}\text{-}R_2$$
$$\leftrightarrow R_1\text{-}R_{acid}\text{-}CO\ HN\text{-}R_{amine}\text{-}R_2\ +\ H_2O$$

Figure 1 - Condensation reaction between a diacid and diamine monomer.

Of the different types of polyamides that exist, polyamide 66 is one of the most common. The 66 denotes the presence of 6 carbon atoms on both the diacid and diamine monomer species. Polyamide 66 is referred to as an aliphatic polyamide as the carbons are in a linear chain.

Polyamide 66 has a glass transition temperature of 50°C and a crystalline melting temperature of 260°C [4]. When reinforced with 30% glass fibre, a typical elastic modulus versus temperature profile is given in **Figure 2** [5]. The initial large drop in modulus occurs near the glass transition temperature of 50°C. The modulus drops off to near zero at the crystalline melting temperature of 260°C:

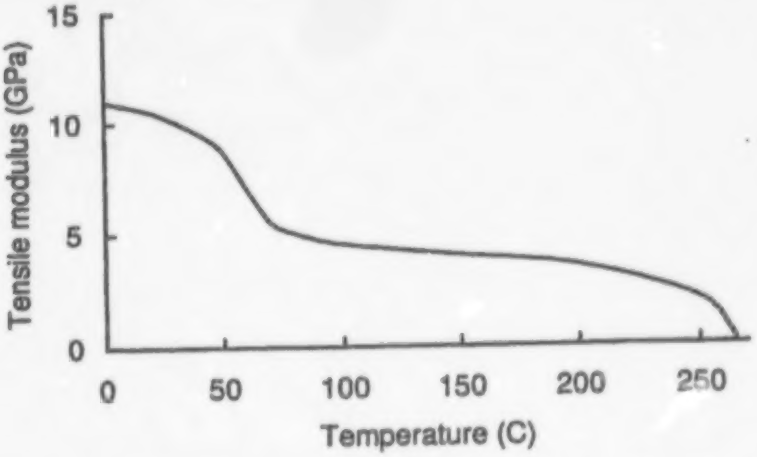

Figure 2 - Tensile modulus as a function of temperature of a 30% glass reinforced polyamide 66 compound [5].

In order to expand the market of aliphatic polyamides towards higher temperature applications, it is necessary to increase the glass transition temperature and/or the crystalline melting temperature of the polymer. In the last 15 years a number of new polyamide polymers have been developed by incorporating either aromatic diamine or diacid monomers (**Table 1**). These semi-aromatic polyamides (as opposed to fully aromatic polyamides such as Kevlar®, Nomex®...) exhibit higher glass transition temperatures, and higher or lower melting temperatures depending on the crystalline structure and amide/amide interactions [3].

Commercial trade name	Polymer producer
AMODEL®	Amoco (USA)
GRIVORY®	EMS Chemie (CH)
IXEF®	Solvay (B)
RENY®	Mitsubishi Gas Chemical (J)
ULTRAMID® T	BASF (D)
ZYTEL® HTN	Dupont (USA)

Table 1 : Partial list of commercialized semi-aromatic polyamides

An example of such a semi-aromatic polyamide is polyamide mXD6 which is polymerized using an aromatic diamine. A comparison of the elastic modulus of comparably reinforced polyamide 66 and mXD6 is shown in **Figure 3** [2]. The semi-aromatic polyamide's higher elastic modulus in the temperature region below 125°C is due to its higher glass transition temperature. The superior stiffness of the polyamide mXD6 in this temperature region has allowed it displace aliphatic polyamide 66 in many applications such as the diesel engine valve cover shown in **Figure 4**. The central bolting of this part to the engine block necessitated excellent high temperature stiffness along the cover edge to prevent oil leakage.

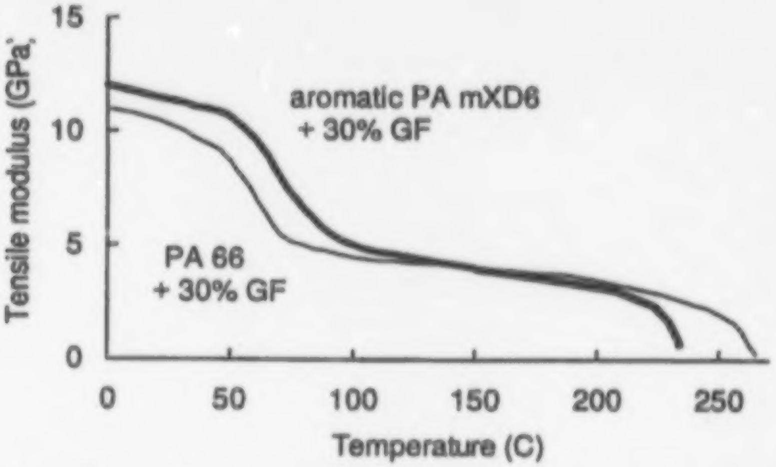

Figure 3 - Tensile modulus as a function of temperature for a 30% glass reinforced polyamide 66 compound and a 30% glass reinforced semi-aromatic polyamide mXD6 compound [2].

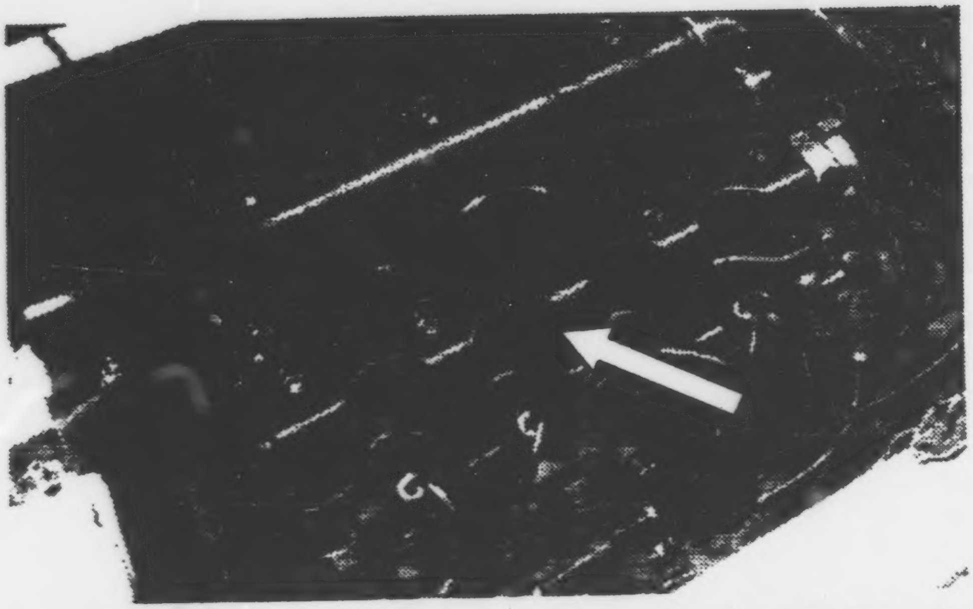

Figure 4 - Peugeot TUD3 motor valve cover moulded by Mecaplast (F) using semi-aromatic polyamide mXD6 reinforced with 50% glass fibre (IXEF® 1022 from Solvay).

4. GLASS FIBRES

Reinforcing fibres used in the thermoplastic industry can be divided into inorganic (glass, boron ....) and organic (carbon, aramid ....) groups. On a mass basis, inorganic glass fibres make up over 99% of the reinforcement used currently in thermoplastics [1].

4.1 Glass fibre parameters

Glass fibres, like any reinforcement, play a predominant role in determining the mechanical and physical properties of the composite material and of the finished part. They also influence the processing technique that can be used. The glass fibre parameters affecting properties are :

- ***glass composition*** : There exist several different glass compositions denoted by letters : E - general purpose; D - improved dielectric properties; R or S-improved mechanical properties. E type glass is used almost exclusively with reinforced thermoplastics [6].
- ***glass fibre sizing*** : Sizing is the chemical coating applied to the individual glass monofilaments immediately after they are formed. Sizing chemistry is tailored for the polymer and the processing technique. Sizing permits coupling between the polymer matrix and the reinforcement, adhesion among the individual glass monofilaments prior to processing, and lubrication between the monofilaments and any solid surfaces encountered during handling or processing [6]. The sizing composition is generally a closely guarded secret of glass fibre manufacturers as it is one of the major methods of product differentiation.

- ***glass monfilament diameter*** : The diameter of the individual monofilaments used in glass fibres is usually in the range of 10 to 24 μm [6, 7]. The actual diameter of a given glass fibre product is a compromise between mechanical properties, price, and ability to produce the glass product. To a certain point, smaller diameter monofilaments improve the strength of reinforced thermoplastics by increasing the surface area for a given reinforcement level [7]. Conversely, larger diameter monofilaments are generally lower in cost due to the higher production throughput during the fibre manufacture.

- ***reinforcement form*** : Glass fibres are available in several different forms (**Figure 5**) : *rovings* composed of several hundred to several thousand near parallel continuous monofilaments, *chopped fibres* composed bundles of parallel monofilaments of length 5 mm to 30 mm, and glass *mat*. Glass mat can be composed of randomly oriented fibre (shown in Figure 5), woven rovings or dispersed chopped fibre.

  The reinforcement form will dictate, to a large extent, the type of processing that can be used to make the finished part. In addition, the reinforcement form will also determine how the reinforcement should be combined with the polymer prior to final processing. This necessary combination step is often referred to as compounding.

  Currently most of the glass fibre used with thermoplastic polymer is of the chopped fibre form. The compounding of the polymer with the chopped fibre is done predominantly using a single or twin screw extruder (section 4.2). The resulting compound is then usually processed using the injection moulding process (section 5.2).

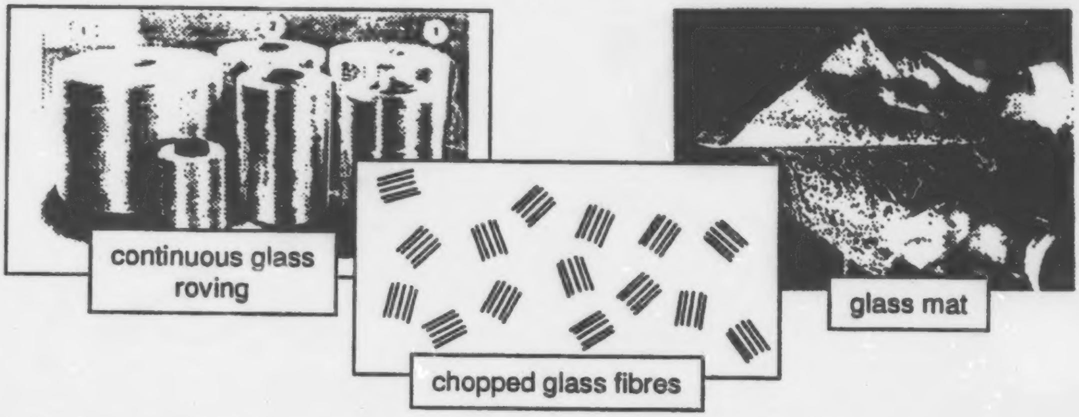

Figure 5 - Illustration of the various forms of glass fibre that can be used with glass reinforced thermoplastics.

4.2 Thermoplastic-Glass Fibre Compounding

Compounding of the glass fibre and the thermoplastic polymer is a necessary step prior to final part processing. The compounding of thermoplastic polymers with glass fibres is more difficult than compounding similar reinforcement with thermosetting resins. This is due to the lower viscosity of the thermoset resins prior to curing than that of most thermoplastic polymers in the melt state.

Many different techniques are used to compound thermoplastic polymers and glass fibres. They are often inspired from those used with thermosetting resins. Some of these techniques and their axes of development are discussed in the following sections.

4.2.1 Compounding of thermoplastic polymer in the melt state

4.2.1.1 Extrusion compounding

The most common technique used to compound glass fibres and thermoplastic polymer is extrusion compounding [8]. The process is shown schematically in **Figure 6**. It involves using the shearing action of an extruder or static mixer to distribute and disperse glass monofilaments throughout a polymer melt. The fibres are introduced into the extruder either in chopped or roving form. A *discontinuously reinforced composite strand is extruded* and chopped to form pellets which are then used in downstream processing such as injection moulding.

Extrusion compounding is an economical means of mixing most polymers with glass fibres as well as other additives. Its major disadvantage is the degradation of glass monofilament length during the extrusion process. For this reason, extrusion compounding is often referred to as short fibre compounding and the resulting material is called short fibre compound. The average residual monofilament length and length profile in the composite strand depend on extrusion conditions [9]. However, a number average value of the order 300 μm is typical. The glass monofilaments will undergo further degradation during the final processing.

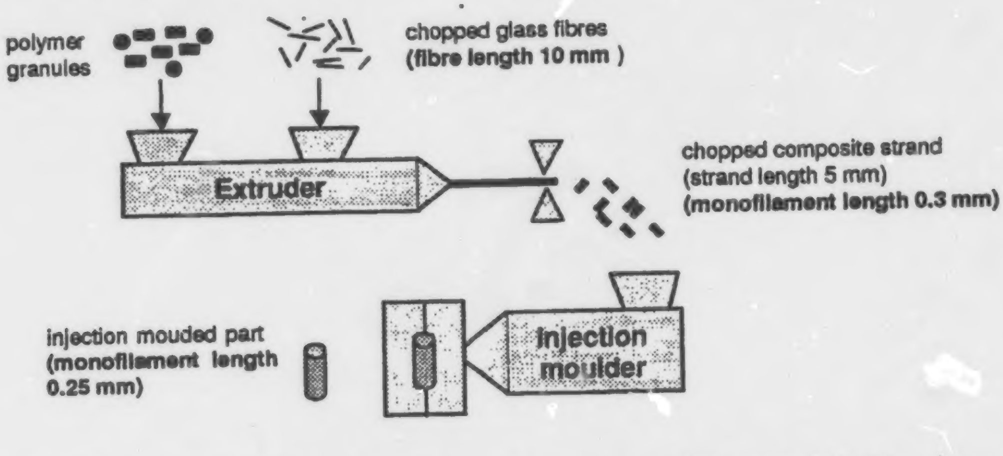

Figure 6 - Schematic diagram of a typical extrusion compounding operation using chopped glass fibres. The compounding is followed by injection moulding processing.

4.2.1.2 Pultrusion compounding

A number of alternative compounding techniques have been developed to minimize the fibre length degradation during compounding [10, 11, 12]. Most of these techniques use glass fibres in roving form. The roving is often impregnated by molten polymer in a specially designed die (**Figure 7**). A *continuously reinforced strand is then pulled from the die* and then chopped to form pellets for downstream injection moulding processing.

Although monofilament length degradation will still occur during the injection moulding process, the average monofilament length in the finished part is generally higher than that of parts made using short fibre compounds. For this reason, this pultrusion compounded material is often referred to as long-fibre compound.

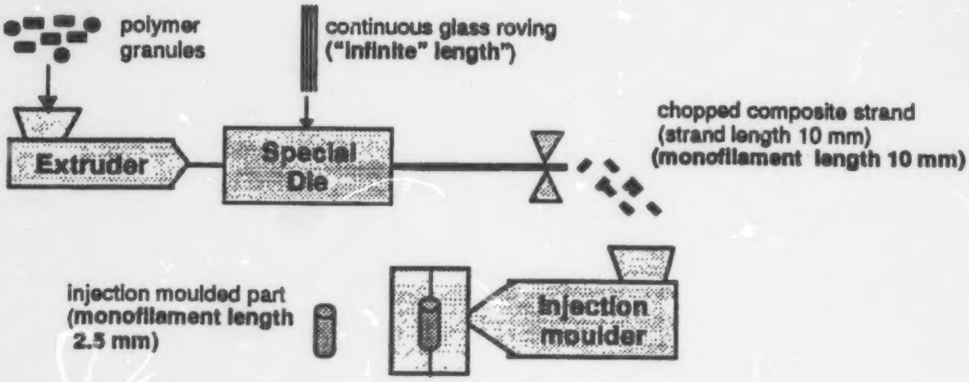
polymer granules
continuous glass roving ("infinite" length")
chopped composite strand (strand length 10 mm) (monofilament length 10 mm)
Extruder
Special Die
injection moulded part (monofilament length 2.5 mm)
injection moulder

Figure 7 - Schematic diagram of a typical pultrusion compounding operation using glass roving. The compounding is followed by injection moulding processing.

The ability to achieve higher residual glass monofilament lengths in the injection moulded parts translates to improved mechanical properties. **Figure 8** shows that notched IZOD impact resistance of 50% glass reinforced polyamide 66 is improved dramatically when long fibre compounds are used [13]. This increase in impact strength is obtained without a drop in modulus. This latter point is important as it is also possible to improve the impact performance of glass reinforced compound via rubber addition. This results, however, in a decrease in modulus.

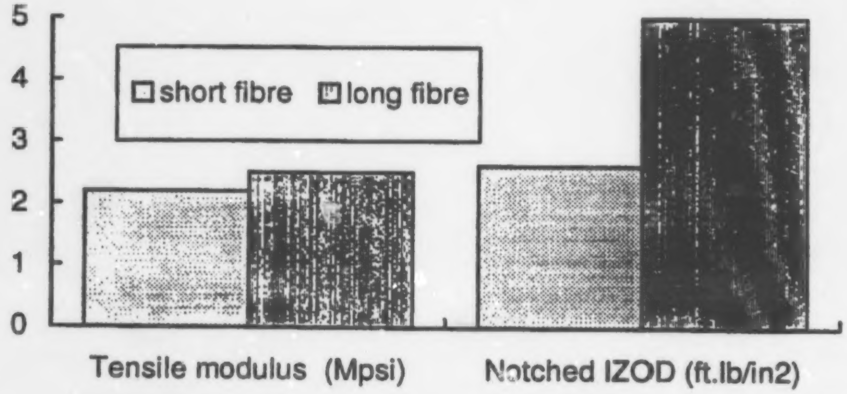

Figure 8 - Comparison of the room temperature tensile modulus and notched IZOD impact properties of polyamide 66 reinforced with 50% (wt) glass short and long fibres [13].

Several long fibre materials are currently commercially available : Verton (LNP) and Celstran (Hoechst Celanese).

4.2.1.3 Compression/lamination

Extrusion and pultrusion compounding are used to manufacture compounds containing either discontinuous or continuous monofilaments. In order to manufacture reinforced thermoplastic polymer compound in sheet form, a technique similar to that used in making thermoset sheet moulding compound (SMC) [4, 14] is often used. In such a process, glass mat is combined with several molten polymer sheets. The composite mixture passes through a lamination process where an applied compressive stress forces the molten polymer to penetrate the mat. The impregnated mat is then cooled and cut into blanks. This type of composite material is generally processed into the final part in a compression moulding operation [15].

AZDEL® is the trade name of such a polypropylene based glass reinforced mat. It is manufactured by a joint venture of GE and PPG.

4.2.2 Compounding of thermoplastic polymer in the solid state

The techniques described in section 4.2.1 all involve combining a molten thermoplastic polymer with reinforcement and applying pressure to force the two components into intimate contact. It is also possible to combine polymer in the solid state with the reinforcement, and then use the heat and pressure during final part processing to achieve intimate contact of the two materials.

4.2.2.1 Co-mingling

One of the most recent techniques for compounding of thermoplastic polymer and glass reinforcement is the co-mingling of continuous polymer and glass fibres (**Figure 9**).

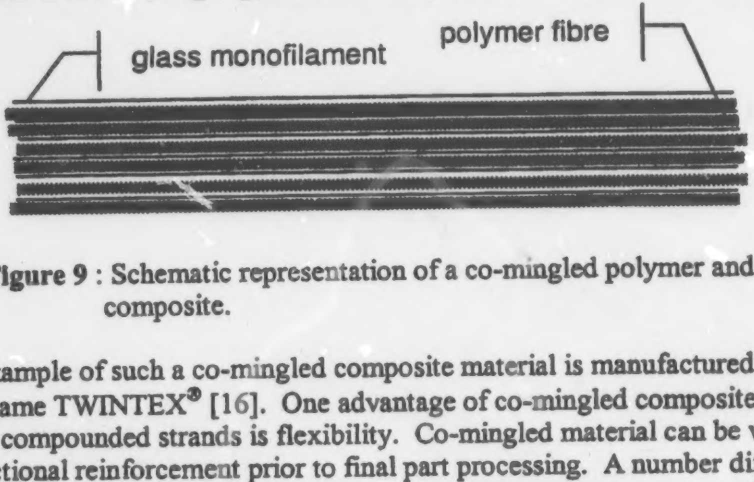

Figure 9 : Schematic representation of a co-mingled polymer and glass fibre composite.

A new example of such a co-mingled composite material is manufactured by Vetrotex under the trade name TWINTEX® [16]. One advantage of co-mingled composite strands versus pultrusion compounded strands is flexibility. Co-mingled material can be woven or assembled as unidirectional reinforcement prior to final part processing. A number different processing operations are under evaluation with this material. They include compression moulding, vacuum forming and filament winding.

4.2.2.2 Powder impregnation

Prior to the introduction of co-mingled composite fibres, an alternative technique was often used to obtain flexible composite strands. It involved incorporating polymer powder between reinforcing monofilaments. This compounding operation was often performed in a specially designed fluidized bed [17, 18]. This material is frequently filament wound over metal pressure vessels to increase their burst pressure [19].

5. PROCESSING TECHNIQUE

5.1 Introduction

The processing technique used to manufacture the finished part will depend largely on the form of the glass fibre as well as the thermoplastic-glass compounding technique. These combinations have been briefly discussed in the previous sections and are summarized in **Table 2.**

Glass fibre form	Compounding technique	Typical final processing
chopped fibre	extrusion	• injection moulding
continuous roving	pultrusion	• injection moulding
	co-mingling	• filament winding • compression moulding • vacuum forming
	powder impregnation	• filament winding
mat	compression/lamination	• compression moulding • vacuum forming

Table 2 : Typical final processing as a function of the glass fibre form and compounding.

Although a wide variety of fibre forms, compounding and processing techniques exist, injection moulding of extrusion compounded chopped glass fibre and thermoplastic polymer is today the most common combination [20]. Injection moulding's popularity is the result of its ability to manufacture complex small to medium sized parts at high production rates in an automated process. In spite of these strengths, this process presents a number of important weaknesses that need to be considered when designing a glass reinforced thermoplastic part for injection moulding or when selecting the appropriate processing technique.

5.2 Injection moulding process

In order to better understand the issues relating to injection moulding, it is important to first understand the process itself. The process is divided into a number of sequential operations :

- ***Plastification*** - the reinforced thermoplastic pellets are introduced into the plastification unit (**Figure 10**) which consists of a rotating screw inside a cylindrical barrel. The polymer matrix is melted and the composite mixture accumulates in front of the screw until the required volume for injection is available.
- ***Injection*** - the mould is closed and the screw quickly moves forward to push the molten material through a series of channels into the mould cavity(ies).
- ***Holding*** - the screw then applies pressure to the melt for a specified time. This creates a slow flow of material from the plastification unit to the mould cavity(ies). This additional material compensates for material shrinkage inside the cavity(ies).
- ***Cooling/Ejection*** - the material is left inside the cooled mould until sufficient solidification has occurred for the part(s) to be ejected without significant deformation.

The plastification, injection and holding phases cause a number of process limitations. These issues are described in the following sections.

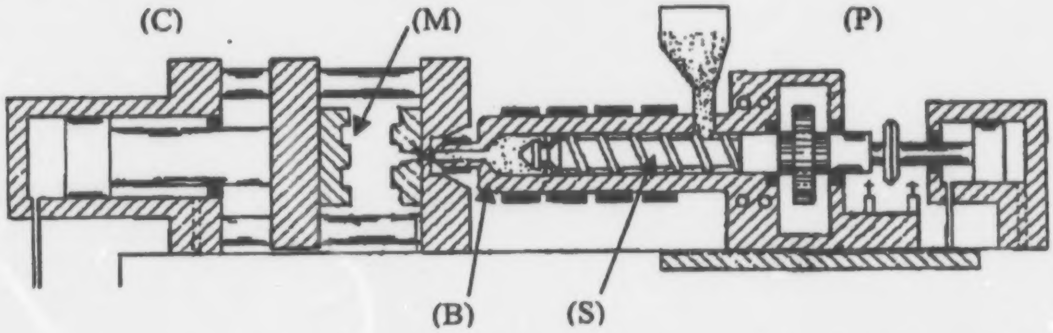

Figure 10 - Schematic diagram of an injection moulding machine showing : (P) plastification unit, (B) barrel, (S) screw, (C) clamping unit and (M) mould in the open position.

5.3 Injection moulding issues

5.3.1 Fibre length degradation

The shearing action of the plastification unit's screw will cause a degradation of the glass monofilament length [20]. Decreases in length will lead to a drop in mechanical properties of the part. As discussed in sections 4.2.1.1 and 4.2.1.2, degradation during injection moulding is critical if pultrusion compounded material is used, but is generally less important when using extrusion compounded material.

The monofilament degradation during the injection moulding step may be attenuated, but not eliminated, by the judicious choice of low shear injection moulding conditions [21].

5.3.2 Monofilament orientation

The glass monofilaments injected with the molten polymer will be oriented in the cavity by the shear stresses created during mould filling. The estimation of the orientation from mould geometry and injection moulding conditions is the subject of much research [22, 23]. In the absence of converging and diverging flows, monofilaments will be oriented preferentially in the direction of flow. The mechanical properties of the part will therefore be a maximum in this direction.

To illustrate the effect of glass monofilament orientation on mechanical properties, flexural specimens were cut at various angles from plates moulded using a 50% glass reinforced nylon compound [2]. The flexural modulus of these samples as a function of the angle is given in **Figure 11.** It is observed that the modulus is a maximum when the sample is cut from the plate the direction of flow (direction of preferential monofilament orientation).

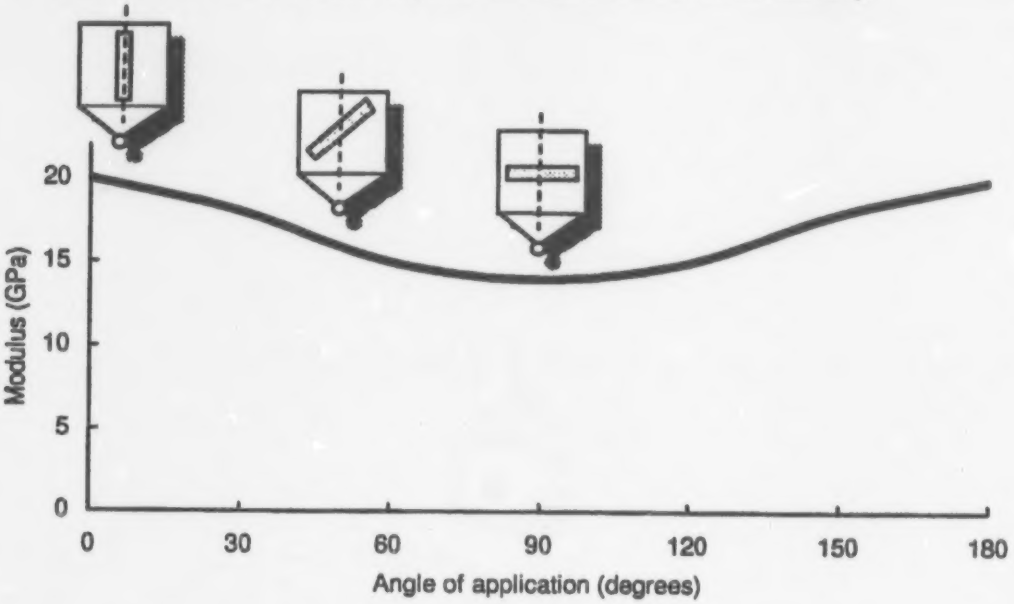

Figure 11 : Flexural modulus as a function of application angle for a plate injection moulded using a 50% glass reinforced PA mXD6 [2]

The monofilament orientation in injection moulded parts must be accounted for during part design as well as during the interpretation of property data sheets. Most data sheet properties of glass reinforced materials are measured in the direction of flow and hence in the direction of preferential glass orientation.

A second orientation related weakness of glass reinforced injection moulded thermoplastics occurs at weldlines. Weldlines are the interface created when two fronts of molten material meet during the injection phase. This can occur if multiple gates are used or if the cavity contains cores or inserts around which the molten material must flow. The flow induced shear stresses at the weldline are small as little flow occurs across this interface. Few glass monofilaments will therefore be oriented across the weldline and the mechanical properties perpendicular to the weldline plane are reduced to near those of the unreinforced polymer.

Figure 12 compares the tensile strength of injection moulded samples which contain no weldlines and those containing a central weldline. The central weldline sample was injection moulded using a cavity containing two end gates. Both materials are 50% glass reinforced PA mXD6 [2]. The tensile strength of the sample containing the weldline is comparable to that of the unreinforced polymer - 100 MPa [24].

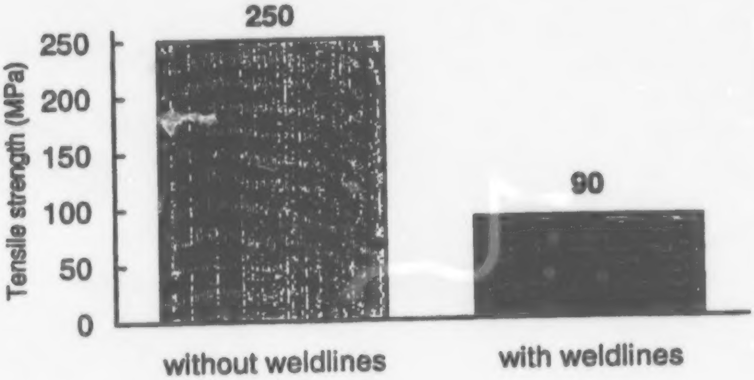

Figure 12 : Tensile strength of 50% glass reinforced PA mXD6 using samples with and without central weldlines.

Although weldlines are difficult to eliminate in most injection moulded parts, the weldline strength of the fibre reinforced thermoplastic polymer can be maximized by :

- *correct gating* : In general, the designer should minimize the number of gates to minimize the number of weldlines. The gate should also be positioned to move the weldlines to locations in the part which are under low stress.
- *correct venting* : It is necessary to allow evacuation of the air trapped between the melt fronts just prior to the formation of the weldline. This air can become trapped in the material upon solidification and can reduce the strength of the weldline. Air evacuation occurs through passages called vents that are machined into the mould usually along its parting line.
- *correct processing* : For maximum weldline strength, it is important to inject the hot material quickly to minimize cooling of the material prior to weldline formation.

5.3.3 High pressures during the injection moulding cycle

The injection moulding process requires high melt pressures to inject the material into the mould and to hold the pressure. Large clamping forces are thus needed to keep the mould closed. The injection moulding machine clamping force is an important factor in determining machine cost. **Figure 13** shows the relative price of injection moulding machines as a function of the clamping force in tons. [2]

Although high pressures are required for most injection moulding materials, the pressure (hence clamping force) is often higher for glass reinforced polymers versus the non-reinforced variety due to their higher melt viscosity.

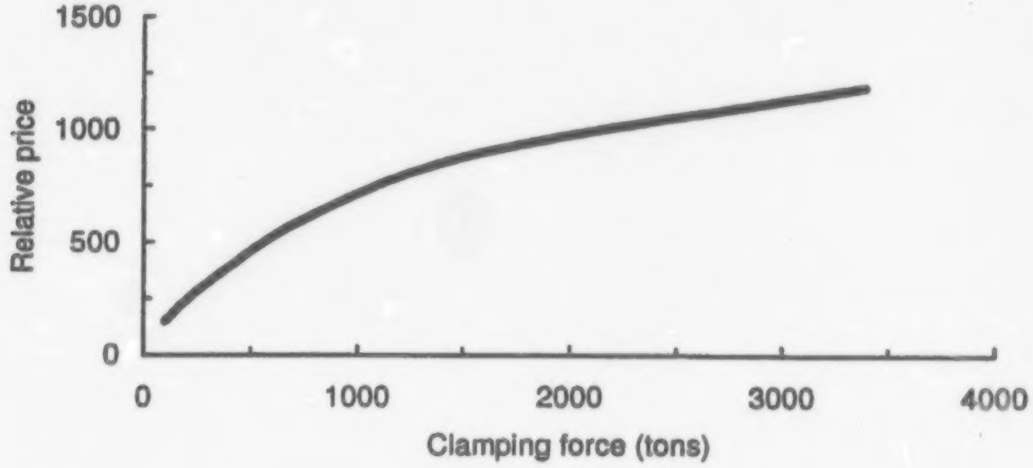

Figure 12 : Relative price versus clamping force for injection moulding machines [2].

Minor reductions in injection moulding pressure can be made by using several gates or centrally positioning the gate to minimize the flow length. Both these options have, however, implications on weldlines and glass monofilament orientation in the part.

Modified injection moulding techniques such as gas-assist injection moulding can also reduce both the injection and holding pressures [25, 26]. Gas-assist involves injecting an inert gas into the molten polymer to complete the injection and holding phases. The gas forms a hollow channel in the centre of the part.

5.4 Alternative processes

Although minor improvements can be made to the injection moulding process to address the various issues outlined in section 5.3, eliminating them involves using alternative processing techniques such as compression moulding, vacuum forming and filament winding. These techniques are commonly used for reinforced thermoset resins.

These alternative processes generally use continuous reinforcement (see table 2) and involve a more controlled placement of the reinforcement during processing. Although compression moulding involves high pressures, the pressure is generally lower than that observed during injection moulding due to the lower flow length and absence of a gate and runner system [15]. The lower pressure of these processes therefore reduces the equipment costs compared with injection moulding.

In spite of these advantages, there remain many challenges in using these alternative processes. They can be broadly grouped into two categories :

- ***compounding*** : The compounding cost associated with manufacturing thermoplastic polymer with either continuous roving or glass mat is significantly higher than classic extrusion compounding. New techniques must be developed and older ones improved if these costs are to decrease.

- ***processing*** : Many of the techniques used to process continuously reinforced thermoplastics are relatively new or have been adapted from thermoset processing. More work is needed to optimize these processes for thermoplastic polymers.

The Royal Military College of Canada (RMC) is actively involved in continuous glass reinforced thermoplastic research. Two research projects are currently underway :

- ***Experiments and modeling of a pultrusion compounding process*** : The objective of this research is to model the thermoplastic melt impregnation of continuous glass roving in a pultrusion compounding process as non-newtonian fluid flow through porous media. Bench scale experiments are performed to estimate the model parameters. Model results are compared with existing pilot scale pultrusion compounding data.

- ***Low pressure forming of glass fibre reinforced thermoplastic mat*** : Co-mingled glass and polymer fibres can be woven to form mats which can be processed using a variety of techniques. The objection of this research is to study the suitability of this type of material to low pressure forming of large panels to be used as part of a ballistic protection system. The experimental and modeling work will involve all stages of the part manufacture process: heating, vacuum forming, composite consolidation and part cooling.

For further information on any of these subjects, please contact the authors.

6. REFERENCES

1. Plastics Business, pg. 19, May 1989.
2. IXEF Manuel Technique, Solvay SA, Brussels, 1995.
3. Kohan M.I., "Nylon Plastics", John Wiley & Sons, New York, 1973.
4. Charrier J.M., "Polymeric Materials and Processing", Hanser Publishers, Munich, 1991.
5. Bates P.J., Dubois M., "Mechanical Properties of Glass Fibre Reinforced Thermoplastics", Injection Moulding of Plastics Conference, Technolgisch Instituut KVIV, April 1994.
6. Verre Textile Pour Renforcement des Matières Plastiques, Vetrotex Saint-Gobain.
7. Sato N., Kurachi T., Sato S., Kamigaito O., "Mechanism of Fracture of Short Glass Fibre Reinforced Polyamide Thermoplastics", Jour. of Mat. Sci. 19:1145, 1984.
8. Folkes M.J., "Short Fibre Reinforced Thermoplastics", John Wiley & Sons, New York, 1982.
9. Turkovich R.V., Erwin L., "Fibre Fracture in Reinforced Thermoplastic Processing", Polym. Eng. and Sci., 23:743, 1983.

10. U.S. Patent 4,549,920
11. U.S. Patent 4,559,262
12. U.S. Patent 4,439,387
13. Cianellli D.A., Travis J.E., Bailey R.S., "Processing of the New Long Fiber Reinforced Thermoplastics", 43rd Annual Conference, Composites Institute, The Society of the Plastics Industry, Feb. 1-5, 1988.
14. Lee S.M., "International Encyclopedia of Composites", vol. 5 pg. 510, VCH Publishers, New York, 1991.
15. Technopolymer Structures - Design and Processing Guide AZDEL, GE Plastics, 1989.
16. Osten S., St. John C., Guillon D., Zanella G., Renault T., "Compression Molding of Twintex and Random Fiber Thermoplastic Molding Materials", ANTEC Conference Proceedings pg. 2432, SPE, Brookfield Conn, 1997.
17. U.S. Patent 3,703,396
18. Brevet Français 81 21545
19. Long Fiber Unidirectional Thermoplastic Tapes, Baycomp product bulletin.
20. Lunt J.M., Shorthall J.B., "Extrusion Compounding of Short-Glass-Fibre-Filled Nylon 66 Blends", pg 37-44, Plastics and Rubber Processing, June 1980.
21. Bailey R., Kraft H., "A Study of Fibre Attrition in the Processing of Long Fibre Reinforced Thermoplastics", pg 94-101, Intern. Polymer Processing 2, 1987.
22. Lee S.C., Yang D.Y., "Prediction of Fiber Orientation in Injection Molded Parts Considering Compressibility and Phase Change", ANTEC Conference Proceedings pg 642, SPE, Brookfield Conn, 1997.
23. Gerard P., Raine J., Pabiot J., "Characterization of Fiber and Molecular Orientations and their Interactions in Composite Injection Molding", ANTEC Conference Proceedings pg 526, SPE, Brookfield Conn, 1997.
24. MX Polyamide mXD6 Nylon Technical Manual, Mitsubishi Gas Chemical, Tokyo.
25. Kirland C. "New Molding Methods Increase Design Freedom", Pg 37-40, Plastics World, Feb 1991.
26. Becker O., Karsono D., Koelling, K., Altan T., "Gas-assisted Injection Molding of Long Glass Fiber Reinforced Thermoplastics", ANTEC Conference Proceedings pg 615, SPE, Brookfield Conn, 1997.

#507211 ⑧

Applications of Composites for C5 Sonar Dome Components

By Dr. T.S. Koko[1], Mr. M.J. Connor[2] and Mr. G.V. Corbett[3]

[1]Martec Limited, 1888 Brunswick Street, Suite 400
Halifax, N.S., Canada, B3J 3J8

[2]Composites Atlantic Limited, 71 Hall Street
Lunenburg, N.S., Canada, B0J 2C0

[3]DMSS 7-3-5, National Defence Headquarters
Ottawa, Ontario, Canada, K1A 0K2

ABSTRACT

Composite materials have seen increasing use, within the past decade, in many structural applications which exploit their superior specific strength and stiffness properties. In the marine community, their excellent corrosion resistant properties can also be exploited for use in corrosion sensitive components. This paper presents one such study. The study was undertaken to replace the stainless steel fairing band assembly components of the C5 hull mounted sonar dome with composite material, in order to eliminate the corrosion problems associated with the use of the stainless steel material.

The fairing band assembly is used to wrap around the dome-hull interface to provide a smooth surface so as to reduce turbulence and flow noise. The fairing band assembly consists of two stainless steel bands (4400 mm x 140 mm x 0.9 mm) and a stainless steel tail cap which are fastened to the mild steel hull structure by means of stainless steel bolts. In the presence of moisture, a cathodic corrosion mechanism is created between the stainless steel fairing band components and the mild steel dome spacer. The resulting corrosion ruins the mounting threads in the dome spacer and this results in loss of the fairing band assembly. This requires the ship to be brought frequently to dry dock in order to perform corrective measures, thereby increasing the maintenance cost as well as reducing the operational readiness of the ship.

Glass reinforced plastic (GRP) composites were selected for the application because of their superior corrosion resistant properties. Each fairing band was fabricated from four plies of plain weave E-glass epoxy prepreg, laid up on a solid surface and cured with a pressure plate. The mounting blocks at the ends of the band were integrally fabricated from many layers of the same material. These blocks are used to support as well as transfer loads from the mounting bolts to the fairing band. The screw threads in the fastener holes in the mounting blocks were also fabricated integrally using removable threaded inserts. Details of the investigations, which includes material selection, detailed design, tooling and fabrication requirements are presented in this paper. Results on the performance of the composite fairing band assembly, as well as the challenges encountered in undertaking the study discussed.

#567212 (9)

Impact Properties of Composite Sonar Dome Materials

J.P. Szabo, A.J. Russell*, and J.A. Hiltz

Defence Research Establishment Atlantic
P.O. Box 1012, Dartmouth, N.S. B2Y 3Z7

***Esquimalt Defence Research Detachment**
CFB Esquimalt, P.O. Box 17000, Station Forces
Victoria, B.C. V9A 7N2

ABSTRACT

In an effort to reduce the costs associated with the repair and overhaul of the C5 stainless steel sonar dome, DMSS-7 is examining the feasibility of using composite materials in the C5 dome. As part of the project, DREA was tasked to study the acoustic and mechanical properties of glass and Spectra® reinforced composites panels. This paper discusses the effects of impact damage on the acoustic properties of the composite panels. A total of six 30 cm x 30 cm panels were impacted using a drop tower until damage was evident both visually and ultrasonically. The six panels were fabricated using various combinations of reinforcing fibre, resin system, and weave. The normal incidence insertion loss in the 1 - 10 kHz range was measured for both damaged and undamaged panels using a parametric array source and a PVDF hydrophone. The effect of water uptake on the insertion loss, and the implications for sonar performance will be discussed.

Impact Properties of Composite Sonar Dome Materials

J.P. Szabo[†], A.J. Russell*, and J.A. Hiltz[†]

[†]Defence Research Establishment Atlantic

*Esquimalt Defence Research Detachment

BACKGROUND

- C5 Sonar Dome is currently double walled stainless steel
    - high initial cost
    - high R&O cost due to corrosion and impact damage

- DMSS   C5 Composite Sonar Dome Project

- DREA tasked by DMSS to study Spectra and Glass composites:
    - Acoustic
    - Mechanical
    - Effect of impacts
    - Effect of environment

Test Laminates

Laminate ID	988PT/ BTCY-3	988PT/ BT250E	985PT/ BTCY-3	985PT/ BT250E	BROWN GRP	BLUE GRP
Fibre	Spectra	Spectra	Spectra	Spectra	Glass	Glass
Matrix	Cyanate-Ester	Epoxy	Cyanate-Ester	Epoxy	Cyanate-Ester	Epoxy
# of Plies	28	28	28	28	36	36
Thickness	9.6 - 9.9 mm	9.4 - 9.7 mm	9.3 - 9.6 mm	9.6 - 9.8 mm	9.2 - 9.6 mm	8.3 - 9.2 mm
Weave	4 harness satin	4 harness satin	8 harness satin	8 harness satin	8 harness satin	8 harness satin
Porosity	Very Low	Very Low	Very Low	Very Low	High	High
Colour	Brown	White	Brown	White	Brown	Blue

Spectra fibre pre-pregs manufactured by Bryte Technologies. Cyanate-ester cured 5 hours at 121°C.

All fibres run in x and y directions. Every second layer of woven cloth is rotated 90° (or flipped upside down) with respect to the others.

Impact Damage - Approach

1 Determine elastic property coefficients of material

2 Investigate impact behaviour using simple but representative conditions. ie. Characterize material response to impact

3 Model impact experiments and use test data from 1 & 2 to set-up and validate damage model parameters

4 Model structure using shell elements and validated damage model

5 Apply dynamic impact loads to model

Impact Tests

• Drop Weight Tester	maximum height = 2.4 m maximum velocity = 7 m/s
• Instrumented Tup	measure load vs time
• Displacement gage	measure displacement vs time
• Strain gage	back-surface strain vs time

Impact Test Parameters

- 50 mm diameter aluminum tup
- 9 mm thick laminates simply supported on 250 mm diameter ring
- Masses of 7, 11 and 21 kg Used for initial tests
- Impact at centre of support

Base of drop tower showing cross-head, tup, laminate support and displacement gage.

8H Glass/ Epoxy 289 J Impact

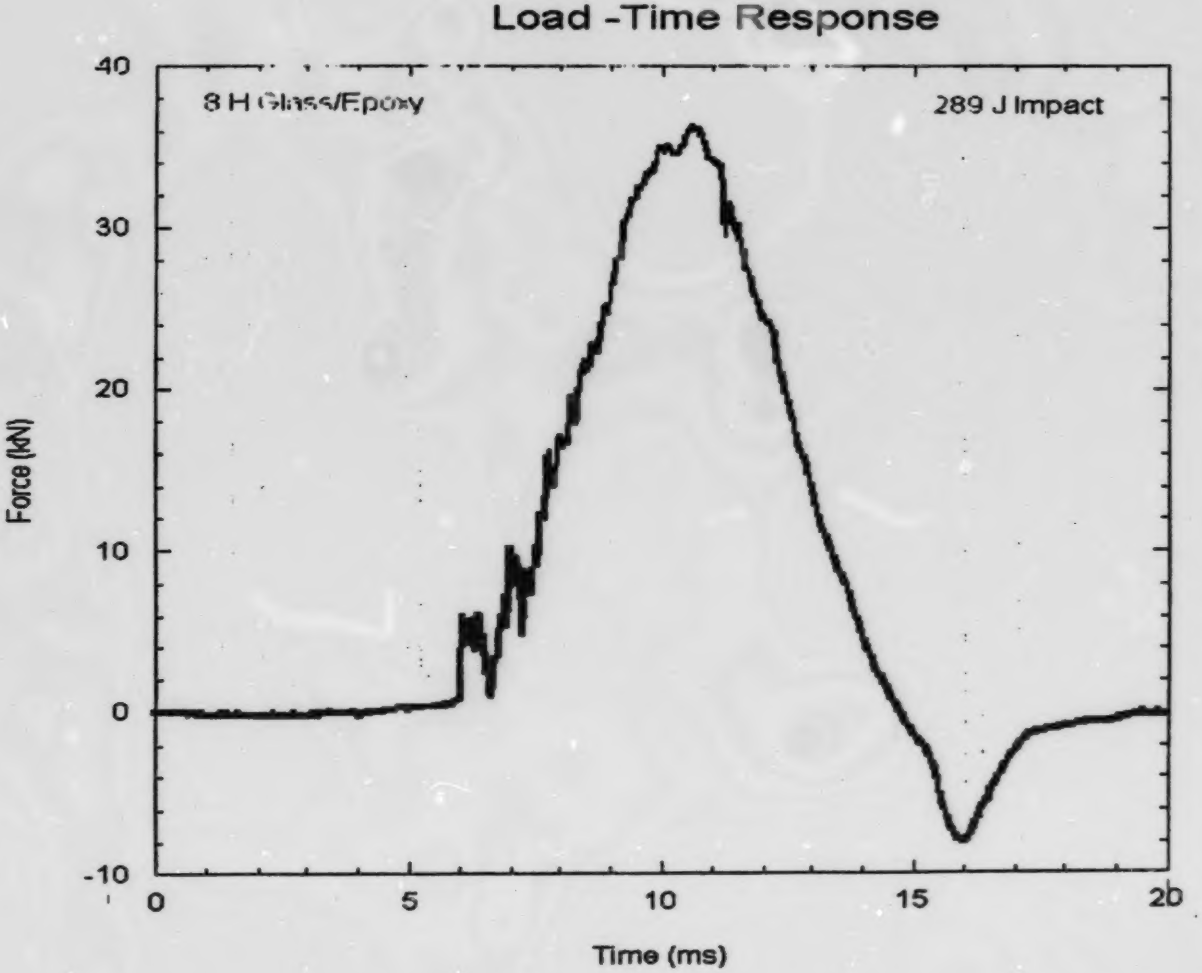

8H Glass/ Epoxy 289 J Impact

Load - Displacement Response

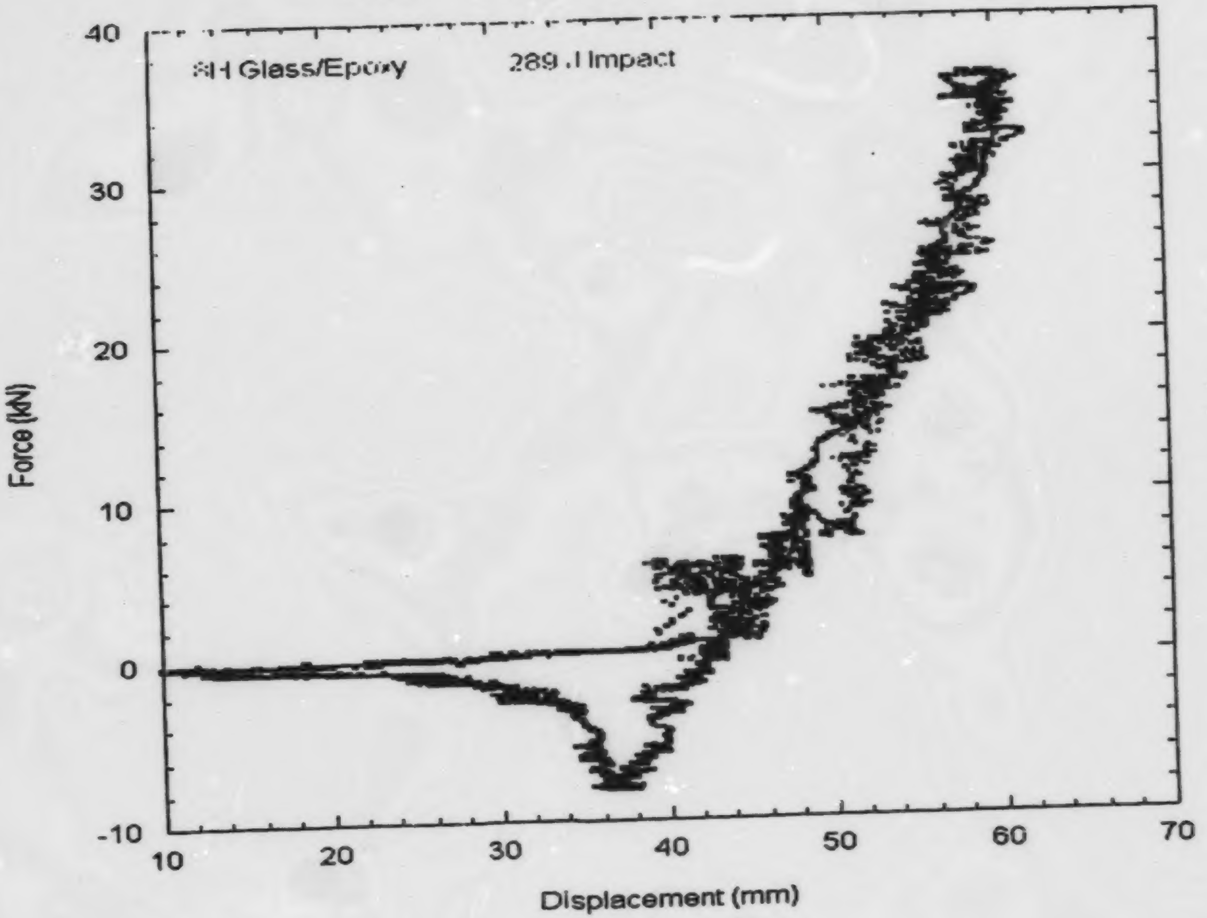

4H Spectra/ Cyanate Ester 236 J Impact

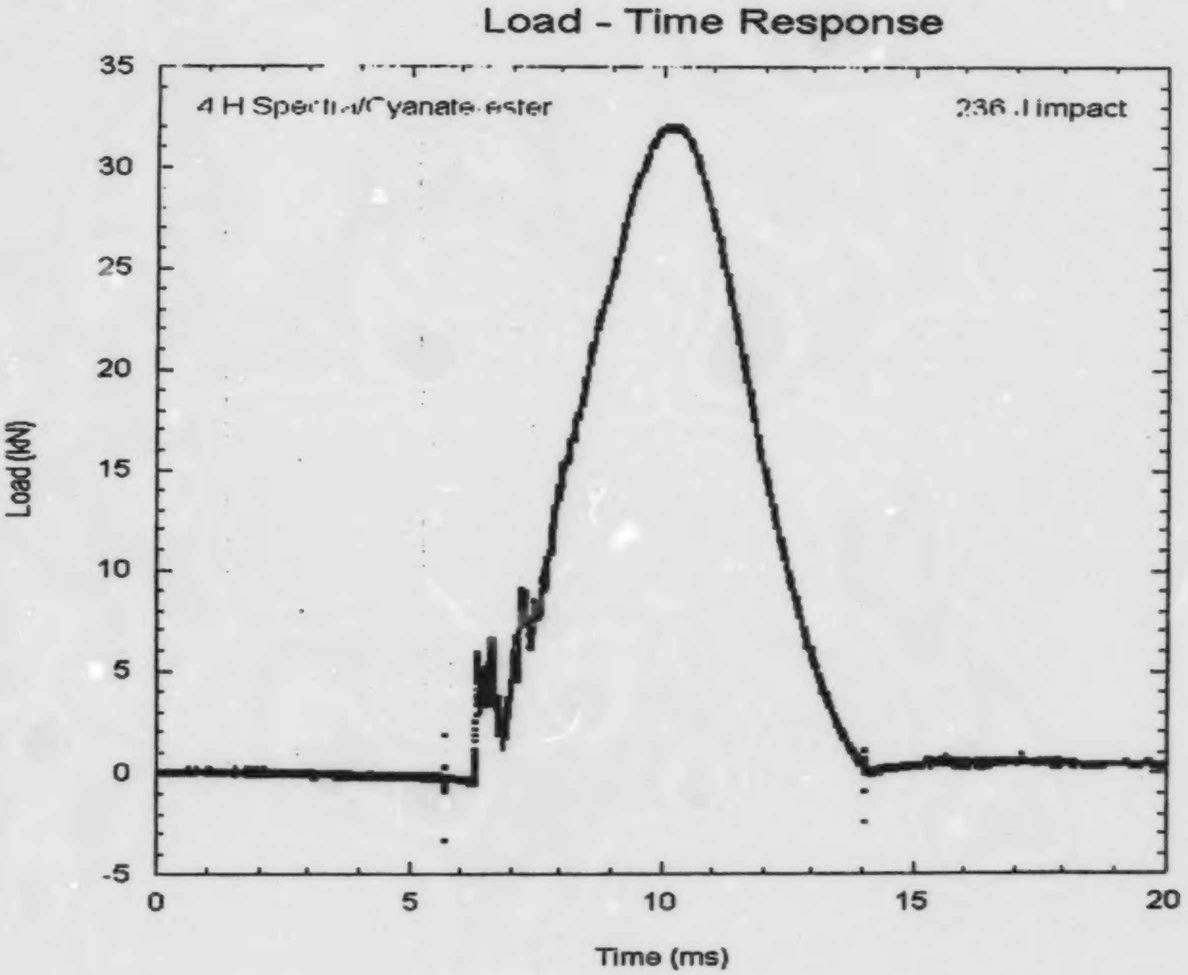

4H Spectra/ Cyanate Ester 236 J Impact

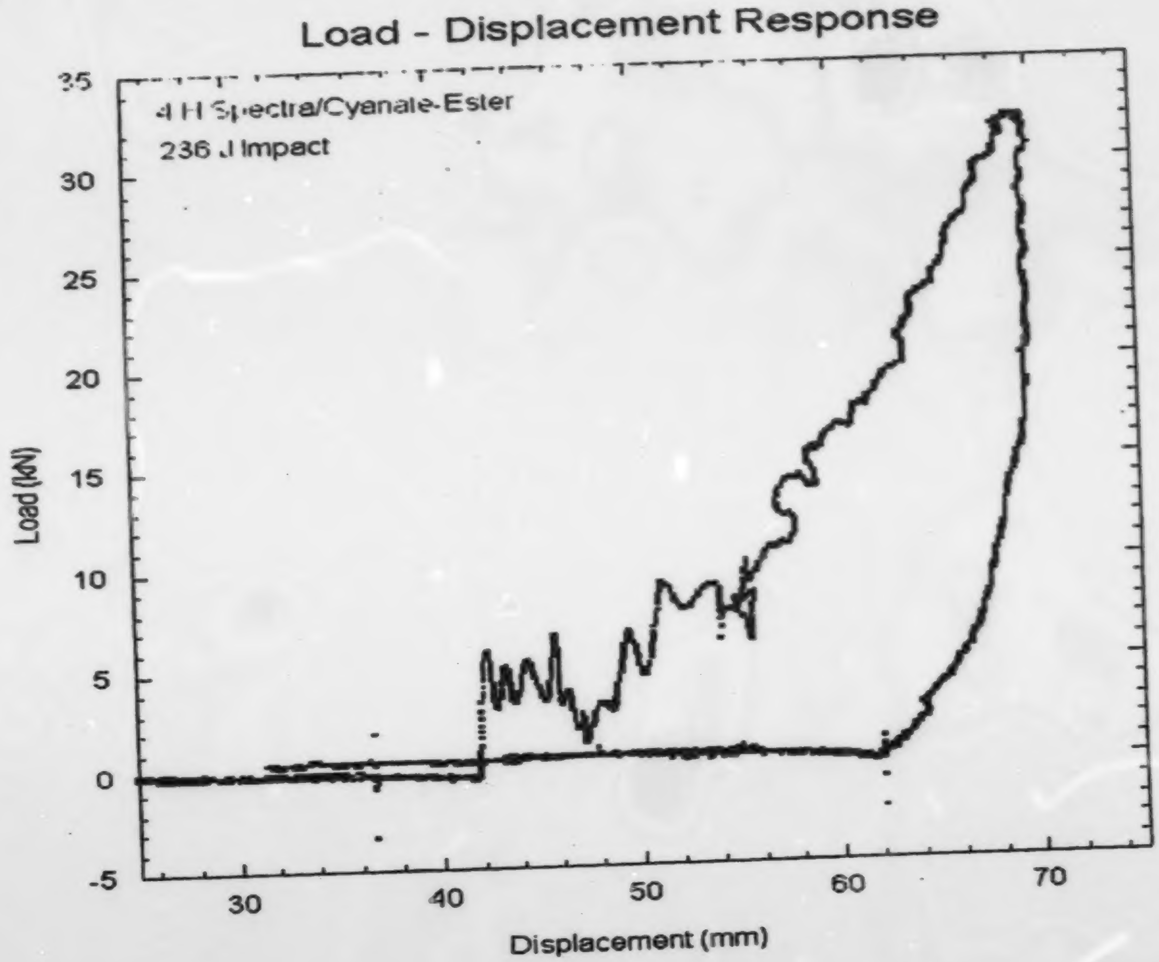

Deformation of Spectra Fibre Laminates

Spectra Laminate	Thickness (mm)	Permanent out-of-plane deformation (mm)	
		156.5 J Impact	236.4 J Impact
4 H Cyanate/Ester	9.86	3.53	7.90
8 H Cyanate/Ester	9.40	4.42	8.18
4 H Epoxy	9.58	3.61	7.65
8 H Epoxy	9.63	3.84	6.93

Damage Characterization

- Visual inspection
- Ultrasonic C-scan
- Acoustic attenuation
- Optical Microscopy

Back-lit photographs of
Spectra/cyanate-ester panels impacted
with 156 J (top) and 235 J (bottom)

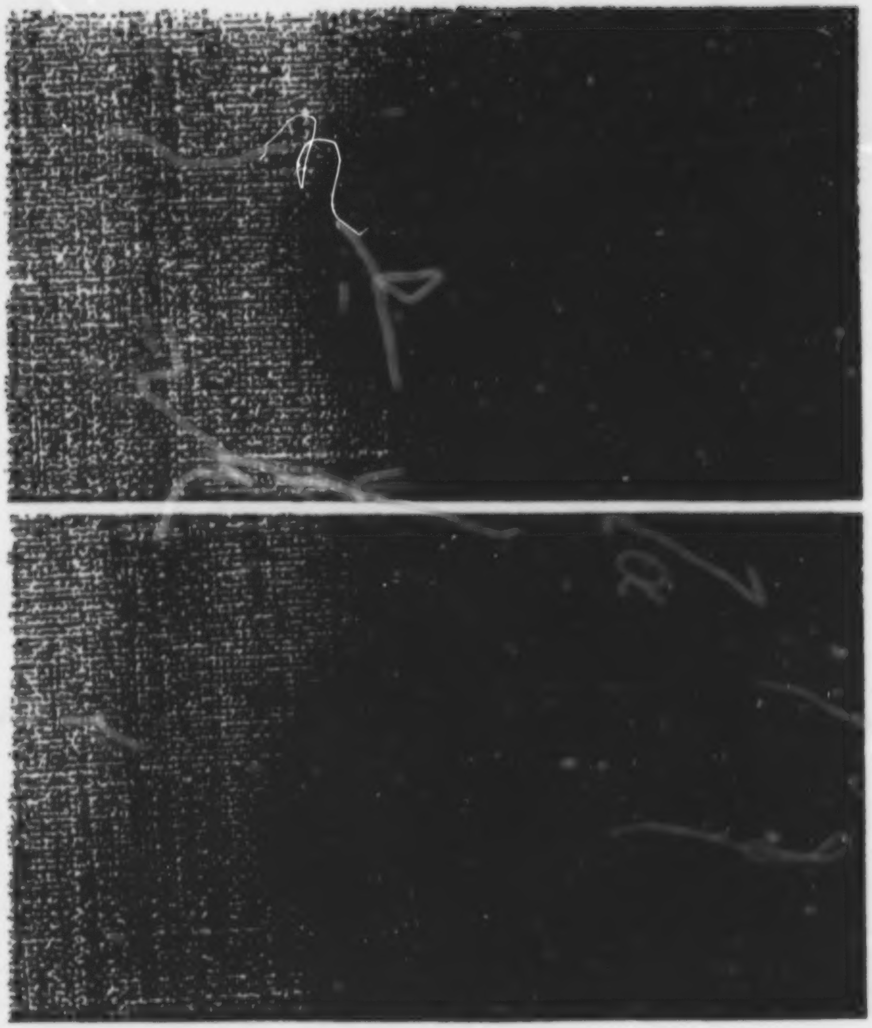

Back surface of impacted (289J) glass/epoxy panel showing tensile failure of surface ply and delamination

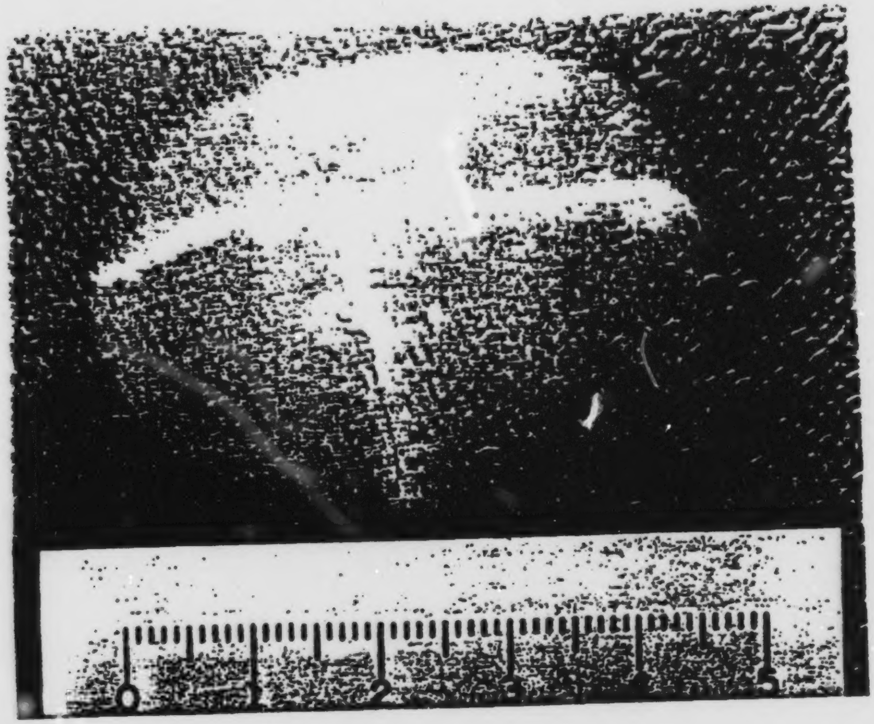

Glass/ Epoxy: Microcracking

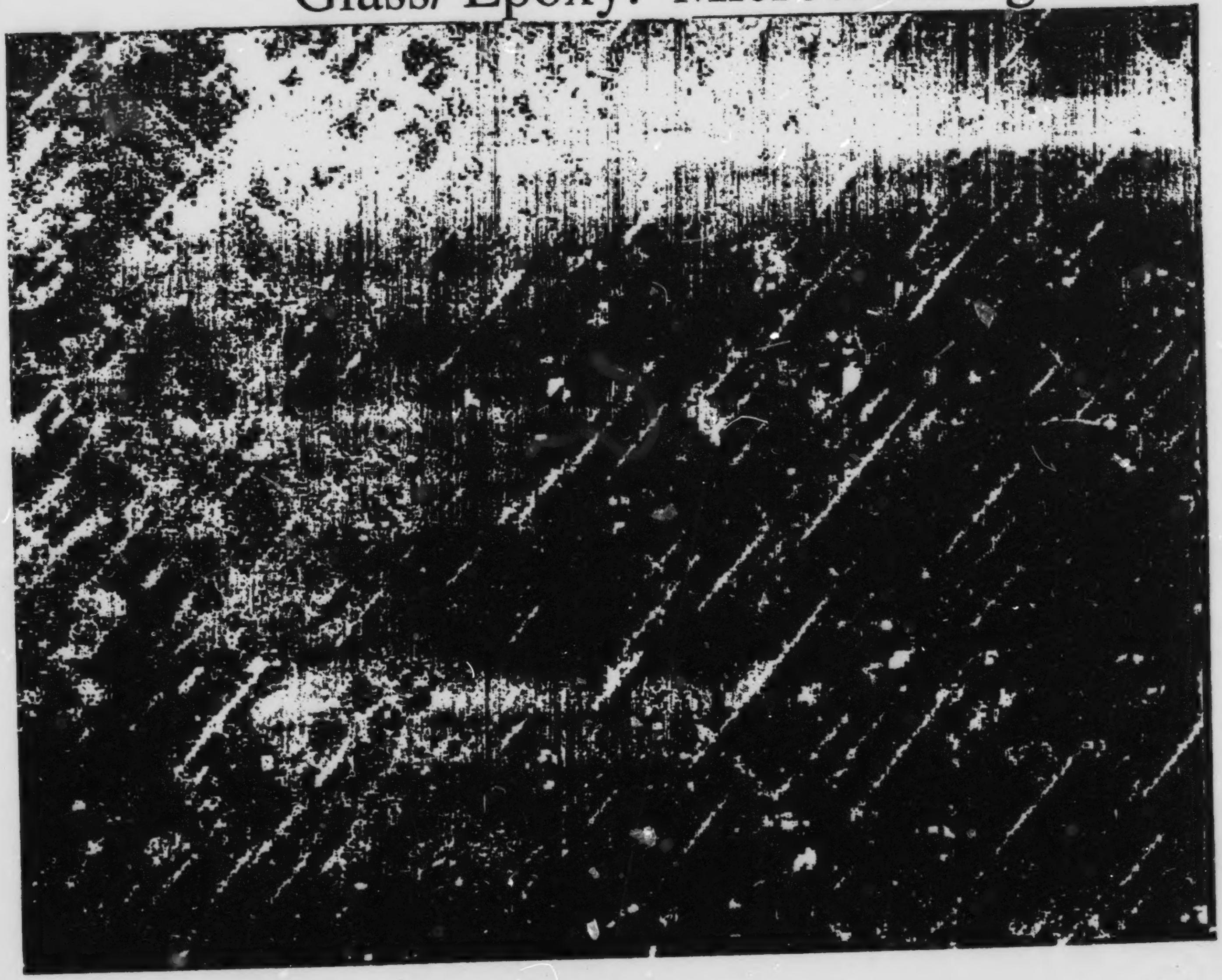

4H Spectra/ Cyanate Ester 156 J + 236 J Impacts

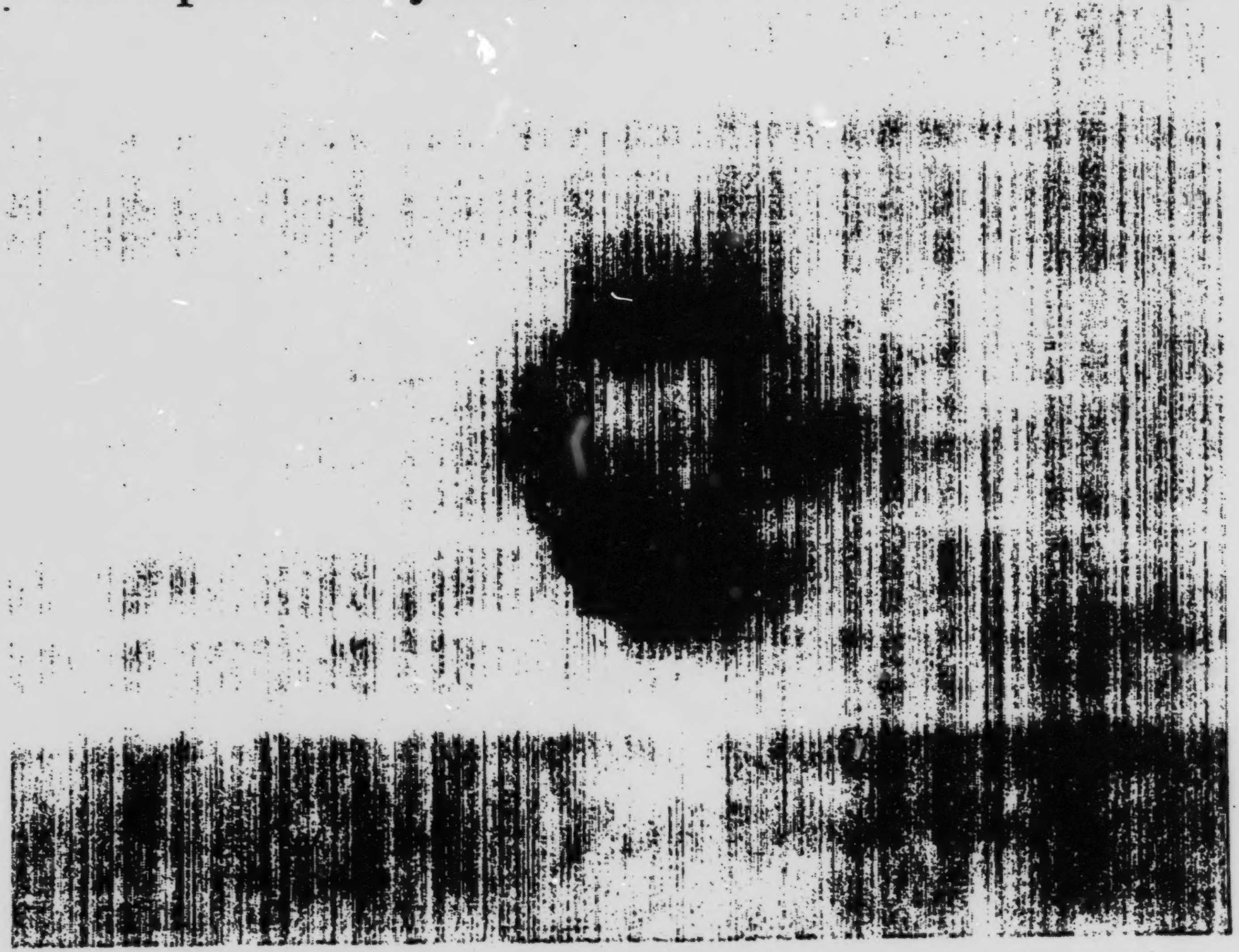

4H Spectra/ Epoxy 156 J + 236 J Impacts

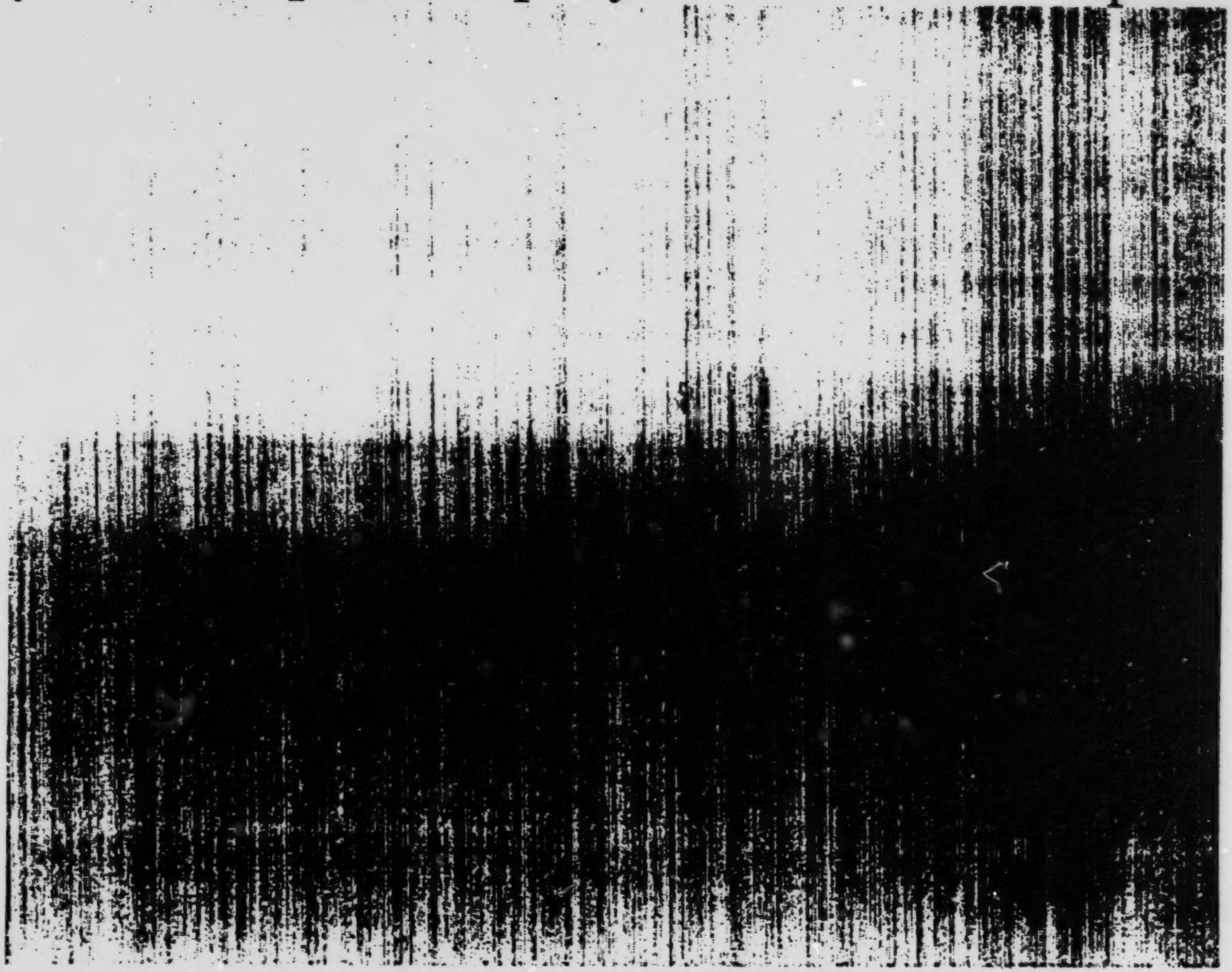

8H Glass/ Epoxy 289 J Impact

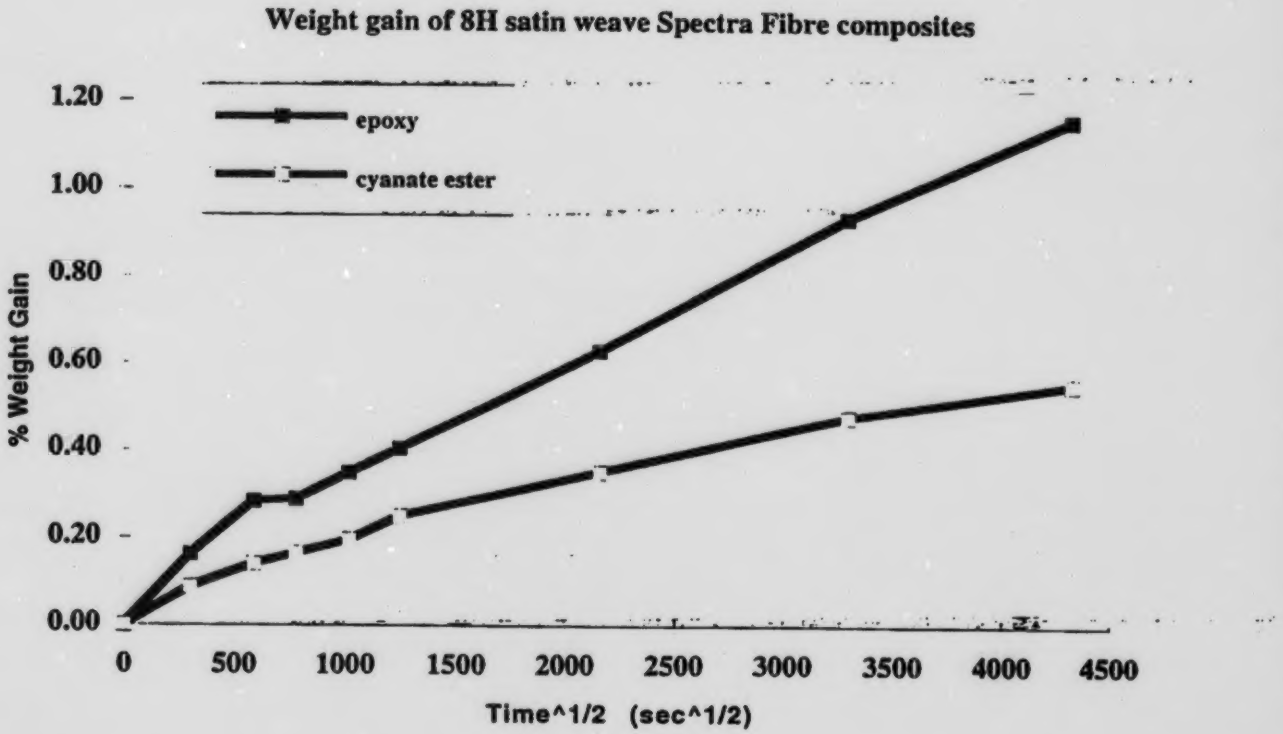
Weight gain of 8H satin weave Spectra Fibre composites

WHY IS INSERTION LOSS OF SONAR DOME IMPORTANT?

Consider very simplified model of active sonar in noise limited environment (cylindrical spreading loss, 1/R dependance):

A sonar window with insertion loss of x dB will decrease detection range by a factor $10^{(-x/10)}$.

Insertion Loss (dB)	Range (arb units)
0	1
1	0.79
2	0.63
5	0.32
10	0.10

PLANE WAVE MODEL

Panel with	density	ρ
	thickness	d
	longitudinal sound speed	c
	attenuation coefficient	α

Response of panel to normal incidence plane wave of frequency ω:

$$\mathrm{IL} \quad = \quad -20\log\left|\frac{4Ak^*}{(A+k^*)^2\exp(ik^*d)-(A-k^*)^2\exp(-ik^*d)}\right|$$

where

$$A \quad = \quad \rho\omega/Z_w$$

$$k^* \quad = \quad \omega/c-i\alpha$$

INSERTION LOSS

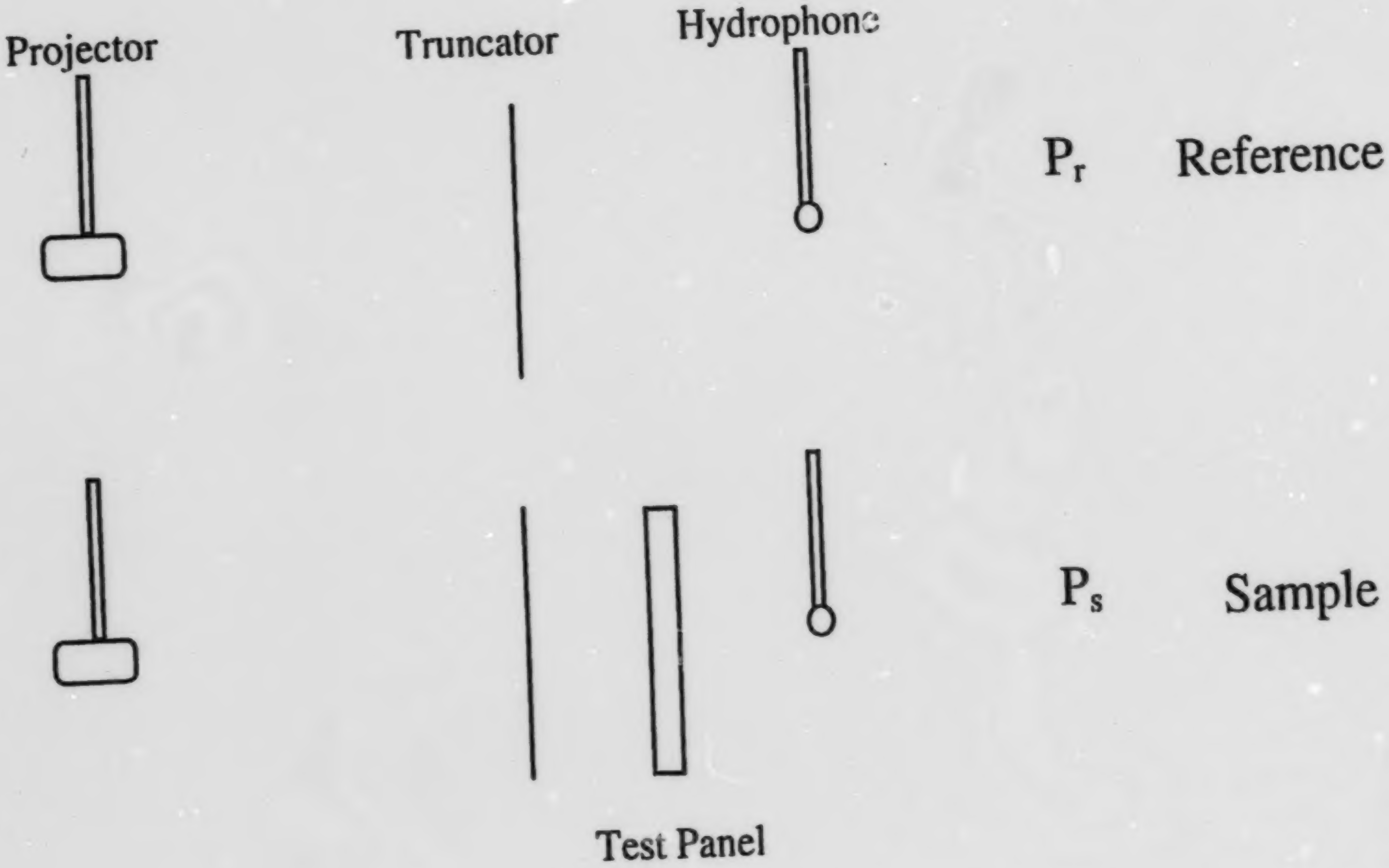
Projector
Truncator
Hydrophone
P_r Reference
P_s Sample
Test Panel

$$IL = -20 \log (P_s/P_r)$$

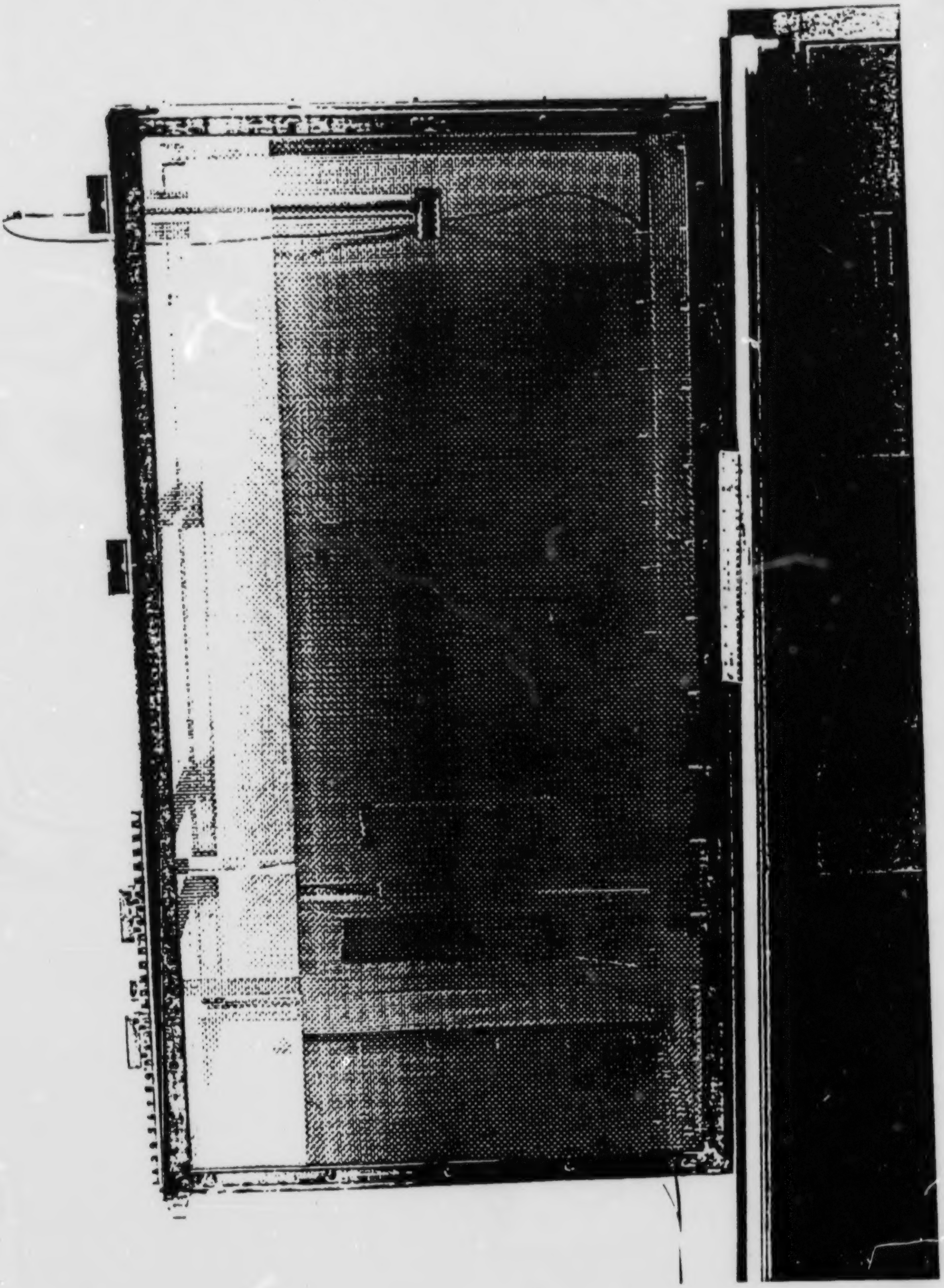

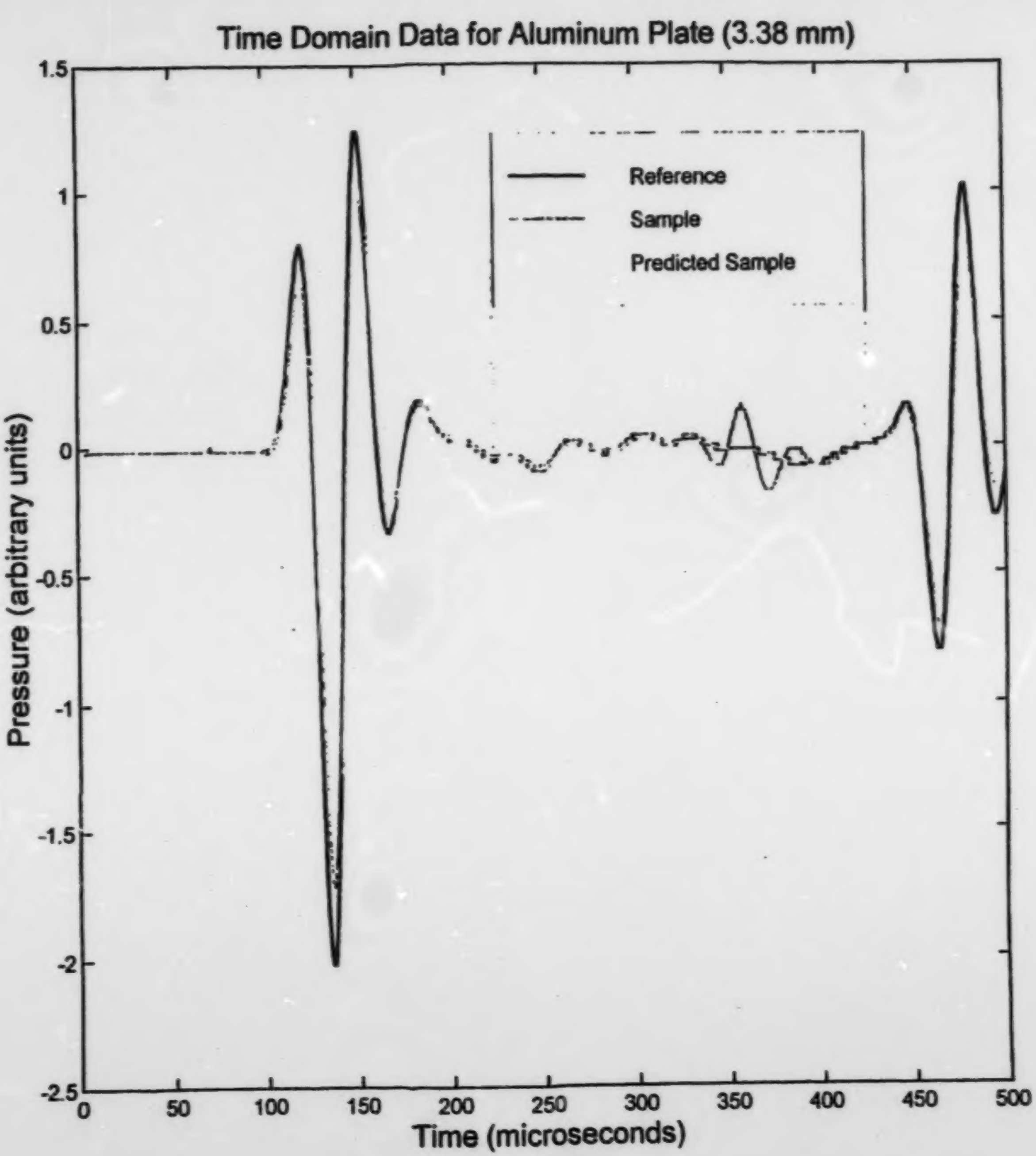
Time Domain Data for Aluminum Plate (3.38 mm)
Reference
Sample
Predicted Sample
Pressure (arbitrary units)
1.5
1
0.5
0
-0.5
-1
-1.5
-2
-2.5
0
50
100
150
200
250
300
350
400
450
500
Time (microseconds)

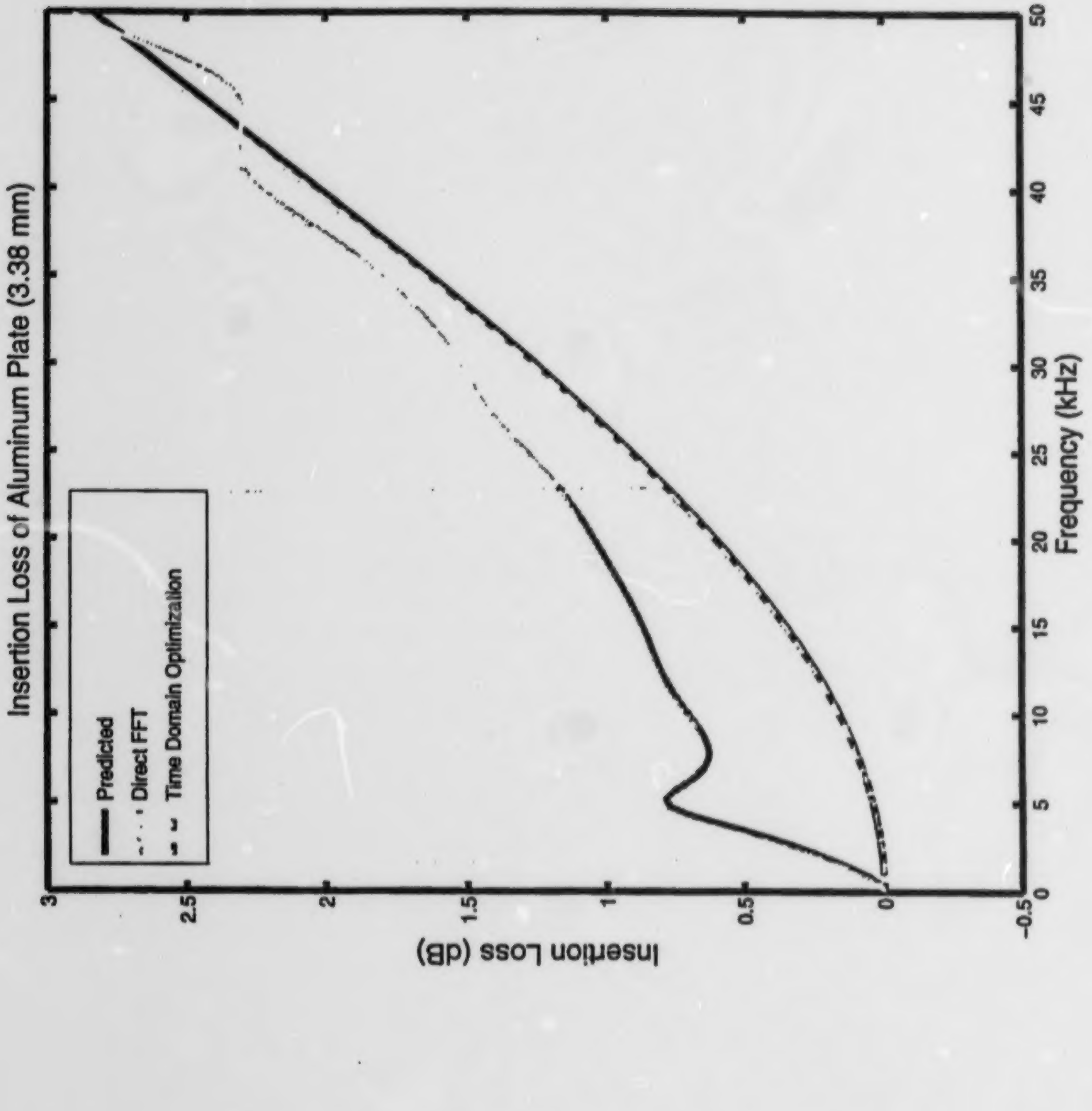
Insertion Loss of Aluminum Plate (3.38 mm)
Predicted
Direct FFT
Time Domain Optimization
Insertion Loss (dB)
Frequency (kHz)
-0.5
0
0.5
1
1.5
2
2.5
3
0
5
10
15
20
25
30
35
40
45
50

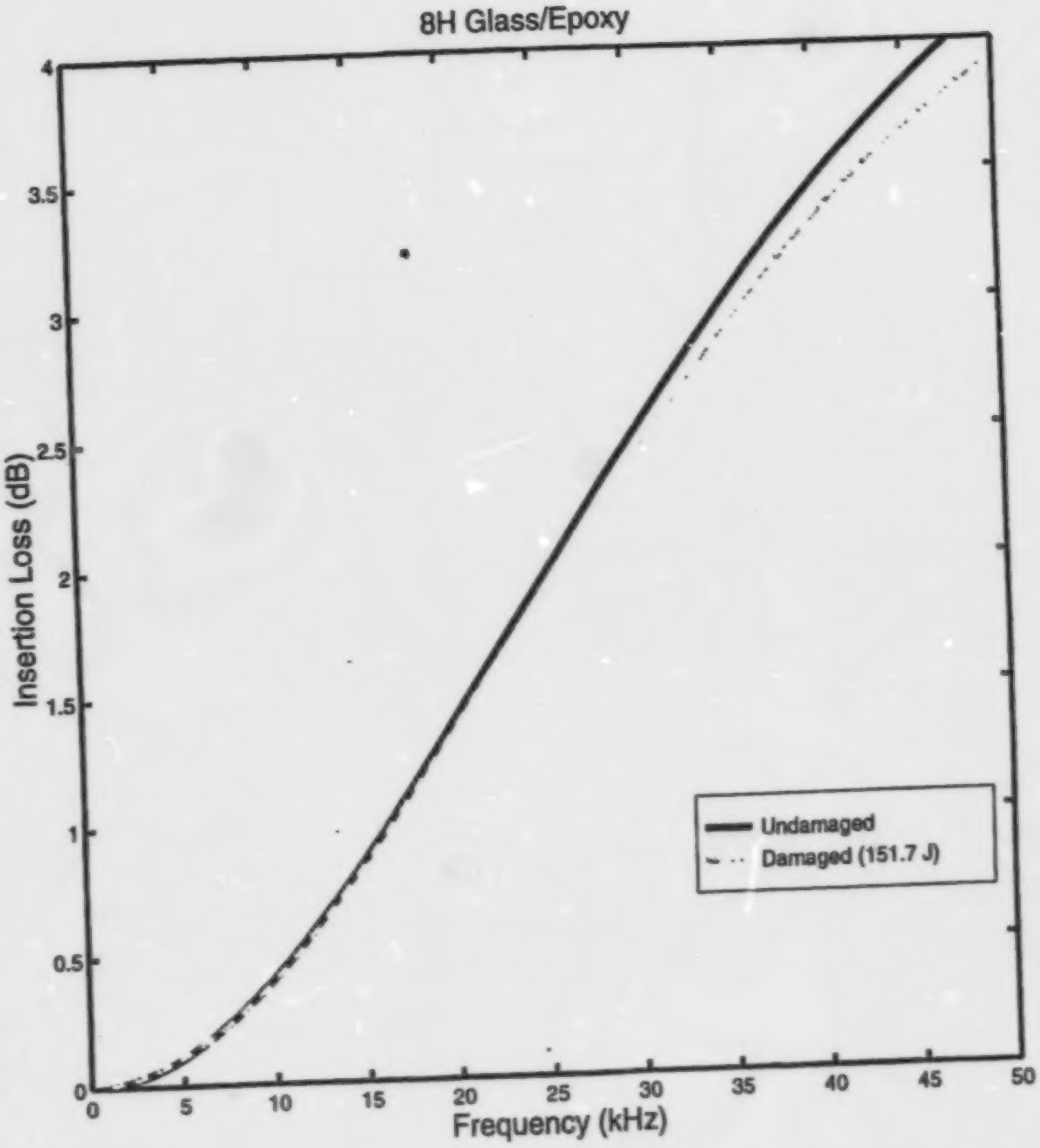
8H Glass/Epoxy
Insertion Loss (dB)
0
0.5
1
1.5
2
2.5
3
3.5
4
Frequency (kHz)
0
5
10
15
20
25
30
35
40
45
50
Undamaged
Damaged (151.7 J)

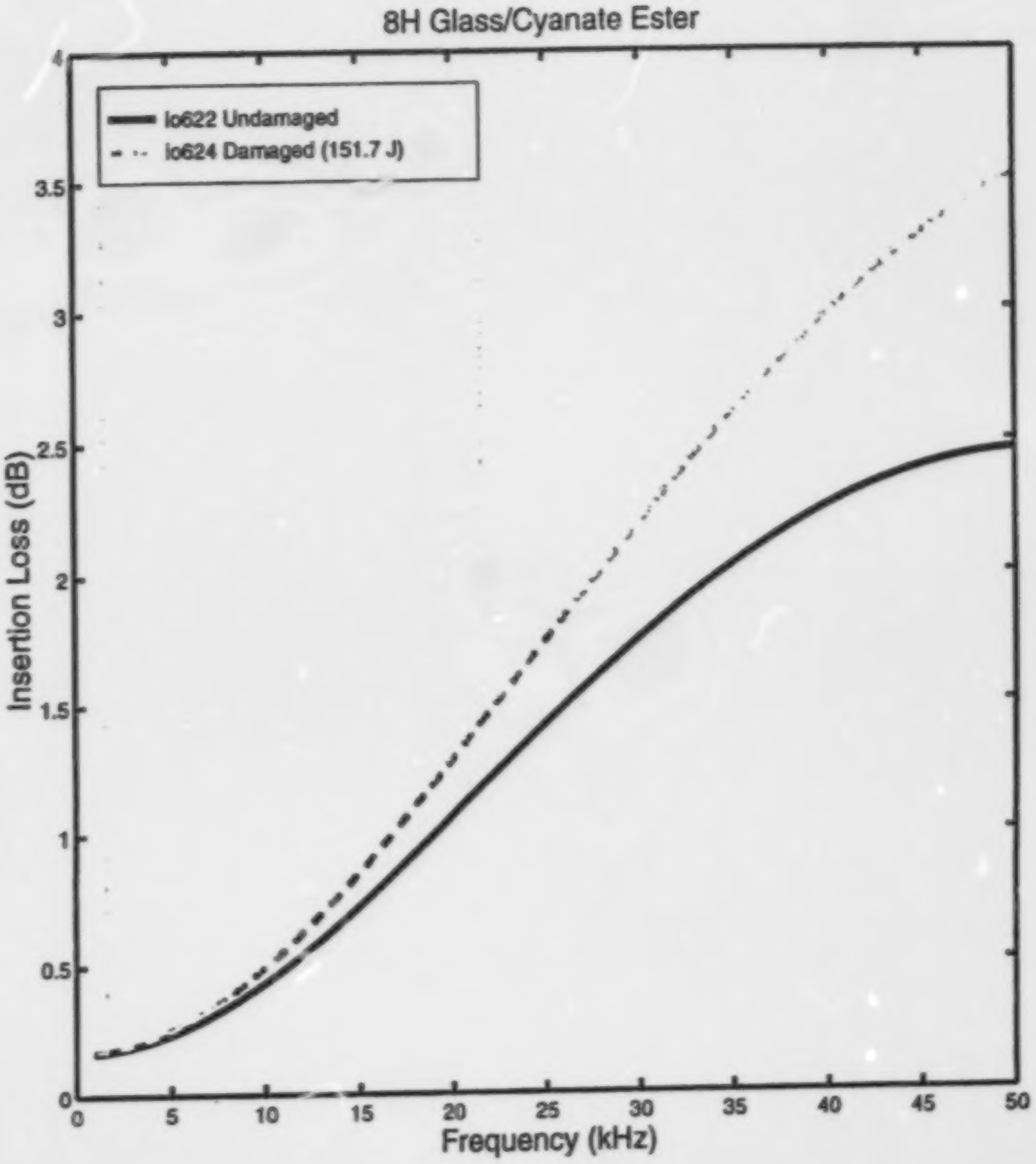
8H Glass/Cyanate Ester
Io622 Undamaged
Io624 Damaged (151.7 J)
Insertion Loss (dB)
0
0.5
1
1.5
2
2.5
3
3.5
4
Frequency (kHz)
0
5
10
15
20
25
30
35
40
45
50

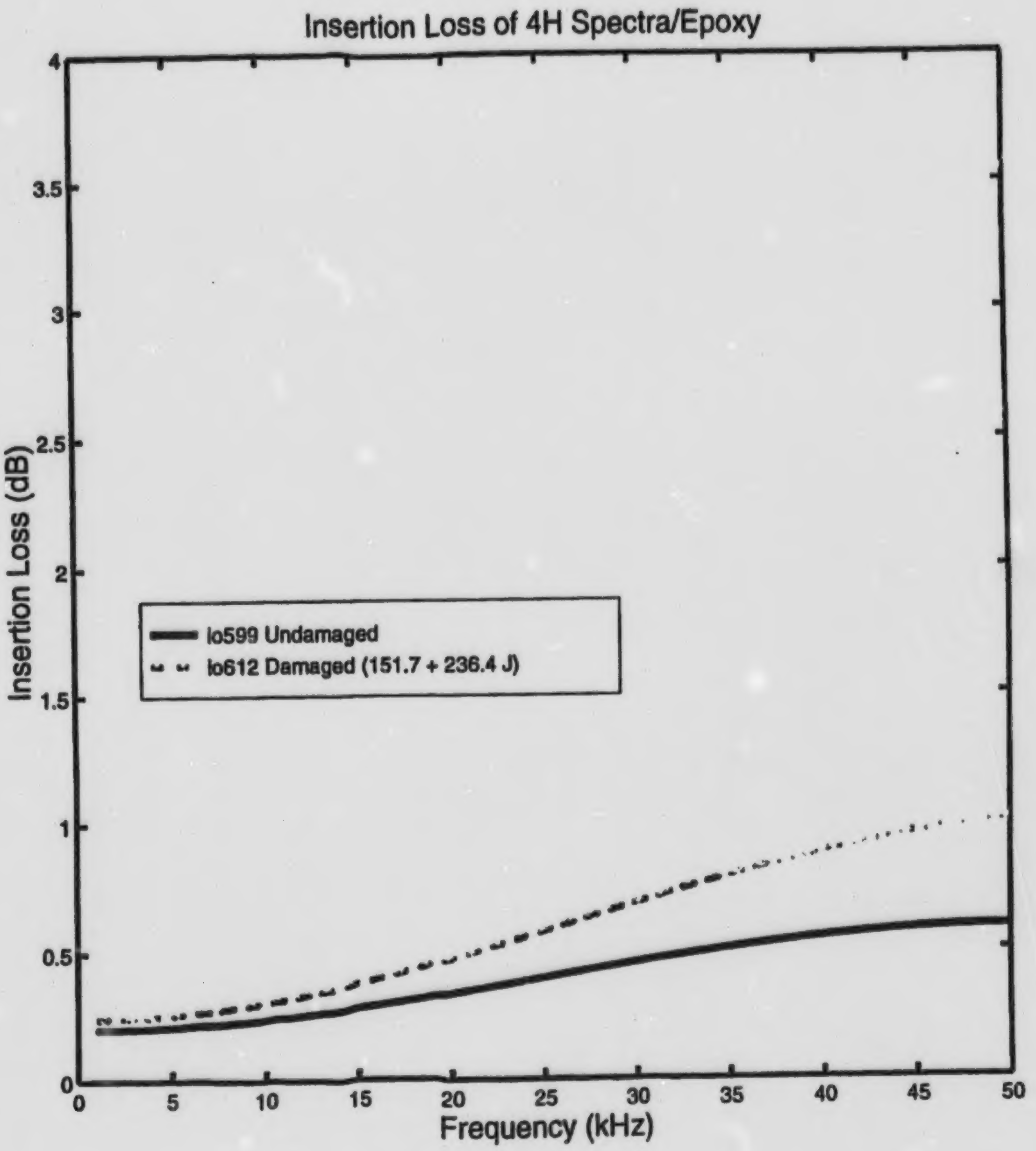
Insertion Loss of 4H Spectra/Epoxy
Insertion Loss (dB)
4
3.5
3
2.5
2
1.5
1
0.5
0
Frequency (kHz)
0
5
10
15
20
25
30
35
40
45
50
lo599 Undamaged
lo612 Damaged (151.7 + 236.4 J)

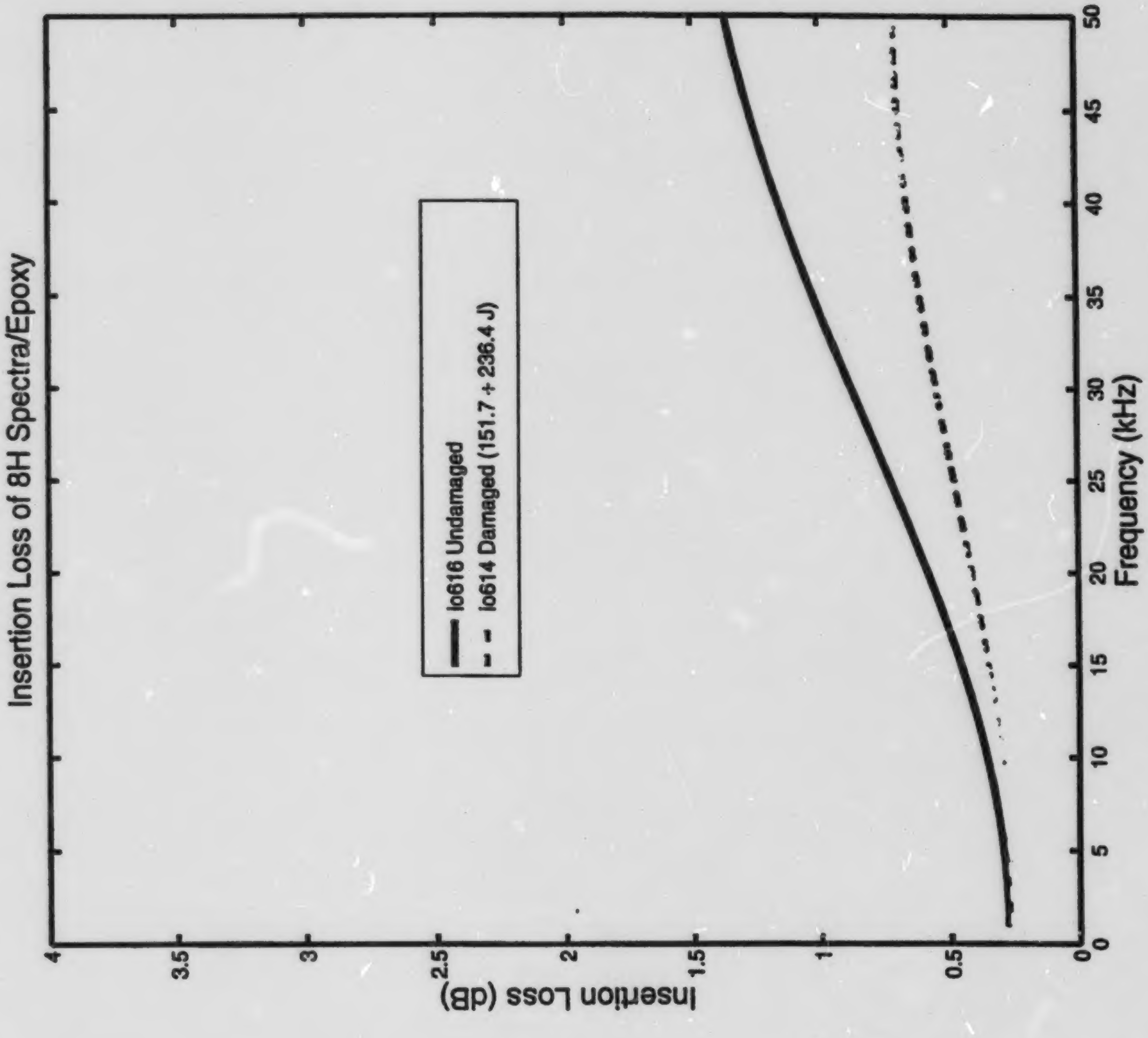
Insertion Loss of 8H Spectra/Epoxy
Insertion Loss (dB)
Frequency (kHz)
lo616 Undamaged
lo614 Damaged (151.7 + 236.4 J)
0
0.5
1
1.5
2
2.5
3
3.5
4
0
5
10
15
20
25
30
35
40
45
50

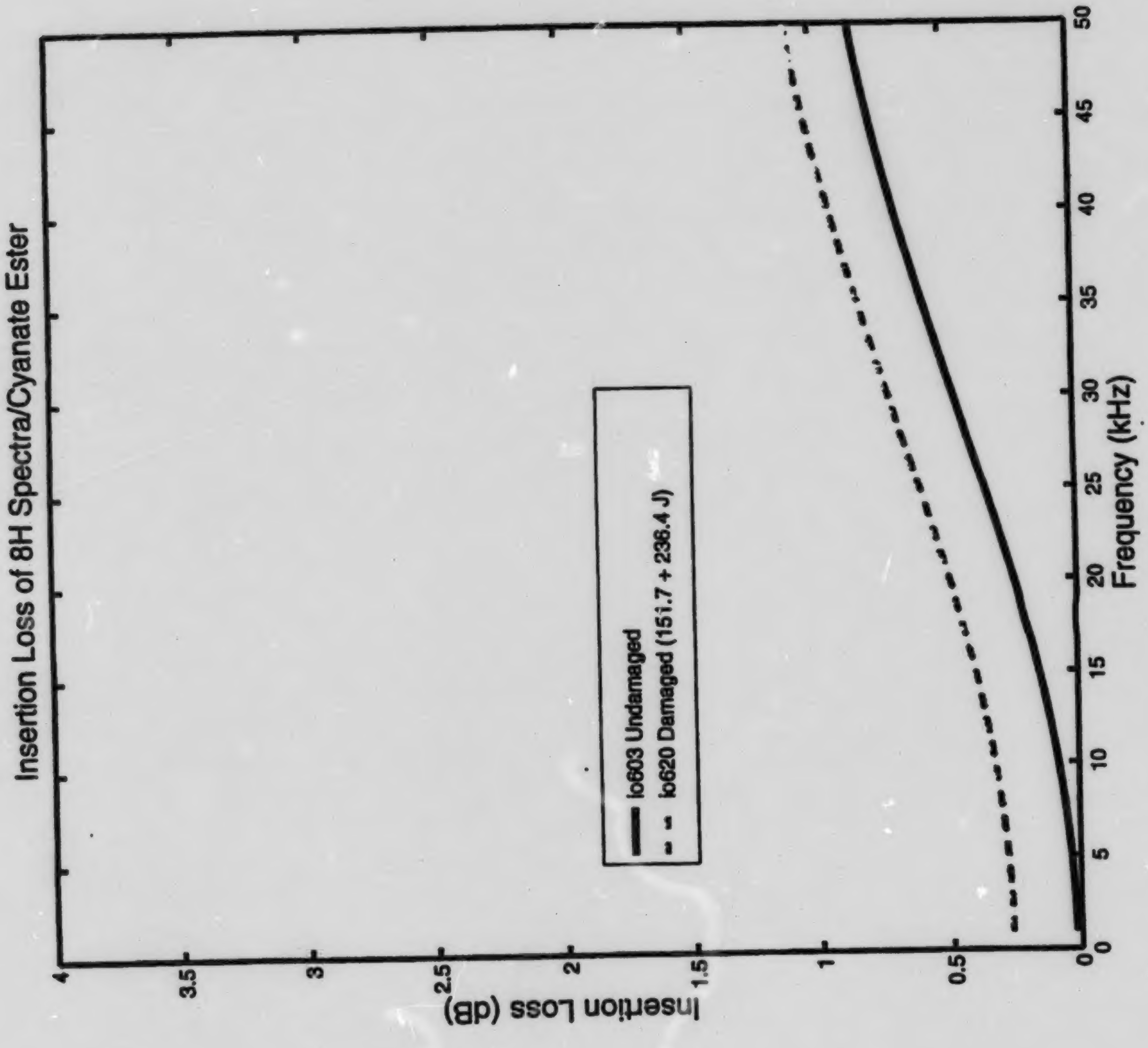
Insertion Loss of 8H Spectra/Cyanate Ester
Insertion Loss (dB)
Frequency (kHz)
lo603 Undamaged
lo620 Damaged (151.7 + 236.4 J)
0
0.5
1
1.5
2
2.5
3
3.5
4
0
5
10
15
20
25
30
35
40
45
50

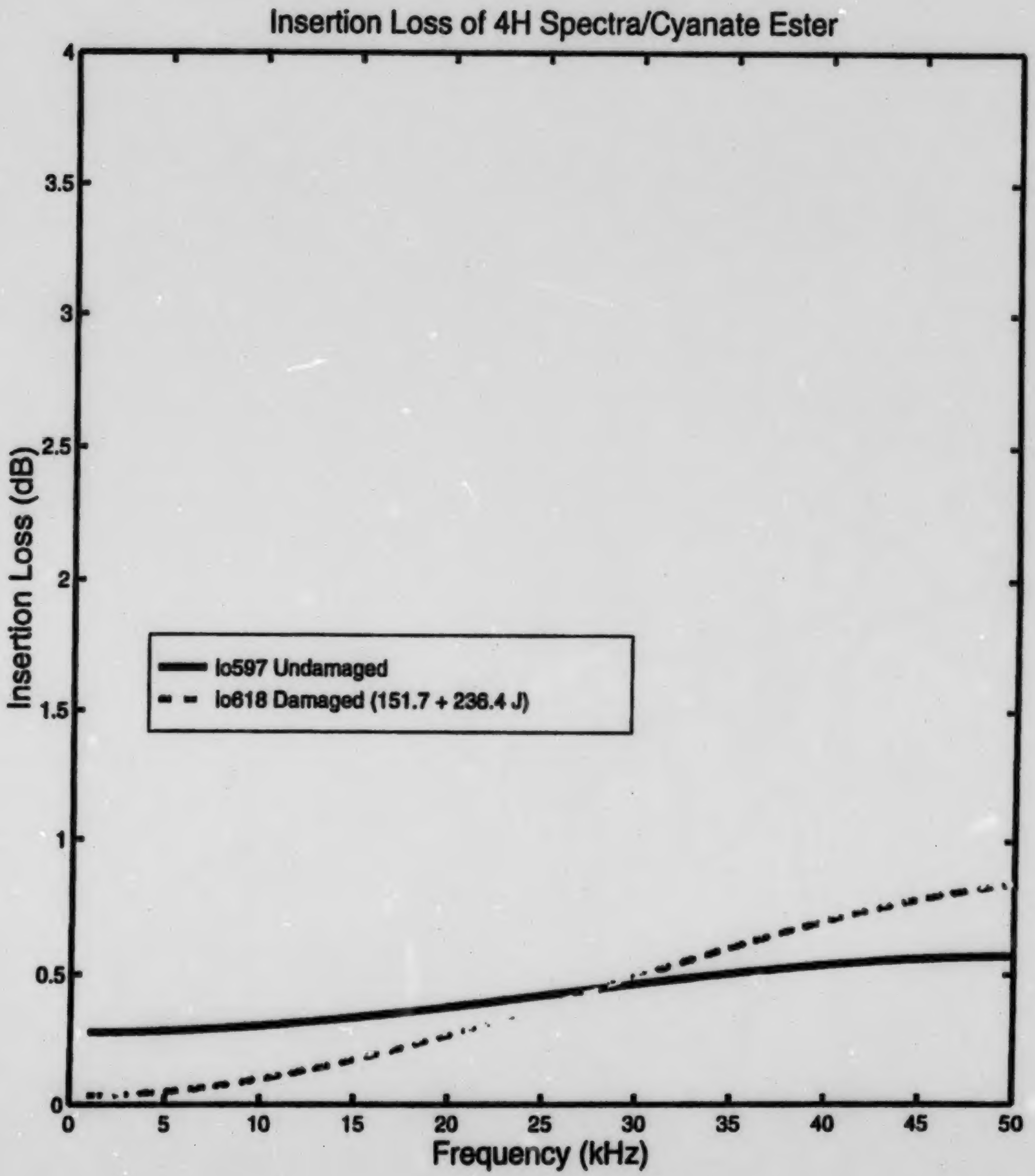
Insertion Loss of 4H Spectra/Cyanate Ester
Insertion Loss (dB)
0
0.5
1
1.5
2
2.5
3
3.5
4
Frequency (kHz)
0
5
10
15
20
25
30
35
40
45
50
lo597 Undamaged
lo618 Damaged (151.7 + 236.4 J)

CONCLUSIONS

- Low energy impacts resulted in microcracking under contact region
- High energy impacts resulted in: permanent deformation for Spectra panels
  tensile failure for glass panels
- Ultrasonic C-scans ⇒ localized changes in acoustic properties (MHz)
- Insertion loss ⇒ change < 0.25 dB due to impacts (0 - 20 kHz)
  ⇒ Spectra is superior to glass > 10 kHz
  ⇒ 8H Spectra/ cyanate ester 0.08 dB at 10 kHz
- Water uptake faster for epoxy than cyanate ester

ACKNOWLEDGMENTS

Gary Corbett	DMSS - 7
Irv Keough	DREA
Gerald Piercey	DREA
Dan Liesch	EDRD

#507213 ⑩

An Introduction to Fiber Optic Sensing for Composite Materials

by

D.O. MacDonald

INNOVACORP
P.O. Box 790
Dartmouth, Nova Scotia
B2Y 3Z7

ABSTRACT

In the last decade, the focus of application for advanced composite materials has slowly turned from aerospace to marine, civil, construction, and transportation industries. The properties of composite materials which make them attractive for such applications include their high strength to weigh ratio and resistance to corrosion. Composites have recently been used in civil engineering applications including rehabilitation projectors, prestressing tendons, reinforcing bars, and most recently as innovative structural members of bridges. As well, they have found many applications in the quest to reduce the top side weight of marine vessels. Composite sandwich panel hulls are also becoming more common.

The use of composite materials on such applications has been slowed somewhat due to the fact that they are the "new kid on the block," and because there is a lack of reliable long term field data, as compared to the traditional structural materials such as steel. Designers also need larger and more standardized databases of material properties for the multitude of existing composite materials.

For these reasons, composite materials lend themselves as prime candidates for another rapidly expanding field of research known as "smart materials." A smart material is a structure which contains a built in sensing device that can be used to continuously monitor the current state and serviceability of the structure. This is referred to as a "passive" smart material which has many applications in both marine and civil structures. More sophisticated smart structures have embedded sensors to monitor performance; the ability to compare the measured data to specification; and the means to apply corrective forces through embedded actuators. These structures are called "active" smart materials (intelligent materials) and have the most potential for application in high precision engineering structures. Composites are also good candidates as smart materials because their "build up" fabrication techniques inherently allow for the embeddement of sensors and communication lines.

The internal sensing of a smart composite material is achieved with optical fibers which function as both a sensing element and data transmitter. There are a variety of fiber optic sensors which can measure such external forces as pressure, temperature, strain, and vibration. Two types of fiber optic sensors which appear to have the most promising commercial benefit include the Fabry Perot extrinsic sensor, and the Bragg Grating sensor. A key advantage with embedded optical fibers and sensors is that their small size does not greatly effect the mechanical properties of the composite material.

The benefits of optical fiber sensing techniques as compared to the traditional foil gauges include: low weight, corrosion resistance, resistance to electromagnetic interference, reduced cabling, and excellent sensitivity.

Key issues which need to be addressed to allow for the successful production of smart composite materials include:

- embeddement of optical fibers, sensors, and connectors within a composite material;
- removal and protection of optical fiber leads from within a composite;
- survivability of optical fibers during processing of composite materials;
- effects of optical fibers, sensors, and connectors on the strength of composite materials; and
- adaptation of the above issues from hand layup fabrication to more automated processes such as pultrusion, filament winding, or tape laying.

Acknowledgement

This work has been supported by the ISIS-CANADA NCE, and Dalhousie Polytechnic's Smart Material Centre directed by Dr. Alexander Kalamkarov.

#507214 ⑪

A Reference Electrode Data Acquisition System For Cathodic Protection Studies

by

Dr. Derek Lenard
Dockyard Laboratory (Esquimalt)
Esquimalt Defence Research Detachment
Defence Research Establishment Atlantic

ABSTRACT

Aluminum vinyl anti-corrosive paints and impressed current cathodic protection, both of which were subjects of extensive development in Canadian defence research laboratories, have substantially increased the length of time between dockings for hull maintenance on HMC Ships. Unfortunately, at least in Canada, the transfer of cathodic protection expertise to the private sector does not appear to have been completely successful. For example, the original cathodic protection system on the DDH 280-class ships did not provide enough protection in the stern, with resultant corrosion of rudders and A-brackets. When a new anode and reference electrode were finally placed in the stern, the initial current demand was so high that circuit breakers were blown, clearly indicating the need for additional protection in that area. Given the general lack of knowledge concerning the cathodic protection current distribution around the hull of a ship at sea and specific concerns about the systems in use on HMC Ships, the Esquimalt Defence Research Detachment initiated a research project to design and build a self-contained reference electrode data acquisition system. These electrode systems could be mounted at locations of interest around the ship hull without the need for through-hull penetrations or over-the-side cables.

The electrode unit can measure and record the potential of the hull/sea water interface at its location, along with a time/date stamp, every hour for up to one year, or every fifteen seconds until its memory is full. A prototype unit will be displayed and the results of trials on a simulated ship hull will be presented. Each electrode system would be connected to the hull by way of a mounting stud that was friction welded to the hull by divers. Issues involving the welding procedure, such as fire hazards and possible damage to internal coatings, will also be discussed. The data retrieval unit, which can be used by divers to program or download data from up to thirty electrode units, will be displayed and its underwater communications capabilities will be demonstrated. The information gained from these electrodes would identify any weaknesses in existing cathodic protection systems and provide vital data for the development of computer models to improve future designs.

A REFERENCE ELECTRODE DATA ACQUISITION SYSTEM FOR CATHODIC PROTECTION STUDIES

BY

DR. DEREK LENARD
DOCKYARD LABORATORY (ESQUIMALT)
ESQUIMALT DEFENCE RESEARCH DETACHMENT

EDRD IS A DIVISION OF THE DEFENCE RESEARCH ESTABLISHMENT ATLANTIC

R&D Branch / Bureau de R&D

OUTLINE

- NEED
- DESCRIPTION OF EQUIPMENT AND SOFTWARE
- TRIAL OF PROTOTYPE ON SIMULATED SHIP HULL
- DEMONSTRATION OF DATA RETRIEVAL
- POTENTIAL EXPERIMENTS

1. Aluminum vinyl anti-corrosive paints
2. Cathodic protection

- Substantially increased the length of time between dockings for hull maintenance.
- Transfer of expertise to the private sector not completely successful
- Original CP system on DDH 280-class did not provide enough protection in the stern: corrosion of rudders and A-brackets

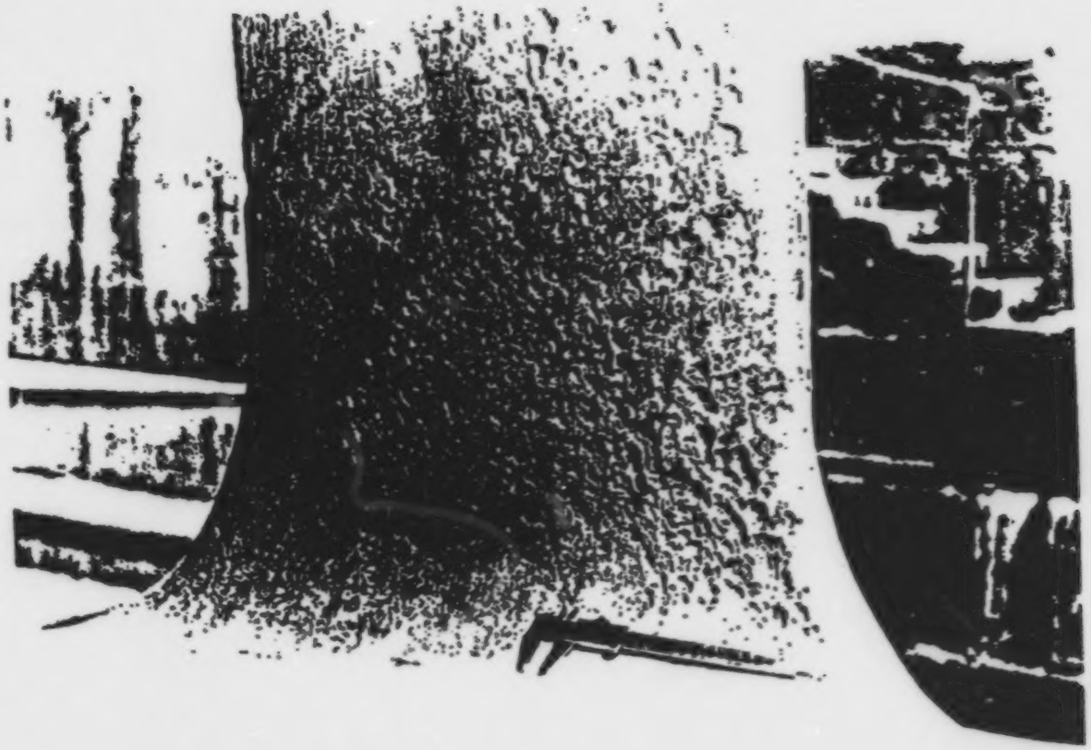

Before CathodicProtection:
Cavitation damage on A-bracket of HMCS Cayuga (1956)

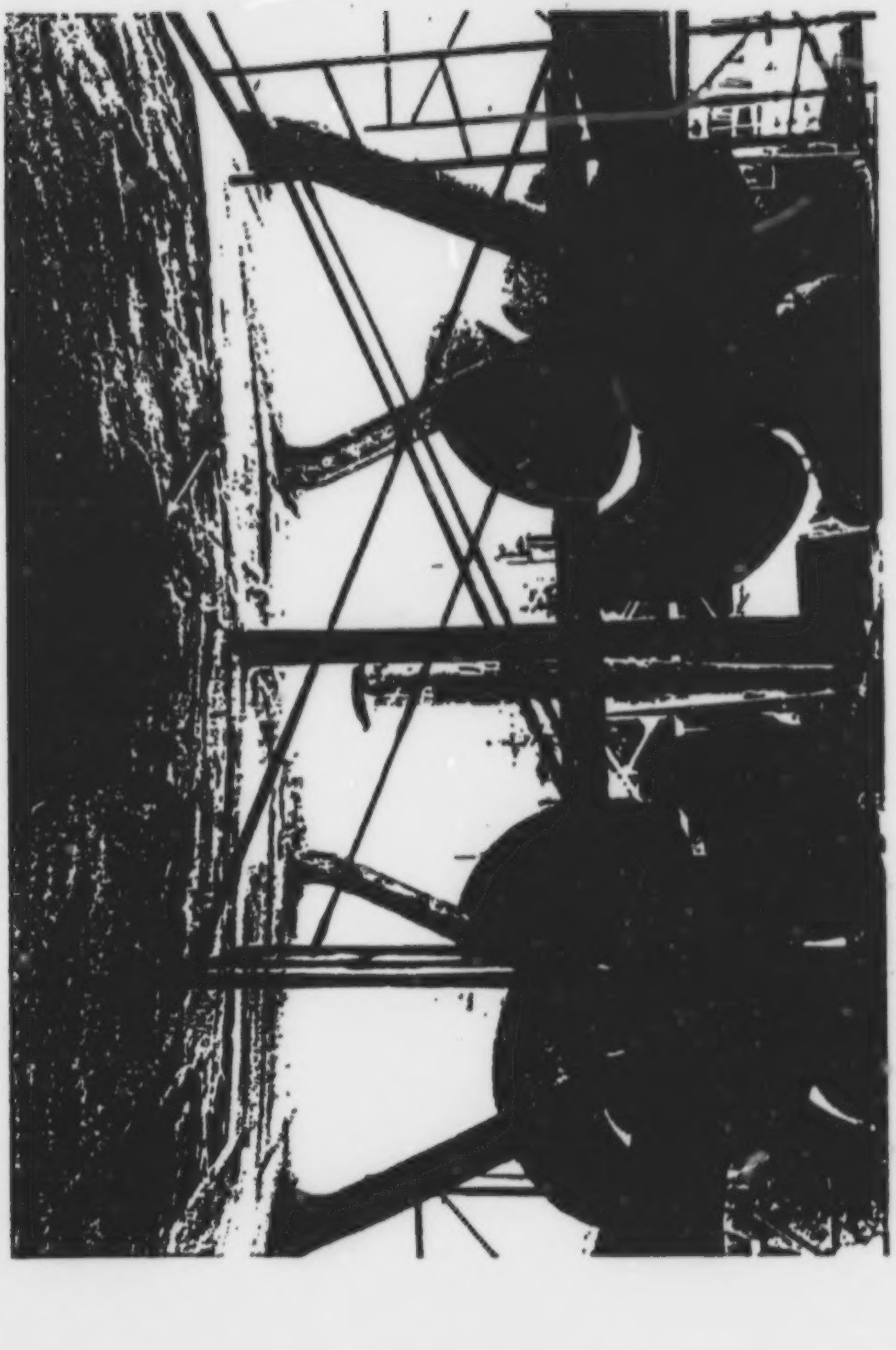

Stern Anode on Canadian Patrol Frigate

Aft Reference Electrode on CPF

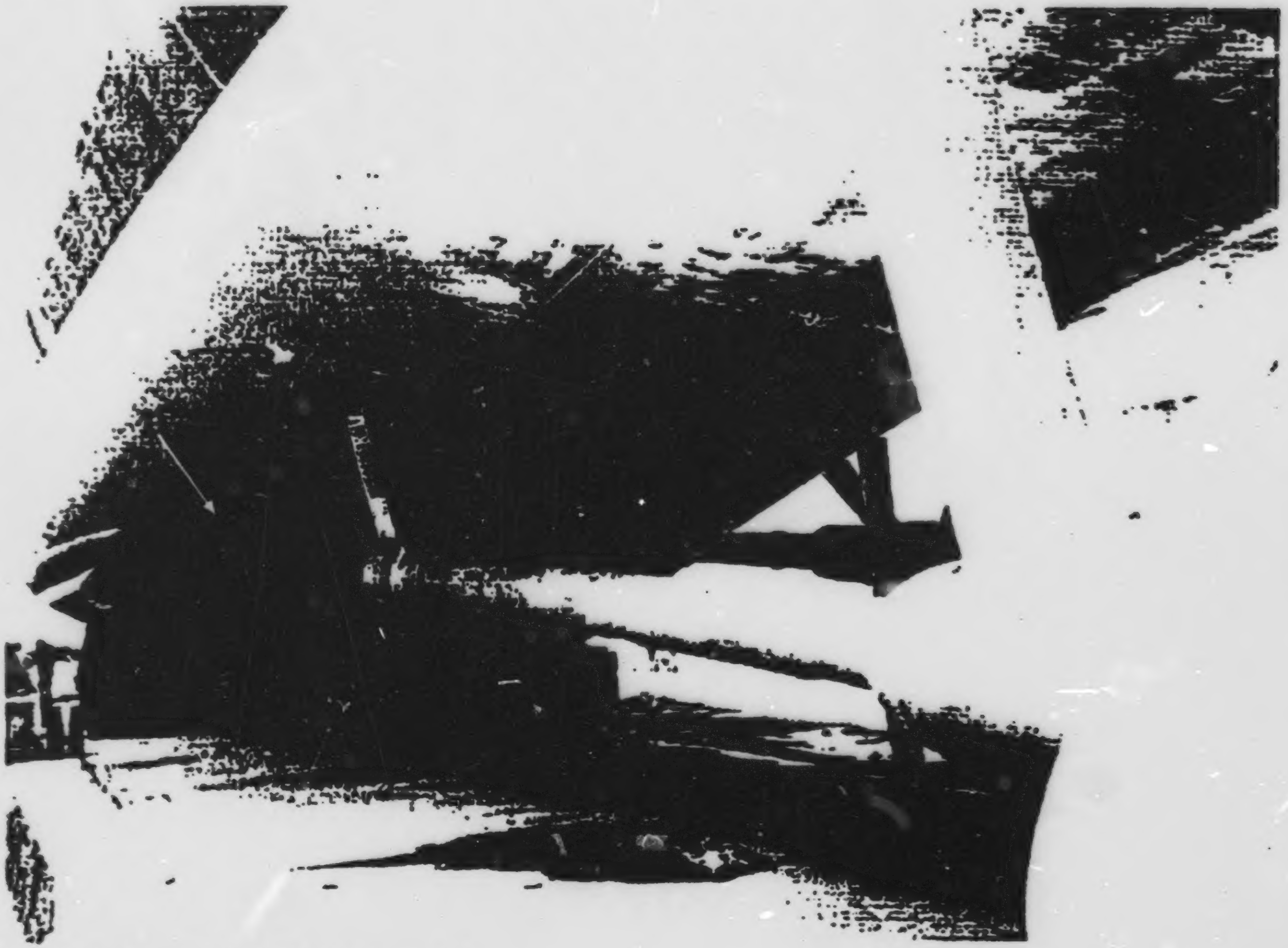

Forward reference electrode for all anodes

- Question: Is the stern area of the CPF adequately protected if the “forward” reference electrode is used to control the current output from the aft anodes?

- Computer Modelling of Cathodic Protection
  - cost-effective design tool once model is developed
  - requires knowledge of the relationship between current output and “hull potential”
  - this relationship is dependent on the velocity of the ship
  - very little data for a ship at sea

- “HULL POTENTIAL” really means:
- The potential of the steel/sea water interface with respect to a silver/silver chloride reference electrode.
- The potential of this interface varies with the amount of current passing through it. The variation is not linear.
- Experience has shown that a “hull potential” of -850 millivolts will prevent corrosion of the steel without damaging the paint.
- Need to place the reference electrode (which controls the amount of current from the anode) and the anode in locations which protect as much of the hull as possible.

- **AIM:**
- **Place a number of stand-alone reference electrodes at locations of interest around the ship hull to measure the “hull potentials” at those locations.**

- **REQUIREMENTS:**
  - no through-hull penetrations or over-the-side cables
  - low profile to minimize turbulence
  - ability to acquire data for up to one year
  - data retrieval and system programming by divers
  - operation should be invisible to ship staff
  - ship hull easily returned to original condition after experiments completed

Self-contained Reference Electrode Data Acquisition System (Rhocraft R&D Ltd.)

1) Reference electrode module
   - records time/date, hull potential and water flow rate every hour for up to one year or every 15 seconds until memory is full or unit switched back to hourly measurements.
   - mounted on the hull using a stud attached to the hull by a diver with a friction welder
   - quickly removed in an emergency with stud ground off without damaging hull integrity

2) Data retrieval/Programming module
   - diver points the face of the retrieval unit at the electrode module and the two units establish communications
   - complete data transfer in 1 to 2 seconds at a distance of up to 1 m from the electrode.
   - data from up to 30 electrodes can be downloaded in a single session
   - reprogramming the electrodes in a similar fashion

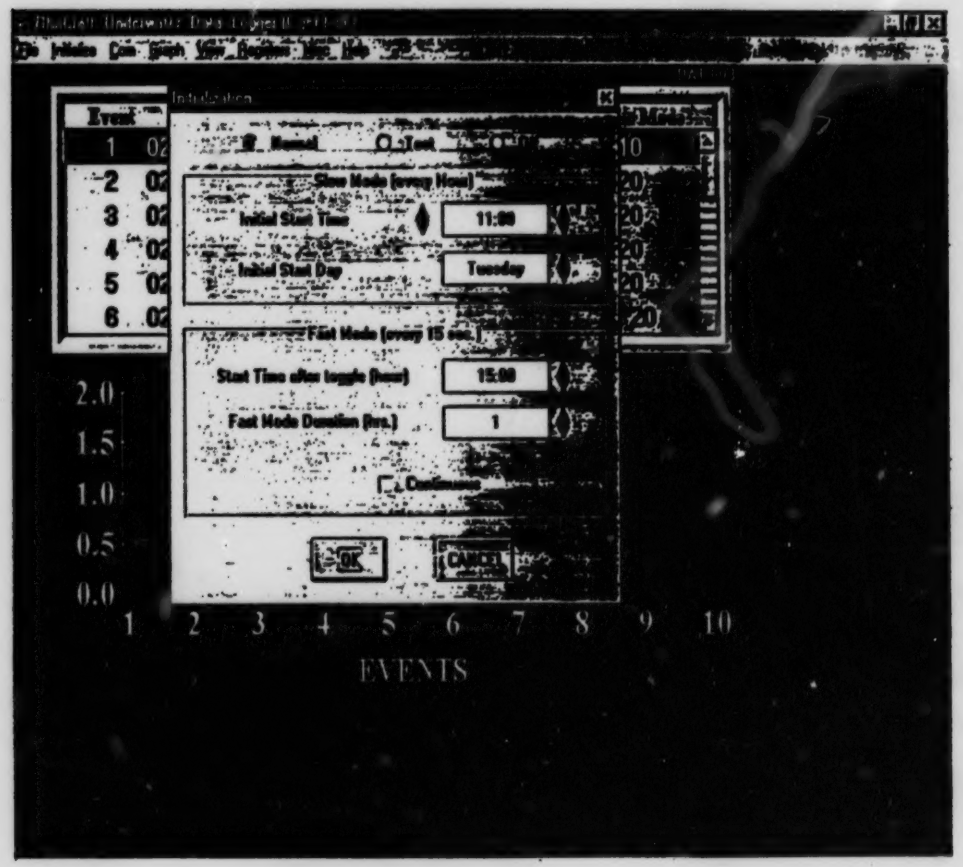
Underwater Data Logger
File
Initialize
Com
Graph
View
Registers
Help
Event
1
2
3
4
5
6
2.0
1.5
1.0
0.5
0.0
1
2
3
4
5
6
7
8
9
10
EVENTS

Initialization

● Normal ○ Test

Slow Mode (every Hour)

Initial Start Time: 11:00

Initial Start Day: Tuesday

Fast Mode (every 15 sec.)

Start Time after toggle (hour): 15:00

Fast Mode Duration (hrs.): 1

☐ Continuous

OK CANCEL

Programming the Underwater Data Logger (UDL)
(This is the self-contained reference electrode unit)

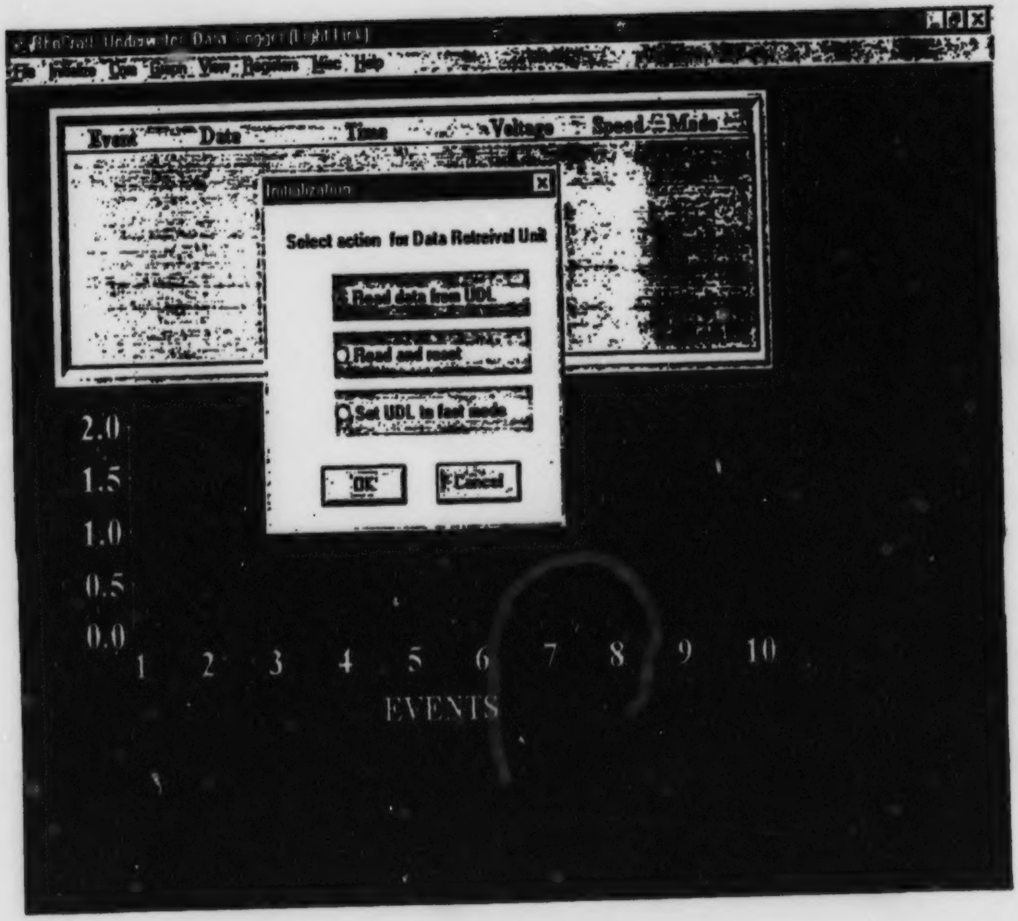
Underwater Data Logger (LightLink)
File
View
Registers
Misc
Help
Event
Date
Time
Voltage
Speed
Mode
2.0
1.5
1.0
0.5
0.0
1
2
3
4
5
6
7
8
9
10
EVENTS

Initialization

Select action for Data Retreival Unit

● Read data from UDL

○ Read and reset

○ Set UDL to fast mode

OK Cancel

Programming the Data Retrieval Unit

Simulated Ship hull partially immersed in sea water (arrow at water line)

Friction Welding equipment

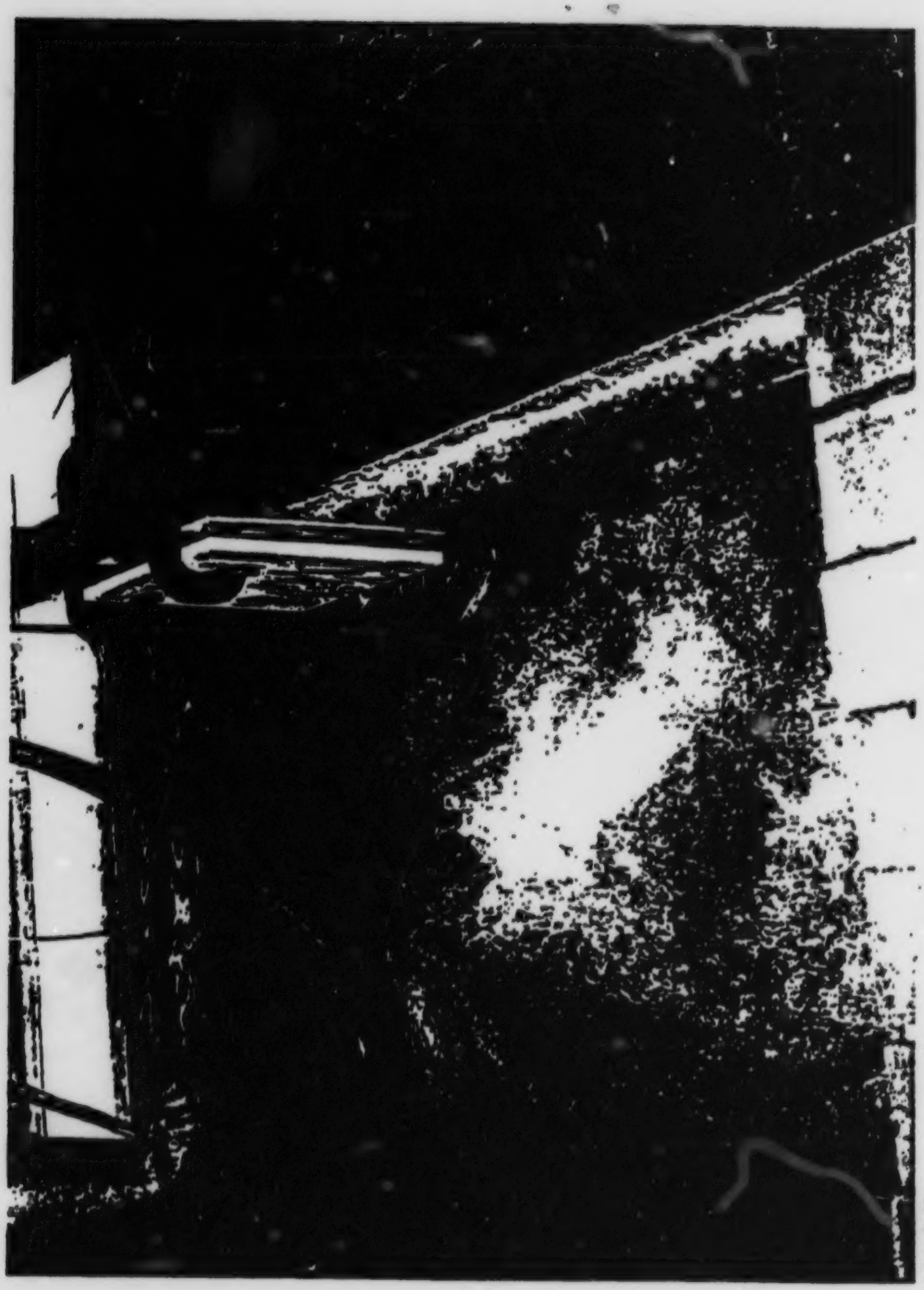

Welding operation

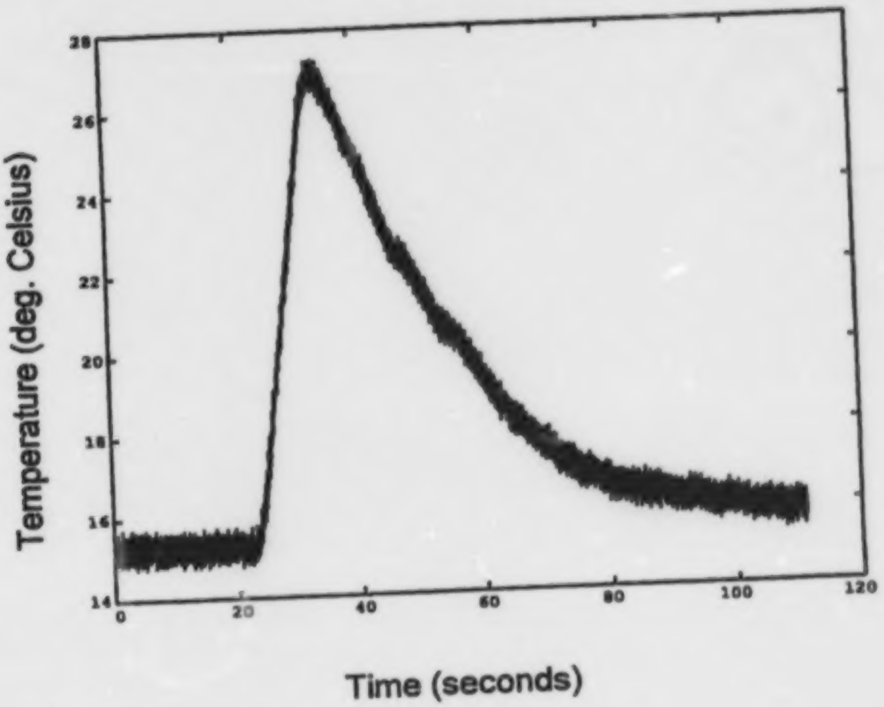

Temperature change on back (dry) side of hull plate 2.5 cm away from the centre of the friction weld.

Back side of weld: no paint damage

Back side of stud that was friction welded in air

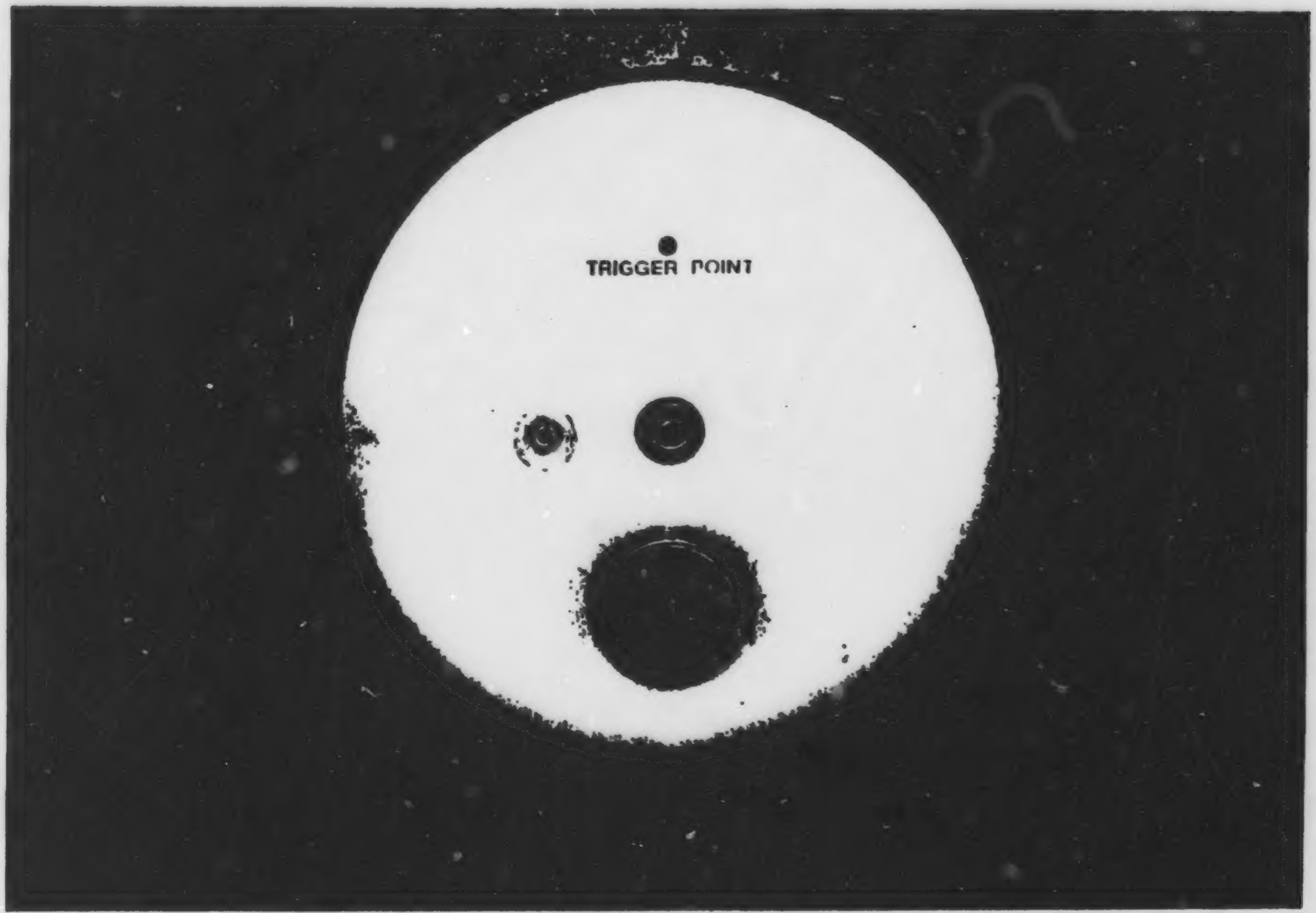
TRIGGER POINT

Reference Electrode System mounted on simulated ship hull

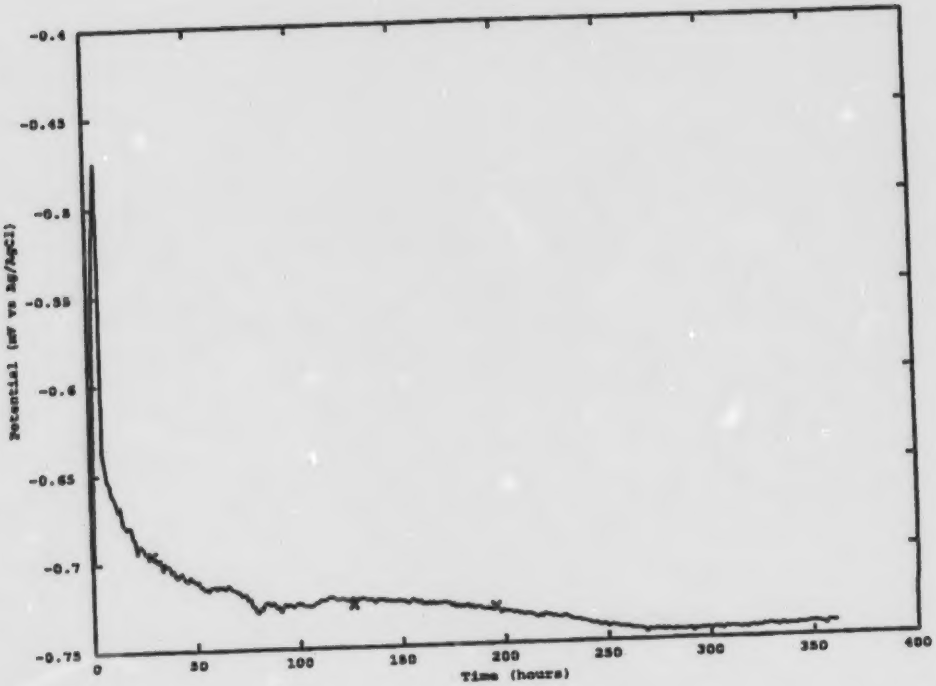

Solid line represents the output from the reference electrode data acquisition system mounted on the simulated ship hull. Note that the true output involves a time and date stamp. The time scale has been converted for graphical presentation. The "x" marks indicate the potential as measured with a conventional reference electrode and digital multimeter.

USES

- EFFECTIVENESS OF CATHODIC PROTECTION SYSTEM
- RATE OF POLARIZATION / DEPOLARIZATION AT DIFFERENT LOCATIONS AROUND HULL
- EFFECTS OF TEMPERATE VERSUS TROPICAL WATERS
- EFFECTS OF VELOCITY - PROVIDE DATA FOR COMPUTER MODELS

#507215 (12)

Corrosion Sensors for Field Applications

by

M. Tullmin and P.R. Roberge

Department of Chemistry and Chemical Engineering
Royal Military College of Canada
Kingston, Ontario, K7K 7B4

ABSTRACT

Corrosion damage is recognized as a serious problem in naval operating environments, leading to significant cost penalties, reduced safety and unavailability of equipment. In order to manage corrosion control programs more effectively, quantitative information on the nature of corrosive attack is needed. Such information is a fundamental requirement for condition and predictive/prognostic based corrosion maintenance strategies.

Numerous industrial corrosion measurement techniques are available, each with specific advantages and limitations. In order to obtain maximum information on complex corrosion problems, a multi-technique approach is advocated. The multi-technique corrosion measurement approach can often be applied to single corrosion sensor units, constructed of multiple sensing elements. Many of the commonly applied techniques provide semi-quantitative corrosion information only, a factor that is often overlooked.

Corrosion sensors are a vital element of corrosion surveillance systems, utilized to generate information for effective decision making in corrosion control programs. These sensors have emerged as highly specialized devices for technically challenging field applications. The highly sensitive variety can provide early warning of imminent corrosion damage, long before it is observable by visual means. Sensors for corrosion surveillance under aqueous as well as atmospheric corrosion conditions are described. Recent corrosion sensor developments in the domain of "smart structures" is also discussed.

Corrosion Sensors for Field Applications

M. Tullmin and P.R. Roberge
Department of Chemistry and Chemical Engineering
Royal Military College of Canada

Overview

- ☐ Role of Corrosion Sensors
- ☐ Three Main Application Areas
  - Smart Structures
  - Inspection and Maintenance Scheduling
  - Testing under Operating Conditions
- ☐ Examples of emerging technology
- ☐ Summary

Role of Corrosion Sensors

- ☐ Is corrosion control effective if corrosion damage cannot be predicted ?
- ☐ Can corrosion damage be predicted if it cannot be detected ?

Corrosion Surveillance

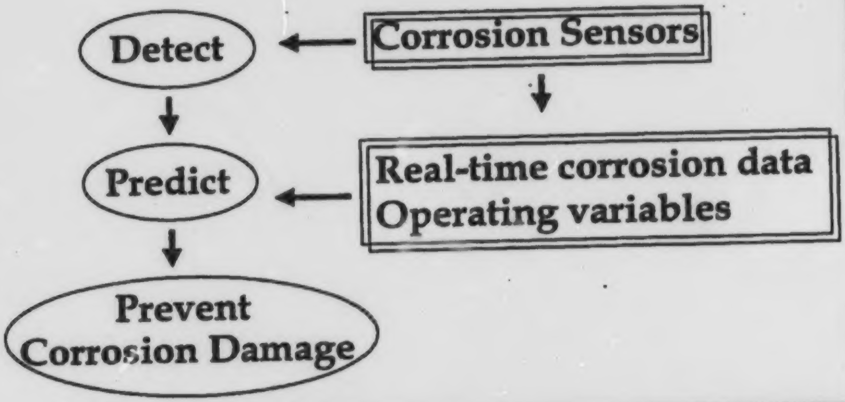
Detect
Corrosion Sensors
Predict
Real-time corrosion data
Operating variables
Prevent Corrosion Damage

Corrosion Sensor Types - Field Use

☐ Passive Sensors (Coupons)
☐ Electrical Resistance
☐ Electrochemical
☐ Fiber Optics
☐ Chemical
☐ Surface Activation (Radiometry)
☐ Electrical Field Mapping
☐ Piezo-electric Crystals

Three Application Areas

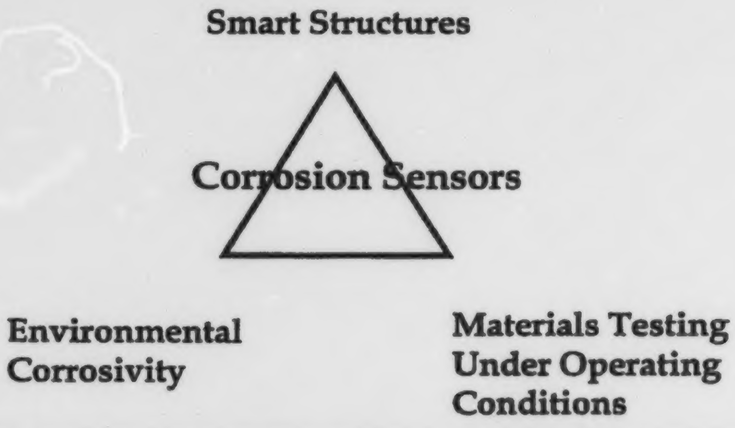

Smart Structures

Corrosion Sensors

Environmental
Corrosivity

Materials Testing
Under Operating
Conditions

Macro → Micro

Environment

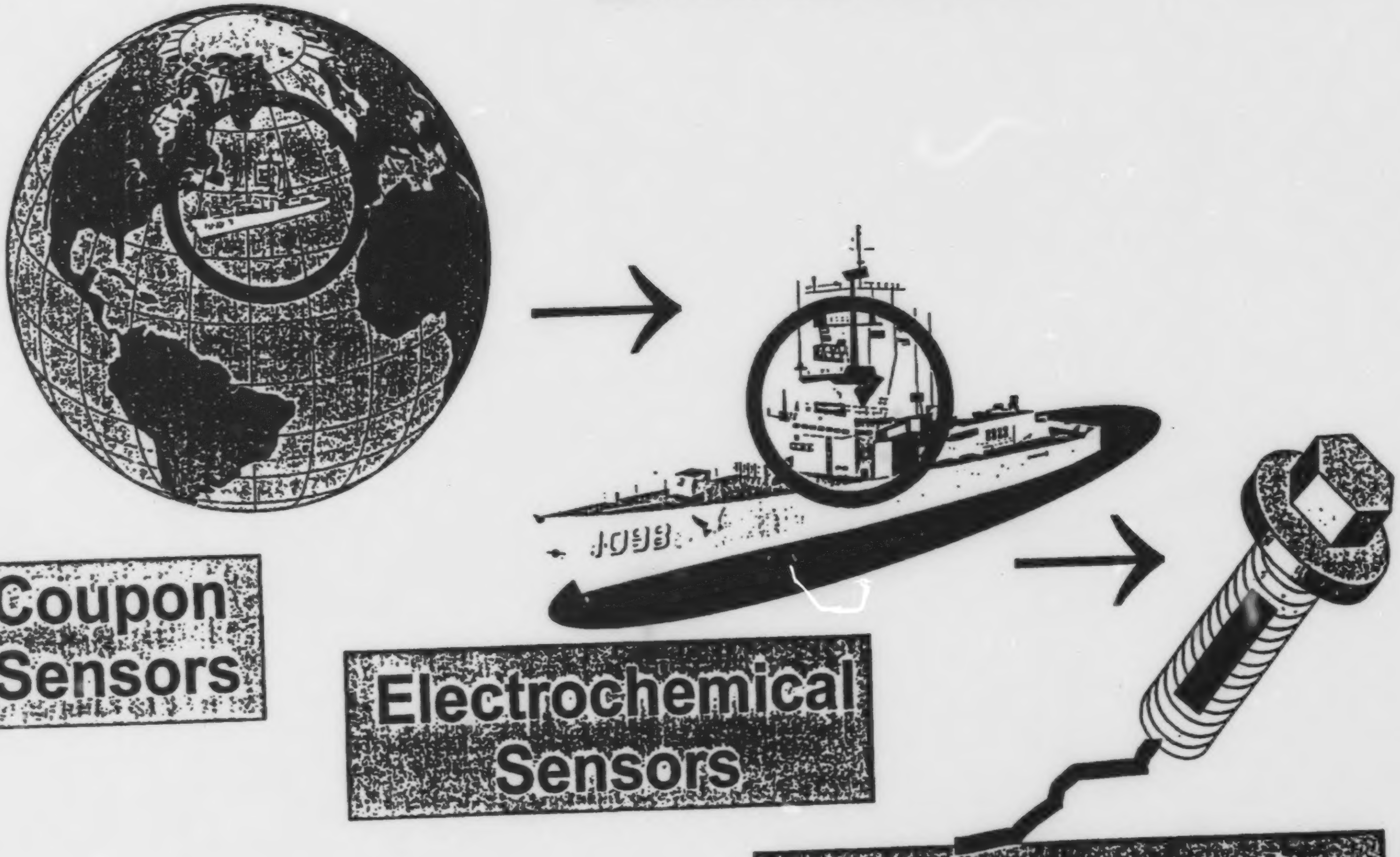

Coupon Sensors

Electrochemical Sensors

Micro Ion Selective Electrodes

Shipboard Corrosivity

(V.S. Agarwala, ASTM STP 965, 1988)
(E.Tankins et al., JOM, Sept.1995)

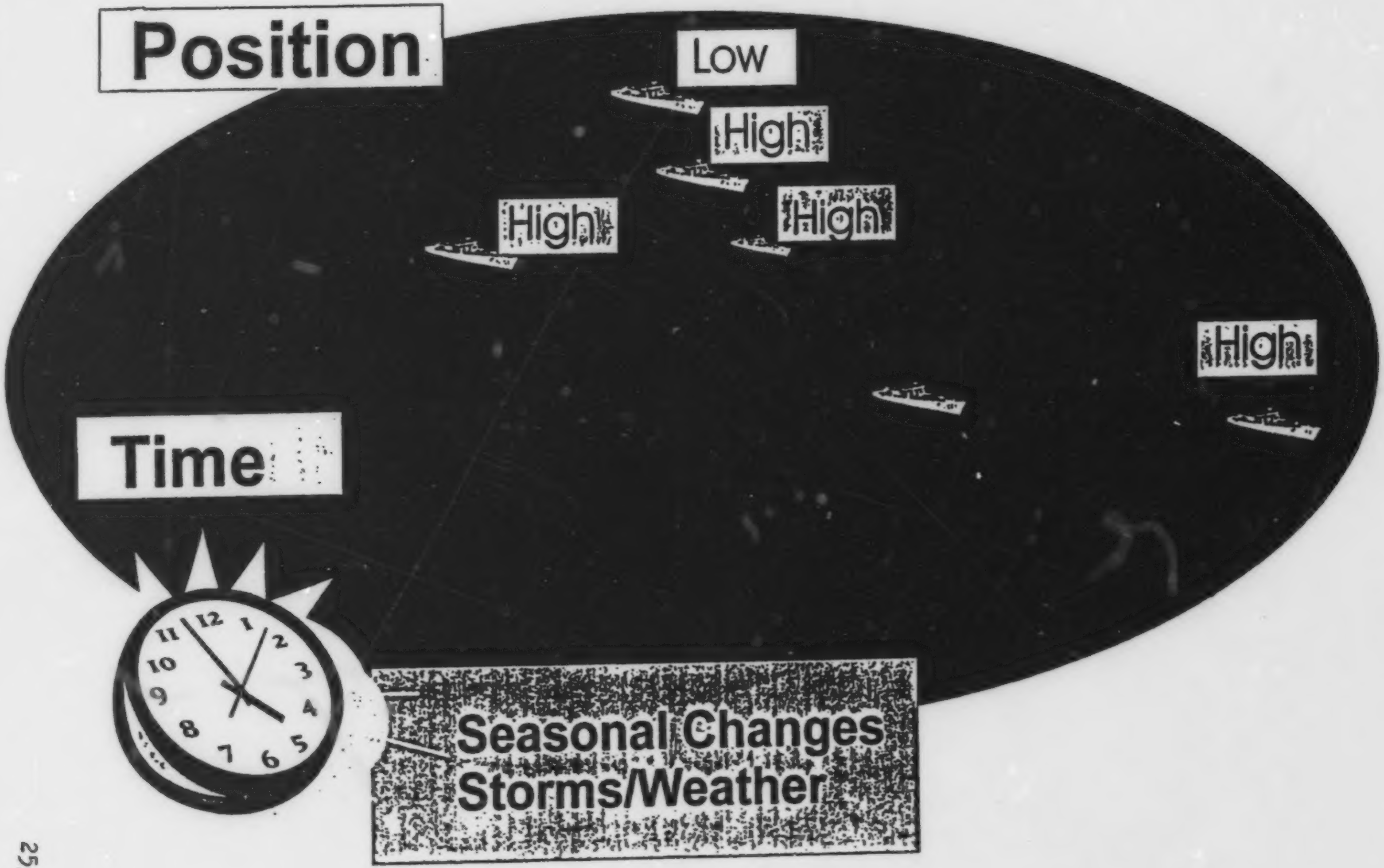
Low
High
High
High
High

Position

Time

Seasonal Changes
Storms/Weather

Corrosivity of Operating Environment

- Micro-environment most important
- Changes with time, position
- Link to inspection and maintenance scheduling
- Cleaning, inhibitor application, paint repair, repainting

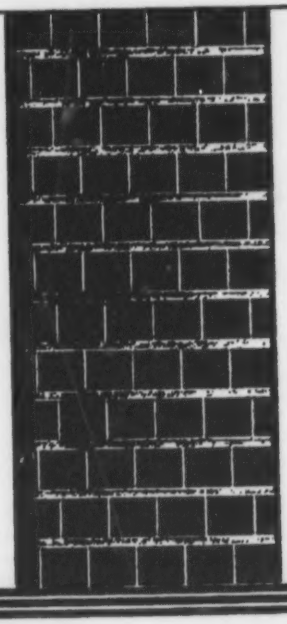

Corrosivity of the (Micro) Environment

Maintenance and Inspection Schedules

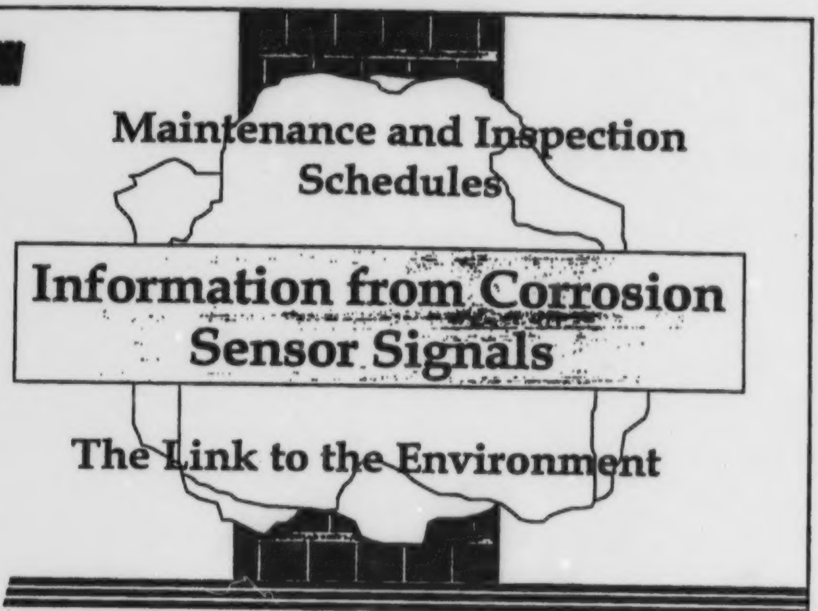

Maintenance and Inspection Schedules

Information from Corrosion Sensor Signals

The Link to the Environment

Smart Structures

- ❑ Sensors reveal when and where inspection and maintenance is required
- ❑ Condition based vs time based
- ❑ Cost driven
  (50-80% maintenance cost savings)*
  (>30% reduction in spares inventory)*

* Survey of 500 plants, Modern Power Systems, July 1994.

Smart Structure Corrosion Sensors - Paint Coating Degradation

- ☐ **Recent Electrochemical Initiatives**
  - Elimination of sensor leads
    (Zollars et al. 1997, Kelly et al. 1997)
  - Flexible thin film devices
    (Agarwala, 1996)
- ☐ **Chemical Color Changes**
  (Agarwala, 1992)
- ☐ **Fluorescence**
  (Johnson and Agarwala 1994; 1997 Miller et al. 1995)

Electrochemical Sensors

Principle

- ☐ Current and/or potential measurements on closely spaced metallic sensor elements

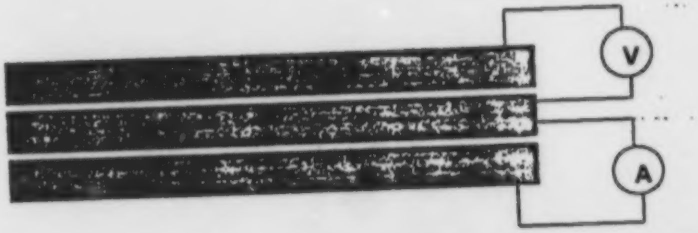

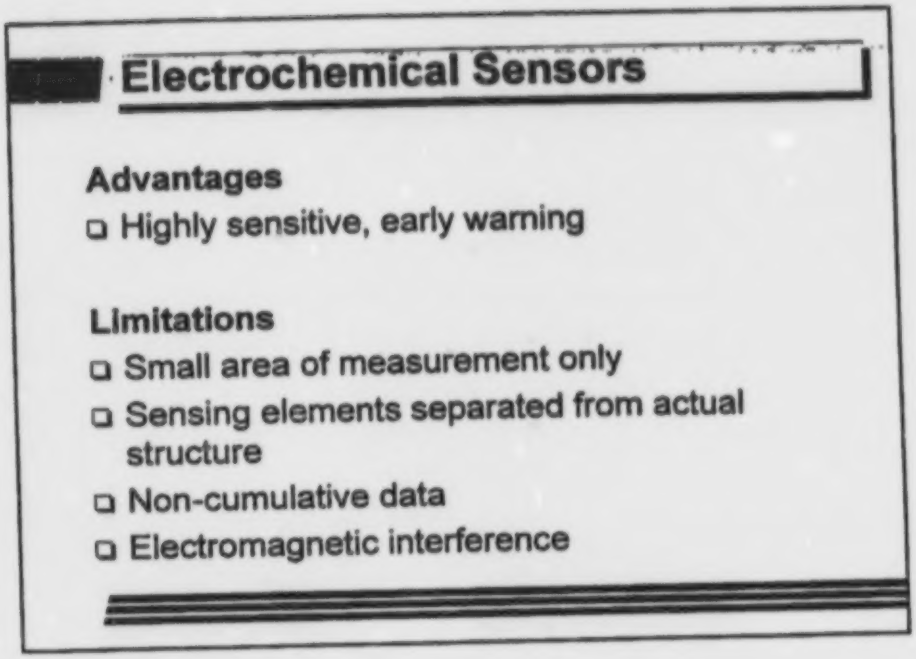

Electrochemical Sensors

Advantages

- Highly sensitive, early warning

Limitations

- Small area of measurement only
- Sensing elements separated from actual structure
- Non-cumulative data
- Electromagnetic interference

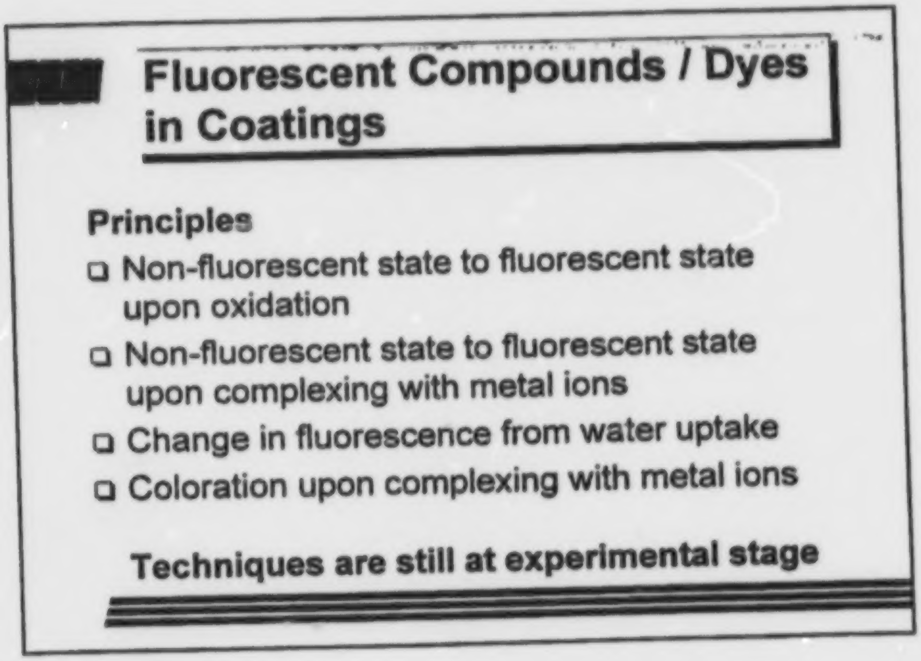

Fluorescent Compounds / Dyes in Coatings

Principles

- Non-fluorescent state to fluorescent state upon oxidation
- Non-fluorescent state to fluorescent state upon complexing with metal ions
- Change in fluorescence from water uptake
- Coloration upon complexing with metal ions

Techniques are still at experimental stage

Fluorescent Compounds / Dyes in Coatings

Advantages

- ❑ Large surface areas monitored
- ❑ Integral part of coating system, structure

Limitations

- ❑ Development and validation is required

Materials Performance Testing, Process Control

Condenser Tubing

(M.A. Winters et al., ASTM STP 1277, 1996)

- ❑ Major technical challenge
- ❑ Multiple forms of corrosion
- ❑ Corrosion and scaling under heat transfer
- ❑ Erosion effects
- ❑ Representative sensor !

Benefits

- ☐ Selection of most cost-effective material
- ☐ Reduced maintenance
- ☐ Extended service life
- ☐ Operating in "safe" windows
- ☐ Early warning of problems e.g. "overpickling" in acid descaling

#507216 ⑬

A Laboratory Simulation of the Galvanic Corrosion of a Ship Hull Plate by Shaft Grounding Systems

by

Trisha Huber
DREA Dockyard Laboratory (Esquimalt), Victoria, BC

ABSTRACT

The use of modern impressed current cathodic protection and shaft grounding systems have substantially reduced the corrosion of the underwater hull and propellers of HMC Ships. However, there have been circumstances in which the shaft grounding system has been left on while the cathodic protection system has been turned off. This has led to increased corrosion of the hull plate, both because of the inherent difference in potential between the steel hull and bronze propellers and because of the differences in the rates of delivery of oxygen to these surfaces. A laboratory simulation has been developed in an effort to determine the extent of galvanic corrosion that occurs under these circumstances.

The effects of different relative velocities of impinging natural sea water on the galvanic corrosion of hull steel (350WT) coupled to a bronze propeller were quantified with a zero resistance ammeter data acquisition system. The effects of relative surface area and different propeller materials were also measured. The results were extrapolated to estimate the length of time the cathodic protection system could be shut off before hull perforation could occur.

INTRODUCTION

Metal corrosion or oxidation is a natural phenomenon, as illustrated by the fact that ores are the most common source of metals. The abundance of ores indicates that these metals are more stable as cations than in their elemental state. Since the natural tendency of anything is to spontaneously move to a lower energy state, there is an intrinsic (or inherent) driving force for metals to corrode. This is an unfortunate situation for the Navy.

Metals and alloys exhibit varying physical, chemical, and mechanical properties. When constructing ships, we take advantage of this by utilizing materials which are well-suited to a particular purpose.

For example, when choosing materials for propellers, high tensile strength and resistance to various forms of corrosion rank high in importance. In addition the material must be readily cast in heavy sections. To satisfy these criteria bronzes, such as nickel aluminum bronze, are usually employed.

Hull materials are chosen based mostly on cost, strength, and toughness properties with much less regard to corrosion-resistance. Steels, such as 350WT, which is a tough, weldable steel are used for this purpose.

The most important criteria when choosing heat exchanger materials are resistance to a number of types of corrosion (general, localized, selective), high thermal conductivity, and high ductility. Copper-nickel alloys, such as 70-30 or 90-10, are usually used for heat exchangers.

In order to construct our ships with the most appropriate materials, we encounter an unavoidable situation of having different alloys in contact with each other in seawater, which is a corrosive environment. Thus, in addition to the occurrence of inherent corrosion, we have the perfect setting for what is known as galvanic corrosion.

A definition of galvanic corrosion is corrosion which occurs as a result of dissimilar metals in contact in a corrosive solution. This is exactly what we have with hull steel and bronze propellers which are in contact via the shafts.

When the metals or alloys are not in contact with each other but are immersed in a corrosive solution, both will undergo inherent corrosion. However, when in a corrosive solution and in contact with each other, we observe different behaviour. As the metals or alloys are dissimilar, one will be more reactive (less noble) than the other. The more reactive of the couple acts as an anode, while the less reactive material behaves as a cathode. Current flows from the anode to the cathode.

In the hull/propeller case, the hull acts as an anode and the steel is oxidized to produce ferrous ions and electrons (see Figure 1). The current flows to the propellers where the major cathodic reaction is oxygen reduction, which consumes the electrons and produces hydroxide ions.

The galvanic couple causes the steel to suffer accelerated corrosion, while the bronze is protected by the preferential corrosion of the steel. The driving force of the galvanic corrosion is the potential difference and the rate determining step is usually O_2 reduction.

It is obvious that we are unable to avoid circumstances which lead to galvanic corrosion, so we must employ methods which eliminate or at least reduce the extent of corrosion. Several methods, including those known as cathodic protection methods, are used to accomplish just that.

The simplest is the use of sacrificial anodes. This involves electrically connecting a more reactive metal to the material to be protected. The more reactive species corrodes preferentially, resulting in cathodic protection.

Another method which is slightly more complicated is known as impressed current cathodic protection (ICCP). This is the method which is used on the frigates. Current from a DC source is supplied to the ship via the hull and serves to decrease the potential of the ship as a whole. The aim is to lower the potential of all components such that they have the same or similar potentials, thereby reducing the driving force for current flow. With all components being held at a more negative potential than their respective free corrosion potentials, all act as cathodes.

A very site-specific method is the shaft grounding system, which maintains an electrical connection between the shaft and the hull. The shaft grounding system consists of metal brushes firmly connected to the hull, which surround the shaft and maintain contact with it, even when the shaft is rotating. The current flows from the ICCP anode, through the hull, and out through the shaft back to the anode via the seawater (see Figure 2).

When properly maintained, these methods are highly effective in eliminating or least significantly diminishing galvanic corrosion, however, there are occasions when the cathodic protection must be turned off. If each time the cathodic protection is turned off care is taken to ensure that it is turned back on as soon as possible, there will not be a problem in the short term. Unfortunately there is always the chance that the requirement to turn the cathodic protection back on may be forgotten.

The aim of this project was to determine the time for hull perforation under the circumstances in which the cathodic protection has been turned off and the shaft grounding system is functioning well. If the cathodic protection system is off and the shaft is not grounded, then the circuit is not complete; there will be no galvanic corrosion due to hull/propeller coupling.

EXPERIMENTAL

In order to estimate the time for hull perforation, the rate of corrosion of hull steel must be determined. The true corrosion rate of the steel is a combination of the rate due to galvanic corrosion and that of inherent corrosion. Experimentally the galvanic and inherent corrosion rates must be determined independently, but the experimental setup is similar.

The metal specimens used in the experiments are thin 1"x8" plates. To simulate the hull, 350WT, the actual hull steel, was used, while the propellers were simulated using Al bronze alloy D, a typical propeller bronze.

Surface preparation of the bronze samples involved blasting, while the steel samples were surface ground to a 25 - 30 µin finish. Early experiments, in which the steel samples were only blasted, resulted in an inconsistent surface area, as indicated by the data, so although this is how actual hull steel is treated, a more consistent finish was desired for these experiments. The specimens were then painted with an insulating paint such that only a nominal 1 in^2 (6.45 cm^2) of metal was exposed to seawater.

The seawater is natural seawater, pumped directly from the Strait of Juan de Fuca, which is less than 40 m from the lab, and used on a once through basis. The temperature of the water varies from 7 - 13 °C throughout the year, and was approximately 9 °C during the experiments discussed today.

The intake of the pump system is shown in Figure 3; there are two pumps, each with its own basket filter used to exclude large particles. Once in the lab, the water is filtered again through a 30 mesh filter to remove smaller particles. The intake is nowhere near any sewage or freshwater outlets, thus the seawater used for these experiments is very representative of natural open seawater.

Figure 4 shows the experimental setup. The manifold has 6 lines, each with its own pressure regulating valve, and calibrated pinch clamp. The velocity of seawater travelling through each line can be adjusted independently. One experiment requires two lines, one for the steel and one for the bronze, so this manifold can handle three experiments running simultaneously. Since the experimental conditions, such as T and [O_2], vary with time it is important to be able to run several at the same time in order to be able to compare the data.

A close-up of the samples immersed in the seawater tank is shown in Figure 5. Each water line ends with a small glass tube which fits into the sample holder such that the water is impinging on the sample from the same distance for each one.

The water velocities chosen for impinging on the samples were based on information obtained from crew on one of the frigates. The low end of slow cruising speed is 10 knots, with the shaft rotating at a frequency of 63 rpm. This translates roughly to a ship velocity of 17 ft/s (5.2 m/s), and a maximum velocity of 50 ft/s (15.2 m/s) at the tip of the propeller blade. Most of the hull would not experience direct impingement at 17 ft/s, nor would the entire propeller blade experience 50 ft/s. Moreover, there were limitations to the maximum velocity obtainable in the lab, so a velocity of 5 ft/s (1.5 m/s) was chosen as the slow ship velocity, and 20 ft/s (6.1 m/s) was chosen as the fast propeller velocity.

DATA & CALCULATIONS

Galvanic Corrosion Rate

For determining the galvanic corrosion rate, the steel and bronze specimens were electrically connected through a zero-resistance ammeter (ZRA, see Figure 6), which determines the current flow without altering the current. The ZRA is connected to a computer which initiates data acquisition at preset time intervals, and stores the current-time data. The ZRA is capable of acquiring current-time data for several experiments running simultaneously. In addition, the ZRA also measures the potential between each specimen and its own SSC electrode.

Figure 7 shows a typical current-time plot. The data were acquired every 30 min for ca. 1 week. The current increases to a maximum and then remains at ca. the same value. The oscillations reflect how the oxygen concentration fluctuates with demand by biological activity. The average current is obtained by averaging the data from where the current appears to have reached a maximum to the end of the experiment. For this experiment shown the average current was determined to be 2815 µA.

In order to calculate the galvanic corrosion rate, the following equation (derived from Faraday's Law) is used:

$$\frac{W}{t} = \frac{I(EW)}{F} \qquad 1$$

where W is mass lost (g), t is time (s), I is current (A), EW is equivalent weight of the material (g/mol e), and F is Faraday's constant (96487 C/mol e). The average current determined in the ZRA experiment used for I, EW of iron used for EW, since 350WT is more than 98.5% Fe.

Thus for an average current of 2815 µA, the corrosion rate was calculated to be 8.147×10^{-7} g/s per 6.45 cm^2 bronze. The surface area of the bronze is critical to the overall corrosion rate for galvanic corrosion. When the steel is coupled to two propellers (each with a surface area of 9.5 m^2 or 95000 cm^2),the corrosion rate is calculated to be 2.400×10^{-2} g/s. Converting to volume per unit time, using the density of steel (d = 7.8 g/cm^3) yields a corrosion rate of 3.077×10^{-3} cm^3/s. The calculation may be halted at this point since we can combine the galvanic corrosion rate with the inherent corrosion rate, which will be discussed next.

Inherent Corrosion Rate

A technique known as linear polarization was used to determine the inherent corrosion rate. The technique involves measuring the polarization resistance of the steel. The polarization resistance is the slope of a potential versus current plot. To obtain this type of data a potentiostat holds the potential of the sample at a range of values slightly removed from the free corrosion potential (within ± 20 mV). The potentiostat also measures the current at each of the potential values, and a potential-current plot can then be constructed.

The experiment was set up concurrently with ZRA experiments, so that the conditions would be the same, and the polarization resistance was measured periodically. The polarization resistance values were plotted versus time, and the average R_p was determined by averaging the data which had reached a stable value (see Figure 8). The average R_p was determined to be 67.9 Ω.

The polarization resistance, R_p, is inversely proportional to the corrosion current, according to:

$$I_{corr} = \frac{B}{R_p} \qquad 2$$

where: B is a constant (which depends on electrolyte, material, temperature, time, *etc.*), I_{corr} is the corrosion current, and R_p is the polarization resistance. Using a B value of 21.7 mV (corresponding to cathodic and anodic Tafel constants of 100 mV), the corrosion current was calculated to be 319.6 μA per 6.45 cm^2 of exposed steel (49.6 μA/cm^2 of exposed steel). Unlike the galvanic corrosion rate, which depends only on the propeller surface area, the inherent corrosion rate depends only on the surface area of exposed steel.

Using the loss rate equation (equation 1), the inherent corrosion rate was calculated to be 1.435×10^{-8} g/s per cm^2 exposed steel, or 1.840×10^{-9} cm^3/s per cm^2 exposed steel.

TIME TO PERFORATION CALCULATION

In order to calculate the time to perforation, the area of exposed steel must be known. The time to perforation was calculated for 1 m^2 to 20 m^2, and the data presented in the form of a plot of time to perforation, in months, versus exposed steel area, in m^2 (see Figure 9).

The calculations were based on a hull thickness of 3/8" (0.9525 cm). For each exposed steel area, the inherent corrosion rate for a given area is the product of the area and the inherent rate per cm2 exposed steel (calculated from the polarization resistance). The true corrosion rate is simply the sum of the inherent corrosion rate for a given area and the galvanic corrosion rate. To calculate the time to perforation, the volume (product of area and hull thickness) is simply divided by the rate of corrosion. The mass of steel lost may also be calculated (product of volume and density).

For example, for 10 m^2 of exposed steel,

inherent corrosion rate = 1.84×10^{-4} cm^3/s
true corrosion rate = 1.84×10^{-4} cm^3/s + 3.077×10^{-3} cm^3/s
= 3.261×10^{-3} cm^3/s
mass lost = 743.0 g steel
time to perforation = 11.1 months

CONCLUSIONS

There are several assumptions which were made when calculating the time to perforation which result in overestimating the time to perforation dramatically. One of the major assumptions is that the rate of corrosion is consistent across the exposed surface. In reality, there will be areas which suffer accelerated corrosion, while other areas corrode at rates less than calculated. Although the calculated time to perforation is based on consistent thinning, it is highly unlikely that the hull will not perforate until almost all of the exposed area has corroded.

Another assumption made is that the exposed area remains constant. That is, there is no buildup of corrosion products on the exposed steel. The buildup of corrosion products serves to decrease the effective surface area, which decreases the inherent rate of loss but has no effect on the loss rate due to galvanic. The inherent loss rate is significantly less than the galvanic loss rate (an order of magnitude), even at exposed steel areas as great as 15 m^2, so the reduction in surface area has little effect on the true corrosion rate. However, the time to perforation is directly proportional to the exposed area, so any reduction in surface area will have a dramatic effect on the time to perforation. For example, if the effective exposed steel area is 5 m^2, the calculated time to perforation is 5.7 months.

Other experiments, under similar experimental conditions, resulted in lower average galvanic currents (approximately 2100 µA). As mentioned previously, the experimental conditions vary, especially with respect to oxygen concentration, and this substantially affects the current flow since the rate-determining step is oxygen reduction. For a 10 m^2 exposed steel area, a current of 2100 µA results in a galvanic corrosion rate of 2.295×10^{-3} cm^3/s, and a calculated time to perforation of 14.2 months. This again is highly overestimated due to the assumptions outlined above.

In conclusion it is absolutely critical that the cathodic protection remain on as much as possible, and if it must be turned off, care must be taken to ensure that it is turned back on as soon as possible.

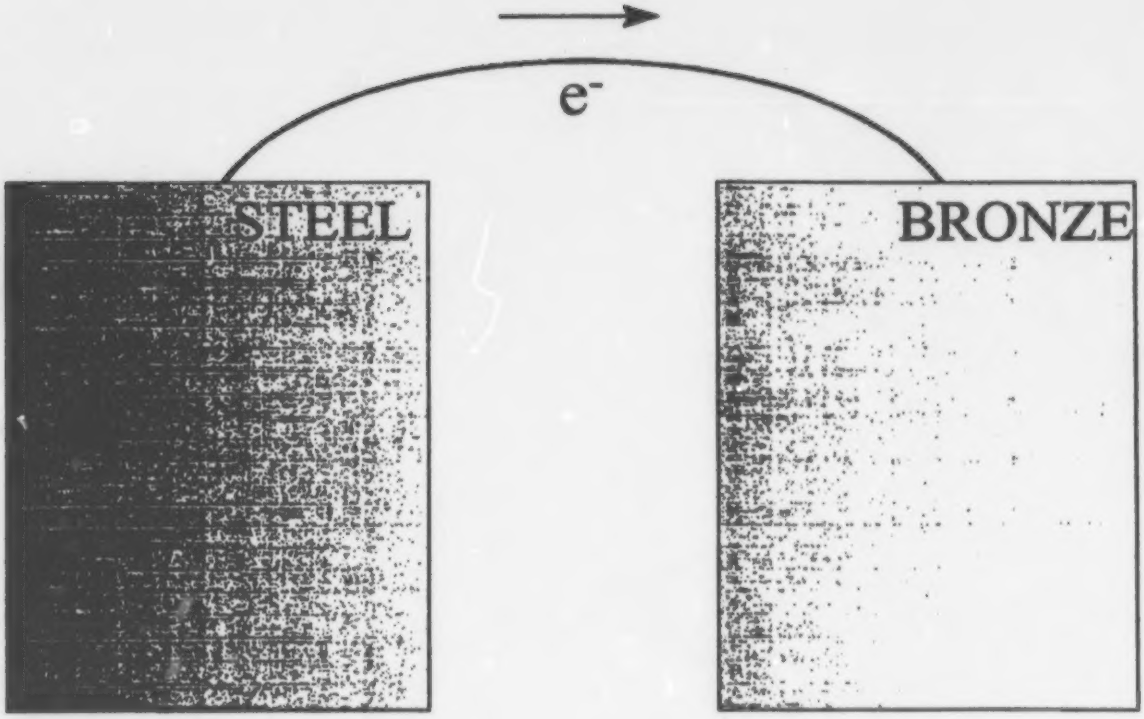
e⁻
STEEL
BRONZE

$$Fe \rightarrow Fe^{2+} + 2e^{-} \qquad O_2 + 2H_2O + 4e^{-} \rightarrow 4OH^{-}$$

Figure 1: Galvanic Current Flow

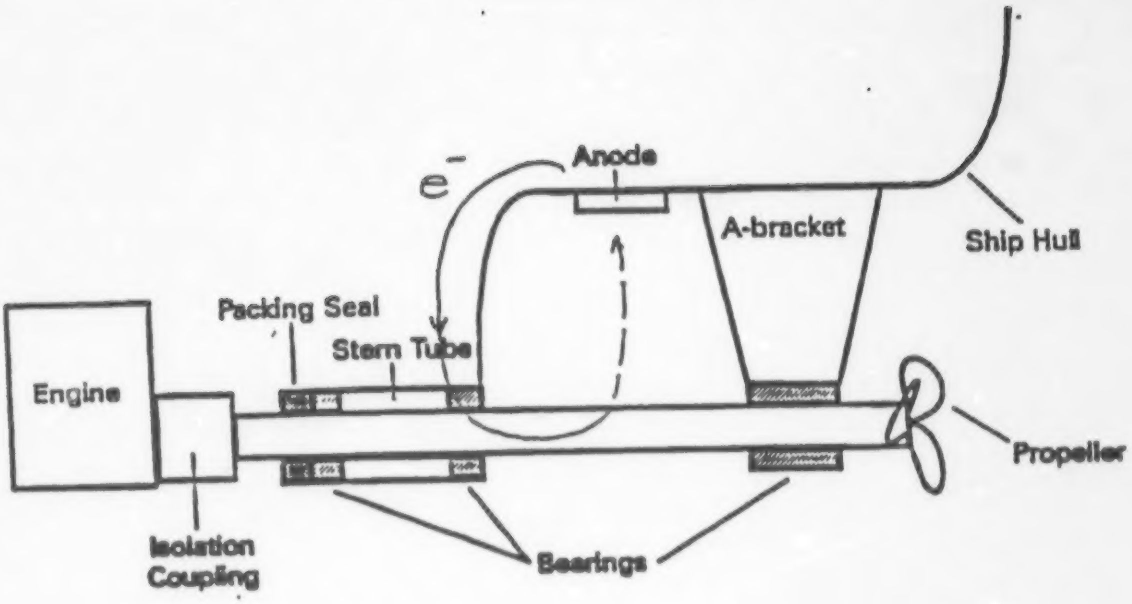
e⁻
Anode
A-bracket
Ship Hull
Packing Seal
Stern Tube
Engine
Propeller
Isolation Coupling
Bearings

Figure 2: Ship Diagram

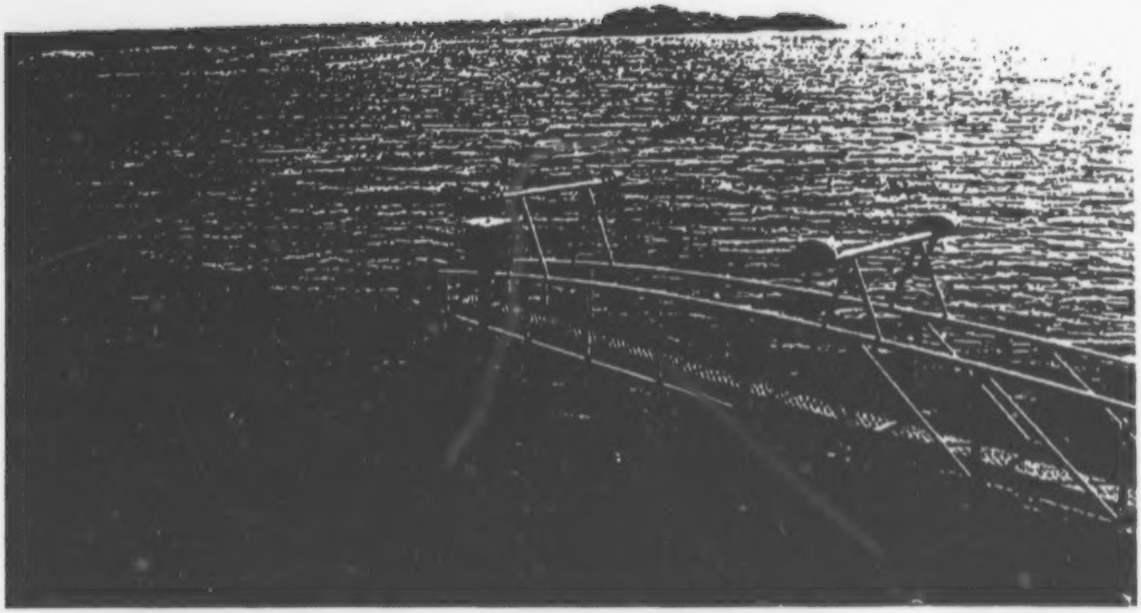

Figure 3: Seawater Intake

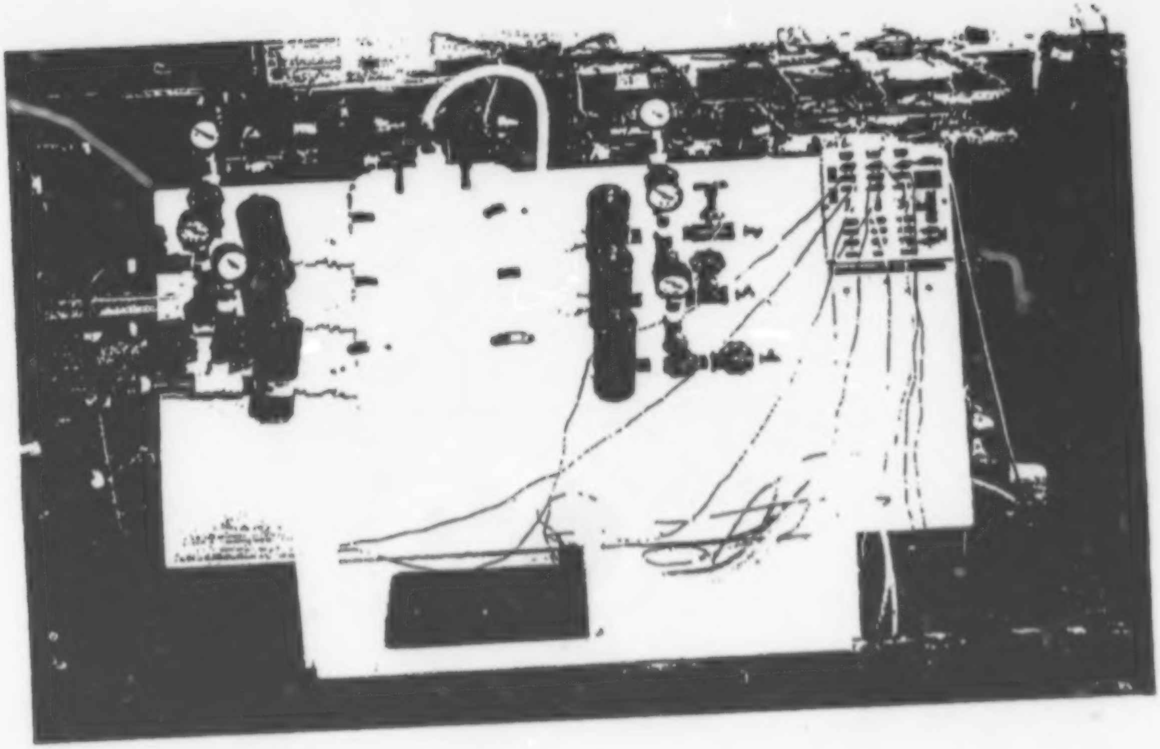

Figure 4: Experimental Setup

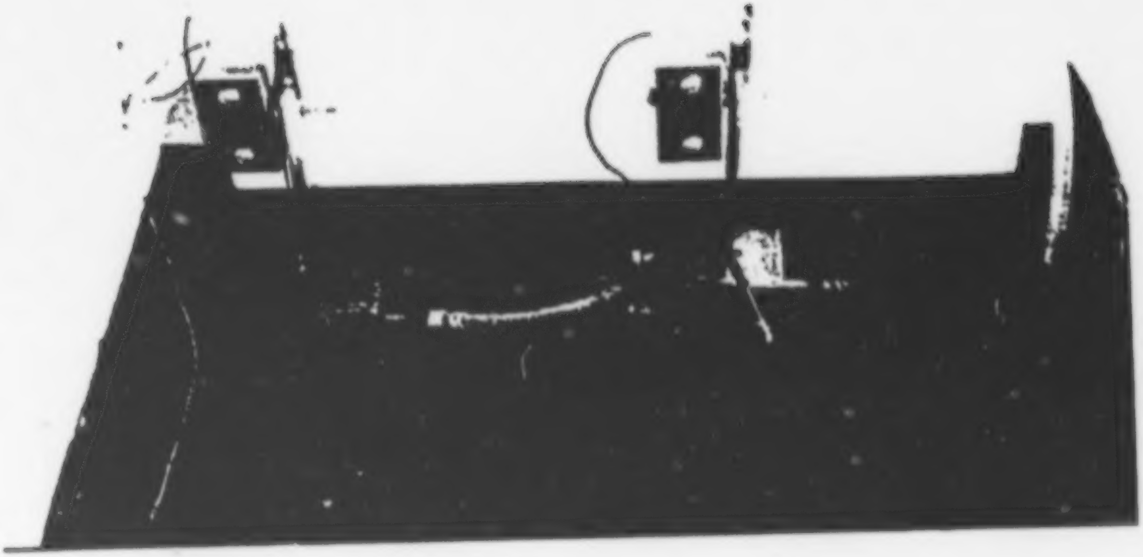

Figure 5: Immersed Samples

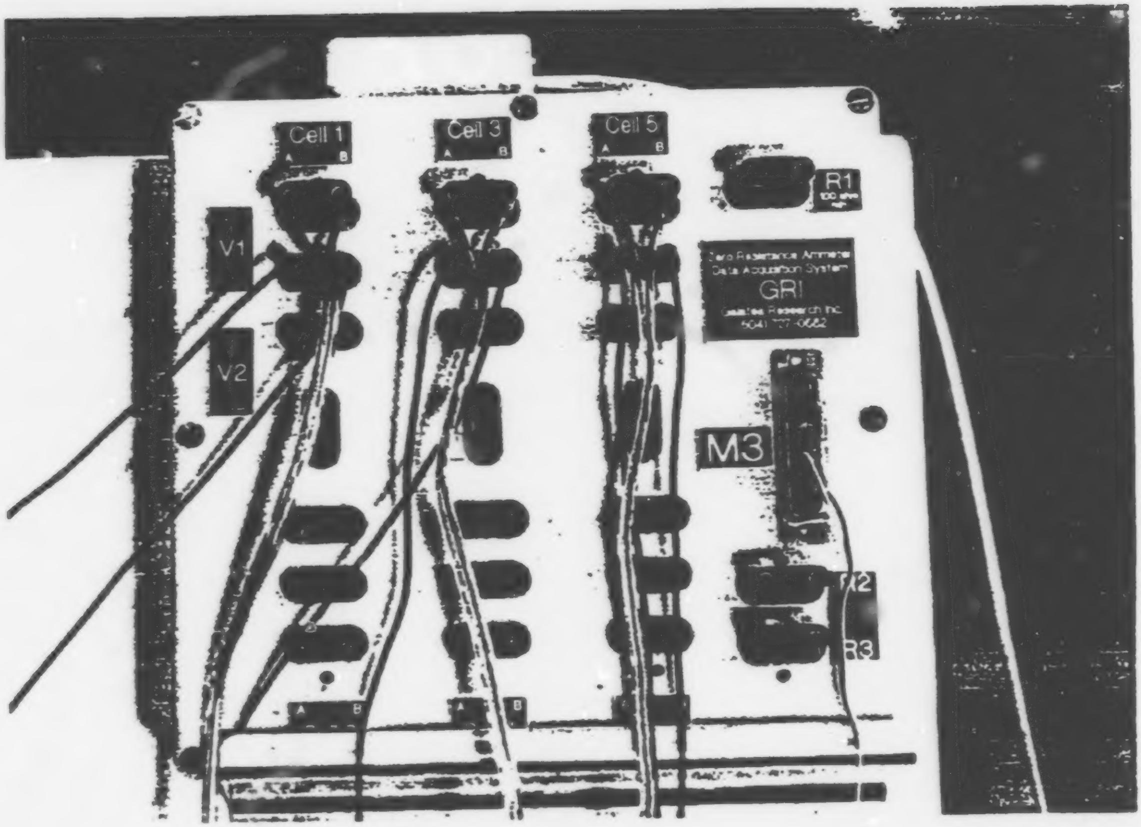
Cell 1
A
B
Cell 3
A
B
Cell 5
A
B
R1
100 ohm
V1
V2
Zero Resistance Ammeter
Data Acquisition System
GRI
Research Inc
M3
R2
R3
A
B
A
B

Figure 6: ZRA Module

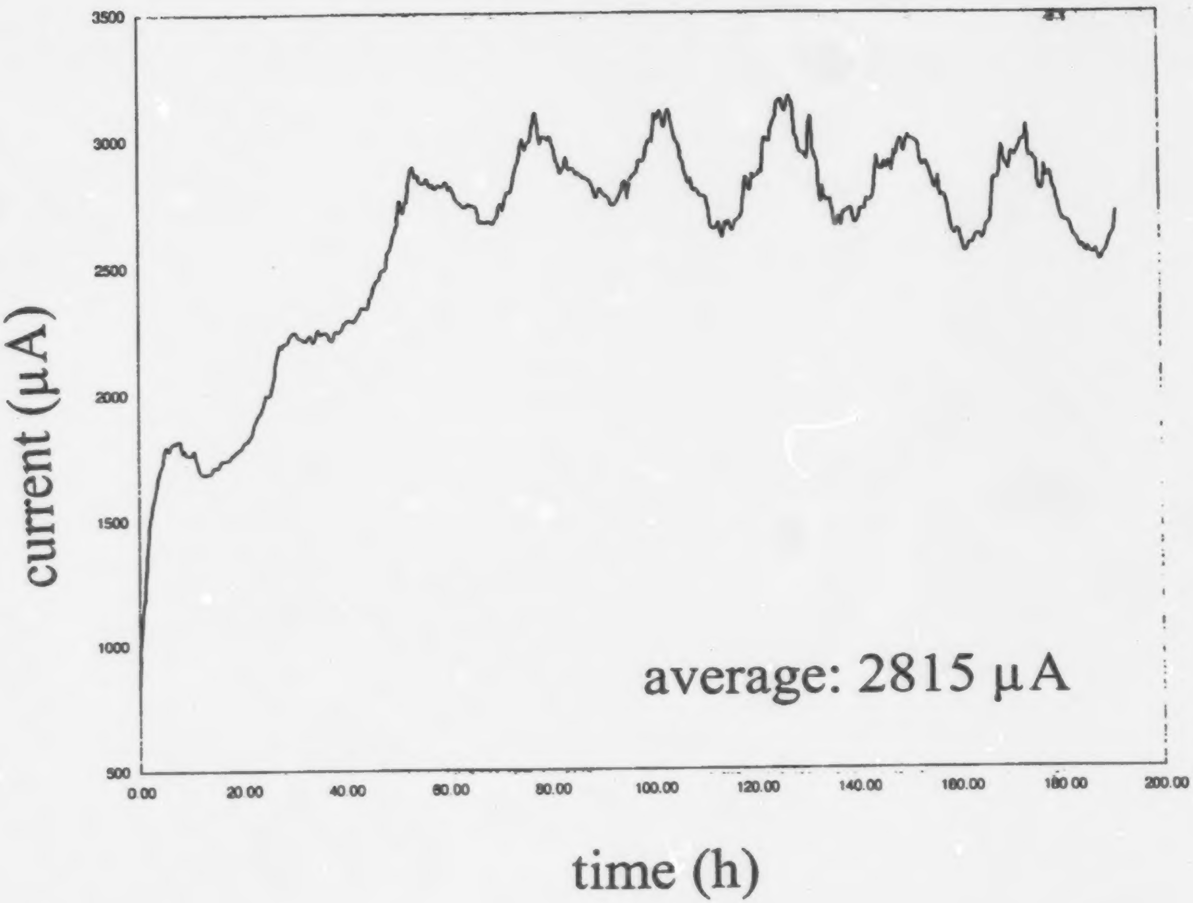

Figure 7: Plot of Current vs. Time

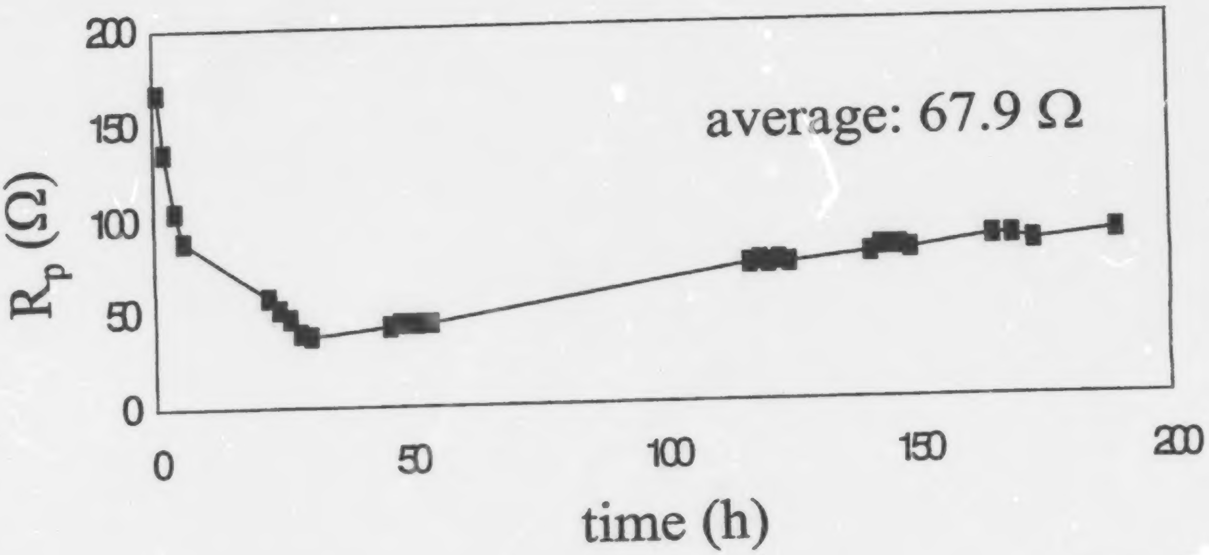

Figure 8: Plot of R_p vs. Time

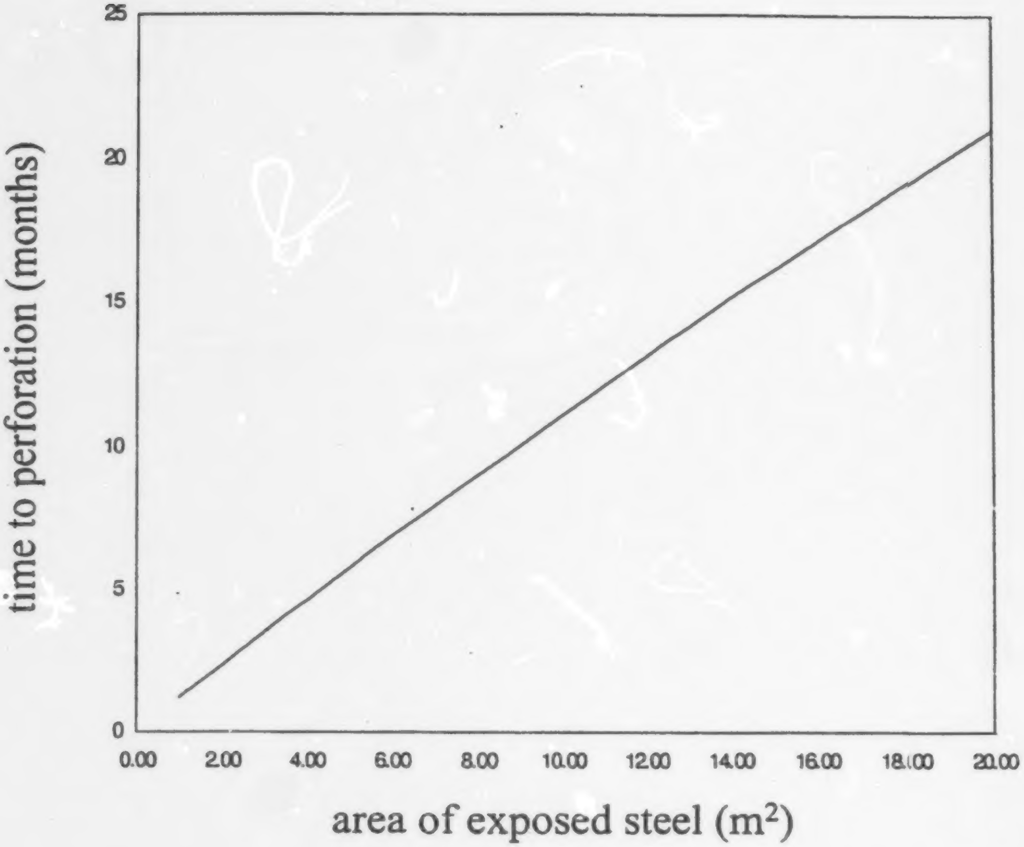

Figure 9: Plot of Time to Perforation vs. Area of Exposed Steel

#507217 (14)

CORROSION AND COATINGS IN THE RAN

M. J. SIM

Naval Materiel Requirements Branch
Department of Defence, Australia

Mr Sim is Assistant Director Materials in the Directorate of Naval Platform Systems Engineering. He has been involved with materials, corrosion and coatings for many years and has participated in international information exchange and the Internaval Corrosion Conferences.

The presentation gives a broad outline of a number of issues on corrosion and coatings that are being examined in Australia. Several of these are being actively discussed in the international information exchange program which will replace IEP ABCA-8.

Organisation

Like many other countries, Australia is reviewing and changing its Defence organisation. The Defence Efficiency Review has recently been completed, with major changes to uniformed and civilian activities.

The Naval Materiel Requirements Branch, combining Naval Engineering Services and Naval Engineering Requirements branches, came into being in April 1997. It is responsible for providing engineering advice to a wide range of Defence customers, from concept through acquisition to in-service support. It is positioned to meet the expected requirements of the Defence Efficiency Review.

Materials

The RAN operates in the same marine environment as other Navies and experiences the same problems, which may also be inherited from overseas designs. The Defence Science and Technology Organisation (DSTO) has various tasks and consultancies evaluating some of these problems. The Conference has other examples of lessons not learnt, so there is little need to list more. Instead, I would mention studies that can provide useful information exchange.

The surface treatment of nickel aluminium bronze to improve the corrosion resistance of components is of major interest. DSTO is undertaking and extending some work on alloy characterisation, laser melting and heat treatments.

Crevice corrosion testing of stainless steels is another ongoing program to evaluate materials for corrosive marine applications.

Underwater Hull Painting

The RAN uses organotin self-polishing copolymer antifouling for the underwater hull of its major units, though copper-based antifouling is used on support craft and vessels under 40 metres. The Defence Science and Technology Organisation (DSTO) has a task to evaluate tin-free and non-toxic alternatives to organotin.

Because of the requirement to extend docking intervals to five years a satisfactory alternative has not been found. A number of ships have test strips of antifouling paints, which are also being tested on rotor apparatus and rafts. One product shows promise but others deteriorate too rapidly.

One non-toxic fouling release coating has been applied to a workboat and has performed satisfactorily for about three years. The product is being used on the more recent of the new COLLINS Class submarines, which are covered with elastomeric tiles. Because the submarines are still undergoing trials there is fouling buildup while they are stationary and this has to be cleaned off by divers. After a few teething problems the coating system and the cleaning procedures seem to be working well.

The standard anticorrosive coatings under the antifouling on ships has been a vinyl anticorrosive, which is single pack, easy to apply, recoat and repair. Because it is relatively soft it is easily damaged particularly at the wind and waterline area. Consequently the RAN has adopted an abrasion resistant epoxy for damage prone areas. Initially this was used at the wind and waterline area where ships were prone to fender damage etc. Soon it was extended to the entire wind and waterline area and to ship sides of patrol boats.

The use of the abrasion resisting epoxy requires a controlled sequence of overlaps to the underwater paint system and the ship side system. It is now likely that the epoxy will be adopted for the entire hull, provided relative costs and performance estimates are satisfactory.

Painting of Tanks

Several years ago requirements for painting of tanks etc. included a total dry film thickness of 300 µm. In 1994 the RAN Painting Manual changed to specifying generic paint schemes applied in accordance with manufacturers data. This gave rise to possible problems where the manufacturers typical thickness and number of coats could turn out to be the maximum thickness applied and the actual thickness could be too low to provide adequate service.

Painting Manual - ABR 19

ABR 19 was revised in 1994 to provide a basic guidance document with generic paint systems and manufacturers approved schemes. When it was issued there was essentially only one major manufacturer listed, but other suppliers are now being included. The generic schemes referred to specifications of the Government Paint Committee, now the Australian Paint Approval Scheme, which incorporates manufacturer accreditation and audit, and product or system approvals. For predominantly naval applications ABR 19 allows Navy approvals.

It had been hoped that this would free up the painting requirements, relying on manufacturers recommendations instead of detailing hundreds of schemes to fit every need. Unfortunately this has not been entirely successful.

In the revision of the Painting Manual currently under way it is intended to subdivide schemes into build/refurbishment, major maintenance and onboard maintenance. The difficulty is that the categories overlap depending on the extent of work and it is impossible to cater for all contingencies. It would be preferable to require the application of common sense before the application of any paint.

Exterior Painting - Visual Signature and Infra-red Reflection

Comments have often been made that the RAN exterior colour of Storm Grey (Light Grey) is not suitable because it is a greenish grey. United States Navy Haze Gray has been suggested as a better colour match to sea colours. The use of full gloss paints has also been criticised, since current alkyd paints lose gloss on weathering and are polished or overcoated to restore gloss.

Consequently a trial is underway to evaluate a low gloss Haze Gray polyurethane paint on a patrol boat, HMAS WHYALLA. There was little significant difference seen from flyovers, but a large reduction in visibility for ship to ship observation. Ship staff has early concerns with the low gloss because it appeared to get dirty more quickly but they have found it easy to clean.

In addition to changing the colour and gloss of the exterior paint scheme the trial system has also changed the solar heat reflectance. This has been achieved by eliminating carbon black pigment and substituting near infra-red reflecting pigments. This has dramatically reduced the heat build up in the vessel, with a substantial reduction in airconditioning requirements. It is possible to walk on the decks in bare feet.

The low solar absorption properties and the consequent reduction in airconditioning requirements has prompted a request that all exterior painting be changed to near infrared reflecting.

Environment and Health and Safety

So far Australia does not have specific restrictions on Volatile Organic Compounds (VOC) for paints. The Australian Paint Approval Scheme has adopted limits, mainly for building paints. Navy has an informal requirement to lower VOC but may accept products with similar or even higher VOC if performance is better.

Water based paints are attractive because of the reduction in VOC and solvent cleanup. Single pack paints are attractive because there is not the problem of disposing of part containers of mixed paints beyond pot life.

The majority of paints in use are alkyd or epoxy. Polyurethanes are used for patrol boat exterior painting and for interior deck coatings, although there are some concerns on isocyanates. The urethanes are high performance coatings and can be applied safely in the right conditions but because of the OH&S concerns it may be necessary to use other materials. For example, ship exteriors are likely to get damage and touch up, and are painted in the open, so acrylics may be preferred. A change to water-based acrylic would give a better topcoat performance than alkyd even though not as good as polyurethane.

Cathodic protection

ABR 5023, the RAN Cathodic Protection Manual, gives policy and design guidance for cathodic protection. It is in need of an update and a draft revision has been made. This is in abeyance awaiting resources. Like the Painting Manual it was intended that the Cathodic Protection Manual would porvide overall policy and guidance, but leave detailed design to contractors and ship designers. Discussions with other Navies suggest that this may not be practicable.

DSTO has a task including physical scale modelling of cathodic protection and this may lead to defining various design parameters. Experimental reference electrodes designed and made in Canada are also being purchased to measure actual cathodic protection potentials underway.

#507218 (15)

Development of an Optimum Consumable Alloy for Low Heat Input Welding of Nickel Aluminum Bronzes

by

C.V. Hyatt[1], J.C. Bennett[2], G. Pelletier[1], B. Armstrong[1], K. KarisAllen[3], J. Hewitt[4], T. Betancourt[6]
J. Gianetto[5] and M. Sahoo[5].

ABSTRACT

Nickel aluminum bronzes are used in ship and submarine sea water handling, propulsion and combat systems equipment, as well as in a range of commercial high performance components. Usually, when these alloys fail, they fail by a surface sensitive mechanism such as wear, corrosion, dealloying, cavitation-erosion or corrosion fatigue. To determine if these surface properties could be improved with laser cladding, a laser cladding method was developed and the processing-structure-property relationships were studied. Microstructures and properties were found to be highly dependent on heat input. To reduce this sensitivity to heat input and further improve properties, work to develop an optimum consumable alloy was undertaken. The effects of additions of chromium, zirconium, and titanium were investigated along with the effects of composition variation within the range allowed by various standards. Work so far reveals three possible alloying approaches. Using these alloying approaches, reductions in the sensitivity of microstructures to heat input and property improvements are possible.

1. Defence Research Establishment Atlantic, Dartmouth, Nova Scotia, Canada
2. Acadia University, Wolfville, Nova Scotia, Canada
3. FACTS Engineering, Halifax, Nova Scotia, Canada
4. The Laser Institute, Edmonton, Alberta, Canada
5. Materials Technology Laboratory, Ottawa, Canada
6. Nova Scotia Research Foundation (now retired)

1.0 INTRODUCTION

Nickel aluminum bronzes are, and will remain for the foreseeable future, the most important alloy used in ship and submarine propulsion and sea water handling systems[1,2]. They are also extensively used in combat systems equipment. In all marine applications the performance of these alloys is limited by surface sensitive properties—corrosion-fatigue for propellers, crevice corrosion for valves, cavitation-erosion for pumps and wear for bearings[3-8]. It is also significant that many high value-added components made of nickel aluminum bronzes cannot be reclaimed by current welding methods because of some localized corrosion problems as well as distortion problems[5-8]. These problems are believed, at least in part, to be caused by poor understanding of effects of heat input and composition (especially residual elements) on the microstructure and properties of nickel aluminum bronze weldments. Clearly large improvements in performance are possible by improving the surface properties of nickel aluminum bronzes. Recent analysis' of the through life costs of warships show that extending the life of nickel aluminum bronze components would also have cost benefits as well. Low heat input welding and weld cladding methods such as laser welding are promising means to improve the surface properties of nickel aluminum bronzes and to make repairs which we cannot make now[9-25].

To overcome the problems just mentioned, DREA has been investigating the surface engineering and clad welding of nickel aluminum bronzes. The goals of this project are to develop means to improve equipment performance and reduce operation and maintenance costs. This can be done by engineering the surfaces of components to make them last longer and by making possible repairs which are impossible with current technology. Goals of the work include:

1. Developing low heat input laser welding methods for cladding complex shapes with minimal distortion, as well as higher heat input processes;

2. Evaluating the properties and in-service performance of laser clad materials and components, which involves the development of new experimental techniques;

3. Developing optimum alloys, with high hardness, ductility and resistance to all forms of corrosion when deposited with a range of heat inputs; and

4. Seeing the procedures and materials put into practice, first for repair and later for the treatment of new components.

Previously, we reported that a low heat input laser cladding method had been developed and showed that complex parts of ships and submarines could be clad for a reasonable cost [21,28,29]. We also reported on the structure of deposits and on the effect of heat input in laser cladding[21,22,30].

In the heat input study, nickel aluminum bronze castings were clad with a consumable of composition Cu-9.0 Al-4.6 Ni-3.9-Fe-1.2 Mn and a range of heat inputs from 42.5 to 595

J/mm. At the lowest heat input, the deposit microstructure was almost entirely martensitic. Increases in heat input caused the amount of α to increase. Depending upon heat input, the α was present as grain boundary allotriomorphs, secondary Widmanstätten α sideplates and intragranular Widmanstätten α precipitates. The reheated zones were of lower hardness, and at all heat inputs consisted of a mixture of grain boundary allotriomorphs and Widmanstätten α and martensite. Laser cladding improved the corrosion and cavitation erosion resistance of the surfaces but reduced their ductility. Properties of the clad surfaces depended on heat input [30]. Other work showed that deposit composition also effects microstructure [31].

Laser cladding would be more useful for nickel aluminum bronzes if the microstructures and properties were less sensitive to heat input, if further property improvements could be made and if reductions in ductility could be eliminated through the development of a nickel aluminum bronze consumable alloy, optimum for the low heat input welding. Such an alloy should be insensitive to heat input (hopefully though not likely, even in conventional welding), have high hardness and better ductility, high resistance to corrosion, de-alloying, wear, cavitation and erosion corrosion, pitting and corrosion fatigue and have a corrosion potential similar to that of nickel aluminum bronze

There is good reason to believe this goal is achievable. First, as mentioned above, microstructural response to heat input and probably properties, do depend on heat input. Second, data on solid state quenching shows that nickel and iron content and the Ni/Fe ratio as well as Al content affects hardenability [32]. Third, a variety of additions including Zr, Ti, and Cr give hardening in other copper alloys including bronzes. These elements are particularly interesting, because some early patents suggest these elements inhibit both dealloying and stress corrosion in cast and wrought aluminum bronzes[2 and references therein]. Finally, data on ternary intermetallics suggests a number of potentially useful strengthening precipitates might form from the addition of these elements [33, 34].

To identify an optimum alloy composition, 28 experimental alloys, laser surface melted with eight different heat inputs were examined. So far microstructures, microhardnesses, cavitation erosion behaviors, corrosion potentials and temper resistance by resistivity have been investigated. These are the topics of this paper. Wear, erosion-corrosion, long term immersion (including crevice corrosion), potentiodynamic corrosion, differential thermal analysis and corrosion-fatigue studies are planned.

2.0 MATERIALS AND METHODS

The compositions of the experimental alloy castings used in this work are shown in Table 1. To simply investigate heat input effects, surface melting (autogenous welding) was performed using the conditions listed in Table 2. Optical metallography and some transmission electron microscopy was also carried out using the preparation techniques summarized in Refs. 30,35,36. We describe the resolidified laser melt as the remelted material (analogous to the as-deposited in a clad deposit) and the heat affected zone in the remelted material produced by the next pass as the reheated zone (analogous to the reheated zone in a clad deposit)

⊕ Table 1. Nickel Aluminum Bronze Alloy Compositions

Series	Melt #	Sample	Cu	Ni	Fe	Mn	Al	Cr	Ti	Zr	Ni/Fe
C	103.95-2	1	76.45	5.06	6.20	0.35	9.70		2.24		0.82
B	125.95-3	2	79.60	3.80	5.50	1.00	10.10				0.69
B	128.95-1	3	80.10	5.00	4.70	1.10	9.10				1.06
B	125.95-1	4	81.20	3.80	3.90	1.00	10.10				0.97
B	128.95-2	5	78.60	6.50	4.60	1.10	9.20				1.41
B	133.95-1	6	78.00	4.70	3.80	1.30	12.20				1.24
B	132.95-3	7	77.95	4.00	5.80	0.95	11.30				0.69
A	124.95-1	8	80.20	4.60	4.80	1.10	9.30				0.96
A	124.95-3	9	77.30	4.60	4.60	1.00	12.50				1.00
C	103.95-3	10	75.44	4.95	6.10	0.36	9.60		3.55		0.81
A	124.95-2	11	78.80	4.70	4.70	1.10	10.70				1.00
B	132.95-1	12	79.30	4.10	4.30	1.00	11.30				0.95
B	133.95-2	13	76.40	5.90	4.20	1.30	12.20				1.40
C	103.95-1	14	77.20	5.05	6.30	0.31	10.00		1.06		0.80
B	133.95-3	15	74.00	6.10	6.50	1.20	12.20				0.94
B	132.95-2	16	78.60	4.10	5.00	1.00	11.30				0.82
B	128.95-3	17	77.60	6.50	5.70	1.00	9.20				1.14
C	114.95-1	18	77.83	4.95	6.02	0.83	9.40			0.97	0.82
A	136.95-1	19	79.30	4.60	6.20	1.10	8.80				0.74
C	137.95-2	20	77.23	5.16	5.60	1.10	9.76	1.15			0.92
C	137.95-1	21	78.71	5.19	4.78	1.10	9.61	0.61			1.09
A	136.95-3	22	78.40	4.60	6.20	1.10	9.70				0.74
D	140.95-2	23	78.95	4.70	5.00	1.00	8.90	0.60	0.44	0.41	0.94
	140.95-3	24	80.60	3.70	4.40	0.91	7.80	1.12	0.79	0.68	0.84
C	137.95-3	25	76.14	5.10	6.30	1.10	9.64	1.72			0.81
A	136.95-2	26	78.90	4.60	6.10	1.10	9.30				0.75
D	140.95-1	27	78.63	4.90	5.30	1.10	9.30	0.31	0.23	0.23	0.92

Table 2. Laser Surface Melting conditions

Condition (#)	Laser	Heat Input (J/cm)	Ave. Power (w)	Speed		Melt Pool	Defocus
				(cm/s)	(ipm)	Width (um)	(mm)
1	Mits	25	800	32.0	756	275	0.00
2	Mits	100	800	8.0	189	360	0.00
3	CE5000	650	5000	7.7	182	1100	10.80
4	CE5000	800	5000	6.3	148	1100	10.80
5	CE5000	1000	5000	5.0	118	1200	10.80
6	CE5000	1500	5000	3.3	79	1500	10.80
7	CE5000	3000	5000	1.7	39	1800	11.30
8	CE5000	3000	5000	1.7	39	1700	10.80
9	CE5000	650	5000	7.7	182	1100	10.80
10	CE5000	3000	5000	1.7	39	1800	11.30

Corrosion potentials (E_{corr}) were determined by the ASTM G5 method [37]. Briefly, after wires were attached to the surface melted specimens, the specimens were mounted in epoxy so that only the laser surface melted face was measured. Except in a few cases where deliberate exceptions were made, the surface melted face was ground to remove the oxide layer prior to testing. The corrosion potentials were measured with respect to a standard calomel electrode in de-aerated sea water at 25 °C. Measurements were made after 1 hour of immersion.

Cavitation erosion measurements were made according to ASTM standard G-32 [38]. The experimental test apparatus consisted of a Branson Model No. 108 connected to a 184V power supply/function generator. A 1:1 booster was attached between the titanium horn and the converter. The specimens were attached at the lower extremity of the horn which was submerged in sea water during testing. Sea water temperature was maintained at 25 °C ± 2 °C during testing. As well, a peak to peak amplitude of 0.05 mm was maintained throughout the test and the operating frequency of the horn was maintained at 20 kHz. For each run, a two liter beaker was filled with naturally occurring sea water and placed in the water bath. A 316 stainless steel specimen was run in the sea water for 30 minutes to stabilize the gas content. The specimen was then screwed into the horn tip and pretorqued to 120 in-lbf with a torque wrench. The test apparatus holder slid vertically on a rod at the back of the cabinet. The holder was positioned so that the face of the test specimen was immersed approximately 10 mm in the test liquid. The power was activated and the voltage adjusted to between 152 Vdc and 154 Vdc.

Test duration was approximately 16-20 hours. For the first half of the test, the specimen was removed from the horn every hour, washed with acetone, blown dry and weighed using an analytical scale. For the second half of the test, this procedure was repeated every two hours. When the test was completed, the weight of the specimen was recorded and the specimen stored in a desiccator.

Temper resistance of the different alloys was assessed by electrical resistance measurements. Samples approximately 1.00 mm thick, 3.00 mm wide and 40.00 mm in length were heat treated at 1000°C for one hour, quenched in an iced brine solution, and then tempered at temperatures from 400°C to 900°C for various times.

3.0 RESULTS

3.1. Metallography and Microhardness

Work on the metallography of the alloy set is in progress. So far optical metallography has been completed on all specimens for laser surface melting conditions 10, 65 and 300 J/mm. This work will be reported in detail in a DREA report [39]. A report on the base casting structures is also to be available shortly.

Briefly, work on the laser melted experimental alloys showed remelted and reheated zone microstructures were affected strongly by composition and heat input. Hardness as a function of the alloy numbers listed in Table 1, for several different heat inputs is shown in Fig. 1. Replotting this as a function of aluminum content (Ni/Fe ratios are shown beside each point), shows that higher aluminum favors a both higher remelted hardness and increased resistance to softening of the reheated zone. As well Ni/Fe ratio seems to affect hardness. This requires further investigation, though it appears that above 10 % Al, Ni/Fe greater than 1 favors higher hardness while below 10% Al the effect is reversed. .

The non-standard additions provided some hoped for increases in hardness. First, in the remelted material, both Ti and Cr increase remelted hardness relative to an otherwise similar alloy without these additions. Of significance relative to the design of an alloy which will retain high hardness over a range of heat inputs is the observation that for Ti additions a peak in the hardening effect occurred at 65 J/mm while for Cr additions hardness as a function of heat input was still increasing at 300 J/mm. It is also clear from the data that Cr, Zr, Ti all reduce sensitivity of the reheated zone to tempering, and give harder reheated zones than for otherwise equivalent alloys which do not contain these additions. The results show Cr and Ti additions are particularly effective additions for improving resistance to tempering.

The reason for the observed reversal in the effect of Ni/Fe ratio as aluminum content increases is unclear. Possibly at low aluminum, the Ni/Fe ratio may be more important in determining hardenability and whether or not lower hardness bainites or α phases form, while at high aluminum only martensitic microstructures form so the effect of Ni/Fe on martensite structure, order, and precipitate type and coherency probably becomes more important. Alternatively, in the low aluminum case, the Ni/Fe ratio may affect precipitate type, size and density. Electron microscopy studies now in progress may clarify this issue.

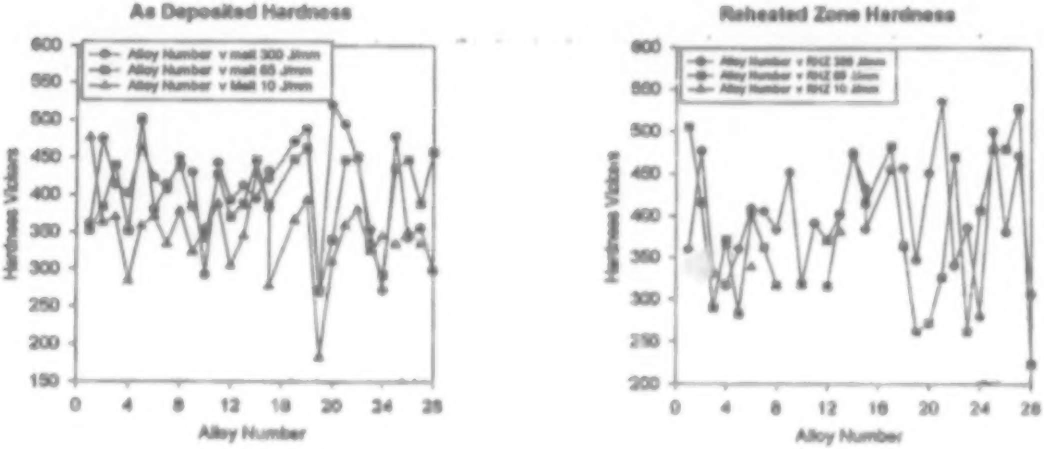

a. b.

Figure 1. Hardness of as deposited (a) and reheated zones (b) as a function of heat input.

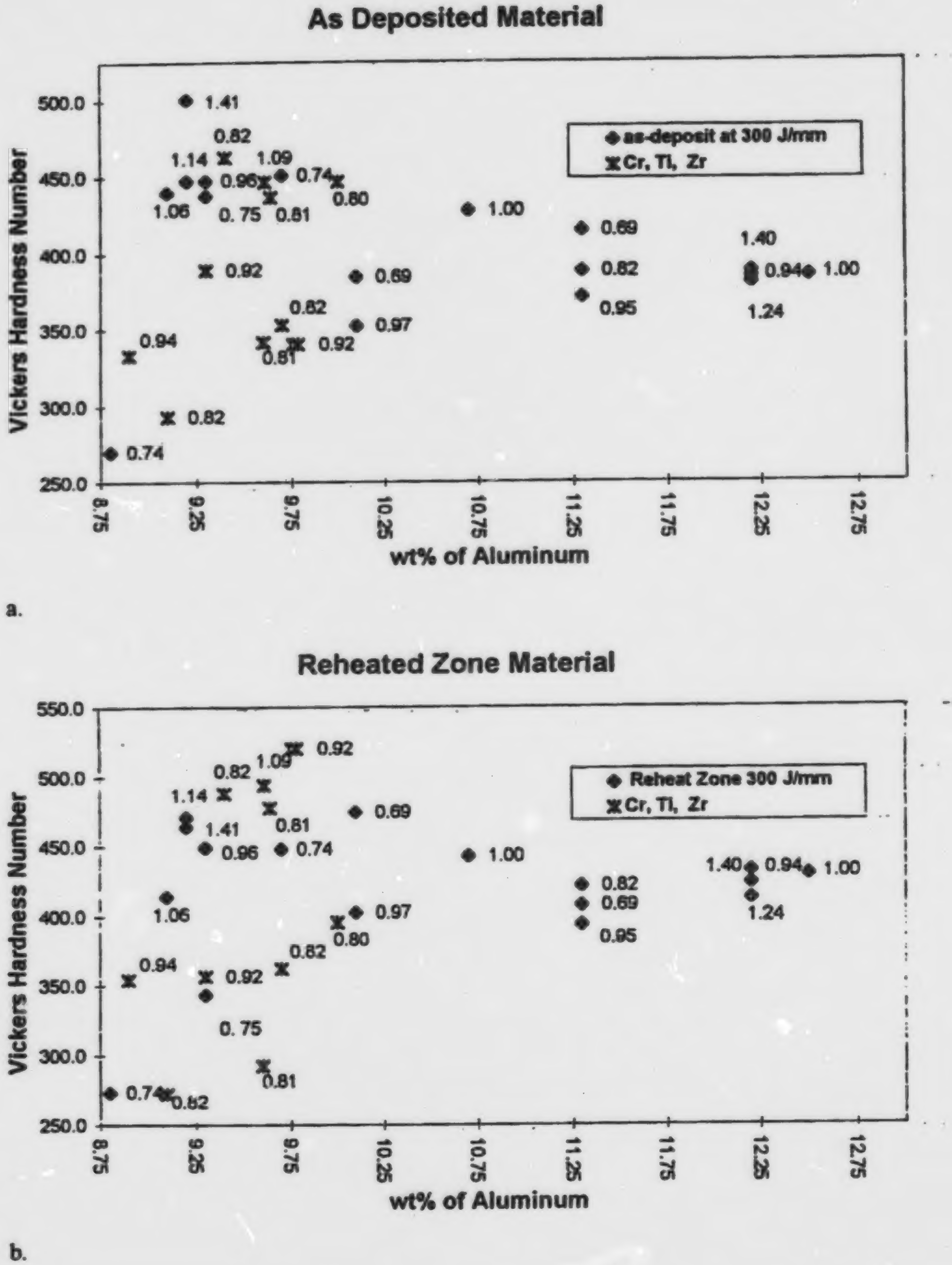

Figure 2. Remelted (a) and reheated (b) zone hardness as a function of aluminum content

We plan to discuss the details of the effects of heat input and composition on the microstructure of these alloys in several future papers. Work so far has revealed some

F4

interesting trends. First, as the aluminum content is increased, the volume fraction of α becomes lower. Above 11% Al, no α is present in the deposit, even at relatively high heat inputs of 300 J/mm. For Al contents of less than about 9 %, little high temperature β phase forms so there are few β transformation products, only a dendritic solidification structure. Examples of these two extremes are shown in Figs. 3 and 4. We also noticed that at constant aluminum and heat input, high Ni favors martensite (and perhaps bainitic high temperature β transformation products) while high Fe favors the formation of α in various forms. The addition of Cr helps to suppress α, in both the deposit and reheated zone and reduces differences between those two zones. This is shown in Fig. 5. Titanium and zirconium additions produced laser surface melted microstructures which were similar to each other and much different from other structures. Both additions seemed to support the formation of α and a multiphase equiaxed structure (this is shown in Fig. 6.).

Figure 3. Optical micrograph of remelted material on Alloy 19 which contained 8.8-Al, 4.6-Ni, 6.2-Fe, 1.1-Mn.

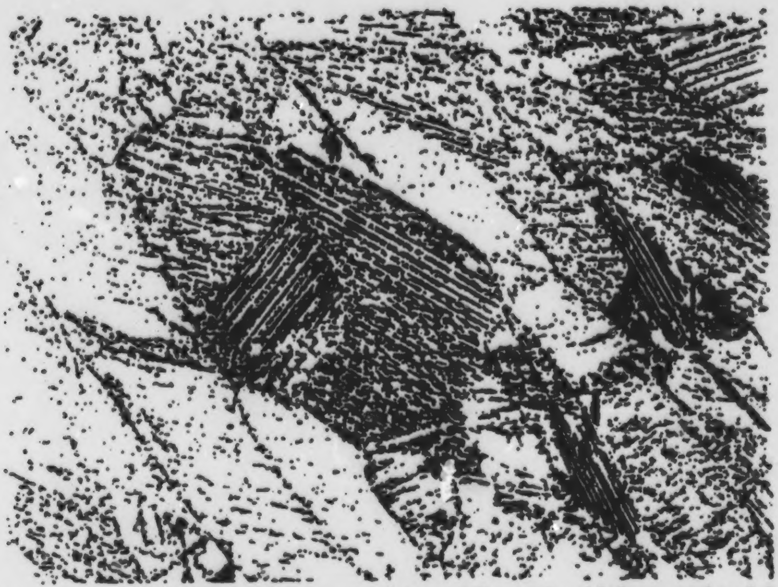

Figure 4. Optical micrograph of remelted material on Alloy 16 which contained 11.3-Al, 4.1-Ni, 5.0-Fe, 1.0 Mn.

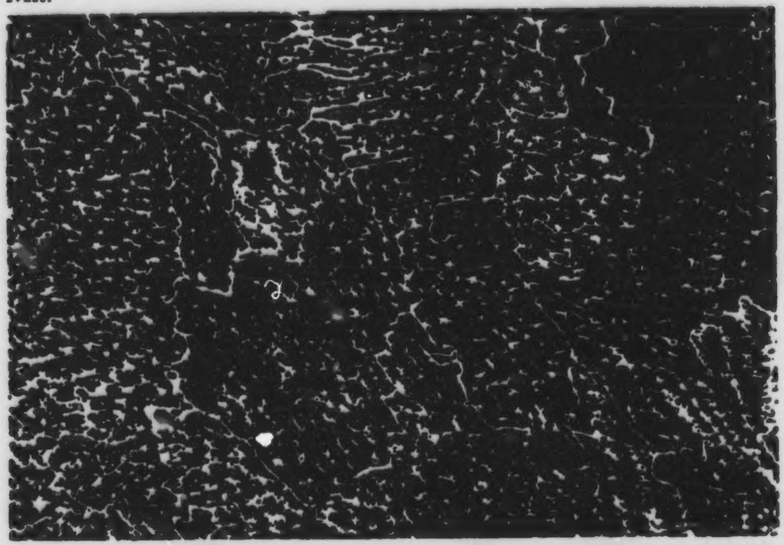

Figure 5. Optical micrograph of remelted material on Alloy 21 which contained 9.61-Al, 5.16-Ni, 5.6-Fe, 1.1-Mn, 0.61 Cr.

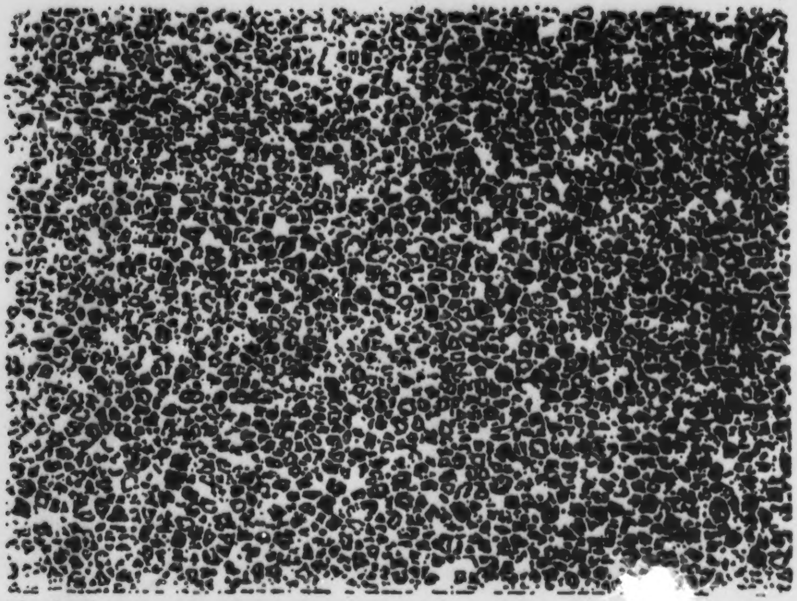

Figure 6. Optical micrograph of remelted material on Alloy 14 which contained 10.0 Al, 5.05 Ni, 6.3 Fe, 0.31 Mn, 1.08 Ti.

Limited electron microscopy on these alloys has been carried out. Examination of Alloy 21, laser surface melted with a heat input of 300 J/mm showed that this alloy contained predominately martensite and bainite with structures similar to those found in a Cu-9.0Al-4.6Ni-3.9Fe-1.2Mn laser cladding deposit produced with a heat input of 150 J/mm [36]. A typical region is shown in Fig 7. This Figure reveals a predominately two-phase microstructure containing martensite plates along with α or bainite. Numerous small (~20 nm) precipitates are also present. In-situ x-ray microanalysis indicated these precipitates are Fe and Cr rich, containing up to 20 % Cr. In contrast, Alloy 27 which contains Ti and Zr as well as Cr additions, exhibits a different microstructure when laser surface melted with the same 300 J/mm heat input. As shown in Fig. 8, the microstructure again consists mainly of α and martensite. However in this alloy, α is present with a more equiaxed morphology and a greater volume fraction. Several additional phases are also observed including small Fe/Cr rich precipitates similar to those found in Alloy 21 as well as somewhat larger Fe/Zr-rich particles. Further TEM studies are in progress to characterize the crystallographic structure of the precipitate phases in these alloys.

3.2. Corrosion Potential Measurements

The results of the corrosion potential measurements are summarized in Table 3. The results for Alloy 4, which was tested in both the as received condition (i.e. with the high temperature oxides still intact) as well as after grinding shows that the corrosion potential of the oxide film from welding is different from that of a ground sample. This supports suggestions in an earlier paper that oxides from welding may play a role in localized corrosion [30]. It is also interesting that the corrosion potential of surfaces produced at a lower heat input of 65 J/mm was generally more negative than those produced at a higher heat input 300 J/mm. This may be a result of a higher volume fraction of more metastable phases or of less tempering of the metastable phases in the more rapidly cooled lower heat input case. Further investigation of this observation is being carried out. The corrosion potentials of the higher heat input specimens, for all alloys examined, are similar to those of other marine copper alloys.

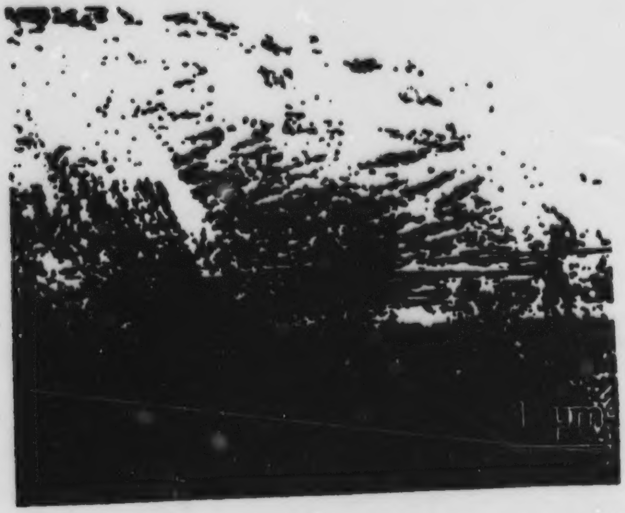

Figure 7. Transmission electron micrograph of remelted material on Alloy 21 revealing a predominately two-phase microstructure of martensite (dark irregular plates) and α (light rod like features). A high density of cuboidal Fe/Cr-rich precipitates is also present.

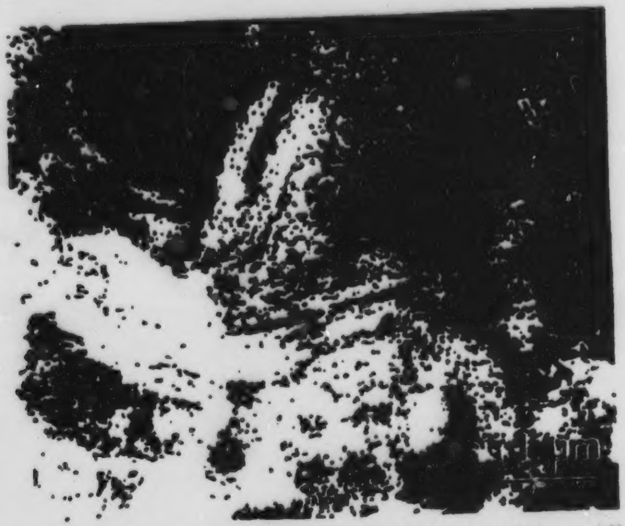

Figure 8. Transmission electron micrograph of remelted material on Alloy 27 revealing an α plus martensite structure. Compared with the microstructure shown in Fig. 7, there is more α and the α is more equiaxed. A high density of precipitates is also present.

In making the corrosion potential measurements, we noticed that the oxide films from welding in many cases were very hard and electrically resistant. Measurements were made with a hand held electrical resistivity meter. Those listed in table 1 as having high resistance generally could not be penetrated with the pointed steel prods of the hardened steel probes. With a few exceptions, the higher resistivity surface film seems to be favored by higher aluminum and higher heat input as well as by the presence of the experimental alloying additions Ti, Zr or Cr.

Table 3. Corrosion Potentials E_{corr} of Various Experimental Alloys with Laser Treated Surfaces in Deaerated Sea water at 25°C

Alloy Number	Laser Treatment					
	Heat Input = 65 J/mm			Heat Input = 300 J/mm		
	E_{corr} versus SCE [mV]		Surface Resistance	Ecorr versus SCE [mV]		Surface Resistance
	1st Reading	2nd Reading		1st Reading	2nd Reading	
1	-387	-385	Low	-335	-336	High
2	-381	-381	Low	-336	-335	High
3	-454	-454	Low	-354	-356	High
4	-412	-410	Low	-324	-325	High
4(a)	-394(a)	-	Low	-285(a)	-	-
5	-438	-438	Low	-	-	-
6	-	-	-	-	-	-
7	-	-	-	-	-	-
8	-378	-377	Low	-342	-342	Low
9	-479	-478	Low	-353	-355	Low
10	-425	-425	Low	-332	-332	Low
11	-457	-457	Low	-347	-348	Low
12	-	-	-	-	-	-
13	-	-	-	-	-	-
14	-397	-396	High	-287	-288	High
15	-	-	-	-	-	-
16	-	-	-	-	-	-
17	-	-	-	-	-	-
18	-435	-435	High	-339	-340	High
19	-	-	-	-	-	-
20	-311	-312	Low	-349	-349	High
21	-404	-403	High	-339	-340	High
22	-	-	-	-	-	-
23	-411	-410	High	-319	-319	High
24	-409	-409	High	-299	-300	High
25	-412	-412	High	-340	-340	High
26	-	-	-	-	-	-
27	-415	-415	High	-315	-316	High

3.3. Cavitation Erosion

So far in the evaluation of cavitation erosion behavior we have examined specimen topography and erosion performance. Often in cavitation erosion experiments , a porous surface is produced with fairly general attack. For nickel aluminum bronze this is true of both castings and conventional welds. However in a previous study [3], we noticed laser welds were preferentially eroded at the reheated zones during cavitation erosion. This allowed each laser pass to be seen and as a result the specimen appeared to have a raster pattern on its surface. In the cavitation erosion tests on the experimental alloys, four basic surface morphologies were observed on the specimens. Table 4 lists the morphologies which dominated for each specimen tested. Morphology (c) indicates that the tested surface exhibited a raster pattern with dispersed cracks. These cracks were often faintly visible on the pretest polished specimen surface. Three alloy compositions (6,9,13) exhibited cracking. Table 1 indicates that the aluminum content in these three specimens was over 12 weight percent. The only specimen with more than 12.0 percent Al which did not crack was specimen 15. Of these four specimens, specimen 15 was the only alloy where the percentage of Fe exceeded the percentage Ni. The only alloy composition to exhibit the porous morphology (p) expected on cavitation eroded nickel aluminum bronze was Alloy 19. This alloy had the lowest amount of Al content (8.8 percent) of any studied. It was also the only alloy which had a cellular dendritic microstructure. All the remaining specimens exhibited the raster wear pattern (r) observed in previous studies [6]. The zirconium bearing specimens tended to be much smoother (r/s), though the raster pattern could still be seen.

Table 4 and Figure 9 indicate that the overall erosion performance of an alloy depended strongly on its aluminum content. All alloy compositions containing in excess of 10.7 percent Al performed exceptionally well regardless of the visual appearance of the tested surface of the specimen. The only composition producing equivalent performance with less than 10.7 percent Al was specimen 25 which contained 9.64 percent Al and 1.72 percent Cr. The lowest performing alloys of the compositions listed in Table 1 were either low in Al (less than 9 percent) or contained additions of titanium of greater than 2 percent.

For the alloys tested, it is observed that chemistries which produce above average overall performance (i.e. time to 25 μm penetration) generally have both above average incubation times and above average erosion rates. Several of the alloy compositions have exceptionally low erosion rates (low slope) when compared to the standards recommended in ASTM G-32. The low erosion rates observed tend to reduce the sensitivity of the linear extrapolation method used by ASTM G-32 to determine the incubation time. As well, the surface is not homogenous. Thus, on some specimens the reheated zones and the as deposited material behaved differently. As a result, in simplification the measured curves could be considered a sum of the curves for each weld zone.

We are looking forward to the results of transmission electron microscopy studies on these alloys, because these may help us to understand what role the type and density of planar boundaries and other microstructural features played in determining the topography and cavitation erosion resistance of different weld zones and alloys.

Table 4 - Summary of the cavitation results contained in Appendix B.

Specimen ID	Incub Time (hrs)	Max. Rate (um/hr)	Specimen ID	Incub Time (hrs)	Max. Rate (um/hr)	Avg Incub Time (hrs)	Rank	Avg Rate (um/hr)	Rank	Elapsed Time to 25 um (hrs)	Rank
1A(r/s)	1.01	2.53	1B(r/s)	1.14	2.35	1.075	22	2.44	21	11.3209	21
2A(r)	2.55	1.42	2B(r)	2.56	1.49	2.555	7	1.455	11	19.7371	10
3A(r)	1.77	1.97	3B(r)	1.44	1.97	1.605	17	1.97	19	14.2954	19
4A(r)	2.62	1.59	4B(r)	2.55	1.56	2.585	6	1.575	14	18.458	12
5A(r)	2.00	1.82	5B(r)	1.45	1.76	1.725	13	1.79	16	15.6915	16
6A(c)	3.32	1.21	6B(c)	3.25	1.09	3.285	2	1.15	6	25.0241	4
7A(r)	2.49	1.04	7B(r)	2.30	1.05	2.395	9	1.045	2	26.3184	3
8A(r)	1.83	2.04	8B(r)	1.91	1.79	1.87	12	1.915	17	14.9248	17
9A(c)	3.06	1.07	9B(c)	1.94	1.22	2.5	8	1.145	5	24.3341	6
11A(r)	2.01	1.13	11B(r)	2.06	1.09	2.035	10	1.11	4	24.5575	5
12A(r)	4.45	1.44	12B(r)	4.03	1.27	4.24	1	1.355	8	22.6902	7
13A(c)	2.53	1.01	13B(c)	3.80	1.11	3.165	3	1.06	3	26.7499	2
14A(r/s)	2.02	1.56	14B(r/s)	f/t	f/t	2.02	11	1.56	13	18.0456	14
15A(r)	2.64	0.98	15B(r)	3.09	0.99	2.865	4	0.985	1	28.2457	1
16A(r)	2.78	1.33	16B(r)	2.50	1.48	2.64	5	1.405	9	20.4336	9
17A(r)	1.40	1.93	17B(r)	1.78	1.94	1.59	18	1.935	18	14.5099	18
19A(p)	1.07	5.59	19B(p)	0.93	5.87	1	24	5.73	25	5.363	25
20A(r)	1.71	1.45	20B(r)	1.21	1.37	1.46	19	1.41	10	19.1905	11
21A(r)	1.71	1.46	21B(r)	1.71	1.59	1.71	14	1.525	12	18.1034	13
22A(r)	1.86	1.70	22B(r)	1.48	1.73	1.67	15	1.715	15	16.2473	15
23A(r/s)	1.17	2.70	23B(r/s)	1.20	2.60	1.185	21	2.65	22	10.619	22
25A(r)	1.67	1.31	25B(r)			1.67	16	1.31	7	20.754	8

() letter in brackets refers to specimen surface morphology.
n/t - indicates weight loss numbers were influenced by porosity in specimen.
f/t - indicates a fatigue crack formed in the specimen before enough useful data could be recorded.

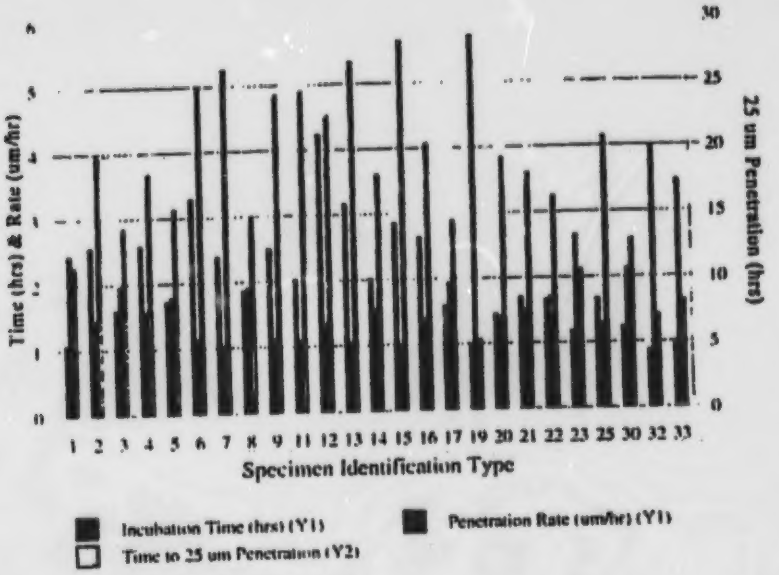

Figure 9. Cavitation erosion behavior

3.4. Temper Resistance

Typical results of the tempering experiments are shown in Figure 10. Briefly, specimen sets with higher contents of aluminum (≥ 11.30%) appear to have the greatest resistance to tempering. These sets also had high manganese contents (≥ 0.95%) and high nickel to iron ratios. In terms of the additions of Cr, Ti, Zr, the results suggest that Cr has little effect and Ti and Zr may have an effect in modifying behavior at long times and a temperature of 600°C. Here a tempering reaction seems to be occurring in the Zr containing alloy long after it is complete in the conventional one. This latter observation could be significant if a standard corrosion inhibiting heat treatment were applied to alloys containing Ti or Zr. These experiments are summarized in more detail elsewhere. Further work on the tempering and phase transformation behavior of these alloys, by metallography, hot stage microscopy, differential thermal analysis and quench dilatometry is planned. Eventually it is hoped that tempering-transformation diagrams will be developed, along with a clearer understanding of the reactions involved in tempering of these alloys.

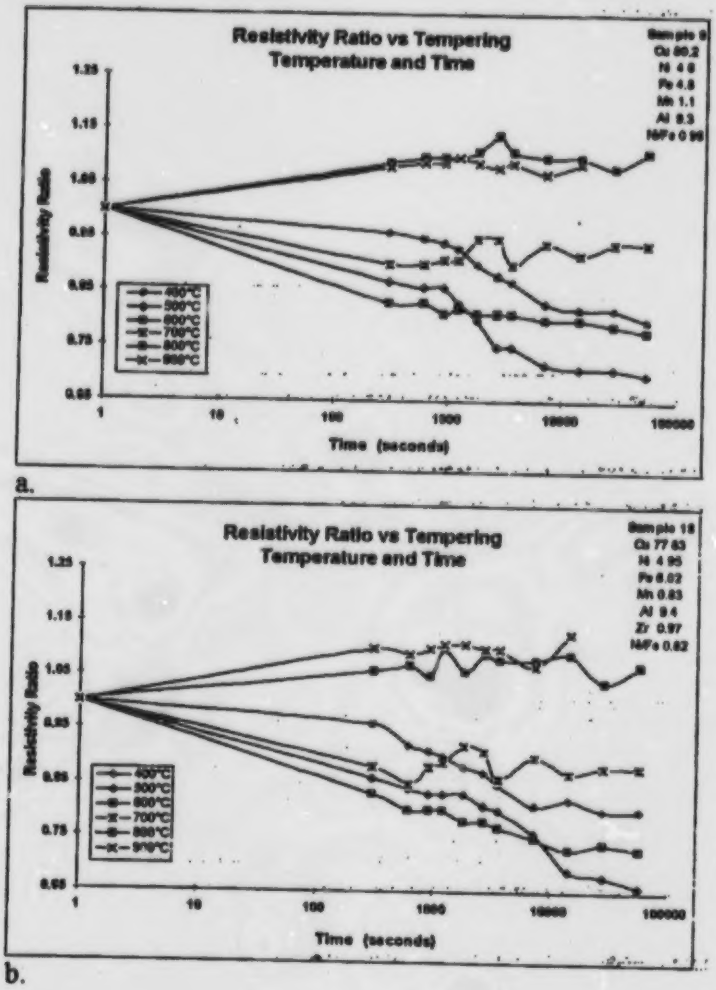

Figure 10. Typical results of resistivity measurements for otherwise similar specimens with (a)and without Zr (b).

4.0 CONCLUSIONS

Work to develop an optimum alloy for low heat input welding of nickel aluminum bronze has been started. Metallography shows that the structure and hardness of the remelted material and the reheated zones are sensitive to Ni/Fe as well as aluminum content. At the lowest aluminum content studied, the as deposited microstructure was cellular dendritic, the hardness was low and the cavitation erosion resistance was the worst measured among the alloy sets. As the aluminum content increased, the tendency of the reheated zone to soften was reduced, the hardness increased and the amount of α in the remelted and reheated zones was reduced. Also as aluminum content increased, the cavitation erosion resistance increased. High nickel seemed to favor a martensitic and bainitic high temperature transformation products, while high iron seemed to favor the formation of α in the remelted material. The addition of chromium seemed to increase the hardness of both remelted and reheated zones, suppressed the formation of α, and improve cavitation erosion resistance over that in otherwise equivalent alloys without chromium. The role of titanium and zirconium is less clear. Zirconium at least seems to promote the formation of a two phase α plus martensite structure in the remelted material. Cavitation erosion resistance seems to be lower, but it is interesting that the presence of this alloying element promotes a smoother surface during cavitation erosion. Technologically this could be useful from the perspective of the interaction between cavitation erosion and corrosion fatigue.

In summary, earlier work showed that laser welding is a technically viable means of improving and repairing high value components. It also showed that even with conventional consumable compositions, property improvements could be achieved. The work reported here reveals there are several routes by which an optimum alloy for low heat input welding of nickel aluminum bronzes might be developed and that results so far are promising.

5.0 REFERENCES.

1. P.J. Macken and A.A. Smith, *The Aluminum Bronzes, Properties and Production Processes*, CDA Publication 31, Herts, England, 1966.
2. F.L. LaQue, *Marine Corrosion*, Wiley, New York, 1975.
3. *Rules for Building and Classing Steel Vessels*, American Bureau of Shipping, Paramus, New Jersey, 1990, Section 37/2.
4. *Rules and Regulations for the Classification of Shipping*, Lloyds Resister of Shipping, London, England, 1978, Part 5, Chapter 7, Sections 2.1 and 3.1 and Part 2, Chapter 9, Section 1.
5. C.F. Zanis and R.J. Ferrara, *AFS Trans*, 1974, vol. 53, pp. 71-78.
6. J.C. Rowlands,., *Proc. 8th International Congress on Metallic Corrosion*, Mainz, Germany, 1981, pp.1346-1351.
7. R.J. Ferrara and T.E Caton, 1981, *Proc of Corrosion 81*, NACE, Houston, Texas, 1981, Paper 198.
8. E.A. Culpan and G. Rose, *British Corrosion Journal*, 1979, vol. 14, pp. 160-166.
9. C.W. Draper, *Lasers in Metallurgy*, The Metallurgical Society, Warrendale, PA, 1981, pp. 21-31.
10. C.W. Draper, *J. Mat. Sci*, 1981, vol. 16, pp. 2774 to 2780.

11. C.W. Draper, J.M. Vandenberg; C.M. Preece, and C.R. Clayton, *Rapidly Solidified Amorphous and Crystalline Alloys*, 1982, Elsevier, New York, pp. 529-533.

12. C.W. Draper and S. P. Sharma, *Thin Solid Films*, 1981, vol. 84, pp. 333-340.

13. C.W. Draper, S. P.Sharma, J. L. Yeh, and S. L. Bernasek, *Surface and Interface Analysis*, 1980, Vol. 2, pp. 179-182.

14. R.J. Taylor; D.A. Weston, G.M. Wright, and B.W. Turnbull, Sept. 1987, *Corrosion Australasia*, pp. 12-17.

15. N. Dubnyakov, I. B. Malysheva, and S. F. Pulim, *Sov. J. Friction and Wear*, 1986, vol. 7, Translation, New York, Allerton Press, pp. 70-76.

16. F. Hasan, A. Jahanafrooz, G.W. Lorimar, N. and Ridley, *Met. Trans.*, 1982, vol 13A, pp. 1337-1345.

17. Y. Liu, J. Mazumder, and K. Shibata, *Met. Trans.*, 1994, vol. 25A, pp. 37-46.

18. Y. Liu, M.E. Mochel, J. Mazumder and K. Shibita, *Acta Met.*, 1994, vol. 42, pp. 1763-1768.

19. Y. Liu, J. Mazumder, and K. Shibata, *Met.Trans. B*, 1994, vol. 25B, pp. 749-759.

20. C.V. Hyatt, K.H. Magee, J. Hewitt and T. Betancourt, Laser Weld Cladding of Nickel Aluminum Bronzes, in *Abstracts and Summaries of the 2nd CF/CRAD Meeting on Naval Applications of Materials Technology*, 1995, J.R. Matthews, ed., Defence Research Establishment Atlantic, Dartmouth, Nova Scotia, pp. 226-252.

21. C.V. Hyatt, and K.H. Magee, in *Proceedings of Advanced Methods of Joining New Materials II*, The American Welding Society, Miami, Florida, 1994, pp. 111-126.

22. D.E. Bell, Master of Science Thesis, *Microstructural Development and Corrosion Resistance of Laser-Welded Nickel Aluminum Bronze*, Pennsylvania State University, 1993.

23. K. Petrolonis, *Laser Welding and Continuous Cooling Studies of Nickel Aluminum Bronze*, Master of Science Thesis, The Pennsylvania State University, 1993.

24. P.J. Oakley and N. Bailey, in *Proc. International Conference on Power Beam Technology*, 1986, The Welding Institute, Cambridge, England, pp. 301-314.

25. F. Hansan, G.W. Lorimar and N. Ridley in *Proceedings Conference on Phase Transformations*, 1987, Cambridge, U.K., pp. 131-134.

26. D.E. Bell, K. Petrolonis and P.R. Howell, in *Proc. International Trends in Welding Science and Technology*, S.A. David and J.M. Vitek Eds, Gatlinburg, TN, pp. 301-305.

27. D.E. Bell, T.A. Marsico, K. Petrolonis, P. E. Denney and P.R. Howell, *Metallography: past, Present and Future*, ASTM STP 1165, 1995, G.F. Vander Voort, F.J. Warmoth, S.M. Purdy and A. Szirmae, Eds., ASTM, Philadelpia, Penn., pp. 327-434.

28. J. Hewitt, Laser Weld Overlaying of Marine Components and Alloys, DREA CR/95/525, Defence Research Establishment Atlantic, Dartmouth, Nova Scotia.

29. J. Hewitt, V.E. Merchant, C. Hyatt, and D.O. Morehouse, Laser Beam Welding of Nickel Aluminum Bronze with a Fine Wire Feeder, Presented at the 78th Annual AWS Convention, Written Version of the Paper is being prepared for the Welding Journal.

30. C.V. Hyatt, K.H. Magee, and T. Betancourt, The Effect of Heat Input on the Microstructure and Properties of Nickel Aluminum Bronze Laser Clad with a Consumable of Composition Cu-9.0Al-4.6Ni-3.9Fe-1.2Mn, In internal review, for submission to Metallurgical Transactions.

31. K.H. Magee, "Laser Cladding of Marine Copper Alloys," DREA CR/94/424, Defence Research Establishment Atlantic, Dartmouth, Nova Scotia 1994..

32. P. Brezina, *International Metals Reviews*, 1982, vol. 27, pp. 77-120.

33. S. Kumar, International Metals Reviews, 1990, 35, 6, 294-327.

34. C.V Hyatt, *Review of Literature Related to Microstructural Development During Laser Surface Engineering of Nickel Aluminum Bronze, DREA Technical Memorandum*, TM/96/227, 1996, Defence Research Establishment Atlantic, Dartmouth, Nova Scotia.

35. J.C. Bennett, Microstructural Characterisation of Laser-Clad Nickel Aluminium Bronze Alloys by Transmission Electron Microscopy, DREA/CR/96/442, Defence Research Establishment Atlantic, Dartmouth, Nova Scotia, 1996.

36. J.C. Bennett and C.V. Hyatt, *TEM Study of NiAl Bronze Laser-Weld Claddings*, Proceedings of the 1997 Microscopical Society of Canada General Meeting, 1997, vol. 24. pp70-71.

37. *ASTM Standard G5-87, Standard Reference Test Method for Making Potentiostatic and Potentiodynamic Anodic Polarization Measurements*. 1987 Annual Book of ASTM Standards, Vol. 03.02. pp. 124-131, Philadelphia, PA.

38. *ASTM Standard G32-85, Standard Method of Vibratory Cavitation Erosion Test. 1987 Annual Book of ASTM Standards*, Vol. 03.02, pp. 187-194. ASTM, Philadelphia, PA.

39. C.V. Hyatt and B. Armstrong, Metallographic Characterization and Microhardness Testing on Experimental Alloys Laser Surface Melted With Heat Inputs of 10, 65 and 300 J/mm. DREA Lab Note, In Prepartion.

40. G. Pelletier, C.V. Hyatt, "Tempering Resistance of Experimental Nickel Aluminum Bronze Alloys", DREA DL/RN/97/6.

#567219 ⑯

Laser Processing of Nickel Aluminum Bronze for Use in Propeller Fabrication and Repair

by

Dr. T.A. Marsico

Applied Research Laboratory
The Pennsylvania State University
165 Applied Science Building
University Park PA 16802

ABSTRACT

Laser beam materials processing technology was first employed on nickel aluminum bronze (NAB) cast components by the Applied Research Laboratory, The Pennsylvania State University (ARL Penn State) in 1989 to meet the stringent tolerance requirements of newly designed components and to provide a viable economic means of repairing existing damaged components. Laser beam welding (LBW) offers a low heat input process resulting in much less distortion of the workpiece as well as reduced residual stresses when compared to that observed in components welded using GMAW. Laser beam cladding (LBCL) is the process of melting alloying elements onto the surface of a metal to repair mechanically-induced structural damage and it can also be used to improve the wear and corrosion resistance of the base alloy.

Techniques have been developed for laser beam welding and cladding NAB cast and wrought materials using both high power carbon dioxide ($C0_2$) and neodymium yttrium aluminum garnet (Nd: YAG) laser systems respectively. The specifics of these techniques will be presented. Also, two approaches for LBCL NAB material onto NAB cast substrate have been developed by: i) melting NAB powder onto the substrate using a rather low power density rastering beam, and ii) melting NAB wire onto the substrate using a defocused high density beam. The resultant macro and microstructures of the two types of clads will also be presented.

PRESENTATION OUTLINE

- Program Objectives (Original)
- Program Objectives (Redirected)
- Work Accomplished (through FY '95)
- Ongoing Work (FY '96)
- Future Plans

PROGRAM OBJECTIVES
(Original)

- Development of LBW processes and procedures for use on the SSN 21, SSN 688, and SSBN 726
  - minimize distortion of component
  - minimize residual stresses in component
  - reduce manufacturing costs
  - improve corrosion-resistance
  - improve cavitation-resistance
- Qualification of developed processes
- Transfer of technology to Navy facilities

BENEFITS OF LASER MATERIALS PROCESSING ON PROPULSOR COMPONENTS

- Due to low heat input, starting and stopping minimized - continuous welding
- Parts can be welded in near final dimensions - machining costs reduced
- Less residual stress associated with laser welding process

PROGRAM OBJECTIVES
(Redirected FY '93)

- Development of laser-based repair and refurbishment processes and procedures for NAB components
  - LBW procedures
  - LBCL procedures
  - Development of processes using portable Nd:YAG
  - Robotic systems
- Qualification of developed processes
- Transfer of technology to Navy facilities

WORK ACCOMPLISHED
(through FY '95)

- Laser Beam Welding Procedures
- Laser Beam Cladding Procedures
- Thermocouple Studies
- Accelerated Corrosion Testing
- Long Term Corrosion Testing
- Cavitation Testing
- Fatigue Studies
- Tensile Test Results
- X-ray Residual Stress Analysis
- Microstructural Analysis

WORK ACCOMPLISHED (cont.)
(through FY '95)

Laser Beam Welding:

- Development of LBW techniques for NAB wrought plate and cast materials
  - 14 kW and 25 kW CO2 industrial lasers coupled to LARS units
  - thicknesses up to 5/8", with or w/out filler wire (e.g., 5/8" @ 23 kW, ~35 ipm)
  - LARS vision system/seam tracking for contoured surfaces

WORK ACCOMPLISHED (cont.)
(through FY '95)

Laser Beam Welding:

- Microstructural analysis of the metals meeting MIL 24480 has shown great variations in structure due to compositional fluctuations (w/in spec.) and thermal processing history
- Weld metal consists of proeutectoid α + martensite (same as that seen in conventional welds but on a much finer scale)
- Fatigue studies have shown that the laser welds fall w/in the same strength levels as the base metal casting while conventional welds were found to fail at significantly lower strength levels

WORK ACCOMPLISHED (cont.)
(through FY '95)

Laser Beam Welding:

- Long term corrosion tests have shown laser welds will perform at least as well as conventional welds
- Accelerated corrosion tests have shown that in the HAZ, martensite is anodic with respect to the surrounding α phase (less martensite is produced in laser welds when compared to that of conventional welds) and in areas adjacent to the base metal, α phase is anodic with respect to κ_{iii} phase
- Ultra-high speed cavitation tests (in fresh water) have shown that the laser weld will perform at least as well as the base metal casting and conventional weld materials

WORK ACCOMPLISHED
(through FY '95)

Laser Beam Cladding:

- Developed 3 techniques for laser beam cladding NAB onto NAB
  - rastering laser beam with powder deposit
  - nonrastering laser beam with powder deposit
  - nonrastering laser beam with wire deposit
- Each technique has unique advantages
  - maximum deposition rate = rastering beam w/powder
  - out-of-position cladding = nonrastering beam w/wire
- Each technique produces unique microstructures
  - rastering beam w/powder = primarily proeutectoid α (relatively soft, corrosion-resistant)
  - nonrastering beam w/wire = martensite + proeutectoid α (harder, wear-resistant)

WORK ACCOMPLISHED (cont.)
(through FY '95)

Laser Beam Cladding:

- Thermocouple studies indicate a maximum temperature at the fusion line of 1331 °C and a preheat of ~80 °C between passes when cladding using a nonrastering beam w/wire deposit
- Dilatometry and DTA analyses have been used to better determine the melting and solidification temperature ranges of the base metal and the temperature ranges where critical phase transitions occur
- Ultra-high speed cavitation tests indicate that the laser beam clad (rastering beam w/powder) will perform at least as well as the base metal casting

WORK ACCOMPLISHED
(through FY '95)

Thermocouple Studies:

Peak Temperature and Cooling Rate

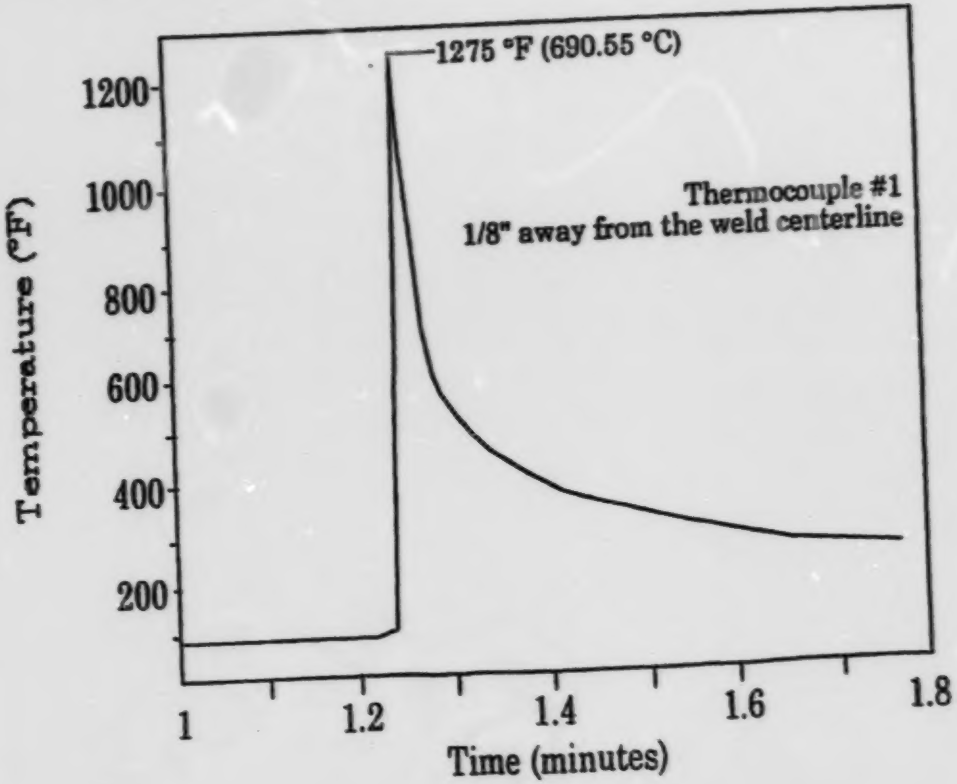

WORK ACCOMPLISHED
(through FY '95)

Corrosion Studies:

- Long Term Testing (300+ Days)
  - NRL Key West Facility
  - Flowing Sea Water
  - Base, LBW, MIG Welds Tested
  - LBW's will behave at least as well as the conventional welds
- Accelerated Testing
  - Two Methods
    - > weight loss
    - > electrochemical
  - Two HAZ areas susceptible to corrosion but less HAZ area in LBW when compared to conventional weld

WORK ACCOMPLISHED
(through FY '95)

Cavitation Studies:

- Fresh Water
  - ARL Penn State Ultra-High Speed Water Tunnel
  - Base, LBW, MIG Welds, and LBCL
  - Laser Beam Processed NAB Behaved at Least as Well as the Base Metal
- Salt Water
  - Water Jet Hammer (ASTM G32)
  - Cavitation Erosion
  - Base and Laser Processed NAB
  - Laser Beam Processed NAB Behaved at Least as Well as the Base Metal Casting

WORK ACCOMPLISHED
(through FY '95)

X-ray Residual Stress Analysis:

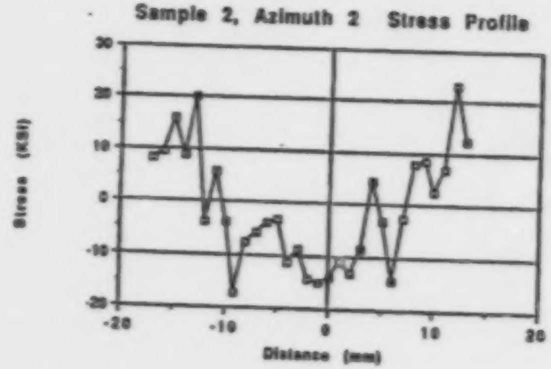

Conventional Arc Weld

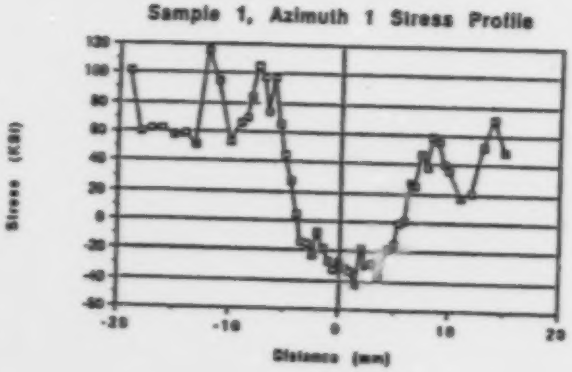

Laser Weld

- Transverse scans across laser and arc weldments
- Both laser and arc welds were in compressive stress states
- Machining stresses were detected
- Laser welded material experiencing residual stress was 1/2 the volume of that seen in arc weldments

WORK ACCOMPLISHED
(through FY '95)

Tensile Test Results:

- Tensile Testing
  - Base metal casting = 55.7 ksi ys
  - LBW ~ 66.4 ksi ts, ~34.3 ksi ys
- Microhardness
  - Base metal casting ~ 150 VHN
  - LB Processes (wire) ~ 260 VHN
  - LB Processed (powder) ~ 170 VHN

WORK ACCOMPLISHED

(FY '96)

- Welding procedures and joint configurations have been demonstrated that include autogenous and filler-added LBW of as-cast to as-cast and as-cast to wrought NAB in joint thicknesses up to 5/8" with join gaps up to 1/8"
- LBCL processes and procedures have been developed for depositing Inconel 625 onto NAB and for NAB deposited onto steel substrates
- LBCL processes and procedures have been developed for depositing NAB onto Al alloys (shear strengths ~ 22 ksi, NAB on NAB shear strengths ~28 to 30 ksi)
- LBW Distortion Measurements (NSWC)
  - Mock "conventional" joints compared to conventional welding processes
  - LBW distortion ~0.094" in the longitudinal direction, less than any other welding process
  - Mock "laser" joints produced ~0.031" longitudinal distortion, significantly less than any other welding process

WORK ACCOMPLISHED
(FY '96)

- LBW was included in the fabrication of the LSV
- Laser beam welds can be made within 1/8" of temperature-sensitive material (adhered to 3/8" thick NAB) without degradation of the material or the adhesive (3 different adhesives were tested)
- The 3c demo piece was LBW for NSWC using the LARS
- A full scale 688 blade was seam tracked and laser welded using the LARS
- ARL Penn State was awarded a Laser Line Bending Program by ARPA with Rocketdyne, Newport News, Ingalls, Boeing, and MIT for forming complex shapes using differential laser heating techniques
  - "Dishing" of 0.25" thick NAB wrought plate has been demonstrated

WORK ACCOMPLISHED
(FY '96)

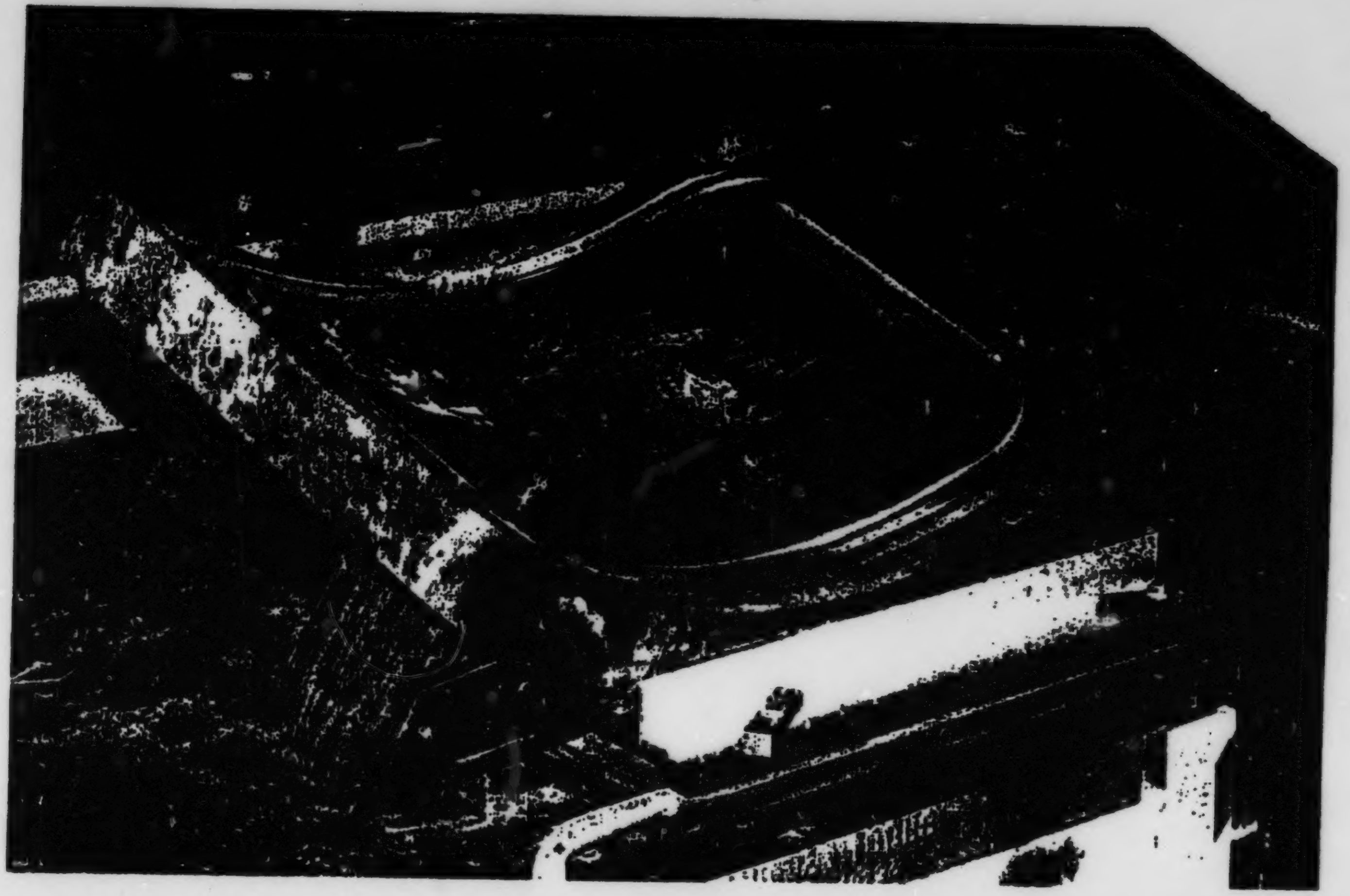

Laser beam welded mock joint for NSWC, seam tracked using LARS

WORK ACCOMPLISHED
(FY '96)

Laser beam welded SSN 688 blade, seam tracked using LARS

WORK ACCOMPLISHED
(FY '96)

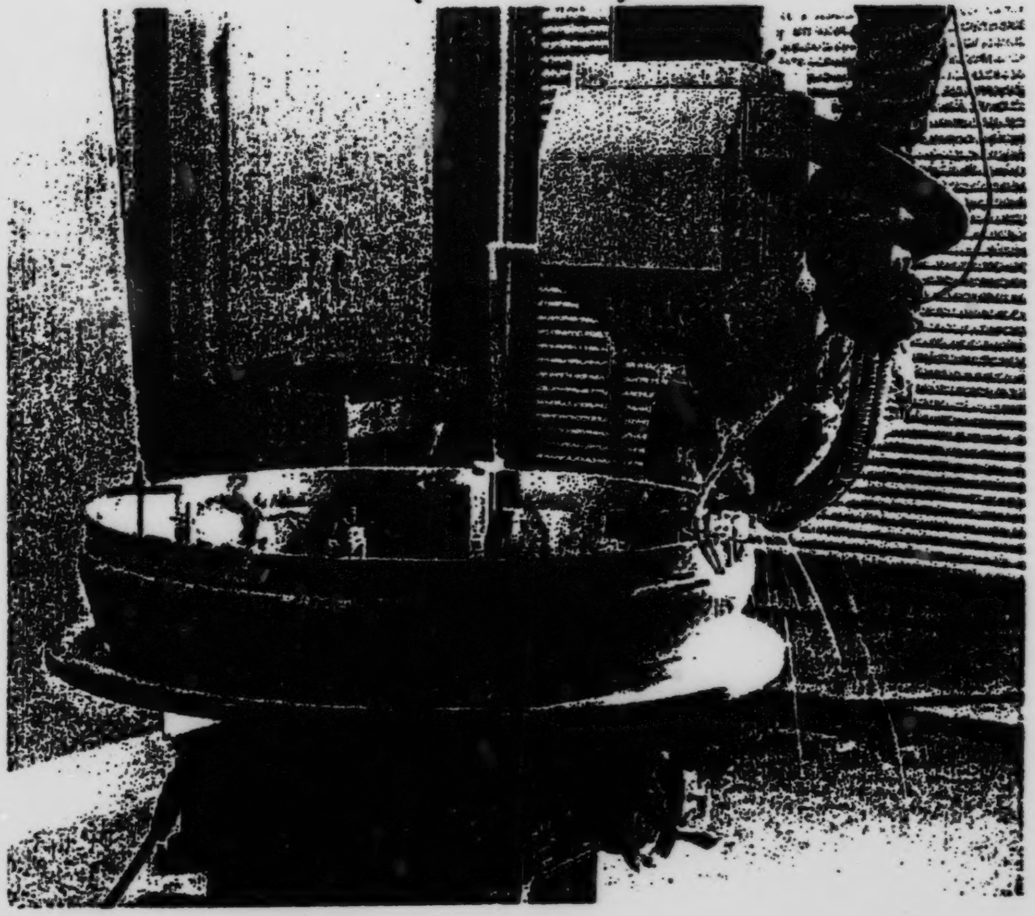

Laser beam welded circular component for LSV, welded using LARS

FUTURE PLANS

- Qualify LBW processes using the LARS and CE 25 kW CO_2 Systems
- Qualify LBCL processes using the LARS and CE 25 kW CO_2 Systems
- Qualify LBW processes using the Hobart 3 kW Nd:YAG System (at 2.4 kW power levels)
- Qualify LBCL processes using the Hobart 3 kW Nd:YAG System (at 2.4 kW power levels)
- Write NAB Technical Reports

#507220 ⑰

Microstructural Characterization of Laser-Clad Nickel Aluminum Bronze Alloys by TEM

by

J.C. Bennett, Department of Physics, Acadia University

and

C.V. Hyatt, Defence Research Establishment Atlantic

ABSTRACT

Recently, the use of high power lasers for surface melting and cladding of nickel aluminum bronze (NAB) components has stimulated renewed interest in the microstructural development of these alloys. In this study, a laser-clad NAB weldment of nominal composition Cu - 9 wt. % Al - 5 wt. % Ni - 4 wt. % Fe - 1 wt. % Mn, provided by DREA was examined using transmission electron microscopy. Significant variations in the microstructure were observed between the weld deposit and heat affected zone of the clad. In the weld deposit, the microstructure predominantly consisted of two phases which are the product of martensitic or possibly bainitic phase transformations. A high density of Fe-rich precipitates, ranging up to 200 nm in size, are also distributed throughout both matrix phases. In the heat affected zone, the microstructure typically contained three major phases: a martensitic phase similar to that observed in the deposit region, the fcc α phase, and an $(\alpha + \kappa)$ eutectoid. The small Fe-rich precipitates are retained in the martensitic phase. The observed phase relationship and morphologies will be discussed in terms of the transformation behaviour of the NAB clad.

Microstructural Characterization of Laser-Clad Nickel Aluminum Bronze Alloys using Transmission Electron Microscopy

INTRODUCTION

Nickel aluminum bronze (NAB) alloys are used for many marine applications due to their excellent sea water corrosion resistance and good mechanical properties. At the Defence Research Establishment Atlantic, laser surface modification techniques such as cladding and surface melting are being investigated for the repair and surface engineering of NAB alloy components [1]. In these processes, a high intensity laser is focussed to melt a thin surface layer [2]. Since the melting occurs over a very short time, the bulk of the component remains cool and acts as an infinite heat sink. The consequent very rapid self-quenching and resolidification which occurs may in turn generate metastable phases. Currently, there is little data available concerning the microstructures produced in laser processed NAB alloys. In this paper, transmission electron microscopic (TEM) observations of the microstructure developed in a commercial (C95800) NAB alloy cladding are reported.

NAB alloys of interest for marine applications typically contain from 8 to 13 wt.% Al, 4 to 5 wt.% Ni, and 4 to 5 wt.% Fe along with smaller amounts of Mn and Si. To facilitate discussion of the microstructural features found in these alloys, the relevant vertical section of the equilibrium phase diagram is shown in Figure 1 [3]. For NAB alloys with Al contents near 10 wt.%, the solid solution β phase with bcc crystal structure is stable at high temperatures. Upon cooling, proeutectoid α with fcc crystal structure precipitates along with several ordered intermetallic phases, collectively referred to as κ. In quenched samples, a metastable β' phase may also be observed with a volume fraction dependent on the degree of undercooling. Several previous studies [4,5] have indicated that the β' phase is the product of a martensitic phase transformation. The crystallographic data reported for the various phases in the NAB phase diagram are summarized in Table 1.

Several previous investigations of the microstructure of NAB alloys in the as-cast and tempered condition have been carried out using TEM [6-8]. However, for laser clad and laser surface melted NAB alloys, only limited microstructural data is currently available [5,8,9]. These studies indicate that laser processed NAB alloys contain novel precipitate and matrix phases whose stability is sensitively determined by alloy composition and cooling rate from the β field. It is thus important to characterize laser processed materials under conditions corresponding as closely as possible with actual metallurgical practice.

EXPERIMENTAL

The NAB weldment studied was supplied by DREA and produced using a laser cladding technique described previously [1]. Briefly, a coupon of composition Cu - 8.6 wt.% Al - 4.8 wt.% Ni - 4.0 wt.% Fe - 1.1 wt.% Mn was clad by scanning a laser beam while simultaneously feeding a welding wire of composition Cu - 9.0 wt.% Al - 4.6 wt.% Ni - 3.9 wt.% Fe - 1.2 wt.% Mn into the melt pool. The resultant deposit was composed of small overlapping beads which were directly related in size to the dimensions of the melt pool during the single scan of the beam. A laser beam heat input of 1.2 kJ/cm was used for these experiments. Figure 2 shows schematically a section of the clad deposit with the location of the as-deposited, reheat and heat affected zones indicated.

Specimens for TEM were obtained by sectioning the coupon parallel to the clad surface using a low speed saw. A surface layer from 0.1 - 0.3 mm thick was removed and then the sections were backed thinned to 0.1 mm using a range of SiC grinding papers (240-600 grit). After punching the 3 mm diameter disks required for TEM, further mechanical polishing reduced the thickness to ~100 μm. Since the deposit region is known to extend to a depth of at least 1000 μm under these laser processing conditions, the above procedure limited examination to the as-deposited and reheat zones of the cladding.

The 3 mm disks were thinned to electron transparency in a Tenupol-3 jet electropolisher using a 33 % nitric acid/methanol solution. It was observed that attainment of the polishing condition depended very sensitively on the experimental parameters. For example, cooling of the electrolyte in the range -30 to -40 °C was essential to avoid extensive pitting of the specimens. The optimum polishing condition was obtained with a potential difference of 11 V and a slow to moderate electrolyte flow speed which resulted in a polishing current of 0.2 - 0.25 A. Larger currents invariably resulted in etching rather than polishing of the specimens.

The position of the electron transparent region with respect to the as-deposited and reheat zones was established by visual inspection using a stereomicroscope. The procedure consisted of replacing the polished 3 mm disks within the sections which had been previously etched in $FeCl_3$/HCl/methanol solution to reveal the zones of interest. In addition, the sections were also mounted for optical microscopy in plan view.

Electron microscopy of the thin foils was carried out with either PHILIPS EM300 or CM20 transmission electron microscopes operating at 100 and 200 kV, respectively. Microanalysis of selected phases in the thin foil specimens was performed with the CM20 microscope using an energy-dispersive x-ray detector. Quantitative analysis was obtained using the ratio technique [11] and calculated k-factors.

RESULTS

Typical optical micrographs obtained for the as-deposited and reheat zones are shown in Figure 3. The observed microstructures are similar to those reported previously for laser clad NAB alloys [1,2,12]. Light etching material is generally observed on the prior β grain boundaries and as elongated rods within the grains, corresponding to allotriomorphic and Widmanstatten α, respectively. The dark etching regions have usually been interpreted as martensite. For the claddings, comparable microstructures were observed in the as-deposited and reheat zones, however the Widmanstatten α plates were considerably coarsened in the latter case. The results of the optical metallography confirmed that all of the specimens examined in the TEM were representative of either the as-deposited or reheat zones of the cladding.

Figure 4 shows a typical TEM micrograph of the as-deposited region and reveals a predominantly dual phase microstructure consisting of lighter contrast (more electron transparent) rods separated by irregular, darker contrast plates. A pronounced acicular morphology for the rods was evident within the former β grain interiors. In addition, a high density of small (~20 nm), roughly cuboidal precipitate particles were dispersed throughout both the rods and plates. X-ray microanalysis of the rods and plates yielded similar results, close to the nominal composition of the bulk coupon, with only small differences in Al and Ni content between the two regions. Conversely, the precipitates were substantially enriched in Fe and Ni in comparison to the bulk (Table 2).

Selected area electron diffraction (SAD) and diffraction contrast imaging of the acicular rods suggests several variants may be present in the as-deposited region. A relatively small fraction of the rods were distinguished by varying numbers of stacking faults appearing in isolation or in clusters (Figure 5). Analysis of the SAD patterns revealed a crystal structure based on the fcc unit cell with a lattice parameter of ~0.375 nm, confirming that these rods are composed of Widmanstatten α. Convergent beam electron diffraction (CBED) patterns obtained using a probe ~15 nm diameter (Figure 6) are consistent with the space group Fm3m expected for the fcc α phase. The CBED analysis also revealed no orientational change occurred on crossing the positions of the faults, confirming their displacive nature. No evidence of solute ordering was detected in the SAD or CBED patterns.

The majority of the rods in the as-deposited region contained a uniform density of stacking faults spaced about 0.6 nm apart (Figure 7). Superimposed on this regular array of defects, random faulting was also observed. The SAD patterns from the rods revealed pronounced streaking of the diffraction spots, associated with the random faulting, as well as additional satellite reflections. As a result, the observed SAD patterns could not be indexed as any simple close-packed crystal structure such as fcc or hcp (hexagonal close-packed). The presence of the stacking fault array indicated that the most suitable crystallographic description for this phase was in terms of an interface modulation of the fcc structure of the parent α phase via the periodic insertion of stacking faults on every third close-packed plane. Similar interface modulated superstructures have been reported for martensitic phases arising in some NAB and related alloys [9,13,14].

The interface modulated superstructure described above is generated through the periodic repetition of modules consisting of close-packed layers separated by stacking faults on the $\{111\}_{fcc}$ planes. For such an interface modulation, satellite reflections occur at positions shifted relative to those of the parent structure by an amount inversely related to the period of the faulting [15]. Rather than using an fcc unit cell, it is convenient to specify the satellite shifts based on a primitive hexagonal unit cell with the c-axis chosen perpendicular to the close-packed plane. Using this approach, the position of the parent (1100) reflection is located geometrically and taken as a reference point for measurements of the fractional shifts. In the observed SAD patterns, the $k = 1$ and $k = -1$ satellites were shifted in opposite directions, indicating a rhombohedral symmetry for the modulation. Information on the stacking mode can also be deduced from the intensity distribution of the satellites. SAD patterns calculated on the basis of a 9 layer stacking module (ABCBCACAB where A, B and C are close-packed planes) were found to be in good agreement with the experimental intensities (Figure 8). The SAD patterns can thus be indexed as an unordered 9R structure.

TEM observations of the irregular, dark plates revealed that these were composed of narrow, acicular lamellae ranging in width from 10-50 nm (Figure 9a). Stacking faults spaced ~0.6 nm apart may also be observed within the twin lamellae in high magnification images (Figure 10). While the streaking of the diffraction spot renders SAD patterns difficult to measure accurately, the results were generally consistent with an interface modulated 9R superstructure. In addition, SAD showed that the lamellae were twin-related with twinning occurring on the $\{200\}_{fcc}$ planes (Figure 9b). Elongation of the diffraction spots along the direction of twinning suggests the interface is not fully coherent. Similar finely twinned martensites have been previously observed in quenched NAB alloys [4].

The martensite lamellae and the 9R α phase rods were crystallographically identical, however the difference in scale suggests these features formed under differing thermal regimes. In addition, EDX microanalysis indicated that the martensite was enriched in Al relative to the 9R α phase. Note also that the observed similarity in electron transparency, morphology and chemical composition indicates a close relationship exists between the fcc and 9R α phases. Hence, the TEM observations would appear to be consistent with a bainitic origin for the 9R α phase. However, due to the presence of several precipitation reactions which complicate the interpretation of the compositional data, further studies are needed to definitively establish the nature of the 9R α phase.

A high density of small, cuboidal precipitates were characteristically observed in both the martensite and 9R α phases. The precipitates ranged from 20-50 nm in size and were Fe-rich according to EDX microanalysis. A typical distribution of precipitates in the 9R α phase (orientated with the stacking faults out of contrast) is shown in Figure 11. For precipitates very near the edge of the foil, it was occasionally possible to obtain electron microdiffraction (MD) patterns, which were free of intensity contributions from the surrounding matrix. (Figure 11 inset). The MD patterns were indexed in terms of an ordered B2 crystal structure, suggesting that these precipitates are related to the κ_{IV} or κ_{II} particles previously reported to occur in cast NAB alloys. The precipitates in the martensite exhibited a similar size distribution, chemical composition, morphology and crystal structure as those in the 9R α phase.

It was not possible to deduce a consistent orientational relationship between the precipitate and matrix phases based on the MD studies. However, it was very difficult in practice to locate high symmetry zone axes for all but the largest of the precipitate particles, i.e. those approaching 50 nm in size. In the TEM images, characteristic "lobe" diffraction contrast associated with coherency strain fields was often observed around the smaller precipitates. This suggests that there exists a critical precipitate size for loss of coherency in this system. Such a critical size effect would normally occur if the surface energy of the precipitates becomes small relative to the coherency strain energy as the particle size increases. A coherency size effect of this type may account for the observation of ring diffraction patterns formed by the precipitates in SAD patterns obtained using a large area-selecting aperture (Figure 12). The intensity in these ring patterns would be expected to be dominated by contributions from the largest precipitate particles, which are incoherent with the matrix phases. Further studies are in progress to ascertain the influence of precipitates on mechanical properties and grain refinement in NAB alloys.

The microstructure observed in the reheat zone of the cladding is broadly similar to that described above for the as-deposited region. However, in the reheat zone, the α phase contained very few precipitates, was largely free from stacking faults and in many areas adopted an equiaxed rather than rod-like morphology. SAD and CBED analyses indicated an fcc crystal structure with space group $Fm\bar{3}m$ for the α phase in the reheat zones. No α particles having the 9R crystal structure were detected. The martensite in the reheat zones is crystallographically identical to that in the as-deposited regions, retaining the 9R structure and a high density of Fe-rich precipitates. While the average plate size was somewhat reduced, the martensite still consisted of narrow, twin-related lamellae ranging from 10-50 nm in width. The size, morphology and crystal structure of the precipitates found in the martensite was also unchanged.

In many parts of the reheat zone, a microstructure consisting of a light contrast phase containing numerous elongated precipitate particles was observed (Figure 13). SAD, CBED and EDX microanalysis indicated that the matrix corresponded to the fcc α phase described above while the elongated precipitates were considerably different from those observed elsewhere. SAD patterns from the precipitates were indexed in terms of a B2 structure with lattice parameter a = 0.26 nm. EDX microanalysis yielded an average composition of 24 wt.% Cu - 27 wt.% Al - 29 wt.% Ni - 20 wt.% Fe, indicating that the elongated precipitates were Ni-rich in contrast to the cuboidal, Fe-rich precipitates found in the martensite, 9R α and fcc α phases. The morphology, unit cell and composition of the elongated precipitates is similar to that reported by Hasan et al. for κ_{III} particles in as-cast NAB alloys [6]. The TEM observations are consistent with the formation of $(\alpha + \kappa_{III})$ eutectoid in the reheat zone. Within these eutectoid areas, the α phase was predominantly present as grain boundary allotriomorphs rather than Widmanstatten plates. Note that limited eutectoid formation also occurred in the vicinity of prior β grain boundaries within the as-deposited regions of the cladding.

DISCUSSION

The phases observed in the present TEM study are consistent with the results of previous studies of laser-processed NAB alloys. The most extensive work has been performed by Liu and co-workers [5,9,16] who examined a NAB laser-cladding produced on an aluminum substrate. These workers identified two types of martensite which were designated sheet or lath based on their morphology. The sheet martensite had a 9R structure and corresponds to the martensitic phase identified in the present study while the lath martensite, which had a fcc crystal structure, would appear to correspond to either the 9R or pro-eutectoid α phase reported here.

The formation of Fe-rich precipitates in NAB alloys has been reported by several workers [6,8,16]. Most of these studies have concluded that the Fe-rich precipitates form prior to the martensitic transformation. In the current study, the observation in SAD patterns of "spotty" diffraction rings produced by the precipitates, suggesting some degree of preferred orientation, supports this conclusion. Hence, the TEM results indicate that the decomposition of β to α + κ_{IV} occurs well above the martensite start temperature, M_s.

No direct evidence regarding the role of solute diffusion in the transformation producing the α phase is currently available. However, the results of Hasan et al. [6] for cast NAB alloys indicate that Widmanstatten α precipitates from the β phase under conditions where diffusion is likely to be important. From a crystallographic point of view, the 9R α phase and martensite have similar interface modulated superstructures with a high density of randomly occurring stacking faults. EDX analysis indicates that the Al content of the 9R α phase is slightly lowered while the plate size is much larger relative to that of the twin-related lamellae in the martensite, implying these features formed under different temperature conditions. The TEM observations are therefore consistent with a bainitic origin for Widmanstatten α having the 9R structure. Similar bainitic phases have been reported in the Cu-Al-Ni [14] and Cu-Al-Zn [17] alloy systems.

Due to the steepness of solubility lines, the mechanisms governing the phase stability in both the as-deposited and reheat zones of the cladiing depend sensitively on composition as well as cooling rate. Although further studies are required to obtain a detailed understanding of these processes, the TEM results point to the following general model. NAB initially solidifies as the bcc β phase and, upon further cooling, decomposes to the α phase precipitates from β, probably via a bainitic transformation. The presence of Ni and/or Fe alloying elements apparently lowers the temperature for the β to α + κ_{III} eutectoid reaction below that required for the formation of the Fe-rich, κ_{IV} type precipitates. Nucleation of the Al depleted 9R bainitic α phase, perhaps aided by the presence of stress gradients around the κ_{IV} precipitates, produces a supersaturation of Al in the remaining parent β phase, depressing M_s. [3]. As a result, the martensitic transformation probably occurs at a relatively low temperature. The observation of substantial amounts of martensite in the as-deposited region indicates that a high cooling rate prevails during laser cladding. This rapid cooling gives the α plates little opportunity to coarsen and produces a fine Widmanstatten morphology in the as-deposited region of the cladding.

A short heating pulse from the scanning laser beam, which is again followed by fairly rapid cooling, is responsible for the microstructural changes occurring in the reheat zone. The reheat temperature profile produced during cladding has not yet been established. However, the similarity of the martensite in the as-deposited and reheat zones indicates that the martensite retransformation temperature is increased above the peak reheat temperature, possibly due to stabilization by the Fe-enriched particles. This is consistent with the results of Liu et al. [5] who observed no noticeable change in the sheet martensite on heating between room temperature and 673 K. It would appear that the maximum reheat temperature is sufficient to dissolve the κ_{IV} type precipitates in the α phase. . Although further studies of the tempering behaviour of ternary NAB alloys are required, it seems likely that the bainite transforms to the stable fcc α phase through a gradual reduction in the stacking fault density. Elimination of the bainite proceeds via a diffusion-controlled disordering mechanism and could occur at relatively low reheat temperatures. The TEM observations suggest this process also occurs in the as-deposited region but is often only partially completed.

The results of the present study demonstrate that TEM can provide considerable new insights into the complex microstructural phenomena occurring in laser processed NAB alloys. It is evident that diffusionless and diffusional transformations, precipitation reactions, twinning and long-range ordering all play important roles in forming the microstructures.

REFERENCES

1. C.V. Hyatt, K.H. Magee, J. Hewitt and T. Betancourt, Proc. Of 2nd CF/CRAD Meeting on Naval Applications of Materials Technology, J.R. Matthews, ed., Halifax, 1995.
2. C.V. Hyatt and K.H. Magee, Proc. Of Advanced Methods of Joining New Materials II, The Am. Weld. Soc., Miami, 1994, 111-126.
3. P. Bezina, Int. Metals Rev., 27, 1982, 77-121.
4. F. Hasan, G.W. Lorimer and N. Ridley, J. de Physique, C4, supp. 12, 43, 1982, 651-657.
5. Y. Liu, J. Mazumder and K. Shibata, Metall. And Mat. Trans. A, 25A, 1994, 37-46.
6. F. Hasan, A. Jahanafrooz, G.W. Lorimer, and N. Ridley, Metall. Trans., 13A, 1982, 1337-1345.
7. F. Hasan, G.W. Lorimer and N. Ridley, Metals Sci., 17, 1983, 289-295.
8. D.E. Bell, M.Sc. Thesis, Penn. State Univ., 1993.
9. Y. Liu, J. Mazumder and K. Shibata, Acta metall. mater, 42, 1994, 1755-1762.
10. J. Hewitt and V.E. Merchant, Proc. Of 2nd CF/CRAD Meeting on Naval Applications of Materials Technology, J.R. Matthews, ed., Halifax, 1995.
11. G. Cliff and G.W. Lorimer, J. Microscopy, 103, 1975, 1397-1399.
12. J.A. Gianetto, M. Sahoo, M.W. Letts and C. Bibby, DREA report CR/95/435, Defence Research Establishment Atlantic, 1995.
13. P. Ratchev, J. Van Humbeeck and L. Delaey, Acta metall. mater., 41, 1993,2441-2449.
14. Y.S. Sun, G.W. Lorimer and N. Ridley, Metall. Trans.,21A, 1990, 575- 588.
15. S. Amelinckx and D. Van Dyck, Electron Diffraction Techniques, J.M. Cowley, ed., Oxford Univ. Press, 1995.
16. Y. Liu, M.E. Mochel, J. Mazumder and K. Shibata, Acta metall. mater., 42, 1994, 1763-1768.
17. K. Takezawa and S. Sato, Metall. Trans., 21A, 1990, 1541-1545.

Phase	Structure Prototype	Schnoeflies Designation	Space Group	Lattice Spacing (nm)
α	Cu	A1	Fm3m	0.365
β'	Cu_3Al	9R	R$\bar{3}$m	—
κ_{II},κ_{IV}	Fe_3Al	B2	Fm3m	0.571
κ_{III}	NiAl	B2	Pm3m	0.288

Table 1: Crystallographic data for the various phases observed in as-cast NAB alloys [6].

Description	Cu	Al	Ni	Fe	Mn
fcc α phase (reheat zone)	0.846 ±.019	0.070 ±.014	0.046 ±.012	0.031 ±.004	0.007 ±.001
9R α phase (deposit)	0.865 ±.014	0.076 ±.003	0.041 ±.007	0.013 ±.003	0.005 ±.002
martensite	0.821 ±.030	0.097 ±.011	0.053 ±.014	0.016 ±.006	0.008 ±.001
κ_{III} precipitates	0.243 ±.015	0.268 ±.014	0.292 ±.024	0.197 ±.010	
κ_{IV} precipitates	0.449 ±..117	0.105 ±.014	0.119 ±.044	0.268 ±.135	0.006 ±.003

Table 2: Results of chemical analysis (wt. %) by EDX of Phases in NAB Laser Cladding.

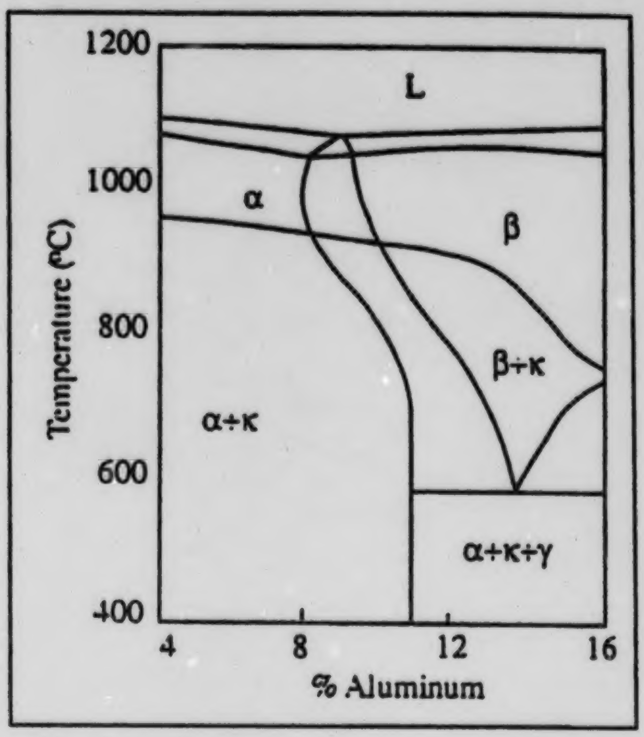

Figure 1: Vertical section of the Cu-Al-5 wt. % Ni-5 wt. % Fe equilibrium phase diagram [3].

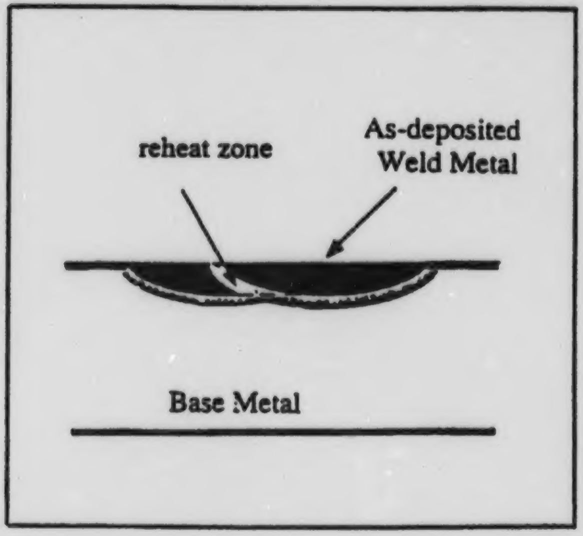
reheat zone
As-deposited
Weld Metal
Base Metal

Figure 2: Schematic diagram of the various zones of the laser-clad weldment.

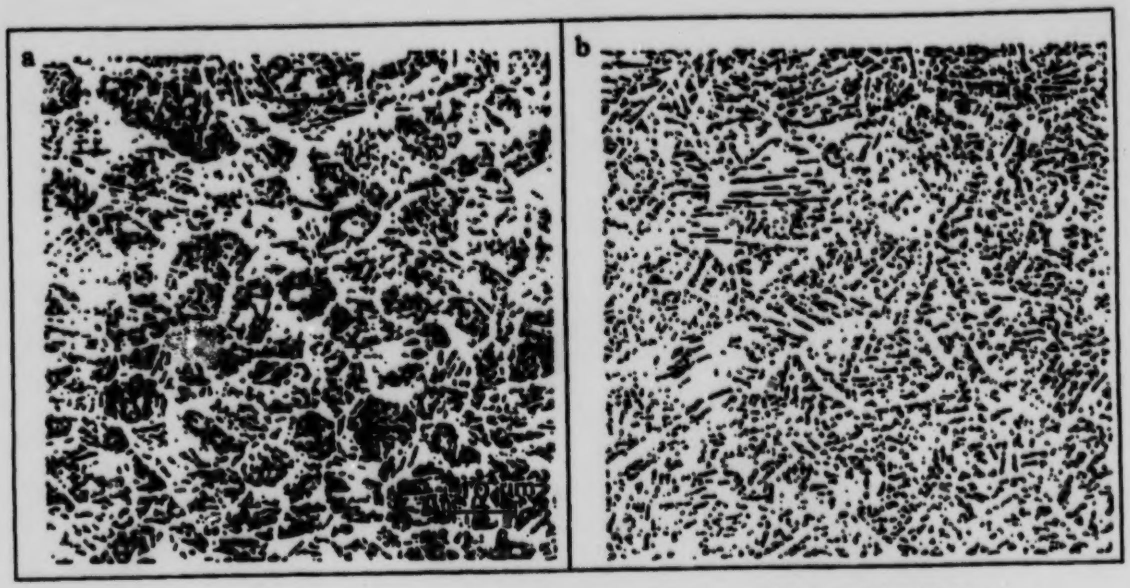

Figure 3: Optical micrographs showing typical microstructures for (a) the as-deposited and (b) reheat zones of a NAB laser cladding.

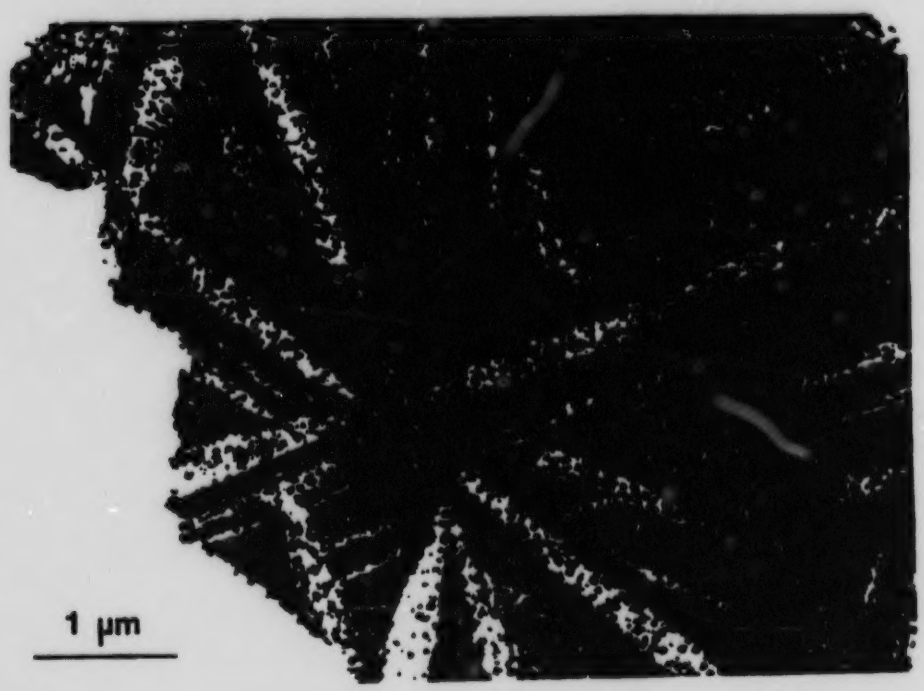

Figure 4: Typical TEM micrograph of the as-deposited region-of a NAB laser cladding showing Widmanstatten α rods (light) and martensite plates (dark).

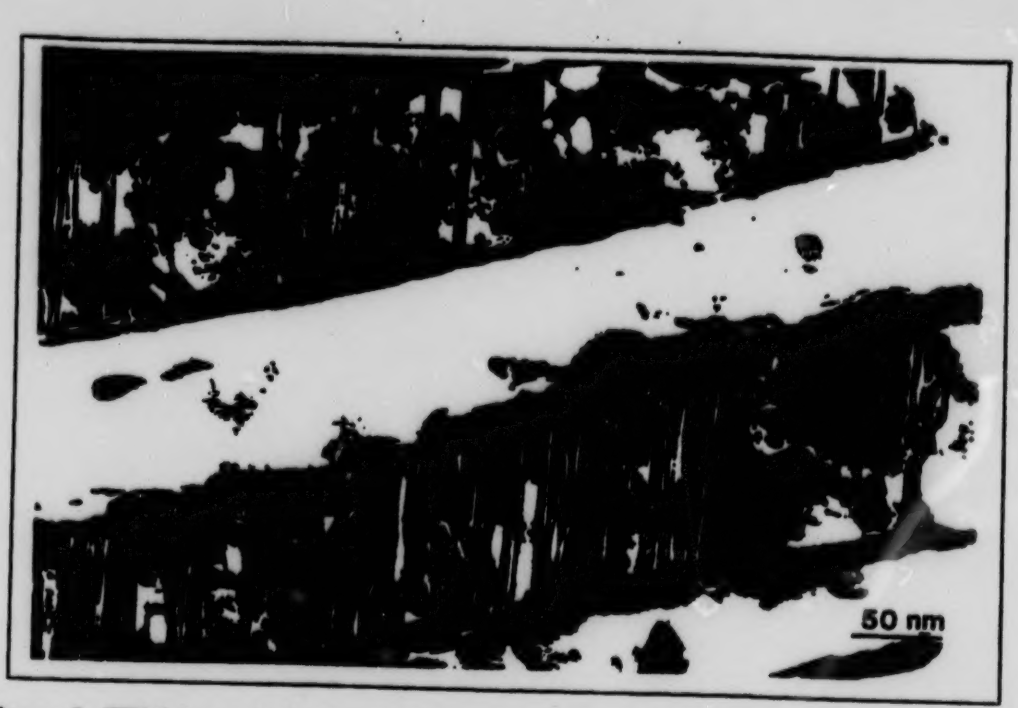

Figure 5: TEM image of a fcc α rod in the as-deposited region showing clusters of stacking faults. Moire ringes, arising from double diffraction, are frequently observed.

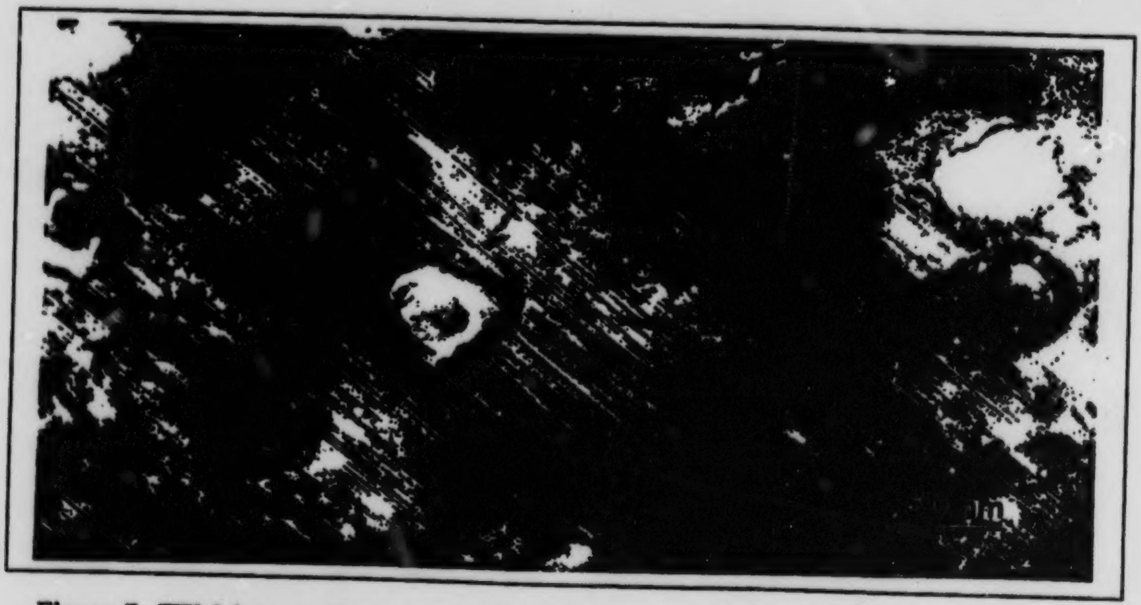

Figure 7: TEM image of an α rod with 9R long-range order. Closely spaced, parallel striations visible in the image are a periodic array of stacking faults on the $\{111\}_{fcc}$ planes..

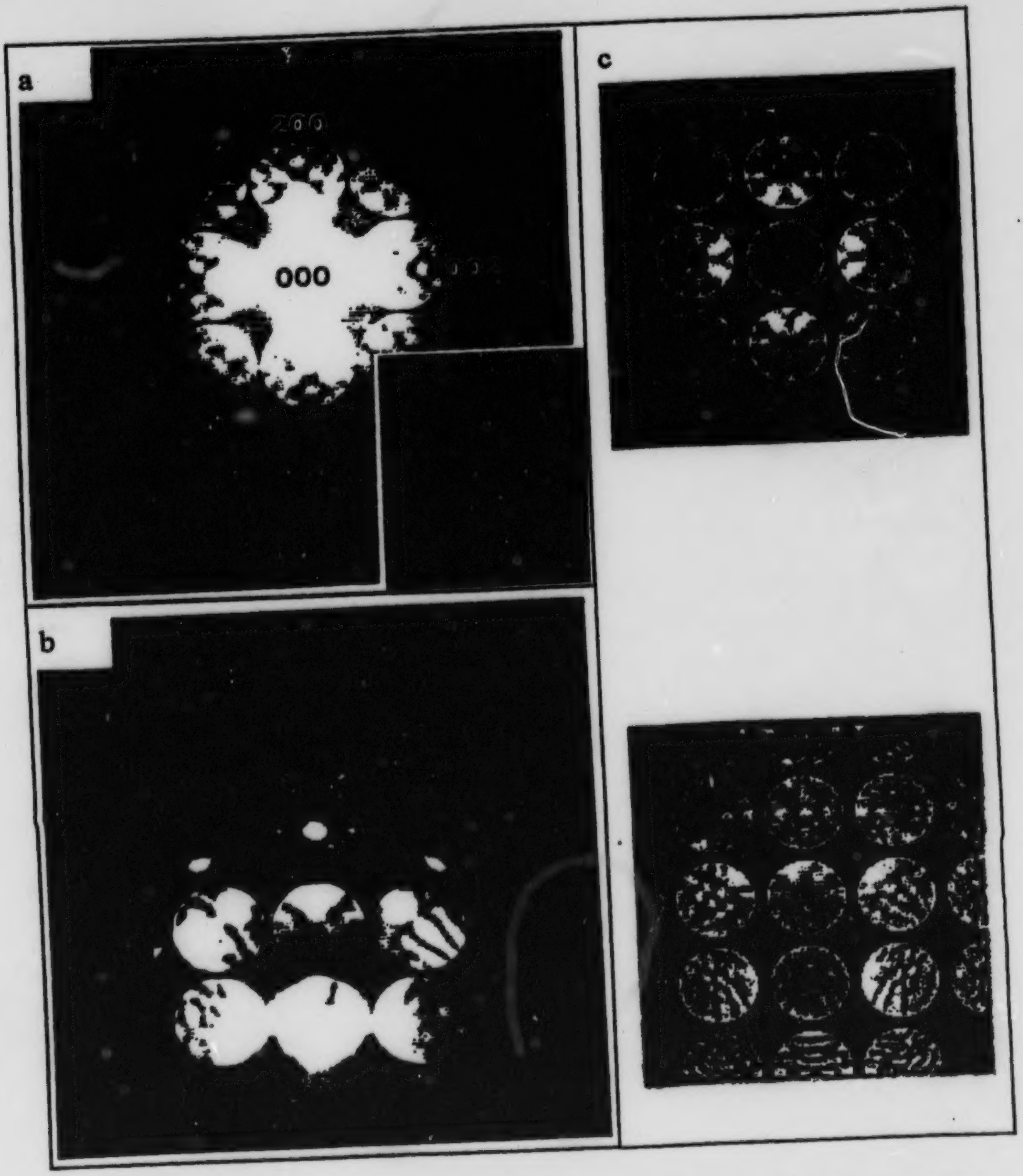

Figure 6: [100] zone axis CBED patterns for the Widmanstatten α phase. (a) On-axis pattern showing 4mm symmetry (the central disk is shown in the insert). (b) Dark-field pattern tilted such that the center of the Laue circle is at the position of the (200) disk. (c) Simulated CBED patterns for space group $Fm\overline{3}m$.

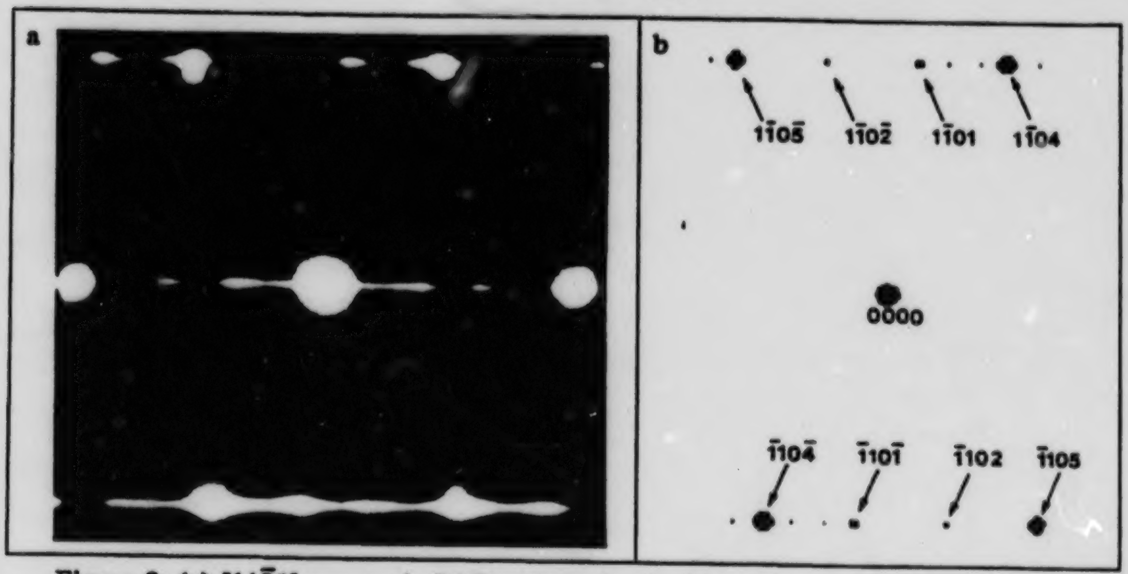
a
b
$1\bar{1}0\bar{5}$
$1\bar{1}0\bar{2}$
$1\bar{1}01$
$1\bar{1}04$
0000
$\bar{1}10\bar{4}$
$\bar{1}10\bar{1}$
$\bar{1}102$
$\bar{1}105$

Figure 8: (a) $[11\bar{2}0]$ zone axis SAD pattern for the long-range ordered 9R α phase. (b) Corresponding calculated pattern for a ABCBCACAB stacking module.

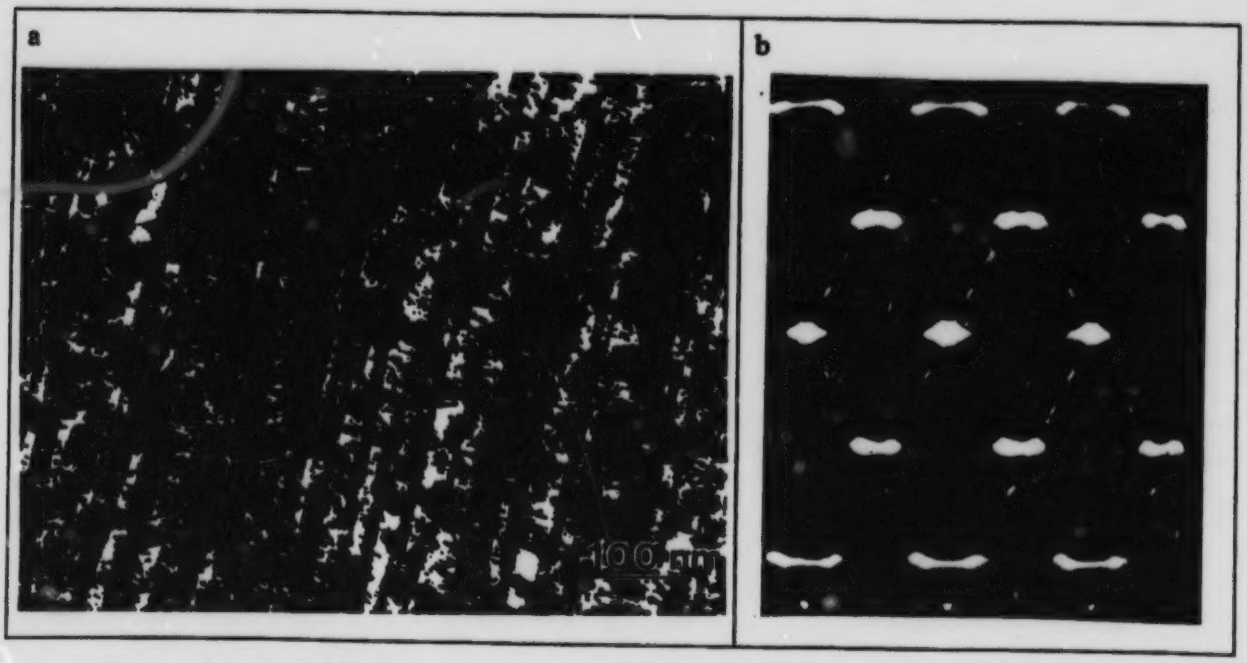

Figure 9: (a) TEM micrograph of martensite in the as-deposited region showing parallel-sided, acicular twins. (b) Corresponding $[11\bar{2}0]$ zone axis SAD pattern for the martensite revealing the presence of 9R order and twinning

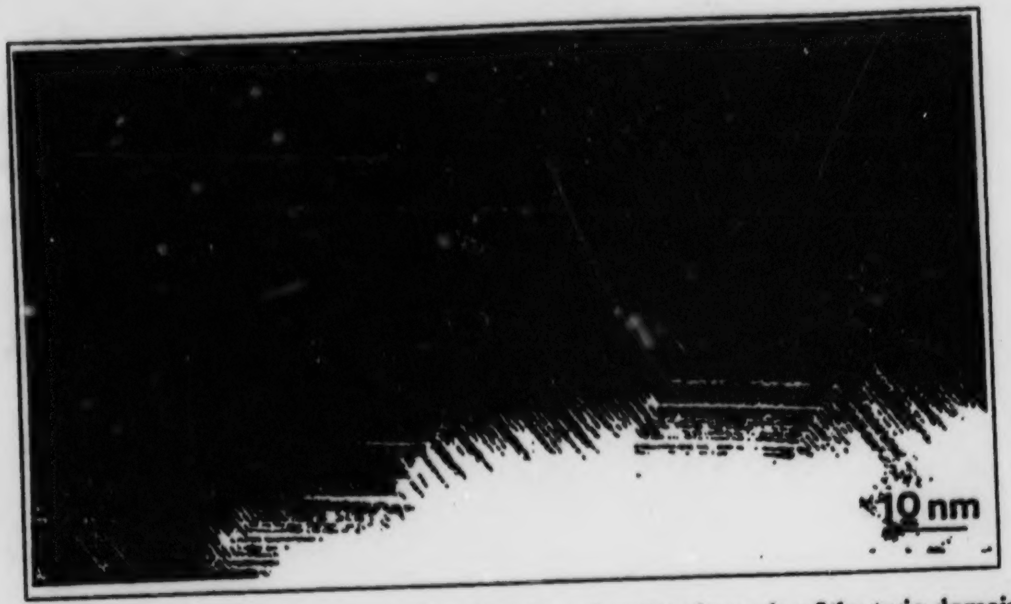

Figure 10: TEM image of the martensite lamellae showing the scale of the twin domains and numerous stacking faults.

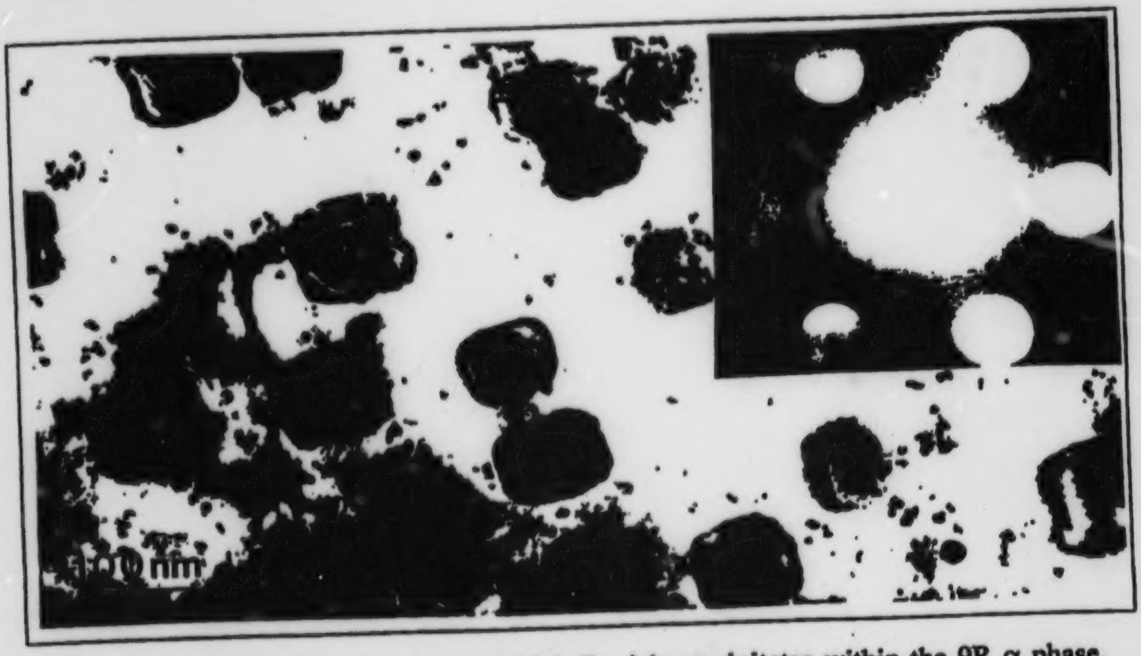

Figure 11: TEM image showing cuboidal, Fe-rich precipitates within the 9R α phase. Microdiffraction patterns (inset, [111] zone axis) indicate the precipitates possess B2 crystal structure.

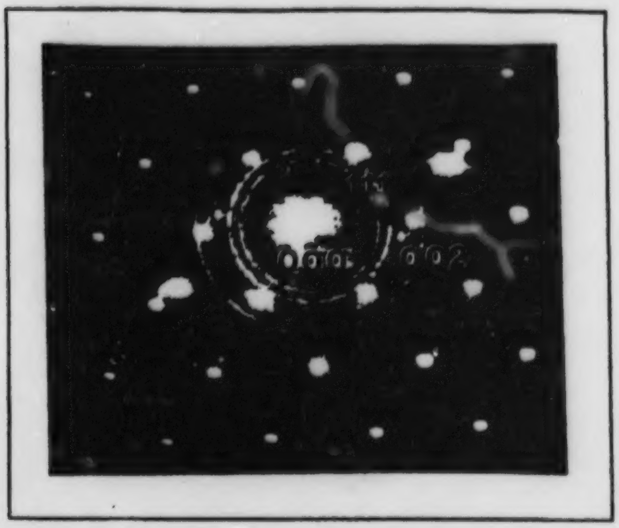

Figure 12: A "spotty" ring diffraction pattern produced by a collection of precipitates within a large SAD area-selecting aperture. The rings are superimposed on the [110] zone axis SAD pattern of the surrounding α matrix.

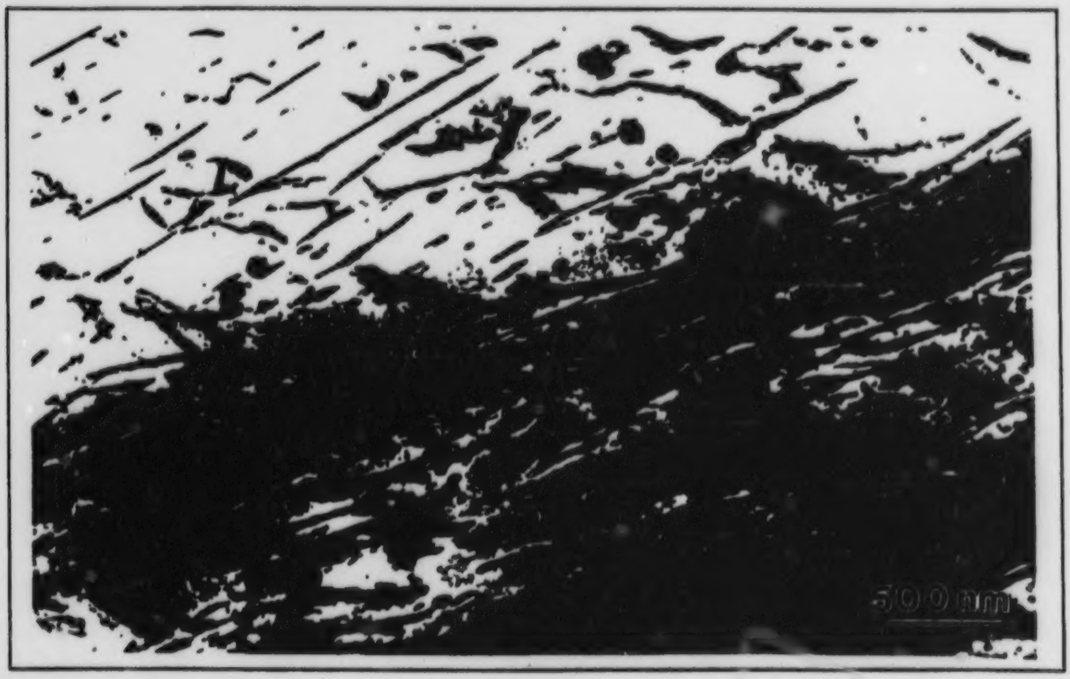

Figure 13: TEM image of a typical ($\alpha+\kappa_{III}$) eutectoid region in the reheat zone. The elongated particles are Ni-rich and have a B2 crystal structure.

#507221 (18)

LIBURDI
engineering

LIBURDI
PULSWELD.

VARIABLE POLARITY PLASMA ARC WELDING OF ALUMINUM ALLOYS

Robert J. Pistor - Gaëtan R. Labbé - Wayne H. Tuttle

Liburdi Engineering Limited
400 Highway 6 North • Dundas, Ontario • L9H 7K4 • Canada

ABSTRACT

When compared with gas tungsten arc welding (GTAW), plasma arc welding (PAW) has significant advantages. These advantages include: complete joint penetration, less joint preparation, improved weld quality and soundness, decreased distortion and reduction in the number of weld passes. The welding of aluminum alloys is aggravated by the formation of an oxide layer which has generally a high free energy of formation. Previous attempts to weld aluminum with Direct Current Electrode Positive (DCEP) or Direct Current Electrode Negative (DCEN) were unsuccessful due to severe cutting through the joint, weld metal porosity, electrode degradation, and incomplete fusion. To overcome aluminum's strong tendency to form an oxide an alternating current (AC) power supply is used. The success of the AC power supply is limited due to electrode deterioration, lack of weld pool control, the need for superimposed high frequency and decreased amperage capability of the welding torch. The final solution in plasma arc welding of aluminum alloys is achieved by using a "VARIABLE POLARITY" (DC) power supply. This approach produces cyclic changes of DCEN and DCEP polarities with independent control of current amplitude and duration. This "state-of-the-art" technology allows for proven superior results in all parameters.

Sub-pulsing is a new area of VPPAW technology that resulted from advances in power engineering developed by Liburdi Engineering Limited. The arc penetrating force encountered during the high pulse has the effect of producing a deep narrow weld, while the role of the low pulse is to average out the heat input to reduce overheating of the weld. As a result, the continuous improvement of this technology shows that VPPAW welds using square butt joint preparation have demonstrated superior penetration and narrower heat affected zones.

Liburdi ***Pulswald*** has engineered this unique technology to meet demanding high performance welding applications such as aerospace, automotive, milling tools, high speed tube welding.

INFORMATION

Pure Current:
The Liburdi ***Pulsweld*** current source provides pure DC current with less than 0.5% peak to peak ripple. This provides ideal arc characteristics such as a narrow, constrained arc which produces exceptional arc force. This feature allows for lower heat input while welding of critical components. The high purity also ensures that all work cells equipped with Liburdi ***Pulsweld*** current sources will provide identical welding results with no need to adjust parameters from machine to machine.

Drift Free Operation:
Unlike conventional current sources designed for manual welding, Liburdi ***Pulsweld*** current sources are designed for accurate and repeatable performance with accuracy better than 1% of the programmed value. Our current sources are factory calibrated with instrumentation traceable to ISO and NIST. Their performance has made them the industry standard for aerospace, nuclear power, high production tube mills, turbine engine component repair, research laboratories, and other industry where the cost of compromise cannot be tolerated.

Control Loop Bandwidth > 10 kHz:
The performance of the Liburdi ***Pulsweld*** current source is largely due to its exceptional control accuracy. With small and large signal bandwidth greater than 10 kHz, the current source can respond to current commands and regulate precisely, in spite of such external forces such as power line interference. Pulsed current always maintains its sharp rise times and does not overshoot or undershoot the programmed value before steady state is reached. The Liburdi ***Pulsweld*** current source is never the limiting factor in weld procedure development or production welding operations.

High Frequency Switching Regulator:
The pulse width modulation frequency of the Liburdi ***Pulsweld*** current source is 150 kHz *(150,000 times per second)*. This means that the current source is controlled and adjusted approximately every 6 micro-seconds. This feature provides assurance that the current is always correct and regulated in spite of such conditions as abrupt changes in arc gap, surface contamination, or change in parent metal mass. Commercial current sources simply do not have the current stability and reaction that is provided by the state of the art power control employed by Liburdi ***Pulsweld*** products.

Computer Compatibility:
The Liburdi ***Pulsweld*** current source is designed specifically for use with computer control. They eliminate interference associated with conventional HF arc starter operation, as well as conducted EMI through communication cables *(the Liburdi **Pulsweld** products hold the "CE MARK" certification for EMC and Safety Voltage Engineering)*. These types of interferences, common in conventional GTAW/PAW power source can cause an alias of analog signals from computer systems resulting in set-point errors and in some cases computer lock-up. True-differential inputs eliminate any potential ground loops between computer ground and the power source.

Reliability Designed-In:
Implementing military style derating of components ensures that the current source has the highest possible MTBF and the lowest maintenance requirements possible. For more than fifteen years, our track record of trouble free service has stood as a statement to our dedication for overall quality and maximum system up-time.

Direct Factory Support:
Unlike large scale manufacturers of conventional current sources, Liburdi ***Pulsweld*** fully supports its customers with electronic, control, and welding process support. Even when supplied through a separata OEM systems integrator, Liburdi ***Pulsweld*** precision current sources are fully supported by our trained factory personnel and warranted against defects for one full year past purchase. Offices in Hamilton, Ontario *(International Office)* - Los Angeles, California - Detroit, Michigan - Paris, France - Bristol, United Kingdom and Singapore ensure that we provide responsive, timely attention to our customer's needs.

The How's & Why of Variable Polarity Welding:
Variable Polarity Arc Welding is a type of AC welding that is specifically designed to provide defect free welds with a minimum of preparation for use in commercial and aerospace production.

It is capable of welding materials such as aluminum, nickel, cobalt, titanium alloys, as well as other materials that produce tenacious oxide layers and/or are subject to hydrogen/porosity problems.

The following explanation of the application of variable polarity welding will deal only with the welding of aluminum alloys and some of the problems that are solved with this type of arc welding.

Aluminum readily forms oxides. These can become oxide inclusions that will cause for rejection and/or rework. The oxides are difficult to remove and must be chemically etched or physically scraped off the surface prior to welding. If the removal process is not immediately followed by welding, the oxide layer will re-form. The heat of welding has no effect on the aluminum oxide as its melting temperature is more than three times the melting temperature of aluminum.

The "cathodic etch" of variable polarity welding removes the aluminum oxide layer during the weld process. It cleans the weldment in front and around the weld puddle. This prevents the oxides from entering the molten pool and, therefore, prevents oxide inclusions from occurring in the first place.

Another problem is porosity. Porosity in aluminum welding comes from hydrogen being absorbed into the molten weld puddle, otherwise known as "hydrogen solubility". Aluminum alloys, in their molten state, have high levels of hydrogen solubility. As the weld puddle cools and changes to a solid, the solubility level drops to nearly zero. This means that if there is hydrogen available near the puddle, it will be absorbed.

When the metal solidifies, the hydrogen is forced out of solution and form bubbles. The bubbles cannot escape since the material is solidifying. Reheating the material will drive the hydrogen back into solution, but will not liberate it. Therefore, the only way to eliminate porosity is to eliminate exposure to hydrogen during the welding process.

The contaminating hydrogen has two main sources: water and oils. The water come from moisture on the surface of the weldment in the shield gas *(leaks in the torch cooling system, for example)*, or even from water stains on the surface of the parent material. Elimination of the water can be handled with proper care of the equipment and careful cleaning of the parts. Variable Polarity welding can also eliminate most of the problems as the cathodic etch can remove the water stain prior to the area being elevated to the melting point *(when hydrogen absorption occurs)*.

The other source of hydrogen is hydrocarbon contamination. In other words, oils on the surface of the part. During exposure to the high temperature and electrical stresses of arc welding, oils are broken down into hydrogen and carbon. Of course, we have all seen the carbon that forms on dirty welds, but we have not always connected it with the problem of porosity. If any oil is present *(even a single fingerprint)*, the molten aluminum will be exposed to hydrogen and will develop porosity.

The amount of porosity and whether or not it is acceptable depends on many factors, but to guarantee defect free with so called "water-clear" X-Rays, surface contamination must be eliminated prior to the weld.

Variable Polarity welding accomplishes this with the cathodic etch. Surface hydrocarbons are removed in the area of the weld and the puddle is not exposed to hydrogen. In Variable Polarity welding, the surface of the weld is cleaned. In GTAW welding this may only be the front side of the part, while in Plasma key hole, the surface of both sides and the edges of the butted pieces are exposed to the cleaning etch.

The "etch" of the Variable Polarity is the key to making these defect-free welds. In order to understand what this etch is, we must delve into how the arc works. Electrical current is the flow of electrons. Electrical conductors are materials that have the ability to have their electrons move from one atom to the next. Non-conductors are materials whose electrons cannot readily flow from atom to atom. Nevertheless, given the right circumstances, most materials will become conductive.

Argon and Helium shield gases are not normally conductive but, under the right condition, can become ionized and conduct. This ionization process consists of the molecules being torn apart and having their electrons removed. This yields a supply of negatively charged electrons and a supply of positively charged particles called ions. This gas consisting of an equal amount of positive ions and negative electrons is called plasma. Once the shield gas is a plasma, it can conduct electricity. While conducting electricity, the arc remains in a state of plasma.

In normal straight Polarity welding, the electrode is negative. This simply means that it has an excess of electrons. The workpiece is positive, meaning it has too few electrons and electrons will travel from the electrode to the workpiece.

The electrons have very little weight and accelerate to an extremely high velocity. When they strike the workpiece, they create heat that melt the aluminum. At the same time as the electrons are moving toward the workpiece, the positive ions are being accelerated toward the electrode. Since they have much more weight, they do not accelerate as quickly and are travelling slower when they strike the electrode. With their lower speed, the heat generated is lower.

During reverse polarity *(electrode positive)*, the opposite happens, with the electrons heating the torch and the heavy ions striking the work. It is the heavy ions striking the work *(much like grit blasting)* that causes the cleaning that we need to remove oxides and oils from the surface.

An interesting and important phenomena of the reverse polarity is that the electron emissivity of the bare aluminum *(the ability of the bare aluminum to give off electrons)*, is much lower than the aluminum oxide and oil contaminates. This means that the arc seeks out the dirty areas of the aluminum and concentrates there. This makes the blast of ions concentrate on the precise areas where it is needed. It could be thought of as an automatically directed grit blast of the areas that need cleaning.

As can be seen from this explanation, periodically changing the current's direction will clean the weld and give superior weld results. This is similar to the AC welding. In typical AC welding, there is a problem in that the heat during the reverse time is around the periphery of the weld area, because the contaminates are outside the weld pool area. This heating creates shallow, wide weld beads that may not be satisfactory.

It also creates an excessive amount of heat in the welding electrode and torch. The degradation of the electrode causes changes in the weld heat input that are somewhat independent of the current and AVC setting. For the reason of short electrode life and customary use of continuous high frequency radiation to keep the arc "alive", AC welding is not normally used for automated welding.

Variable Polarity welding is a special type of AC welding in which the straight and reverse current periods are carefully matched to provide proper cleaning with the least amount of torch overheating possible. In typical use, the reverse is 20% or less of the straight time. The Liburdi ***Pulsweld*** system provides patented technology that allows the reverse current to be reduced below the level of the straight current to further minimize torch and electrode degradation. This feature also reduces the widening of the pool associated with reverse polarity welding current.

The cleaning is mostly a function of time. One to four milliseconds are sufficient to properly clean the area adjacent to the weld. The absolute value of the reverse polarity current is less important that the duration to the level of cleaning attained.

When comparing torch heating between AC and VP welding, consider that in standard AC welding, half of the heat enters the electrodes and torch assembly. In VP, 80% of the heat goes to the work and only 20% goes to the torch assembly. Furthermore, even less heat goes to the work when the reverse current can be programmed below the level of straight current. This creates several advantages but the main one is the increased electrode life and the inherent ability to make more consistent welds.

PROCESS DESCRIPTION

Definition of Plasma:

Plasmas are electrically neutral ionized gasses or conductive vapours which are in a highly exited thermal state. In the normal state, a gas is an electric insulator. It does not contain '*free*' charged particles, but only neutral atoms or molecules. The addition of significant amounts of energy to a gas (say through a tungsten electrode) raises the energy state of the gas, ultimately releasing electrons from their base states. This ionization effect of the gas renders it a conductor of electricity. It is this state that is known as a plasma.

Plasma Arc Welding:
In GTA welding, a plasma forms the greater part of the arc column, across which the electric current is passed. Only when the arc column is constricted is the technique referred to as plasma arc welding. This constriction is obtained mechanically by means of a water cooled orifice which forms an essential part of the plasma arc welding torch see (figure 1). When the combined arc forces and gas impingement forces of the plasma jet become strong enough to penetrate the substrate, this is know as "Keyhole" welding.

When operating in keyhole welding mode, this constricted plasma column has many significant advantages over traditional GTA welding.

1) The plasma jet is much less sensitive to contamination of the workpiece because the plasma gas flushing through the open heyhole easily entrains gases that would, under other circumstances, be trapped as porosity in molten metal. To the user of plasma arc welding this means: a) joint preparation is easier and less expensive; b) rework costs are reduced; and c) inspection procedures may be relaxed.

2) The more symmetrical fusion zone of the keyhole weld reduces the tendency for peaking distortion.

3) The greater joint penetration may permit a reduction in the number of passes required for a given joint.

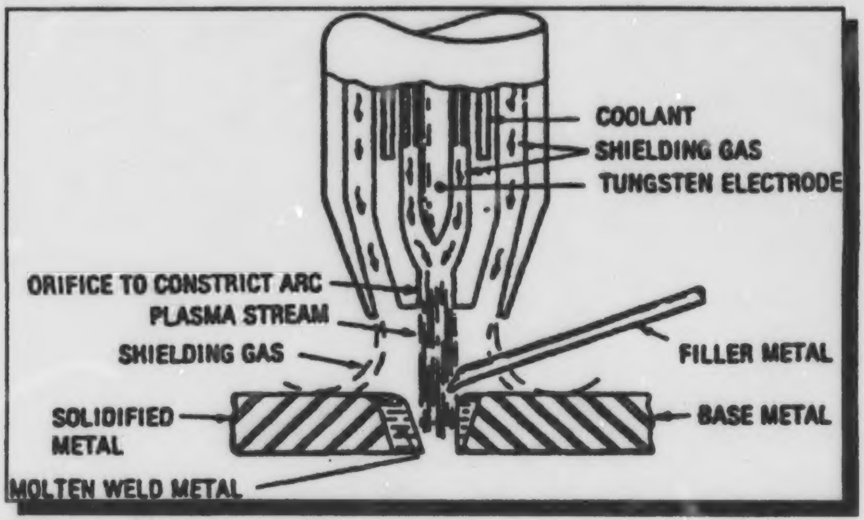

Figure 1 -*Plasma arc welding*

Torch:
A PAW torch consists of a cylindrical chamber, equipped at its lower end with a detachable nozzle, having a central orifice of the ejection of plasma (Figure 1). The degradation of the nozzle is prevented usually by water cooling. Mounted within the cylinder is a non-consumable tungsten electrode.

Arcs:
There are two types of arcs in plasma welding, non-transferred and transferred plasma arc (see figure 2). The non-transferred arc occurs when the piping constriction of the torch completes the circuit of the arc. Likewise, the transferred arc occurs when the non-consumable electrode and the work piece close the circuit of the arc.

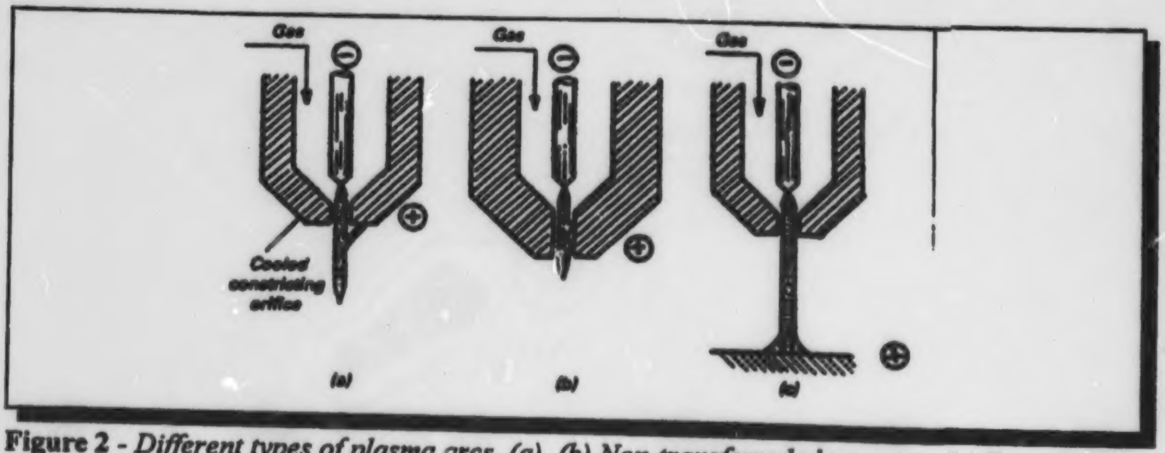

Figure 2 - *Different types of plasma arcs. (a), (b) Non-transferred plasma arc. (c) Transferred plasma arc.*

The constriction imposed in PAW reduces the profile of the column considerably when compared to the free arc in GTA. The high gas velocity through the orifice in the torch head produces a jet which further constricts the arc. Typically, the space occupied by the arc can be reduce to 20-50% of the orifice cross-section. This, in effect, forms a highly localized heat distribution in the centre of the plasma core. This high temperature core of the plasma column is well suited to the needs of welding. However there is a problem with this arrangement. The arc restriction caused by the jet of gas causes the plasma column to be surrounded by a mass of relatively cool gas moving at high speed. This cool gas is detrimental to weld because it widens the arc pool and leads to increased porosity. It is for this reason that a variety of welding torch designs have been formed to cope with this problem.

Variable Polarity Plasma Arc Welding:
Variable polarity in a power source allows the user to fine tune the current wave form in PAW. The variable polarity plasma arc welding technique integrates two features; a plasma arc and variable polarity. It is this integration that provides the uniquely superior welds common to this technique.

Power Supply:
The main function of a VPPAW power supply is to provide the user with a fully adjustable current wave form. Figure 3 shows referenced typical wave forms needed for 1/4" aluminum alloys.

As can be seen from the figure, the power supply can provide an adjustable amplitude and cycle for both DCEN and DCEP currents.

Recent advances in power supply technology have increased the operating range and improved the characteristics of the current wave form. Figure 4 demonstrates the "State of The Art" in current wave form technology. Some of its characteristics are mentioned;

- Forward currents ranging from 3 to 400 Amps;
- Reverse currents ranging from 50 to 400 Amps;
- The addition of high frequency sub-pulsing *(0-10,000 Hz)* in the forward current;
- Ramping currents; and,
- A truly square wave form.

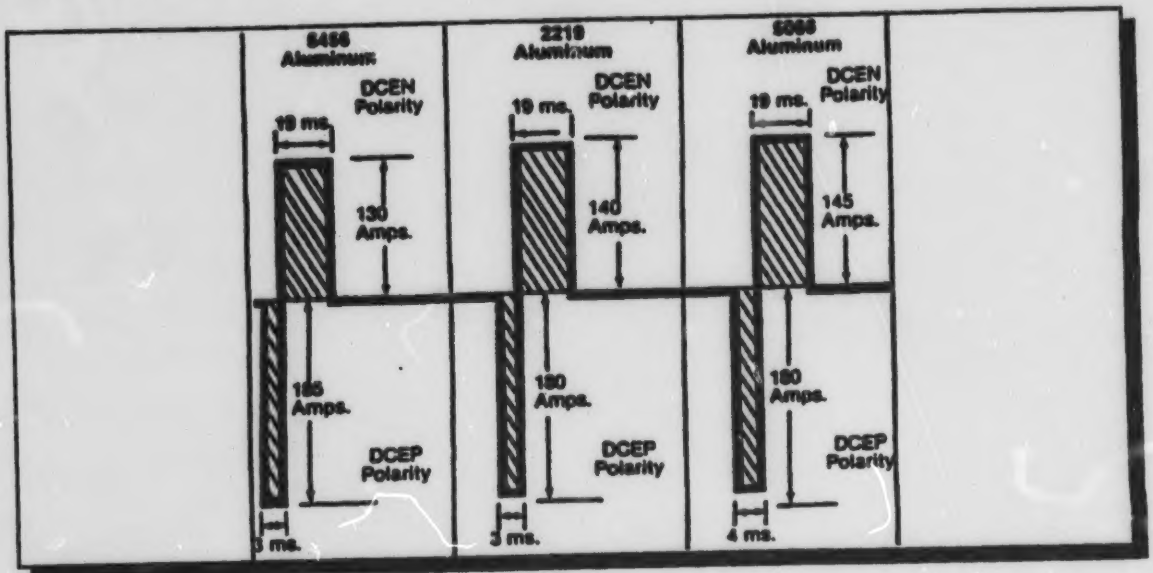
5456 Aluminum
DCEN Polarity
19 ms.
130 Amps.
185 Amps.
DCEP Polarity
3 ms.
2219 Aluminum
DCEN Polarity
19 ms.
140 Amps.
180 Amps.
DCEP Polarity
3 ms.
5086 Aluminum
DCEN Polarity
19 ms.
145 Amps.
180 Amps.
DCEP Polarity
4 ms.

Figure 3 - *Variable polarity current wave form*

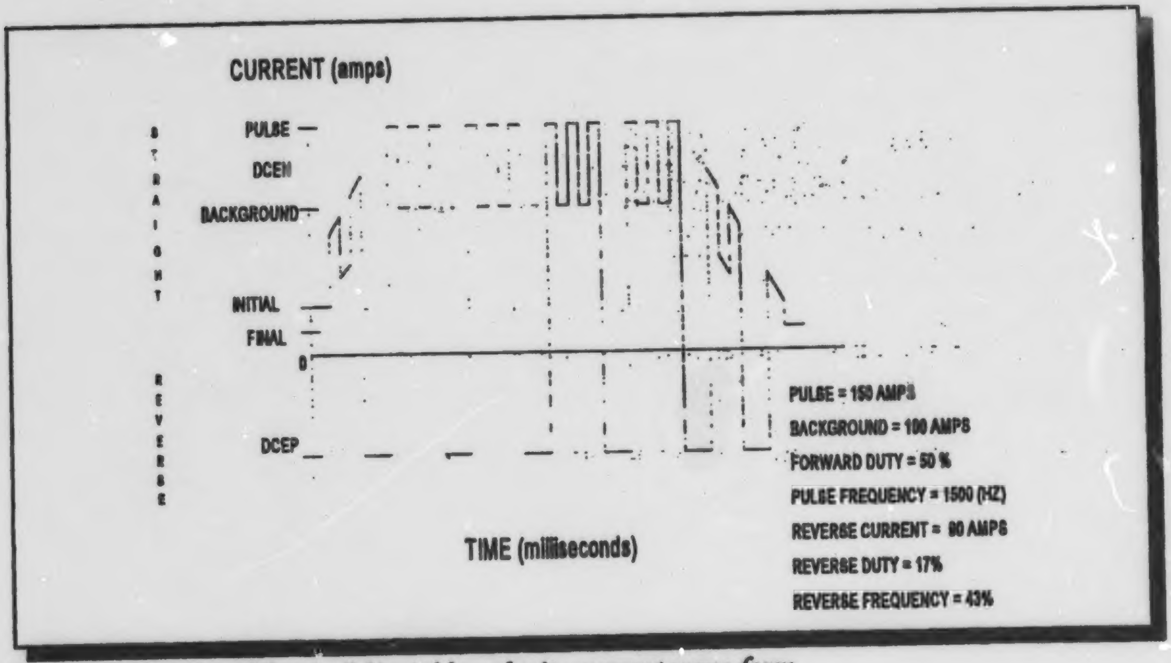
CURRENT (amps)
STRAIGHT
REVERSE
PULSE
DCEN
BACKGROUND
INITIAL
FINAL
0
DCEP
TIME (milliseconds)
PULSE = 150 AMPS
BACKGROUND = 100 AMPS
FORWARD DUTY = 50 %
PULSE FREQUENCY = 1500 (HZ)
REVERSE CURRENT = 80 AMPS
REVERSE DUTY = 17%
REVERSE FREQUENCY = 43%

Figure 4 - *"State of the Art" Variable polarity current wave form*

Welding of Aluminum:
Aluminum has a high free energy of formation of aluminum oxide (Al_2O_3) when compared to other metals. In terms of welding, this tenacious oxide layer frustrates the welding of aluminum significantly. Generally, the welder complains that the metal doesn't flow properly. Preventing the oxide layer from forming by using an inert shielding gas has met with very limited success. Metallurgically, the oxide layer also tends to contaminate the weld with oxide inclusions. Clearly a method to '*break*' the aluminum oxide layer must be devised.

The Role of Electrode Polarity:
Figure 5 shows the two types of polarities in arc welding. Straight polarity (DCEN) gives higher arc efficiencies for both GTAW and PAW when compared to reverse polarity (DCEP). In DCEN welding, much of the heat transferred is by electrons. In DCEP welding, the electrons are transferred to the electrode. This causes the electrode to degrade at a higher rate and a significant heat reduction to the weld. The advantage of DCEP welding is to give a cleaning effect on aluminum. This is possibly due to a combined effect of the bombardment of gas ions on the weld pool and the sputtering of the weld pool surface.

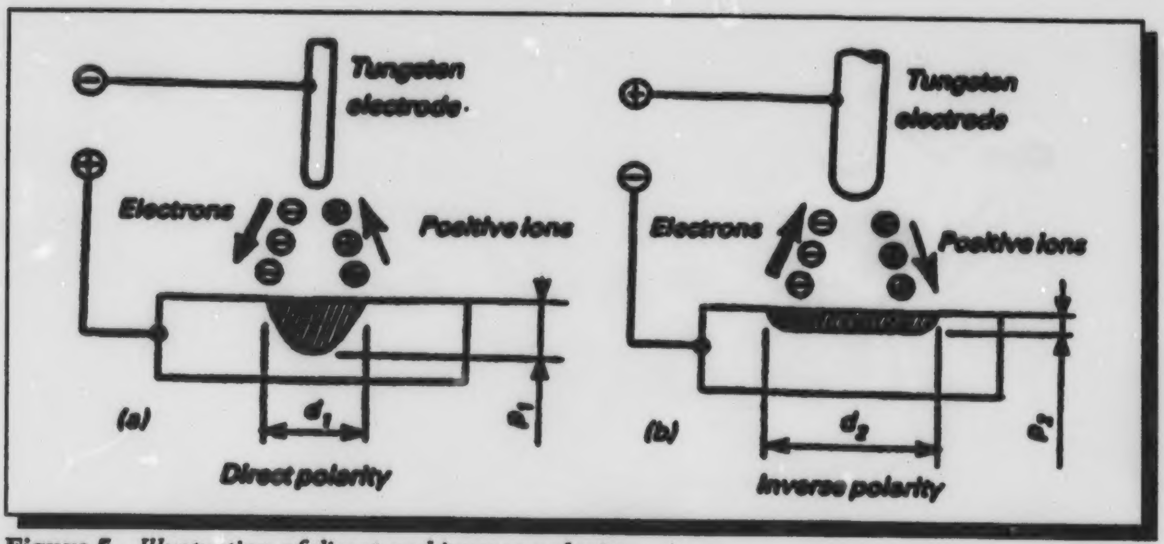

Figure 5 - *Illustration of direct and inverse polarity.*

In GTA welding practice, DCEP welding, generally obtained through use of alternating current, has long been used to take advantage of the cleaning effect produced as heavy, positively charged gas ions sputter off the surface oxide film. Successful application of DCEP PAW to the welding of 1/4" thick aluminum plate has been performed since 1965.

The lower heat input, due to DCEP welding, reduces the penetration of the weld. Therefore, it is necessary to consider a process that can combine the effects of the high input due to DCEN welding and the cleaning effects of DCEP welding. This is where the variable polarity power supply finds its niche.

The Role of Sub-Pulsing:
Sub-pulsing is a new area of VPPAW technology that resulted from advances in power engineering. Currently there is little or no published data on its effects and should be perused at the research level to gain better fundamental understanding. High frequency sub-pulsing has been claimed to refine grain structures in the weld as well as to further constrict the heat affected zone. It is believed that refined grain structures result from the changing electromagnetic fields inherent in high frequency sub-pulsing during weld pool solidification. The smaller heat affected zones are believed to be due to the higher arc penetrating force encountered in a sub-pulsed

weld. For example, to weld a plate without sub-pulsing, the forward current may be 100 Amps. In sub-pulsing the forward current's root mean square value may be 100 Amps, but the forward current may be as high as 150 Amps on the high pulse and as low as 50 Amps on the low pulse. The arc penetrating force encountered during the high pulse has the effect of producing a deep narrow weld, while the role of the low pulse is to average out the heat input to reduce over heating of the weld.

Gas Contamination of Aluminum Welds:

Gas contaminants typically found in aluminum welds are oxygen, hydrogen, nitrogen and methane which arise in both the arc and shielding gas. These contaminates lead to porosity and incomplete fusion.

Other tell tale signs of gas contamination can be found on the welding equipment. Inside the torch, oxygen from water vapour decomposed by the arc can produce a visible oxide stain on the tungsten electrode. The plasma jet may sputter and exhibit a green colouration from copper eroded for the nozzle under erratic flow conditions.

It has been found in a fairly recent study that VPPAW welds are particularly sensitive to gas contamination (much more than GTAW). The following are some of conclusions that Torres, et al made after performing an exhaustive investigation on gas supply contamination in VPPAW:

1) Hydrogen levels of 25ppm in the shielding gas produce micro porosity and the associated surface features caused by bubbles of gas reaching the surface just as it solidifies;
2) Methane concentrations of 100ppm produce fine porosity;
3) Nitrogen concentrations of 300ppm were required to produce fine porosity and undercutting;
4) Oxygen contamination of 250ppm can be detected by rough backsides on keyhole welds;
5) Incomplete fusion is a result of removal of only portions of the thin oxide on the aluminum surface by either disassociated or ionized hydrogen. The remaining oxide is free to move and forms wetting barriers at the back of the weld pool; and,
6) Asymmetrical undercutting is a result of slight arc misalignment , sometimes in combination with gas contaminants, which may preferentially enter one side of the weld pool and increase Marangoni flow on that side.

As a result of the gas contaminating effects, very close attention must be paid when changing gas lines and sufficient purging of gas lines is mandatory. The move to ultra pure gas or a gas purifier is also recommended.

VPPAW The Aluminum Welding Technology Break Through:

An excellent reference paper by Nunes, et al describes the development of VPPAW and its application to the welding of the 2219 aluminum external tanks for the space shuttle. After acquiring a VPPAW system in 1979 at the Marshal Space and Flight Centre, a 6 month study concluded that:

1) VPPAW welds in aluminum were essentially porosity-free, as noted by radiography. This characteristic would reduce weld repair costs appreciably, compared to GTA welds.
2) The cleaning of flaying by scraping and then draw filing of adjacent surfaces of the joint as required for DCEN GTA welding could be eliminated. This would reduce joint preparation costs significantly, compared to GTA.
3) A significant reduction in peaking was noticed. This would reduce costs. Peaking reduction, usually by magnetic hammer, is required on GTA welds where peaking measured as the complement of the dihedral angle across the weld exceeds 6.5°.

The success of the experiment gave VPPAW the leading position in welding 2219 aluminum for the space shuttle external tanks. It is interesting to note that more than 1820 ft of welds have been produced with zero rejectable internal defects for the space shuttle external tank.

Results:
The introduction of VPPAW has greatly increased weld quality, porosity and weldability of aluminum alloys. Its success in the space shuttle external tank program has demonstrated that it is definitely superior to GTAW. When compared with GTAW, time and money are saved in the long run.

The extent of VPPAW's success can be attributed to its constricted plasma arc jet and cleaning effect or "cracking" of the oxide layer found on aluminum. The highly focused arc leads to high penetration or keyhole welding and the cleaning of the oxide layer leads to increased weldability.

Although superior to GTAW, VPPAW is more sensitive to gas contaminates found in the shielding and plasma gas lines. Special care must be taken concerning the supply and purity of the gases.

Conclusion:
For over fifteen years, Liburdi ***Pulsweld*** current sources have been raising the standard of industries that employ either the GTAW or PAW processes. With pioneering capabilities such as Variable Polarity Welding that allows lower heat input to the weld zone beyond that provided by conventional AC power sources. Liburdi ***Pulsweld*** stands unprecedented in the field of non-consumable arc welding.

References

① Tomsic, M., Barhorst, S., "*Keyhole Plasma Arc Welding of Aluminum with Variable Polarity Power*" Welding Journal, February 1984, pp. 25, 32.

② Nunes, A.C., Bayless,E.O., Jones, C.S., Munafo, P.M., Biddle, A.P., Wilson, W.A., "*Variable Polarity Plasma Arc Welding on the Space Shuttle External Tank*" Welding Journal, September, 1984, pp. 27, 34.

③ Cornu, J., "*Advanced Welding Systems Tig and Related Processes*" ISF Publications/Springer-Verlag, Berlin, Vol. 3, 1988.

④ Torres, M.R., Mcclure, J.C., Nunes, A.C., Gurevitch, A.C., "*Gas Contamination Effects in Variable Polarity Plasma Arc Welded Aluminum*" Welding Research Supplement, April, 1992, pp. 123-s, 131-s.

Note: This presentation is condensed from an article published in the Welding Journal. All questions, comments, or suggestions should be referred to the authors for clarification.

#567222 (19)

Laser Welding in Ship Construction

By: **J Bird**, Ministry of Defence, Abbey Wood, Bristol, UK
A Furio, Naval Warfare Centre, Carderock Division, Bethesda, Maryland, USA

Introduction

The need to remain competitive in an ever increasingly competitive market is of paramount importance in the shipbuilding industry where far eastern fabricators, with significantly lower labour costs compared with those in Europe, compete aggressively. It has been stated that structural rework accounts for anything up to 25% of basic man hour fabrication costs as a result of misalignment and distortion resulting from welding and other fabrication related problems. Consequently anything that can be done to save some or all of the 25% of the currently expended rework man hours will go a long way to allowing European shipyards to remain competitive in the world market.

Large scale structural distortion and poor fit up can be effectively counteracted by use of CAD/CAM techniques. With accurate laser cutting of the individual structural steel components, a truer structure can be fabricated. This relies on individual accurately cut structural steel components being carefully positioned and firmly located for welding. However, using arc welding procedures, when considerable amounts of weld metal are used to join the individual items together, large scale restraint stresses may be generated due to weld metal contraction. The structure consequently can and usually does suffer unwanted distortion. In contrast, laser welding uses small welds, with little or no filler, and as a consequence contraction is reduced and thus the potential for large restraint stresses and the accompanying distortion.

By using accurately cut steel plate and sections, with precise alignment and great attention being paid to the positioning and location of the components to be laser welded, a structurally efficient fabrication can be manufactured exhibiting minimal distortion. The means of joining the various components, plate, sections, etc by laser welding is achieved using butt welds, stake welds and what has been called skid (1) welding.

The object of the paper is to illustrate what has been achieved using laser welding with respect to warship structures. In addition to the general use of laser welding for fabricating conventional ship structures, laser welding of lightweight stiff structures illustrates the potential for novel structural development. This may have specific applications, in the fast ferry industry (2), where designs with respect to increasing size, is outweighing the capability of aluminium to fulfil the materials role, whilst still producing a cost effective acceptable power to weight ratio vessel.

Overall it has been suggested that the use of Laser welding will result in:

1. decreased imperfection levels, due to more precise and controlled heat input;
2. increased joining rates;
3. less consumable costs, due to the reduced need for filler material;

4. more precise structural fabrication reducing design margins, allowing for inaccuracies;
5. improved reproducibility.

Laser Fabrications

1. Frame Stiffened Panels

Frame stiffened panels in naval vessels have the frames fillet welded on both sides, either continuously or intermittently, to form a rigid structure which has a lower weight compared with simple plate of equivalent stiffness. In order to produce a structurally efficient frame stiffened panel from plate segments, the plate must be flat, be accurately cut and carefully positioned for arc welding with the minimum quantity of weld metal to minimise distortion. To manufacture such a panel by laser welding requires accurate cutting of the plate, as with the arc welding, but using laser cutting under CAD/CAM control the accuracy of the cut this is readily achieved. Fit up then must be equivalent to standard panel manufacture and it must be guaranteed to a gap tolerance of 1mm. The joint can be formed using a single pass, full thickness, frame to plate laser weld, adequate to carry the design load. For thick framing, laser welding can be carried out from both sides of the frame to form a fully fused joint. Consequently the distortion do to weld contraction is not only minimised but directed in one direction as compared with the more usual fillet welds. This will clearly produce over a large structure, a significant decrease in distortion and the fit up of individual fabricated structural sections can be expected to be vastly improved, with total distortion of some 10% of that of arc welded structures being quoted.

The proposal to use welds without fillets to help transfer the load may at first seem to be counter productive as regards induced stress level and in consequence fatigue performance and overall ductility. In order to investigate the effect of replacing a two sided fillet weld with one which in essence joined only the stiffener thickness to the plate, a number of large scale tests were fabricated and tested in tensile, bending and fatigue. These included:-

a) Large scale ductility tests
b) Large scale crack arrest tests
c) Large scale buckling tests
d) Large scale fatigue tests
e) Fracture mechanics tests

a) Large scale ductility tests

It is a requirement of the classification authorities that 22% elongation be developed in constructional welds. However because of the small size of the laser welds it is very difficult to identify a tensile test which will reliably measure the ductility of a laser deposit. Consequently, in order to show that in construction adequate levels of ductility could be developed, large scale tensile tests were devised to demonstrate that such levels of ductility could be achieved.

The specimen developed for large scale ductility testing, figure 1. measured 1000mm wide by 850mm wide and 12mm thick containing a longitudinal butt weld and two transverse stiffeners. The arc welded version of the test carried out for comparison purposes was made using a four pass single-sided procedure whilst the laser panel was constructed with a single pass laser weld made at 1m/min. The panels in both cases were made from the same plate of Grade A steel.

The stress was applied to the specimens via a heavy cross pieces loaded by two large hydraulic jacks, in a rig used for wide plate testing, the elongation being measured by four extensometers with a gauge length of 1100mm. Because the extensometers were limited to 50mm travel the overall plastic strain for the panel was estimated on the basis of machine displacement and a particular gauge length , the parallel length of the panel, 940mm. The overall elongation produced significant lateral contraction, which caused buckling of the transverse frames and plate dishing between the frames. There was no evidence of damage to the longitudinal weld. In spite of the buckling of the frames, especially in the laser panel which was taken to a higher elongation, there was no signs of local tearing in the welds attaching the frames to the plating. The overall elongation was estimated as 7.5% for the arc panel and 10.5% for the laser welded panel.

The structural relevance of requiring 22% elongation from the weld is unclear. What matters is the structural response as a whole. In context, the 10.5% overall elongation achieved on the large laser welded panel tested is considered to demonstrate a more than adequate level of structural ductility and consequently to show that laser welding does possess adequate ductility for ship construction.

b) Large scale crack arrest tests

Brittle fracture has from time to time been a major problem in ship steels, as indicated in the liberty ship failures and more recent failures, a significant contribution to which has been brittle fracture. In the current laser welding trials Grade A was used as the test material. Consequently it was thought relevant to determine if fast fractures could develop and propagate in the molten zone or HAZ of the laser welds as it was known that such areas would, due to the high cooling rate, be very strong and as a result likely to be of low toughness. In order to determine how the laser welds were performing compared with currently used equivalent tests were carried out on arc welded panels.

The test sample is shown in figure 2. and with a central test section 1000mm wide by 850mm high comprising four equally sized 12mm thick plates butt welded together using arc or laser welding. The arc welds were deposited using Flux Cored Wire welds for the root and a submerged arc fill resulting in a total of 4 passes per arc weld. In contrast the laser welds were made using a single pass at 1m/min. The object of the test was to present the transverse (horizontal) weld in assembly with a fast running crack whilst the test section was subjected to a remote stress representative of what might be encountered in a ships deck. The longitudinal (vertical) weld was included with the intention of including realistic residual stresses. The load was applied to the test piece via a tapered transition piece bolted at its ends into a heavy cross member loaded as for the previously described tensile tests.

The fracture toughness of low strength ship steels and weldments are generally found to be sensitive to strain rate. A brittle crack will only initiate under static loading if the temperature is below the minimum encountered in ship structures. Because dynamic loading is difficult to apply to large test pieces crack initiation was achieved by cooling the central portion of the test piece down to -120°C before driving a small wedge device into the centre of the plate. The region remote from the crack initiation point was held at a more realistic ship design temperature, -30°C to

0°C using solid carbon dioxide in aluminium trays. The resulting temperature gradient was monitored using contact thermocouples.

In all cases running cracks were initiated in the horizontal welds of the arc and laser welded panels. For the arc welds, the remote stress at initiation was 151MPa and 178MPa. The cracks ran for a small distance in the weld, a maximum of 150mm before deviating into the plate and arresting at temperatures between -5°C and -15°C. The cracks initiated in the laser welded panels, which were subjected to remote stresses of 146mpa and 62mpa, immediately deviated into the plate material before arresting at temperatures between -15°C and -30°C. One laser welded panel was ground flush 50mm either side of the central hole in an attempt to confine the crack to the weld, side grooving was not practical, but this only resulted in the crack remaining in the weld for 6mm before deviating into the plate.

The large scale crack arrest tests provide an encouraging demonstration of the defect tolerance of laser welds in comparison with standard arc welds with crack deviation dominating. The applied nominal stress 150MPa is an extreme level and there is only a small probability of it being encountered in a ship's lifetime. Later charpy testing indicated that this Grade A steel would have qualified as Grade D steel with a minimum charpy toughness level of 27J.

c) Large scale buckling tests

These tests were an initial attempt to obtain structural information which would allow the ship designer to confidently use laser welded structures in place of more conventional arc welded structures. Three principal areas were to be assessed:

1. residual stresses due to welding
2. plating imperfection levels due to welding
3. overall structural performance

The design of the panel used for comparing the structural performance of arc and laser welded structures is shown in figure 3. After welding both panels an assessment of the structural distortion developed in the panel together with residual stress measurements determined via strain gauges positioned midbay on the plating and the frame web tables was made. This was followed by longitudinally compressing the panel until buckling failure occurred.

The comparison indicated that the laser welded panel had lower imperfection levels, lower residual compressive stress levels, but similar levels of sub-component misalignment to the arc welded structure. Thus it might be expected that the structural performance of the two panels would differ. This was highlighted by the fact that the laser welded panel behaves linearly figure 4. up to a greater portion of the structural crush load compared with the conventional panel and exhibited a more catastrophic failure mode see figure 5. Both panels failed at the same peak load with the laser welded panel showing lower post-collapse levels of strength.

It has been suggested that by modifying the structural slenderness of the plating in the laser welded panel it may be possible to constrain the failure mode of the structure to a smoother elasto-plastic failure. This will produce a lighter structure of a similar ultimate strength, with a safe failure mode, which will be of great value to the ship designer. Further work is required to assess the parametric performance of such variations in panel design but it should be possible, using current design methods adapted for laser welded structures, to design safe satisfactory laser welded structures.

d) Large scale fatigue tests

Structural fatigue testing was carried out using the sample shown in figure 6. to compare laser and arc welded panels. The details of primary concern in the ship are the transverse stiffeners and these have been incorporated on both sides of the test piece for convenience. The two laser welded panels contained two single pass fillet, one double pass fillet and one single pass butt weld. The arc welded panels were made using single pass fillets and single sided four pass butt weld. The test section measured 1100mm by 550mm wide and 12mm thick, the test section having been reduced from the original 1600mm width. All butt welds attaching the end sections to the test rig were ground flush with the plate surface to reduce stress concentration effects.

The test were undertaken in air at a frequency of 1Hz. Strain being measured by strain gauges located as shown in figure 6. The stress ranges used for the pairs of panels were 6 to 106MPa and 6 to 156MPa. The arc welds failed as might be expected with fatigue cracks spreading from the toes of the fillet welds. None of the laser welded panels failed in the test section. The more lowly stressed (100MPa) laser welded panel survived twice the number of cycles of the arc welded equivalent and the more highly stressed laser panel (150MPa) survived to five times its arc welded equivalent before the test was prematurely terminated.

In the above tests the plain transverse butt weld and the non load carrying transverse fillet weld can be classified according to the British Standard on fatigue design in welded structures as Class D and Class F respectively. The SN data for the tests are plotted in figures 7. and 8. If mean stress is used both arc weld results lie below the minus two standard deviation Class F design curve. But using maximum strain the results are more in line with the expected behaviour of Class F welds. The surprisingly short life of the arc welded panel may be due to the large length of weld tested. For the laser welds, the specimens are unbroken and the results lie above the Class D line. In the case of one of the laser welded panels the arc welded supporting fixture (Class D) failed and in consequence provides strong circumstantial confirmation that laser fillet welds can be classified as Class D or better in contrast to arc fillet welds which barely meet Class F for this type of specimen.

The most likely explanation for the superior fatigue performance of the laser welded panel is the much neater weld profile. It is known that the stress concentration effect of a transverse fillet becomes more severe as the leg length of the fillet increases.

e) Fracture mechanics toughness tests

Dynamic CTOD tests were carried out on the test plates in order to obtain a more direct link between laboratory tests and structural performance than can be achieved using charpy energy. The necessity to use dynamic CTOD tests is because most ship steels and welds are sensitive to loading rate. If static fracture mechanics testing is used, a ship steel which maybe brittle under dynamic loading may appear misleadingly ductile if slowly loaded. The dynamic CTOD test is performed on a sample of the same thickness and crack sharpness (fatigue cracked) as the structure, at a structurally relevant temperature and loading rate. Using the structurally relevant parameters, temperature, strain rate and stress level fracture mechanics will give an unambiguous answer on whether the steel or weld is suitable for use in ship construction.

In the testing described a number of sample types were used see figure 9:

1) a deep machine notch on weld centre line;
2) a deep machine notch on weld HAZ;
3) a deep machine notch in the plate;
4) a shallow notch on weld centreline;
5) a shallow notch on weld fusion line.

The result of the tests can be summed up in figure 10. for the weld centreline where the laser weld results are superior to those for single and multipass arc welds. For the weld HAZ the dynamic toughness of the laser welds figure 11. are equivalent to those for the single pass arc welds but somewhat less than for the multipass arc HAZ. The defect tolerance of the laser weld zone is greater than that of conventional arc welds and that of the laser weld HAZ is equivalent to that of the single pass arc weld. It is clear therefore that the laser welds tested have adequate toughness for use in ship structures (3). Where the fatigue crack is located in the weld the crack deviated and propagated by cleavage along the fusion boundary whereas a crack initiating in the fusion boundary continued in that plane.

2. Corrugated Core Structures

An alternative concept to frame stiffened panels is LASCOR a lightweight metal corrugated cored structure which has been under development since the late seventies. Test and evaluation is continuing in the areas of static and dynamic strength, fire, corrosion, fatigue and ease of manufacture. The concept originally developed for reduced weight and survivability, was focused on top side structures above the main strength deck where there is the highest payoff. However , there are many other applications below topside and above the ships centre of gravity where there could be advantages in weight savings such as decks, bulkheads, ramps, hatch covers, etc. Although reduced strength is not ruled out in main strength decks it would require a significant test and evaluation program to validate its use.

Originally a number of cored structures were considered to give designers options over conventional ship structures at affordable cost. Lascor does not require conventional stiffening until you get to major transverse supports and the designers by taking advantage of the self stiffening configuration can increase the usable compartment volume. This provides more usable space and uninterrupted flat surface areas for supporting marine systems which results in reduced fabrication costs over conventional plate beam construction.

Lascor sandwich panels are a type of stress-skin construction in which the face sheets resist nearly all of the applied edgewise loads (i.e. in-plane compression and tension) and flatwise bending moments and shear. The corrugated core spaces and stabilises the face sheets and transmits the shear. The concept relies on two strong, thin face sheets far enough apart to achieve a high ratio of stiffness to weight, using a strong core that provides the spacing and also provides the required shear resistance and face sheet stability. Because of its basic corrugated core configuration, the structure can be optimised on the basis of weight and/or cost by varying one or more of the design variables: core height, core pitch, core angle, core landing, core thickness, face sheet, and material height, figure 12. For example, if high stiffness is required, as with the case of vibration concerns, then more closely spaced corrugations are required. However, this necessitates increased welding time because of the increased number of corrugations which require to be welded. To reduce cost and weight, a non-symmetrical design may be generated by reducing the bottom plate thickness. It should be noted that in bending of thin plates alone, LASCOR is about 10 times stiffer than steel.

Lascor is orthotropic and thus it was necessary to develop a parametric FEM study to establish its response in to bending moments, shear forces, membrane forces and deflections. The developed theoretical equations required validation and this has been carried out using small scale tests of in-plane compression, bending and shear. The test data allows reliable equations to be developed which predict the critical buckling strength of the face sheet and core under these conditions. Based on this data the initial structural failure of the panel can occur by local buckling of either the face sheet or the core. This has been confirmed many times but what is not fully understood is what the global buckling behaviour is and how to predict its behaviour.

a) Results of Small Scale Testing

The Lascor concept is a departure from the norm and equal confidence must be developed in the reliability and performance of these structures before designers will consider using such structures as a viable alternative in ship construction. In order to develop confidence in Lascor structures it is necessary to examine the performance of the proposed structures. This can best be achieved with small scale panels the eventual transition to large structures and finally a full scale construction on the form of a ship. What the designer wishes to know is, having designed a Lascor panel for a particular purpose to meet certain strength and stiffness requirements, will the panel perform in the predicted manner? Equally important, will the laser weld stand up the imposed stresses.

The US and UK navies have developed a number of designs for laser panels with a variety of dimensions, testing them both statically and in fatigue. The static tests were carried out in order to determine the Longitudinal and Transverse Bending Strength, the Longitudinal and Transverse Shear Strength, the Flatwise Compression Strength and the Longitudinal and Transverse Edgewise Compression Strength. Additionally, a number of fatigue tests were carried out using of the above test directions.

The tests described here were carried out on laser welded panels with the dimensions shown in figure 13. Although panels have been manufactured using single, twin, triple and sinusoidal laser welds per corrugation, the results quoted here refer to panels welded only using a single linear run per corrugation.

The results of the longitudinal and transverse bend tests are shown in figure 14. plotting deflection, as measured by a displacement transducer located in the centre of the panel against load, measured directly from the testing machine. It is clear, as might be expected, that in the longitudinal direction, the maximum bending load achieved is considerably greater then in the transverse direction. The loading in both test directions increases to a maximum before falling away as bowing commences in the core adjacent to the face plate below the loading points. As bowing develops through the core, as in the case of the longitudinal bending test, the load remains high before falling as the core collapses.

For the comparison of the longitudinal and transverse shear strength tests, figure 15. there is again a considerable difference between the two test directions.

After reaching a maximum the load, in the case of the longitudinal test sample, remains high as bowing occurs in the core, before collapse of the structure takes place below the loading points, as indicated by the fall off load. The load thereafter rises again as the structure becomes rigid due to the local interaction of the buckling and bowing modes of failure.

The collapse of the flatwise compression test sample was characterised by two peaks in the load deflection curve, figure 16. The load initially rises as the panel resists the imposed deflection before falling off as the core succumbs to failure by buckling. Following the initial failure mode there is a further increase in load as the realigned core continues to resist the increased deflection before the load ultimately falls again with the final buckling of the vertical core members Clearly deformation of the panel in the through thickness direction has the potential for absorbing a considerable amount of energy as the core collapses. This could be beneficial in some circumstances, such as blast loading.

Longitudinal and Transverse Edgewise compression tests also show considerable variation in performance, figure 17. Once again the results for the load carrying capacity of the longitudinal sample is much greater than that for the transverse sample The small flat portion of the transverse curve is the result of the early buckling which is not evident in the longitudinal sample.

The final failure in all the static tests was by core buckling. In no case did any of the laser welds fail even though in some extreme cases the surface plates showed signs of ductile tearing. The modes of collapse varied somewhat but generally followed the forms shown in figure 18.

In addition to the static loads tests some fatigue testing has been carried out using similar loading regimes. Here, it was assumed that there was equivalence between a "longitudinal welded attachment loaded parallel to the weld," (British Standard Classification C (BS5400 Part10, 1980 Steel, Concrete and Composite Bridges, Code of Practice for Fatigue)) and the Lascor samples tested in longitudinal compression. It was also assumed that the Lascor transverse bend, longitudinal edgewise compression and the transverse edgewise compression fatigue tests were equivalent to a "longitudinal welded attachment loaded transverse to the weld" (BS5400 Classification F). The results for these tests, figure 19., indicate that the various requirements are attainable. It has also been shown that, as might be expected, multiple welded panels perform better than panels with single linear welds and that panels using sinusoidal laser welds to attach the face plates to the core exhibit the best performance.

b) Service Requirements

1. Fire.

In general Lascor type structures have an advantage when it comes to fire, as compared with steel plate beam structures which require insulation, in that the open volume acts as an insulation barrier in the transmission of heat from one side to the other. This barrier contributes to a significant temperature differential when Lascor panels are subjected to ASTM E-119 slow temperature rise versus time type fire tests. The E-119 criteria requires that the temperature on the non-fire side remains below 232°C (the accepted temperature for the ignition temperature of common consumable materials) for the first 30 minutes. For the E-119 fire tests a bare 51mm thick Lascor panel took twice as long to reach 232°C as the flat plate equivalent, eight times as long if the voids are filled with foam (polyisocyanate) and will never reach 232°C in a 60 minute E-119 test with 25.4 mm of standard insulation on one side; no foam filled voids.

2. Noise

Lascor panels are effective in reducing the transmission of high frequency sound but less effective in attenuating low frequency sounds.

3. Corrosion

Lascor was never intended to be submerged in water as is the case of a hull structure, but rather used topside (exposed weather) and internal structure above and below the main strength deck. When Lascor is manufactured from a suitable stainless steel there is no corrosion problem. However, when it is made from carbon steel corrosion protection of the inner core must be considered because of the inaccessible void. For deckhouse structures and other applications exposed to the weather corrosion protection is advisable. For internal non-weather applications corrosion protection may not be required. For cases where corrosion protection is required the use of lightweight close celled foam (polyisocyanate) could potentially solve the problem. This foam can be sprayed into the inner core after fabrication and expands to a given volume filling up the entire void volume. From preliminary corrosion testing this foam has shown considerable promise in eliminating internal corrosion. It completely seals all the hidden volume within the core and it does not absorb water. It also shows promise in providing an effective fire barrier and in some cases may even reduce the amount of fire insulation required.

3. Applications

There are a number of examples in service where corrugated core panels have been used:

a. Close in weapons system enclosure, 8' x 8' x 21', on a destroyer comprising a weather exposed deckhouse made up of a magazine, repair compartment and gun control room. Lascor deckhouse resulted in a 25% reduction in weight.

b. A large avionics workshop complex and stowage platform on board a carrier the former measuring 60' 45' x 10' and the latter 12' x 60'.

c. Deck edge elevator hanger bay door on a carrier. It is reported that there is a decrease in the required maintenance for the machinery which operates the door as a result of a 50% decrease in weight of the door. This door has been exposed to aircraft, forklift, truck traffic and wave slap loads without incident.

d. Large 36' x 12' x 3" antenna platforms on a Navy combattant resulting in a 33% weight saving and adequate structural stiffness.

e. Currently a number of 42' x 22' Lascor hatch covers, which will experience severe static and dynamic loads from stowage and movement of vehicles (tanks, trucks, forklifts, etc.) are being fabricated for the sealift ship programme. It is proposed to fabricate future deckhouses in US Naval and Coast Guard vessels.

f. Primary structural applications are also being considered including flight decks, strength decks, athwart ship watertight subdivision and longitudinal bulkheads.

g. The UK Navy have recently constructed a Lascor 8' x 8' carrier flight deck panel which is about to undergo rigorous testing including buckling. Further tests of this type of structure for both UK and US authorities are planned.

4. Lessons learned

1. No flame straightening of Lascor structure required.
2. Straight orderly routing of marine systems can be achieved.
3. Thermal insulation requirement reduced in Lascor structures due to air space between face sheets.
4. Requirement for structural painting and coating reduced as less surface area exposed.
5. Flatness of Lascor panels minimises deck tiling difficulties associated with conventional decking.
6. Installation of equipment and machinery foundations less complicated.
7. Fire blocking ability of Lascor structures is of great value.

5. Summary

Tests on laser welded ship structural samples has shown that their performance in respect to strength, toughness, fracture mechanics and fatigue is equivalent or superior to similar conventional arc welded structures. Some further work needs to be undertaken to investigate the buckling behaviour of laser welded structures. It is believed that with the appropriate design changes, modifying the structural slenderness of the plating, it will be possible to constrain the failure mode to a smoother elasto - plastic failure.

Laser welded Lascor corrugated core structures have demonstrated acceptable performance via a variety of strength and fatigue tests. Significant weight reductions have been achieved in the structures that have been designed for use in existing classes of warship. The reported performance of these structures to date is very encouraging. Further benefits will accrue from the use of Lascor structures with respect to fire, insulation, flatness, ease of painting and coating etc.

References

1. Brooke S J	High Power Laser Welding of T Joints in Ship Production. Transactions of North East Coast Institution of Engineers and Shipbuilders. Vol. 104, No 3, June 1988.
2. Furio A J Bird J	Lightweight Metallic Corrugated Core Structures an Option for the Future. Proceedings of the Fast Ferry Conference, Singapore 25th - 27th February 1997.
3. Sumpter J D G	Fracture Toughness of Laser Welds in Ship Steel. Advanced Performance Materials 3, 393-405 (1996). Editor F H Froes, Kluwer Academic Publihers.

LARGE DUCTILITY TEST PANEL DIMENSIONS

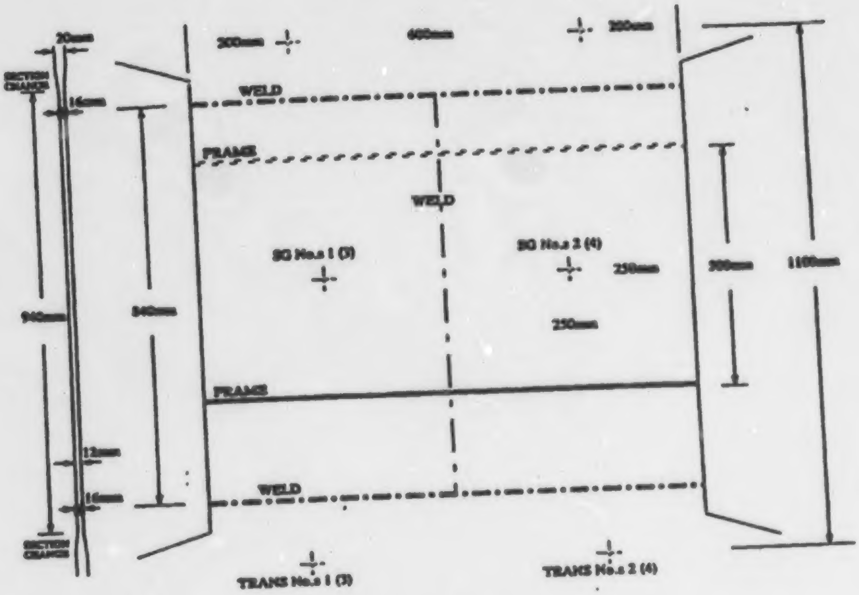
20mm
300mm
600mm
300mm
SECTION CHANGE
16mm
WELD
FRAME
WELD
SG No.s 1 (3)
SG No.s 2 (4)
250mm
300mm
1100mm
940mm
840mm
250mm
FRAME
12mm
WELD
16mm
SECTION CHANGE
TRANS No.s 1 (3)
TRANS No.s 2 (4)

Figure 1.

DIMENSIONS of WIDE PLATE CRACK ARREST TEST

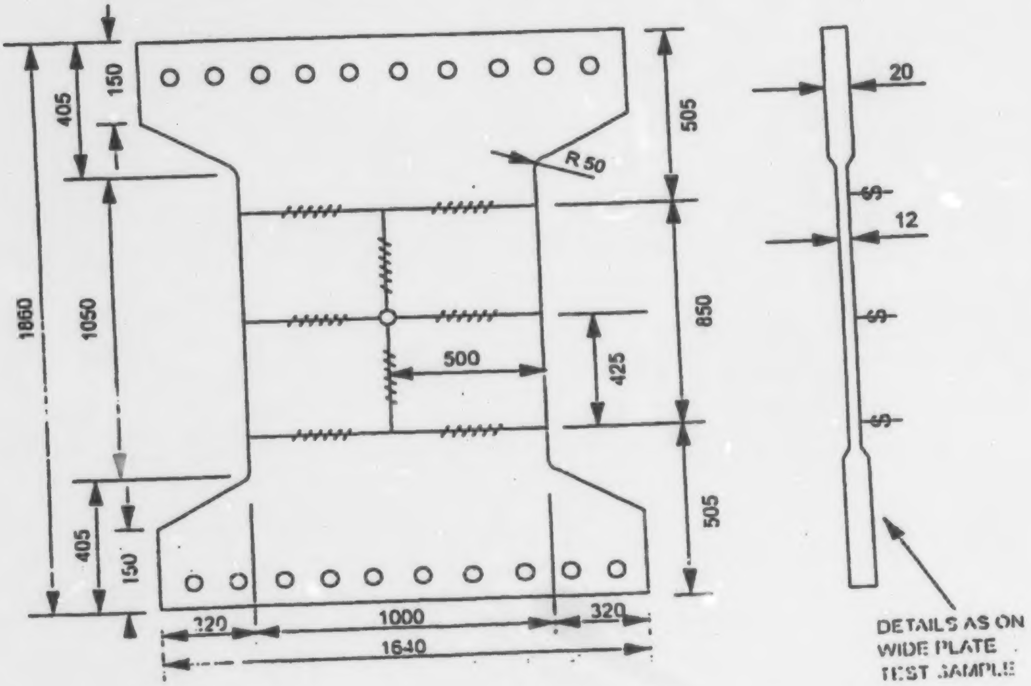
150
405
1860
1050
405
150
R 50
505
850
425
500
505
320
1000
320
1640
20
60
12
60
60
DETAILS AS ON
WIDE PLATE
TEST SAMPLE

Figure 2.

PLAN VIEW of STRUCTURAL PANEL

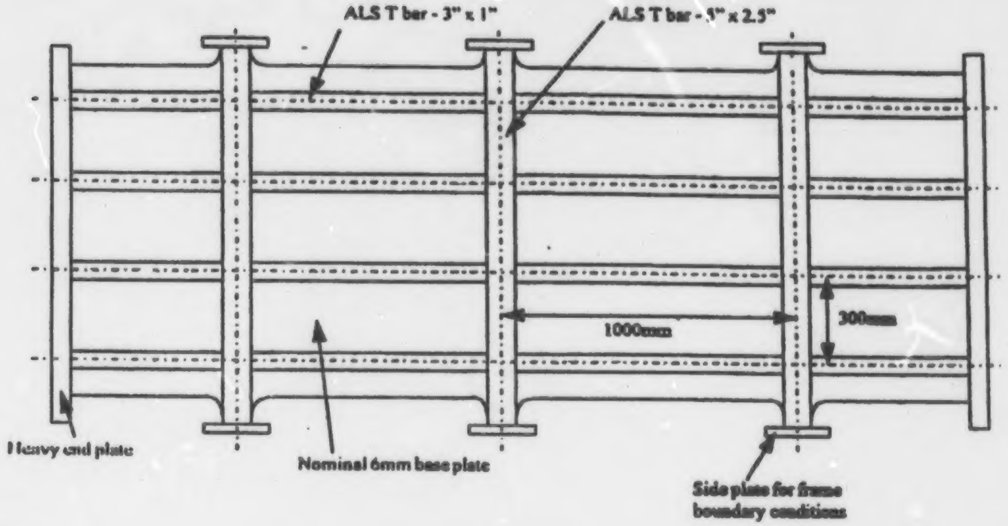
ALS T bar - 3" x 1"
ALS T bar - 5" x 2.5"
1000mm
300mm
Heavy end plate
Nominal 6mm base plate
Side plate for frame boundary conditions

Figure 3.

LASER WELDED PANEL LOAD DEFLECTION CURVE

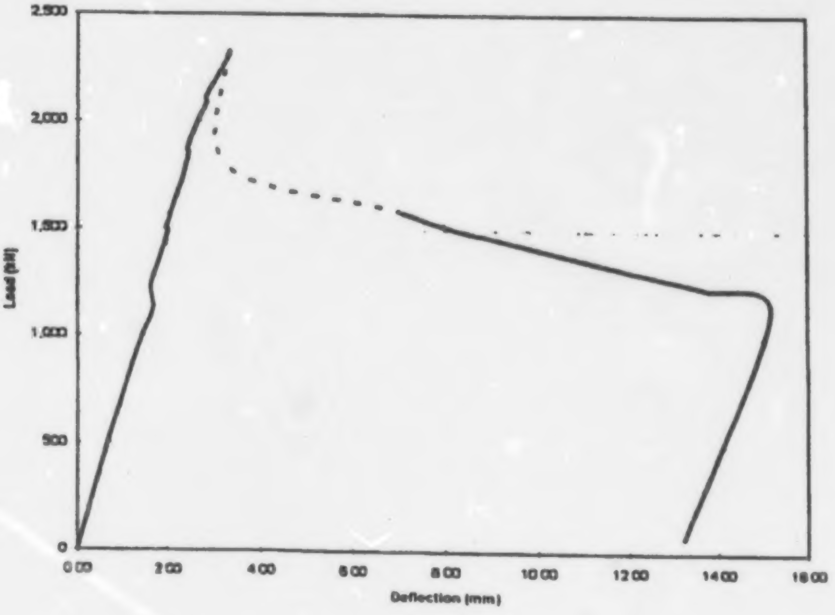

Figure 4.

ARC WELDED PANEL LOAD DEFLECTION CURVE

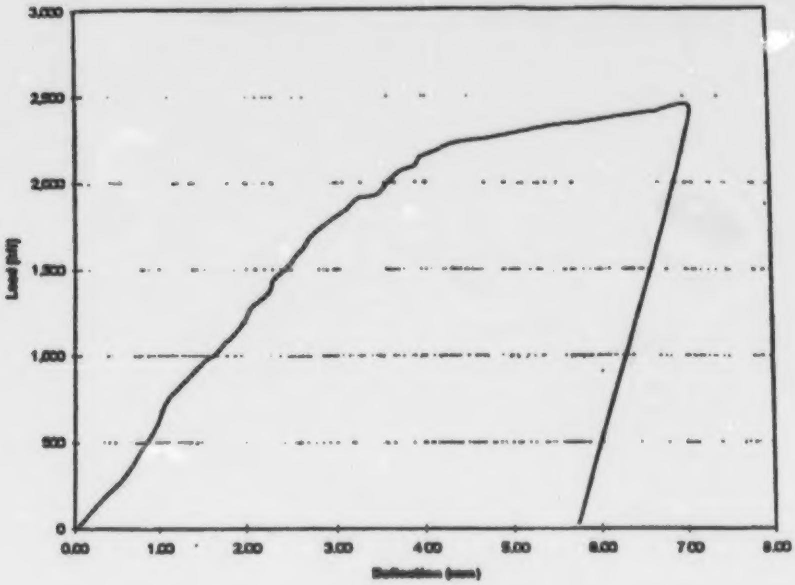

Figure 5.

FATIGUE TEST PANEL DIMENSIONS

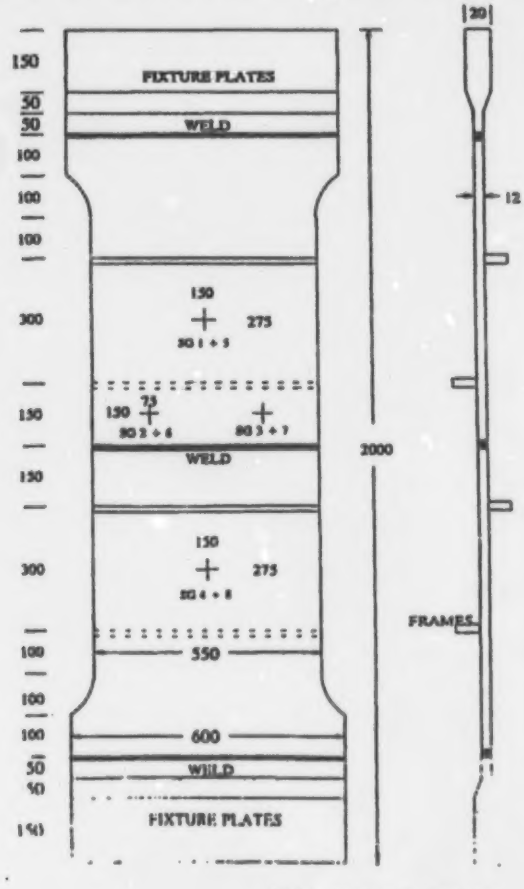
20
150
FIXTURE PLATES
50
50
WELD
100
100
12
100
150
300
275
SG 1 + 5
150
75
150
SG 2 + 6
SG 3 + 7
WELD
2000
150
150
300
275
SG 4 + 8
FRAMES
100
550
100
100
600
50
WELD
50
150
FIXTURE PLATES

Figure 6.

DIMENSIONS IN MILLIMETERS

MEAN CURVE CATAGORIES for FILLET and BUTT WELDS

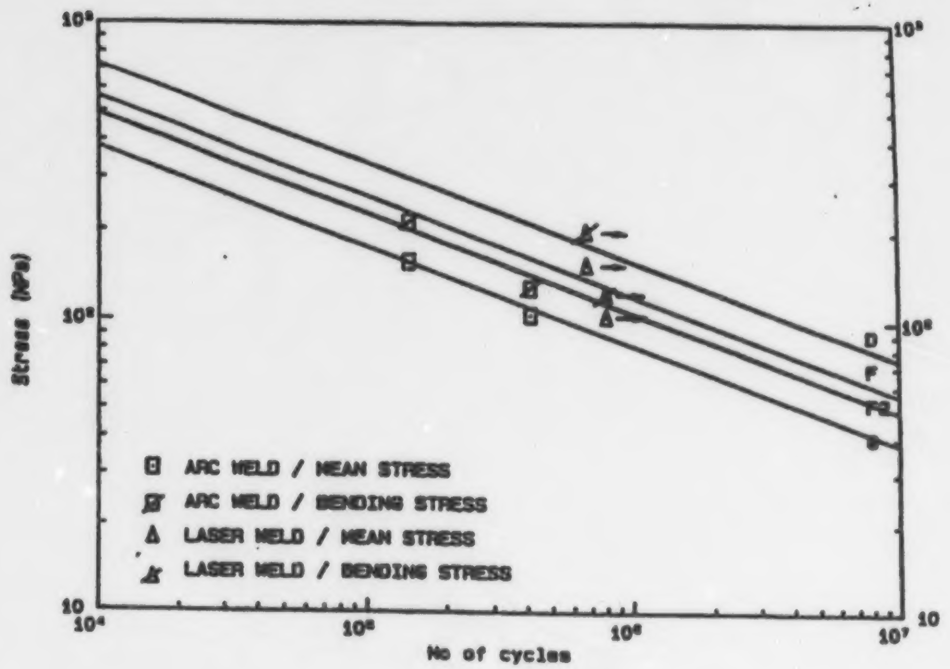

Figure 7.

-2sd CURVE CATAGORIES for FILLET and BUTT WELDS

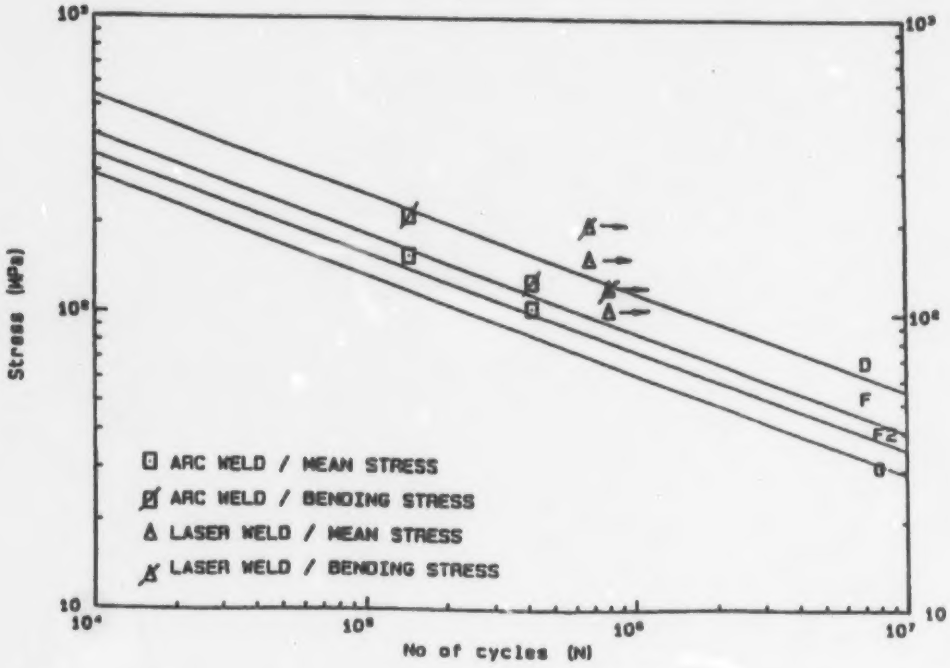

Figure 8.

FRACTURE MECHANICS SPECIMEN DESIGNS

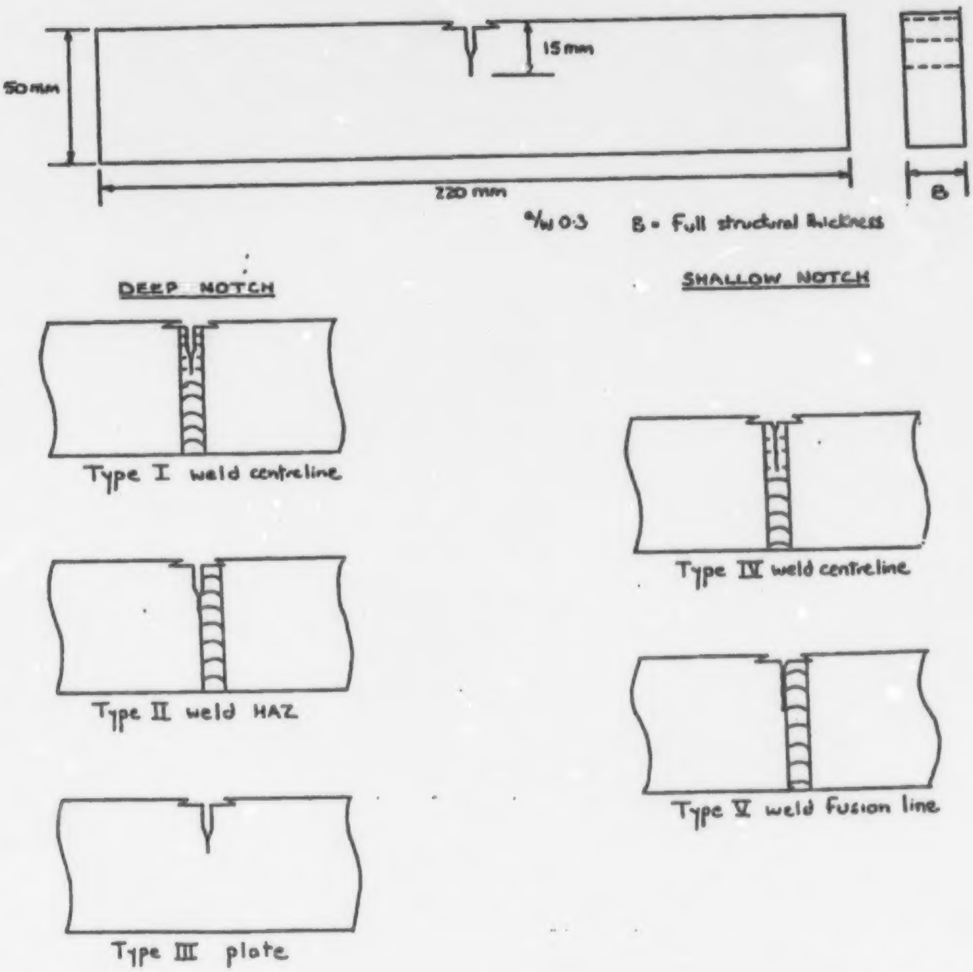
15mm
50mm
220 mm
B
a/w 0.3
B = Full structural thickness
DEEP NOTCH
SHALLOW NOTCH
Type I weld centreline
Type II weld HAZ
Type III plate
Type IV weld centreline
Type V weld fusion line

Figure 9.

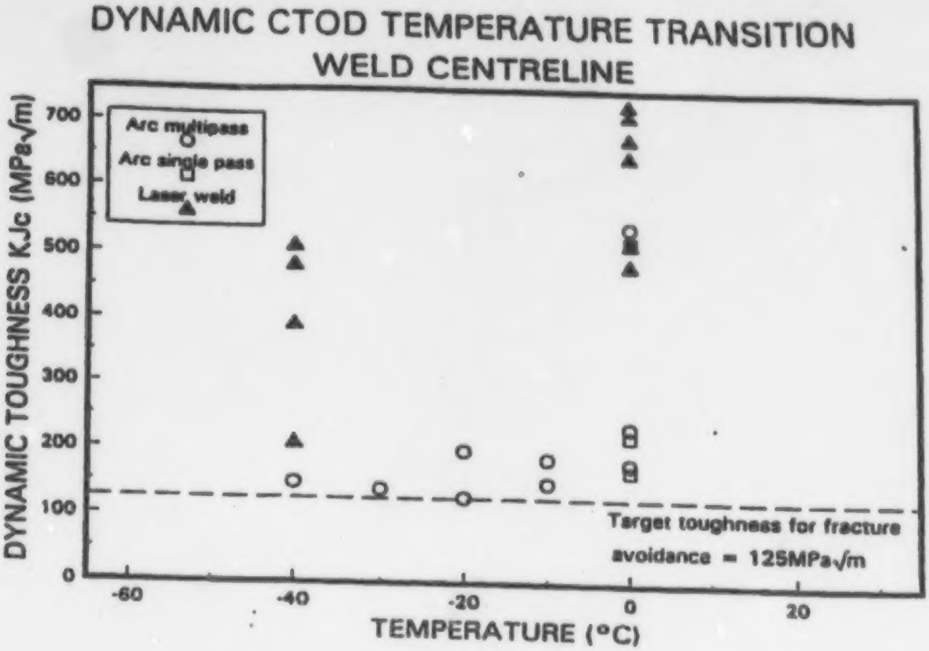

Figure 10.

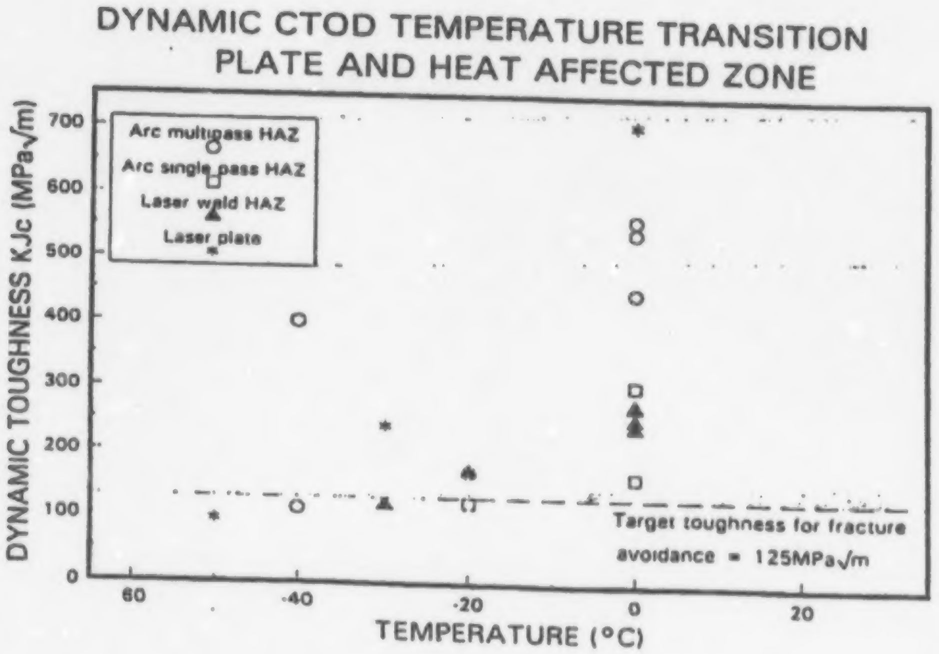

Figure 11.

CORRUGATED CORE SCANTLINGS

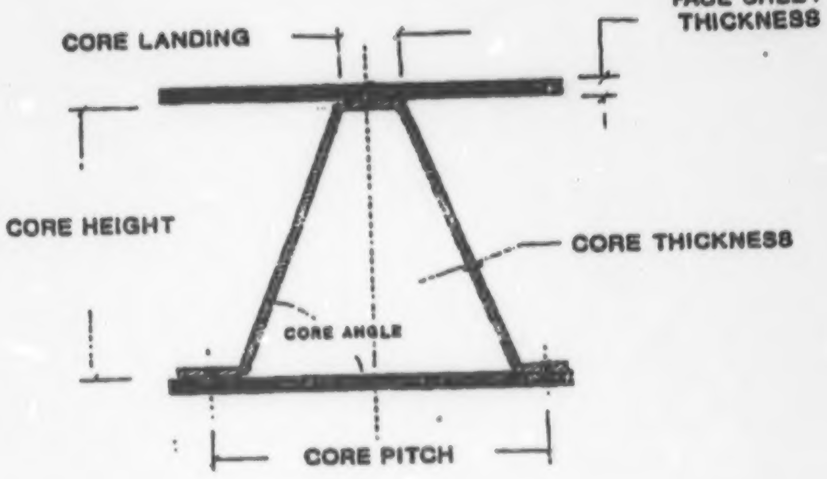
FACE SHEET THICKNESS
CORE LANDING
CORE HEIGHT
CORE THICKNESS
CORE ANGLE
CORE PITCH

Figure 12.

TEST PANEL CONFIGURATION

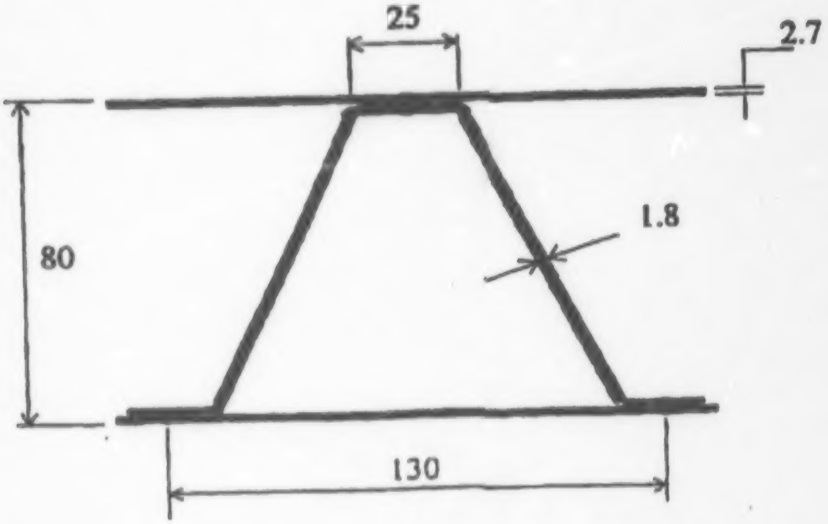
25
2.7
80
1.8
130

Figure 13.

BENDING STRENGTH

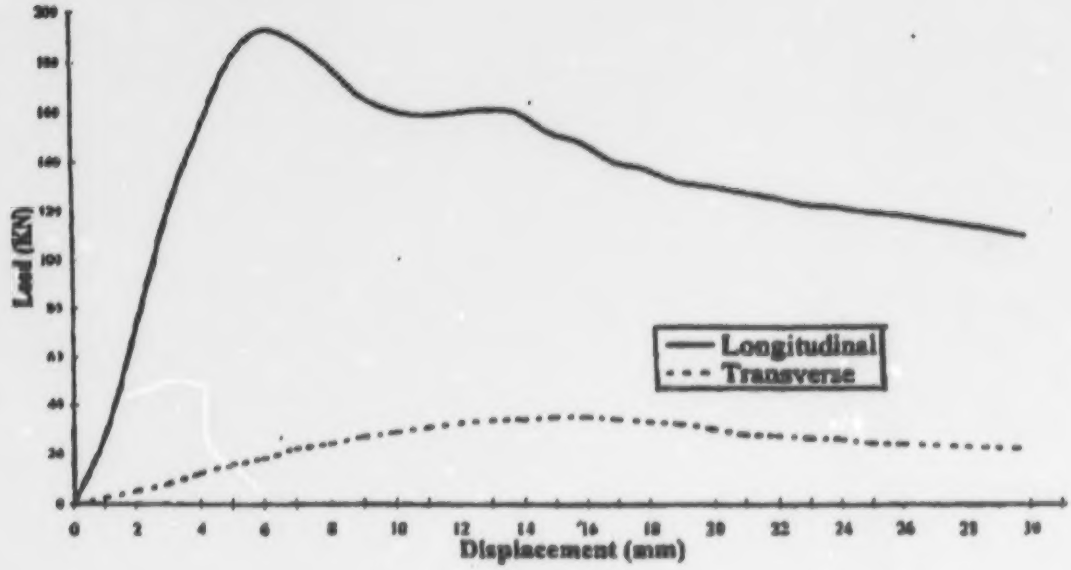

Figure 14.

SHEAR STRENGTH

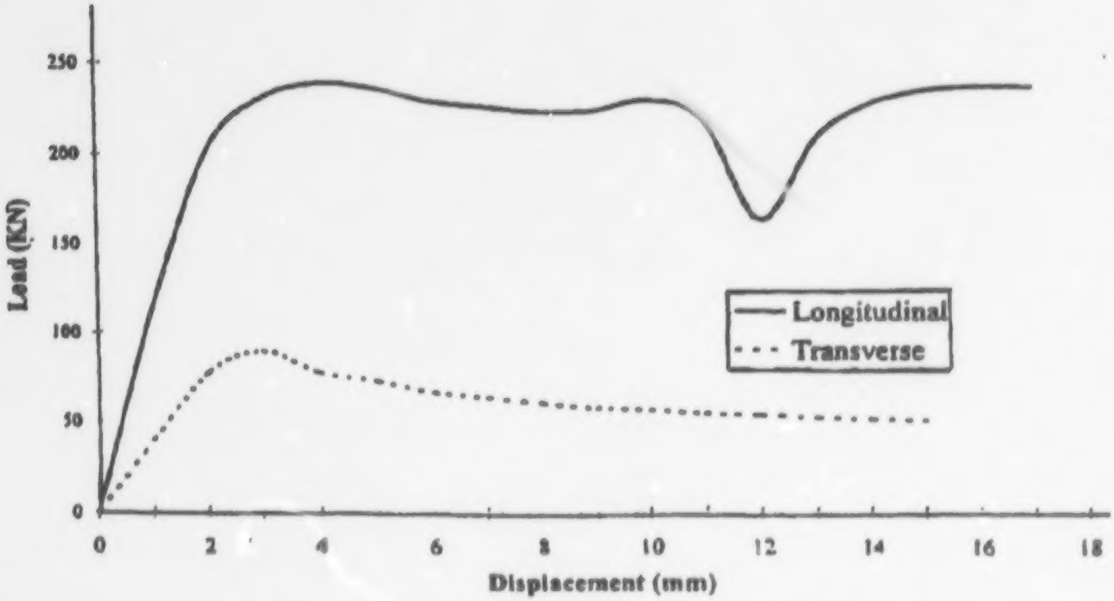

Figure 15.

FLATWISE COMPRESSION STRENGTH

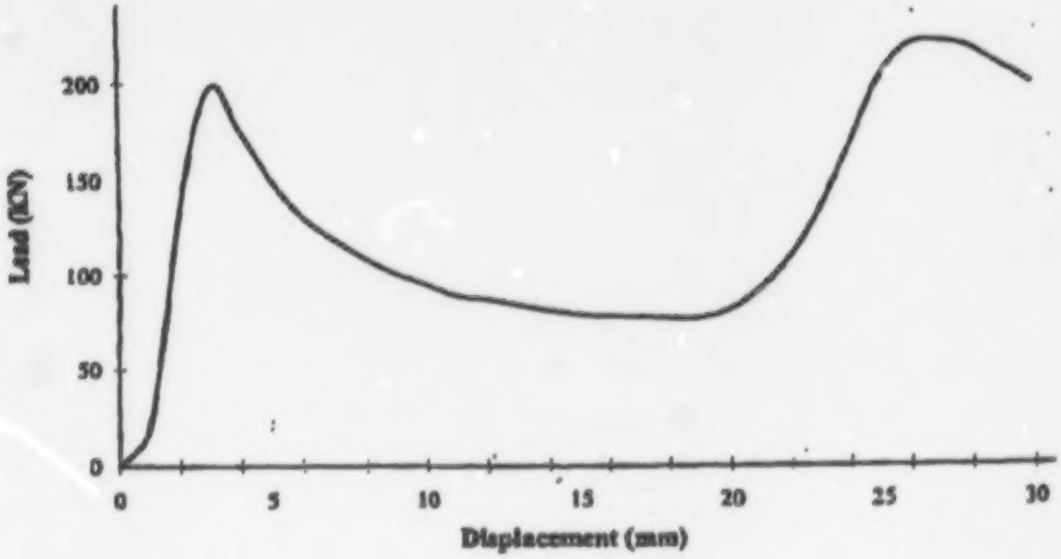

Figure 16.

EDGEWISE COMPRESSION STRENGTH

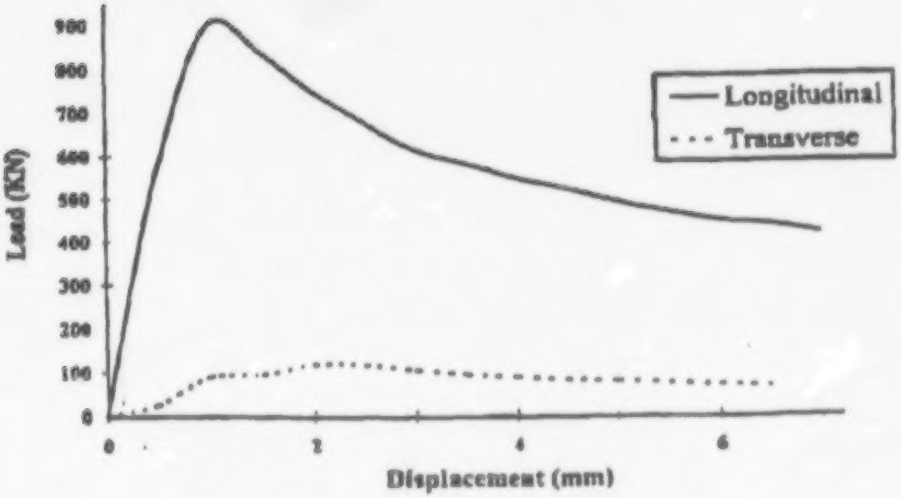

Figure 17.

FATIGUE PERFORMANCE

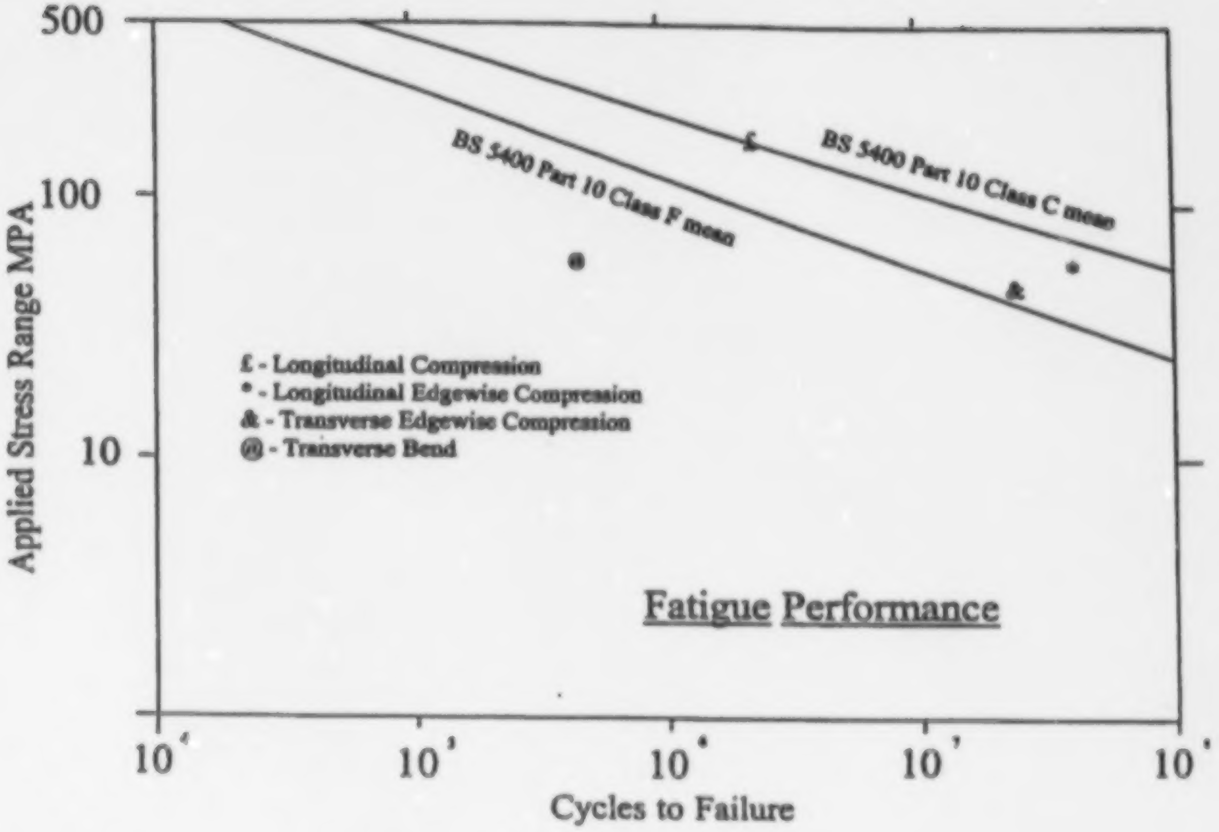

Figure 18.

#507223 ⑳

Tail Shaft Struts on an Aluminum Planing Craft: Problems and Repairs

by

J.C. Thornley
K.G. Sedman and J.W. Carter
RPC

ABSTRACT

The m/v "Marine Courier" was built for passenger transport along the southern coast of Newfoundland, from Port-aux-Basques to Terrenceville, serving such intermediate communities as Burgeo, Ramea and Grey River. The vessel is a triple screwed all aluminum planing craft with a normal operational speed of about 18 knots. Each of the three tail shafts is supported, at its after end, by a strut from the bottom plating. Two of these three struts failed after only a few weeks of service. This article describes the continuing problems with the breaking of the struts by fatigue cracking and with measures taken to prevent them from breaking. These measures included strut design changes, propeller balancing and propeller changes and local weld treatment. The design changes and propeller modifications did reduce the cyclic stresses on the struts. Also, the local treatment of aluminum alloy welds showed that this treatment could be successful in increasing resistance to fatigue cracking at welds. However, success depended on the simultaneous elimination of even minor welding flaws. This flaw elimination could not be achieved sufficiently consistently to provide reliable service and, eventually, stainless steel struts replaced the aluminum struts.

#507224 (21)

Inorganic Intumescent Coatings for Improved Fire Protection of GRP

K.B. Langille, D.T. Nguyen and J. O Bernt
J.O. Bernt & Associates Limited
Mississauga, Ontario

D.E. Veinot
Defence Research Establishment Atlantic
Halifax, N.S.

ABSTRACT

Glass reinforced polymer (GRP) has been identified as a potential structural for naval superstructures and offshore platforms. Although GRP has been used in commercial and pleasure crafts and other areas for the past 30 years, it has limited applications in the military due to its flammability.

Despite its poor fire resistance, GRP has advantages over metals that include high strength-to-weight ratio, stiffness-to-weight ratio, and excellent corrosion resistance. In marine applications, these advantages could result in lighter naval vessels, better performance and lower cost. The present challenge of GRP manufacturers is to resolve the problems of fire, smoke and smoke toxicity of vinylester or polyester based GRP. It must meet the requirements of military standards and building codes in order to expand the market share over metal alloys and other materials.

This paper examines the use of an inorganic coating to improve the fire resistance of vinylester resin based GRP. The selected coating is a totally inorganic system which does not release any organic gases or contribute to the fireload during the fire. The test data will include flame spread index (ASTM E162), smoke generation (ASTM E662), the cone calorimeter test (ASTM E1354), and the Navy Quarter Scale Room Fire Test.

Outline

- Background
- Organic vs Inorganic Systems
- Compositional Development
- Small and Large Scale Evaluations
- Video of US Navy 1/4 Scale Test
- Tech Transfer/Commercial Opportunities
- Summary

Background

- Fire at Sea / Falklands Conflict
- Aim to Minimize Spread of Fire
- Protection of Vulnerable Substrates
- Use Non-toxic Non-combustible Coatings
- Low Cost and Retrofit Capability
- Commercialization

Organic Intumescent Coatings

- Can Add to Fire Load
- Uncontrolled Release of Blowing Agent
- Produce Smoke and Toxic Gases
- Ablation of Surface Char
- Expensive

Inorganic Intumescent Coatings

- Non-combustible / No Added Fire Load
- No Toxic Gases or Smoke
- Strong Rigid Intumesced Structure
- Inexpensive

Silicate Compositions

- Sodium Silicate
- Potasium Silicate
- Litium Silicate
- Sodium/Potassium/Lithium Phosphosilicate
- Mixtures of the Above Silicates

Formulations

- Dried From Solution
- Powdered Granules in Silicate Solution Binders
- Powdered Granules in Latex Binders

Small Lab Scale Evaluation

- Degree of Intumescence
- Water Solubility
- Hygroscopicity
- Efflorescence
- Flexibility
- TGA and DSC for Weight Loss vs Temp

Large Scale Evaluations

- Modified ASTM E 119
- Standard Room Fire Test at NRCC Ottawa
- US Navy 1/4 Scale Fire Test
- Underwriters Lab Test of Fire Door

Technology Transfer

- To J. O. Bernt and Associates Limited
- DREA Research Contracts
- Canadian and US Patents
- DIR Assisted Research and Pilot Plant Setup
- DIPP Assisted Manufacturing

Commercialization

- Fire Doors
- Fireproof Penetration Sealants
- Fire Protective Coatings
- Filled Aluminum Siding (Reynolds)

Summary

- Non-combustible, Non-toxic, Inorganic Intumescent Coating Developed
- Passed Large Scale Testing and US Navy 1/4 Scale Test for Ships and Subs
- Technology Transferred to Canadian Industry
- Fire Doors, Sealants, Coatings and Filler for Aluminum siding

#507225 (22)

Development of Novel High-Performance Protective Coatings for Applications in Severe Environments

S. M. Aouadi and K. L. Yan
Cametoid Advanced Technologies Inc., 1451 Hopkins St., Whitby, Ontario L1N 2C2

ABSTRACT

Cametoid Advanced Technologies Inc. is a member of a group of coating companies which specialise in the development and production of specification coatings for the aerospace, defense and other high-technology industrial sectors. Its research and development capability in functional coatings was initially established in the mid-1980's focusing on conceptual and experimental development of inhomogeneous narrow-band optical filters. Subsequent research efforts have been extended to other coatings for protective functions under severe service environments. Two examples of the ongoing development programs at Cametoid are (a) rare-earth element modified aluminide diffusion coatings for corrosion resistance at ambient and high temperatures, and (b) nitride coatings for erosion and wear resistance applications.

While these two types of protective coatings are being primarily developed for aerospace uses, such as in gas turbine engines, they are finding significant spin-off applications in other market sectors. The fabrication processes employed for these coatings are based on ion assisted physical vapour deposition, one by electrical resistive heating with a subsequent heat treatment, and the other by electron beam reactive evaporation technique. Extensive characterization and test results on these experimental coatings have been generated and will be discussed.

1. Company profile

Cametoid Advanced Technologies Inc. (CATI) is a subsidiary of a private, wholly Canadian owned company, Newman Aerospace Incorporated. It is a company recently formed and incorporated in 1993 as a spin-off sister organization of Cametoid Limited. At present, CATI takes over all research and development activities of Cametoid Limited in advanced materials and coating technologies, and is starting its own manufacturing business using its in-house expertise and technologies.

The mission of Cametoid Advanced Technologies Inc. (CATI) is to identify new and emerging materials and process technologies, develop appropriate capabilities and expertise, and utilize them to provide services of superior quality to the aerospace, space and other high technology industries. CATI's business is based on the development and commercialisation of coatings and surface modification using advanced, environmentally friendly processes with major emphasis on physical vapour deposition (PVD). The areas of expertise of CATI's staff include fabrication of coatings and thin films (optical and metallurgical) by various physical vapour deposition (PVD) processes, computer modelling and design of coatings, advanced materials (metals and alloys, ceramics, polymers, adhesives, ceramic matrix and polymer matrix composites, and functionally gradient materials), material characterization and testing, among others.

The company has the essential facilities for the development of advanced coatings and materials. It possesses a number of dedicated experimental vacuum deposition equipment exclusively for developmental purposes, including those for electron beam evaporation, ion beam sputtering and electrical resistive heating. Most of these deposition systems are equipped with ion beam assisted deposition (IBAD) set-up. Over the past years, it also developed a sophisticated computer software and hardware capability for modelling and designing of coatings and for automated process control. Furthermore, various characterization instruments and test facilities are dedicated or available for R&D use. These facilities include metallurgical and scanning electron microscopes, energy dispersive X-ray analyzer, infrared and VIS spectrophotometers, Betascope for coating thickness measurements, hardness tester, profilometer, precision cutting and polishing equipment for preparation of samples, annealing furnaces, thermal cycling furnace, corrosion test furnace, and environmental test chambers, scratch and erosion testing facilities.

CATI has undertaken both short-term and long-term development projects. The short-term development work is normally focused on process and product enhancement to support the company's current production operation, while the longer term activities are aimed at the development of new processes and products according to the company's strategic plan. CATI has implemented a number of multi-year development programs. Two programs were completed recently: (1) Development of compositional gradient thermal barrier coatings for the protection of hot-section components in aero gas turbine engine applications, in partnership with a major gas turbine engine manufacturer, and with the collaboration of Industry Canada, National Research Council Canada, and University of Toronto; (2) Long durability protective coatings for low-Earth-orbit space applications, under contract with the Canadian Space Agency, in co-operation with the University of Toronto, York University, CANMET of Natural Resources Canada. Three projects are ongoing: (1) Ultra-narrow bandpass filters for defence and space applications; (2) Erosion and wear resistant graded nitride coatings for aero propulsion and energy generating systems; and (3) Yttrium-modified aluminide diffusion protective coatings against high temperature oxidation and hot corrosion.

This paper focuses on two of the above-mentioned projects, namely, yttrium-modified aluminide diffusion coatings and graded nitride coatings.

2. Yttrium-Modified Aluminide Diffusion Coatings

2.1 Introduction

The need for protective coatings in processes involving high temperature (i..e. typically between 600°C and 1200°C) arose when improved performance criteria could not be met adequately in spite of new materials with superior physical, mechanical, and metallurgical properties. An increase in service temperature leads to a higher overall efficiency, e.g. in the conversion of thermal to mechanical energy and subsequently to other forms of power. Protective coatings have been developed to extend the service life of existing materials under the severe operating environments commonly encountered in the aircraft, gas, petrolum, and chemical industries.

The use of aluminide coatings has resulted in significant progress in the protection of components for gas turbines, fuel cells, and equipment in the coal and gas industries. These coatings may be further enhanced through the addition of reactive elements such as yttrium, lanthanum, and cerium. The beneficial effects of the addition of the reactive elements are widely recognized at the present time. For instance, yttrium accumulates mostly on the surface region, adjacent to the alumina scales, and enhances the adhesion of these scales to the bulk diffusion zone.

Conventional techniques for the fabrication of these coatings include plasma spraying, pack cementation, and organo-metallic chemical vapour deposition (CVD) followed by diffusion heat-treatment. Over the past decade, ion vapour deposition (IVD) processes have proliferated in industry owing to their versatility in applications and the environmental friendly nature of the processes. The use of large-scale equipment for these processes has been instrumental in the production of coatings with high quality and performance, while at the same time, meeting the commercial goals with respect to service life, reliability, and cost.

2.2 Fabrication process

In ion vapour deposition or ion plating, coating source material is vaporized in a manner similar to an evaporation process. The substrate is electrically biased at a high voltage to form the cathode of a glow discharge from a gas (usually argon) which is backfilled into the chamber. A schematic diagram of a vapour deposition apparatus is shown in Figure 1. The high discharge potential first ionizes argon gas atoms in its plasma, thus sputter cleaning the substrate by removing oxides and other contaminants from its surface, and later ionizes evaporant atoms, which are then accelerated toward the substrate. This continuous sputtering of the surface results in a cleaner, more adherent deposit, but also a decrease in the net deposition rate. The high gas pressure leads to considerable scattering of the deposit vapour, and results in a much more uniform deposit on the substrate than that observed in normal evaporative processes.

2.3 Results

Figure 2 shows a cross-section of the yttrium-aluminide coating formed after diffusion heat treatment at 1050 °C. Three different microstructural zones are revealed. Zone I contains a NiAl matrix with Cr-Al and Ni_3Al precipitates. Yttrium accumulated mostly on top of this zone (coating surface) to enhance the alumina scale adherence. Zone II is an intermediate layer of intermetallic NiAl and Cr, Co, Mo, Ti, and some other alloying elements in solution. Zone III is the diffusion-substrate interface which contains a Cr-rich lamellar structure with a few TiC and Co, Mo, Ta-rich phases.

Figures 3 and 4 show micrographs of aluminide and modified aluminide coatings subjected to a thermal cycling test at 1100 °C obtained on IN 738 test pins. After 643 cycles, the modified aluminide coated test pins have lost approximately 1.5 mg/cm^2 compared to the almost 2 mg/cm^2 lost by the aluminide coated test pins after 300 cycles, an improvement in the predicted service life of more than two times.

The superior cyclic oxidation performance of the modified aluminide coated pins may be explained by discussing the benefits of the addition of yttrium. Reactive elements have been reported to affect the growth of alumina and/or chromia scales by the following mechanisms:

(i) In alloys without reactive element additions, oxidation occurs primarily through outward cation diffusion from the substrate to the metal/scale interface, although there is some inward oxygen diffusion. In alloys with reactive element addition, the primary transport mechanism is reversed with outward cation diffusion being slowed while inward diffusion is enhanced.[2-4]

(ii) In alloys with reactive element additions, the grain growth of the alumina and chromia scales is reduced via grain boundary pinning resulting in an oxide scale with a small mean grain size.[2,5] Alloys without reactive element additions have oxide scales with larger mean grain sizes as growth is not impeded during high temperature exposures.

3.4 Status

The promising results of this investigation have prompted CATI to file applications for U.S. and International PCT patents. In the meantime, researchers at CATI have embarked on a follow-on project through the addition of transition metals such as chromium, titanium, and silicon to the aluminide coatings to further enhance the high temperature corrosion resistance of the modified aluminide coatings, especially in a sulphate environment.

3. Graded Nitride Erosion Resistant Coatings

3.1 Introduction

Deterioration of the compressor components of aero gas turbine engines under combined corrosion/erosion aggression is one of the main problems influencing turbine efficiency. Existing industrial protective hard coatings, like individual nitrides, carbides, and borides of the transition metals often do not provide the required protection under severe erosion/corrosion conditions.

New progressive types of hard coatings, multi-component coatings such as M-TiN (where M=Al, V, Cr, Hf, etc.), and multilayered composite coatings exhibiting high hardness, high erosion resistance combined with good corrosion resistance and good adhesion may provide reliable protection for aero gas turbine components under severe service conditions. Most promising results have been achieved using compositionally and functionally graded (CFG) technology.

In this work, the following coatings were selected as candidates for protection in aero gas turbines:

- Single component, compositionally and functionally graded coatings, from titanium (Ti) to titanium nitride (TiN)
- Multi-component, compositionally and functionally graded coatings, from TiAlV alloy to (Ti,Al,V)N alloy nitride.

3.2 Fabrication Process

Hard coatings were deposited using a custom-made plasma-asssisted electron beam physical vapour deposition chamber. A schematic diagram of the chamber is shown in Fig. 5. It consists of two electron beam sources, a substrate holder, and a thermionic emitter. The chamber is diffusion-pumped with a cold trap and a Polycold chiller. Two quartz crystal monitors, one for each gun, provide in-situ readings of the deposition rates and coating thicknesses.

Titanium atoms are evaporated by focussing an electron beam onto a titanium rod. Nitrogen is introduced into the chamber to produce compound deposits. A thermionic emitter is used to improve the ionization efficiency of the titanium-nitrogen mixture. A bias voltage is applied to the substrate to provide bombardment of the growing surface to produce dense and adherent coatings.

3.3 Results

A number of characterisation and testing techniques were used to examine the physical characteristics and performance of the coatings. Erosion tests were among the most crucial ones. An uncoated substrate, a standard industrial sample, and several coated samples were tested for comparison (Fig. 6). According to the test results, experimental coatings performed better than the standard sample. Moreover, (Ti,Al,V)N coatings showed better erosion resistance than corresponding TiN coatings (Fig. 7).

3.4 Status

A laboratory scale process to produce functionally graded and compositionally graded nitride coatings was developed. CATI is embarking in the next phase to develop a production-scale process.

REFERENCES

1. G. Kleinert, Sermatech Reviews 33, 3 (1990).
2. P. Kofstad, "High Temperature Corrosion", Ellsevier Applied Science, London 389-424 (1988).
3. R. J. Hussey and M. J. Graham, Oxidation of Metals 45, 349 (1996).
4. E. W. A. Young and J. H. W. De Wit, Solid State Ionics 16, 39 (1985).
5. M. K. Loudjani, A. M. Huntz, and R Cortes, Journal of Materials Science **28**, 6466 (1993).

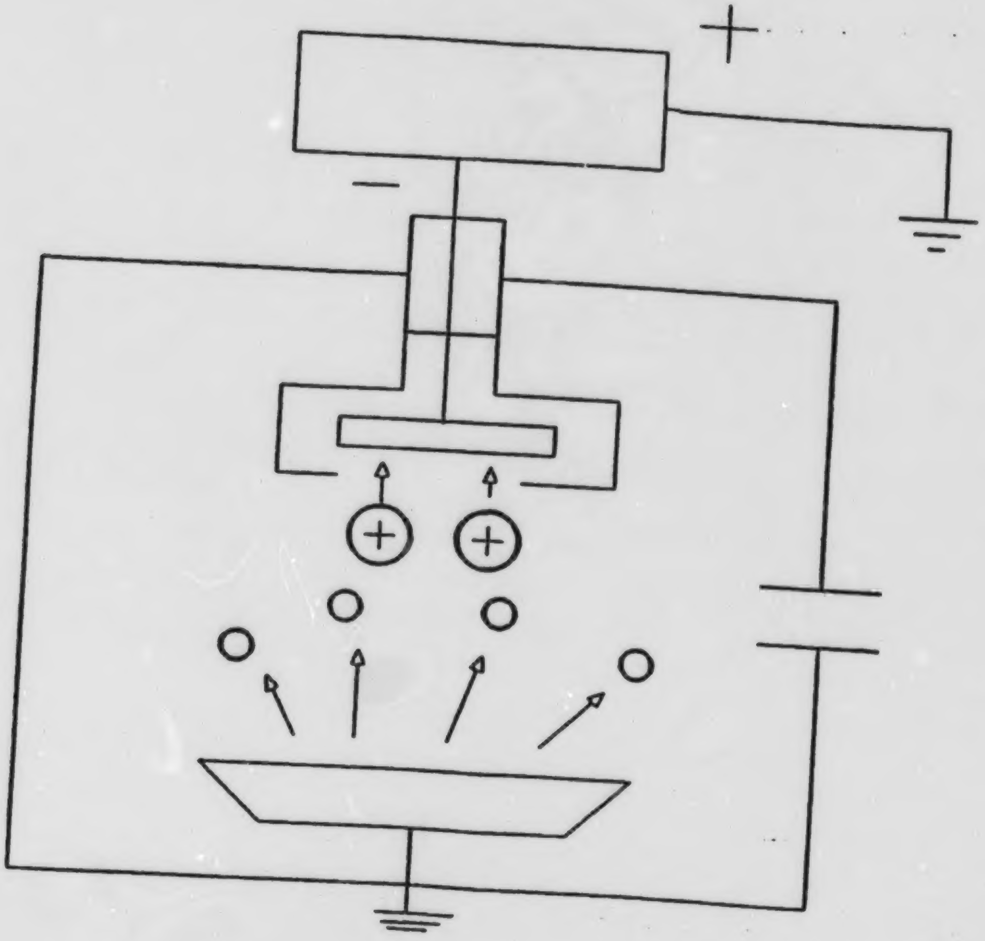

Figure 1: Schematic of ion vapour deposition system.

Figure 2: Cross-sectional micrograph of an yttrium modified aluminide coating on IN 738.

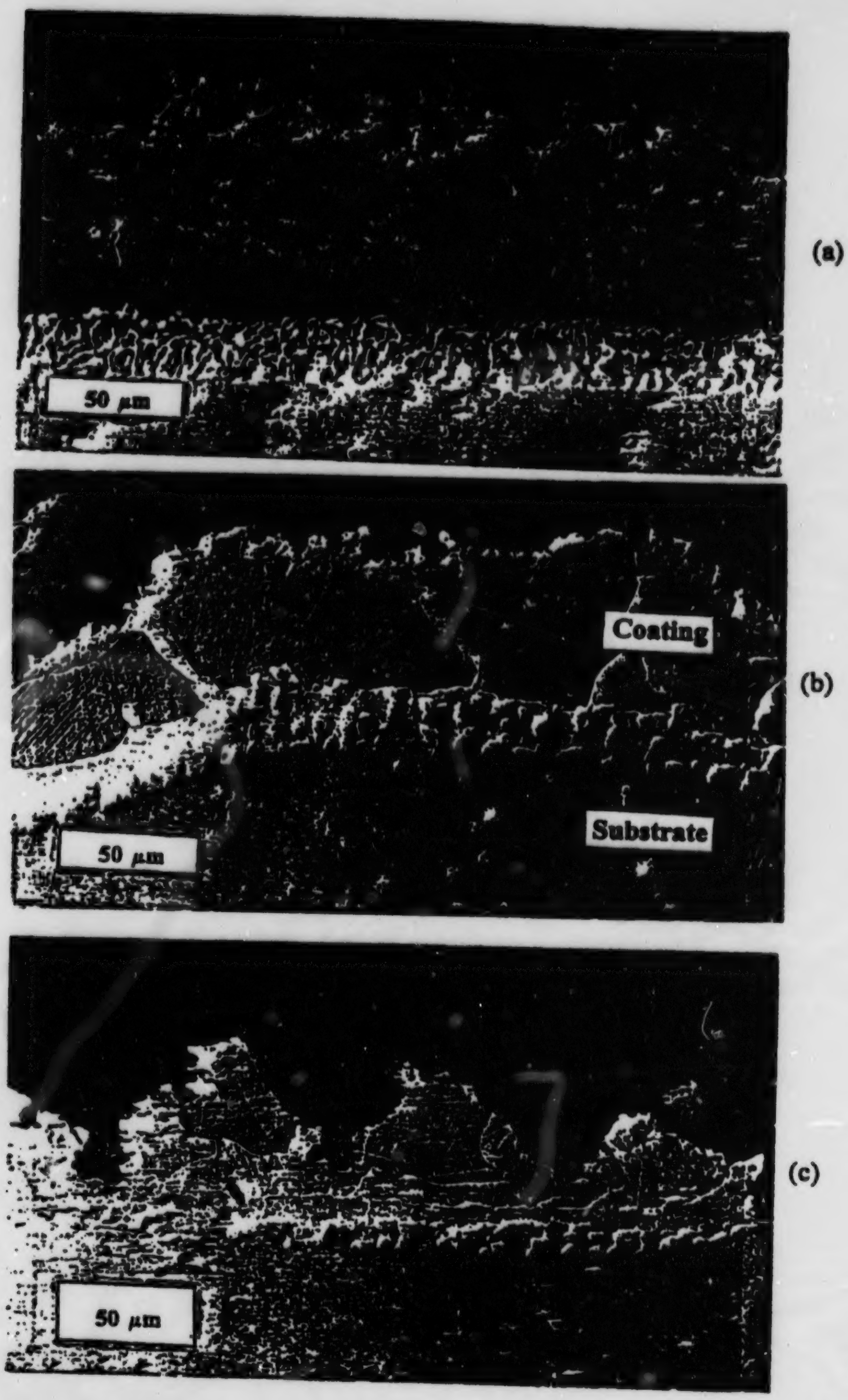
50 µm
(a)
Coating
(b)
50 µm
Substrate
(c)
50 µm

Figure 3: Micrographs of the aluminide coatings heat treated at 1050 °C for 3 hours after thermal cycling test for: (a) 100 cycles; (b) 500 cycles; (c) 800 cycles.

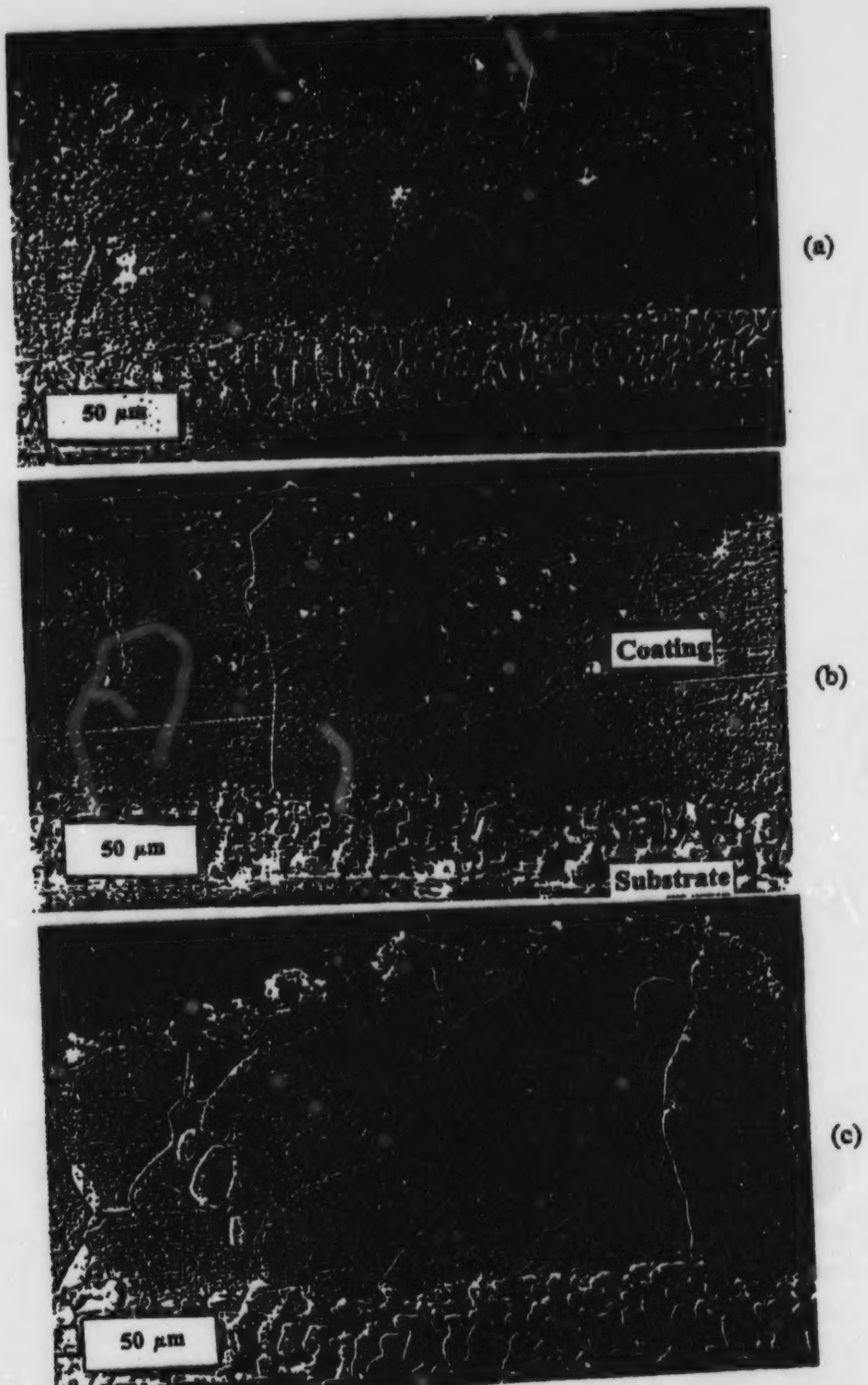
50 µm
(a)
Coating
(b)
50 µm
Substrate
50 µm
(c)

Figure 4: Micrographs of the yttrium-aluminide coatings heat treated at 1050 °C for 3 hours after thermal cycling test for: (a) 100 cycles; (b) 500 cycles; (c) 800 cycles.

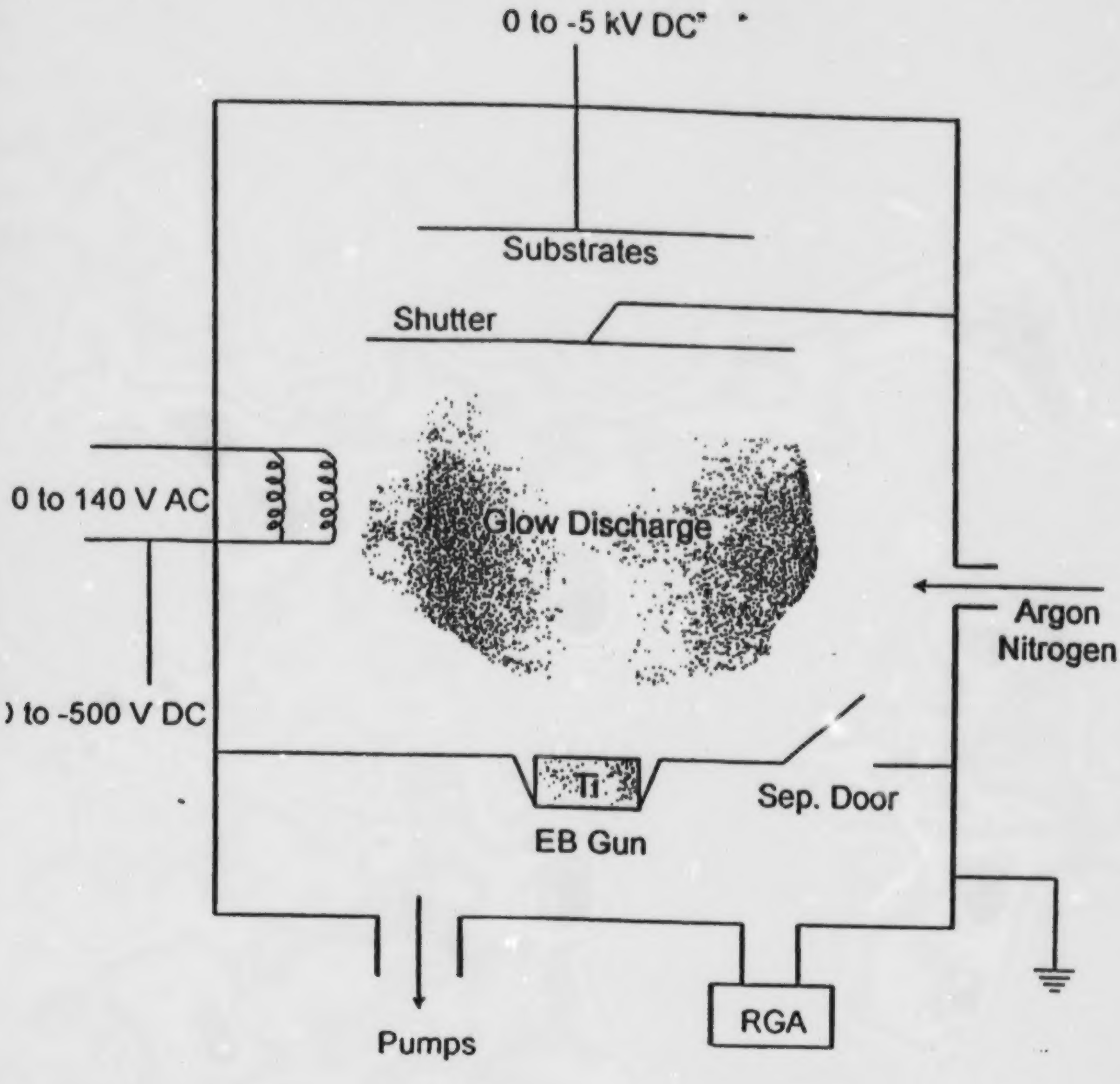
0 to -5 kV DC
Substrates
Shutter
0 to 140 V AC
Glow Discharge
Argon
Nitrogen
0 to -500 V DC
Ti
EB Gun
Sep. Door
Pumps
RGA

Figure 5: Schematic diagram of a plasma-assisted electron-beam physical vapour deposition chamber.

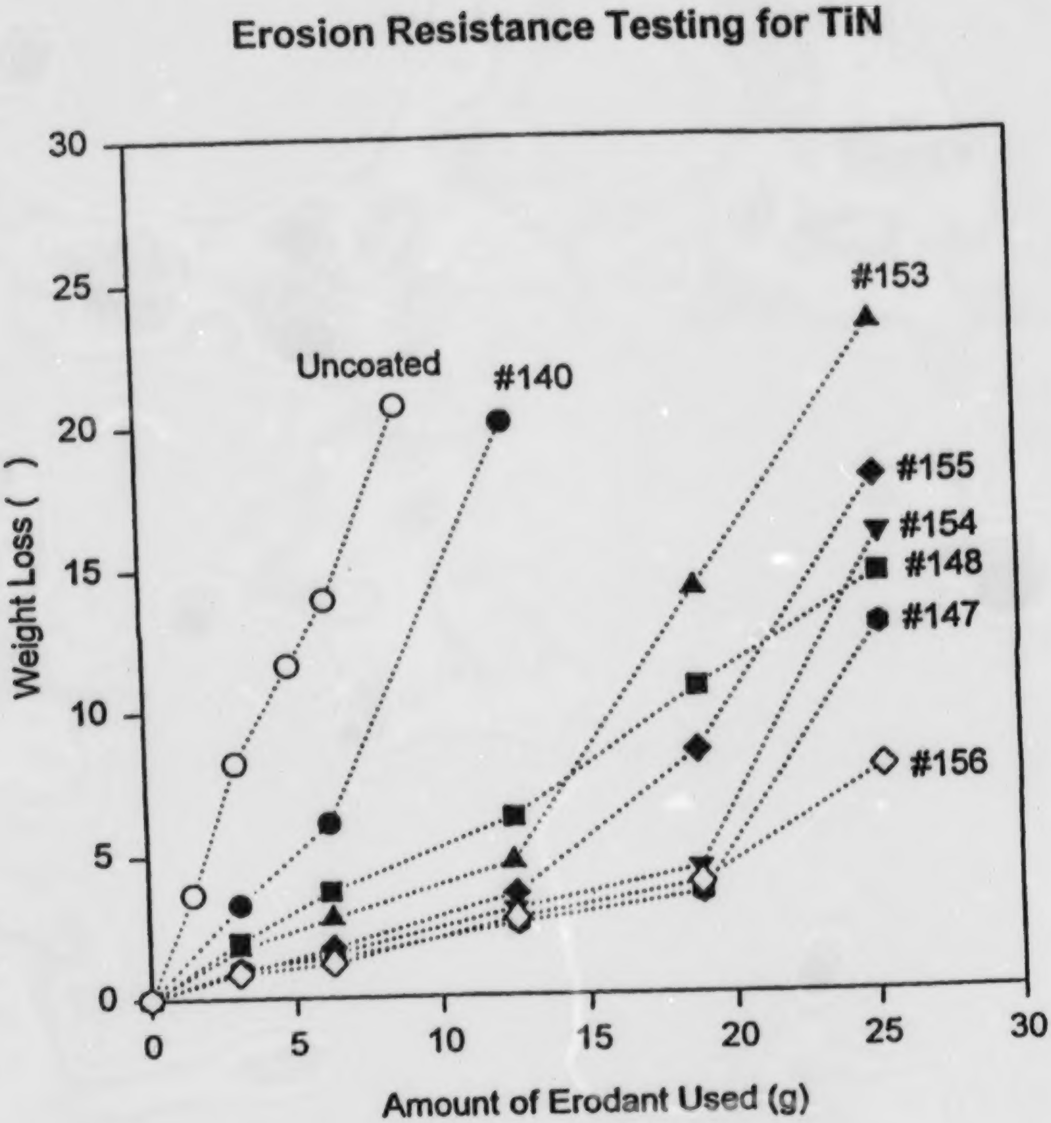

Figure 6: Erosion resistance test for TiN coatings.

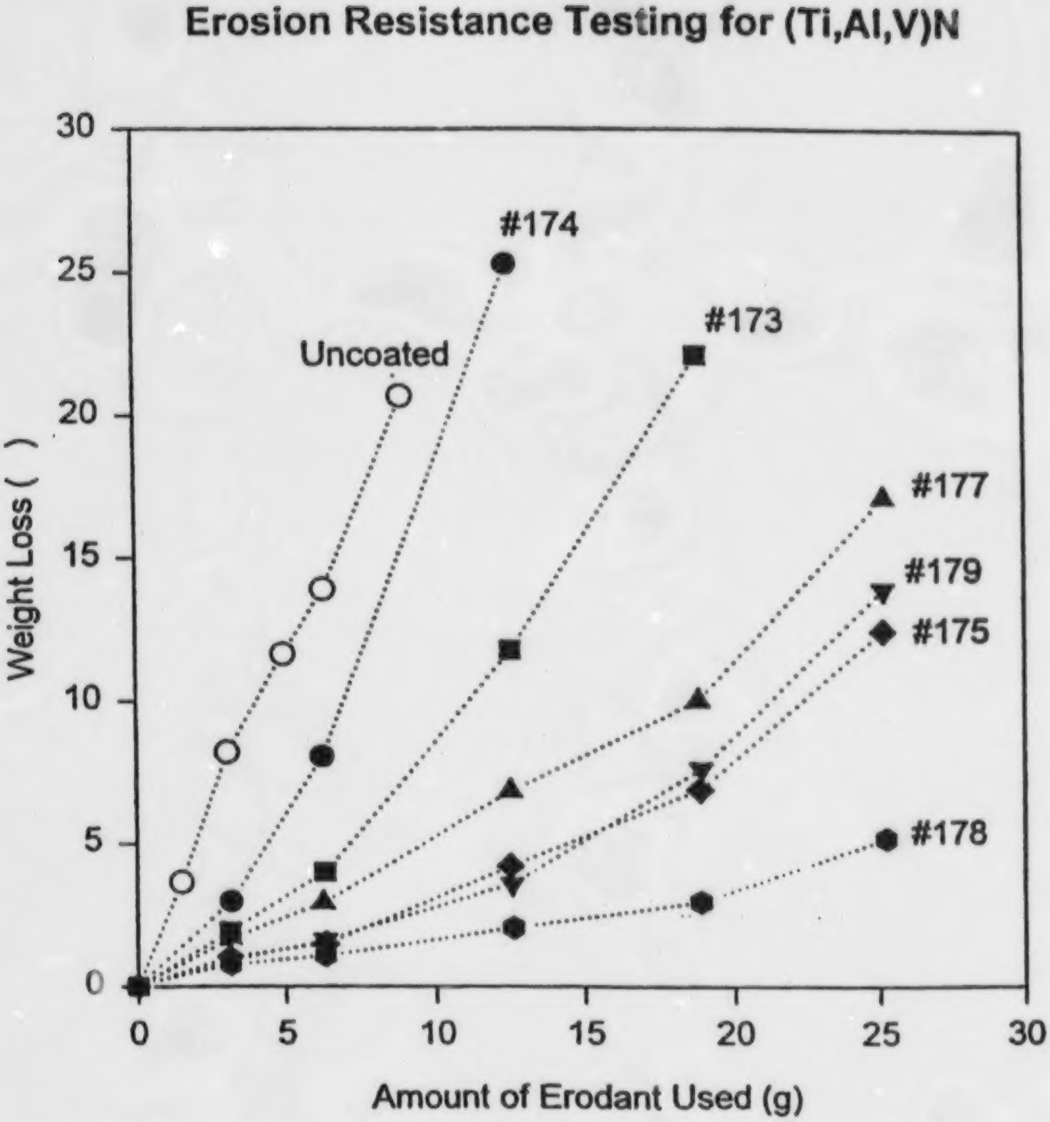

Figure 7: Erosion resistance test for (Ti,Al,V)N coatings.

"AN OVERVIEW OF WATERJETTING ON U.S. NAVY VESSELS AS AN ALTERNATIVE TO DRY ABRASIVE BLASTING"

DR. BRENDA S. HOLMES
U.S. NAVY
NAVAL SEA SYSTEMS COMMAND

JOHN TANNER
AMERON INTERNATIONAL

APRIL 23, 1997
HALIFAX, NS CANADA

WHY USE HYDROBLASTING?

- TECHNIQUE FOR CLEANING SURFACES WHICH RELIES ON ENERGY OF WATER STRIKING A SURFACE TO REMOVE COATINGS
  - CLEANER AND HEALTHIER METHOD
- AVOIDS DUST POLLUTION AND DISPOSAL OF SPENT ABRASIVES
  - SIGNIFICANT REDUCTION IN HAZARDOUS WASTES

EQUIPMENT

- **CLOSED LOOP SYSTEM**
  - NSWC/PRATT & WHITNEY ULTRA HIGH PRESSURE HYDROBLASTING
- **OPEN SYSTEM**
  - CAVI-TECH CAVI-BLAST HIGH PRESSURE HYDROBLASTING SYSTEM
  - UHP PROJECTS, INC.
  - AMCLEAN, INC.

HIGH PRESSURE (HP) HYDROBLASTING

- 10,000 - 25,000 PSI (680 - 1700 BAR)

- EFFECTIVE IN REMOVING LOOSE PAINT, LOOSE RUST, MILL SCALE, AND SOME, BUT NOT ALL, TIGHTLY ADHERENT PAINT

- DOES NOT PRODUCE SURFACE PROFILE

ULTRA HIGH PRESSURE (UHP) HYDROBLASTING

◆ ABOVE 25,000 PSI (ABOVE 1700 BAR)

◆ ABLE TO COMPLETELY REMOVE ALL PAINT FROM A SUBSTRATE

◆ DOES NOT PRODUCE A SURFACE PROFILE (LEAVES EXISTING PROFILE INTACT)

WATER JETTING IS DONE ON MANY TYPES OF VESSELS

AREAS DONE USING WATER JETTING INCLUDE:

* UNDERWATER AREAS
* FEEBOARD AREAS, INCLUDING DECKS
* SUPERSTRUCTURES
* VOIDS, BALLAST TANKS

EXISTING COATING ROMOVAL MAY BE COMPLETE OR PARTIAL

CONCERNS ABOUT HYDROBLASTING

- **FLASH RUSTING**
  - SURFACE CONTAMINANTS
  - HUMIDITY
  - TEMPERATURE
  - TIME OF CONTACT WITH BLAST WATER
- **BLISTERING**
  - PREMATURE COATING FAILURE

INPUT FROM THE COATING MANUFACTURER

- * INTERNATIONAL / COURTAULDS COATINGS SUPPLIED SURFACE STANDARDS

- * DEVOE (AMERON) AND INTERNATIONAL HAD EXPERIENCE WITH WATER JETTING IN THE COMMERCIAL MARINE MARKETPLACE

- * COATINGS SPECIFIED WERE THOSE CURRENTLY APPROVED BY THE U.S. NAVY

- * EXCEPTIONAL RESULTS ARE OBTAINED WHEN MATERIAL IS APPLIED OVER *PROPERLY* WATER JETTED SURFACES

OFFICIAL GUIDANCE

- MESSAGES TO THE FLEET
  - INTERIM GUIDANCE FOR SURFACE PREPARATION BY HYDROBLASTING
    - 120328Z DEC 94
  - GUIDANCE FOR ADHESION PULL TESTS FOR HYDROBLASTED SURFACES
    - 220328Z MAR 95

INTERIM HYDROBLASTING STANDARDS

INTERNATIONAL/COURTAULDS MARINE PAINT COMPANY HYDROBLASTING STANDARDS

- C - STEEL SURFACE COMPLETELY COVERED W/ RUST BUT W/ LITTLE OR SLIGHT PITTING
- HB 2 1/2 - VERY THOROUGH HYDROBLAST (SSPC-SP-10)
- L - LIGHT FLASH RUSTING
  - EXCESSIVE RUST MUST BE REMOVED BY SWEEP BLAST OR HP HYDROBLAST

- **BRESLE METHOD OR EQUIVALENT SENSITIVITY**
  - MINIMUM OF THREE READINGS
- **SURFACE CHLORIDE LEVELS**
  - IMMERSED SURFACES
    - LESS THAN 3 MICROGRAMS/SQ CM
  - NON-IMMERSED SURFACES
    - LESS THAN 5 MICROGRAMS/SQ CM
  - EXCESSIVE CHLORIDES MUST BE REMOVED BY HP HYDROBLAST

ADHESION PULL TESTS

- AW ASTM D4541
- FOR PNEUMATIC ADHESION TESTERS
  - NO LESS THAN 1000 PSI
- ELCOMETER MODEL 106/2 OR EQUIVALENT HAND-HELD ADHESION TESTERS
  - NO LESS THAN 500 PSI
- ADHESION TESTS ON FIRST COAT OF EPOXY PRIMER
  - MINIMUM OF 24 HOURS AT AMBIENT CONDITIONS

UNIFORM INDUSTRIAL PROCESS INSTRUCTION

- FOR USE OF CLOSED-LOOP AND OPEN CYCLE HIGHPRESSURE WATERJETTING EQUIPMENT
- VARYING DEGREES OF COATING REMOVAL
  - COLOR VISUAL STANDARDS
  - WRITTEN DESCRIPTIONS

This page is left blank

This page is left blank

NOMENCLATURE

s	maximum width of shear lip (the average of two sides is used)
a	crack length
Δ_{ac}	critical crack blunting
b	uncracked ligament
B	thickness of sample
W	sample width (specimen dimension parallel to notch)
r_{yc}	critical plastic zone size
K_{Ic}	plane strain fracture toughness
σ_y	yield strength
σ_u	ultimate strength
J_{Ic}	elastic-plastic fracture toughness
DT_E	dynamic tear energy value
Cv_E	Charpy energy value
σ_{flow}	flow stress, $(\sigma_y + \sigma_u)/2$
T - L	specimen orientation transverse (T), notch longitudinal (L)
L - T	specimen orientation longitudinal (L), notch transverse (T)
EDM	electrostatic discharge machining

Introduction

Prediction of ductile behaviour in welded structures requires a knowledge of the structural transition behaviour for the steel and weldments, the minimum service temperatures for the environments surrounding the structure, and the temperature of the steel and weldments themselves taking into consideration any heating and insulation. From this information it can be determined if the structure will exhibit ductile behaviour under all service conditions. Material selection, quality control, weld consumable approval, weld procedure qualification and design are all guided by this information.

Design of structures against fracture therefore requires, at the simplest level, that the minimum service temperature coincide with the upper shelf of the structural ductile to brittle transition curve for the steel and weldments. Material specifications in shipping standards often have no requirement for notch toughness (ie grade A steels) and when they do specify toughness (grades B, C, D, etc.) the specimen (Charpy) is of insufficient size and notch acuity to guarantee that the small scale test transition curve (Charpy transition curve) will reflect the structural transition behaviour and that the structure will be ductile at the lowest service temperatures.

Many commercial ships are built to grade A with no requirement for toughness. It has been estimated that up to 90% of shipping falls into this category. There have been approximately 1000 commercial shipping losses since World War II and many of these losses could have been prevented if notch tough steel had been used. The losses are usually associated with significant events such as collisions, groundings and heavy seas. Poor maintenance and corrosion are often cited as contributing factors. Naval vessels have also been involved in collisions, groundings and severe weather but there have been almost no naval vessel losses in this period. While some of this is attributable to the difference in design, large open tankers, vs small compartment construction etc., all those parts of the ship, exposed to an environment that places the structure on the lower shelf of the plate or weld transition curve, will be subject to brittle fracture.

Historical data on ship fractures and losses is shown in Figures 1a and 1b. The bulk of the data in Figure 1a comes from the final report of the board of investigation into the design and methods of construction of welded steel merchant vessels (i.e. Liberty ships) [1]. For comparison data on the World Concord, the Kurdistan and BS4360 43A (a Lloyd's A steel) are included.

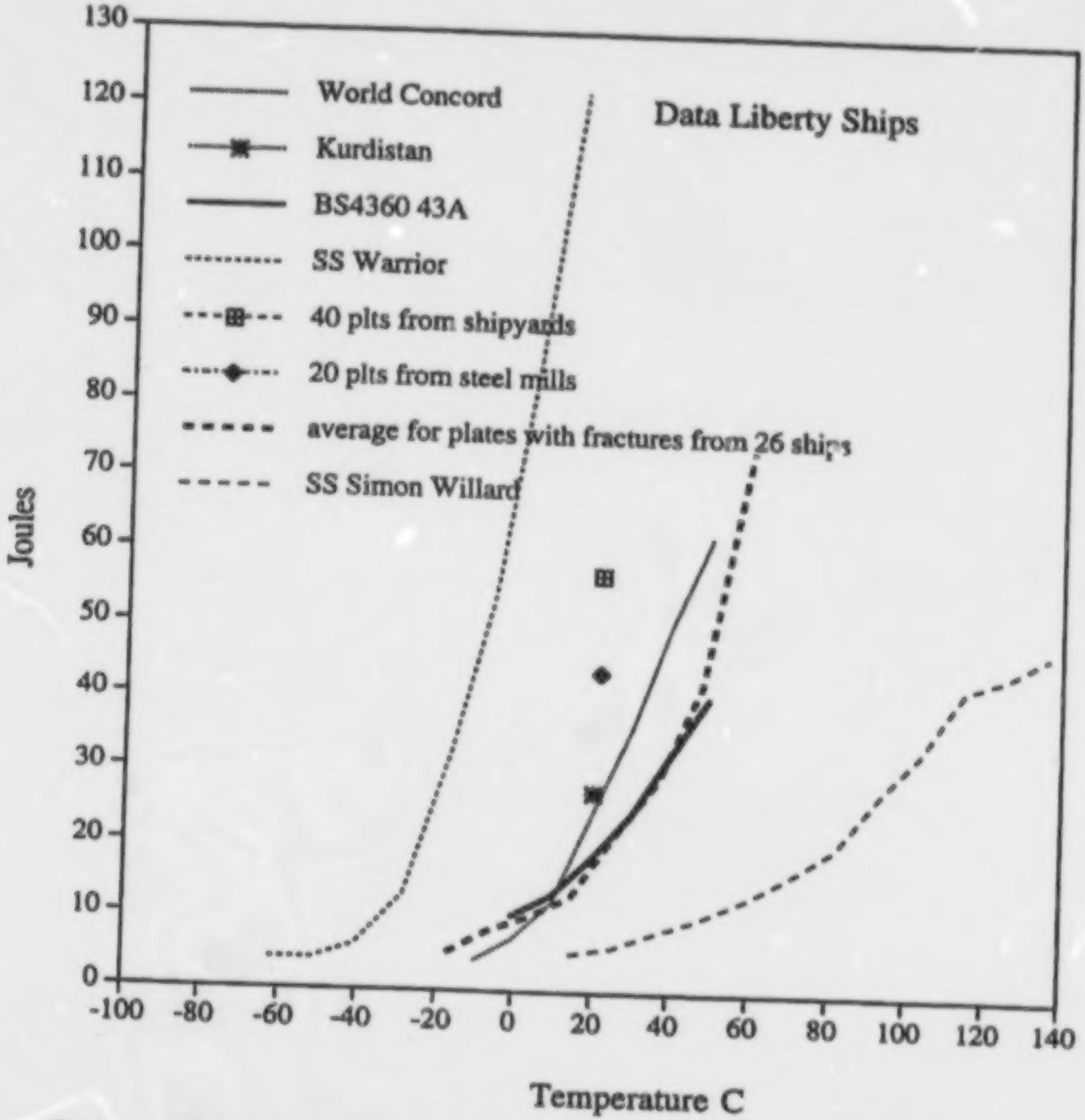

Figure 1a: Charpy transition curve data for Liberty ships[1], BS 4360 43A (a Lloyd's grade A steel) and two recent ships losses.

To compare this data to steels used to construct Canadian Naval vessels, and to other commercial grades of ship steel (B, C, D and E), Figure 1b is included. The area on these two graphs between the transition curve for SS Warrior and SS Simon Willard encompasses most losses. This area also encompasses standards for grades B, C and D. For interest, data for the piece of steel retrieved from the Titanic is also shown. While the requirement for the Canadian Navy (Naval in Figure 1b) and the 350WT steel transition behaviour lie outside the zone of losses, that does not guarantee that our ships are not subject to brittle fracture given the worst conditions. The balance of this report quantifies the risk for our ships.

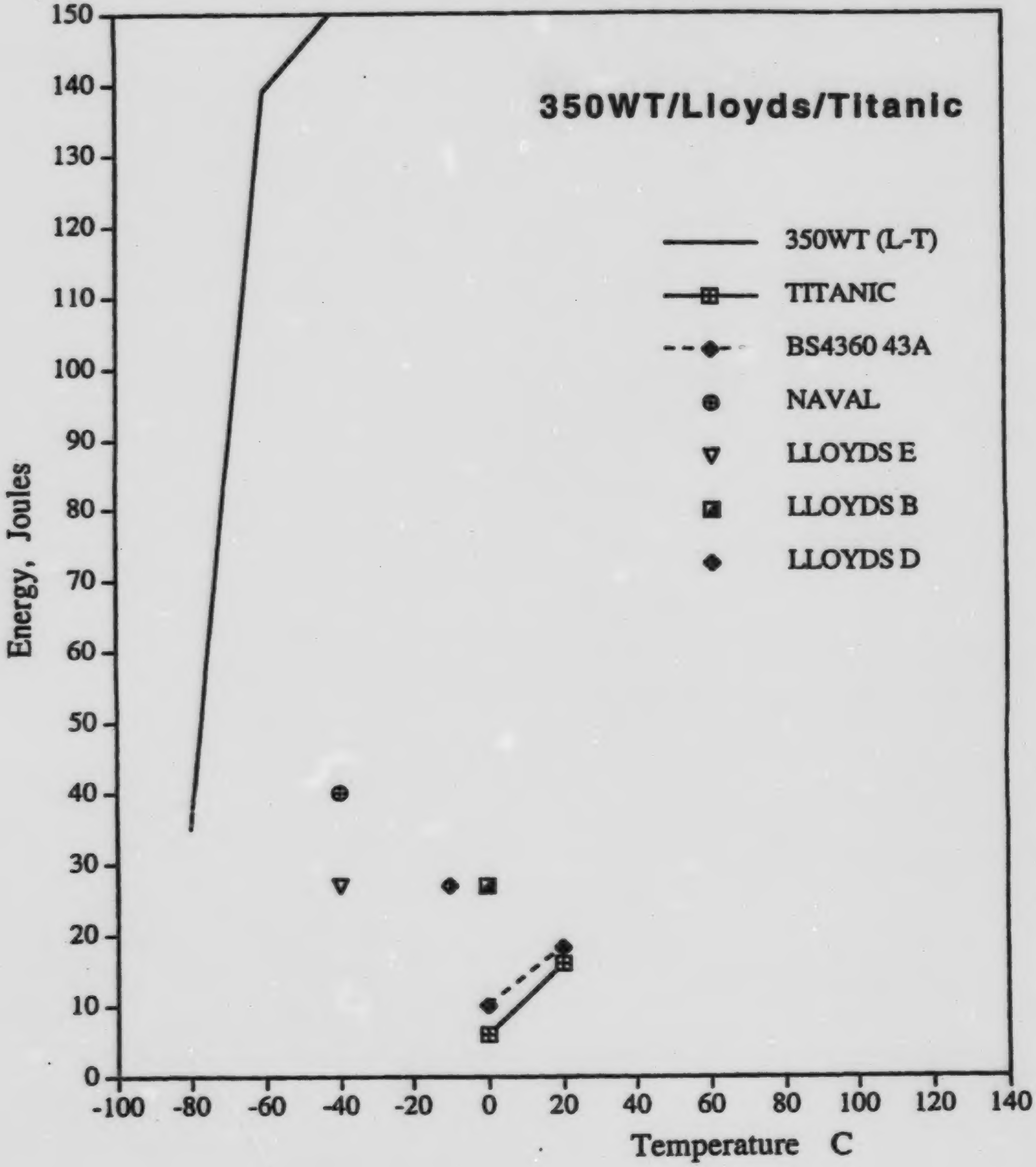

Figure 1b: Charpy transition data for steels used to construct Canadian Naval vessels, and commercial grade standards for grades B, C, D and E steels.

While naval vessel design and material control is better than commercial, it is not perfect. In smaller naval vessels some countries use commercial practice. For frigates and destroyers a minimum Charpy value, Cv_E, is specified for a test temperature typically -40°C. Nevertheless, the latter have suffered small brittle fractures which stop as they enter areas of higher temperature. The brittle fractures occur because the Charpy requirement does not guarantee ductile behaviour. The Charpy specimen does not behave like the structure. The specimen is too small.

The Welding Institute in England[2] has indicated in the past that the arbitrary values derived from Charpy V notched testing have proved adequate for many of the purposes intended (that is, evaluation of SMAW welded mild steel plate in thicknesses up to 38 mm). However, outside these limits, they concluded that the test is not sensitive to all the factors which influence brittle susceptibility. The Institute also pointed out that when weld deposits were made by different processes or different conditions within a process, the Charpy impact test, Cv, provided no real comparative guide to the brittle fracture risk of the weld metal in low strain rate conditions. Charpy transition curves continue to be obtained, however, in order to provide correlation with more meaningful tests so that the Charpy test may hopefully be used for quality control. These limitations were defined to limit errors resulting from use of the Charpy.

In this paper, we go further to not only identify the limitations of (i) often having no impact requirement, and (ii) of using the Charpy as the vehicle for material selection and evaluation but to (iii) suggest that a switch to a structurally comparable impact specimen (Dynamic Tear, DT[3], being the most appropriate of the common specimens) be made.

In this paper; the general use of transition curves in material design for ships will be reviewed; specific design requirements for commercial shipping and naval vessels will be highlighted; the relationship between Cv and DT will be given for 350WT and A517; the effect of altering Cv with an EDM notch will be presented; the relationship between shear lip width and energy in DT specimens will be presented; comparison of shear lip width results for several steels and their weldments will be given (to show that the DT test can provide valuable information without the need for the expensive instrumentation required to obtain the energy results); and finally the thickness independence of the correlation between shear lip and DT_E will be shown (this makes the test even more attractive).

Design

In design of commercial ships there is often no requirement to use notch tough steel. It has been estimated that 90% of ships fall into this category. The implications for fracture are considerable. Steel taken from ships which have fractured and sunk is generally of the same notch toughness as the steel used to fabricate most of these vessels [4]. Even steel from the Titanic exhibits transition behaviour in the range of these steels [5,6]. From a materials perspective the conclusion here is simple, if there is no requirement for impact toughness, brittle fracture will accompany most losses which result from collision, grounding or extreme seas.

For naval vessels, a minimum Cv at a design service temperature has been used to specify steel and weldments for some 50 years. In our case, ships built since 1960 were built to a requirement of 40 ft lbs @ -40°C. Metric conversion seems to be responsible for a more recent change to 28 ft lbs (40 joules) @ - 40°C. Fabrication and repair are rigorously controlled to this requirement as well. Weld consumables are approved and quality control for plate are driven by this simple requirement.

In more recent years, naval architects have been asking materials people to provide methods to predict probability of fracture in fatigue cracked ships and also damaged ships. While it has been tempting to launch into a dissertation on ductile fracture, elastic-plastic fracture mechanics, plastic collapse etc., it was quickly recognized that service temperatures exist where the structure will be brittle. Accordingly instead of fracture control the focus becomes temperature control:

a. there is a temperature where the ship will be subject to brittle fracture

b. if cracks appear, move to warmer water and heat affected areas to 15°C.

c. when areas have known fracture problems, move thermal insulation to outside

d. when fracture analysis is required, temperatures where linear elastic fracture will apply are identified and basic equations provided.

The first step in the process is clearly an upgrade to material requirements so that ships will always behave in a ductile manner. Then ductile fracture prediction and prevention can be considered in detail.

Finally, material specifications in shipping standards (in addition to often no requirement for notch toughness) rely on test specimens of insufficient size and notch acuity to guarantee that the structure will be ductile at the lowest service temperatures. This problem is contributory to the brittle issue and must be simultaneously resolved. Minimum standards must be adopted and specimen size and notch acuity requirements chosen to consistently predict ductile behaviour. In Figure 1c, the problem of specimen size is presented. The designer needs a materials approach that will guarantee good structural performance. The Charpy does not predict the structural performance and must be corrected for. The corrections are different for different types of steel, and are affected by thickness. On the other hand a larger specimen like a DT would be expected to predict the structural performance directly without empirical temperature corrections. The testing cost may be greater but the education and engineering analysis costs would be less. From our perspective the issue is the simplest, cheapest way to predict structural performance (ie DT transition curves), new requirements for all shipping (ie minimum transition temperatures for steel and weldments), and temperature control in the interim.

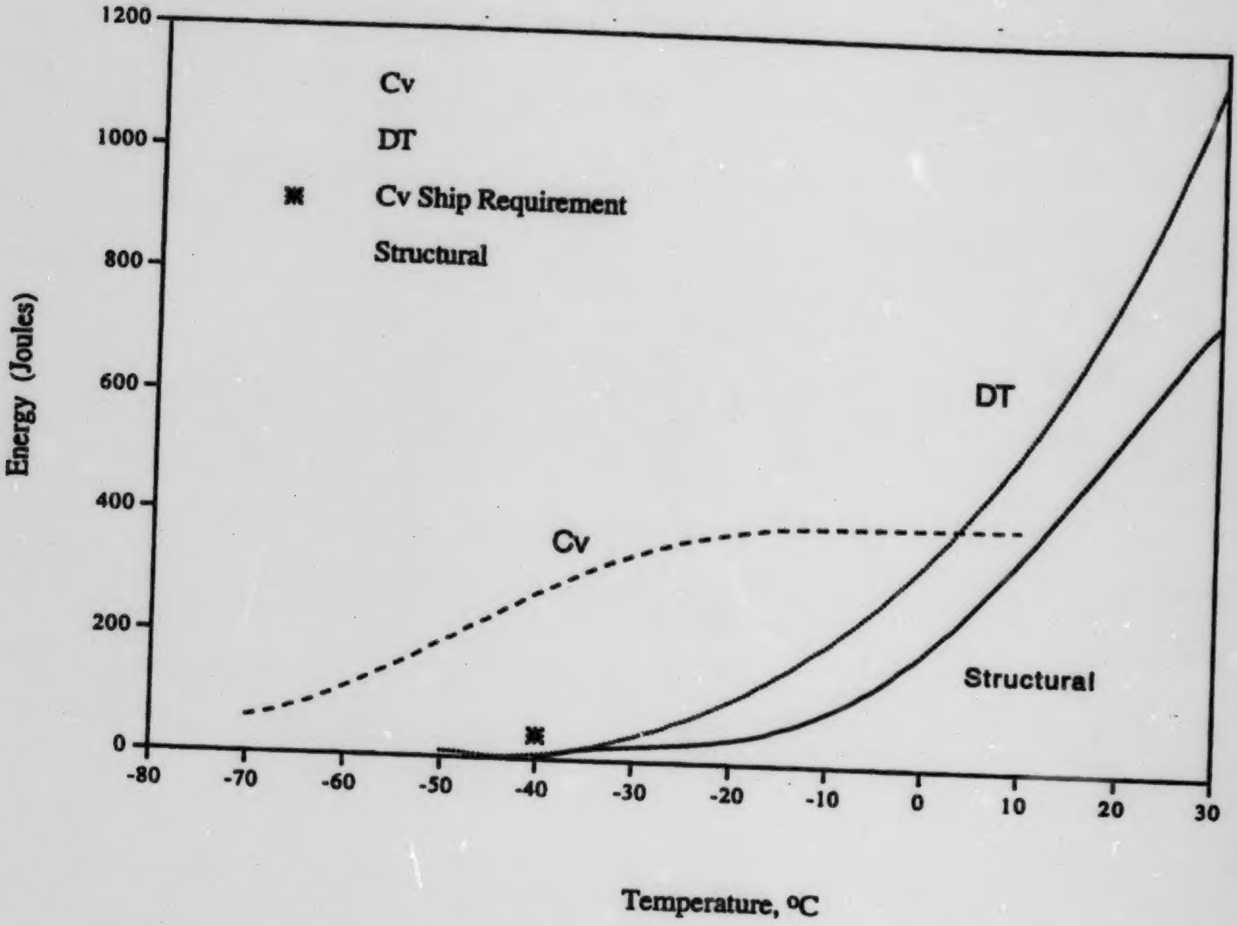

Figure 1c: Schematic of Basic Material Design to Guarantee Ductile Behaviour. (In this schematic, the requirement seems reasonable; the material (Cv) seems much better than the requirement; but the structure is unacceptable: this is typical)

Materials

The materials mentioned in this paper include 25 mm HY80 and HY100 steel plate, 15 mm 350WT steel plate (CSA G40.21-350WT), 9.3 mm ASTM A517 Grade F steel plate and various GMAW weldments of HY80 and HY100 [7,8,9]. The chemical composition for the steels and welding consumables are given in Tables 1 and 2.

Table 1: Chemical Composition of Plates and Welding Wires.

	C	Mn	P	S	Si	Ni	Cr	Mo	Cu
350WT	.22	.8-1.5	.03	.04	.15-.4				
A517 (F)	.1-.2	.6-1.0	.035	.04	.15-.35	.7-1.0	.4-.65	.4-.6	.15-.5
HY100	.12-.20	.1-.4	.02	.02	.15-.35	2.25-3.5	1-1.8	.2-.6	.25
HY80	.12-.18	.1-.4	.025	.025	.15-.35	2.0-3.25	1-1.8	.2-.6	.25
100S1	.08	1.25-1.8	.01	.01	.2-.5	1.4-2.1	.3	.25-.55	.25
120S1	.1	1.4-1.8	.01	.01	.25-.6	2.0-2.8	.6	.3-.65	.25

Table 2: Composition of Welding Gases

gas	Ar	CO_2	He	O_2
95/5	95	5		
T.I.M.E. 1	65	8	26.5	0.5

The steel plates are typical of those used to fabricate naval vessels.

The welding processes mentioned are all GMAW. TIME welding [7] was conducted with either a standard GMAW L-Tec 650 welding machine or a Fronius Transarc pulsed welding machine. The 95% Ar 5% CO_2 gas was used with the Fronius machine only. The TIME process is a gas metal arc welding process which employs a special gas and a specially designed nozzle. The process produces welds that are very clean with reduced sulfur and phosphorous levels and enhanced weldment toughness. The transfer characteristic is effective in the short arc mode as well as the globular and spray modes. Weldments mentioned in this work were all produced in the spray arc mode. The Fronius is a synergic pulsed system which uses variable speed wire feed to compensate for rate of metal transfer requirements.

The dynamic tear specimens were tested in a drop tower loading frame from a height of 1.52 m. The base plate specimens were cut with the notch oriented in the longitudinal direction or the transverse direction, and the weldment specimens were cut with the notch located in either weld metal or in the heat affected zone. An instrumented tup was connected to a signal conditioner and from there to a digital oscilloscope to capture the load-time data. The data were converted to load-displacement with a velocity-energy balance, and the energy under the load deflection curve was calculated numerically. The shear lip measurements were made with calipers and an optical microscope.

Charpy specimens for the base steels were cut from the DT specimens after testing. The tests were conducted from room temperature to liquid nitrogen temperature.

Ductile to Brittle Transition Behaviour

Transition behaviour for Charpy size specimens is sometimes 50 to 100°C below that for larger DT specimens. Figure 2a shows the Charpy and DT behaviour for 350 WT steel. Figure 2b includes transition data for EDM notched Charpys and Figure 2c shows results for the L-T orientation alone. The basic shift between Charpy and DT transition is some 60°C, while the EDM notch transition is 20°C above the standard Charpy and only 40°C below the DT.

Transition behaviour for A517 is less clear possibly because of the thinner (B) plate. Figure 3a shows the lower bound Charpy and DT behaviour for the A517 steel. Figure 3b includes transition data for EDM notched Charpys and Figure 3c shows results for the T-L orientation alone. The basic shift between Charpy and DT transition for the T-L orientation is some 40°C, while the EDM notch transition is 20°C above the standard Charpy and may be 20°C below the DT. In the L-T orientation the lower bound data is less clear mainly because so few of the specimens tested exhibited brittle behaviour. Many more tests would be necessary to clarify the relationship.

Confusion related to the A517 data supports use of the larger specimen. Simply modifying the notch of the Charpy will not make it reflect the structural behaviour. With the A517 steel, thickness and crack size effects may have competed significantly with reducing temperature. The basic behaviour is that as specimens decrease in thickness apparent toughness increases as plane strain gives way to plane stress and apparent toughness drops off as notches and ligaments decrease in size. Accordingly, without fully explaining the A517 behaviour, the DT specimen is probably the simplest existing specimen whose transition behaviour would approximate that of a structure.

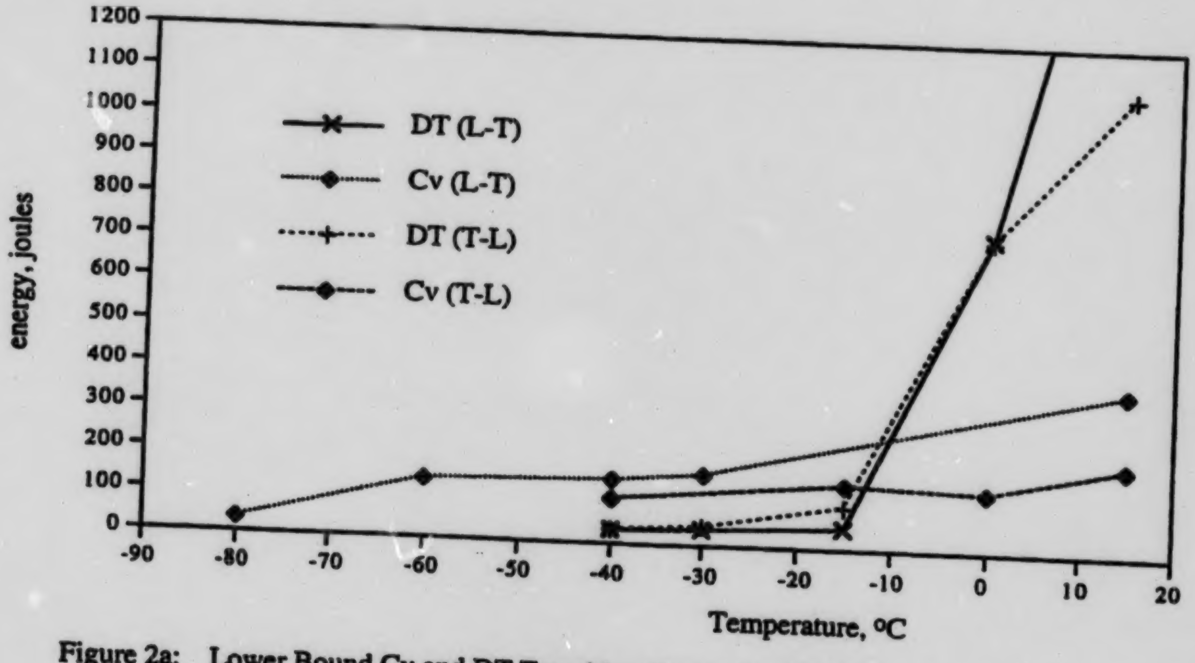

Figure 2a: Lower Bound Cv and DT Transition Curves for 350 WT.

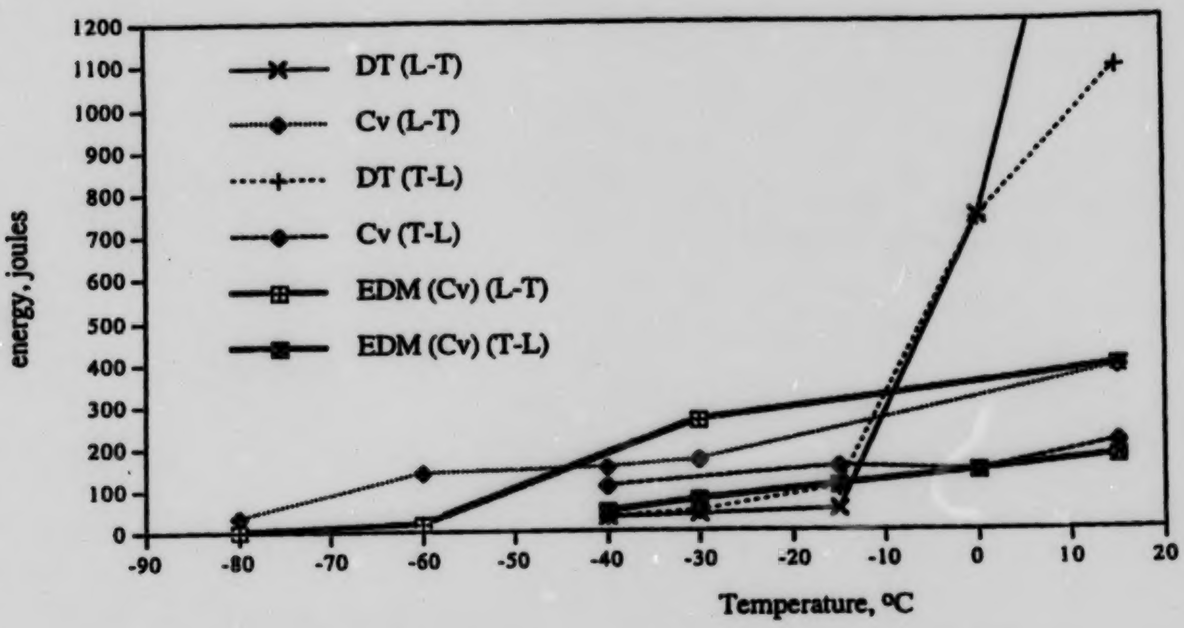

Figure 2b: Lower Bound Cv, EDM (Cv) and DT Transition Curves for 350 WT.

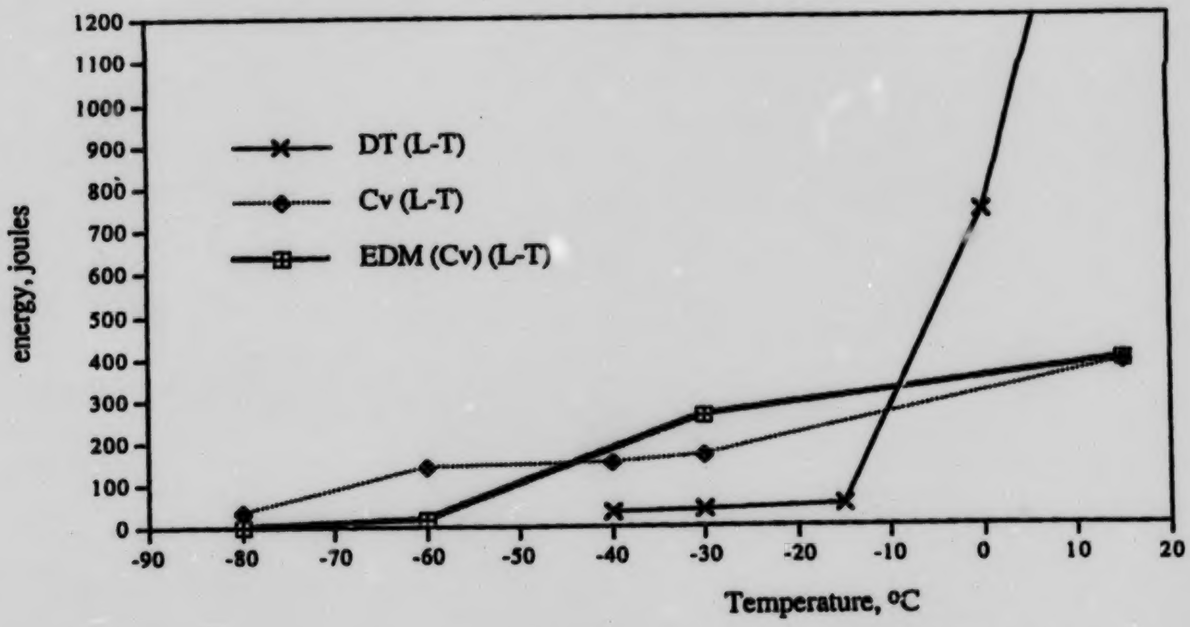

Figure 2c: Lower Bound Cv, EDM (Cv) and DT Transition Curves for 350 WT (L-T).

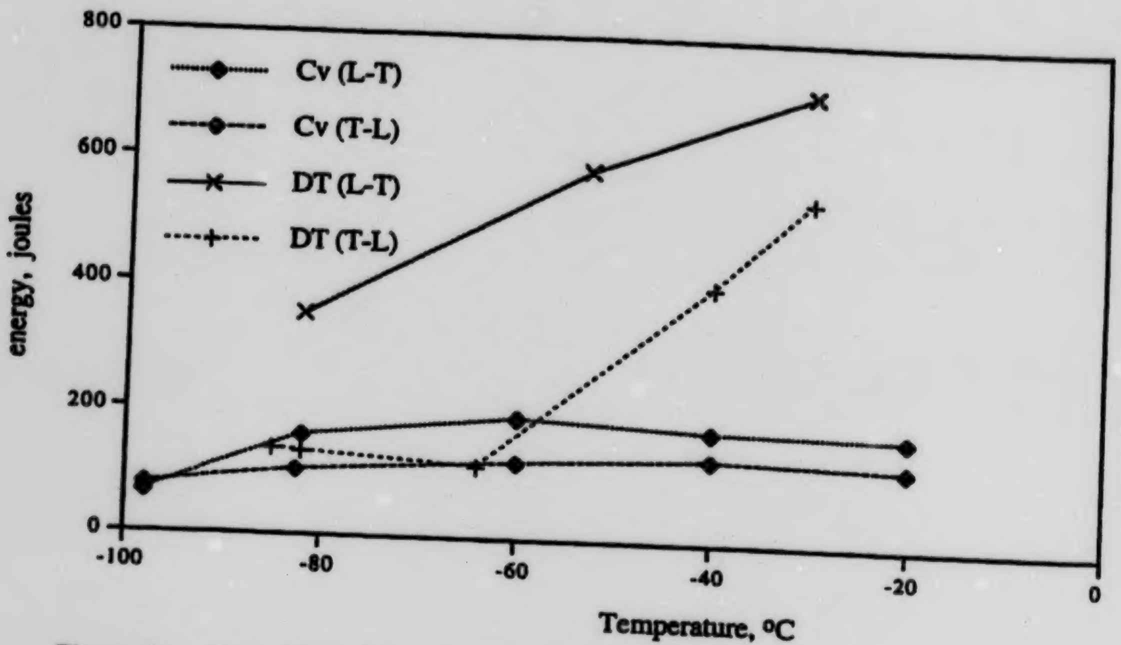

Figure 3a: Lower Bound Cv and DT Transition Curves for A517.

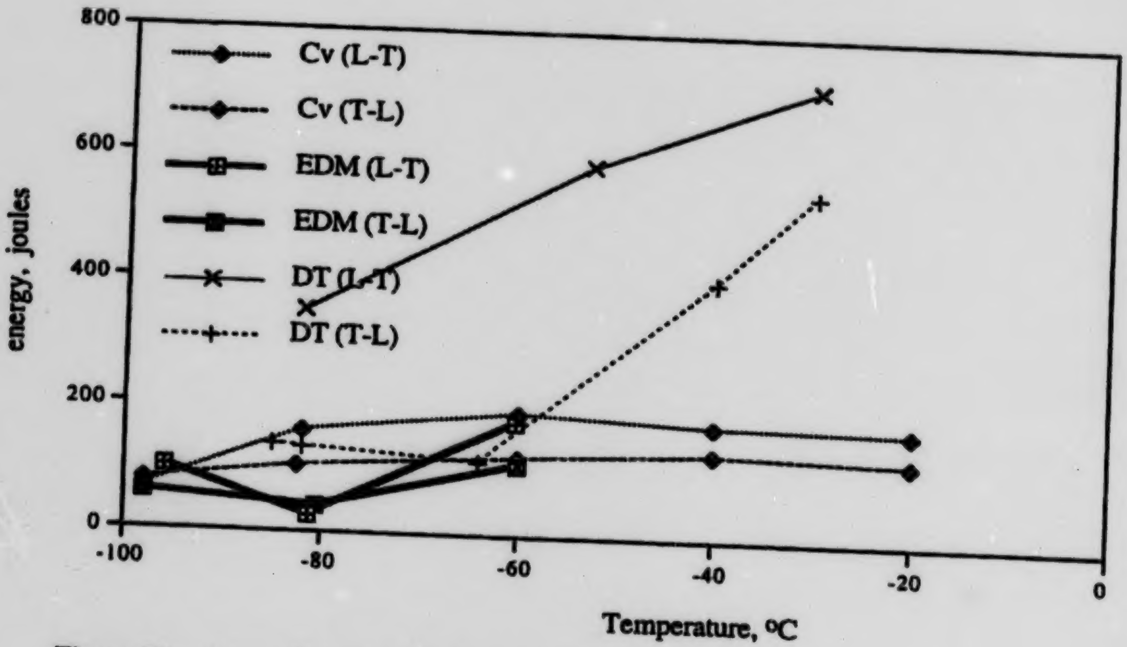

Figure 3b: Lower Bound Cv, EDM (Cv) and DT Transition Curves for A517.

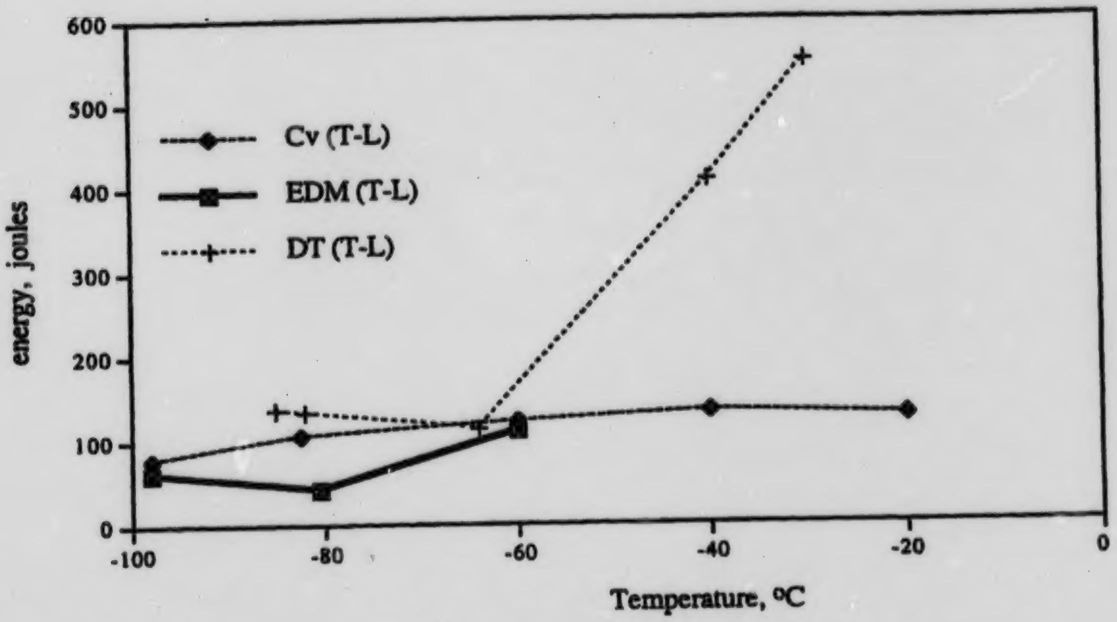

Figure 3c: Lower Bound Cv, EDM (Cv) and DT Transition Curves for A517 (T-L).

Shear Lip Transition Curves

One of the main road blocks to specifying a DT requirement in place of a Charpy requirement is the increased cost of the DT test. The cost comes from the cost of machining, the cost of a tower and the cost of the electronics for load capture and computer analysis. The last cost which is perhaps the greatest can be eliminated by relying on shear lip [8,9] in place of energy to produce transition curves. In addition to reduced cost, the perpetual preservation of results and the potential for elimination of errors that can show up (sometimes undetected) with strain gage instrumentation and computer data logging, plus the elimination of notch effects [8] make shear lip transition curves a very attractive alternative.

Morphology of fracture surfaces has long been used as an indication of how brittle or ductile a material is at a given temperature[10]. The morphology can range from flat when no shear lips are present, to a shear index of one, when the shear lips on either side of the specimen are developed to the point of touching each other, Figure 4. In many fracture tests such as the Charpy V notched (Cv)[1] and Dynamic Tear (DT)[3] standard test methods, measurement of percentage shear which is somewhat related to the shear lip size is optional, while in the Drop Weight Tear Test (DWTT)[11], it is the basic physical measurement required.

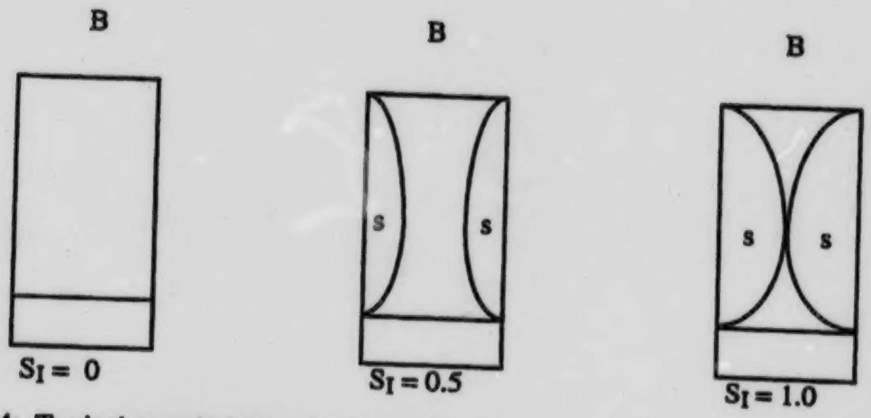

Figure 4: Typical morphologies for dynamic tear impact samples (shear index is measured at the point of the closest contact between the two shear lips: $S_I = 2s/B$).

The rules applied to drop weight tear percentage shear measurements cannot be applied to the 16 mm dynamic tear specimen because the specimen is narrower (W). Accordingly, it was decided in our earlier work[8] to make one measurement on the specimen at the location of closest contact between the two shear lips. This would ensure that the measurement reflected the toughness of the material rather than the flow stress. In practice, the distance between the two shear lips was measured, subtracted from the original width and divided by two to obtain an average shear lip estimate.

DT Data for HY80, HY100 and a lower strength low alloy steel taken over a wide range of temperatures were used to determine the relationship between energy and shear lip size, Figure 5.

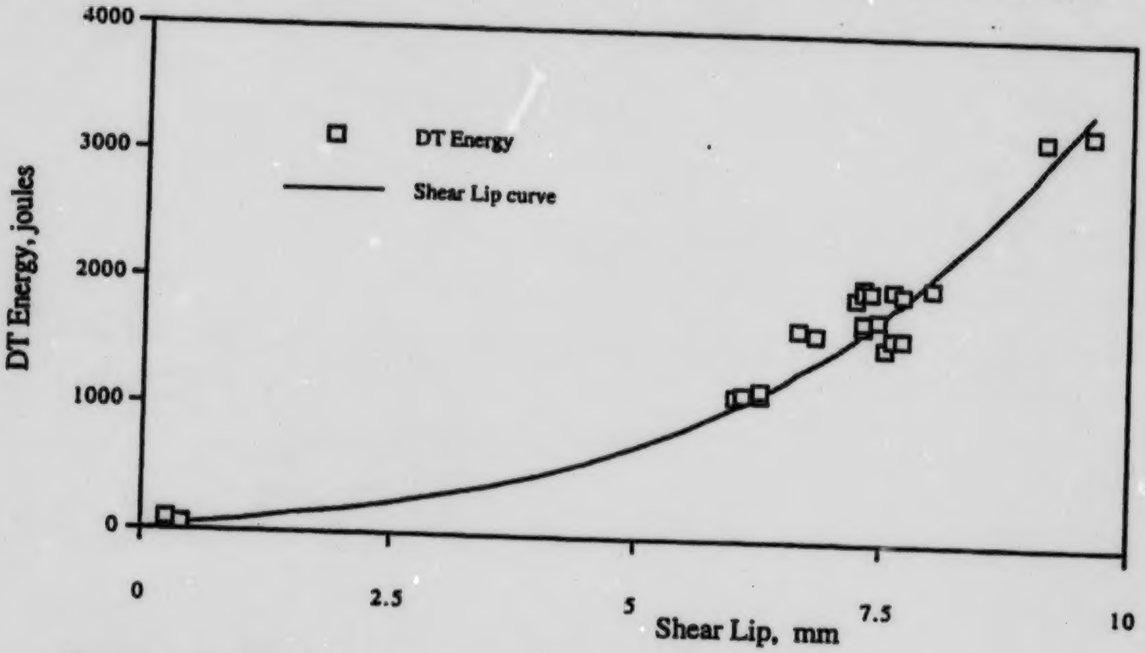

Figure 5: Graph of Shear Lip "s" vs DT Energy.

The influence of yielding on the relationship between shear lip "s" and energy is generally nonlinear except at low values of toughness, in the elastic range, where it is linear. It was found [8] that DT_E in joules can be determined from shear lip in mm by the following:

$$DT_E = 105\,s - 12.96\,s^2 + 4.096\,s^3. \quad (1)$$

This curve is shown with basic data in Figure 5. It was found that this curve fits equally well for steel and weldments. With weldments there is more scatter but this is due to the inherent variability of the welds and weld defects. Scatter caused by notch variability was isolated to be showing up in the energy values only. The shear lip size was independent of the notch acuity.

Attempts to produce an analytical relationship between energy, toughness and shear lip size is extremely complex and covers the whole range of mechanics, elastic through plastic. At low toughness, an elastic analysis would be used to analyze the fracture and determine the relationship, while at very high toughness, a fully plastic analysis would be relevant. As the procedure is not used to measure a specific toughness property, but the energy of total separation, edge and hinge effects exist to complicate any analysis effectively requiring elastic, elastic-plastic and plastic analysis at some stage in the fracture analysis of all but the most brittle samples.

In previous work [8,9] we noted the following

(i) *Elastic*

For plane strain elastic conditions to exist in a DT specimen, just after crack advance at least, the following would apply:

$$a, b, B > 50\, r_{yc} = 2.5 \left(\frac{K_{Ic}}{\sigma_y}\right)^2 \quad (2)$$

Estimating shear lips to be of the order of the critical plastic zone size gives:

$$s = r_{yc} = \frac{1}{6\pi}\left(\frac{K_{Ic}}{\sigma_y}\right)^2 \quad (3)$$

(ii) *Elastic-plastic*

For elastic-plastic conditions to exist in a DT specimen, just after crack advance, the following conditions would apply:

$$a, b, B > 50\,\frac{J_{Ic}}{\sigma_{flow}} \quad (4)$$

Critical crack blunting could be calculated from

$$\Delta a_c = \frac{J_{Ic}}{2\,\sigma_{flow}} \quad (5)$$

The shear lip size would be related to this critical blunting but not to the specimen size as originally suggested[8]. The shear lip would be about 50 times the critical crack blunting.

$$s = 50\,\Delta_{ac} = \frac{25\,J_{Ic}}{\sigma_{flow}} \qquad (6)$$

Slightly larger values would exist for thicker specimens but shear indexes of one would not be expected as specimens get larger and larger. This explains why the shear lips in thicker specimens that we tested (25 mm) tended to peak out at 8 to 9 mm.

(iii) *Plastic*

When the elastic-plastic toughness is exceeded the mode of failure appears to be plastic. In the case of plastic fracture, the flow stress should dominate and energy should be related to it and the specimen size. Hinge effects alter this condition and edge and hinge effects cause plastic dominance at lower toughness values. What this means is that even though elastic-plastic conditions might exist for a short part of the separation, the beginning end and sides are predominantly plastic and overall dominating. This is the case for shear indexes of 0.90 to 1.00 (or shear lips of 7 to 8 mm) for our materials.

In our previous work, it was determined that the correlations only faltered in the presence of significant defects such as gross slag or porosity. Also, it was noted in the previous studies [8,9] in the case of poorly pressed notches, that even though an excessive energy over that with a properly pressed notch occurred that there was no discrepancy in the shear lip values. This contributes significantly to the reliability of the shear lip data and transition curves obtained and also indicates that a lot of the scatter in the relationship between shear lip and energy is due to factors which only affect the energy component.

In Figures 6a and 6b energy and shear lip data are presented for 350WT. It is clear that both measurements tell the same thing about the transition behaviour. Figures 7a and 7b show energy and shear lip data for A517. Once again both measurements tell the same thing about the transition behaviour.

In Figures 8,9 and 10 data for gas metal arc welds of HY80 and HY100 steels show that the energy and shear lip curves impart the same knowledge about the material performance. Also, these three figures show that the relationship between shear lip and energy is independent of specimen thickness between 16 mm and 25 mm thickness.

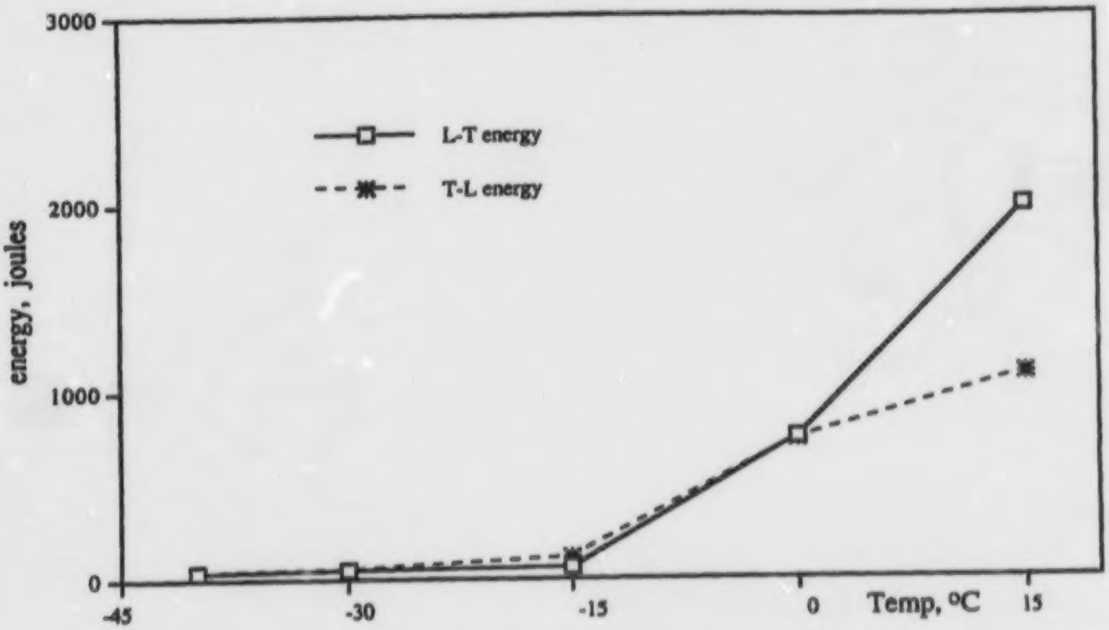

Figure 6a: Dynamic Tear Energy for 15 mm 350WT steel.

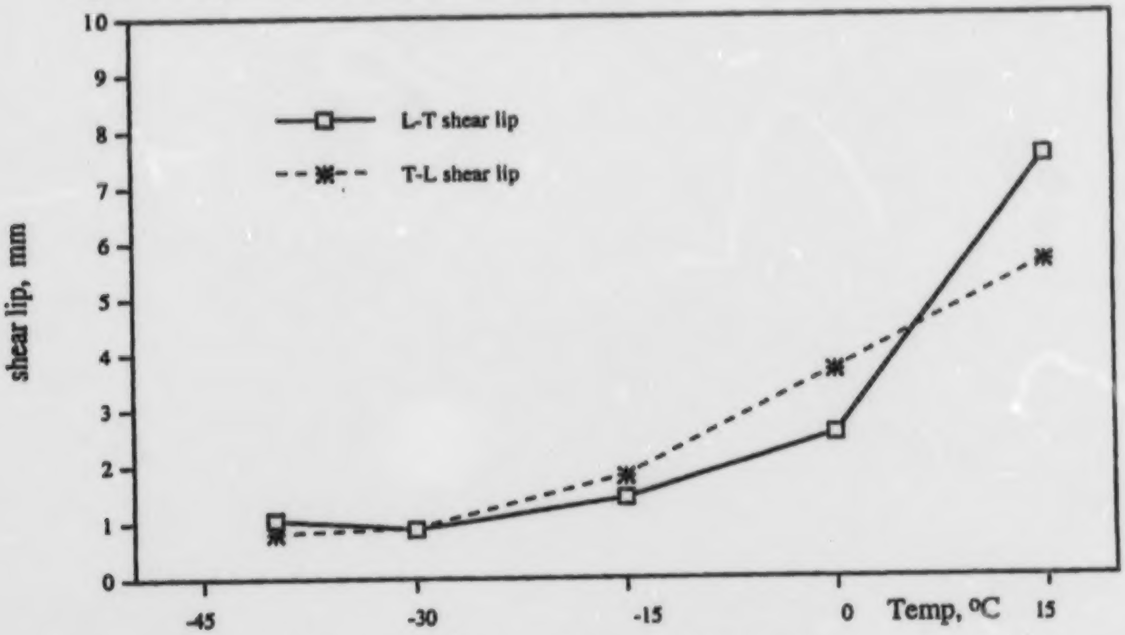

Figure 6b: Shear Lip Transition Curves for 15 mm 350 WT steel.

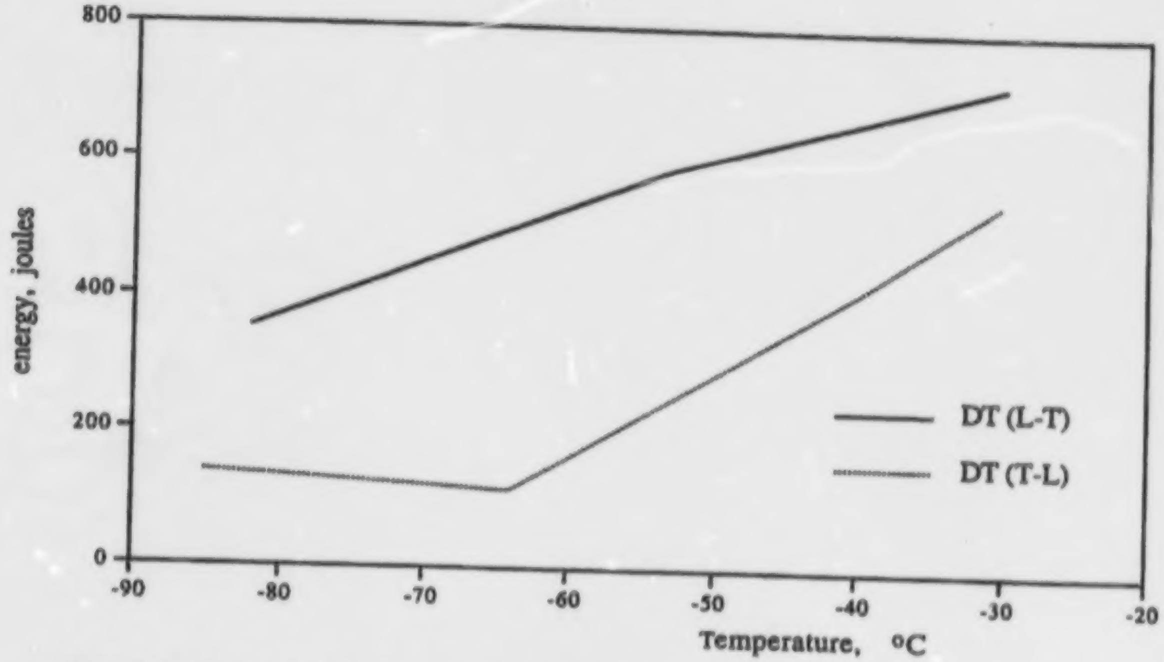

Figure 7a: Dynamic Tear Energy for 9.3 mm Thick A517 grade F steel.

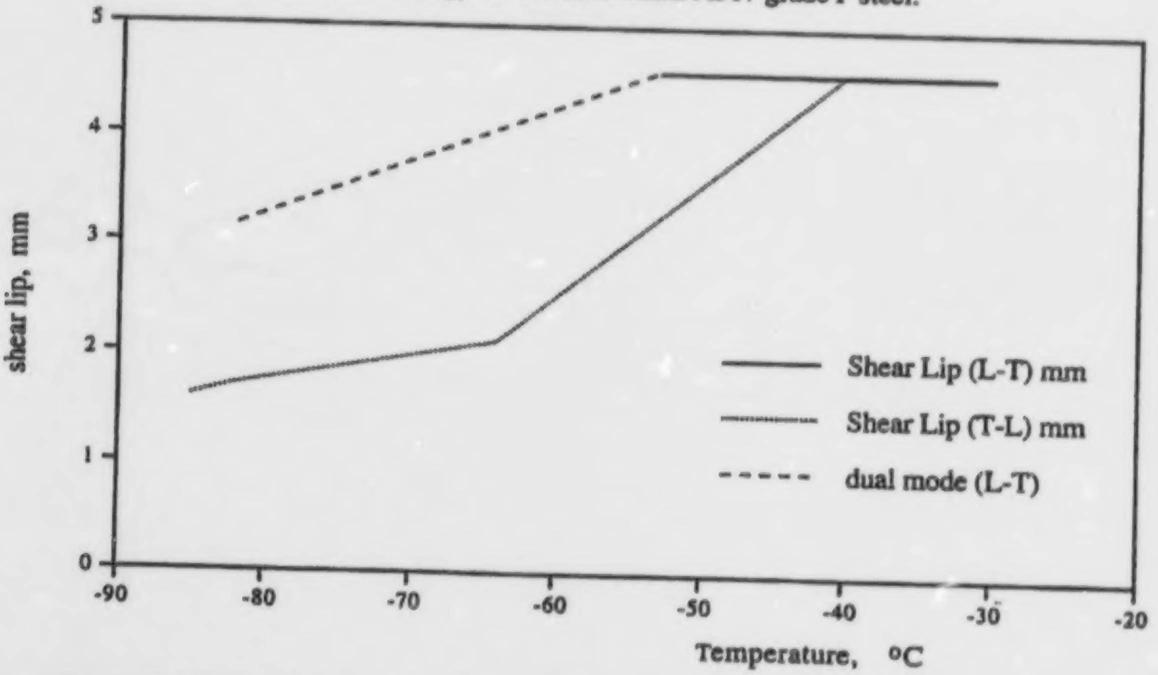

Figure 7b: Shear Lip Transition Curves for 9.3 mm Thick A517 grade F steel.

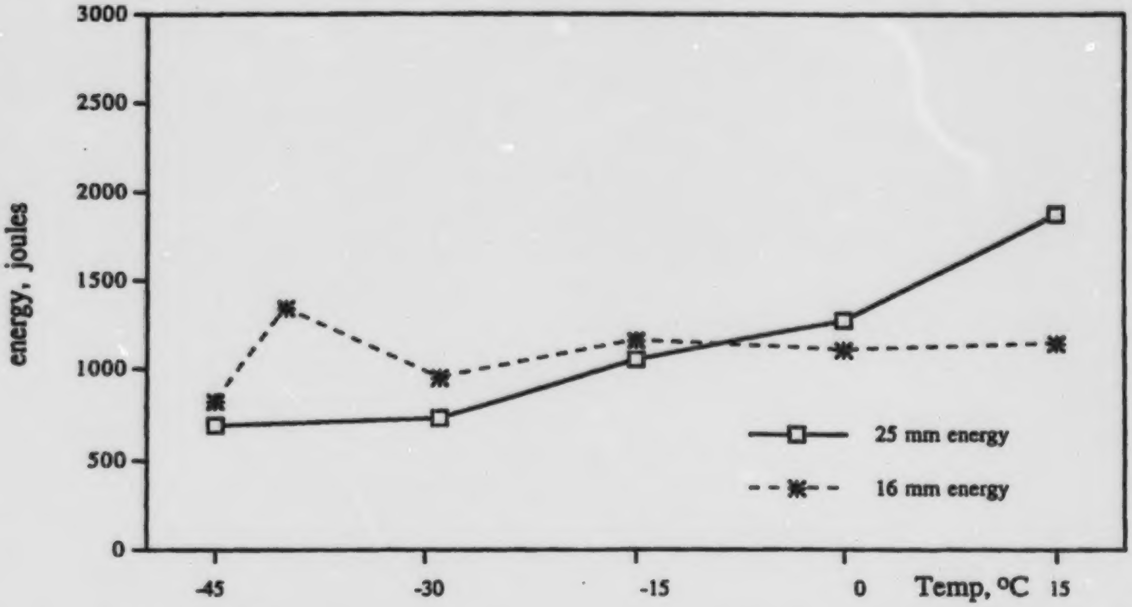

Figure 8a: Dynamic Tear Energy for HY80 GMAW Weld Produced With Standard L-Tec Machine, TIME gas, in the Vertical Position.

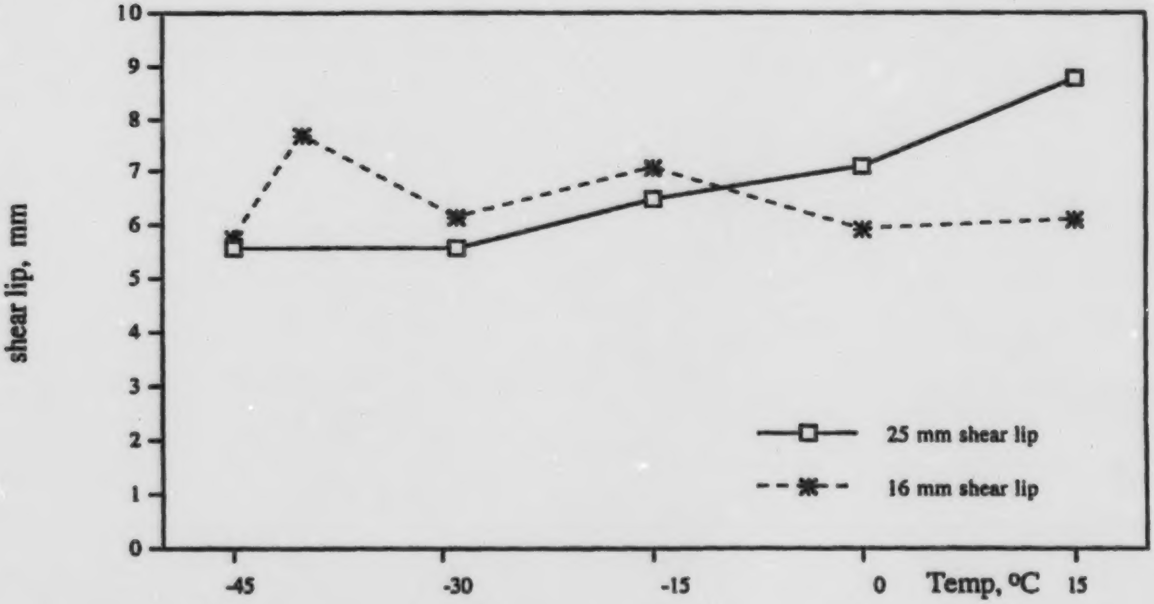

Figure 8b: Shear Lip Results for HY80 GMAW Weld Produced With Standard L-Tec Machine, TIME gas, in the Vertical Position.

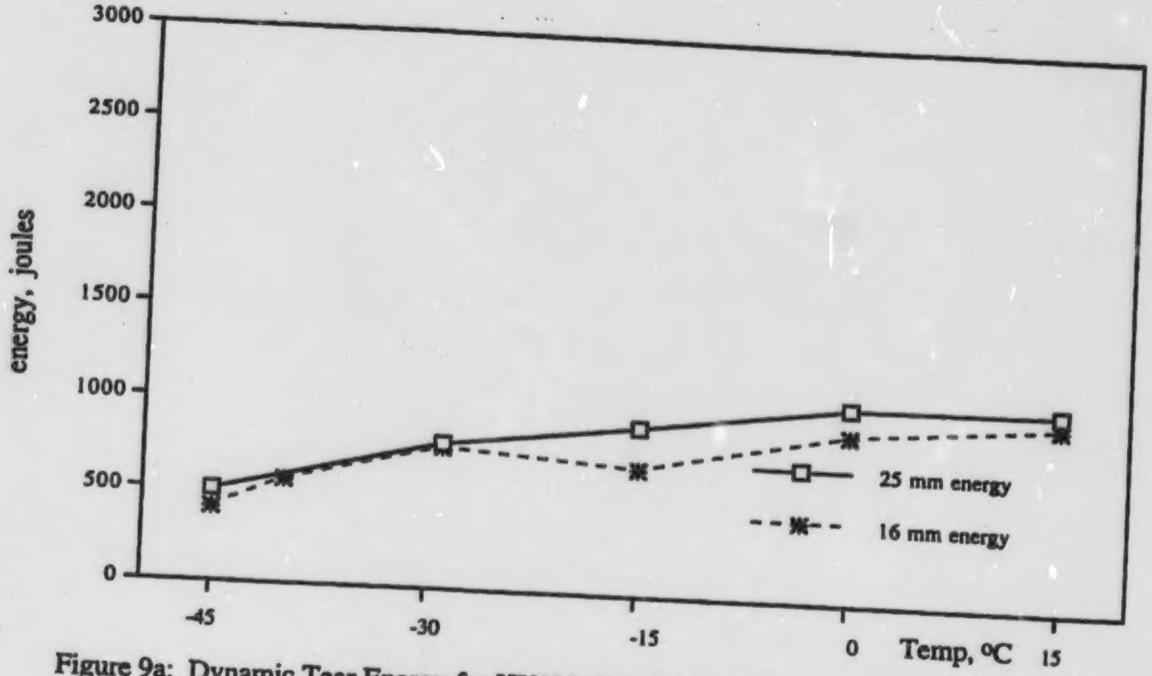

Figure 9a: Dynamic Tear Energy for HY100 GMAW Weld Produced With Standard L-Tec Machine, TIME gas, in the Overhead Position.

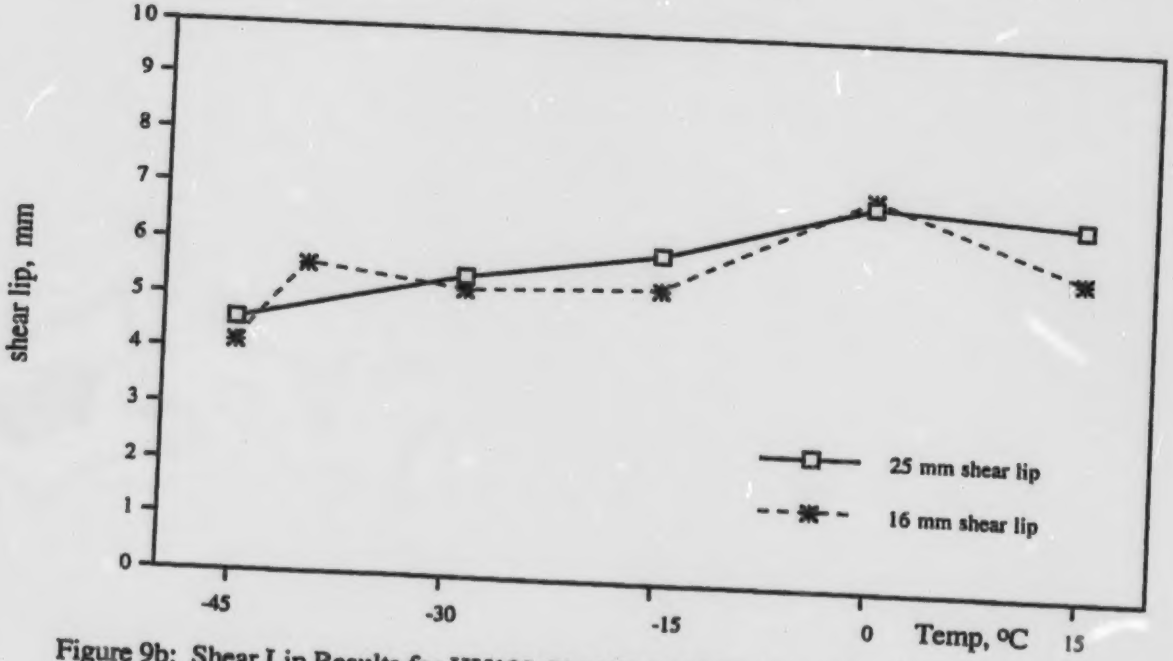

Figure 9b: Shear Lip Results for HY100 GMAW Weld Produced With Standard L-Tec Machine, TIME gas, in the Overhead Position.

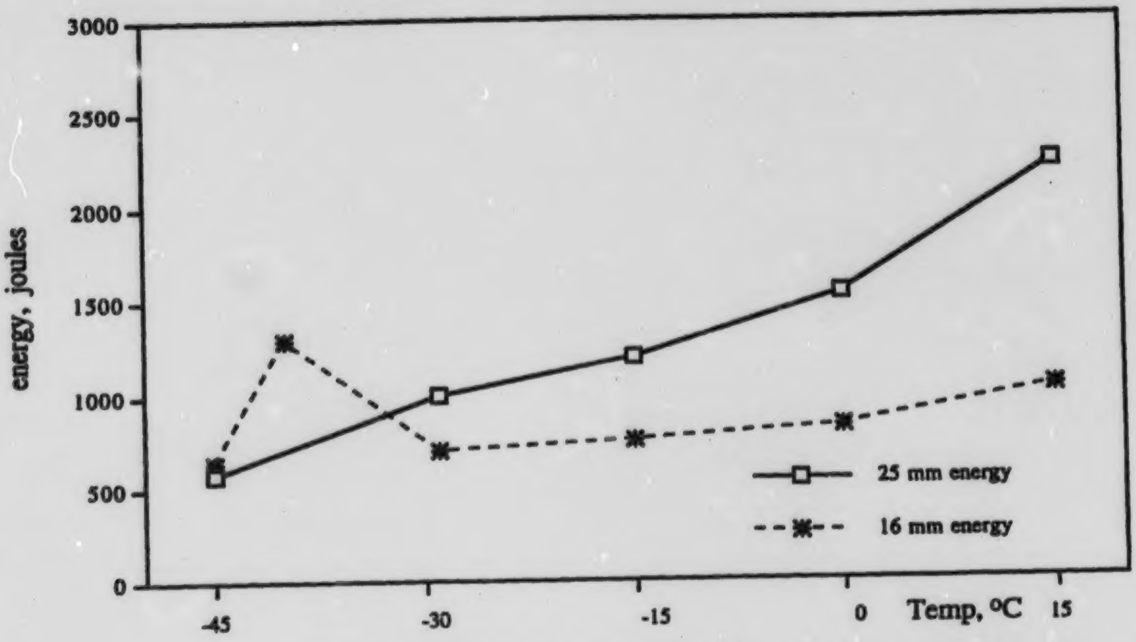

Figure 10a: Dynamic Tear Energy for HY100 GMAW Weld Produced With Pulsed Fronius Machine, 95/5 gas, in the Overhead Position.

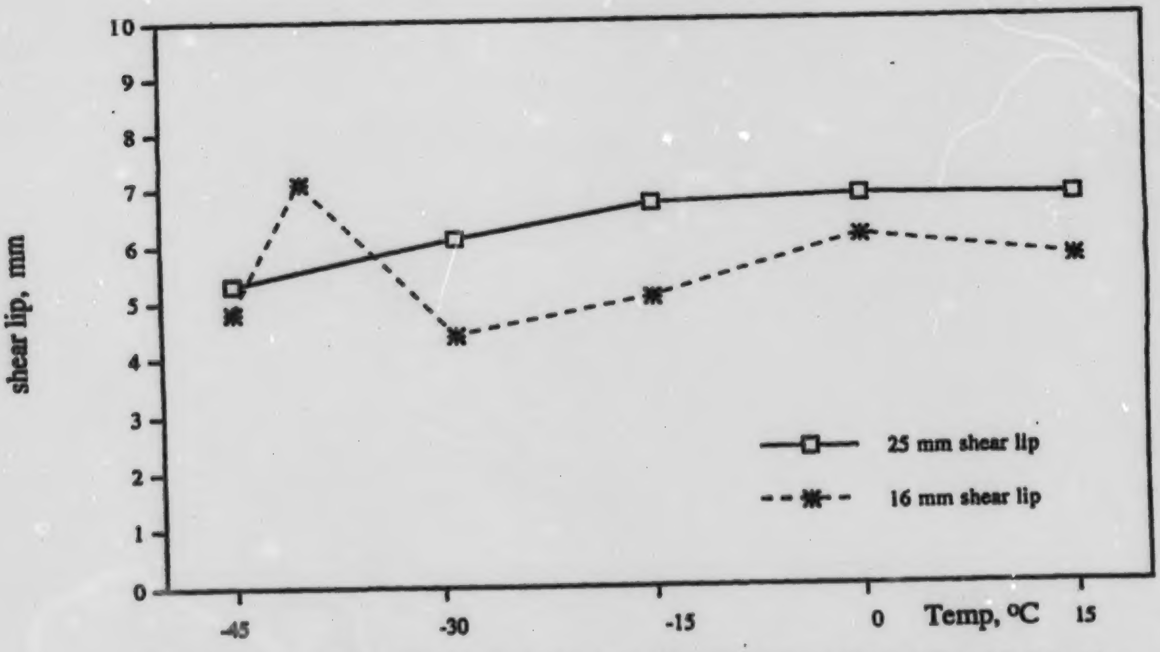

Figure 10b: Shear Lip Results for HY100 GMAW Weld Produced With Pulsed Fronius Machine, 95/5 gas, in the Overhead Position.

CONCLUSIONS

1. Prediction of ductile behaviour in welded structures starts with selection of material and fabrication control that guarantee the structure will exhibit upper shelf behaviour at the lowest service temperature.

2. The Cv specimen is too small to effectively and economically serve as a test vehicle to control structural quality.

3. DT is the simplest existing specimen whose transition behaviour approximates that of a structure.

4. The data presented shows that shear lip information is equivalent to energy information for characterizing the toughness of carbon and low alloy steel and their weldments. As the shear lip data is considerably cheaper to acquire and permanently available for accurate re-examination it is considered the preferential test for transition behaviour evaluation of ship steel and weldments.

5. The correlation between shear lip and energy is independent of thickness for 16 mm and 25 mm specimens of low alloy steels and their weldments. The 25 mm size test specimen shows no increase in energy over the 16 mm specimen except on the extreme upper shelf. Therefore the two tests can be used interchangeably dependent solely on machining costs. Toughness requirements for the one inch specimen will be identical to the 16 mm specimen.

6. The shear lip criterion for determination of toughness does not appear to be affected by poorly pressed notches in DT tests.

REFERENCES

[1] "The design and methods of construction of welded steel merchant vessels", the final report of the board of investigation, convened by order of the Secretary of the Navy, Government Printing Office, Washington, 15 July 1946.

[2] D.N. Shackleton, "Welding HY100 and HY130 Steels", Welding Institute Report, Cambridge, England, 1973

[3] *ASTM E604*, Dynamic tear testing of metallic materials. Am. Soc. Testing Mater., Philadelphia, PA, U.S.A., Vol. 3.01, 1987

[4] J.D.G. Sumpter, J. Bird, J.D. Clark and A.J. Caudry, "Fracture Toughness of Ship Steels", Royal Institute of Naval Architects Spring Meeting, Apr 1988

[5] K.J. KarisAllen and J.R. Matthews, "Fracture Control for Surface Ships", Paper Presented at the 2nd CF/CRAD Meeting on Naval Applications of Materials Technology, Halifax, N.S., May 2-4, 1995 pp. 326-341

[6] R. J. Brigham ant Y.A. Lafreniere, "Titanic Specimens", Metals Technology Laboratories, CANMET, Report 92-32(TR), 1992

[7] J.R. Matthews, J.F. Porter, J. Church, M. Macecek, "An Evaluation of T.I.M.E. Welding of HY 80 Plate," The Welding Journal, 70, 1991, pp: 35-41

[8] J.R. Matthews, "On The Relationship Between Shear Index and Energy In Dynamic Tear Specimens", Engineering Fracture Mechanics, Vol. 39, No. 1, 1991, pp. 131-140

[9] J.R. Matthews, "On The Relationship Between Shear Lip, Shear Index and Energy In Dynamic Tear Specimens", Engineering Fracture Mechanics, Vol. 54, No. 1, 1996, 11-23

[10] F.J. Loss and W.S. Pellini, "Dynamic Tear Test Definition of the Temperature Transition from Linear Elastic to Gross Strain Fracture Conditions", Trans. ASME, Series D, Journal of Basic Engineering, Vol. 91, No. 1, 1969, pp. 108-115

[11] *ASTM E436*, Drop-weight tear tests of ferritic steels. Am. Soc. Testing Mater., Philadelphia, PA, U.S.A., Vol. 3.01, 1987

#507227 2F

Fracture Resistance of Canadian Patrol Frigate Hull Steels

by

Jack Morrison
DREA Dockyard Laboratory (Esquimalt), Victoria, BC

and

Stephane Garneau
DMSS 2-4-3, National Defence Headquarters, Ottawa

ABSTRACT

This presentation provides an overview of results to date and work in progress on the determination of the fracture resistance of steels and welds used in CPF hull construction. This data is being generated in support of ship structural integrity assessments and the evaluation of repair procedures. An overview is provided of the steel specifications, the variations in material supplied for both construction and repair, and of the welding procedures used. The results from two series of fracture test programs are included:

a) A preliminary assessment of the steels, welds and heat affected zones in terms of their mechanical properties, and

b) Supplementary experiments to quantify quasi-static and dynamic toughness over the temperature range of interest.

Related programs on crack arrest toughness, ongoing work on the fracture resistance of mismatched welds, and future trends in steel selection are also discussed.

FRACTURE RESISTANCE OF CANADIAN PATROL FRIGATE HULL PLATE

Jack Morrison
EDRD
Victoria, BC

Stéphane Garneau
DMSS
NDHQ, Ottawa

OUTLINE

- background on steel specifications
- properties of materials supplied for CPF
- review of preliminary toughness results
- results of follow-up test program
- future work

Notes - Background on Steel Specifications

There were 2 classes of steel used on CPF hull construction, CSA 350WT and ASTM A517. Since the CSA G40.21 standard does not cover thicknesses below 6 mm, the 4 mm sheet used in the superstructure was specified using the similar ASTM A570 grade.. The latter is of little significance as regards structural integrity assessments.

Both steel types had specified minimum yield strengths, minimum and maximum UTS, and the same impact energy requirements. 15 mm 350WT may exist in both control-rolled and normalized conditions.

The proposed impact requirements originally included a -40C Charpy energy and a Nil Ductility Transition Temperature at some prescribed value below the lowest anticipated service temperature. In 1984 the latter was dropped in favour of additional Charpy energies at 0C and -60C, although these are not always included in the manufacturers data sheets.

STEEL SPECIFICATIONS AND GRADES

- CSA-G40.21 Grade 350WT Category 5
  plate thickness range: 6 - 15 mm (control rolled)
  15? - 50 mm (normalized)
  Category 5 - purchaser specified impact properties
  (4 mm ASTM A570 Grade 50 Structural Sheet with similar requirements also used in superstructure)
- ASTM A517 Grade F
  plate thickness range: 6 - 15 mm
  quench and tempered
  Grade F is defined by chemical composition limits

SPECIFIED PROPERTIES I

350WT CATEGORY 5 PLATE

- Chemical Composition (heat analysis wt %)

C	Mn	P	S	Si
0.22 max	0.8 - 1.5	0.03 max	0.04 max	0.15 - 0.40

- Tensile Properties

Yield Strength	UTS	Elong. (50mm)
350 MPa min.	480 - 650 MPa	22% min.

- Minimum Impact Energy (Charpy V-Notch)

60 J @ 0°C   40 J @ -40°C   20 J @ -60°C

SPECIFIED PROPERTIES II

A517 GRADE F PLATE

- Chemical Composition (heat analysis wt %)

	C	Mn	P	S	Si	Ni	Cr	Mo	B	V	Cu
Min.	0.1	0.6	-	-	0.15	0.7	0.40	0.4	0.0005	0.03	0.15
Max.	0.2	1.0	0.035	0.040	0.35	1.0	0.65	0.6	0.006	0.08	0.50

- Tensile Properties

Yield Strength	UTS	Elong. (50mm)
690 MPa min.	795-930 MPa	16% min.

- Minimum Impact Energy (Charpy V-Notch)

60 J @ 0°C	40 J @ -40°C	20 J @ -60°C

Notes - Supplier's Test Data

The 350WT used during construction is believed to all come from Algoma Steel. In 1994 the Dockyards and 25 CFSD were supplied with Stelco product. Both companies supplied a microalloyed HSLA, control rolled for most thicknesses. Algoma plate below 15 mm thickness has less than 0.1%C. 15 mm plate is known to exist in both low and high (0.15%) carbon variants, though it is not known how extensively used the latter was. 15 mm Stelco plate has the higher carbon, and in this case some of the 7 mm plate appears to have been made from the same heat (properties were not supplied for some of the thinner plates).

Mechanical properties are for the transverse tensile and L-T Charpy orientation, which are greater than longitudinal and T-L respectively. Sub size specimen values from thinner plates have not been factored up. The 350WT is very strong, averaging over 450MPa for 15 mm or less. The starred values on the 15 mm Stelco plate are 50 MPa less than those obtained by DL(E) on the same plate. For control-rolled plate 350WT Charpy values are 5-10 times minimum specified.

All of the A517 was supplied by the same Belgian manufacturer. Charpy values are 2-5 times minimum.

A variety of weld processes were used, but the R&D investigations described in this presentation were carried out on SMAW with the E7018 and E11018 consumables.

SUPPLIERS' TEST DATA I

350WT CHEMICAL COMPOSITION

	C	Mn	P	S	Si	V	Nb	Al	others
• Algoma (1991-93)									
6 mm	0.08	1.3	0.007	0.006	0.21	0.02	0.02	0.04	-
8-15 mm	0.10	1.3	0.007	0.006	0.26	0.04	0.03	0.04	-
37-50 mm	0.15	1.3	0.008	0.009	0.31	0.04	0.03	0.04	0.2Cu
15mm 1988	0.08	1.4	0.017	0.007	0.17	0.03	0.05	0.01	0.2Cr

a high carbon variant also occurs in 15 mm with Nb only

	C	Mn	P	S	Si	V	Nb	Al	others
• Stelco (1994)									
8-12 mm	0.07	1.4	0.01	0.003	0.26	0.06	0.02	0.03	-
7&15 mm	0.16	1.4	0.01	0.004	0.30	0.07	0.02	0.03	0.2Ni

SUPPLIERS' TEST DATA II
350WT MECHANICAL PROPERTIES

	σ_y (MPa)	σ_u (MPa)	Elong. (%)	Charpy @ -40C (J)
● Algoma (1991-93)				
6 mm	458	535	21	$235^{1/2}$
8 mm	476-494	525-560	22-25	$155^{1/2}$ $346\text{-}391^{3/4}$
15 mm	447-472	520-545	23-25	180-333
37 mm	418/436	535/545	31/33	143/158
50 mm	417	540	34	121
● Stelco (1994)				
9 mm	429/490	492/533	23/22	$286/298^{3/4}$
10 mm	443	509	24	$300^{3/4}$
12 mm	477	522	21	358
15 mm	408*/481	543*/588	26/21	117/148

SUPPLIER'S TEST DATA III

A517 COMPOSITION AND PROPERTIES

Fabrique de fer de Charleroi

- Chemical Composition (wt %)

C	Mn	P	S	Si	Cu	Ni	Cr	Mo	V	B	Al
0.13	0.73	0.01	0 .001	0.31	0.23	0.71	0.49	0.41	0.04	0.002	0.028

- Heat Treatment

  Austenitize 920C, water quench, temper 650C

- Mechanical Properties

σ_y (MPa)	σ_u (MPa)	Elong. (%)	Charpy @ -40C
730-790	814-865	20-28	92-185 J 73-92% shear

WELDING PROCESSES

- SAW - primary structure
  - main long. and trans. members
- GMAW - limited access transverse members
- FCAW - secondary members
  - unit assembly
  - module and megamodule assembly
  - erection joints
- SMAW - small brackets, repairs etc.
  - early module assembly, thin joints
  - erection joints

WELDING CONSUMABLES I

350WT/350WT & 350WT/A517

- **SAW**

  AWS A5.23 F7A6-EG-NII (Lincoln LA75 wire/880 flux)

- **GMAW (shielding gas Ar/CO_2 75/25%)**

  AWS A5.18 ER-70S-3 (Linde 82)

- **FCAW (shielding gas Ar/CO_2 75/25%)**

  AWS A5.20 E70-T1 (Trimark TM71)

- **SMAW**

  AWS A5.1 E7018 or CSA W48.1 E46018 (Nuclearc E7018, Liquid Air LA18Plus, Canox MR, Liquid Carbonic E7018)

WELDING CONSUMABLES II

A517/A517

- **SAW**

  AWS A5.23 F11A6-EF6

  (Armco W-25 wire and Oerlikon OP121T1 flux)

- **SMAW**

  AWS A5.5 E11018 or CSA W48.3 E72018

  (Atom Arc 11018, Lincoln Jetweld H-110, Canox 1118-M)

Notes - DND Fracture Tests

Little data was generated prior to 1994. Recently however several relatively small investigations of the toughness of CPF steels have been carried out by the Dockyard laboratories and DMSS. These will be summarized in the following sections. In 1997 a new more comprehensive program to develop a fracture and fatigue data base has been started under the ISSM major project.

1. Technitrol

In 1994 Technitrol was contracted by DMSS to perform a limited number of Charpy tests on both 350WT and A517 plate. Both plate thickness and specimen size effects were investigated.

2. Dockyard Laboratory (Atlantic)

A more broadly based study of both plate and welds undertaken by DL(A using both Charpy and Dynamic Tear tests (J. Matthews and K. KarisAllen). Selected results of these investigations are shown in the next sections. Since the welds were longitudinal, the plate and HAZ orientations used for comparison are from the lower toughness T-L orientations. The primary objective was to establish lower bound transition temperatures.

RECENT DND FRACTURE TESTS

- 1994 Impact testing (DMSS/Technitrol Eco Inc.)
  8 and 15 mm 350 WT and 15 mm A517
- 1995 Impact and DT tests (DREA DL(A))
  15 mm 350WT and 9 mm A517
  welded 350WT/350WT, 350WT/A517 and A517/A517
- 1996 J and K tests (DREA DL(E)/EMR Ltd)
  welded 15 mm350WT/350WT and 9 mm A517/A517
- 1996 Charpy and DTs (DREA DL(E)/Fleet Tech)
  15 mm Stelco 350WT (crack arrest program)

TECHNITROL PROGRAM SUMMARY

CHARPY ENERGY AND CRYSTALLINITY

- 350 WT plate ($\sigma_y = 420$ MPa $\sigma_{\upsilon} = 510$ MPa)
  Effect of Charpy specimen size
  3.3x10 mm, 5x10 mm, 7.5x10 mm, and 10x10 mm
  Effect of plate thickness
  Comparison of 8 mm and 15 mm plates
- 15 mm A517 ($\sigma_y = 705$ MPa $\sigma_{\upsilon} = 775$ MPa)
  Effect of Charpy specimen size
  3.3x10 mm, 5x10 mm, 7.5x10 mm, and 10x10 mm

TECHNITROL 350WT CHARPY DATA

EFFECT OF PLATE THICKNESS AND SPECIMEN SIZE

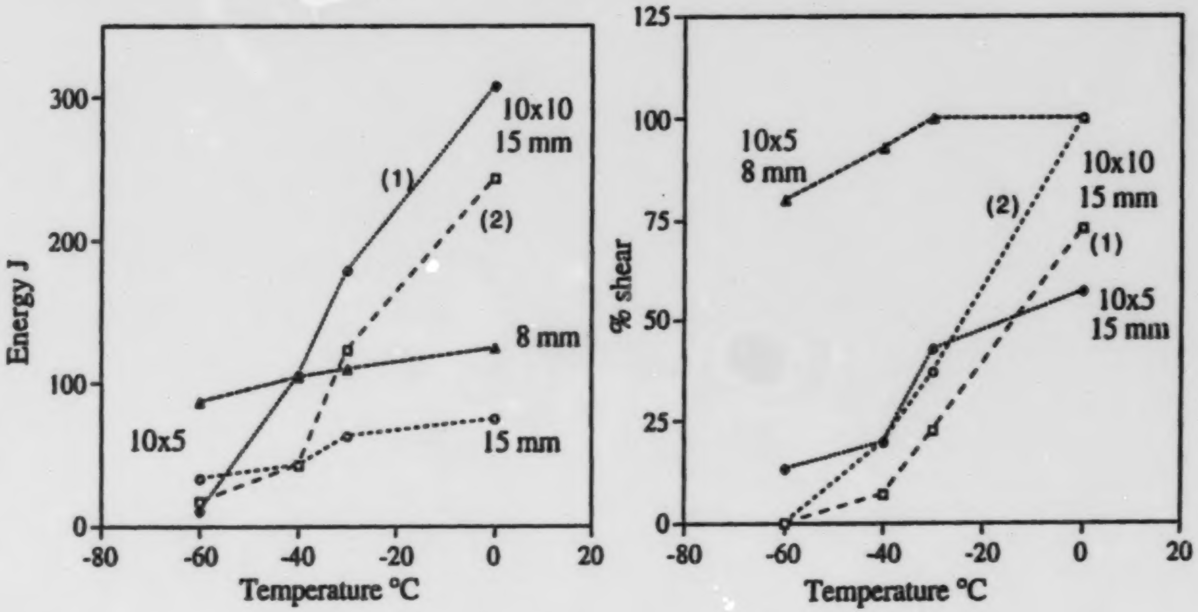

TECHNITROL A517 CHARPY DATA

15 mm PLATE - EFFECT OF SPECIMEN SIZE

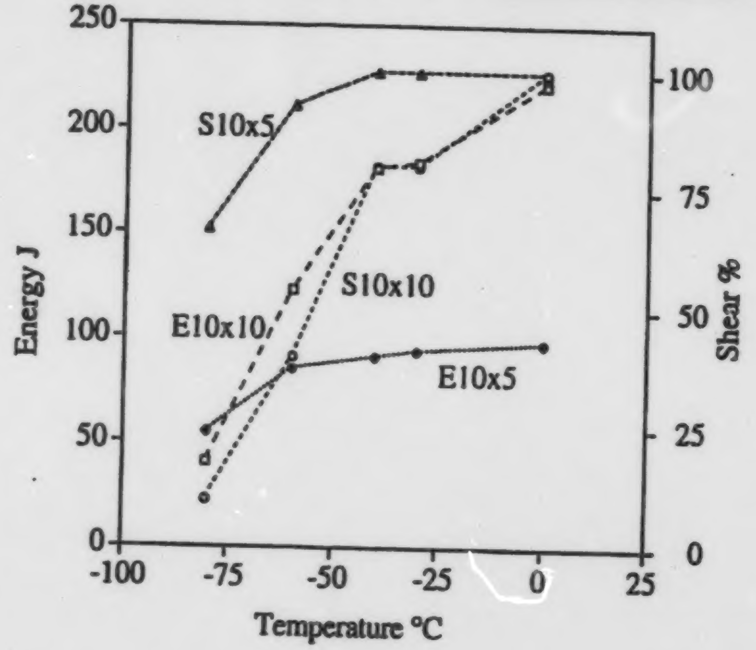

R&D Branch / Bureau de R&D

TECHNITROL PROGRAM

CONCLUSIONS

- 350 WT plate L-T orientation
  15 mm 100 J @ -40°C
  50% shear @ -20°C to -40°C
  8 mm tougher than 15 mm

- 15 mm A517 plate L-T orientation
  Impact energy drops off below -40°C (180J)
  50% shear @ -50°C

DREA DL(A) PROGRAM SUMMARY

LOWER BOUND TOUGHNESS WELDS AND HAZ

- 15 mm 350WT SMAW E7018 electrode
  plate: T-L, T-S, L-T, L-S orientations
  weld: 350WT/350WT & 350WT/A517 (2 heat inputs)
  HAZ: 350WT/350WT, 350WT/A517 & A517/350WT
- 9 mm A517 SMAW E11018 electrode
  plate: T-L, T-S, L-T, L-S orientations
  weld: and HAZ: A517/A517
- Specimen sizes: Charpy 10x10 mm and 7.5x10 mm
  DT: 7.5 mm (A517), 12.5 - 15 mm (350WT)

DREA DL(A) CHARPY DATA

350WT PLATE, WELD, AND HAZ

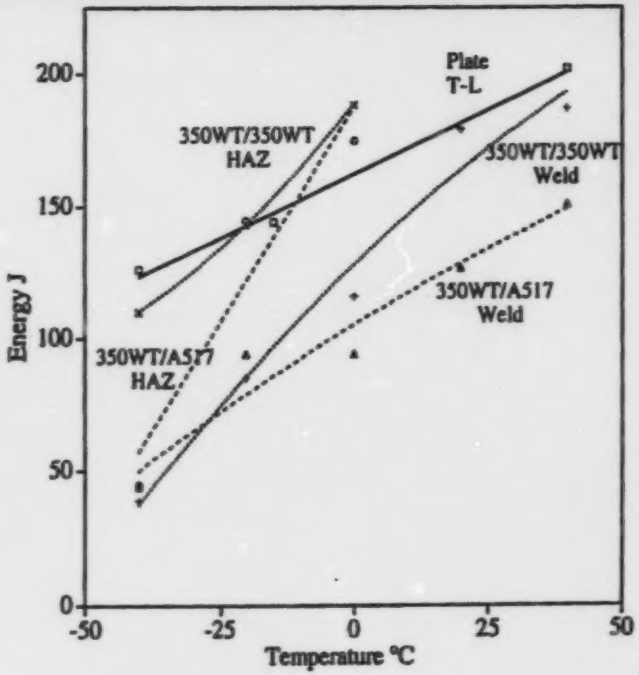

R&D Branch / Bureau de R&D

DREA DL(A) DYNAMIC TEAR DATA

350WT PLATE, WELD, AND HAZ

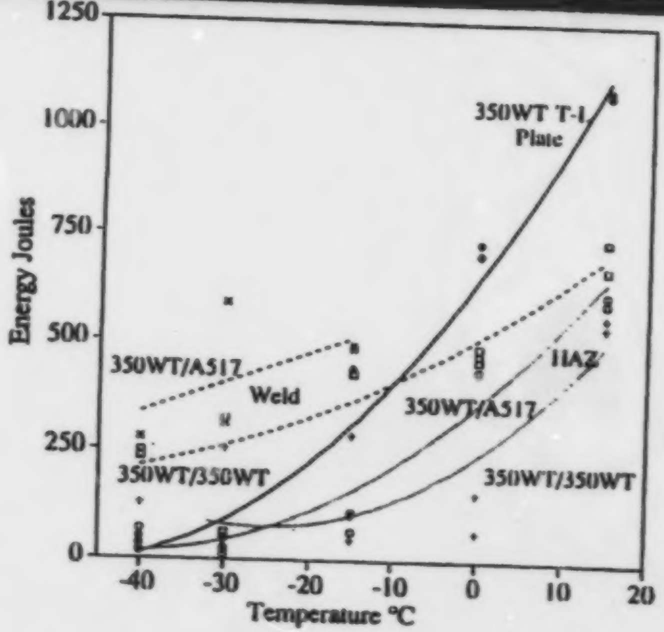

DREA DL(A) CHARPY DATA

A517 PLATE, WELD, AND HAZ

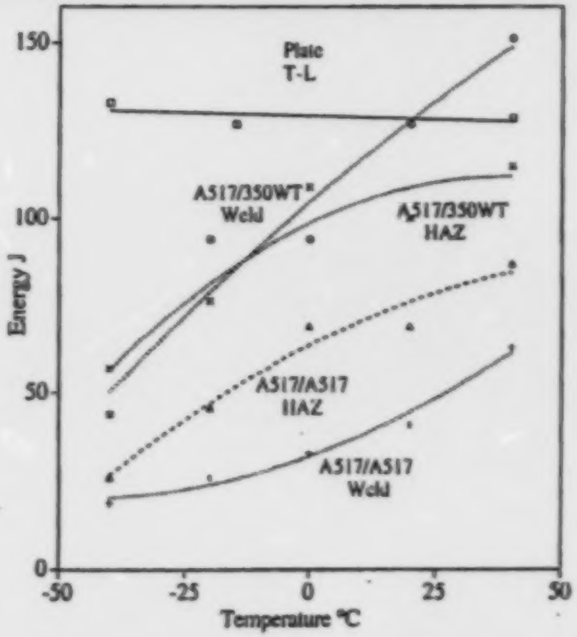

DREA DL(A) DYNAMIC TEAR DATA

A517 PLATE, WELD AND HAZ

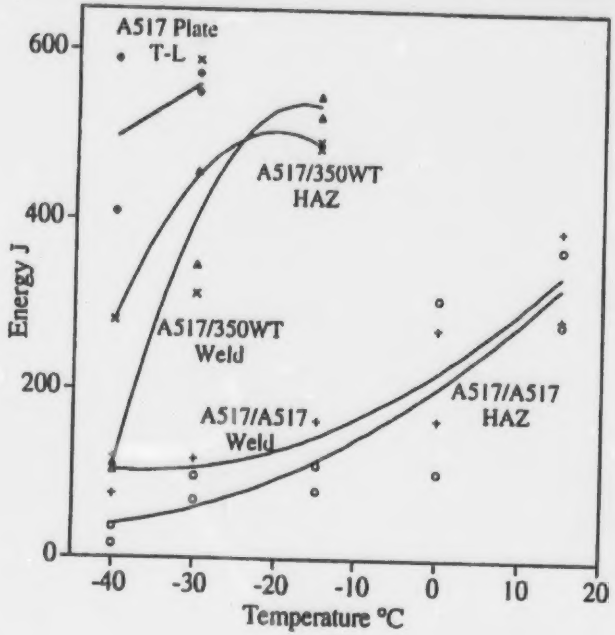

R&D Branch / Bureau de R&D

DREA DL(A) PROGRAM

CONCLUSIONS

- 15 mm 350WT SMAW E7018 electrode
  - plate, HAZ, & weld Charpy all exceed 100 J @ 0°C and 40 J @ –40°C
  - DT energies lowest for HAZ
- 9 mm A517 SMAW E11018 electrode
  - weld Charpy and DT energies relatively low
- DT fracture appearance
  - lower shelf behaviour in E11018 weld below 0°C and in 350WT plate and HAZ below –15°C

Notes - DREA DL(E) Test Program

The DL(A) work indicated that the lowest toughness and/or transition temperatures were exhibited by the A517 weld and the 350WT HAZ. While all had reasonable Charpy values, DT results tended to show lower more abrupt transitions. The follow-up DREA program on the same plate and consumables was carried out by DL(E) (J. Morrison) and Engineering Material Research (A. Hull). This series of tests looked at the 350WT HAZ, and the A517 weld and HAZ. The test procedure was based on ASTM procedures for K, J, and CTOD determination using precracked 3 point bend specimens. Although the results did not in general meet the validity criteria of the standards, the data provided quantitative estimates of toughness over a range of temperatures and at both static and intermediate loading rates.

The welded plate was made by Fleet Technology who had also made the earlier welds. A comparison of Charpy curves was made to demonstrate that the 350WT plate had the same properties. Fracture test responses were characterized as one of elastic-brittle, unstable fracture prior to maximum load, or limit load tearing (with or without a final instability). CTOD values for 350WTHAZ were good. The maximum load K plot shown here grossly underestimates the elastic-plastic K, which based on CTOD and J estimates would be of the order of 300 MPa√m.

A517 HAZ values showed variation between different plates, possibly due to crack path differences (the DL(A) A517HAZ toughness resembled the corresponding weld values). The A517 weld has the lowest toughness and the highest transition temperature.

DREA DL(E) PROGRAM SUMMARY
(ENGINEERING MATERIAL RESEARCH INC)

- Test parameters
  - loading rates

    quasi-static & intermediate (2-4 GPa√m/s)
  - temperatures +5°C to -70 °C
  - 7 mm and 12 mm precracked bend specimens
  - K, J, and CTOD measurements
- Materials
  - 15 mm 350WT/350WT E7018 HAZ
  - 9 mmA517/A517 11018 weld and HAZ

FRACTURE TEST RESPONSES

350WT HAZ (QS @ -70°C, -55°C, -40°C)

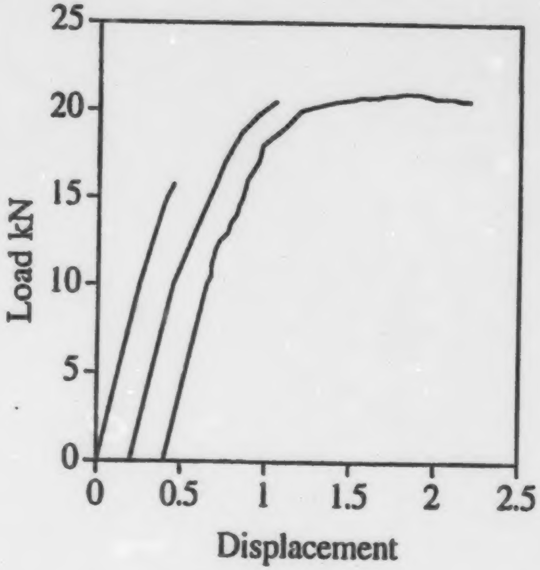

DL(E) - CTOD AT MAXIMUM LOAD

350WT HAZ

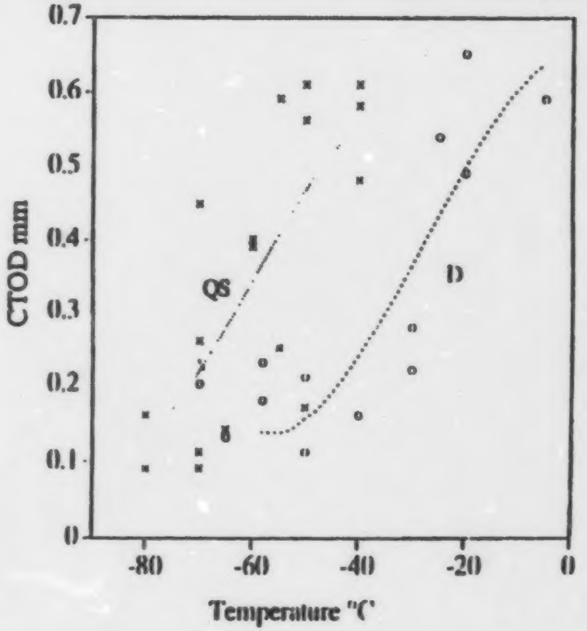

DL(E) - K AT MAXIMUM LOAD

350WT HAZ

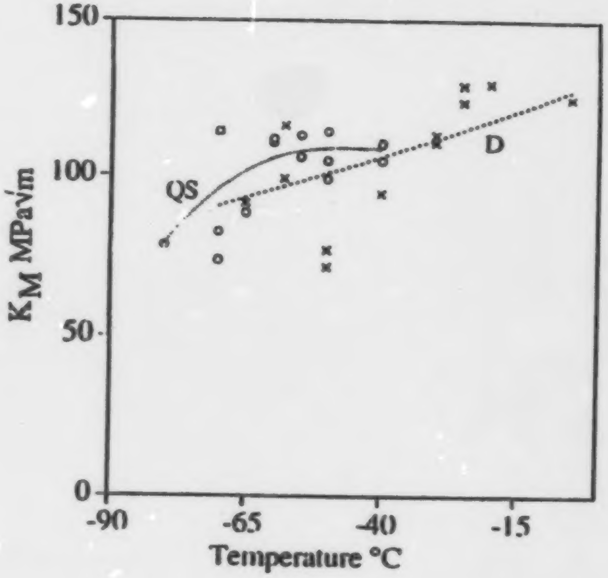

R&D Branch / Bureau de R&D

DL(E) - CTOD AT MAXIMUM LOAD

A517 WELD AND HAZ

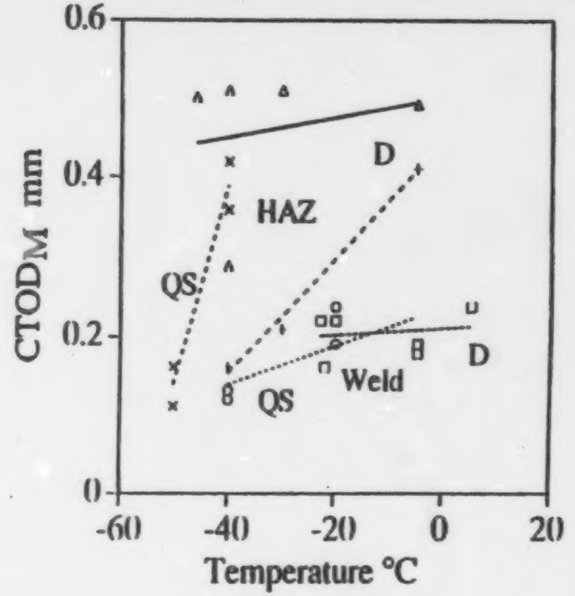

DL(E) - K AT MAXIMUM LOAD

A517 WELD AND HAZ

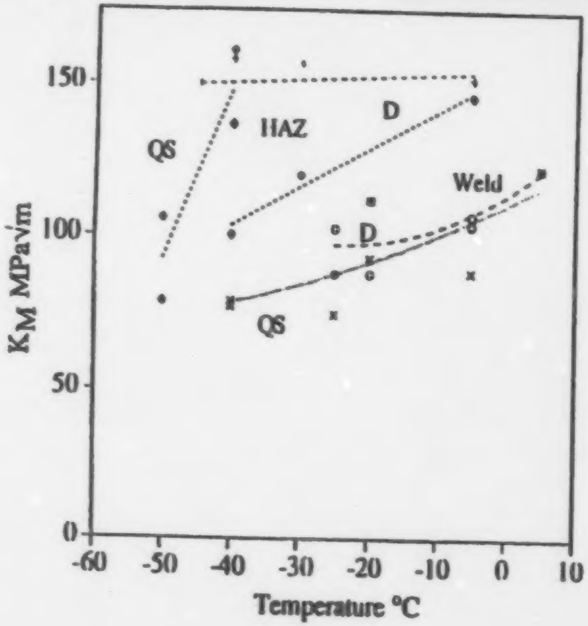

R&D Branch / Bureau de R&D

DREA DL(E) PROGRAM

CONCLUSIONS

- 15 mm 350WT HAZ
  plastic behaviour at ≥-50°C (QS), ≥-25°C (D)
  in plastic regime $K_{Max} \geq 100$ MPa$\sqrt{m}$, CTOD ≥ 0.5 mm
- 9 mm A517 weld
  plastic behaviour at ≥-15°C (QS), ≥0°C (D)
  in plastic regime $K_{Max} \geq 90$ MPa$\sqrt{m}$, CTOD ≥ 0.2 mm
- 9 mm A517 HAZ
  plastic behaviour at ≥-40°C (QS), ≥-25°C (D)
  in plastic regime $K_{Max} \geq 135$ MPa$\sqrt{m}$, CTOD ≥ 0.35 mm

Notes -Comparison of Stelco and Algoma 350WT Plate

A 15 mm plate from Stelco is being used in the DL(E) and DMSS sponsored crack arrest program at Fleet Technology. Both have the same yield strength and meet the specified requirements. The crack arrest program described elsewhere in this proceedings is trying to demonstrate that a proposed procedure for non-plane strain crack arrest toughness measurement can yield useful data for ship structural integrity assessments.

Charpy and DT comparisons with the lower carbon Algoma plate have been carried out. The Stelco plate has much lower Charpy energies, its L-T values being coincident with the Algoma T-L values. Dynamic Tear transition curves are remarkably similar although the Algoma upper shelf values are somewhat higher. Pressing the Charpy notch instead of machining it pushes up the transition temperatures close to those for the DT tests.

CRACK ARREST PROGRAM

COMPARISON OF 350WT BATCHES

- 15 mm 350WT plate

  Algoma   0.09 C 0.04V 0.03 Nb

  Charpy @ -40°C 320 J

  Stelco   0.16 C 0.07V

  Charpy @ -40°C 120 J

  Yield strength 460 MPa for both

- Charpy and DT comparisons L-T and T-L
- Effect of Charpy notch preparation

15 mm 350WT

COMPARISON OF CHARPY CURVES

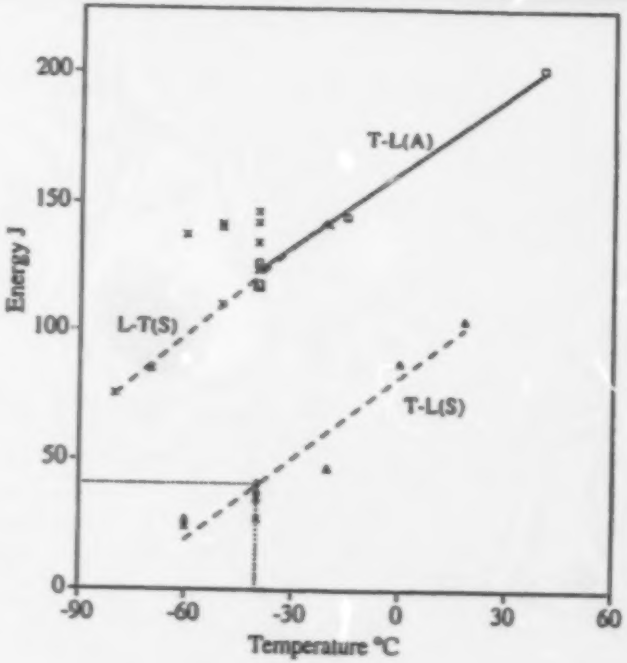

15 mm 350WT

COMPARISON OF CHARPY CURVES

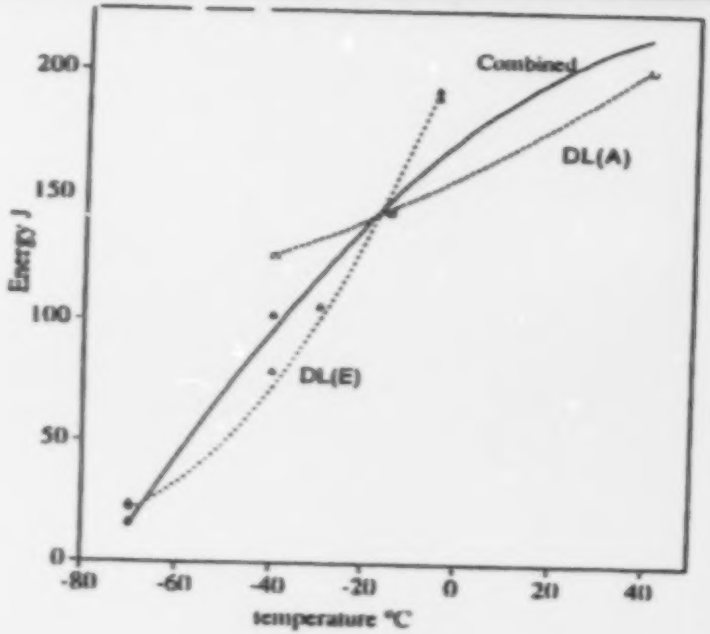

15 mm 350WT

COMPARISON OF DYNAMIC TEAR CURVES

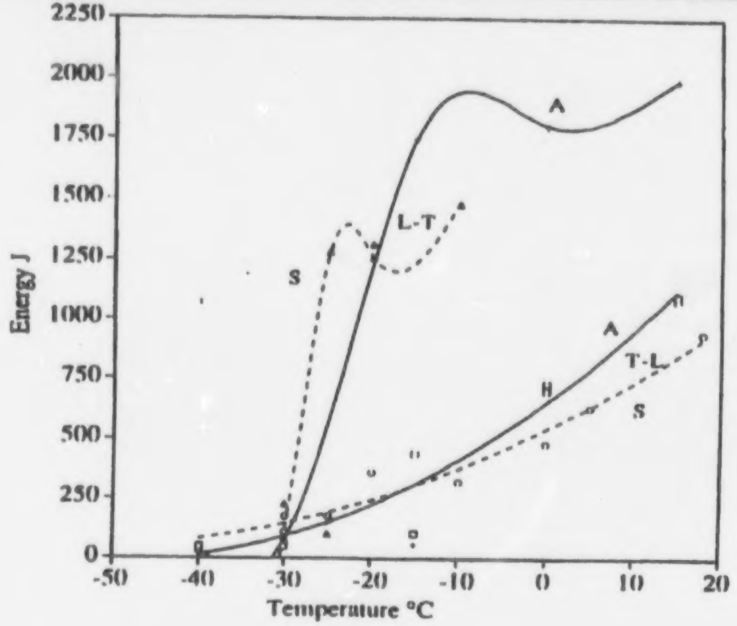

15 mm 350WT (STELCO)

COMPARISON OF CHARPY AND DYNAMIC TEAR 1

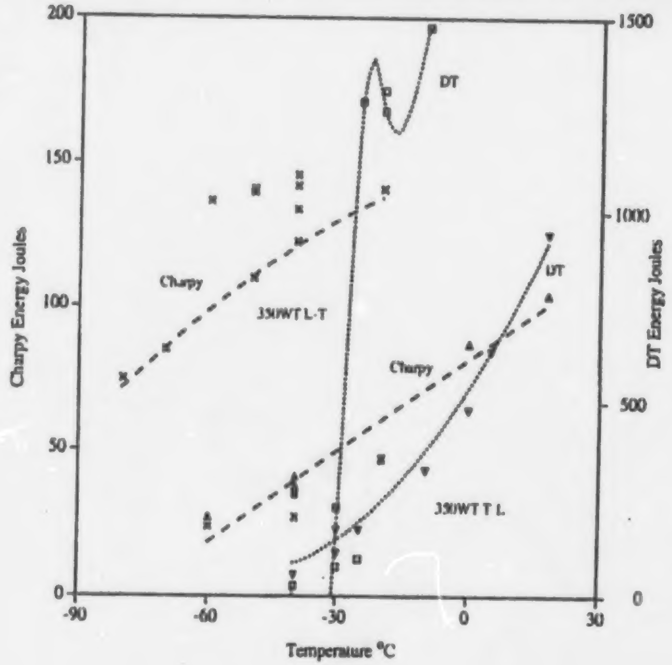

R&D Branch / Bureau de R&D

15 mm 350WT (STELCO)

COMPARISON OF CHARPY AND DYNAMIC TEAR 2

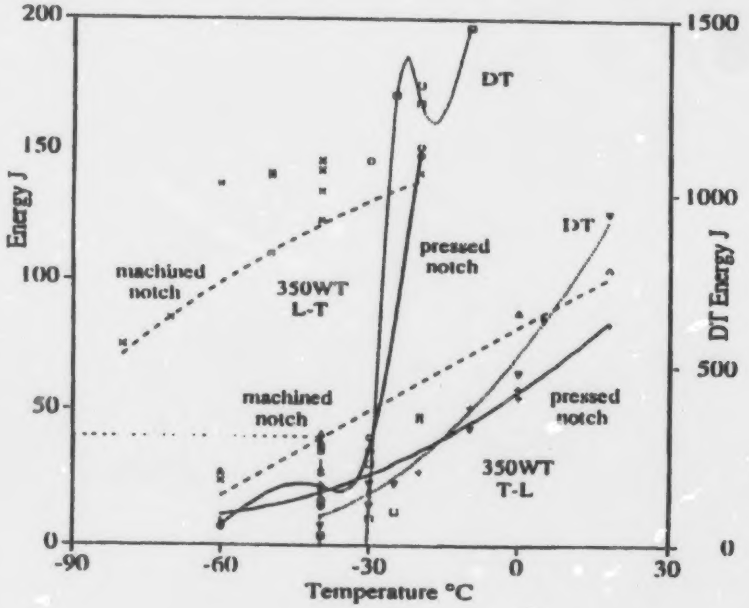

R&D Branch / Bureau de R&D

Notes - Conclusions and Future Work

A series of short investigations has been summarized which provide some indications of the relative toughness and transition behaviour for the CPF steels and welds. The larger data base program currently underway in support of the ISSM development project will provide additional quantitative data for structural modelling.

Future R&D activities include further studies of the transition behaviour using new procedures, comparisons between different batches of 350WT in thinner material, and improved techniques for high rate toughness determination.

FUTURE WORK

- Further data base acquisition being undertaken under ISSM project (DMSS/Fleet Technology)

Related R&D projects include:

- Crack arrest toughness measurement
- Transition behaviour of welded 350WT
- Further comparison of 350WT batches
- High rate J-R curve determinations
- Weld mismatch effects

#507228 (25)

Effect of Notch Acuity on Fracture

by M.N. Bassim* and J.R. Matthews**

* Faculty of Engineering, University of Manitoba, Winnipeg, MB

** Defence Research Establishment Atlantic, Dockyard Laboratory,
Halifax, Nova Scotia

ABSTRACT

Fracture studies of high strength low alloy steels at very high loading rates were conducted using a special Split Hopkinson Bar system equipped with a swing mechanism. Compact tension specimens were used in the investigation. Notch acuity was investigated by performing the tests on several induced notches ranging from spark erosion (EDM) to fatigue precraking followed by fracture.

Both shear lips and stretch zones were measured on the broken speimens as a function of temperature. The effect of notch acuity on toughness (and toughness transition) was studied from the size of the shear lips.

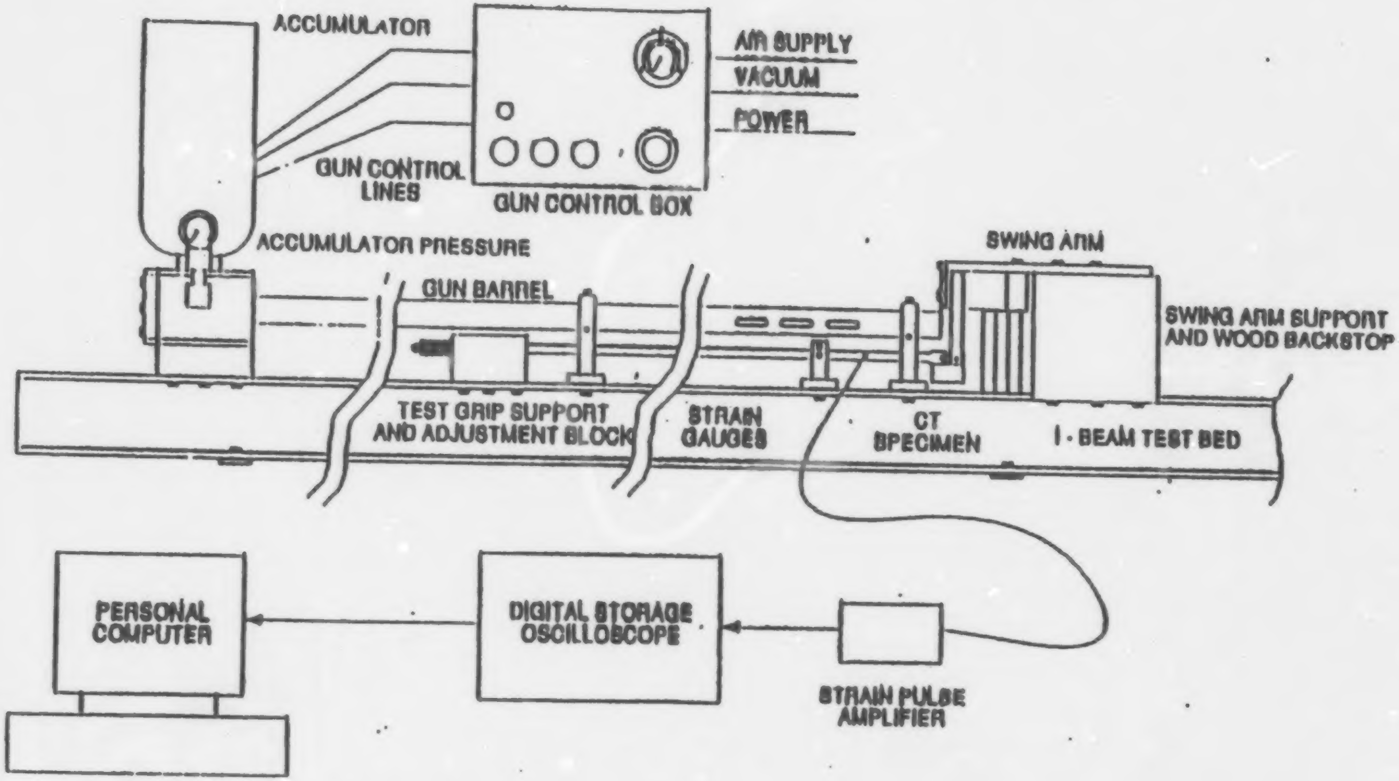
ACCUMULATOR
AIR SUPPLY
VACUUM
POWER
GUN CONTROL LINES
GUN CONTROL BOX
ACCUMULATOR PRESSURE
SWING ARM
GUN BARREL
SWING ARM SUPPORT AND WOOD BACKSTOP
TEST GRIP SUPPORT AND ADJUSTMENT BLOCK
STRAIN GAUGES
CT SPECIMEN
I - BEAM TEST BED
PERSONAL COMPUTER
DIGITAL STORAGE OSCILLOSCOPE
STRAIN PULSE AMPLIFIER

Fig. 2. Split Hopkinson bar assembly for compact tension (CT) specimen testing.

EFM 41/2—K

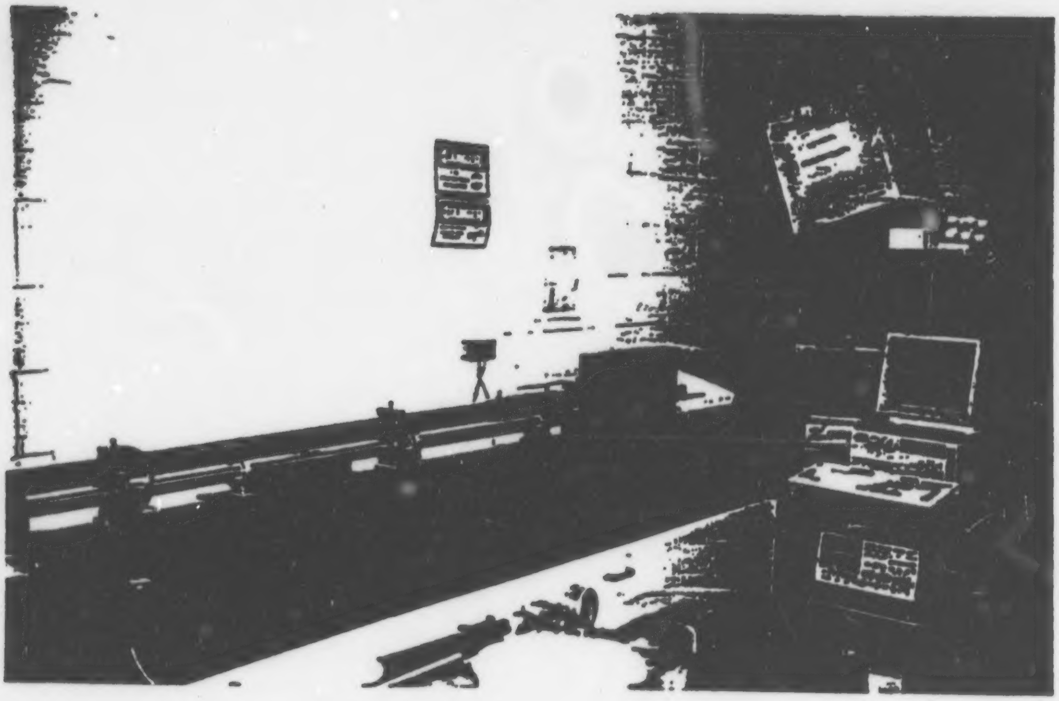

Figure 3.6c Gun barrel, pressure bar, oscilloscope, and computer.

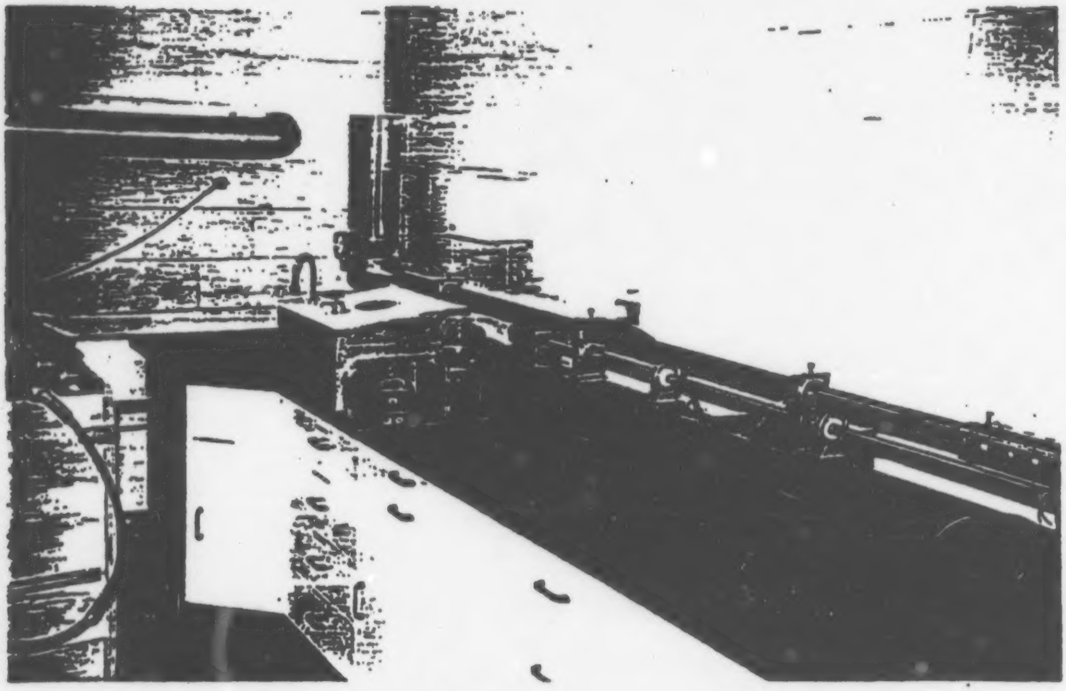

Figure 3.6d Gun barrel, pressure bar, gun control box, and accumulator.

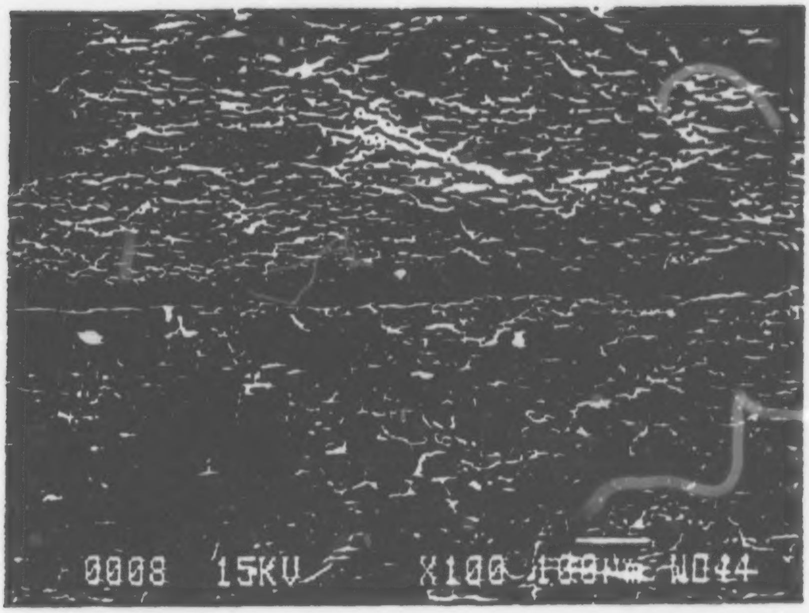
0008 15KV X100 100Mm WD44

Specimen 13

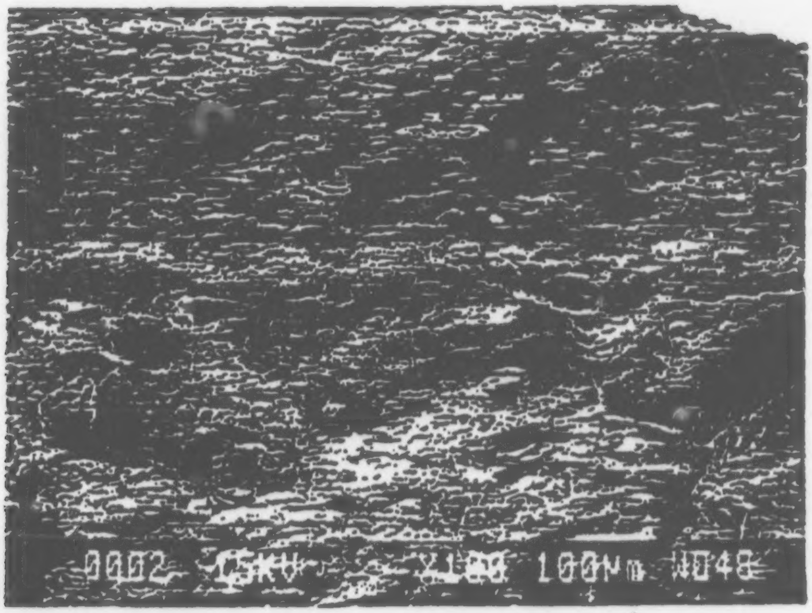
0002 15KV X100 100Mm WD48

Specimen 12

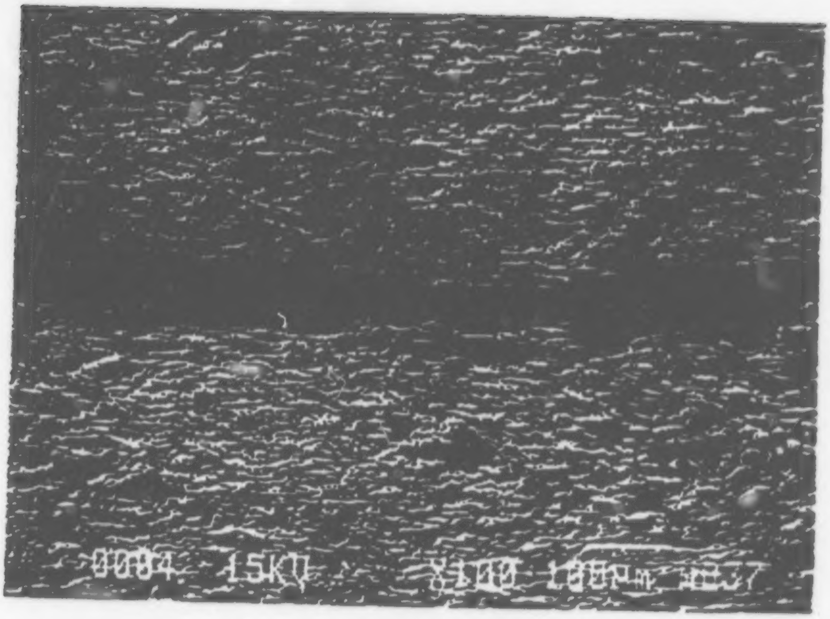
0004 15KV
X100 100µm

Specimen 42

Specimen	Notch	Orientation	Temperature	SZW (μm)
BPA	Fatigue	T-L	-45	56
BPB	Fatigue	T-L	-30	83
BPC	Fatigue	T-L	-15	97
BPD	Fatigue	T-L	0	175
BPE	Fatigue	T-L	15	600
BTA	Fatigue	L-T	-45	46
BTB	Fatigue	L-T	-30	55
BTC	Fatigue	L-T	-15	69
BTD	Fatigue	L-T	0	140
BTE	Fatigue	L-T	15	500

Table 4.2 Stretch zone width results.

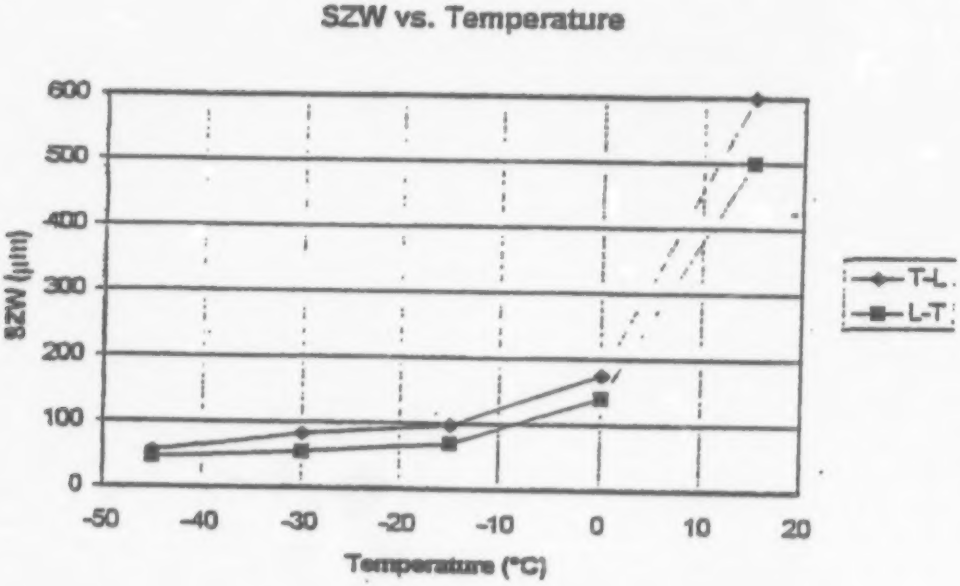

Figure 4.2 Stretch zone width versus temperature.

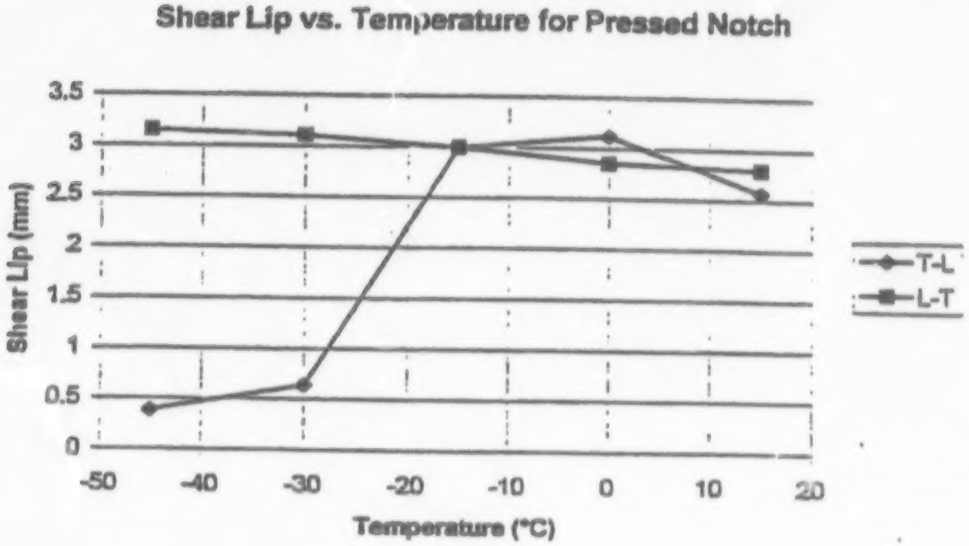

Figure 4.1a Shear lip versus temperature for pressed notch.

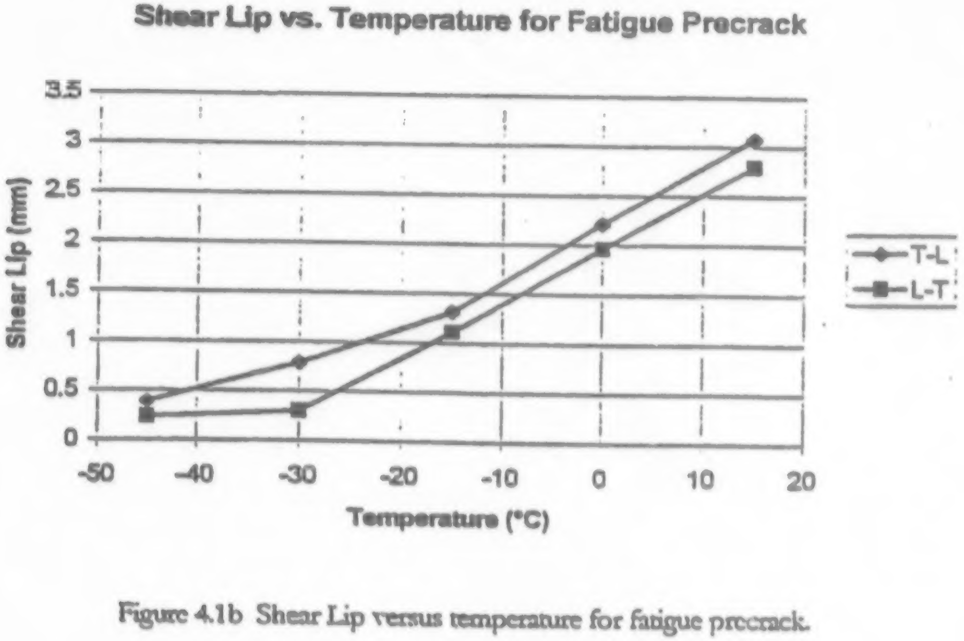

Figure 4.1b Shear Lip versus temperature for fatigue precrack.

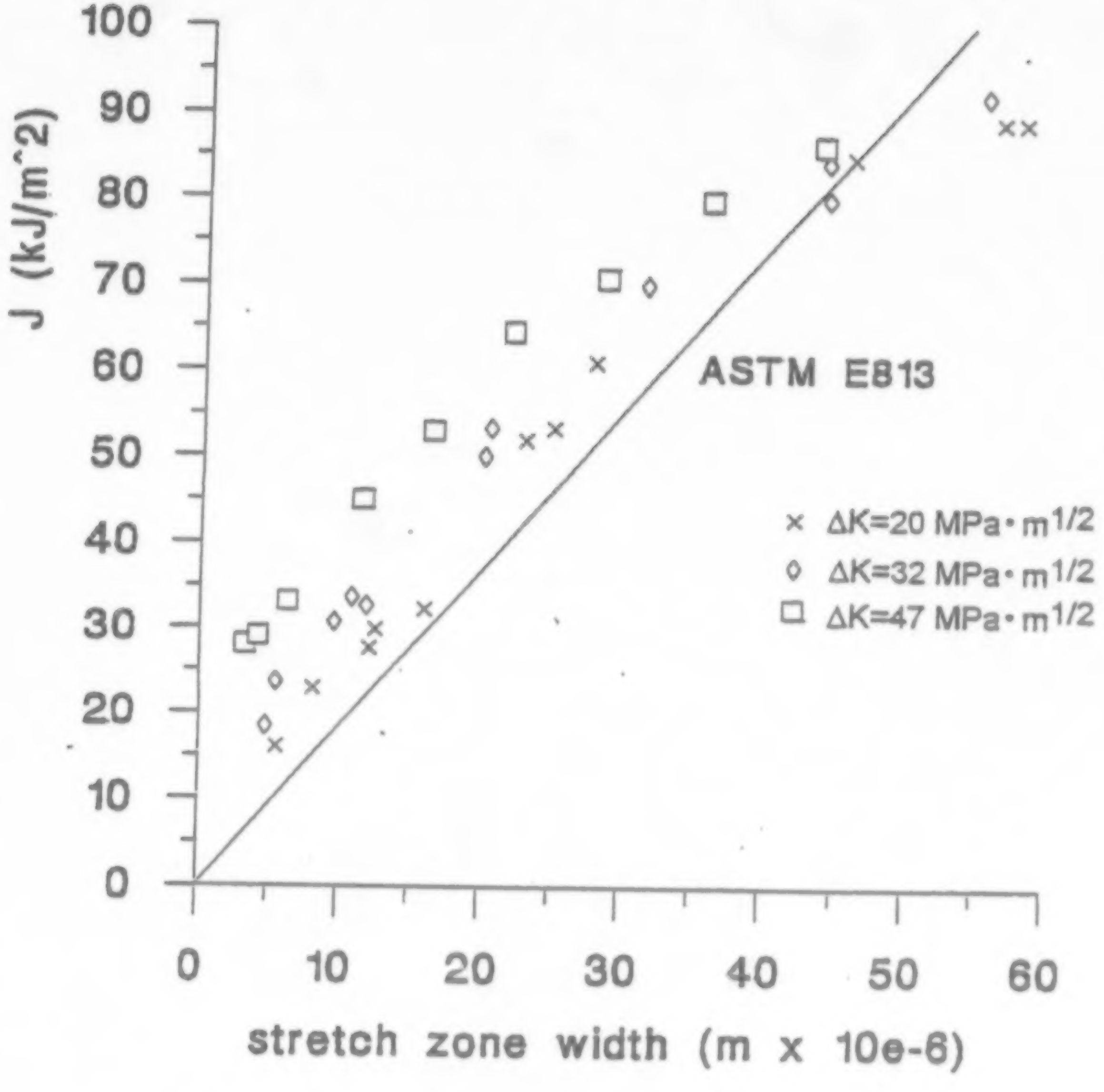

Figure 4.8: Plot of J vs. SZW data for 3 precracking ΔK levels.

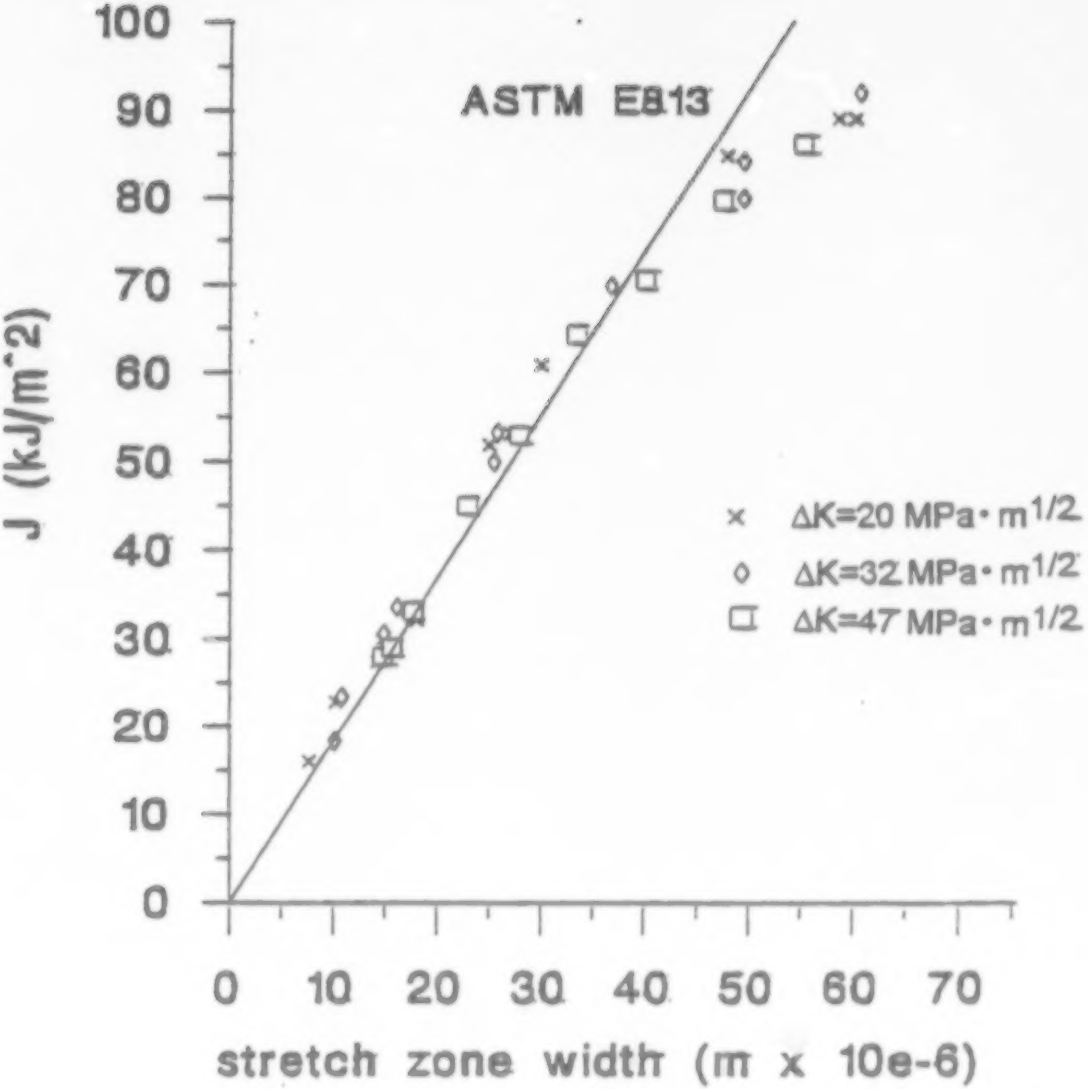

Figure 5.2: Experimental data adjusted to account for fatigue precracking.

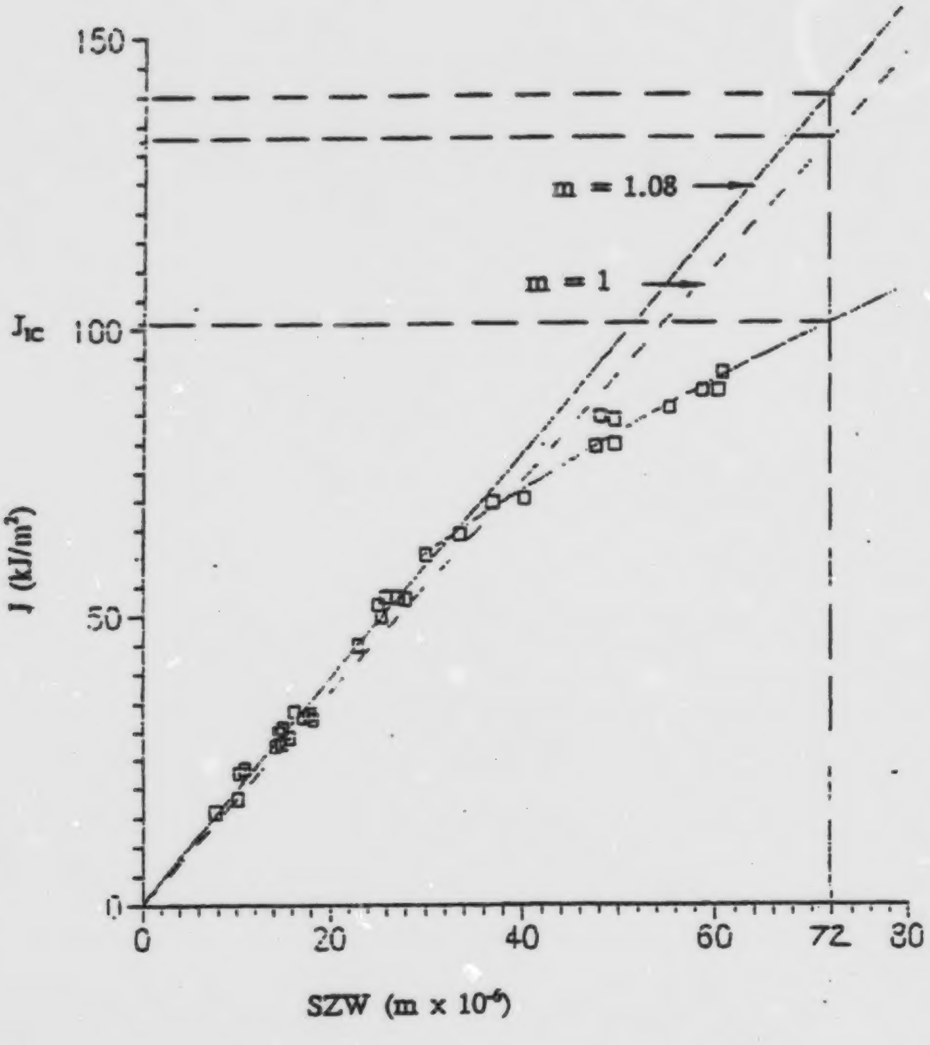

Figure 5.3: Extrapolation from corrected data to J_{IC}.

#507229 (26)

CRACK ARREST TOUGHNESS OF A SHIP STRUCTURAL STEEL

by

L.N. Pussegoda[1], L. Malik[1], J. Morrison[2], and S. Garneau[3]

[1]Fleet Technology Limited, 311 Legget Drive, Kanata, Ontario K2K 1Z8
[2]Dockyard Laboratory (Esquimalt), Esquimalt Defence Research Detachment
P.O. Box 17000 STN FORCES Victoria BC V9A 7N2
[3]National Defence Headquarters

ABSTRACT

Esquimalt Defence Research Detachment and Director Maritime Ship Support have initiated a project to develop procedures and then determine the crack arrest toughness of ship structural steels typical of those used in naval surface ships. In the project to date, a 16 mm thick 350 WT steel has been characterized in terms of its standard mechanical properties (CVN, DT etc.) in both the L-T and T-L orientations. Tests have been performed in the L-T orientation, using the procedure in ASTM Standard E1221 to determine Plane Strain Crack Arrest Toughness but with little success in meeting all of the validity requirements. Full thickness compact crack arrest tests with embrittled chevron notch were then tried using specimens machined in both L-T and T-L orientations, and resulted in improved success. However, further work is required to improve the success rate.

The crack arrest toughness results obtained in the project will be presented and attempts made to relate these to the steel's conventional toughness properties.

Outline

1. Background
2. Objective
3. Methodology of CCA Testing
4. Results
5. Conclusions and Recommendations

FTL FLEET TECHNOLOGY LTD.

Background

- **Test Material**
  - 15.5 mm thick CSA 350WT - controlled rolled microalloyed steel with high strength and toughness
- **Deck plating, shell plating, bulkheads and bottom walls**

i.e. major portion of the CPF hull girder

FTL FLEET TECHNOLOGY LTD.

Objective

- **Measure the arrest toughness in the L-T and T-L orientations, using full thickness compact crack arrest (CCA) specimens.**
  - Dynamic effects are neglected and a static arrest toughness (K_a) of a short (~250 mm long) running crack is measured.

FTL FLEET TECHNOLOGY LTD.

Methodology of CCA Testing

- **Wedge loading - crack run occurs in a diminishing K field**
- **Inject a running crack from locally embrittled zone**
- **ASTM E1221 - Plane strain (K_{Ia}) imposed by two side grooves**

$$K_a = [\delta_f E f(a/W)\ (B/B_N)] / W^{1/2}$$

where: E = Young's Modulus;
δ_f = CMOD at arrest; $f(a/W)$ = compliance function; W = distance from wedge load to back wall of specimen and a = crack length.

$K_a = K_{Ia}$ when conditions for plane strain are met.

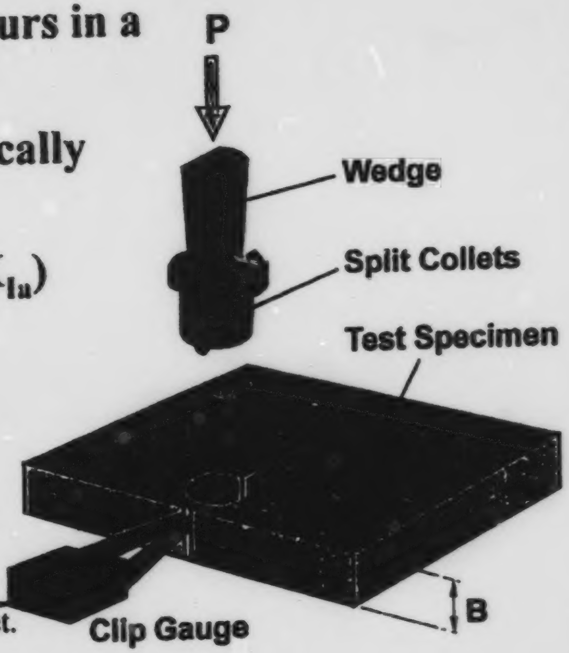
P
Wedge
Split Collets
Test Specimen
B
Clip Gauge

FTL FLEET TECHNOLOGY LTD.

Methodology of CCA testing (cont)

- Modified ASTM E1221 Specimen Design

  Full Thickness (without side grooves)

  - Largest in-plane dimensions specified: (W/B) ratio of 8
  - Anticipated difficulty in obtaining a valid plane strain (K_{Ia}) due to high toughness and small thickness

FTL FLEET TECHNOLOGY LTD.

Methodology of CCA Testing (cont)

- Non-plane Strain CCA Specimen Design Crosley & Ripling

$$W \geq 2.83\ (K_v / \sigma_y)^2$$

Where: K_v = is the "anticipated" crack arrest toughness - typically the minimum required for quality control purposes; σ_y = yield strength.

As test temperature is raised in-plane dimensions (W) increase - no limit for specimen size.

Validity requirements less stringent than ASTM - no check for plane strain.

Specified CMOD limits within which the run-arrest event should occur

- lower limit is based on a minimum crack length (0.5W)
- upper limit is based on a maximum crack length (0.8W)
- if arrest length is below or above these values a lower bound or upper bound estimate of K_a is realized.

FTL FLEET TECHNOLOGY LTD.

Typical Results

- **Modified ASTM E1221 Specimen**
  - Crack starter: brittle weld bead
  - To get a run-arrest event of significance, loading was continued beyond the maximum limit allowed by the standard.
  - Fractures displayed two stage propagation
  - The significant event occurred at the 2nd stage - initiation from the tough HAZ associated with the deposition of the brittle weld bead.
  - All test results did not meet validity criterion.
  - Inferences:
    - a) high stress intensity factor (K_0) for initiation in the second stage
    - b) specimen size limitations ($W/B = 8$).

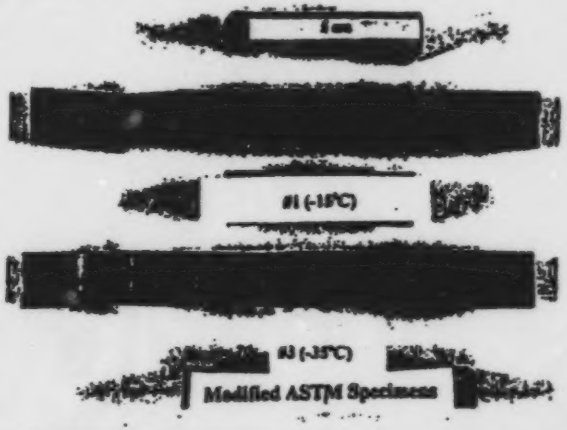

Modified ASTM Specimens

FTL FLEET TECHNOLOGY LTD.

Typical Results (cont.)

- **Non-plane Strain Specimen**
  - Crack starter: strain age embrittled chevron notch
  - More successful in initiating a run-arrest event within the CMOD limits.
  - **L-T Orientation**

    a) Typical fractures

#2 (W - 175mm), (-30°C)

Chevron Notched Specimens

#6 (W = 100mm), (-45°C)

Chevron Notched Specimens

FTL FLEET TECHNOLOGY LTD.

Results (cont.)

- **Non-plane Strain Specimen**

  L-T Orientation

  b) Results

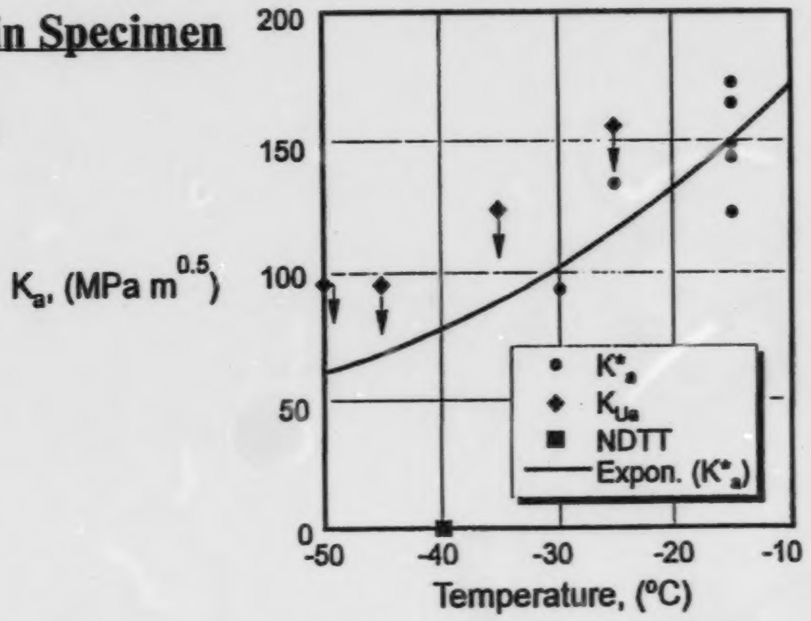

Crack Arrest Toughness vs Temperature
L-T Specimens

FTL FLEET TECHNOLOGY LTD.

Typical Results (cont.)

- Non-plane Strain Specimen
  - T-L Orientation
    - a) Typical fractures displaying the 3 types of behaviour

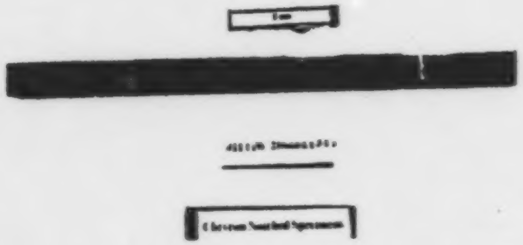
5 cm
Chevron Notched Specimens

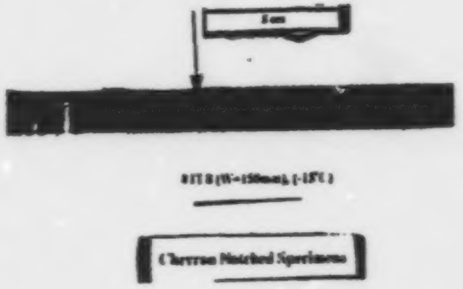
5 cm
8IT 8 (W=150mm), (-15°C)
Chevron Notched Specimens

FTL FLEET TECHNOLOGY LTD.

Results (cont.)

- **Non-plane Strain Specimen**

T-L Orientation

b) Results

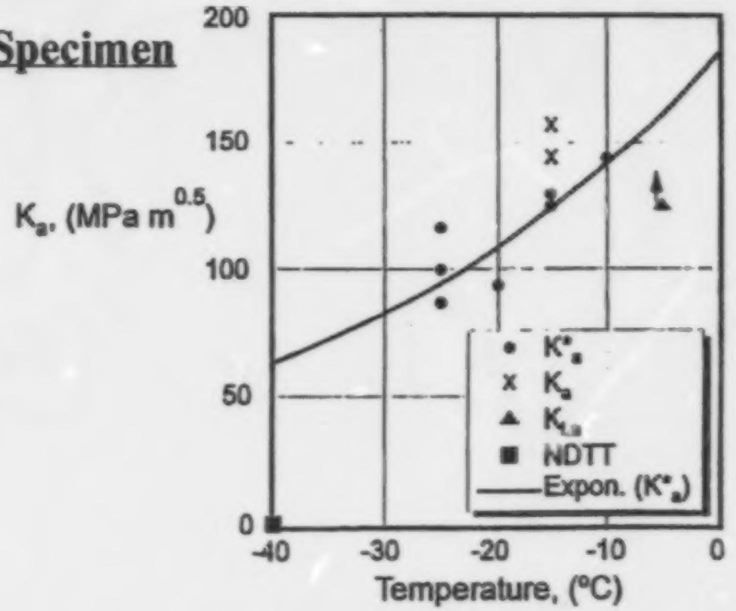

Crack Arrest Toughness vs Temperature
T-L Specimens

FTL FLEET TECHNOLOGY LTD.

Results (cont.)

- **Non-plane Strain Specimen**
  - L-T Orientation

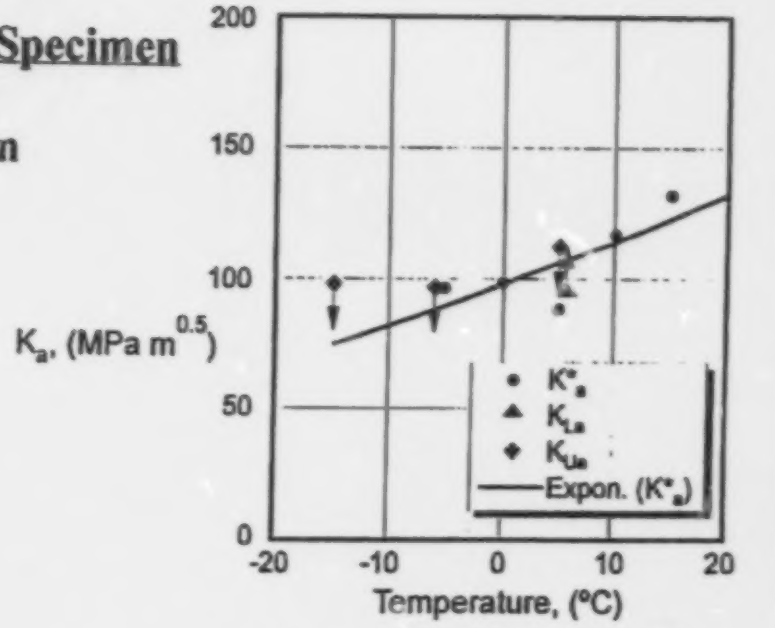

Crack Arrest Toughness vs Temperature
CGHAZ

FTL FLEET TECHNOLOGY LTD.

Conclusions

- **Modified (full thickness) ASTM E 1221 is not suitable -high toughness and small thickness of marine structural plate - anticipated.**
  - – a) size limitation (W/B) ≤ 8
  - – b) failure of the crack starter - brittle weld bead

FTL FLEET TECHNOLOGY LTD.

Conclusions

- **Non-plane strain full thickness CCA specimens were more successful for this plate.**
  - a) no size limitation; in-plane dimensions increase with anticipated increase in K_a with temperature
  - b) more successful crack starter - strain age embrittled

FTL FLEET TECHNOLOGY LTD.

Recommendation

- Study of different degrees of embrittlement of the crack starter - initial findings

FTL FLEET TECHNOLOGY LTD.

#507230 ㉗

J_{Id} Testing of an HY 80 Steel Weldment

by K.D. MacKay[1] and Dr. J.R. Matthews[2]

[1] Martec Limited
Suite 400, 1888 Brunswick St.
Halifax, Nova Scotia, Canada, B3J 3J8

[2] Defence Research Establishment Atlantic,
Dockyard Laboratory, FMO Halifax,
Halifax, Nova Scotia, Canada, B3K 2X0

ABSTRACT

Evaluation of the dynamic elastic-plastic toughness properties of very tough structural steels is an expensive and complicated activity. For military purposes, the dynamic tear test and explosion bulge test have been used in the absence of a simple dynamic elastic-plastic toughness test. DREA has developed a simplified multiple specimen method of determining J_{Id}, which uses a standard drop, tower without instrumentation. A blunting resistance curve is generated, typically from blunting up to complete fracture, by impacting specimens using progressively larger weights and small changes in drop height. The lack of need for instrumentation puts the use of this test into the financial range of many more organisations.

Specific test results will be given for HY 80 welds, prepared at DRA Dunfermline, tested at -5°C.

INTRODUCTION

The Materials Group at DREA have been developing a test method to determine the dynamic elastic-plastic fracture toughness of materials used in naval applications. The ideal test method would incorporate the following features:

- inexpensive
- simple to perform
- little interpretation of data required to generate the toughness value
- test specimens sized to be structurally relevant
- test easily performed at low temperatures

These features would make it possible for the test to be performed at a larger number of facilities and make the test useful as a quality control test.

The elastic-plastic conditions in which the test method is to apply are defined by the central portion of the materials transition curve as shown in Figure 1. At the lower portion of the curve, the materials behaviour can be described by linear-elastic fracture mechanics using a parameter such as K. The upper portion of the curve is dominated by plasticity where failure occurs by plastic collapse and toughness can be described by $\hat{k}$ (flow stress in shear). The central portion of the curve defines the temperature range where elastic-plastic toughness parameters are useful in describing the material behaviour and a toughness parameter such as the J integral can be applied.

BACKGROUND

Static Methods

There are a number of standard test methods for determining the J_{Ic} under quasi-static loading. ASTM standards E813 and E1737 [1] describe three different methods which can be used to determine J_{Ic}. The first method to be used was a multiple specimen technique in which nearly identical specimens were prepared. A specimen is loaded to generate a desired amount of crack extension during which load and displacement are recorded. The area under the load displacement curve is used to determine the energy, U, required to extend the crack. The value of J for each specimen is found using the equation

$$J=2U/Bb_o \quad (1)$$

where B is the specimen thickness and b_o is the size of the original uncracked ligament. The crack is marked after the test by fatiguing or heat tinting and broken open so that the original crack length and the amount of crack extension can be measured. The J-crack extension data pairs are plotted and J_{Ic} is determined by the intersection of a power law fit through the data and an offset blunting line as shown in Figure 2, provided that validity criteria are met.

The second method described by the ASTM standards is a single specimen technique which uses unloading compliance to measure crack length. The specimen is loaded with load and displacement recorded. At various intervals in the test the loading is paused and the specimen is partially unloaded and reloaded to generate an unloading segment in the load displacement record as shown in Figure 3. The slope of the unloading segments are used with a compliance function to determine the crack length at each unloading segment. The value of J is also determined at each unloading segment in terms of its elastic and plastic components. The elastic component is determined from the load, crack length and the specimen dimension and the plastic component is determine by

$$J_{pl}=2U/Bb_o \quad (2)$$

where U is defined by the shaded region under the load displacement curve as depicted in Figure 3. The J-crack extension data pairs at each unloading are plotted and treated in the same manner as the multiple specimen data to determine J_{Ic}.

The third technique described by ASTM E1737 uses electric potential to determine crack size while a single specimen is loaded. A direct current is passed through the specimen while the voltage across the crack is monitored. As the crack grows the current field in the specimen is altered which is indicated by a change in the voltage reading. Crack length is determined from the voltage readings using an experimental or analytical calibration curve. The value of J is determined from the load displacement record in a similar manner as with the unloading compliance method. The J-crack extension data pairs are plotted to determine J_{Ic} as with the first two methods.

Dynamic Methods

The unloading compliance technique is not suitable for a dynamic test because it is undesirable to unload the specimen during the test (pausing to unload the specimen even briefly would affect any time dependant mechanisms and thus reduce the significance of any rate effects).

The electric potential technique has been used to determine the dynamic fracture toughness of materials. However, the complexity and expense of the equipment required to perform the test is significant. The success of the method is dependant on the expertise of the personnel performing the test as there are a number of factors which can produce errors in the measurement including thermal drift, placement of the current input and voltage measurement electrodes, selection of input current magnitude, and electrical isolation of the specimen. Precautions must also be taken to ensure that low level voltage readings are not obscured by induced EMF and improper grounding of equipment.

A number of techniques have been used to determine the crack length during dynamic fracture. Crack growth has been monitored using grids bonded to the surface of the specimen where the crack extension is given by the breakage of the grid elements or the resistance change of the grid. High speed photography has also been used to measure crack growth during dynamic fracture. The difficulty of both these methods is that they are only capable of measuring the crack length at the surface which may not accurately reflect through thickness crack propagation. High speed photography is also expensive due to the equipment required and the large number of photographs to be processed.

Measuring load and displacement during a dynamic test increases the cost of the equipment required to perform the test. Inertial effects can create difficulties in the load and displacement records obtained in dynamic testing. Impact of the specimen with a striker creates vibrations in the specimen which appear as oscillations in the load and displacement records. While some work has been performed on the use of damping the oscillation using absorbers [2-4] there has been concern that the specimen velocity is not constant as the crack grows (due to over damping). Others have used smoothing techniques to remove oscillations from the data record however data smoothing can create errors due to skewing of the data [3, 4].

EXPERIMENTAL (DREA J_{50} METHOD)

Dynamic elastic-plastic fracture toughness tests were performed using the J_{50} test method developed at DREA. The technique uses a number of identically prepared fatigue precracked single edge notch bend (SEN(B)) specimens. The specimens were impacted using a drop tower to generate a different amount of crack extension in each specimen. Crack length and crack extension were measured by marking the crack by post-test fatigue or heat tinting and breaking the specimen to reveal the fracture surface. The 9 point measurement technique, described in ASTM E813 and E1737 [1], was used to measure the original and final crack lengths.

The value of J for each specimen was determined using Equation 1 however in this case the energy term, U, was equated with the potential energy stored in the crosshead of the drop tower:

$$U = w \cdot h \qquad (3)$$

where w is the weight of the crosshead and h is the height of the striker above the specimen. The energy applied to each specimen was adjusted by varying either the weight of the crosshead and/or the height from which the crosshead was dropped.

The J-crack extension data pair from each specimen was plotted to give a dynamic J-resistance curve. The intersection of a data fit through the points and an offset blunting line gives the value of J_{Id}, the dynamic elastic plastic fracture toughness of the material.

The J_{50} test method was used determine the dynamic fracture toughness of an HY 80 weldment that was prepared at DRA Dunfermline [5]. Two SEN(B) specimen configurations were used; one with B=25 mm and W=41 mm and a second with B=75 mm and W=41 mm. Shallow and deep notch specimens were prepared for both specimen configurations. The notch depths for the 25 mm and 75 mm thick specimens are given in Tables 1 and 2 respectively. The dynamic tear transition curves for both shallow notch and deep notch specimens are given in Figure 4. All specimens were tested at -5°C.

RESULTS

The results of the J_{50} tests are given in Tables 1 and 2 for the 25 mm and 75 mm thick specimens respectively. The results are plotted in Figures 5 and 6.

Estimates of the J_{Id} for the 25 mm thick specimens are 1370 kJ/m^2 and 200 kJ/m^2 for the shallow and deep notch specimens respectively. The 75 mm specimens gave J_{Id} values of approximately 400 kJ/m^2 and 40 kJ/m^2 for the shallow and the deep notch specimens. It should be noted that the J_{Id} values given here are approximate due to the limited number of data points.

DISCUSSION

The J_{50} technique offers several advantages over other dynamic test methods. Load, displacement and crack length measurement during the test are not required which reduces the equipment required along with the associated cost and complexity. Low temperature tests are easily performed by cooling the specimen before placing it in the drop tower. Structurally relevant full thickness specimens up to 75 mm have been tested. The calculations to generate the dynamic J-resistance curve are simple and the determination of J_{Id} requires limited data analysis.

One aspect of the J_{50} test which should be noted is that the energy applied to the specimen may be adjusted from specimen to specimen by increasing the drop height and thus the impact velocity is not constant. However the velocity range for the test is typically in the range of 1-3 m/s and errors associated with velocity changes over this range are expected to be minimal. Figure 7 shows data for HSLA 80 steel which was tested over a large range of velocities at two temperatures [6]. Note that the toughness change over the J_{50} velocity range, indicated by the shaded region in Figure 7, is minimal.

New test method

While the J_{50} test method provides a simple method of performing dynamic elastic plastic fracture testing there are some aspects of the test that could be improved. Being a multiple specimen test requires several specimens to be prepared by fatigue precracking for each temperature at which J_{Id} is required. The time to prepare the specimens could be reduced by either replacing the fatigue crack with another notch or by reducing the number of specimens.

A simple test for quality control purposes may be derived from the J_{50} method. The basis of the test would be to define an allowable amount of crack extension when a specimen is impacted. The specimen design and equipment requirements would be the same as with the J_{50} test. Test parameters of crosshead weight, drop height, specimen dimensions, and crack length would define the velocity and the applied J. The drop height would be selected to give a velocity that the structure is expected to experience (for example 1-4 m/s is representative of an explosion). The data from these tests can be plotted as crack extension vs temperature which would be expected to have the form of Figure 8 over the materials transition range.

The amount of allowable crack extension can be based on the desired dynamic J-resistance curve for the material. If the structure design requires that the structure withstand a certain J value at a specified temperature then the J-resistance curve for that temperature would define the amount of crack extension that would be acceptable. Since each specimen will generate a J-crack extension data pair it would also be possible to compare the material to a J-resistance curve by plotting the point on the curve. If the data point falls below the desired J-resistance curve then the material toughness is not acceptable. If the data point is on or above the J-resistance curve then the material meets or exceeds the desired material specifications.

The simple test described above has the advantage over the J_{50} test in that only one specimen is needed at each temperature. Specifying a drop height for all tests eliminates any concern over velocity change effects.

CONCLUSIONS

DREA has developed a simple multiple specimen technique to determine the dynamic elastic plastic fracture toughness of structural steels which offers several advantages over conventional test methods in that it is easy to perform, no instrumentation required, little data interpretation required, and structurally relevant specimens are used. The test method has been used to determine the J_{Id} of an HY80 weldment using both 25 mm and 75 mm thick specimens.

A simple dynamic test for quality control purposes has been proposed which, with further development, may soon be available.

REFERENCES

[1] "ASTM Annual Book of Standards", Vol. 3.01, Philadelphia, PA, 1996.

[2] K.J. KarisAllen, J. Morrison, "Mechanical Reduction of Inertially Generated Effects in Single-Edge Notch Bend (SENB) Specimens Subjected to Impact Loading", *Rapid Load Fracture Testing*, ASTM STP 1130, R, Chona and W.R. Corwin, Eds., ASTM, Philadelphia, 1991 pp. 76-91.

[3] J.A. Joyce and E.M. Hackett, "Dynamic J-R curve Testing of a High Strength Steel Using the Key Curve and Multispecimen Techniques", *Fracture Mechanics: Seventeenth Volume*, ASTM STP 905, J.H. Underwood, R. Chait, C.W. Smith, D.P. Wilhem, W.A. Andrews, and J.C. Newman, Eds., ASTM, Philadelphia, 1986, pp. 741-774.

[4] J.A. Joyce and E.M. Hackett, "An Advanced Procedure for J-R Curve Testing using a Drop Tower", *Nonlinear Fracture Mechanics: Volume I-Tine-Dependant Fracture*, ASTM STP 995, A. Saxena, J.D. Landes, and J.L. Bassani, Eds., ASTM, Philadelphia, 1989, pp. 298-317.

[5] J.D.G. Sumpter, "Production of Q1N Welded Panels for TTCP Operating Assignment on Fracture Control Technology", DRA TM (AWMS) 93217, May, 1993.

[6] N.B. Bassim, J.R. Matthews, and C.V. Hyatt, "Evaluation of Fracture Toughness of HSLA80 Steel at High Loading Rates Using Stretch Zone Measurements", *Engineering Fracture Mechanics*, Vol. 43, No. 2, 1992, pp. 297-303.

Table 1: J_{50} test data and results, B=25 mm

Specimen	Temp. (°C)	a_o (mm)	Height (m)	Weight (N)	Velocity (m/s)	J (kJ/m^2)	Δa (mm)
UK36	-5	5.84	0.114	7993	1.50	2046	22.93
UK25	-5	5.87	0.076	7993	1.22	1365	0.19
UK22	-5	6.40	0.076	2700	1.22	468	0.12
UK7	-5	20.55	0.038	2700	0.86	396	5.09
UK5	-5	20.43	0.064	2700	1.12	656	5.44
UK3	-5	20.10	0.076	2700	1.22	775	6.82
UK18	-5	20.80	0.076	2700	1.22	802	15.12

Table 2: J_{50} test data and results, B=75 mm

Specimen	Temp. (°C)	a_o (mm)	Height (m)	Weight (N)	Velocity (m/s)	J (kJ/m^2)	Δa (mm)
UK42	-5	9.62	0.190	2700	1.93	407	0.65
UK14	-5	9.86	0.305	2700	2.45	656	18.83
UK28	-5	11.17	0.381	2700	2.73	854	27.27
UK12	-5	21.84	0.038	2700	0.86	129	3.92
UK40	-5	21.58	0.076	2700	1.22	254	8.44
UK13	-5	22.25	0.114	2700	1.50	394	15.2
UK27	-5	22.76	0.229	2700	2.12	547	20.04

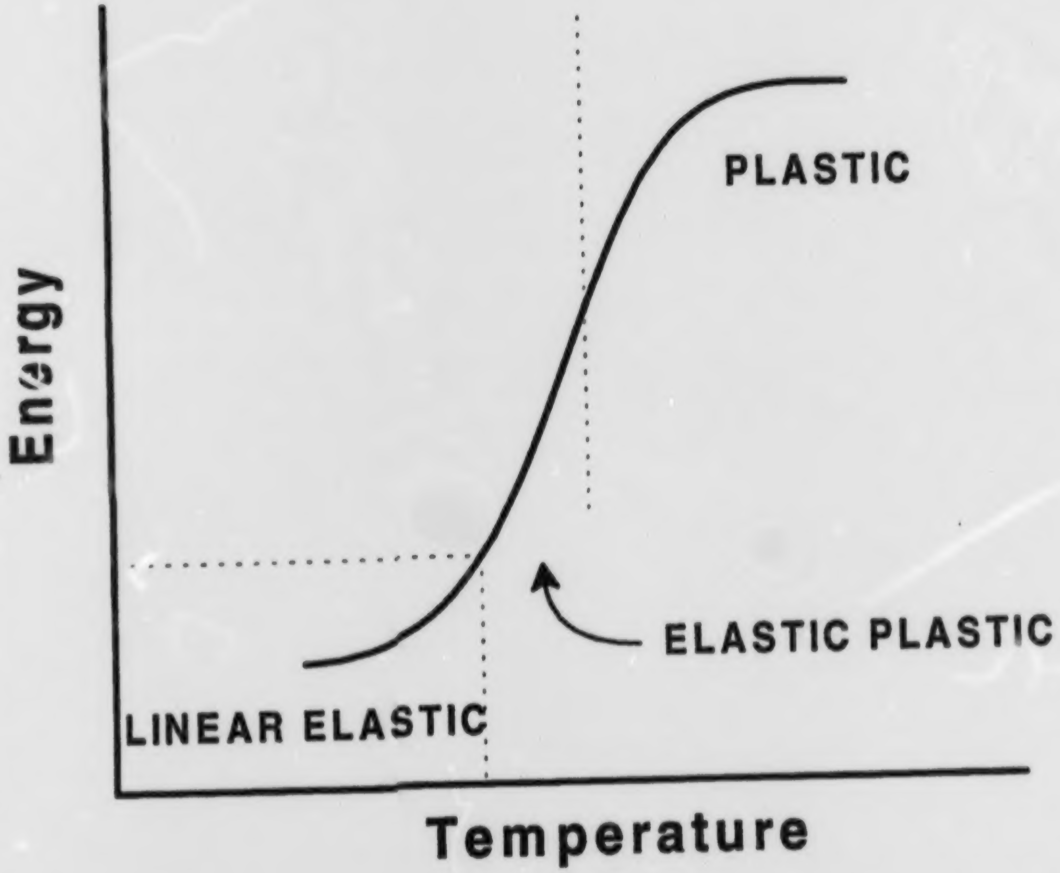

FIGURE 1.: A sketch indicating the fracture behaviour of a material over its transition range.

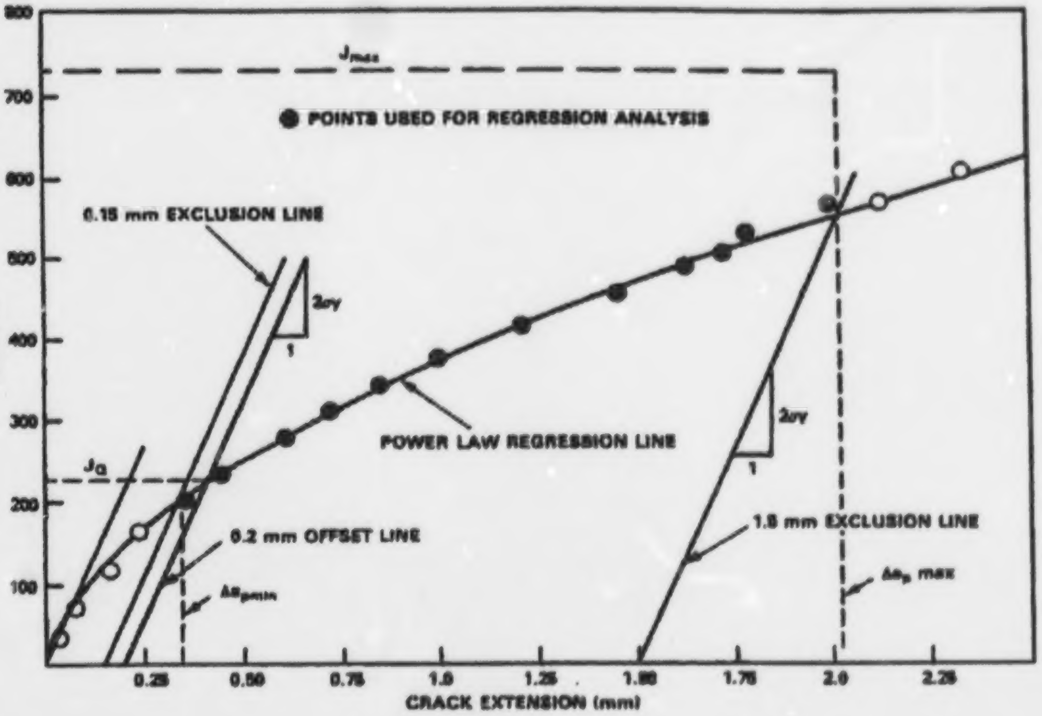

FIGURE 2.: A typical J-crack growth resistance curve [1].

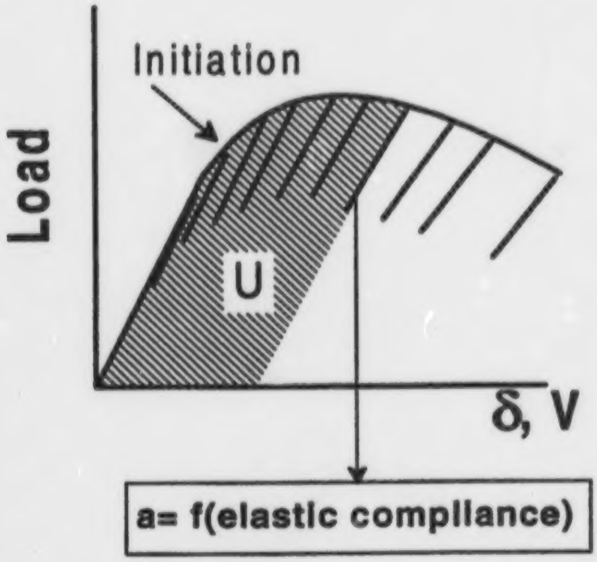
Initiation
Load
U
δ, V
a= f(elastic compliance)

FIGURE 3.: Unloading compliance method load-displacement record.

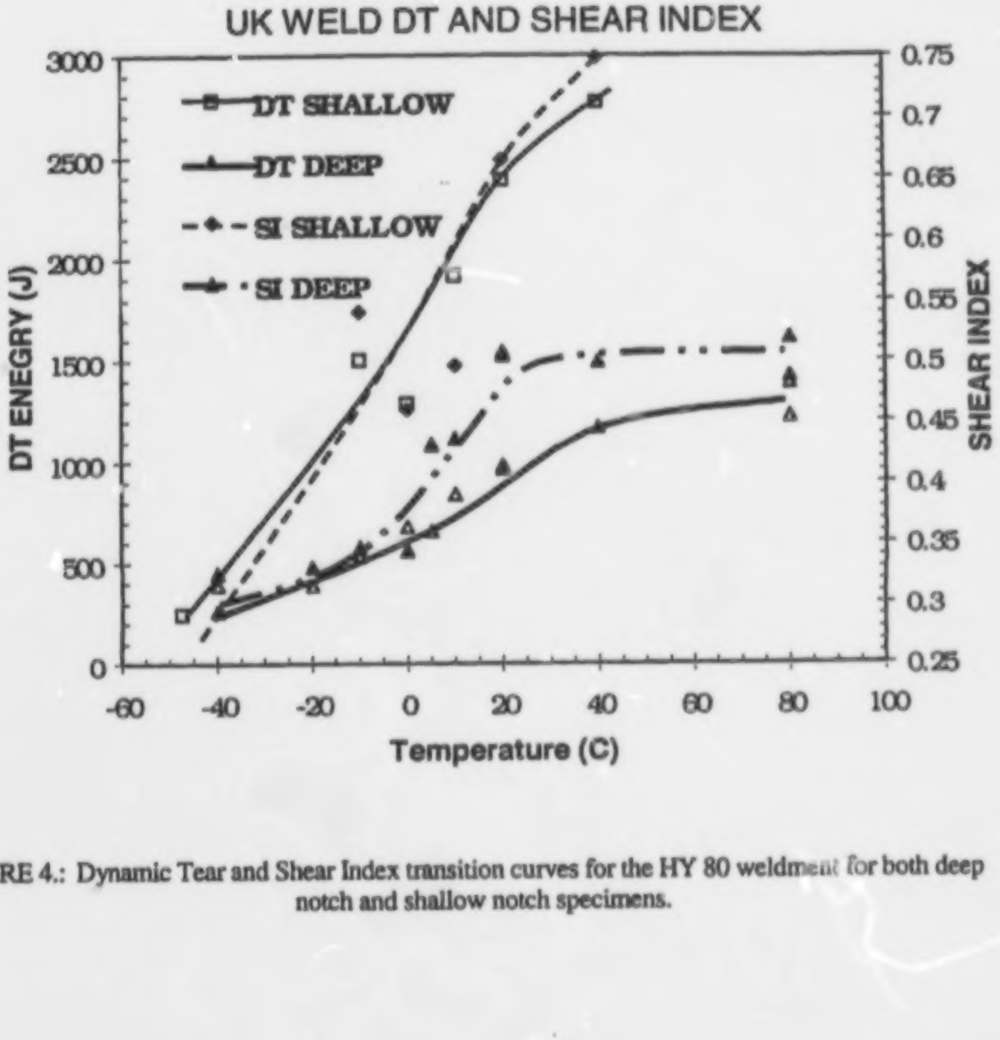

FIGURE 4.: Dynamic Tear and Shear Index transition curves for the HY 80 weldment for both deep notch and shallow notch specimens.

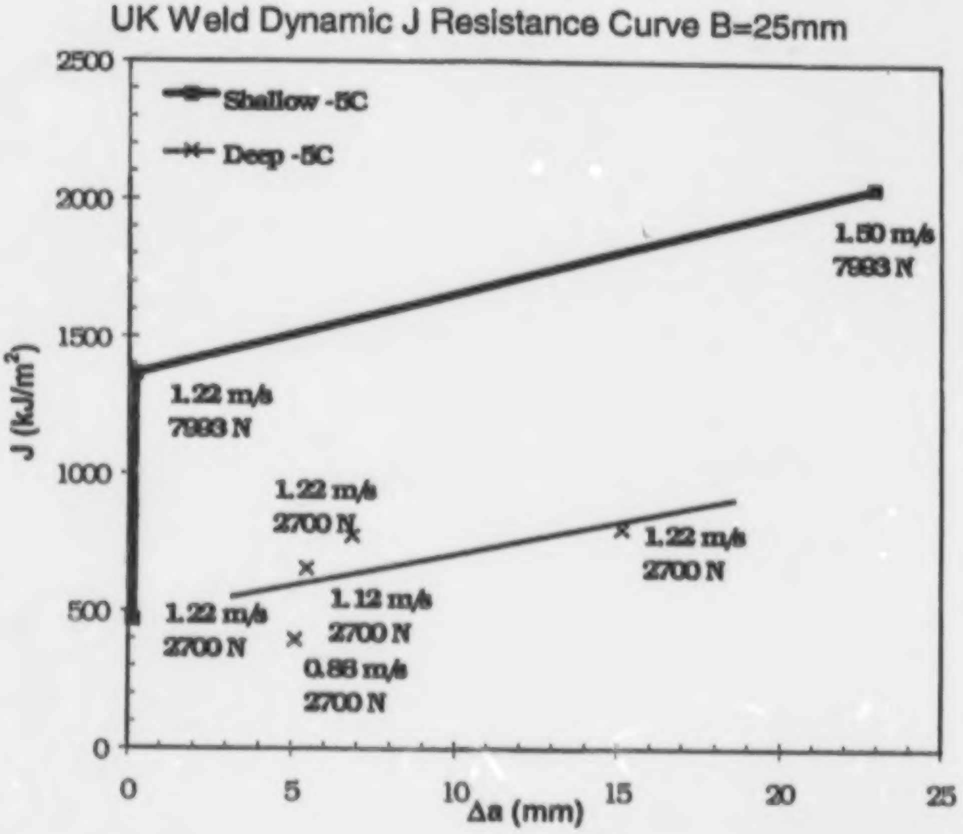

FIGURE 5.: HY 80 weldment dynamic J-resistance curve for 25 mm thick specimens.

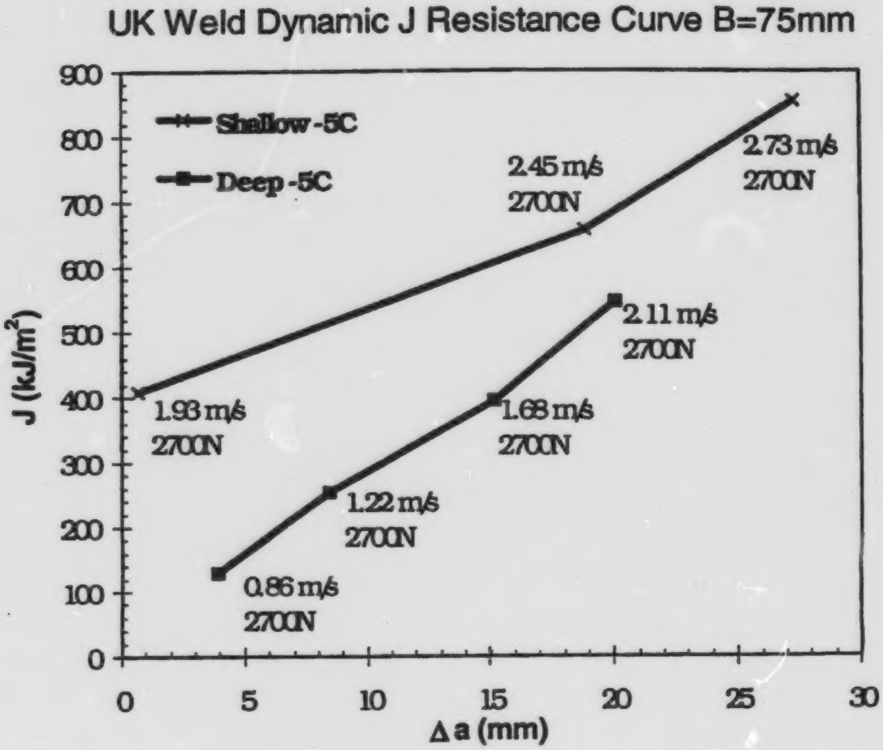

FIGURE 6.: HY 80 weldment dynamic J-resistance curve for 75 mm thick specimens.

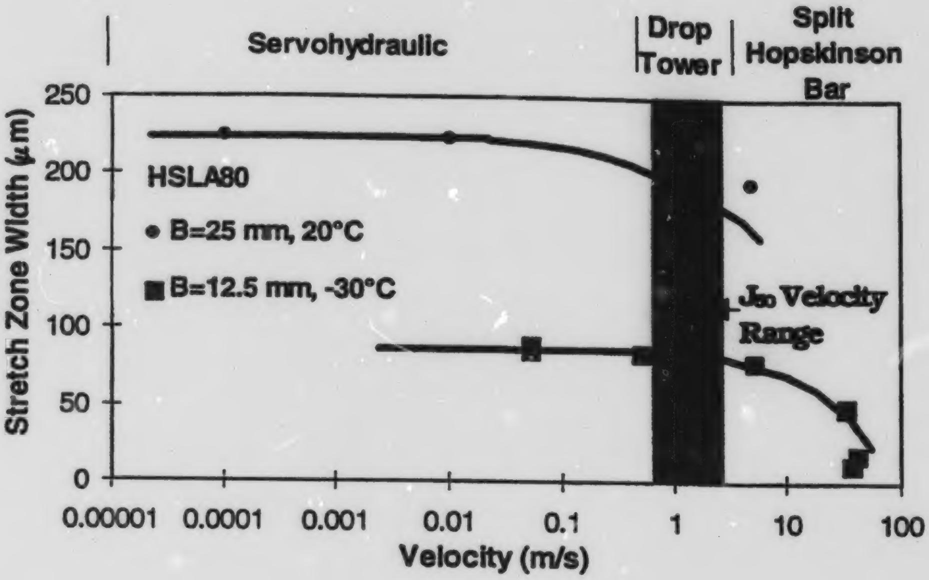

FIGURE 7: The affect of velocity on toughness [6].

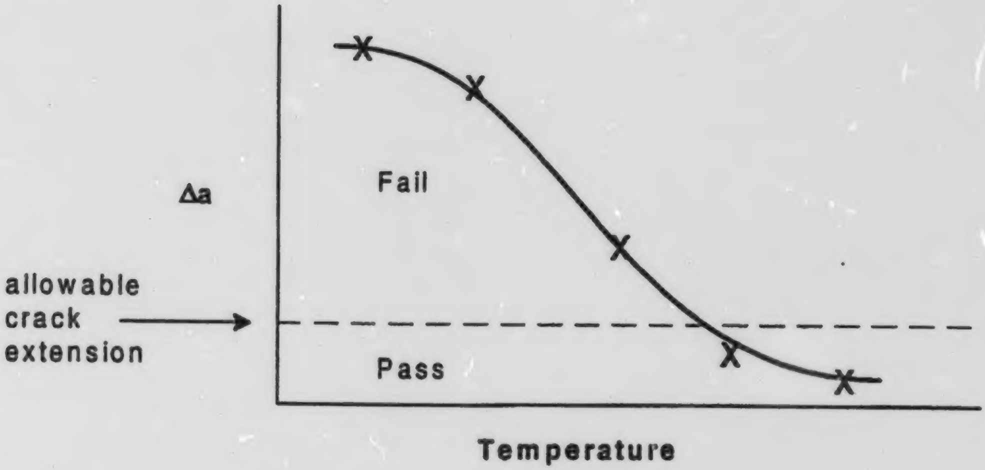

FIGURE 8.: Expected results from proposed test method. Only one specimen is required to produce each data point.

#507231 (28)

Delivering Corrosion Courseware: The Evolution of the RMC Corrosion Short Course

P.R. Roberge
Department of Chemistry and Chemical Engineering
Royal Military College, Kingston, Ontario, Canada K7K 7B4

ABSTRACT

The Corrosion Short Course given at the Royal Military College every second year since 1987 had been requested by the CF Corrosion Committee and designed by some of its scientific members. Typically the course covered topics such as:

- Case histories;
- Fundamentals of metallurgy, thermodynamics and kinetics;
- Paint and coatings, failure analysis; and
- Cathodic protection and design considerations.

The instructors and attendees of the one week long course came from various DND organizations of different parts of Canada. The recent downsizing in DND brought, along with the demise of the Corrosion Committee itself, an erosion of the number of instructors available and of the ability of the system to staff the course with attendees. A new approach had to be considered to deliver the course and advertise its availability. Fortunately the means by which information can be vehicled have improved to a point where it has become possible to deliver complex course materials via simple communication channels. Portable computers have been with us for a decade now, yet we have only just started to unleash their power. In many areas of technology, people have started to invent useful methodologies to support routine human activities. The flexibility provided by computerized information systems is tremendous once the initial investment has been made. This paper will describe the status of the Corrosion Short Course, circa 1997, and discuss the strategy that gradually evolved by considering available software and transmission technologies.

DELIVERING CORROSION COURSEWARE: THE EVOLUTION OF THE RMC CORROSION SHORT COURSE

P.R. Roberge
Royal Military College of Canada

Developing CSC Courseware

- **CSC History**
- **CSC Instructors and attendees**
- **Present status**
- **Distance learning**
- **Publishing tools**

RMC CSC History

- The course was established in answer to a request by the CF Corrosion Committee;
- The one week long course was offered every second year since 1987;
- Instructors and attendees came from various CF organizations.

RMC CSC History

- Criteria for attendance were:
  - Personnel with junior officer rank or above/ or civilian equivalent with at least a degree in post-high school chemistry;
  - Personnel employed in positions involving life cycle material management (LCMM) design, specification preparation or procurement specification of systems and equipment;
  - Personnel employed in positions involving repair and maintenance.

Main Topics of the CSC

- Corrosion case histories;
- Fundamentals of metallurgy;
- Thermodynamics and kinetics;
- Paint and coatings (inorganic & organic);
- Corrosion testing and failure analysis;
- Cathodic protection;
- Design considerations;
- Corrosion information resource.

RMC CSC History: present status

- The staffing organization disappeared in the downsizing process;
- Some instructors have also been downsized;
- The absence of the CF Corrosion Committee also means less recognition of corrosion efforts or needs in the CF;
- Does it mean corrosion problems have also been minimized ?
- And the need for training ?

RMC 427B vs. the CSC

Topics	Army	Navy	Air
1. Aqueous Corrosion	√	√	√
2. Corrosion Testing		√	√
3. Surface Characterization			
4. Life Prediction and Cost Analysis			
5. Failure Analysis	√	√	√
6. Corrosion Monitoring and Inspection		√	√
7. Protective Coatings	√	√	√
8. Corrosion Inhibitors		√	√
9. Cathodic and Anodic Protection		√	
10. Atmospheric Corrosion			√
11. Corrosion of Reinforcing Steel in Concrete	√		
12. Hot Corrosion		√	√

RMC CSC History: future

- **RMC is becoming the center of CF distance learning;**
- **An infrastructure has been created to evaluate the university creditability of present courses offered in the CF;**
- **RMC would like to see the CSC move in these directions;**
- **How can we achieved such goal ?**

TOOLBOOK II INSTRUCTOR

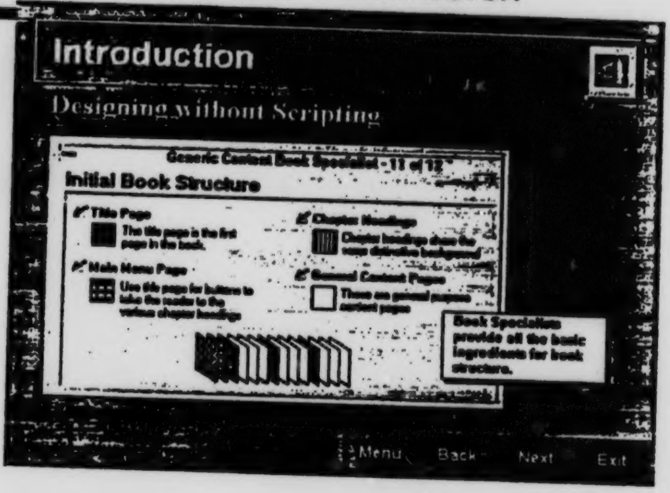

Introduction

Designing without Scripting

Generic Content Book Specialist - 11 of 12

Initial Book Structure

Title Page

The title page is the first page in the book.

Main Menu Page

Use this page for buttons to take the reader to the various chapter headings.

Chapter Headings

Chapter headings share the same distinctive background

General Content Pages

These are general purpose content pages

Book Specialists provide all the basic ingredients for book structure.

Menu
Back
Next
Exit

Corrosion surveillance: internet main screen

ToolBook II - INTERN2.TBK
File
Edit
Text
Page
Help

Aircraft Corrosion:

Corrosion surveillance: corrosion program

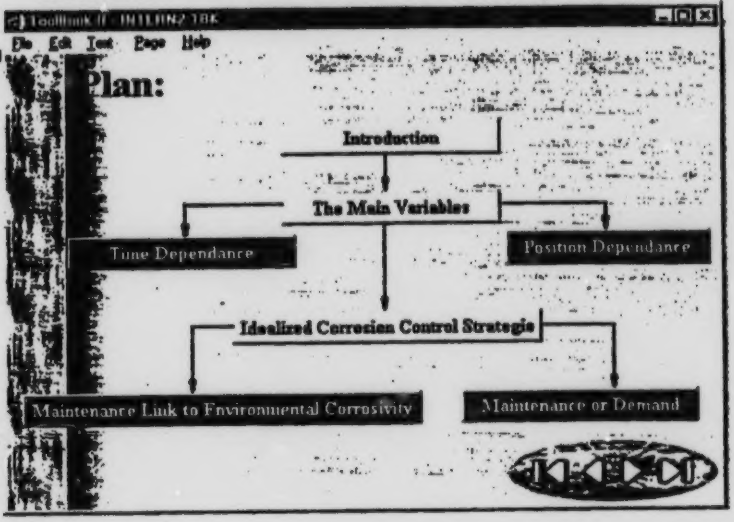
ToolBook II - INTERN2.TBK
File Edit Text Page Help

Plan:

Introduction

The Main Variables

Time Dependance

Position Dependance

Idealized Corrosion Control Strategie

Maintenance Link to Environmental Corrosivity

Maintenance or Demand

Corrosion surveillance: definition

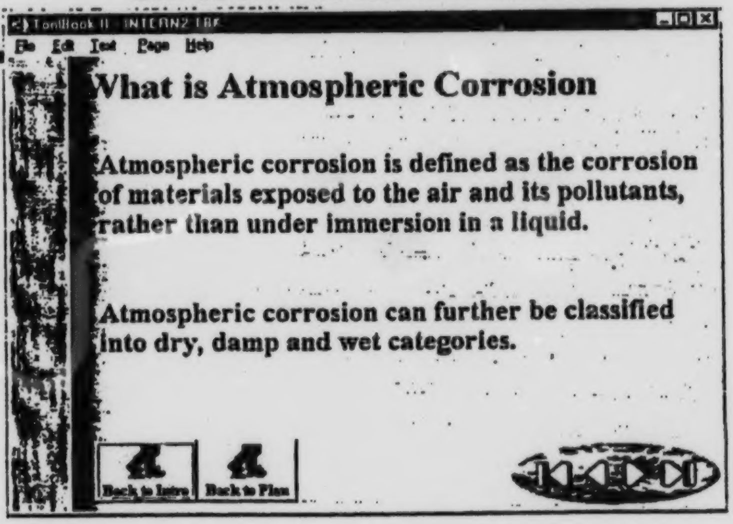
ToolBook II - INTERN2.TBK
File Edit Text Page Help
Back to Intro
Back to Plan

What is Atmospheric Corrosion

Atmospheric corrosion is defined as the corrosion of materials exposed to the air and its pollutants, rather than under immersion in a liquid.

Atmospheric corrosion can further be classified into dry, damp and wet categories.

Visual Studio 97

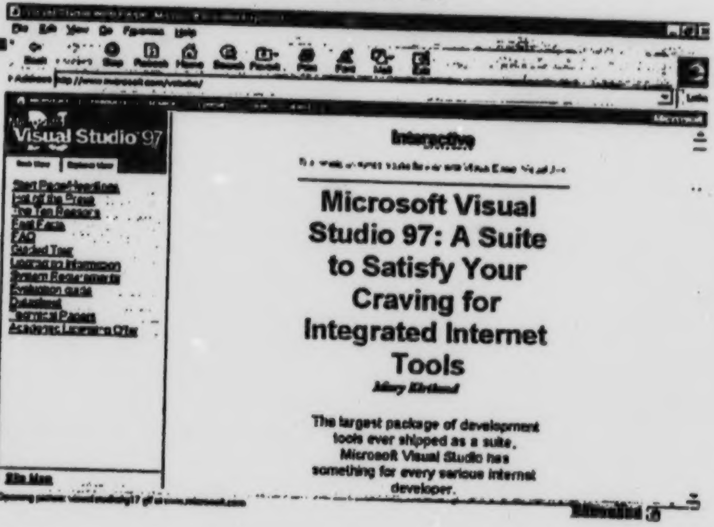
Visual Studio 97
Start Page/Headlines
Hot off the Press
The Ten Reasons
Fast Facts
FAQ
Guided Tour
Licensing Information
System Requirements
Evaluation Guide
Datasheet
Technical Papers
Academic Licensing Offer
Site Map
Interactive

Microsoft Visual Studio 97: A Suite to Satisfy Your Craving for Integrated Internet Tools

Mary Kirtland

The largest package of development tools ever shipped as a suite, Microsoft Visual Studio has something for every serious Internet developer.

ActiveX controls

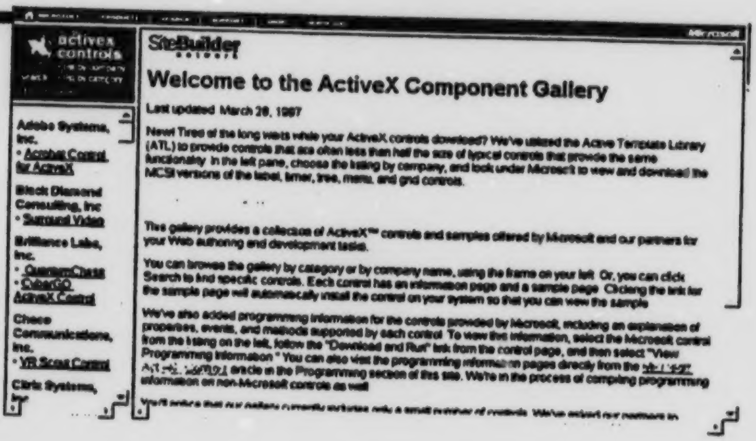
activex controls
SiteBuilder network
Microsoft
Adobe Systems, Inc.
• Acrobat Control for ActiveX
Black Diamond Consulting, Inc
• Surround Video
Brilliance Labs, Inc.
• QuantumChess
• CyberGO ActiveX Control
Chaco Communications, Inc.
• VR Scout Control
Citrix Systems, Inc.

Welcome to the ActiveX Component Gallery

Last updated March 28, 1997

New! Tired of the long waits while your ActiveX controls download? We've utilized the Active Template Library (ATL) to provide controls that are often less than half the size of typical controls that provide the same functionality. In the left pane, choose the listing by company, and look under Microsoft to view and download the MCSI versions of the label, timer, tree, menu, and grid controls.

This gallery provides a collection of ActiveX™ controls and samples offered by Microsoft and our partners for your Web authoring and development tasks.

You can browse the gallery by category or by company name, using the frame on your left. Or, you can click Search to find specific controls. Each control has an information page and a sample page. Clicking the link for the sample page will automatically install the control on your system so that you can view the sample.

We've also added programming information for the controls provided by Microsoft, including an explanation of properties, events, and methods supported by each control. To view this information, select the Microsoft control from the listing on the left, follow the "Download and Run" link from the control page, and then select "View Programming Information." You can also visit the programming information pages directly from the [illegible] article in the Programming section of this site. We're in the process of compiling programming information on non-Microsoft controls as well.

You'll notice that our gallery currently includes only a small number of controls. We've asked our partners to

Atmospheric corrosion: North America

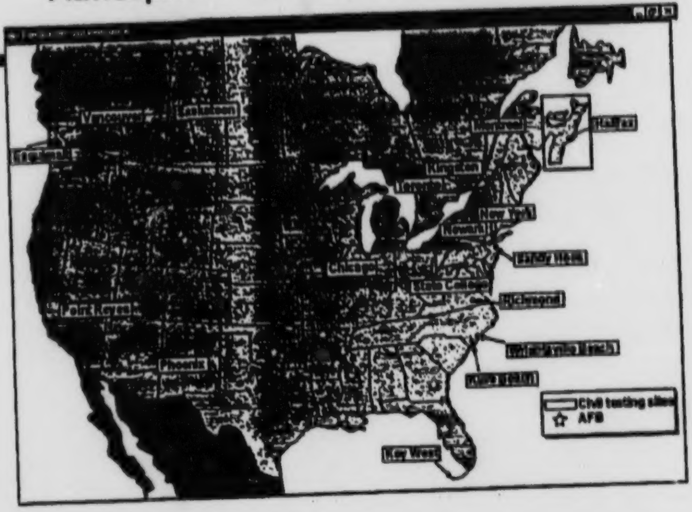
Halifax
Kingston
Toronto
New York
Newark
Sandy Hook
Chicago
Richmond
Wrightsville Beach
Point Reyes
Phoenix
Key West
Civil testing sites
☆ AFB

Corrosion surveillance: CFB Greenwood

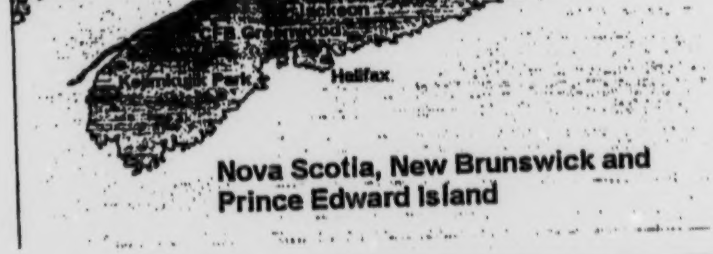
CFB Greenwood
Kejimkujik Park
Halifax
Nova Scotia, New Brunswick and Prince Edward Island

Corrosion surveillance: looking at data

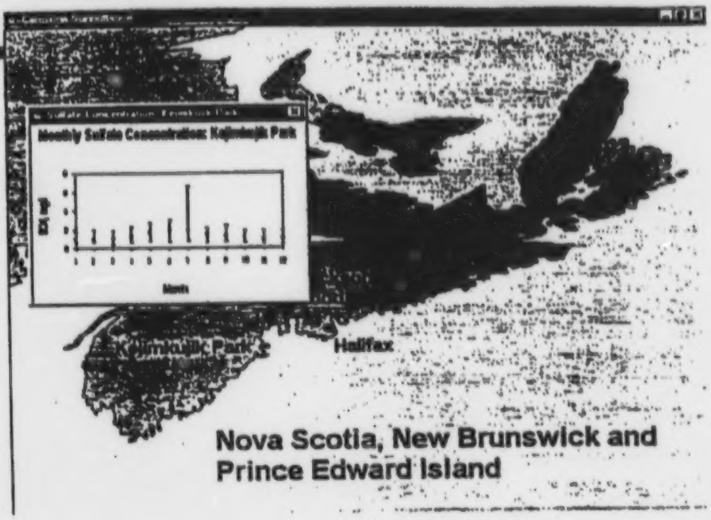
Corrosion Surveillance
Monthly Sulfate Concentration: Kejimkujik Park
Month
1
2
3
4
5
6
7
8
9
10
11
12
Kejimkujik Park
Halifax

Nova Scotia, New Brunswick and Prince Edward Island

Corrosion surveillance: planning field trip

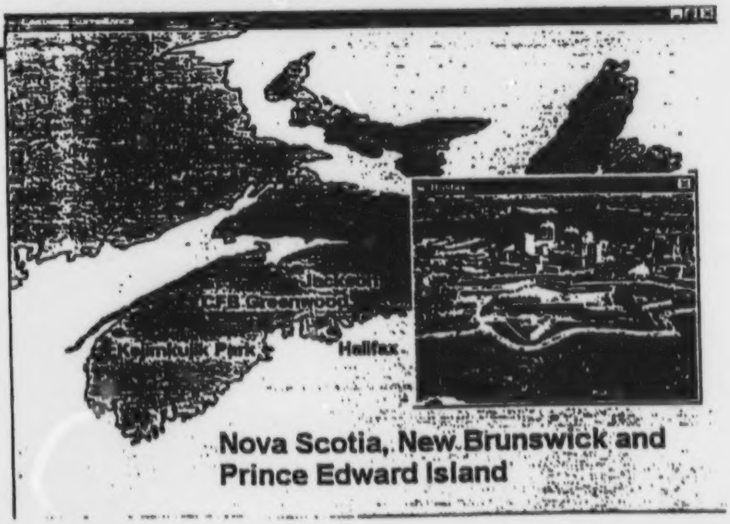
Corrosion Surveillance
Halifax
Jackson
CFB Greenwood
Kejimkujik Park
Halifax

Nova Scotia, New Brunswick and Prince Edward Island

#507232 (24)

Forged copper-nickel-chromium alloy for seawater system components

J C Galsworthy and D Baxter

Structural Materials Centre,
Defence Evaluation and Research Agency,
Farnborough, Hampshire, GU14 0LX, UK

Abstract

The high strength copper nickel chromium alloy, NES824, is a prime choice to replace the current nickel aluminium bronze alloy used in cast seawater system components. Difficulties encountered in casting this alloy has prompted the development of a forging production route for some components. This paper describes the studies undertaken to demonstrate the feasibility of a forging route for this alloy. After initial forging trials to establish forging parameters, two components were fabricated. These components were evaluated for structural integrity. One component was destructively evaluated to determine microstructure and compositional variations; mechanical and corrosion properties; and samples used for welding trials using arc and EB processes. All properties were compared with those typical of the cast version of the alloy. The investigations have demonstrated that the forging of copper nickel chromium components is a viable process. The mechanical properties of the forged material were in all cases at least as high as those of cast material. Tensile properties were significantly better. General corrosion rates of forged and cast material were similar. The forged material was more readily weldable.

Introduction

The nickel aluminium bronze (NAB) castings within the seawater systems of some naval platforms have been found to suffer from selective phase corrosion at both crevices and weld heat affected zones. Such corrosion problems have made it necessary for NAB seawater system castings to be regularly validated to determine their remaining life, resulting in the replacement of a significant number of components.

A number of materials have and are being considered to replace NAB in these seawater systems. One leading contender for these high integrity cast components is an alloy based on IN768, and specified in NES 824 Part 1 [1]. This High Strength Cupronickel alloy (HSCN) is basically a 70/30 cupronickel but contains chromium and silicon to give strengthening by spinodal decomposition. This material is compatible with the cupronickel pipework, is resistant to marine fouling and has mechanical properties broadly similar to NAB

[2]. However, the alloy is prone to linear defects caused by the entrainment of oxide films during casting and due to weld repair restrictions are not always reclaimable.

With NAB not suitable or potentially uneconomic and with NES824 components exhibiting casting defects rendering them unserviceable within the existing specifications, together with potential procurement problems due to foundry closures, an alternative production route was sought. Forging is an alternative production route potentially suitable for the manufacture of valve bodies and other seawater system components. The process can produce components to near finished shape, comparable to the existing cast components, with only finish machining of the flange faces and internal bore necessary. Improved structural integrity is ensured through a more uniform microstructure and the essential absence of orientation effects and compositional variations through the component. This process is widely used for steel components for the offshore industry and in pipelines. Copper alloys are forged to make smaller components in other applications. No work had been conducted on the forging of NES 824 material.

Forging

After initial tests and sub-scale forging trials to determine the characteristics of the material, two forgings were produced from a NES 824 copper nickel chromium as-cast billet. For the purposes of this investigation it was not economic to have dies made for a special naval designed component. Dies for an existing design of valve body which had features similar to current naval components were used. The design had two thick flanges, a tapered body and a central boss.

The fabrication process was conducted in three phases. Initially after a homogenisation and soaking heat treatment, the material from the billet was upset. This was followed by a shaped blocker phase when the larger flange and main body of the component was forged. Forging to the final shape was performed by the piercing of the central bore which forced the remaining material to fill out the full shape and top flange.

The first forging began to show surface cracking after the initial forging stages. The cracked region was removed by machining and processing continued. This component again showed cracks after subsequent forging, particularly in the small flange. These cracking problems were initially assumed to be a result of the material containing the original billet pipe region which could contain a concentration of impurity element from the original casting process. However these cracks are more likely to have been due to too low a forging temperature being used or be associated with the material being in contact with the cold metal dies for too long and the resulting temperature drop in the surface layers of the forging material reducing the metal flow and material ductility. Surface ripples and cracks were to be found where the material was required to flow into abrupt section changes, Figure 1.

The second component was forged with fewer problems leading to a generally acceptable component given the limited process development undertaken. At abrupt section changes the metal surface was still rippled and in some locations cracks had formed. These were found to be shallow and were ground out. Some edge cracks on the small flange were also present, these were machined away to investigate their extent and improve overall appearance, Figure 2.

The forging parameters and processes used in fabricating the two test components were not optimised during this exercise. The problems encountered in surface ripples and cracking would be eliminated with forging parameter and process changes in any final forged components for naval service. The process used proved forging as a possible alternative to produce components in CNC that are currently cast, and was sufficiently developed to produce material in the same metallurgical state that would exist in optimised forged components.

Examination

NDE examination of the forged components by eddy current and ultrasonic techniques found no evidence of internal defects. Metallographic examination of the forging reveals the presence of a relatively fine grained microstructure with mean intercepts varying between 40 and 200 mm depending on the position of the material within the forged component. Previous metallographic examination of cast material, showed that grain size was approximately 2 mm. This would suggest that significant improvements in strength and toughness may result. Grain size was found to vary within the large flange from one position to another. The mean intercept length varied between 130 and 185 mm. This was attributed to local variations in the degree of mechanical work encountered during the forging process. There were no signs of the oxide networks that traditionally cause problems in cast components. Chemical analysis was carried out on each of the two forged components, Table 1. It can be seen that in all cases the composition of the samples were predominantly within the specification.

Mechanical Properties

The tensile properties of the forged material compare favourably with those of the cast material, Figure 3. A 30% improvement in 0.2%PS and a 14% improvement in ductility were found. The tensile properties of the forged alloy therefore far exceed the requirements of the NES824 specification, and offer significant improvements over the cast form of the material.

Higher impact energies than the average value for the cast material were found, Figure 4. The impact energies varied between the different orientations and positions. This was attributed to grain size differences due to different extents of hot working. Specimens taken from the forging body contained the smallest grain size, and exhibited the highest Charpy impact resistance. This inverse correlation between grain size and impact strength is as expected. By controlling the grain size in the material, scope exists for ensuring a significant improvement.

20mm thick compact tension specimens were tested and analysed using multiple specimen and single specimen unloading compliance analyses. Specimens prepared from the forging flange gave consistently higher values of fracture toughness than those prepared from the boss, Figure 5. Both sets of specimens exhibited a significantly higher fracture toughness than those produced from cast material.

Fatigue tests were carried out at a stress ratio of 0.1 at a frequency of 20 Hz. There was no significant difference between orientation and location, nor was there a discernible difference in the fatigue crack propagation rates of the forged and cast materials, all of the data falling predominantly in the same experimental scatter-band, Figure 6.

Low frequency fatigue tests were conducted at a frequency of 0.0083Hz at stress ratios of zero or 0.5 in either laboratory air or natural seawater. The general trend was that fatigue crack growth rates in the forged material were either similar to or marginally slower than cast material when comparative conditions were compared, eg Figures 7&8.

Dynamic tensile tests were conducted using crosshead displacement rates of between 1 mm/s and 3 m/s, Figure 9. The values of proof stress and UTS were similar for forged specimens. The proof stress of the forged material is consistently higher than that of the cast materials, and shows a trend of increasing slightly with increasing strain rate. The UTS of the forged material is higher than that of the cast material. Values of UTS seem to be independent of strain rate.

Corrosion and Erosion Properties

Corrosion tests exposed to fresh, once through seawater flowing at 0.3m/s for nearly one year showed identical general corrosion rates of 0.022mm/year for both forged and cast material. There were similar indications of crevice corrosion on all creviced specimens but of no measurable depth.

In cavitation tunnel tests the average erosion rate of the forged material was 22% less than that of the cast material in the cavitation tunnel tests. In jet cavitation tests a comparison of peak erosion rates showed that the forged material was 9% more erosion resistant than the cast material. Hardness measurements showed that the forged material was approximately 10% harder than the cast and the known correlation between hardness and erosion rate is likely to have accounted for these differences.

Weldability

Hot ductility tests were conducted at elevated temperature between 500-850°C since the cast material has been shown to suffer from problems associated with a ductility trough at temperatures of approximately 700°C. The 0.2% proof stress and UTS progressively decrease with rising test temperature as expected. The specimens from the forged material are also consistently stronger than those from the cast material, Figure 10. Both materials however suffer a marked trough in ductility between 600 and 800°C as shown by the measurements of non-proportional strain to failure. Both forged and cast materials seem to suffer from this type of embrittlement to the same extent.

Welding trials were conducted to compare the weldability of the forged material compared with the cast material. MIG and EB weldments were produced. Metallographic sections of each weldment were prepared and bend specimens were tested in accordance with NES825 [3] and then examined for signs of delamination at the weld-parent metal interface. In all cases except for one, the severe plastic deformation applied to the specimens did not result in any signs of delamination or cracking, Figure 11. Only in one cast material, MIG weld specimens, did any sign of cracking occur.

Discussion

Problems occurred during the forging process with the formation of ripples and cracks on the component surface, especially on the first component. The processing technique and the forging parameters were not optimised in this programme. The forging dies were not specifically made for the CNC material, being originally for a steel component. The problems encountered in the forging of the components used in this investigation are likely to be eliminated by further optimisation. The material and microstructure of the trial components will however be representative of forged copper nickel chromium in any future optimised process.

Grain size was found to have an influence on some of the mechanical properties. Some of the variations in grain size observed can be attributed to the degree of mechanical work encountered during the forging process, together with the different cooling rates of the material within the thick sections of the forged component. No signs of any oxide networks were found in the forged material examined.

During the assessment of mechanical behaviour, all material properties were found to be at least as good as those of the conventionally cast material. Perhaps the most significant advantage of forged material over cast lies in the improvement in tensile properties. A similar improvement is seen in the materials dynamic tensile properties. The fracture toughness of the forged material seems to be sensitive to the local grain size. Fatigue crack growth rates for forged and cast material were found to be comparable for each of the combinations of conditions evaluated. These included high frequency air tests and low frequency tests in laboratory air and natural seawater. The general corrosion behaviour of the two materials was found to be identical. The forged material was found to be slightly more resistant to cavitation erosion. This was associated with the hardness difference.

The hot ductility behaviour of the cast and forged materials were similar, both showing a characteristic ductility trough at around 700°C. The general assumption had been that the smaller grain size of the forged material would increase the amount of available grain boundary for the dispersion of deleterious impurity elements compared with the large grained cast material. However the test results suggest that this effect is not sufficient to cause a change in hot ductility behaviour. In the welding studies conducted in this investigation the forged material appears to be readily weldable, with bend specimens indicating that the welds exhibit very good mechanical performance. Specimens containing both MIG welds and EB welds were crack free after testing.

Conclusions

The forging of Copper Nickel Chromium seawater system type components has been demonstrated as a viable alternative production route, although forging parameters need to be optimised to eliminate problems with surface cracking and to allow more reliable microstructural control. Forged components should be free from deleterious defects. They should have a fine grain size. Their tensile strength should be greater than equivalent cast material. Their fracture toughness, fatigue and dynamic properties should be similar or better than equivalent cast material. Their corrosion behaviour should be similar to cast material. Their weldability should be similar or better than the cast material. It may be possible to optimise the forging parameters and component design to ensure the most favourable microstructural conditions and resulting properties in the final component. Optimisation of process and design variables could ensure a more uniform deformation of the feed stock in the formation of the final component. It will be necessary to ensure that these changes do not adversely effect the material properties and its fitness for purpose.

References

1. NES 824 Part 1, Issue 3, "*Copper nickel chromium sand castings and ingots, Part 1, Production Requirements*", July 1993.
2. Hall B N and Townsend D W. "*Copper nickel chromium casting alloy for Naval applications*", Inter Naval Corrosion Conference, RNEC Manadon, 1988.
3. NES 825 Issue 1, "*Requirements for the Welding of High Strength Chromium Cupronickel Castings*", June 1986.

© British Crown Copyright 1997/DERA
Published with the permission of the Controller
of Her Britannic Majesty's Stationary Office.

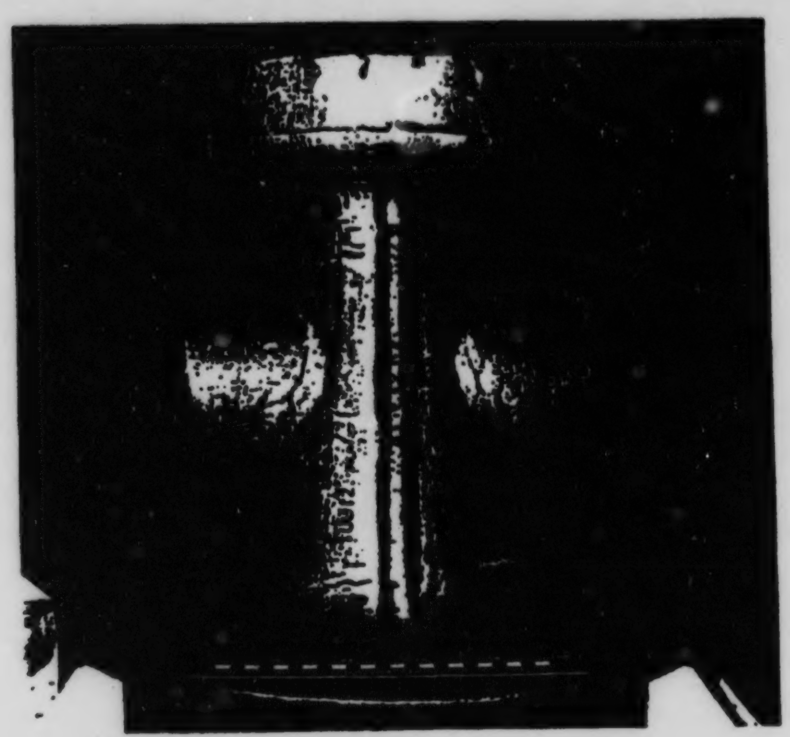

Figure 1. First forged component.

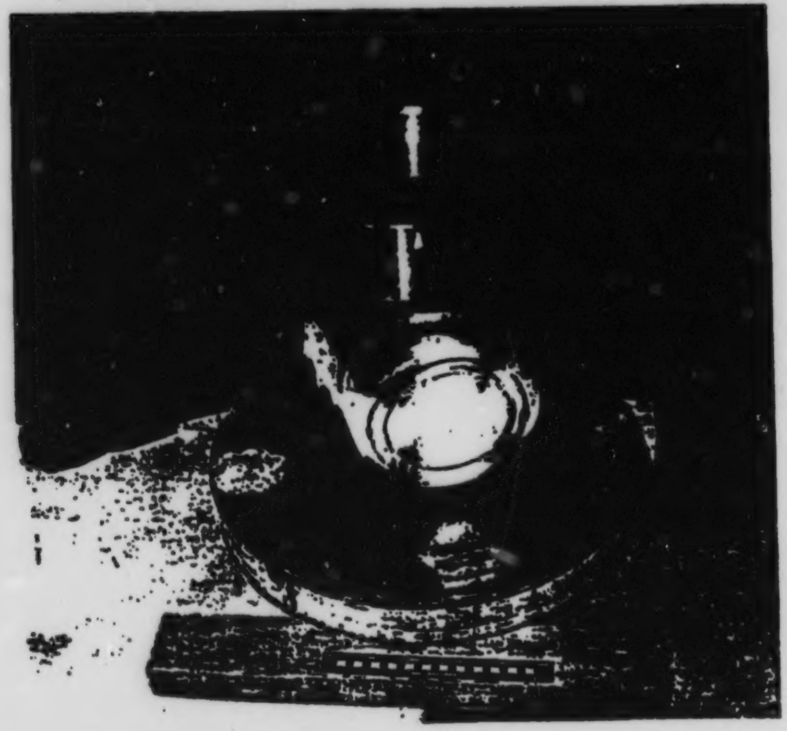

Figure 2. Second forged component.

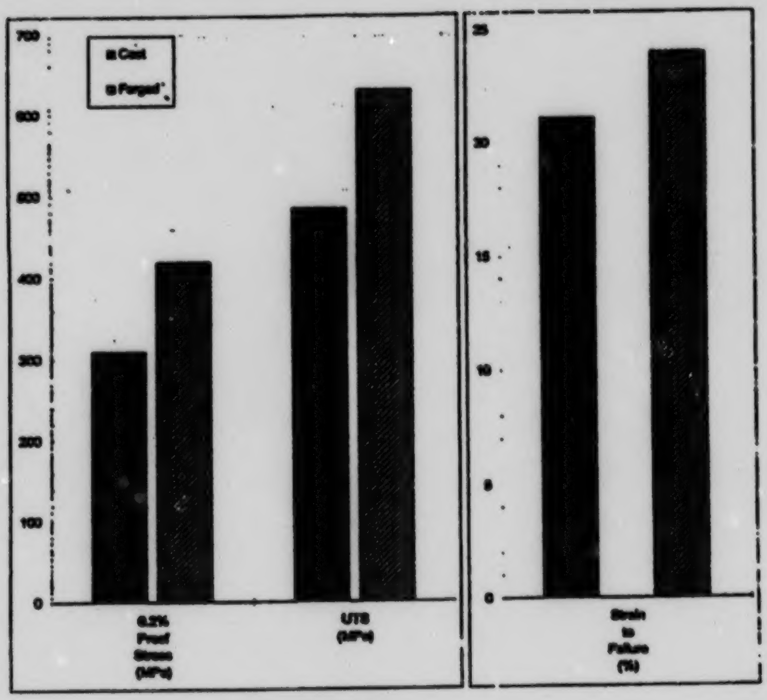

Figure 3. Tensile properties.

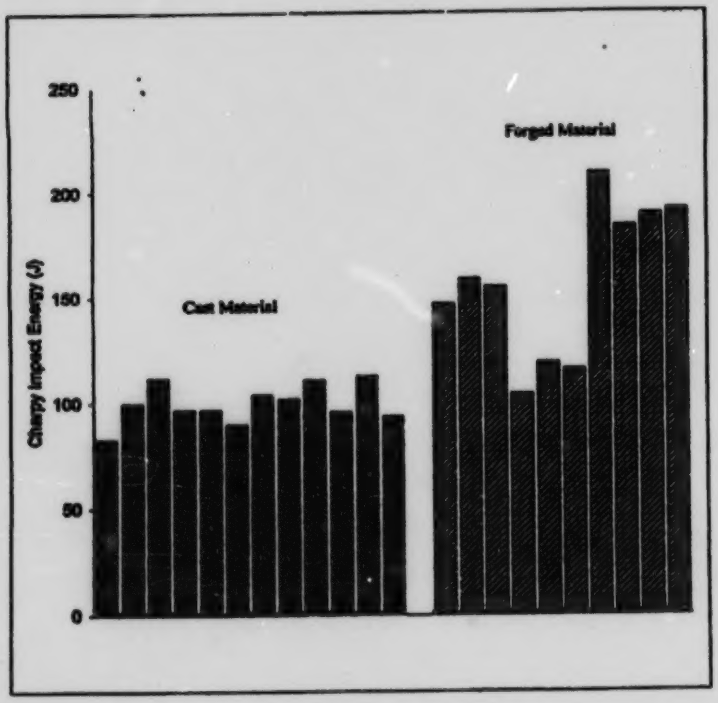

Figure 4. Charpy impact properties.

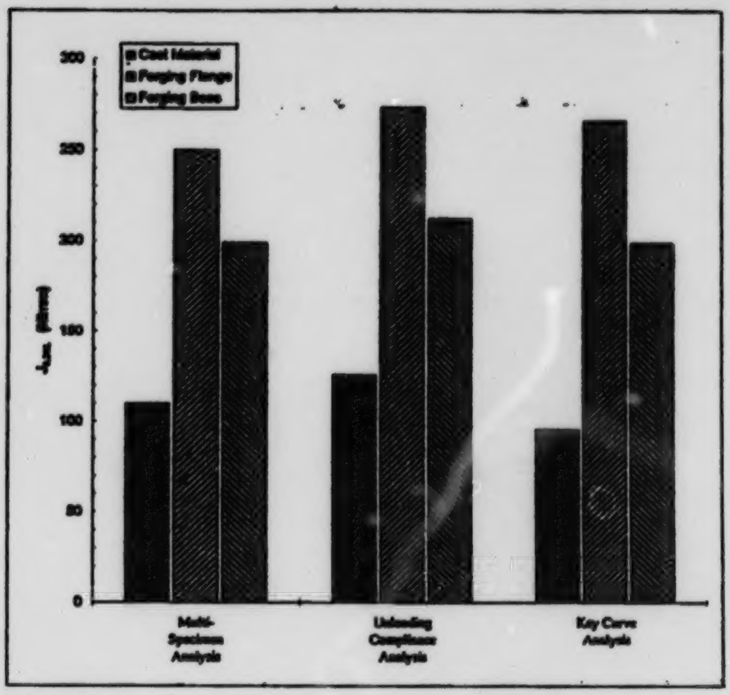

Figure 5. Fracture toughness properties.

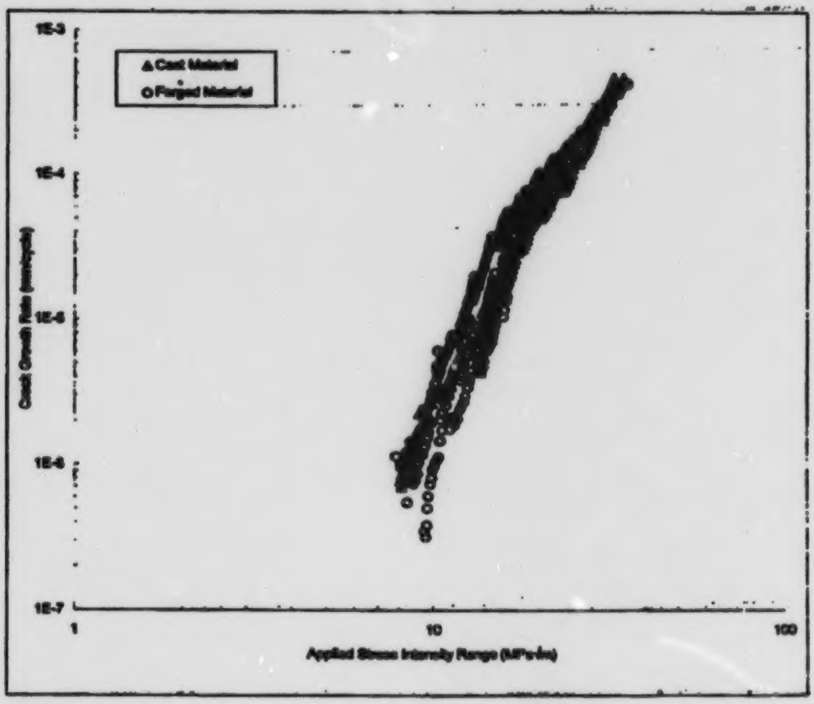

Figure 6. High frequency fatigue (10Hz) in air at R=0.1.

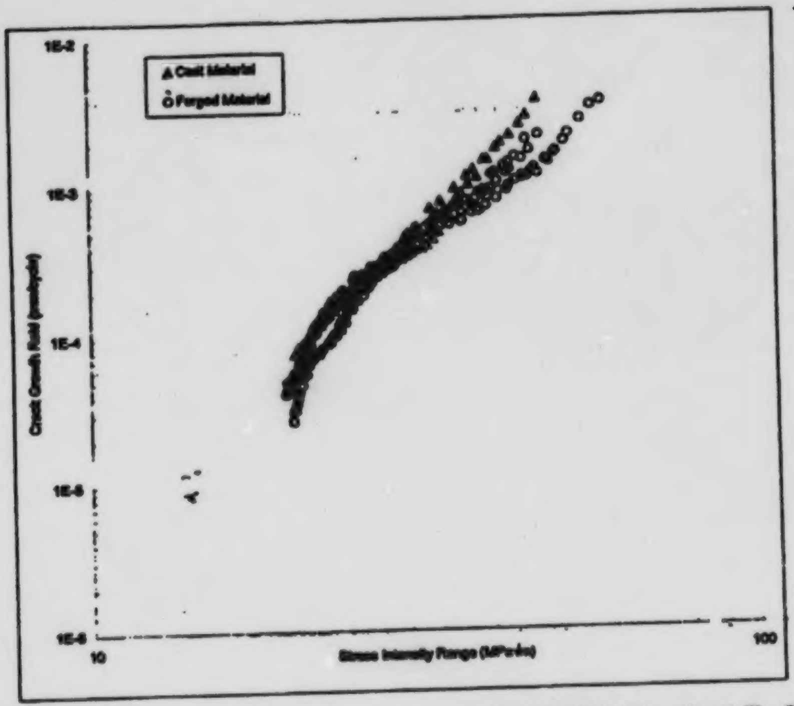

Figure 7. Low frequency fatigue (0.0083Hz) in air at R=0.

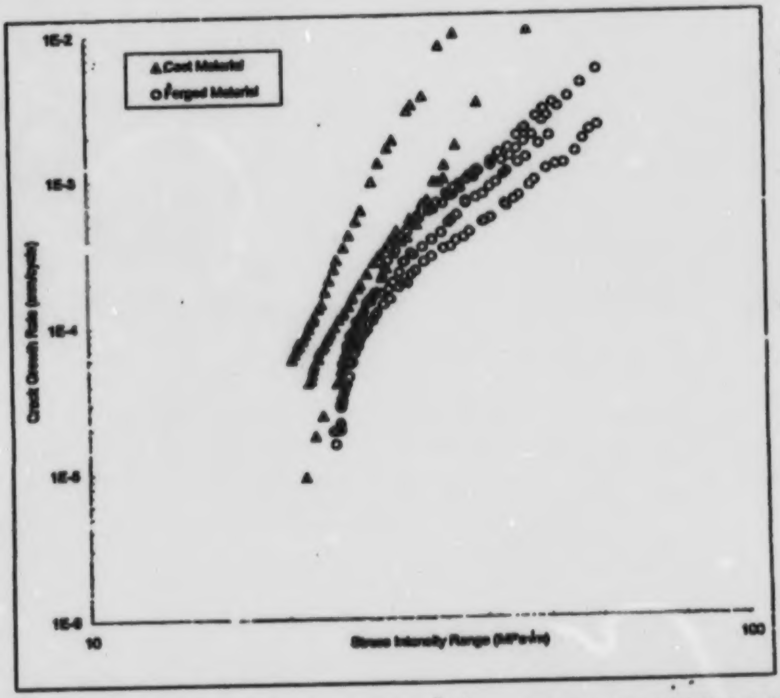

Figure 8. Low frequency corrosion fatigue (0.0083Hz) in seawater at R=0.

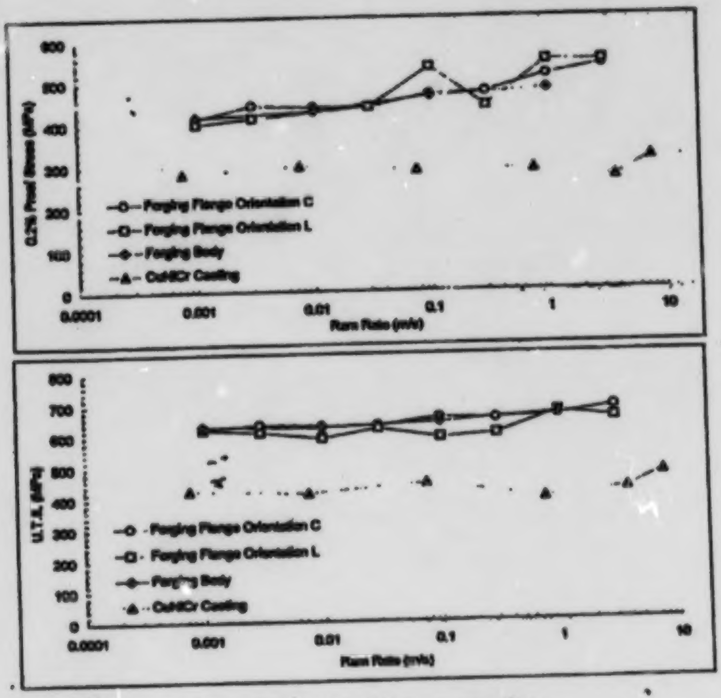

Figure 9. Dynamic tensile properties.

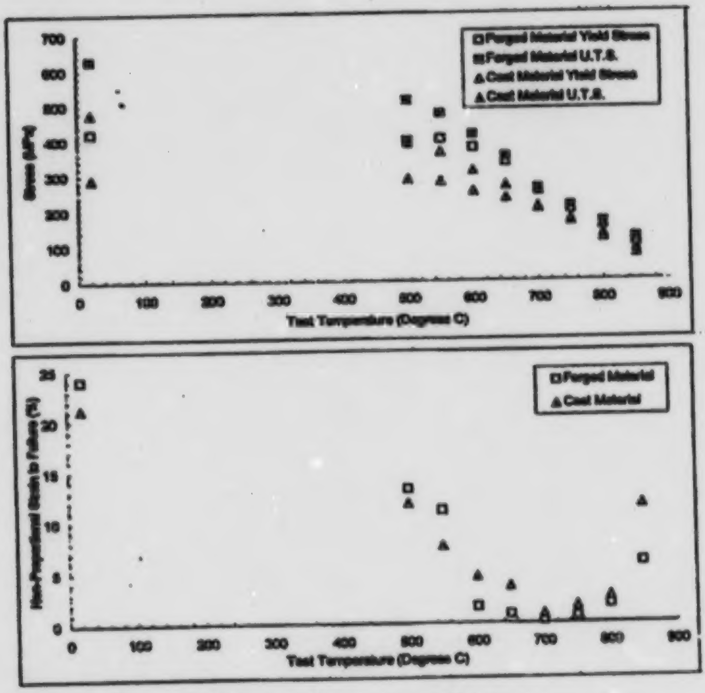

Figure 10. Hot ductility properties.

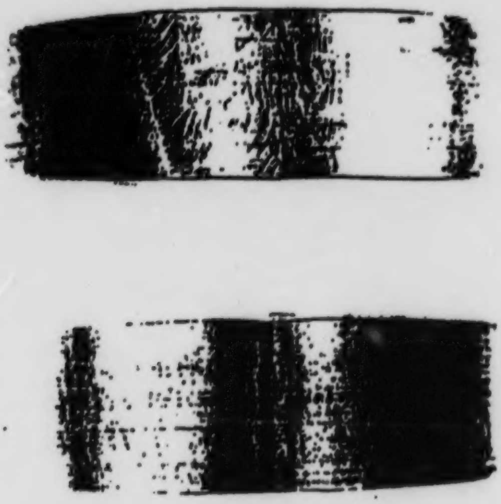

Figure 11. Weld bend tests (a) MIG weld and (b) EB weld.

	TYPICAL CAST	FORGED	NES824[1]
Copper	65.53	66.08 - 67.66	remainder
Nickel	30.75	27.97 - 29.77	29.00 - 32.00
Chromium	1.84	1.66 - 1.81	1.6 - 2.0
Iron	0.59	0.88 - 0.92	0.5 - 1.0
Manganese	0.71	0.74 - 0.78	0.5 - 1.0
Silicon	0.28	0.32 - 0.35	0.2 - 0.4
Zirconium	0.054	0.045 - 0.052	0.05 - 0.15
Titanium	0.099	0.126 - 0.143	0.1 - 0.2
Lead	<0.0005	0.0015 - 0.0022	<0.003
Phosphorus	0.0003	0.0023 - 0.0027	<0.005
Bismuth	<0.0002	<0.0002	<0.001
Sulphur	0.0011	0.0021 - 0.0027	<0.005
Carbon	0.0026	0.0038 - 0.0057	<0.02
Cobalt	<0.005	<0.005	<0.02
Boron	<0.0003	<0.0003	<0.001
Selenium	<0.0002	0.0005 - 0.0006	
Tellurium	<0.0002	<0.0002	
Arsenic	<0.0002	0.0003 - 0.0004	
Zinc	0.0016	0.0068 - 0.0072	

Table 1 - Chemical Analysis of Forged and Cast Components

#507233 ㉚

Development With and Corrosion Performance of Copper Nickel Chrome Castings

by

J BIRD

Directorate of Naval Architecture
Ministry of Defence (Procurement Executive)
Abbeywood, Bristol, ENGLAND, BS12 7DU

Abstract

Nickel Aluminium Bronze NAB has been used over the past thirty years as the material of some naval sea water systems. During that time there has been significant problems relating to selective phase corrosion. This has been particularly true with respect to weld heat affected zones, associated with welding, necessitated by the need to repair casting defects. To overcome these difficulties the use of CuNiCr alloys have been suggested. This route has been pursued in the UK and this paper reports the current position with respect to casting supply. It also records some recent corrosion results which have still to be explained.

Introduction

In some early post second world war vessels the sea water systems were fabricated from gunmetal. This material suffered from corrosion problems and was not really adequate with respect to the 0.2% proof stress requirement. Consequently the various items tended to be heavy and thus the shock resistance was questionable especially the inherent toughness, which was less than ideal. In the 1960's nickel aluminium bronze, which was higher strength and considerably tougher, was introduced into service in order to counteract these problems. Typical composition for currently used NAB is shown in Table 1.

Nickel Aluminium Bronze material although it exhibited a superior 0.2% proof stress and considerably improved toughness to gunmetal was subject to a corrosion problem which came to be described as " selective phase corrosion." (1). The phenomena was encountered in the casting matrix, when it was subjected to prolonged exposure to sea water, but was more severe in the heat affected zones of welds. As the integrity of castings is always suspect, do to porosity resulting from feeding problems, it becomes necessary to weld repair cast items, to a greater or lesser degree, depending on the size and complexity of the product.

In an attempt to ameliorate the selective phase corrosion problem, a heat treatment was developed which greatly improved the corrosion behaviour of weld heat affected zones and was reportedly beneficial for the equivalent matrix corrosion. This procedure, together with the associated restriction for welding on the wetted surface, has enabled the sea water systems to be effectively managed in recent years. However management of the system is tiresome, labour intensive and one is never sure if the described procedure will work in all circumstances. In addition, some weld repaired castings are too large to be effectively heat treated and thus circumstances exist where severe corrosion can be expected to occur. More recently the use of low heat input weld deposits have suggested that selective phase corrosion can be reduced in comparison to high heat input deposits. The beneficial effect has been ascribed to the increased cooling rate in the HAZ and the associated suppression of the development of the corrosive K phase. However in order to ensure this effect is maximised there must be close control of the welding operation which is very costly and consequently nor generally readily applied.

In the most recent past NDE procedures have been developed which will effectively map the area of selective phase corrosion. The principle drawback of the procedure is that the position of the selective phase corrosion must be identified before mapping can take place. As a consequence it has not been possible to develop a surveying technique which will allow items which have been in service to be inspected in situ, and the sea water systems must therefore still be dismantled for revalidation.

With the objective of solving all the aforementioned difficulties and thereby reducing the overall maintenance costs of some naval sea water systems, a high strength copper nickel chrome, CuNiCr, alloy, was proposed to replace the nickel aluminium bronze alloy. This alloy obtained its strength using the chromium addition. The 0.2% proof strength of the alloy, 300MPa, is greater than the 250MPa 0.2% proof strength of NAB and the alloy is also four times as tough.

CuNiCr Alloy Castings

The CuNiCr alloy composition developed for use in Naval sea water systems is given in Table 1. Over the past decade considerable work has been carried out on the castability and weldability of the alloy (2). In addition the necessary NDE procedures have also been developed where gaps in inspection procedures had been identified.

Over the past 12 months the UK copper base foundry industry has been tasked to produce a number of items from the Naval sea water systems in CuNiCr. The items included a small valve body weighing a few pounds through a larger flanged T-piece of some 100-200 pounds in weight to a 1-1.5 ton return end heat exchanger header. These CuNiCr cast items which meet the specified compositional, strength and casting integrity requirements, have now been delivered by two foundries.

The first castings made in the CuNiCr alloy had two drawbacks, the existence of what was described as linear defects and the occurrence of cracking in weld heat affected zones. These cracks associated with the weld fusion line and HAZ were attributed to the impurities in the alloy and the ductility dip associated with CuNi alloys at a temperature of around 600°C.

The linear defects were large entrapped oxides formed as a result of inadequate turbulence during casting. These oxide skins often formed when two independent molten streams interacted without fusion and were originally the surface oxide formed on cool abutting streams, the lack of turbulence and low temperature being insufficient to break up the surface oxide on the streams at the time of interaction. The oxide films were originally very difficult to identify but with the development of a number of eddy current techniques it is now possible to reliably identify such defects down to a depth of 10mm. All the castings delivered were examined and shown to be free from the so called linear defects. It should be noted that these defects also occur in nickel aluminium bronze but they are not regarded as a problem and not inspected for.

The weldability of the CuNiCr alloy was originally thought to be questionable due to the observed impurity levels. Recently alloys with relatively high impurity levels compared with the alloy which was eventually found to be weldable have also been successfully welded. This was the result of modifications to the welding procedure. The actual modification involved amending the weld preparation to give a shallower angle. In addition a procedure has been used which effectively butters the preparation with fine low heat input weld beads before depositing the fill passes at a much higher heat input. Using the procedure modification singularly or in combination has developed confidence that material manufactured to the current CuNiCr specification can be welded. The new weld procedures have enabled the original severe control of impurities to be relaxed without detrimentally affecting the material weldability.

Corrosion Behaviour

A demonstration of the corrosion behaviour of CuNiCr material is probably the most important aspect of the acceptability of the alloy as a replacement for nickel aluminium bronze. Its general corrosion susceptibility should be as good as NAB and it must not suffer from corrosion by any alloy specific mechanism. In addition welding should not increase its corrosion susceptibly in the HAZ to any significant degree.

Confidence in the corrosion behaviour of CuNiCr has been gained recently from the examination of two CuNiCr valve bodies removed from a sea water system after 10 years service. The valve bodies show minimal uniform corrosion in the bores and no evidence of crevice corrosion on the flanges. This includes both a flat faced flange and a flange providing sealing via an O ring groove. Although not considered at the time, it would probably have been possible to reuse the valve bodies using replacements for the internal mechanism. Most importantly there was no evidence of selective phase corrosion as would be expected from the use of this alloy. The items are now used to improve confidence in the alloy by illustrating the superb corrosion performance of the alloy.

In order to confirm the general corrosion behaviour of CuNiCr and to develop confidence in the use of welded items made from the alloy a welded silencer tube was tested in sea water flowing at 1.5m/sec. The welded test item/silencer is shown schematically in Figure 1. The four welds in the test section include two circumferential GMA and one EB weld and one EB weld joining the flange to the tube section. The EB welds are autogenous and the GMA welds were made using a GMA consumable with the composition shown in Table 1. The consumable contains a lower level of iron than the main component. It is usually accepted that CuNi alloys used in flowing sea water systems should contain some 0.7 % Fe in order to prevent inpingement attack.

The test section was subjected to laminar flow for 10,000hrs and turbulent flow for 5,000hrs at a flow rate of 1.5m/sec. When the test section was finally removed from the flow rig after 15,000hrs it was found that there was minimal general corrosion. In addition although the position of the welds was plainly obvious as a depression on the internal bore of the tube, the depression still showed the grinding marks from the time after welding when the weld was flushed. This clearly indicated that the welds had not corroded during testing, thereby creating significant confidence in CuNiCr corrosion performance and weld corrosion performance.

Further tests have been carried out using a conical CuNiCr header, on the exhaust side of a Titanium heat exchanger, which was being tested on a flow rig. The Titanium tube plate of the header was coated with a plastic. The header contained two small weld repaired areas deposited using the same CuNiCr consumable used in the silencer trial. In addition to the weld repaired areas a number of steel plugs were let into the header wall and flushed off. The steel plugs were used to determine the extent to which a galvanic cell would be set up under these conditions.

After 15000hrs under test the system was disassembled and the internal surface of the conical header examined for evidence of corrosion. The main internal surface of the header showed no evidence of general corrosion. The weld areas were covered in a blue deposit. When the deposit was removed the weld surface was seen to have been uniformly corrode to depth of about 1mm. The blue deposit was also present over the area around the steel inserts. The area immediately around the steel inserts was seen to be corroded preferentially to the iron insert, to a depth of 1mm and for about 2mm away from and around the circumference of the insert.

Discussion

The successful production of a number of small items and a return end SW/FW heat exchanger header, at two copper base alloy foundries, has demonstrated that CuNiCr material can be reliably manufactured. The material delivered meets all the required mechanical properties, is chemically compliant and the castings are free from the non metallic defects occasionally seen with the material.

The corrosion tests carried out on the welded silencer clearly indicate that both the weld metal used and the material of the casting are not prone to corrosion under turbulent flow conditions and at the flow velocities used in service. Although the weld metal used in the GMA welds was very low in iron, this has not resulted in any inpingement attack, even though it is generally recognised that CuNi requires some 0.7%Fe to be immune from this type of attack.

There are a number of reasons for the performance seen, one of which is that the welds are small and consequently, because of the of the cooling rate, the deposit is harder than would be normally expected. Secondly, because the alloy contains some 1% Cr, the chromium may be acting as an iron equivalent, thus preventing impingement attack.

The performance of the welded conical header is more difficult to understand. Unfortunately, the blue deposit was removed to examine the weld, before samples of the deposit could be taken for analysis, and thus the material has not been identified to date. However the deposit would be expected to be a copper compound, possible a hydrated chloride or oxychloride. No reason for the increased corrosion susceptibility of the weld deposit has been suggested. The corrosion potential of the cast alloy and the weld metal in sea water should not be significantly different, as the compositions are very similar. Similarly the presence of the Titanium tube plate and tubes should also not directly affect the corrosion performance, as the tube plate has been coated with an inert plastic material. However metallurgically, the casting and the weld deposit will be very dissimilar. The fact that there is preferential attack on the CuNiCr alloy around the circumference of the steel inserts is also puzzling, as it would indicate that the CuNiCr is anodic to the iron, which is at variance with the position of ferritic iron copper base alloys in the electrochemical series.

Conclusions

Castings in CuNiCr can be made successfully, including ones of 1-1.5tons, for use as heat exchanger headers

EB and GMA welds, in a silencer tube, have shown excellent corrosion performance when subjected to turbulent flow at 1.5m/sec for 5,000hrs. This performance was predated by 10,000hrs in laminar flow at the same flow rate.

It is necessary to determine the cause of the unusual behaviour of the alloy, when used as a conical heat exchanger header, in order to develop the necessary confidence to put the alloy into service. The blue deposit, observed on the GMA welds, has not been identified and the apparent anodic behaviour of the CuNiCr, adjacent to the iron inserts, needs investigation.

It is now necessary to repeat the testing with iron containing and low iron weld deposits using both test rigs in order effectively investigate the observed phenomena.

References

1. Rowlands J C. Studies on the Preferential Phase Corrosion of Cast Aluminium Bronze in Sea Water. 8th International Congress on Metallic Corrosion. Mainz. 6th-11th September 1981.

2. Hall B N and Townsend W D. Further Experience with Cast CuNiCr (NES 824). 9th International Corrosion Conference. U.S. Naval Post Graduate School, Monterey, California. 6th-10th April 1992.

© British Crown Copyright 1997/MOD

Published with the permission of the controller of Her
Britannic Majesty's Stationery Office

Material Analysis
Castings

Element	Nickel Aluminium Bronze	Copper Nickel Chrome	CuNiCr Welding Consumable
Alloy			
Nickel	4.5-5.5	29.00-32.00	29.00-32.00
Aluminium	8.8-9.5		
Iron	4.0-5.0	0.5-1.0	
Manganese	0.75-1.3	0.5-1.0	1.4-2.0
Chromium		1.6-2.0	2.0-2.4
Silicon		0.20-0.40	0.20-0.40
Zirconium		0.05-0.15	0.05-0.15
Titanium		0.03-0.15	0.1-0.2
Copper	Remainder	Remainder	Remainder
Impurities			
Iron			<0.05
Zinc	<0.05		<0.0020
Lead	<0.01	<0.005	<0.0015
Tin	<0.05		
Silicon	<0.10		
Magnesium	<0.05		
Chromium	<0.01		
Phosphorus		<0.005	<0.005
Bismuth		<0.001	<0.0005
Sulphur		<0.001	<0.003
Carbon		<0.020	<0.006
Cobalt		<0.050	<0.020
Boron		<0.001	<0.001
Selenium			<0.0005
Tellurium			<0.0005
Arsenic			<0.0010

TABLE 1.

Schematic of CuNiCr Silencer Test Piece

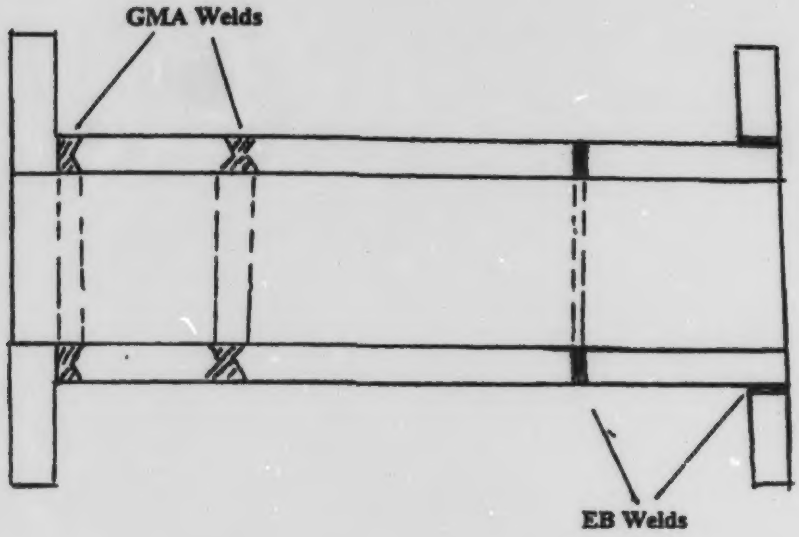
GMA Welds
EB Welds

Figure 1.

]

#507234 (31)

Self Reliance By Commercialisation - A Revolution In Naval Engineering Management

by

P C Conor
Defence Operational Technology Support Establishment
Auckland Naval Base
New Zealand

SUMMARY

The New Zealand Defence Force has been faced by a requirement to reduce operating costs and improve efficiency. A changing operational environment has also led to a need for the Royal New Zealand navy to improve its self reliance. Commercial management methods and commercial technology have been adopted to enhance the technical capability of the RNZN and minimise operating costs.

INTRODUCTION

With a fleet strength of 4 frigates and 3 major auxiliary vessels, the Royal New Zealand Navy is one of the smaller navies of the western alliance. At present the personnel strength of the RNZN is approximately 2,000 officers and men, supplemented by a civilian workforce of about 560. This small force, like allied navies, has been required to downsize in recent years as politicians and the public have sought a peace dividend. The RNZN, again like allied naval forces, has been forced to introduce commercial management to achieve optimum use of resources. However, in the case of the RNZN the drive to reduce costs and improve efficiency has coincided with a period in which the Navy has also had to develop a high degree of self reliance. Engineering elements of the RNZN have led several sectors of the commercialisation process and have been strongly affected by others. This paper outlines the changes and their effect on RNZN maintenance engineering support.

DEFENCE POLICY

At present there is widespread acknowledgment that there is no direct territorial threat to New Zealand (1). The primary concern of the NZDF is therefore seen to be the need to defend New Zealand's wider interests. Current Defence Policy is based on the precept of self-reliance in partnership. Defence is provided with the resources needed to achieve a credible minimum capability. Minimum arises from the need for the Force to be fiscally sustainable, while credibility is to be achieved by reassuring New Zealand's neighbours and allies that the Government has the resolve and capability to meet the aims defined by successive Governments.

PUBLIC SECTOR REFORMS

A series of economic crises in the late 1970's and early 1980's, forced New Zealand to embark on a series of major reforms of the public sector. The primary aim of these changes was to reduce foreign debt but they included major alteration to the structure and operation of the public service. Reform has been based on five key principles:

1. Policy and advisory roles must be separated from administration and operation.
2. Departmental objectives are to be clearly stated to define roles and objectives.
3. Accountability is to be maintained.
4. There should be competitive neutrality. As much of supply as possible should be placed on a commercial basis.
5. Managers should be allowed to manage.

A major review of defence resource management in 1987 paved the way to the restructuring of the Defence Department (2). Reform actions started shortly afterwards: Defence was split into two, policy and advisory roles were taken over by the Ministry of Defence while military operations were placed in the hands of the New Zealand Defence Force (NZDF). Defence outputs have now been defined in terms of quasi-commercial deliverables and the Chief of Defence Force is accountable for meeting these requirements (3). A number of areas of defence activity have been fully commercialised - for example in 1994, management of the naval Dockyard facility was handed over to a consortium of New Zealand and overseas companies.

EVOLUTION OF NAVAL ENGINEERING CAPABILITIES

In the period from WWII to 1984, New Zealand naval operations were tightly intermeshed with those of the US, UK and Australia. Wartime links with the USN were cemented in 1952 when the ANZUS military alliance was signed. This connection provided the core of the strategy which defined the subsequent development of the RNZN's primary capabilities. In the late 1950's the RNZN began the move away from the quantitative capacity offered by a fleet consisting of 3 cruisers and 6 frigates. Instead, the Navy sought improved quality provided by a smaller force consisting of 4 frigates optimised for anti-submarine warfare (4). Two modified Rothesay Class frigates were delivered from the UK in 1960/61 and by 1971 the flotilla had been completed with the addition of two Leander Class frigates. The role of the force was primarily to provide convoy and battle group protection although naval gunnery capabilities were also maintained. Frequent exercises with the US and other navies maintained the skills required to operate in multinational naval operations

These operational connections to the US contrasted to the RNZN's technical background. From its birth until the mid-1970's, the engineering branches of the RNZN effectively operated as remote sectors of the Royal Navy engineering organisation. Most ships and the majority of their equipment were acquired from the UK although Australia provided some products. Maintenance consumables such as paint and lubricants also came from UK sources. Refits and routine engineering activities were carried out in the Devonport (Auckland) Dockyard which was operated on the lines of a UK Naval Dockyard.

Local technical decisions were made by engineering personnel trained in the UK and when unexpected structural or propulsion problems occurred, advice was sought from Admiralty specialists located at Bath or elsewhere in the UK. The communication systems of the time meant that this approach was slow and difficult and moves were made to increase local levels of self reliance. Specifications for the pair of Rothesay Class frigates were different from similar ships in RN service. The break with RN standards represented the first steps towards greater technical independence. Increased engineering self sufficiency was also driven by the need for a sharp increase in local engineering support. Moves were made to develop New Zealand solutions to hull corrosion and component replacement problems. At the suggestion of the RN, a materials function was added to the Naval Research Laboratory. Hull corrosion problems led to the use solid state electronics in a locally designed impressed current cathodic protection system. This development led in turn to trials with coal tar epoxies and other high performance anti-corrosion coatings to make best use of ICCP. Parallel development of manufacturing methods for critical spare components led to significant investment in the Dockyard foundry. The facility was upgraded to enable it to produce high quality corrosion resistant castings and steam system components at short notice.

The four frigates provided the basis for a well established refit cycle driven by requirements for planned preventative maintenance. At any given time, one of the ships was in major refit, two were operational and the fourth was either in post-refit workup or in a maintenance period. After initial teething problems the fleet settled into a routine of reliable operations. Regular refit and repair activity provided a steady flow of work for the Dockyard. However, the cost of maintaining the Rothesay frigates started to rise rapidly as they neared the end of their design life. Various options for ship refurbishment or replacement were explored including removal of the steam turbine plant from one of the ships and its replacement with a gas turbine system. Concerns about the cost and risk of the latter initiative led to it being abandoned when the Royal Navy agreed to transfer two RN Leanders to the RNZN. One of these ships, an IKARA Class vessel, was refitted in the UK. Its arrival served to introduce the RNZN to the demands of operational software maintenance. The second RN Leander was given an extensive modernisation in the Auckland Dockyard.

At about this time, New Zealand entered the phase which culminated in its effective detachment from the ANZUS alliance. Operational contacts with the USN ceased. Links with the RN also began to run down, the process being accelerated by the UK economic reforms which led to the imposition of full market charges for naval personnel training at UK establishments. The trans-Tasman working relationship was strengthened and moves were made to develop closer defence relations (CDR) between New Zealand and Australia. CDR not only encouraged stronger operational links but also emphasized cooperative equipment acquisition. Despite some public opposition, the New Zealand government made the decision to join the ANZAC ship construction program with Australia.

DOCKYARD COMMERCIALISATION

Leander Class frigates were designed for cold war operations: they are optimised for performance but in economic terms are not particularly efficient. Their steam turbine propulsion system requires frequent maintenance to ensure reliability in service. Their hulls are reasonably damage tolerant but their use of evaporators for fresh water production, together with wet bilges, makes for considerable internal corrosion problems in service. RNZN Leanders have not been plagued by the structural defects experienced by their sister ships in the North Atlantic but they have still been expensive to operate, requiring a substantial support organisation. As indicated earlier, the Dockyard had to be progressively expanded as the aging fleet required more and more refit effort.

The RNZN decision to acquire ANZAC frigates signaled an impending crisis for the Dockyard. Replacement of the maintenance-intensive Leanders by ANZAC ships, fitted with commercially-supported diesel and gas turbine engines, palletised systems and digital electronics, was predicted to dramatically reduce the requirement for refit work. Despite the predicted reduced workload the Dockyard would still have to be maintained to provide the necessary engineering support. Initial attempts were made to run the facility on a commercial basis and to attract non-defence work. A number of workplace reforms were undertaken, for example the number of labour unions was reduced from thirteen to two and there was an initial reduction in personnel numbers.

Some commercial work was obtained but a number of factors prevented the early commercial operation from being truly successful. Chief among these were restrictions preventing public sector organizations from borrowing money or making commitments exposing the Crown to financial risk. As a result, the decision was made to hand over the Dockyard to a commercial manager for an initial period of 10 years. The management change took place on August 1, 1994 (5).

The various stages of the commercialisation process have not been without pain. From a peak workforce of over 1020 in 1989, personnel numbers had declined to 780 in 1994 and to 450 in 1997. Specialised industrial facilities such as the dockyard foundry have been closed down and under-utilised plant has been sold off.

Commercial changes have also affected the RNZN itself. The days of the easygoing relationship between the Navy and the Dockyard have gone. A new organisation, the RNZN Fleet Repair Group, has been set up as the project management interface between the navy and the Dockyard. Tasks are now carried out as defined and costed projects and their completion is expected on time and on budget.

Commercial discipline has worked both ways, Dockyard and Naval personnel have both become more focused on financial issues and more conscious about the need for tighter project management and unambiguous task descriptions. As Dockyard staff numbers have shrunk, external contractors have been used increasingly for a wide range of tasks. Naval engineers have become used to the idea of having lawyers routinely involved in contract negotiation and dispute resolution. Greater attention to quality matters has led to widespread adoption of ISO 9000 procedures.

Commercial processes and materials are being used increasingly in place of defence specification products. In many cases major cost savings have proved to be available from use of commercial off the shelf (COTS) technology. For example in the late 1980's when the RNZN acquired a fleet tanker, the vessel was built by a Korean shipyard instead of an accepted naval shipbuilder. The design of the tanker was based on a line of standard commercial vessels modified to meet specific RNZN requirements. The ship cost was substantially less than for an equivalent defence-specification vessel but HMNZS ENDEAVOUR quickly proved to be a critical element of the RNZN fleet.

Paint and coatings provide a more recent case of the use of COTS technology. RNZN engineering materiel authorities have realized that traditional methods of maintaining the paint on its ships are no longer sustainable. Manning levels on ANZAC ships and the auxiliary vessels do not provide the excess personnel resource needed for frequent painting and related maintenance work. Modern surface coating systems are needed to reduce the maintenance burden. Acquisition of military specification paint is not a viable option for an organization as small as the RNZN and the only alternative is for the Navy to use a commercial approach. Paint will be purchased only from companies prepared to stand by their product. The coating will be required to meet a performance requirement rather than a detailed technical specification. Suppliers will be expected to monitor the paint application process to ensure that the coating is applied correctly. Manufacturers will be held accountable if their products fail to meet agreed performance standards.

INDUSTRIAL INVOLVEMENT

In the meantime, New Zealand industry has been heavily involved in the ANZAC ship construction program. Unlike other Western countries, New Zealand has had a very small defence manufacturing base and when NZ involvement in the project was initially considered there was some concern about the ability of local industry to participate effectively in the construction of a modern warship. To their own surprise, a number of manufacturers found that they were fully competitive and once they understood the complexities of the performance certification process, they were able to produce a considerable range of products for the project. At present New Zealand industry has attracted orders worth more than $500 million out of an expected $800 million share of the total value of the ANZAC ship program.

An important benefit of this involvement is that industry can take a more active part in the maintenance of warship systems than in the past. For example, air conditioning systems on the ANZAC ship are fully containerized. The units can therefore removed from the ship and sent to a contractor for overhaul. The Dockyard will not have to maintain a large and expensive air-conditioning refit unit.

The Dockyard is therefore developing two separate sectors. The first concentrates on ship overhaul and repair and treats RNZN ships as just another hull in the mix of military and civilian vessels passing through the drydock. The second, military sector, is concerned with the maintenance of core weapon systems which require specialist knowledge for repair and overhaul.

TECHNOLOGY SUPPORT AND DEVELOPMENT

RNZN requirements for technical support have changed as commercialisation has evolved. Many technical solutions are now obtained from local suppliers of commercial products and services. The technology is often state of the art and highly effective. Its availability represents a key element of RNZN technical self reliance. However, RNZN maintenance engineers sometimes face major difficulties in selecting an appropriate and effective solution from the huge range of available product options. Design requirements represented by military specifications therefore have to be translated into commercial terms and the performance of products on offer has to be assessed against the need.

Additional technical support is also needed when a commercial product fails to meet capabilities claimed for the product. In the naval environment failures have often occurred because the naval application was more demanding than equivalent civilian applications. For example, major paint companies have become well aware that naval vessels spend more time alongside and that standard commercial antifouling coatings can become inactive under these semi-static flow conditions. Specialised products are required to provide the required antifouling properties. Other suppliers may not know about the problem and may offer the cheaper antifouling coatings which are likely fail in service on a naval ship. In order to avoid deficiencies in operational readiness, the procedure used to acquire critical products such as antifouling paint must therefore be set up to avoid purchasing materiel likely to cause problems in service.

In other situations, commercially supplied products may simply be substandard and litigation may be necessary to obtain appropriate remedies. The legal case can often involve a significant technical component and it is important that the technical argument is adequately prepared, based on high quality information and presented by individuals with appropriate qualifications and experience.

The drive to reduce operating costs has also placed more emphasis on condition-based maintenance rather than on preventative maintenance. Far more attention is consequently being paid to systems monitoring. The RNZN is in the process of developing an in-depth capability for machinery condition assessment using vibration and oil analysis methods. The expected life of the RNZN's ANZAC ships is likely to be over 30 years and since these vessels do not have a structural margin for corrosion, it is important that corrosion and fatigue monitoring programs should also be developed to avoid the requirements for expensive structural repairs.

CONCLUSIONS

Incremental and individually moderate reforms implemented over a number of years have collectively led to a revolution in the way the RNZN operates. From an organization which was formerly highly dependent on overseas support, the Navy has become much more self reliant and increasingly capable of independent operation. The process of change has been associated with the introduction of levels of commercialisation which would have been difficult to imagine a few years ago.

The change process may not be over. Downward pressure on the Defence Budget remains intense and the drive to achieve further efficiencies is as strong as ever.

REFERENCES

1. The Defence of New Zealand 1991. New Zealand Government Printer. Wellington, 1991.
2. Quigley, D.F., New Zealand Defence Resource Management Review. Strategos Consulting Ltd. Wellington, 1987.
3. New Zealand Defence Force Annual Report for the Year Ended 30 June 1996. HQNZDF. Wellington, 1996.
4. McDougal, R. J., 'New Zealand Naval Vessels'. NZ Government Printer. Wellington, 1989.
5. Wong, G., 'The Dollar Driven Dockyard', New Zealand Defence Quarterly, Spring, 1994.

#507235 (32)

US Navy Corrosion Presentation

by

Paul Holsberg
Naval Surface Warfare Center

CURRENT CORROSION PROGRAMS
METALS DEPARTMENT
CARDEROCK DIVISION, NSWC

INTERNAVAL CORROSION CONFERENCE
HALIFAX, NS
23 April 1997

Paul W Holsberg
Head, Metals Department
301-227-4401

Carderock Div, Naval Surface Warfare Center
Corrosion Branch - Code 613

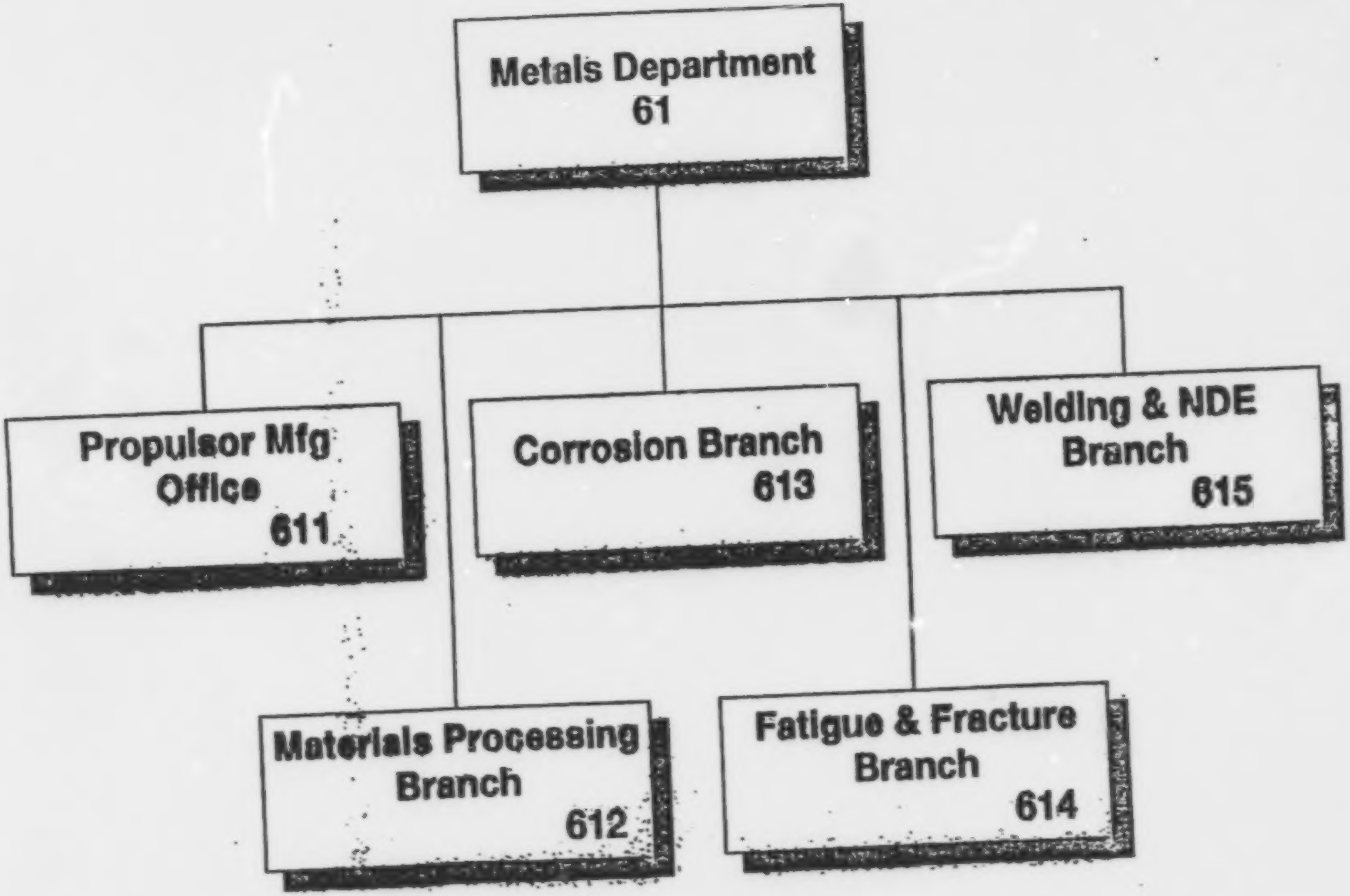

Metals Department
61

Propulsor Mfg
Office
611

Corrosion Branch
613

Welding & NDE
Branch
615

Materials Processing
Branch
612

Fatigue & Fracture
Branch
614

Facilities

- **Electrochemical Test Laboratory - DC and AC Equipment**

- **Stress-Corrosion Cracking Test Laboratory**
  - **Slow Strain Rate Test Equipment - Four Units**

- **Seawater and Marine Atmospheric Corrosion Test Sites**
  - **LaQue Center for Corrosion Technology - Wrightsville Beach, N.C.**
  - **CDNSWC Fort Lauderdale, FLA (Code 683)**
  - **NRL Key West, FLA**

- **High Temperature Corrosion Laboratory**
  - **Low Velocity Burner Rigs (LVBR) - Four Units**
  - **High Velocity Burner Rig (HVBR)**
  - **Thermal Gravimetric Analysis - Three Units**
  - **Stress Rupture/CREEP Test Machines - Four**
  - **Furnaces and Molten Salt Pots**

- **Computer Workstations & Networking to Supercomputer**

Carderock Div, Naval Surface Warfare Center
Corrosion Branch - Code 613

Submarine Shaft Seal Corrosion Control & Repair

POC: E.B. Bieberich (410) 267-2191

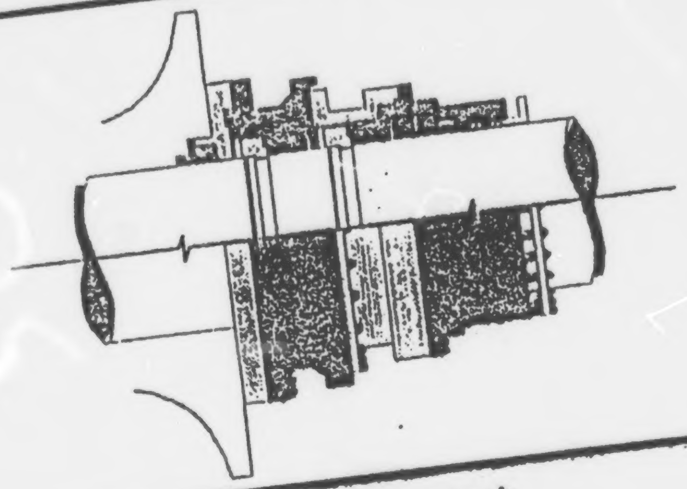

Objective

- Determine cause of corrosion of shaft seal materials which increased seal leakage and repair/replacement costs.
- Identify differences in corrosion performance of shaft seal materials and designs for each submarine class.
- Evaluate effectiveness of corrosion control countermeasures and repair methods for shaft seal components.
- Develop standard methods for corrosion control and repair of shaft seal systems.

Technical Approach

- Perform shaft seal corrosion inspections to establish baseline performance.
- Conduct design analysis for OHIO, LOS ANGELES and SEAWOLF Class submarines.
- Conduct comparative evaluations of shaft seal materials and repair methods through corrosion tests and shaft seal physical scale models.
- Characterize corrosion problem areas and identify effective countermeasures and repairs.
- Implement corrosion control countermeasures and in service and perform fleet evaluations.

Payoff

- Increased reliability of submarine shaft seal systems.
- Extended life of shaft seal system components.
- Standard repair methods and corrosion control countermeasures for shaft seal components.
- Verified performance of repairs and countermeasures through fleet tracking.
- Cost savings through reduced maintenance, repair, and replacement of components.

repair metho

USMC Corrosion Prevention & Control
Background

USMC operates in corrosive salt air / immersion environment

Equipment purchased without corrosion control design guidance

Corrosion repair and maintenance costs are unacceptable

NSWCCD is conducting both O&M and R&D efforts in support of MARCORSYSCOM CPAC program

Goal is to reduce corrosion and associated life cycle costs for existing vehicles and future acquisitions

NSWC
Naval Surface Warfare Center
CARDEROCK DIVISION

USMC Corrosion Prevention & Control

Approach

Corrosion Surveys

Maintenance Procedures

Coatings

Military & Technical Liaison - CPAC

Equipment Protection for Transport

Corrosion Tests - Marine Atmosphere & Accelerated

Alternate Materials & Design

Field Tests

NSWC
Naval Surface Warfare Center
CARDEROCK DIVISION

Carderock Div, Naval Surface Warfare Center
Corrosion Branch - Code 613

Corrosion Control of Double Hull Ships

Objective

- Investigate Approaches To Prevent Corrosion of Double Hull Ships
  - Advanced Double Hull Combatants
  - Commercial Double Hull Tankers

Approach

- Three Phase Program Directed by Code 613 (H. Hack)
- Coordinated Efforts of Various CDNSWC Code 60 Organizational Entities With Expertise in Corrosion and Coatings Technologies:
  - Contract: State-of-Art of Corrosion Control for DH Ships
  - Codes 622 & 624 (Phila.): Corrosion Susceptibility Analysis
  - Code 641 (Annapolis): I.D. Optimum Coating(s) for Long Life
  - Code 68 (White Oak): Investigate Vapor Phase Inhibitors and Dehumidification

Corrosion Control of Double Hull Ships (cont.)

Results

- Established Importance of Design Details To Minimize Corrosion and Make the ADH Concept Economically Feasible.
- Coatings Systems With 15-20 Years Life and Low VOC Content Are a Realistic Goal Assuming Periodic Maintenance Is Provided.
- Use of Vapor Phase Inhibitors or Dehumidification To Reduce Corrosion in Closed Vapor Filled Spaces in the ADH Design Is Feasible.

Deliverable

- Co-Authorized Paper Presented at the Advanced (Unidirectional) Double-Hull Technical Sympossium Held at NIST October 25-26, 1994.

Carderock Div, Naval Surface Warfare Center
Corrosion Branch - Code 613

High Temperature Corrosion and Advanced Ceramic Materials

Current and Future Programs

- ICR Gas Turbine Engine (NAVSEA O3R)
  - -Recuperator Section Alloys
    - 14 Cr - 4 Mo Alloy
    - Alloy 625
    - Alloy 230
  - -Hot Section (Turbine Blades) Coatings
- Alternate Fire Fighting Agents - Corrosion Effects
- Super Conducting Current Collectors
- Shipboard Mobility Fuels Program (Code 859)
  - -Red Dye (Identification)
  - -Vanadium
  - -Sulfur
- Textron-Lycoming: Metallic and Ceramic Coatings
- Westinghouse (Orlando): Thermal Barrier Coatings

EIS

- Electrochemical Impedance Spectroscopy
- A-C Test Technique
- Small Alternating Signal (~ 10 mV)
- Wide Signal Frequencies, 10e5 - 10e-3
- Non-Destructive Test
- Research and Practical Tool

QUANTITATIVE NON-DESTRUCTIVE COATING EVALUATION
BASIS OF NAVY NEED

CURRENT PROCEDURE FOR COATING ASSESSMENT AND REPAINT DECISIONS

- NON-QUANTITATIVE & HIGHLY SUBJECTIVE

  COATING APPEARANCE COMPARED TO VISUAL STANDARDS SHOWING DEGREE AND DISTRIBUTION OF PAINT DAMAGE

- BLAST AND REPAINT OR TOUCHUP DECISIONS BASED ON THE THE JUDGEMENT OF THE INSPECTOR AND HIS INTEREPRETATION OF THE EXTENT OF COATING DAMAGE

- DRY FILM THICKNESS IS ESSENTIALLY THE ONLY QUANTITAIVE DATA PRESENTLY USED IN COATING EVALUATION

- DRY FILM THICKNESS DOES NOT PRVOIDE INFORMATION ABOUT THE PRESENCE/DISTRIBUTION OF PORES AND HOLIDAYS OR THE CONDITION OF THE COATING/METAL INTERFACE

EIS Coating Assessment Parameters

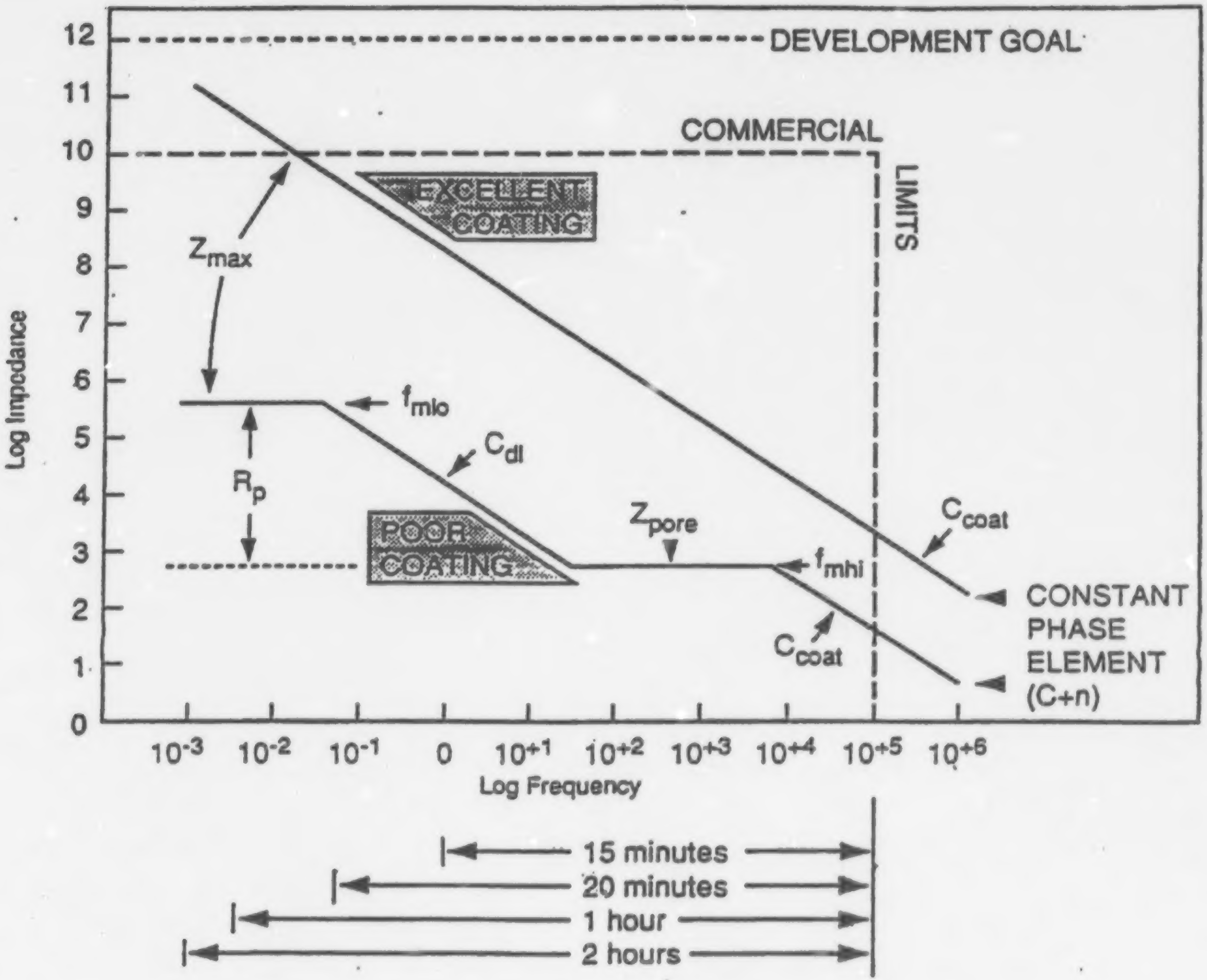

CURRENT CORROSION PROGRAMS

CARDEROCK DIVISION, NSWC

OTHER PROGRAMS

- Aluminum Alloy Sacrificial Anodes
- Cleaning Agents for Pre-Painting Surface Preparation
- Galvanic Interaction of Piping Materials
- High Strength Fasteners
- Materials Selection for Oily Waste Treatment Systems

CODE 613 TASK WRITE-UPS

Non-Destructive Quantitative Coating Assessment System

NSWCCD (Code 6130) has been developing the methodology and improved field portable equipment for quantitative characterization of the use status of painted metals/conductive substrates. A field-portable electrochemical impedance spectroscopy (EIS) system with higher impedance measuring capability has been successfully demonstrated and improvements to the sampling detector are ongoing. The development of a hand-held meter which rapidly records a high frequency impedance, as related to the general coating status, has been initiated. The hand-held unit would allow a mapping of a hull coating or an internal tank coating system within a conventional work day and target the area(s) for more detailed evaluation via EIS. The methodology would establish a quantitative basis for the necessity of repainting.

Aluminum Alloy Sacrificial Anode

NSWCCD (Code 6130) has led the technical effort aimed at implementing the use of aluminum alloy sacrificial anodes for corrosion protection, which is required when hull or tank paint coating systems fail or become damaged; as a weight saving and mission extending measure. While aluminum anodes generally behave reliably, there is some variability in performance which is related to metallurgical factors and foundry practices. A new study is being initiated to establish the casting requirements for a more favorable and larger microstructure which has been shown to allow excellent, uniform anode performance. The joint test effort is being conducted with the Johns Hopkins University, Materials Science and Engineering personnel. The results and casting recommendations will be made available to all three commercial fabricators of the particular aluminum alloy castings.

Cleaning Agents for Pre-Painting Surface Preparation

NSWCCD (Code 6130) is developing an electrochemical and surface chemistry test protocol for determining the effectiveness of commercially available and developmental repainting cleaning agents. Surface (substrate) contamination has been reported to be the leading cause of coating failures in seawater exposure environments. During the last five years, several vendors (some with very limited laboratory capabilities) have marketed products which are claimed to remove contamination and in some cases are claimed to improve paint adherence. The test protocol is being developed and documented to allow a reproducible assessment of the various products and establish, when required, kinetic and mechanistic information. An environmentally benign product for repainting surface cleaning that increased the performance life of Navy coating systems would result in increased system availability as well as decrease life cycle costs.

ICCP/SHT Adhesion Testing

This task is aimed at assessing the effects of impressed current cathodic protection (ICCP) as compared to the effects of seawater exposure under freely corroding (w/o ICCP) on the reliability/adherence, projected life and maintenance requirements of new hull treatment systems intended for use on NSNN. Cathodic protection parameters which could affect the adhesion of special hull treatment (SHT) materials for the NAS are being assessed. These tests are one of several types which are being used to qualify the materials in general for this application. Test results will be used to recommend any necessary alterations to the SHT or cathodic protection systems.

Corrosion Detection and Identification of Material-Upgrades for Shipboard Seawater Valves

The Navy is replacing certain copper-nickel seawater piping systems with titanium on LPD-17 class ships to reduce life cycle costs. Substitution of titanium for copper-nickel piping, while leaving most of the bronze valves in place, could result in premature deterioration of these valves without full system electrical isolation. Even in current copper-nickel piping systems, corrosion induced deterioration of valves is likely to result in their replacement roughly three times in the 40-year life of a surface ship. In order to avoid unnecessary valve replacement and to extend the life of these valves, a condition-based maintenance system needs to be applied and an alternate, more corrosion-resistant material needs to be identified. The objective of this program is to (1) develop an in-situ, non-destructive method for measuring valve deterioration and (2) identify a seawater valve replacement material (with associated trim materials and design considerations) for a 40-year maintenance free service life. The expected payoff is a life cycle cost savings of $1.5 billion (at least $30-40M/yr) for the Firemain and Auxiliary Seawater Cooling systems in a 200 ship Navy, with equivalent additional savings for other systems and additional ships.

Alloy 625 Life Cycle Program

NSWCCD (Code 613) is undertaking a program to develop crevice corrosion data in representative submarine piping system configurations which would stay ahead of the lead ship in the class and provide the technical basis for establishment of inspection and maintenance periodicity for these systems. To accomplish this, an "all metal piping system" loop is operating under prototypical seawater pressure, velocity and treatment levels. The loop contains plain alloy 625 flanged spools and alloy 625 spools overlaid with alloy C-276 (countermeasure), with all flanges greased prior to assembly. Crevice corrosion inspection intervals on this loop are based on anticipated ship schedules. Also under this program, a crevice corrosion remote detection device is being developed and evaluated in an effort to provide a non-destructive method of locating crevice corrosion in the complex system geometries where this type of attack is likely to occur. The current device being evaluated is a flange o-ring incorporating an electrochemical sensor. This o-ring also has the potential to provide the component with impressed current protection from crevice corrosion.

High Strength Fasteners

Alloy K-500 is the currently used high strength alloy for Navy fastener applications in immersion service. Alloy K-500 has performed well as a fastener material in seawater but is susceptible to hydrogen cracking in areas of intense cathodic polarization and is galvanically incompatible with titanium and Alloy 625 components. Due to these inadequacies, it is necessary to identify alternate fastener materials that can suitably replace Alloy K-500. Currently, a joint program is being conducted by NSWCCD Codes 613 and 614 to develop a high strength fastener handbook for 15 alloys, containing data and guidelines on corrosion behavior, mechanical properties, fatigue behavior, and other relevant material properties. The technical information in the handbook will include data generated in this program as well as data reported in the literature by government and industry sources. The fastener handbook will be distributed to Navy designers and engineers to assist in joint design for naval systems. Implementation of proper joint design and utilization of appropriate fastener materials will improve fastener reliability and reduce life-cycle maintenance and cost.

Corrosion Control Methods for Advanced Double Hull Ships

Advanced Double Hull ships present some unique problems with respect to controlling and monitoring corrosion due to limited access to and inability to inspect the cells that comprise the ADH design. NSWCCD Codes 613 (Corrosion Branch) and 683 (Electrochemistry Branch) are conducting a joint investigation of corrosion control methods that offer an alternative or enhancement to the use of coatings for use in Naval and commercial cargo advanced double hull (ADH) ship designs. Alternative corrosion control methods to coatings are being tested because of the high cost of coating application for advanced double hulls, and the difficulty of monitoring the condition of coatings in these areas of limited access. Tests are being conducted at an NSWCCD corrosion test site in Ft. Lauderdale, Florida. Results will be used to select and implement long-term corrosion protection methods for ADH compartments and predict their long term corrosion rates. The corrosion inhibition methods being tested are intended to mitigate corrosion and reduce corrosion control costs (relative to coating) and inspection periodicity; all with reduced environmental impact. Successful implementation of these corrosion control methods will improve ship survivability and reduce maintenance costs.

GALVANIC CORROSION PREVENTION IN PIPING SYSTEMS

(NSWCCD Code 6130) Galvanic corrosion of ships piping due to the use of dissimilar metals is becoming of greater concern because of the increased variety of materials used for piping construction of new ships such as the 688 and 21 class submarines. Current design requires periodic inspections and replacement of waster pieces which is expensive and necessitates shutdown of critical ship systems for maintenance. These inspection pieces are in subsafe systems on the submarines which create a safety issue. Galvanic isolation and electrically isolated separator pieces are not viable control methods due to the complexity or available of system space. Alternative galvanic control methods that would eliminate the need for inspection, improve safety, and control corrosion in piping systems are being investigated. This task will prove the concept and effectiveness of newer galvanic corrosion control methods (barrier coatings, cathodic protection, and bi-electrode) by characterizing their performance of mitigating galvanic corrosion by means of piping mockup tests. A series of piping mockups have been designed to simulate the most probable geometry and existing environmental conditions in naval piping systems. Observation and measurement of any corrosion of the galvanic couples will determine the effectivenes of these control methods. The use of effective galvanic corrosion control methods will furnish ship designers with more piping material options for retrofitting existing systems in the Fleet when necessary and provide greater flexibility for new future submarine and surface ship designs.

MATERIALS SELECTION FOR OILY WASTE TREATMENT SYSTEM

(NSWCCD 6130) This task will evaluate corrosion resistance, erosion resistance, weight, cost, and maintainability for the piping and pump materials presently conceived for a treatment system designed by Code 6330 for the Fleet to process oily waste (200-2000 ppm oil content in seawater) along with a number of heavy metals) to reduce the effluent oil concentration to less than 5 ppm oil (the projected future EPA limit) and some loss of the heavy metals. The waste processing unit operates only when required - on the ship where the system will first be installed, the waste processor will operate about 5 hours every five days; at port the processor would not operate - i.e. the system could lie idle for extended periods of time. The oily waste surge tank is exposed to the atmosphere and may include sulfides. The duty cycle of the system may initiate microbiological corrosion; polluted brackish and seawater may introduce other corrodents to the system. The lack of data on low oil/water media corrosion in the open literature will necessitate testing of different materials in the waste treatment processor at NSWCCD and monitor of. materials performance on a present operating shipboard system.

#507236 (33)

Underwater Acoustic Radiation of an Elastic Rectangular Plate Covered by a Decoupling Coating

Olivier Foin and Alain Berry

Groupe d'Acoustique de l'Université de Sherbrooke
Département de Génie Mécanique
Université de Sherbrooke
Sherbrooke, Québec (CANADA), J1K 2R1

and

Jeffrey Szabo
Defence Research establishment Atlantic

ABSTRACT

The reduction of the sound radiated by a finite structure immersed in water on one side is of concern in this paper. The purpose of this study is to investigate the decoupling effect of adding a compliant layer between a base structure and the fluid. The vibration response and the acoustic radiation of a baffled, elastic plate covered by a decoupling layer immersed in water is analyzed. The theoretical model uses the Love-Kirchhoff theory to describe the motion of the base plate whereas the locally reacting model is used for the behavior of the coating. A parametric study is performed in order to understand the decoupling mechanism and the noise reduction effect of such structures.

The locally reacting model assumes that the decoupling layer behaves like evenly distributed springs in the transverse direction. The unknowns of the problem (i.e. transverse displacement of the base plate and acoustic pressure in the fluid) are expanded with trigonometric functions that satisfy the simply supported boundary condition. The radiation impedances of the plate-fluid system are calculated using a numerical algorithm.

SCOPE

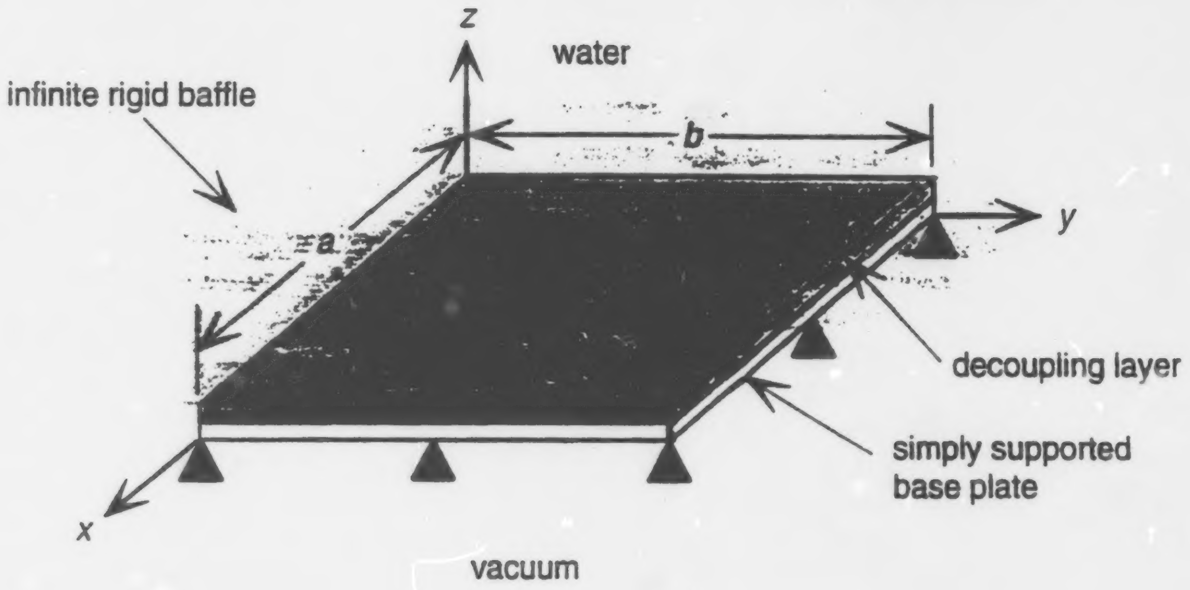
z
water
infinite rigid baffle
b
y
a
decoupling layer
simply supported
base plate
x
vacuum

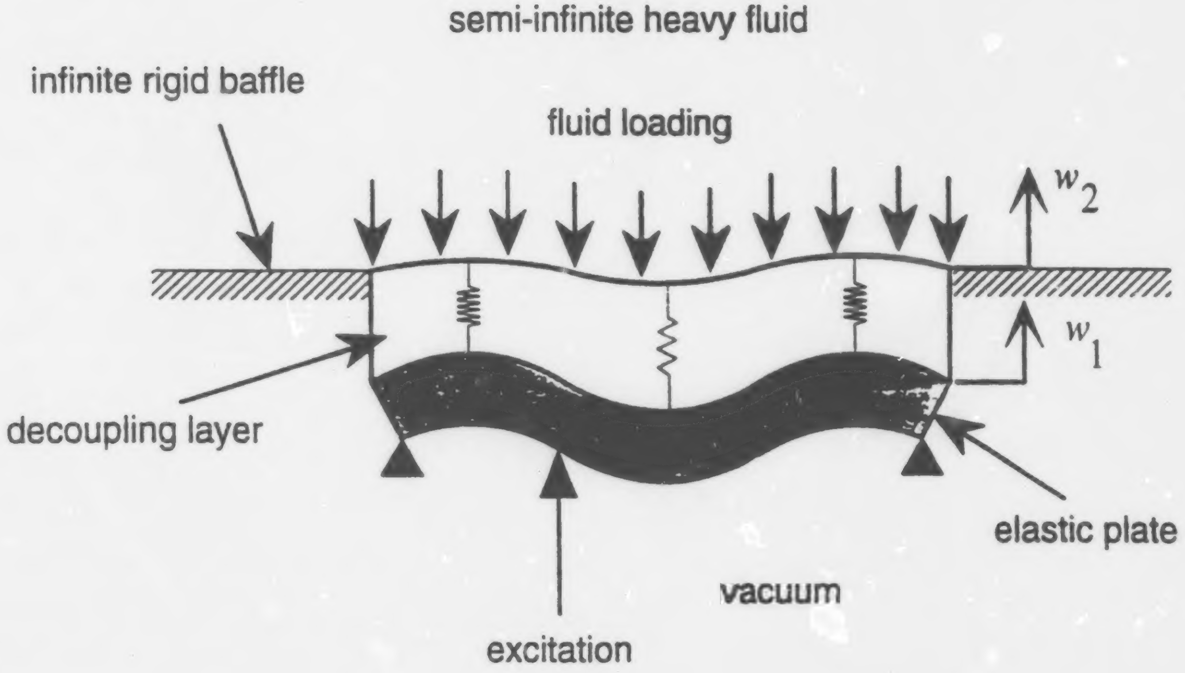
semi-infinite heavy fluid
infinite rigid baffle
fluid loading
w_2
w_1
decoupling layer
elastic plate
vacuum
excitation

MOTIVATIONS AND OBJECTIVES

☐ *Motivations*

- Amount of acoustic attenuation provided by decoupling treatment on ship structure in water ?
- How to relate small scale laboratory experiments to full scale case ?
- What « figure of merit » for acoustic characterization / ranking of decoupling materials ?

☐ *Objectives*

- Develop an exact model of Vibration / Sound Radiation into water from finite plate with decoupling layer
- Provide DREA with simple prediction tool to analyze decoupling treatments
- Suggest a global vibratory indicator to characterize acoustic performance of decoupling treatment, independently of substrate size

THEORY : STRUCTURAL MOTION

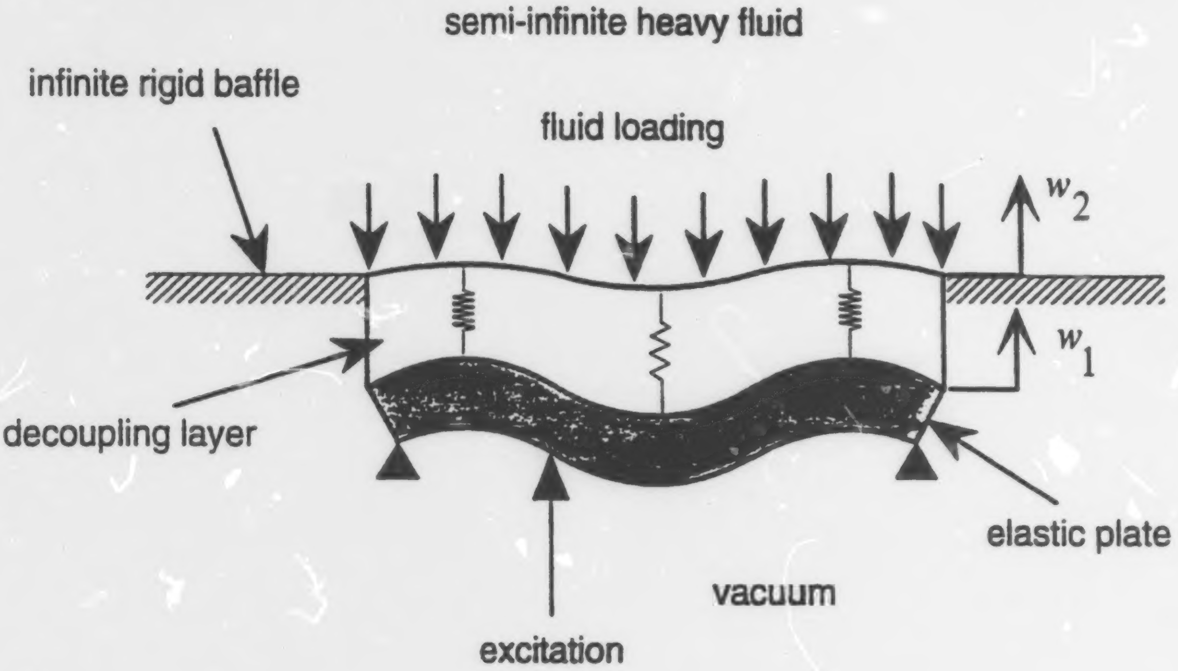
semi-infinite heavy fluid
infinite rigid baffle
fluid loading
w_2
w_1
decoupling layer
elastic plate
vacuum
excitation

☐ ***Assumptions***

- Substrate : Pure bending (Love-Kirchhoff plate)
- Decoupling layer : Locally reacting, massless material (deformation in the transverse direction)
- Fluid loading of the structure

☐ ***Equation of motion of the base plate***

$$\tilde{D}\nabla^4\tilde{w}_1(Q)-\rho h\omega^2\tilde{w}_1(Q)=\tilde{f}(Q)-\tilde{P}(Q)$$

THEORY : STRUCTURAL MOTION (...)

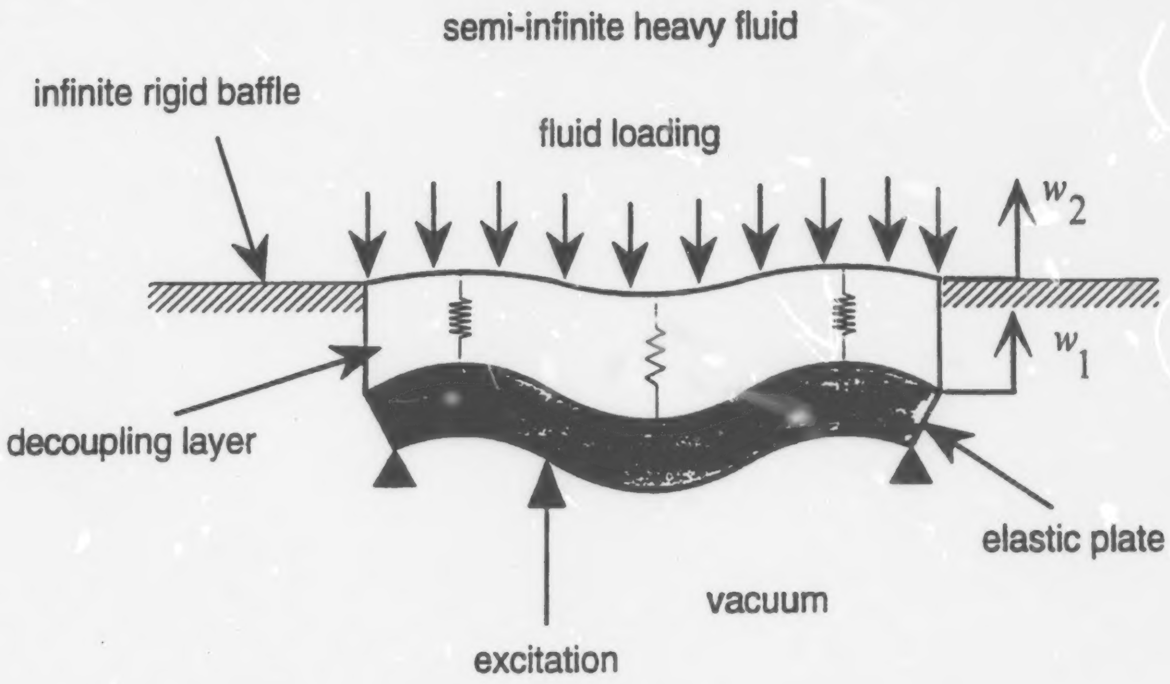
semi-infinite heavy fluid
infinite rigid baffle
fluid loading
w_2
w_1
decoupling layer
elastic plate
vacuum
excitation

☐ ***Equation of motion of the decoupling layer***

$$\widetilde{P}(Q) = Z_c\left(\widetilde{w}_2(Q) - \widetilde{w}_1(Q)\right)$$

Z_c : Impedance of the decoupling material :

$$Z_c = \frac{\widetilde{B}_c}{h_c}$$

$\widetilde{B}_c$: Complex bulk modulus of the decoupling layer : $\widetilde{B}_c = B_c(1 + j\eta_c)$

h_c : Thickness of the decoupling layer

THEORY :: FLUID-STRUCTURE COUPLING

☐ ***Helmholtz equation***

$$\Delta\tilde{P}(M)+k_0^2\tilde{P}(M)=0$$

☐ ***Continuity of the structural and acoustic normal accelerations on the outer surface of the decoupling material***

$$\frac{\partial\tilde{P}(Q)}{\partial z}=\rho_0\omega^2\tilde{w}_2(Q)$$

☐ ***Acoustic pressure in the fluid : Rayleigh integral***

$$\tilde{P}(Q)=-\omega^2\rho_0\iint_S \tilde{w}_2(M)G(M,Q)ds_M$$

Green's function $G(M,Q)$:

$$G(M,Q)=\frac{e^{-jk_0R}}{2\pi R}$$

R : distance between point M and Q

THEORY : COUPLED ELASTOACOUSTIC SYSTEM

☐ ***Elastoacoustic unknowns***

$\tilde{w}_1$: Transverse displacement of the base plate

$\tilde{w}_2$: Transverse displacement of the outer surface of the decoupling layer

$\tilde{P}$: Surface acoustic pressure in the fluid

☐ ***Eliminating $\tilde{w}_2$ using equation of motion of decoupling layer***

$$\tilde{P}(Q) = Z_c\left(\tilde{w}_2(Q) - \tilde{w}_1(Q)\right)$$

☐ ***Expanding*** $\tilde{w}_1(Q)$ and $\tilde{P}(Q)$ ***over in-vacuo modes of the substrate plate***

$$\begin{cases} \tilde{w}_1(Q) = \sum_{m=1}^{\infty} \sum_{n=1}^{\infty} \tilde{a}_{mn} w_{mn}(Q) \\ \tilde{P}(Q) = \sum_{m=1}^{\infty} \sum_{n=1}^{\infty} \tilde{b}_{mn} w_{mn}(Q) \end{cases}$$

where $w_{mn}(Q) = \sin\left(m\pi \frac{x}{a}\right)\sin\left(n\pi \frac{y}{b}\right)$

THEORY : COUPLED ELASTOACOUSTIC SYSTEM (...)

☐ Elastoacoustic system in matrix form

$$\begin{bmatrix}[A] & [B]\\ [C] & [D]\end{bmatrix}\begin{Bmatrix}\widetilde{a}_{mn}\\ \widetilde{b}_{mn}\end{Bmatrix}=\begin{Bmatrix}\widetilde{f}_{mn}\\ 0\end{Bmatrix}$$

$$\begin{cases}[A]=\begin{bmatrix}\ddots & & \\ & \rho\dfrac{ab}{4}\left(\omega_{mn}^{2}(1+j\eta)-\omega^{2}\right) & \\ & & \vdots\end{bmatrix} \text{ (diagonal matrix)},\\[2ex] [B]=\begin{bmatrix}\ddots & & \\ & \dfrac{ab}{4} & \\ & & \ddots\end{bmatrix} \text{(diagonal matrix)},\\[2ex] [C]=\begin{bmatrix} & -j\omega Z_{mnpq} & \end{bmatrix} \text{(full, symmetric matrix)},\\[2ex] [D]=\begin{bmatrix} & -j\omega\dfrac{1}{Z_c}Z_{mnpq} & \end{bmatrix}+\begin{bmatrix}\ddots & & \\ & \dfrac{ab}{4} & \\ & & \ddots\end{bmatrix} \text{(full, symmetric matrix)}.\end{cases}$$

☐ Intermodal radiation impedance coefficients

$$Z_{mnpq}=j\rho_0\omega\iint_{S}\iint_{S} w_{pq}(Q)G(Q,M)w_{mn}(M)ds_Q ds_M$$

Numerical calculation of the radiation impedance coefficients : Sandman method

THEORY :: VIBRO-ACOUSTIC INDICATORS

- ☐ ***Mean square velocity of the base plate***

$$\langle V_1\rangle^2 = \frac{\omega^2}{2s}\iint_s \tilde{w}_1(Q)\tilde{w}_1^*(Q)\,ds_Q = \frac{\omega^2}{8}\sum_{m=1}^{N}\sum_{n=1}^{N}\left|\tilde{a}_{mn}\right|^2$$

- ☐ ***Mean square velocity of the outer surface of the decoupling layer***

$$\langle V_2\rangle^2 = \frac{\omega^2}{2s}\iint_s \tilde{w}_2(Q)\tilde{w}_2^*(Q)\,ds_Q = \frac{\omega^2}{8}\sum_{m=1}^{N}\sum_{n=1}^{N}\left|\frac{\tilde{b}_{mn}}{Z_c}+\tilde{a}_{mn}\right|^2$$

- ☐ ***Radiated sound power in the heavy fluid***

$$W = \frac{1}{2}\mathrm{Re}\left[\iint_s \tilde{P}(Q)(-j\omega)\tilde{w}_2^*(Q)\,ds_Q\right]$$

- ☐ ***Radiation efficiency in the heavy fluid***

$$\sigma = \frac{W}{\rho_0 c_0 s\langle V_2\rangle^2}$$

SIMPLIFIED THEORY FOR LARGE DECOUPLING

☐ Assumptions

- Fluid loading is neglected in the equation of motion of the base plate
- The displacement of the outer surface of the decouling layer can be neglected in comparison to the motion of the base plate :

$$\left|\tilde{w}_2(Q)\right| << \left|\tilde{w}_1(Q)\right|$$

$$\begin{cases} \tilde{w}_1(Q) = \sum_{m=1}^{\infty} \sum_{n=1}^{\infty} \tilde{a}_{mn} w_{mn}(Q) \\ \tilde{w}_2(Q) = \sum_{m=1}^{\infty} \sum_{n=1}^{\infty} \tilde{c}_{mn} w_{mn}(Q) \end{cases}$$

$$\begin{bmatrix} [A] & [0] \\ [E] & [D] \end{bmatrix} \begin{Bmatrix} \tilde{a}_{mn} \\ \tilde{c}_{mn} \end{Bmatrix} = \begin{Bmatrix} \tilde{f}_{mn} \\ 0 \end{Bmatrix}$$

$$\begin{cases} [A] = \left[\ddots \; \rho \frac{ab}{4}\left(\omega_{mn}^2(1+j\eta) - \omega^2\right) \; \ddots \right] \text{ (diagonal matrix)} \\ [E] = \left[\; -\frac{ab}{4} Z_c \; \right] \text{ (diagonal matrix),} \\ [F] = \left[\; -j\omega Z_{mnpq} \; \right] \text{ (full, symmetric matrix)} \end{cases}$$

NUMERICAL RESULTS : LOW DECOUPLING

Bulk modulus of the decoupling layer : $B_c = 10^8$ Pa

☐ *Characteristics*

	Length (m)	Width (m)	Thickness (mm)	Density (kg/m^3)	Young/bulk modulus (Pa)	Loss factor	Poisson ratio
Base plate	0.6	0.6	9	7850	2.1×10^{11}	0.005	0.3
Decpl. layer	0.6	0.6	10	-	10^8	0	-

Excitation : Point force applied at $x_0 = y_0 = 0.06$ m from a corner of the plate

☐ *Mean square velocity*

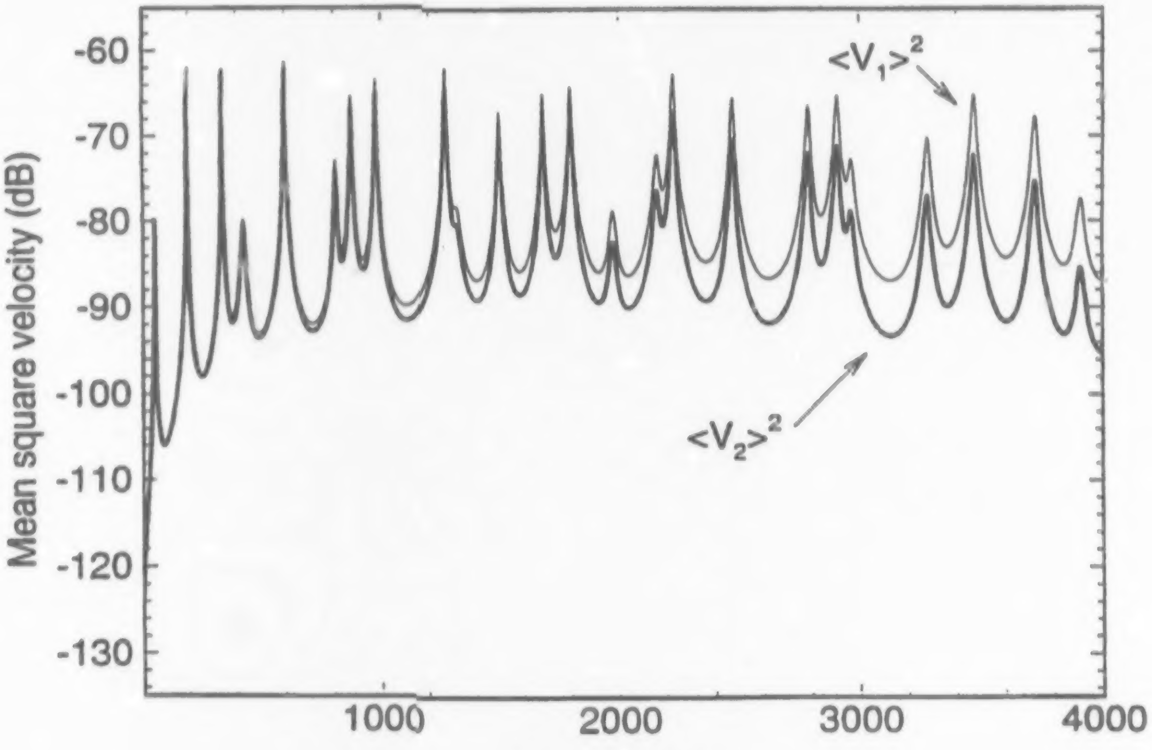

NUMERICAL RESULTS : LARGE DECOUPLING

Bulk modulus of the decoupling layer : $B_c = 10^6$ Pa

☐ ***Characteristics***

	Length (m)	Width (m)	Thickness (mm)	Density (kg/m^3)	Young/bulk modulus (Pa)	Loss factor	Poisson ratio
Base plate	0.6	0.6	9	7850	2.1×10^{11}	0.005	0.3
Decpl. layer	0.6	0.6	10	-	10^6	0	-

Excitation : Point force applied at $x_0 = y_0 = 0.06$ m from a corner of the plate

☐ ***Mean square velocity***

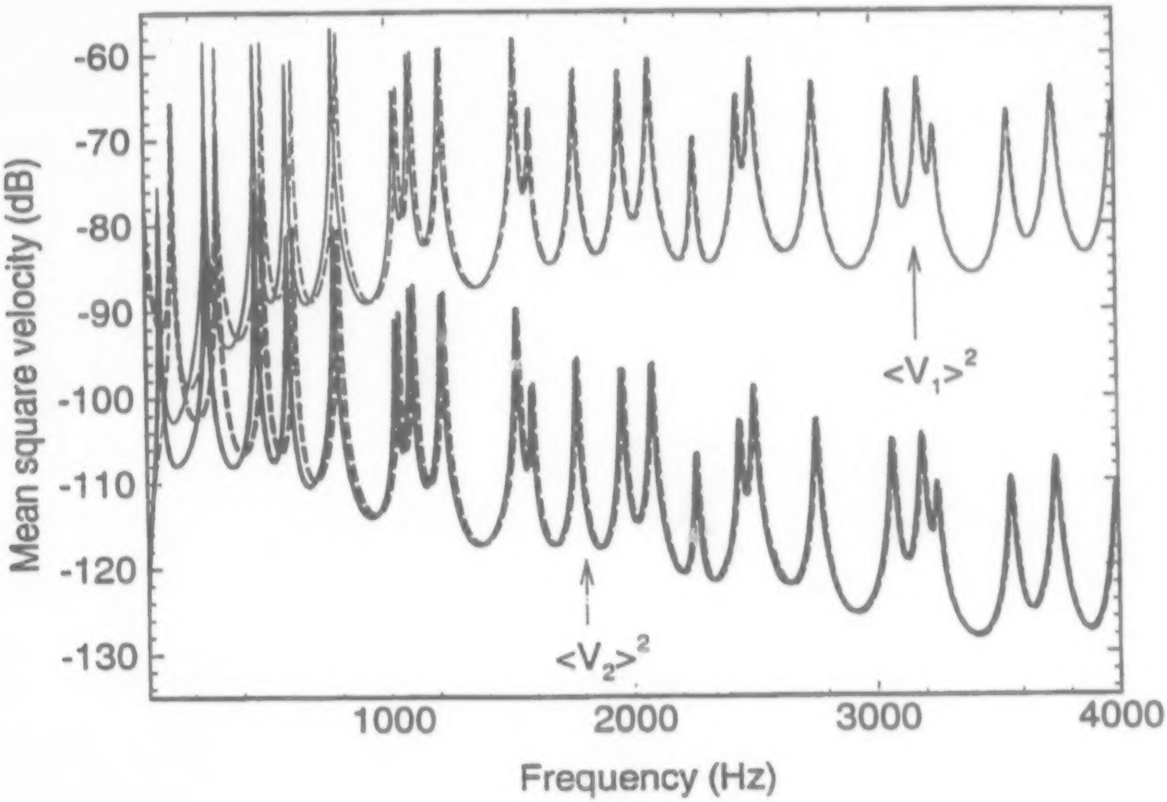

NUMERICAL RESULTS : COMPARISON WITH SANDMAN

Bulk modulus of the decoupling layer : $B_c = 10^6$ Pa

☐ *Characteristics*

	Length (m)	Width (m)	Thickness (mm)	Density (kg/m^3)	Young/bulk modulus (Pa)	Loss factor	Poisson ratio
Base plate	0.6	0.6	9	7850	2.1×10^{11}	0.005	0.3
Decpl. layer	0.6	0.6	10	-	10^6	0	-

Excitation : Point force applied at $x_0 = y_0 = 0.06$ m from a corner of the plate

☐ *Mean square velocity ratio :* $10\log(\langle V_1\rangle^2/\langle V_2\rangle^2)$

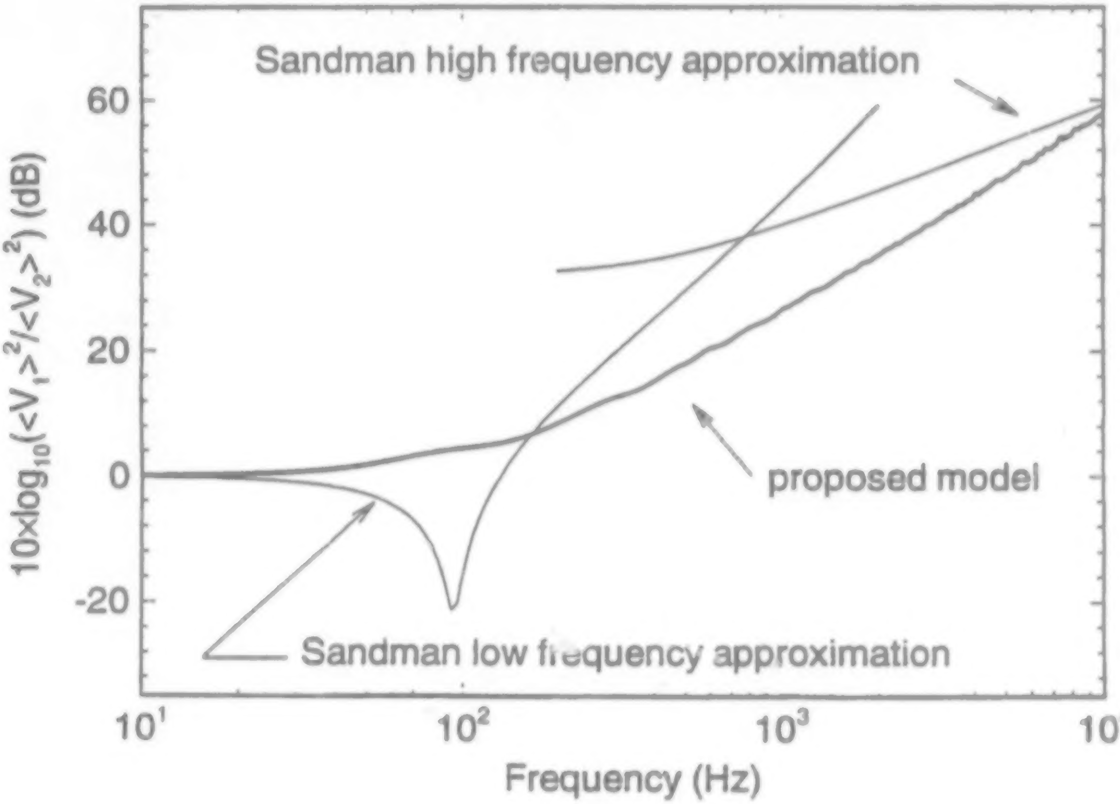

NUMERICAL RESULTS : RADIATION EFFICIENCY

Bulk modulus of the decoupling layer : $B_c = 10^6$ Pa

☐ *Characteristics*

	Length (m)	Width (m)	Thickness (mm)	Density (kg/m^3)	Young/bulk modulus (Pa)	Loss factor	Poisson ratio
Base plate	0.6	0.6	9	7850	2.1×10^{11}	0.005	0.3
Decpl. layer	0.6	0.6	10	-	10^6	0	-

Excitation : Point force applied at $x_0 = y_0 = 0.06$ m from a corner of the plate

☐ *Radiation efficiency*

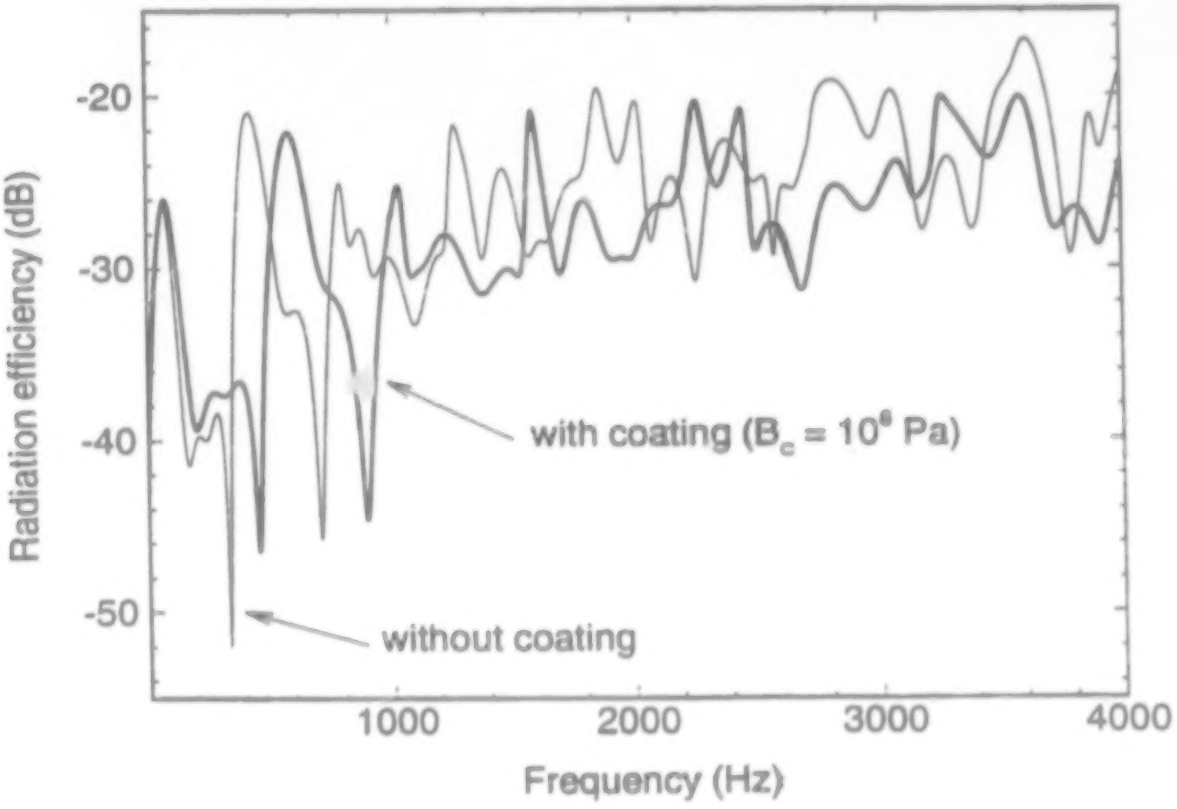

NUMERICAL RESULTS : RADIATED SOUND POWER

Acoustic efficiency of a decoupling layer

☐ *Characteristics*

	Length (m)	Width (m)	Thickness (mm)	Density (kg/m^3)	Young/bulk modulus (Pa)	Loss factor	Poisson ratio
Base plate	0.6	0.6	9	7850	2.1×10^{11}	0.005	0.3
Decpl. layer	0.6	0.6	10	-	10^6	0	-

Excitation : Point force applied at $x_0 = y_0 = 0.06$ m from a corner of the plate

☐ *Radiated sound power*

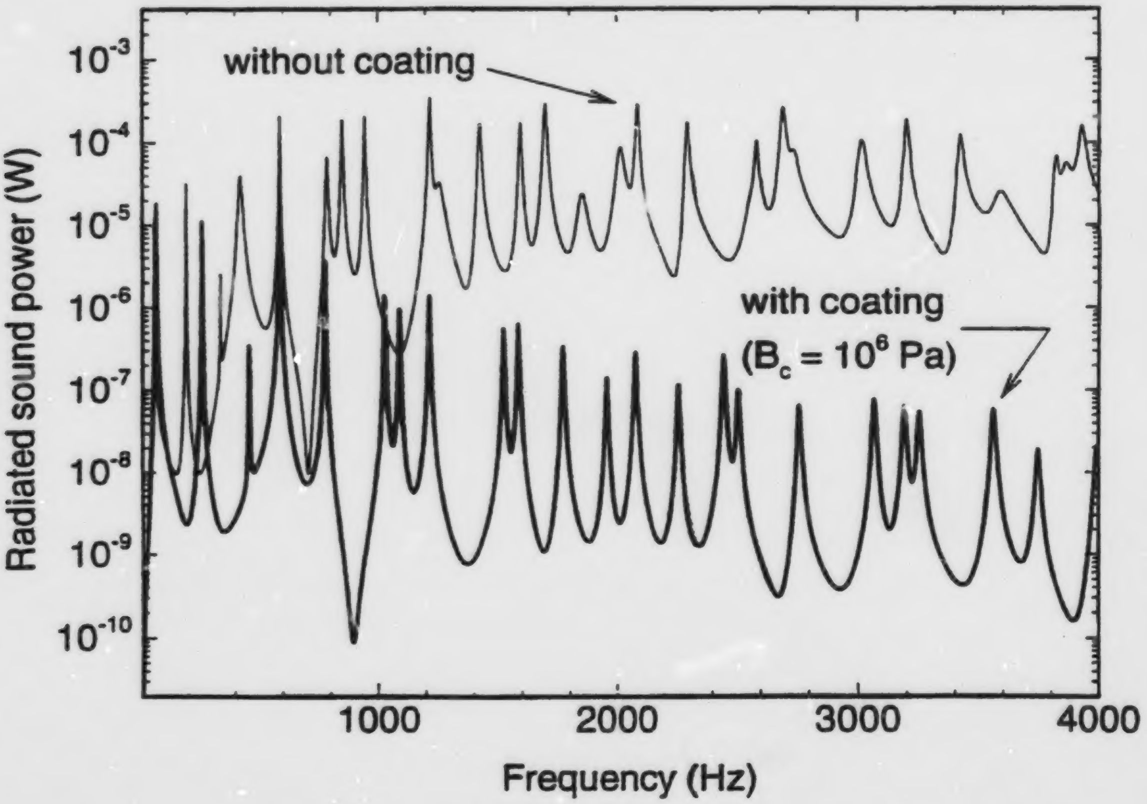

NUMERICAL RESULTS :
VELOCITY RATIO VS. ACOUSTIC INSERTION LOSS

- ☐ ***Looking for a simple vibratory indicator representative of acoustic performance of decoupling treatments***

- ☐ ***Comparison of the mean square velocity ratio*** **$10\log(<V_1>^2/<V_2>^2)$** ***and the acoustic insertion loss***

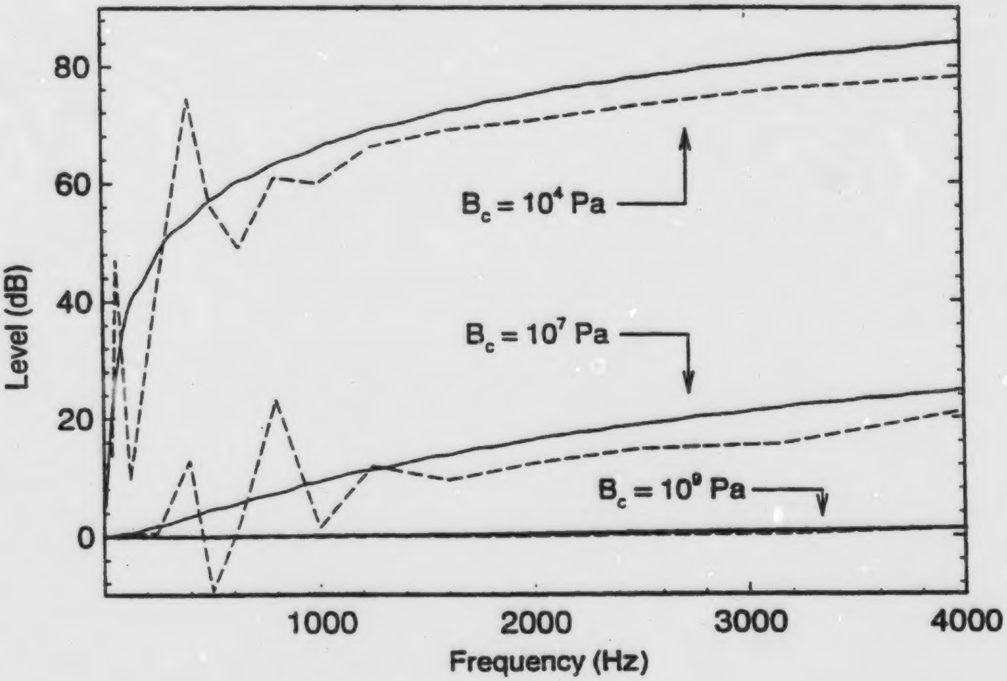

The mean square velocity ratio $10\log(<V_1>^2/<V_2>^2)$ is an appropriate measure of the acoustic performance of a decoupling treatment

NUMERICAL RESULTS : EFFECT OF SUBSTRATE SIZE

- ***Is the proposed decoupling indicator dependent on substrate size ? (cf. small-scale laboratory characterization)***

- ***Comparing the mean square velocity ratio and acoustic insertion loss for 2 plate x- and y-dimensions***

- ***Characteristics***

	Thickness (mm)	Density (kg/m^3)	Young/bulk modulus (Pa)	Loss factor	Poisson ratio
Base plate	9	7850	2.1×10^{11}	0.005	0.3
Decpl. layer	10	-	10^7	0	-

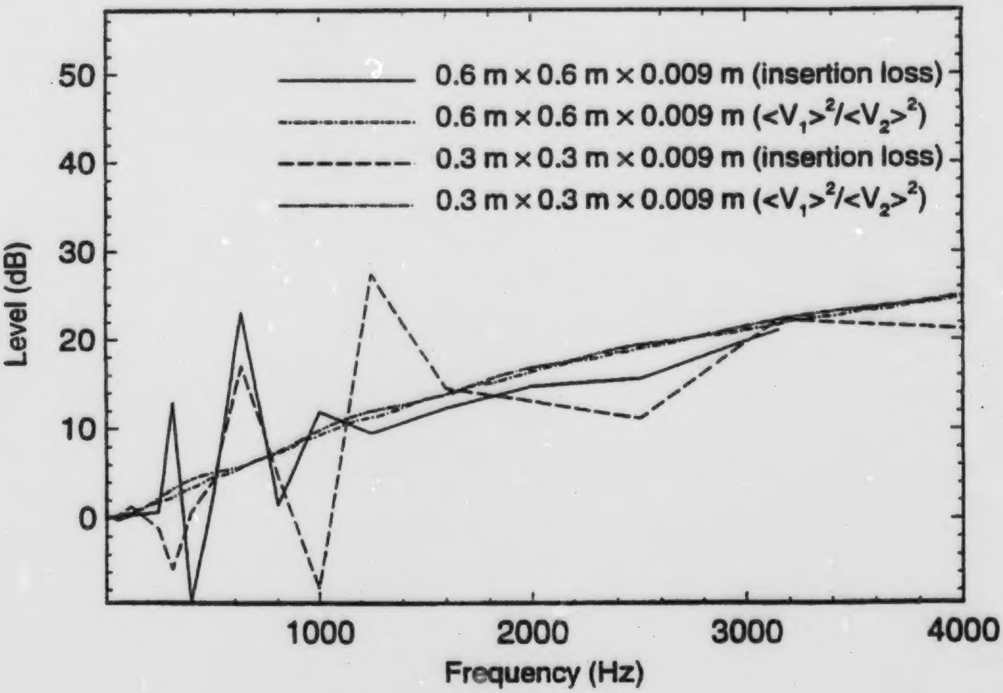

CONCLUSIONS

☐ *A model for Vibration / Sound Radiation into water from baffled, rectangular, S-S Love-Kirchhoff plate covered by compliant, locally-reacting, massless decoupling layer*

☐ *Simplified theory when decoupling effect is large (low impedance / high frequency)*

☐ *The ratio* $10\log(\langle V_1\rangle^2/\langle V_2\rangle^2)$ of *average vibration velocity of substrate to average vibration velocity at layer's free surface :*

- *is a smooth, non-modal indicator approximately independent of substrate dimensions*
- *is representative of the acoustic insertion loss provided by the decoupling treatment*

☐ *Perspectives :*

- *theory of elasticity to account for flexural, shear and extensional strain of decoupling layer*
- *Experimental validations*

#507237 (34)

Vibration Isolation Research for Naval Ships at the Australian Defence Force Academy

by Dr. Hugh Williamson

Acoustics and Vibration Unit
School of Aerospace and Mechanical Engineering
University College, The University of New South Wales
Australian Defence Force Academy
Canberra, ACT, Australia

To avoid detection in times of conflict, it is vitally important for naval ships to be designed so that acoustic signatures are minimised. The primary source of a ship's acoustic signature is on-board machinery. In order to reduce the acoustic signature, the transmission of structure-borne noise from machinery should be minimised. The minimisation of this transmission depends upon careful design of machinery isolators and supporting structures.

This paper will discuss research work in this area at the Australian Defence Force Academy which has been sponsored by Australia's Defence Science and Technology Organization. Part of the work concentrates on the measurement and characterisation of the performance of polymeric vibration isolators. Another aspect of the research concerns the characterisation and optimisation of machinery supporting structures for minimum transfer of vibrational energy to the ship's structure.

Contact between an isolator and supporting structure occurs over a finite contact area. Hence the true structural response is not well represented by the response due to a concentrated force, ie, point mobility. Research is proceeding on the concept of surface mobility, that is the response of supporting structures to forces distributed over a finite area. The ultimate aim is to find methods of predicting, measuring and optimising surface mobility of machinery support structures so that vibration isolation can be maximised.

Vibration Isolation Research for Naval Ships at the Australian Defence Force Academy

Dr Hugh Williamson

Acoustics and Vibration Unit
School of Aerospace and Mechanical Engineering
University College, The University of New South Wales
Australian Defence Force Academy
Canberra ACT Australia

Introduction

The Royal Australian Navy, like most navies, is concerned about reducing the acoustic signature of its ships in order to make detection by an unfriendly force as difficult as possible. In addition to the issue of detection by others, noise and vibration in and around a ship can interfere with sonar and other important equipment. As well, vibration and noise, particularly that from machinery, can be a source of annoyance to the crew of a vessel which in severe cases may become a health and safety problem. Hence in ship design, or in the design of modifications to a ship, effective vibration isolation of machinery is a very important consideration.

This paper gives an overview of a research program on vibration isolation at the Australian Defence Force Academy. The program is supported by Australia's defence research organisation, Defence Science and Technology Organisation, DSTO, through its Aeronautical and Maritime Research Laboratory in Melbourne.

Classical Vibration Isolation Theory

The classical theory of vibration isolation of machinery [1] considers the machine to be a lumped mass mounted on a linear spring and linear damper as shown in Figure 1. As well as assuming linear spring and damper behaviour, the machine and its foundation are taken to be perfectly rigid.

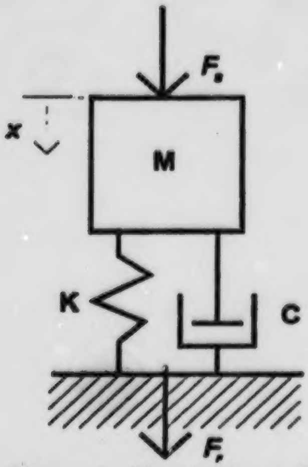

F_s = source force = $F_s \cos 2\pi f t$

M = machine mass

K = isolator stiffness

C = isolator damping

F_F = transmitted force
= $Kx + Cx'$

Figure 1 Classical one dimensional model of machinery isolation

In this simple model F_S represents the source of vibrations, that is all the forces within the machine which cause vibrations, for example out of balance forces generated in rotating parts, and F_F represents the forces transmitted to the foundation by the isolator. Applying the equations of motion to this model leads to the calculation of transmissibility, T, the ratio of the force transmitted to the foundation to the source force.

$$T = \frac{F_F}{F_S} \qquad (1)$$

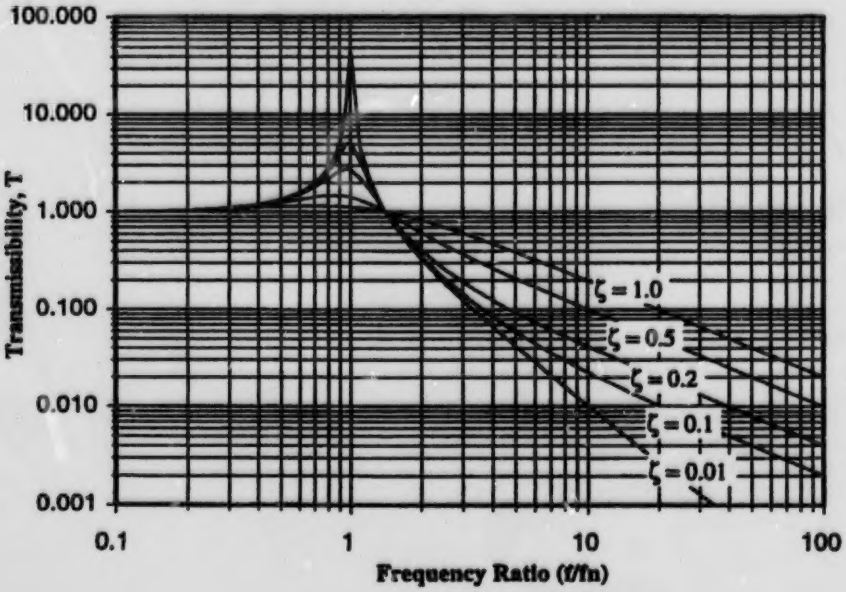

Figure 2 Transmissibility as predicted by the classical theory

Transmissibility, as shown in Figure 2, is a function of frequency ratio, f/f_n, and damping ratio, ζ.

$$f_n = \frac{1}{2\pi}\sqrt{\frac{K}{M}} \qquad \zeta = \frac{C}{2\sqrt{KM}} \qquad (2)$$

As suggested by the shape of the transmissibility curves, isolation should occur when the frequencies of the exciting forces in the machinery are significantly above the natural frequency, f_n, of the machine-isolator system. In many cases this simple approach will lead to adequate vibration isolation, however in many other instances poor isolation is achieved because factors not considered in this simple model have been ignored. Such factors include the following.

- Isolator materials are not adequately modeled by a simple linear spring and linear damper. For polymeric isolators in particular, behaviour is often dependent on applied load, frequency and temperature. Additionally the mass of an isolator needs to be taken into account since this leads to wave effects at higher frequencies.
- The simple lumped mass model for the machinery does not take into account the fact that vibrations can occur in various directions or as rotational oscillations about various axes. Machinery is normally mounted on a number of isolators in various locations in order to accommodate all directions of vibration and rotational oscillation.
- Neither the mounting, points on the machine, nor the foundation are perfectly rigid. This lack of rigidity at the mounting points on the machine and foundation can have a very significant effect on the effectiveness of isolation.

Isolator Model Including Foundation Mobility

The model of vibration isolation discussed below has been developed [2,3] to give a more adequate description of vibration isolation, particularly in terms of accounting for the non-rigidity of the foundation and the non-rigidity of the machinery mounting points. The isolator is represented using the four-pole parameter model which allows a more complete description of isolator behaviour including isolator mass and wave effects.

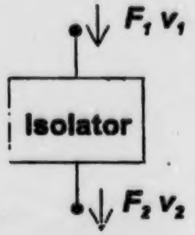

Figure 3 Schematic representation of an isolator

Figure 3 shows schematically, the four-pole parameter representation of an isolator with forces and velocities shown at the input and output of the isolator. Note that in this section, time varying forces, velocities and other quantities are in complex notation. The characteristics of the isolator are then described in terms of the four-pole parameters, α_{11}, α_{12}, α_{21} and α_{22}, as shown in equation (3). Using principles of reciprocity and symmetry it can be shown that $\alpha_{11}\ \alpha_{22} - \alpha_{12}\ \alpha_{21} = 1$ and that $\alpha_{11} = \alpha_{22}$ respectively, thus leaving only two independent parameters [2]. The four-pole parameters are in general complex quantities which depend on frequency. They provide a considerably more complete description of isolator behaviour than K and C of the classical description. In particular they do not assume that force is the same at each end of the isolator, a necessary requirement for considering wave effects in an isolator. Measurements of the four-pole parameter properties of large machinery isolators have been carried out recently by Norwood and Dickens [4] of DSTO.

$$\begin{aligned} F_1 &= \alpha_{11}F_2 + \alpha_{12}v_2 \\ v_1 &= \alpha_{21}F_2 + \alpha_{22}v_2 \end{aligned} \qquad (3)$$

Figure 4 shows schematically, two situations: (a) a machine or source which is mounted on an isolator, and (b) a machine mounted directly to a foundation. The non-rigidities of both the foundation and the machinery mounting points are represented by point mobilities, M_F, and M_F.

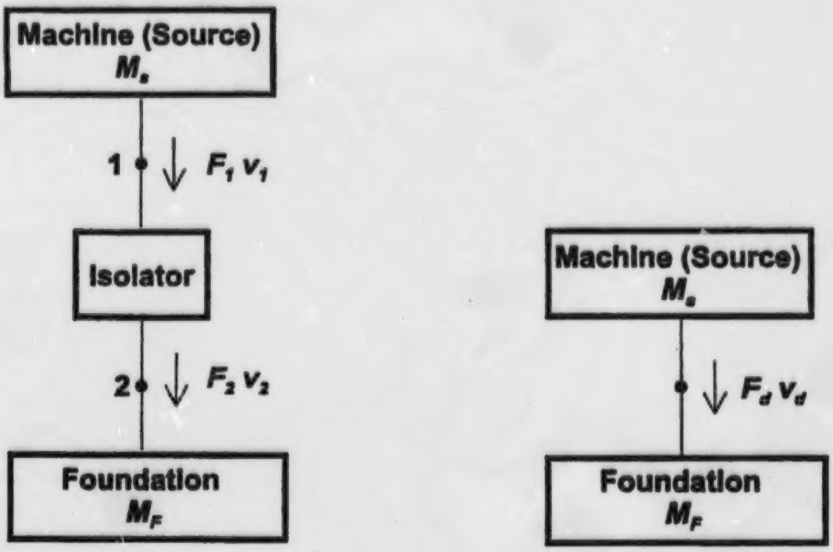

(a) (b)

Figure 4 (a) Schematic of a machine mounted on an isolator, (b) Schematic of a machine mounted directly to the foundation

The non-rigidity of the foundation is represented by its mobility, M_F , where mobility is defined in equation (4).

$$M_F = \frac{v_2}{F_2} = \frac{v_d}{F_d} \qquad (4)$$

The machine (source) is characterised by the free velocity, v_0, at the mounting point, that is the velocity at the mounting point which occurs when the machine is freely suspended and the force at the mounting point is zero. When the machine is connected to the isolator, a force of - F_1 is applied to the machinery mounting point. The free velocity, v_0, is then modified by M_s ($-F_1$) as shown in (5). The same relationship between forces and velocities also applies when the machine is mounted directly to the foundation, also shown in (5).

$$v_1 = v_0 - M_s F_1 \quad \text{or} \quad v_d = v_0 - M_s F_d \qquad (5)$$

Considering the situation where the machine is mounted on an isolator (3), (4) and (5) can be solved to give expressions for the force and velocity at the foundation. One measure of isolator performance is the ratio of the magnitude of the velocity at the foundation with the isolator present to the magnitude of the free velocity (6).

$$\frac{|v_2|}{|v_0|} = \frac{|\text{foundation velocity}|}{|\text{free velocity}|} = \left| \frac{M_F}{\alpha_{11} M_s + \alpha_{12} M_s M_F + \alpha_{21} + \alpha_{22} M_F} \right| \qquad (6)$$

An alternative measure of isolator performance is called effectiveness, E, which is the magnitude of the ratio of the force transmitted to the foundation with the isolator present, Figure 4(a), to the force that would be transmitted if the machine were connected directly to the foundation, Figure 4(b).

$$\mathrm{E} = \left| \frac{F_2}{F_d} \right| = \left| \frac{M_s + M_F}{\alpha_{11} M_s + \alpha_{12} M_s M_F + \alpha_{21} + \alpha_{22} M_F} \right| \qquad (7)$$

Foundation Mobility

Equations (6) and (7) demonstrate that foundation mobility can have a significant effect on the performance of a vibration isolation situation. In a ship or other structure it is normal to design a foundation to be as rigid and substantial as possible, however, there are practical limitations to this and it is clear from the above analysis that foundation mobility can have a major effect on isolation effectiveness.

Research at the Australian Defence Force Academy has been directed towards obtaining a better understanding of foundation mobility, with the long term aim of developing techniques for optimising foundation design from a vibration isolation point of view. Mobility as used in equation (4) is defined in terms of the response of a structure at the point of application of a concentrated force, hence such a mobility is referred to as a *point mobility*. However in a practical case, isolators tend to be of a significant size with contact between the isolator and the foundation occurring over a significant area. Theoretical values of point mobility have been calculated for simple structures such as plates and beams [5], and point mobility can be measured by standard techniques such as an instrumented impact hammer or shaker with an impedance head, however these predictions or measures do not represent the actual situation where contact occurs over a significant area. It will be shown below that a contact region is of significant size when it has a dimension which is larger than approximately 10 percent of the governing wavelength of the foundation. Thus there is a need for considering mobility over a finite region of contact, that is a need for the concept of *surface mobility*.

Hammer and Peterson [6,7] considered a similar problem in building acoustics and vibration where contact between a wall and a floor occurs over a narrow strip. They suggested two approaches to defining surface mobility, an average power definition, designated below as $\mathbf{M}^{ap}$, and a definition based on effective point mobility, designated below as $\mathbf{M}^{ee}$. Current research at the Acoustics and Vibration Unit is developing theoretical expressions, and carrying out measurements, of the surface mobility of simple anechoic plates where the contact region is either circular or rectangular. Techniques and concepts developed in these studies will be later applied to the measurement and prediction of surface mobilities for typical foundation structures.

Definitions of Surface Mobility

The average power definition of surface mobility is based on the vibrational power flow, **Q**, which occurs at the point or region of contact between an isolator and a structure. A schematic diagram of the contact region on an arbitrary body is shown in Figure 5.

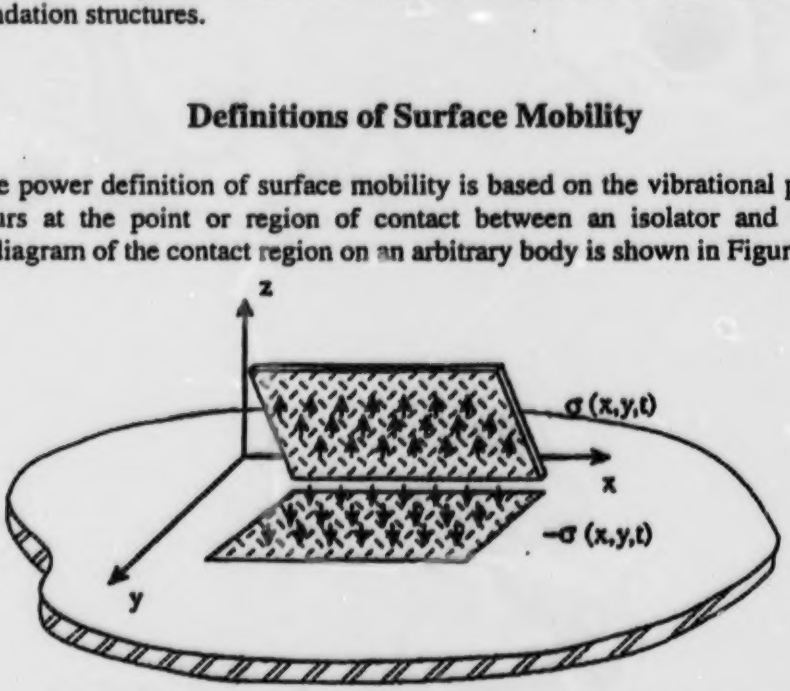

Figure 5 Schematic diagram of a contact region on the surface of a body

For the general case the contact force, represented by stress, $\sigma(x,y)$, and the velocity, $v(x,y)$, vary continuously over the contact region. Note that σ and v are complex amplitudes of time varying quantities which also vary spatially.

For point contact between two bodies, the time averaged power flow can be expressed in terms of mobility as follows.

$$Q = \frac{1}{2}\mathrm{Re}\{F^{*} \cdot v\} = \frac{1}{2}|F|^{2}\,\mathrm{Re}\{M\} \qquad (8)$$

For contact over a region, the time averaged power flow, and the total force, F, are given by the following.

$$Q = \frac{1}{2}\mathrm{Re}\left\{\int_{S} \sigma^{*}(x,y) \cdot v(x,y)\,ds\right\} \qquad (9)$$

$$F = \frac{1}{2}\int_{S} \sigma^{*}(x,y)\,ds \qquad (10)$$

Thus by analogy the surface mobility based on average power is given by (11).

$$M^{sp} = \frac{2Q}{|F|^{2}} = \frac{1}{|F|^{2}}\mathrm{Re}\left\{\int_{S} \sigma^{*}(x,y) \cdot v(x,y)\,ds\right\} \qquad (11)$$

Note that while surface mobility, M^{sp}, and power flow, Q, could be defined as complex quantities, only the real part which is the actual time averaged power flow has physical meaning. (Both the real and imaginary parts of the point mobility have meaning because the phase angle of the mobility is equal to the phase difference between the force and velocity at the point of contact. However with distributed forces and velocities over a contact region, the phase angle of the surface mobility is no longer meaningful.)

The definition of surface mobility, M^{se}, based on effective point mobility is founded on the basis of multi-point contact between two bodies [6]. For power transmission in multi-point coupled systems where there are N contact points, effective point mobility at point j is given by

$$M_i^{e} = \frac{V_i}{F_i} = \frac{\sum_{j=1}^{N} M_{ij}}{F_i} \qquad (12)$$

where M_{ij} = the ordinary transfer mobility between points i and j.

If the contact points are distributed over an area, s, the effective point mobility, M_i^{e}, at the point (x_i, y_i) is given by

$$M^{e}(x_i,y_i)=\frac{\int_s M(x_i,y_i|x_j,y_j)\sigma(x_j,y_j)ds}{\sigma(x_j,y_j)} \tag{13}$$

and the total time averaged power flow through the contact area is given by the following.

$$Q=\frac{1}{2}\int_s\left|\sigma(x_i,y_i)\right|^2\cdot \mathrm{Re}(M^{e}(x_i,y_i))ds \tag{14}$$

Now surface mobility is defined again by reference to (8).

$$M^{se}=\frac{\frac{1}{2}\int_s\left|\sigma(x_i,y_i)\right|^2\cdot \mathrm{Re}(M^{e}(x_i,y_i))ds}{\left|\int_s \sigma(x_j,y_i)ds\right|^2} \tag{15}$$

Implementation of either of the above definitions of surface mobility requires the determination of the force distribution over the contact area.

Surface Mobility of an Infinite Plate

Current research has concentrated on determining the surface mobility for relatively simple situations such as a uniform con-phase force distribution applied over a circular or rectangular region of an infinite (i.e. anechoic) plate [8,9]. These predictions can be duplicated experimentally and following confirmation of the techniques, the theory will form the basis for development of methods for determining surface mobility of practical support structures.

For an infinite plate, the theoretical predictions of surface mobility are based on the solution for the vibration field caused by a point force [5]. The solution of the thin plate vibration equations leads to the following relationship between the exciting force field, $\sigma(x_0,y_0)$, and the velocity, $v(x,y)$, at some arbitrary location [8].

$$v(x,y)=\int_s \sigma(x_0,y_0)\cdot M_0\cdot \Pi(kr)ds \tag{16}$$

where $\Pi(kr)=H_0^{(2)}(kr)-H_0^{(2)}(-jkr)$

$H_0^{(2)}$ is a zero-order Hankel function,

r = distance between (x_o, y_o) and (x, y),
k = wave number,
$M_o = \dfrac{k}{8c_B\rho h}$ is the point mobility of an infinite thin plate,
c_B = bending wave speed in the plate,
ρ = mass density of the plate, and
h = thickness of the plate.

The following plots are examples of the predictions obtained of surface mobility based on the averaged power definition given above. All plots are for cases where it has been assumed that a uniform con-phase force distribution is acting over the contact area.

Figure 6 gives the theoretical prediction of normalised surface mobility, M^{ap}/M_o, for a contact region of radius a. Normalised surface mobility is plotted against Helmholtz Number which physically represents π times the ratio of the diameter of the contact region to the governing wavelength of the bending waves in the plate.

$$\text{Helmholtz Number} = ka = \pi(2a)/\lambda \qquad (17)$$

where $\lambda = 2\pi/k$ = wavelength

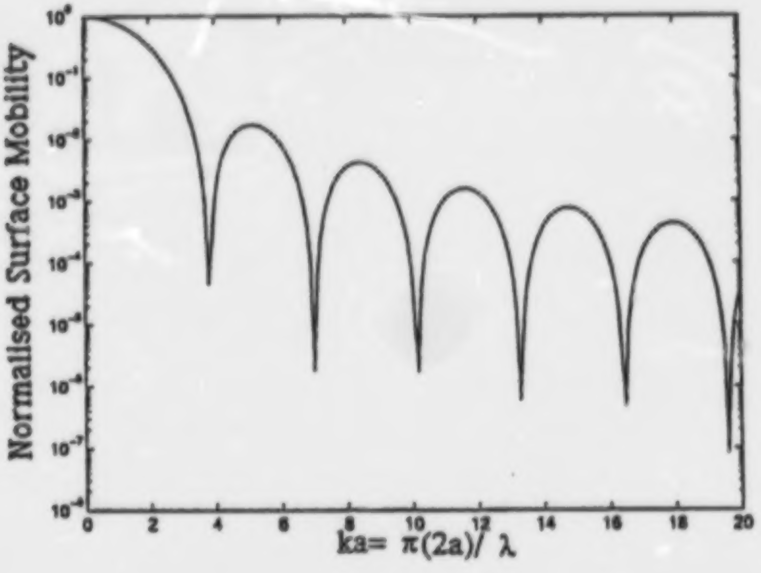

Figure 6 Normalised surface mobility, M^{ap}/M_o, for a circular contact region on an infinite plate subject to a uniform con-phase force distribution [8,9].

It can be seen in Figure 6 that when the contact region is small relative to the wavelength, i.e. small values of ka, the surface mobility approaches the point mobility. However for shorter wavelengths relative to the diameter of the contact region, mobility significantly decreases. Additionally, the mobility exhibits distinct minima or dips whenever a multiple of the wavelength is approximately equal to the contact diameter.

Also in Figure 6 it is clear that once the diameter is greater than approximately 10 percent of the governing wavelength, point mobility is no longer a good approximation for the surface mobility, see also discussion of point mobility of plates in [5].

In a similar way Figure 7 gives the theoretical prediction of normalised surface mobility, M^{sp}/M_o, for rectangular regions, length l and width w, of various aspect ratios. Again it can be seen that when the contact region is small relative to the wavelength, the surface mobility approaches the point mobility, and that for relatively small wavelengths, i.e. higher frequencies, mobility decreases. Mobility also decreases somewhat with higher aspect ratios and again dips in mobility are seen whenever a multiple of the wavelength is approximately equal to the width of the contact region.

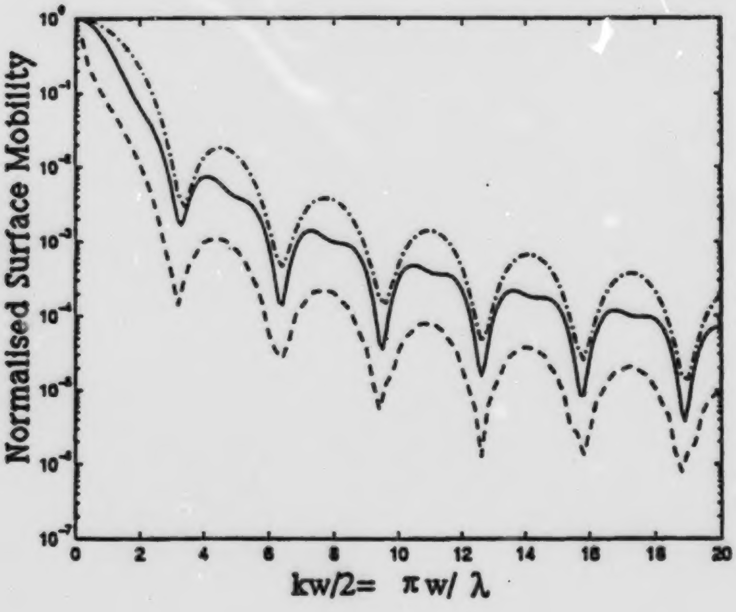

Figure 7 Normalised surface mobility, M^{sp}/M_o, for rectangular contact regions of various aspect ratios on an infinite plate, subject to a uniform con-phase force distribution [9]. Symbols: —·— l/w = 1, —— l/w = 2, - - - l/w = 10.

As well as the above theoretical results for surface mobility, theoretical work [10, 11] is also proceeding on cases where a uniform velocity distribution is assumed. Additionally, experimental work [8, 12] is proceeding which is in the process of confirming various theoretical predictions. Use of the finite element method for predicting surface mobility is also being explored [10] as this could provide a ready tool for predicting the surface mobility of practical foundation structures.

Summary and Discussion

Vibration isolation is a critical issue in naval ships where the generation of excessive underwater noise can lead to detection by an enemy. Additionally, poor vibration isolation in any structure, a vehicle or a building, can lead to unwanted noise and disturbance. A theoretical framework has been set out above for taking into account, not only the characteristics of the vibration isolator, but also the mobility or lack of rigidity in the foundation which supports machinery. Research being carried out at the Australian Defence Force Academy is studying methods of characterising and measuring foundation mobility. The long term aim of the work is to develop better methods of assessing machinery foundations as well as methods for optimising foundation design.

Acknowledgments

The financial and in-kind contributions of the Defence Science and Technology Organisation, the Australian Research Council and The University of New South Wales are gratefully acknowledged. In particular the author's colleagues and collaborators, Chris Norwood, John Dickens, Yuejin Li, Dai Jue and Jiye Zhao are particularly thanked for their support, encouragement and hard work.

References

1. Tse, F.S., Morse, I.E. and Hinkle R.T., *Mechanical Vibrations - Theory and Applications*, 2nd edition, Boston, Allen and Bacon, 1979.

2. Molloy, C.T., *Use of Four-Pole Parameters in Vibration Calculations*, Journal of the Acoustical Society of America, vol. 29, no. 7, pp. 842-853, 1957.

3. Snowdon, J.C., *Mechanical Four-Pole Parameters and their Application*, Journal of Sound and Vibration, vol. 15, no. 3, pp. 307-323, 1971.

4. Dickens, J., Norwood, C. J. and Juniper, R. G., *Four-Pole Parameter Characterisation of Isolator Acoustic Transmission Performance*, Proc. Australian Acoustical Society Annual Conference, Adelaide, Australia, 1993.

5. Cremer, L., Heckl, M. and Ungar, E. E., *Structure-Borne Sound*, New York, Springer-Verlag, 1979.

6. Hammer, P. and Petersson, B., *Strip Excitation, Part 1: Strip Mobility*, Journal of Sound and Vibration, vol. 129, no. 1, pp. 119-131, 1989.

7. Hammer, P. and Petersson, B., *Strip Excitation, Part 2: Upper and Lower Bounds for the Power Transmission*, Journal of Sound and Vibration, vol. 129, no. 1, pp. 132-142, 1989.

8. Norwood, C., Williamson, H.M. and Zhao, J.Y., *Surface Mobility of a Circular Contact Area on an Infinite Plate*, Journal of Sound and Vibration, accepted for publication in 1997.

9. Dai, J. and Williamson, H.M., *Surface Mobility for a Uniform Force over a Rectangular Excitation Area of an Infinite Thin Plate*, Acoustics and Vibration Unit Report No. AVC 9603, Australian Defence Force Academy, 1996.

10. Li, Y. and Williamson, H.M., *Surface Mobility of an Infinite Plate Under Uniform Force Excitation by Finite Element Method*, Acoustics and Vibration Unit Report No. AVC 9615, Australian Defence Force Academy, 1996.

11. Dai, J., Williamson, H.M. and Li, Y., *Investigation of Effective Mobility over Rectangular Excitation Areas of an Infinite Thin Plate*, Acoustics and Vibration Unit Report No. AVU 9617, Australian Defence Force Academy, 1996.

12. Li, Y., Williamson, H.M. and Dai, J., *Determination of Surface Mobility of an Infinite Plate Under Uniform Force Excitation by an Experimental Method*, Acoustics and Vibration Unit Report No. AVU 9621, Australian Defence Force Academy, 1996.

#507238 (35)

Minimization of Vibration Transmission Through Engine Isolation Mounts

by

Stanley G. Hutton
Alexander Muravyov and Guoping Chen

Department of Mechanical Engineering
University of British Columbia
Vancouver, B.C. V6T 1Z4

and

Jeffrey Szabo and David Stredulinski
Defence Research Establishment Atlantic

ABSTRACT

Engine isolation mounts should be designed to provide optimum isolation of the vibrational energy produced by engine operation. In order to achieve such a goal effective modeling of the complete system would be of assistance. Such modeling must include the three dimensional nature of the problem, the vibration characteristics of the engine and its supports and an accurate representation of the response characteristics of the isolator mounts.

The present paper reviews the development of such a model and pays particular attention to the experimental measurement and modeling of isolator characteristics. A comprehensive finite element model is developed by using viscoelastic modeling of the isolators and numerical tools are developed that assist in the choice of optimal isolators for a given installation.

CONTENTS

1. BACKGROUND

- Modelling of Isolator Materials
- Isolation of SDOF Systems
- Specification of Isolation Criteria

2. CONSTITUTIVE MODELLING OF ISOLATOR MATERIALS

- Viscoelastic Constitutive Models
- Experimental Determination of Viscoelastic Characteristics

3. VIBRATION ANALYSIS OF ENGINES ON FLEXIBLE MOUNTS

- Vibration Analysis of Viscoelastic Materials
- Analysis of Forces Produced by a Diesel Engine
- Vibration Analysis of Engines on Flexible Mounts

4. NUMERICAL RESULTS

- Effect of Material Characteristics on Engine Vibration Response
- Effect of Mount Geometry on Engine Vibration Response

5. EXPERIMENTAL MODEL TESTING

- Effect of Material Characteristics on Vibration Response
- Comparison of Numerical and Experimental Results

6. SUMMARY

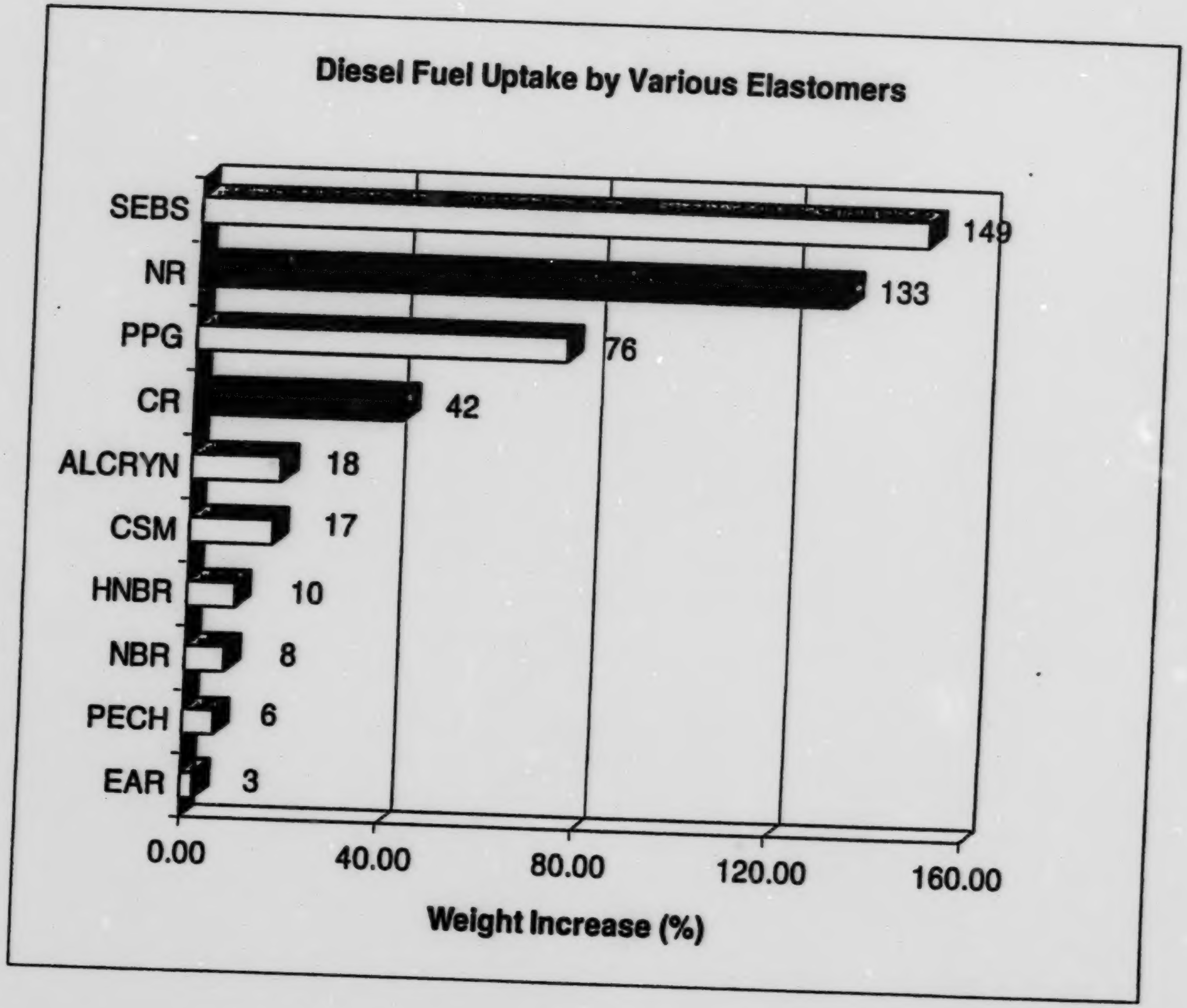
Diesel Fuel Uptake by Various Elastomers
SEBS
149
NR
133
PPG
76
CR
42
ALCRYN
18
CSM
17
HNBR
10
NBR
8
PECH
6
EAR
3
0.00
40.00
80.00
120.00
160.00
Weight Increase (%)

MODELLING OF ISOLATOR MATERIALS:

1. FOR UNIAXIAL TEST WITH SUDDENLY APPLIED STRAIN

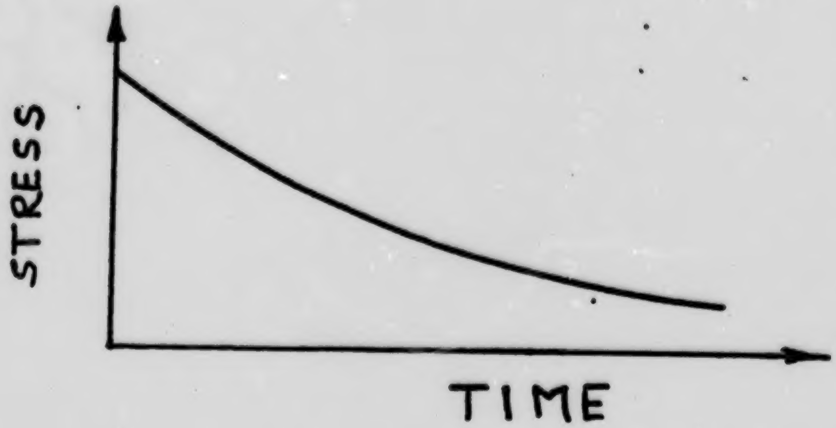

STRESS/STRAIN RELATION IS TIME DEPENDENT

2. FOR UNIAXIAL TEST WITH A HARMONIC EXCITATION $F_0 \sin WT$

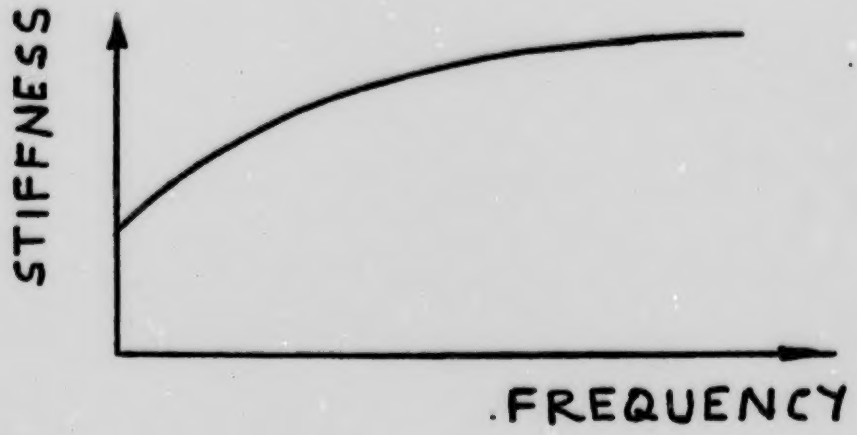

STRESS/STRAIN RELATION IS FREQUENCY DEPENDENT

ISOLATION OF A SDOF SYSTEM

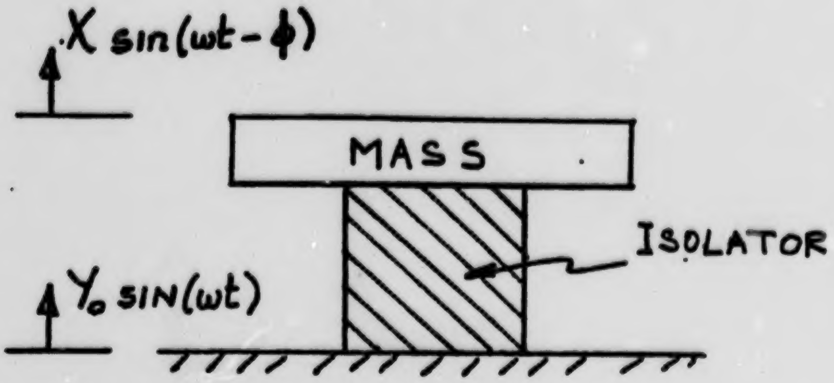

$X \sin(\omega t - \phi)$
MASS
ISOLATOR
$Y_0 \sin(\omega t)$

$$|\text{TRANSMISSIBILITY}| = \left|\frac{X}{Y_0}\right|$$

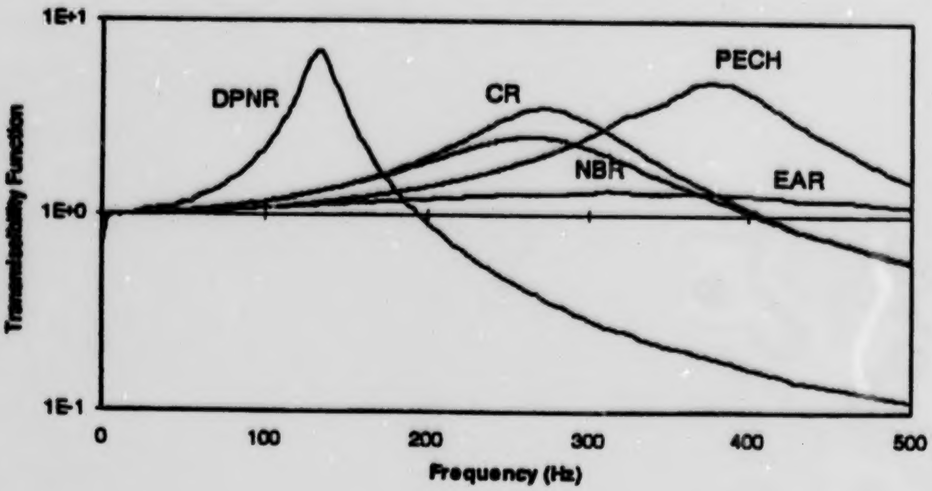

AT LOW FREQUENCY REQUIRE HIGH DAMPING BUT AT HIGH FREQUENCY REQUIRE LOW DAMPING (FOR SDOF SYSTEM)

VISCOELASTIC CONSTITUTIVE MODELS

1. GENERAL ONE DIMENSIONAL STRESS/STRAIN LAW:

$$a_1\sigma + a_1\frac{d\sigma}{dt} + \cdots \quad a_n\frac{d\sigma}{dt^n} = b_0\varepsilon + b_1\frac{d\varepsilon}{dt} + \cdots \quad b_n\frac{d^n\varepsilon}{dt^n}$$

or

$$\sigma(t) = E\left(\varepsilon(t) - \int_0^t \Gamma(t-\tau)\varepsilon(\tau)d\tau\right)$$

where $\Gamma(t-\tau) =$ RELAXATION KERNEL

$$= \sum_{i=1}^{n} c_i \; exp\left[-\alpha_i(t-\tau)\right]$$

where c_i and α_i must be determined experimentally

2. FOR HARMONIC EXCITATION AT *w* R/S

$$\varepsilon = \varepsilon_0 \; exp\left[iwt\right] \quad i = \sqrt{-1}$$

and $\sigma = E^*\varepsilon_0 \; exp\left[iwt\right]$

where $E^*(w) = E_1(w) + i\,E_2(w) =$ COMPLEX YOUNG'S MODULUS

$E_1(w) =$ STORAGE MODULUS

$E_2(w) =$ LOSS MODULUS

NEED TO MEASURE $E^*(w)$ OVER FREQUENCY RANGE OF INTEREST TO BE ABLE TO CONDUCT ANALYSIS

EXPERIMENTAL DETERMINATION OF VISCOELASTIC CHARACTERISTICS

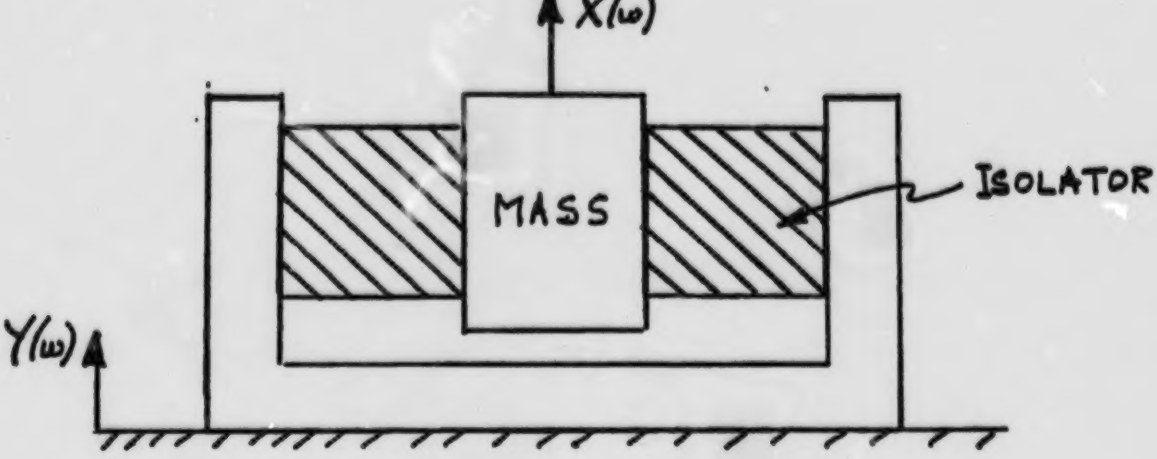

$Y(w)$ = INPUT EXCITATION
$X(w)$ = OUTPUT RESPONSE

1. TRANSMISSIBILITY = $\left|\dfrac{X}{Y}\right| = T^*(w) = T_1(w) + i\,T_2(w)$

2. DEPENDS UPON E^* COMPLEX YOUNG'S MODULUS
   G^* COMPLEX SHEAR MODULUS
   GEOMETRY OF TEST SAMPLES

3. USING FINITE ELEMENT ANALYSIS OF GEOMETRY AND KNOWING $T^*(w)$ CAN CALCULATE E^* AND G^*

CAN EXPERIMENTALLY DETERMINE $E^*(w)$ AND $G^*(w)$ OVER WIDE FREQUENCY RANGE

SPECIFICATION OF ISOLATION CRITERIA FOR MARINE DIESEL ENGINES SUPPORTED ON A FLEXIBLE FOUNDATION

The following factors need to be considered:

1. The Excitation Forces Produced by the Engine

2. The Three Dimensional Nature of the Engine Vibration Response

3. The Three Dimensional Nature of the Isolator Mounts

4. The Material Characteristics of the Mounts

5. The Response Characteristics of the Flexible Foundation

REQUIRE AN ACCURATE PREDICTIVE CAPABILITY TO INVESTIGATE THE ABOVE CHARACTERISTICS

VIBRATION ANALYSIS OF ENGINE ON VISCOELASTIC MOUNTS

1. We have developed a closed form solution to the free vibration response of viscoelastic materials for the case when the relaxation kernel is expressed as a sum of exponentials. This means we do not have to use expensive time stepping numerical integration schemes

2. We have developed a complete three dimensional dynamic analysis of engine forces that includes time dependent inertia terms not previously considered. Under conditions of high unbalance these terms can lead to the occurrence of unstable parametric resonances.

3. We have developed computer programs that

   a) uses finite elements (VAST) to analyse steady state response of an engine supported by viscoelastic isolators on a flexible foundation

   b) uses the engine model to (i) analyze the effect of different engine and isolator properties on response when the isolators are rigidly supported; and (ii) optimize the loss modulus as a function of frequency for given low frequency constraints on isolator displacements.

NUMERICAL RESULTS

EFFECT OF MOUNT GEOMETRY ON ENGINE VIBRATION RESPONSE

Engine Mount Stiffness Model:

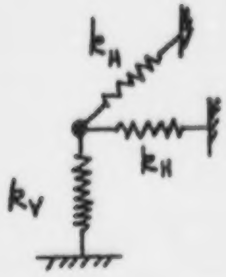

What is the effect of $\lambda = \dfrac{k_H}{k_V}$?

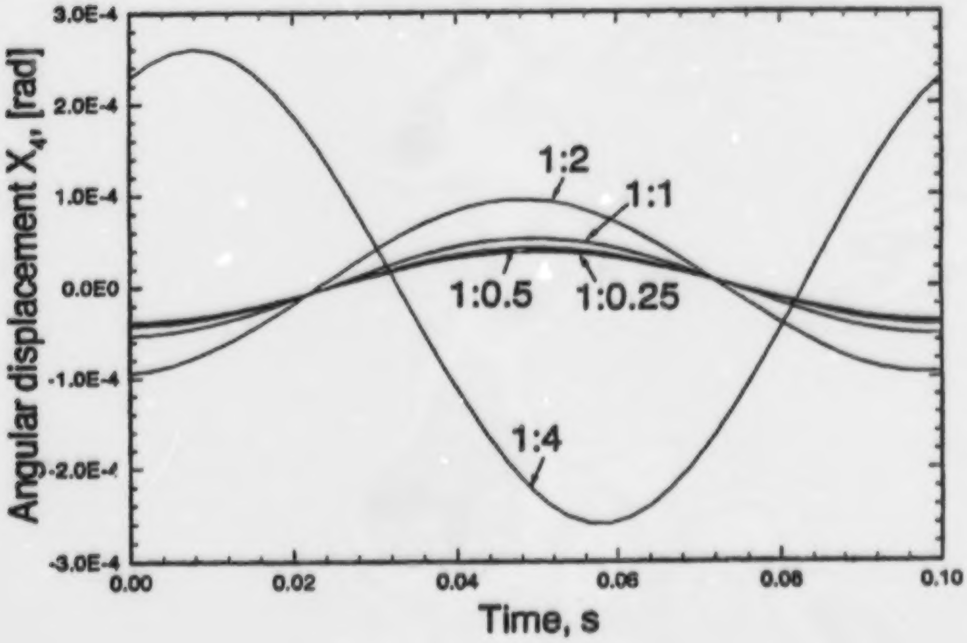

THE THREE DIMENSIONAL CHARACTER OF THE ISOLATION MOUNT MUST BE INCLUDED IN THE ANALYSIS

NUMERICAL RESULTS

EFFECT OF MATERIAL CHARACTERISTICS ON ENGINE VIBRATION RESPONSE

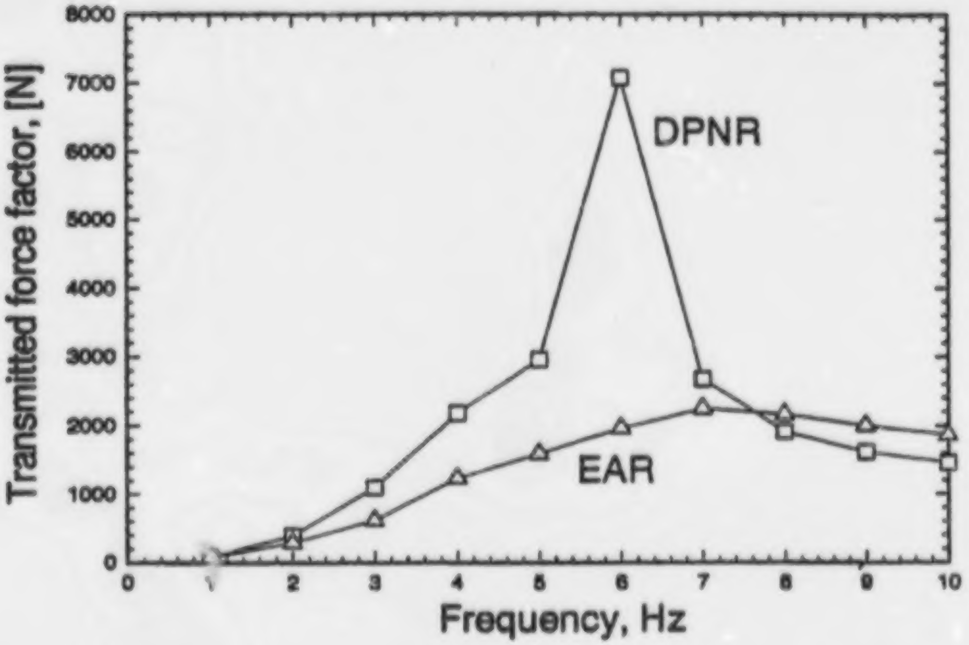

EXPERIMENTAL MODEL TESTING

EFFECT OF MATERIAL CHARACTERISTICS ON VIBRATION VELOCITY MEASURED ON FLEXIBLE FOUNDATION DUE TO SINE FORCE EXCITATION APPLIED TO ENGINE

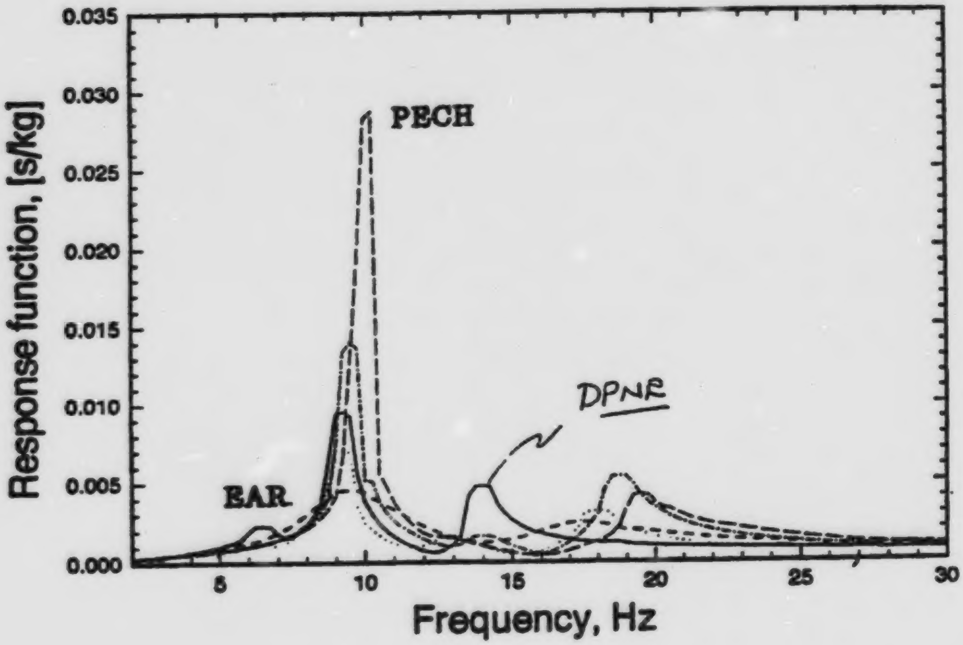

EXPERIMENTAL MODEL TESTING

COMPARISON OF NUMERICAL AND EXPERIMENTAL RESULTS

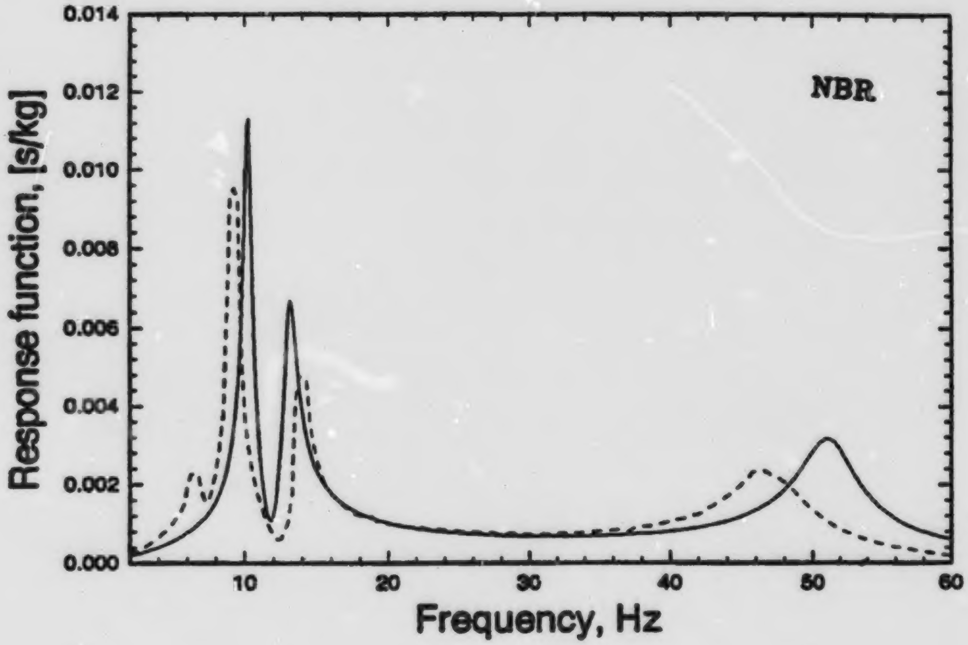

SUMMARY

In order to conduct an analysis of the vibration transmission through engine mounts the following are required:

1) Details of the engine geometry and its inertia characteristics
2) Accurate complex moduli data for the isolators
3) Geometric details of the isolator mounts
4) Foundation support structural details
5) Constraints upon maximum mount vibrations
6) Knowledge of other resonant vibrations that may exist

The work that has been conducted in the present contract has provided fundamental understanding of the issues involved and has developed the basic tools required to compare the behaviour of different mount materials

#587239 (36)

Modelling and Analysis of Active Vibration Control of Naval Structural Components

By Dr. T.S. Koko, Dr. I.R. Orisamolu, Dr. M.J. Smith and Dr. U.O. Akpan

Martec Limited, 1888 Brunswick Street, Suite 400
Halifax, N.S. Canada, B3J 3J8

ABSTRACT

Control of structural behaviour is often required in many naval applications. Examples include vibration control of ship machinery and noise suppression in ship and submarine structures. In the marine community, control is traditionally achieved by the use of passive controllers, such as externally attached absorbers or damping materials, which store or dissipate the energy of vibration. However, although passive control is desirable, it is insufficient in itself in preventing excessive vibration or the propagation of disturbances to remote regions of the structure. On the other hand active control techniques, which involve the use of sensors, actuators and control laws, are suitable when the disturbances to be suppressed excite a number of vibration modes or are of an uncertain or evolving character.

This study is concerned with the modelling and analysis of active vibration control of beams and plate structures. The sensors and actuators are made of piezoelectric materials which are bonded on to the surface of the structures. When subjected to mechanical strain the piezoelectric sensors produce an electric potential, which is first amplified using a suitable control law, and then applied to the actuators. The applied actuator electric potential is converted to a mechanical force which is used to control the structure. An integrated finite element based design/analysis tool, called SMARTCOM, has been developed to model the response and control behaviour of actively controlled structures. The method is based on a twenty-node piezoelectric finite element and control algorithms based on the independent modal control strategy and the linear quadratic regulator (LQR). The integrated finite element-control method is applied for simulating the open-loop and closed-loop responses of beam and plate structures subjected to transient loads. The results of the study have shown that SMARTCOM can be efficiently used for the design/analysis of actively controlled naval structural components.

#507240 (37)

Residual Stress Determination by Non-Destructive Methods
Sensors: Numerical Modeling and Construction

by

Dr. George Roy
CANMET/Materials Technology Laboratory
Ottawa, Ontario, Canada, K1A 0G1

ABSTRACT

Three methods of nondestructive residual stress determination, X-ray Diffraction (XrD), Magnetic Barkhausen Noise (MBN), and Electromagnetic Acoustic Transduction (EMAT) were used to determine known applied (through four-point jigs) stress states or residual stress states in steel and aluminum specimens and parts of steel engineering components. The results were compared with the stress states determined by two destructive methods, Hole Drilling Method (HDM), and Cut-and-Section Method (CSM).

There was a two-part objective of this study: 1) to assess the accuracy of the methods on known stress states, and 2) apply the methods to unknown stress states. The known stress states were applied to steel and aluminum specimens with simple geometries, such as slender bars and/or plates, instrumented with strain gauges, subjected to four-point bending, so that the surface stress components were calculated directly from strain readings and the unknown stress states were determined in such parts of engineering components as angled strips that are used to make high voltage transmission towers in Canada, and rolled steel that is used to make thin-wall pipes.

The known stress states in the instrumented steel plates were determined by MBN and XrD, and in the aluminum bars by EMAT and XrD, whereas the unknown stress states were determined in the rolled steel by XrD and HDM, and in the angled strips by XrD, MBN, HDM, and CSM. The results indicate an adequate correlation between the determined stress states within acceptable engineering error bounds of 5-10%.

To be able to tune EMAT sensors to work in steels, numerical modeling was applied to understand better their (EMAT's) impulse generation in magnetostrictive materials and acoustic wave propagation caused by the impulse.

Nondestructive Methods:

1) X-ray Diffraction;
2) Magnetic Barkhausen Noise;
3) Acoustoelastic -
   Electromagnetic Acoustic Transducers

Destructive Methods:
1) Hole Drilling; and
2) Cutting

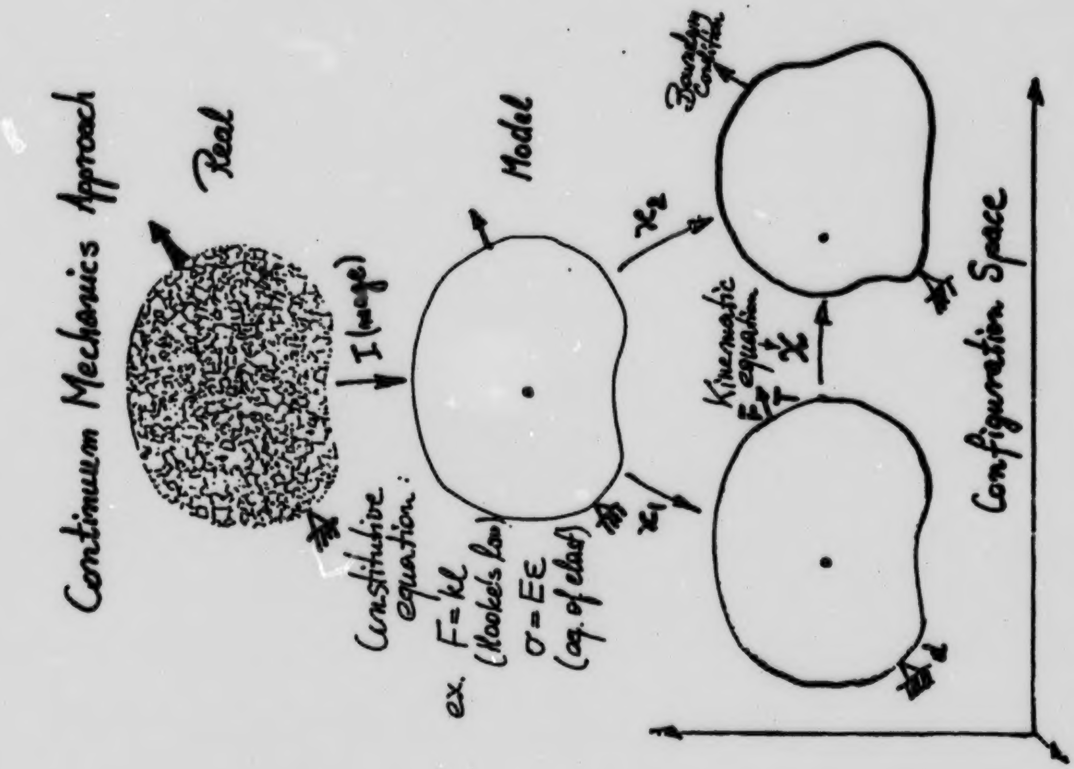
Continuum Mechanics Approach
Real
I(mage)
Model
Constitutive equation:
ex. F=kl (Hooke's law)
σ=Eε (eq. of elast)
χ1
χ2
Boundary Condition
Kinematic equation
χ
Configuration Space

Stress State

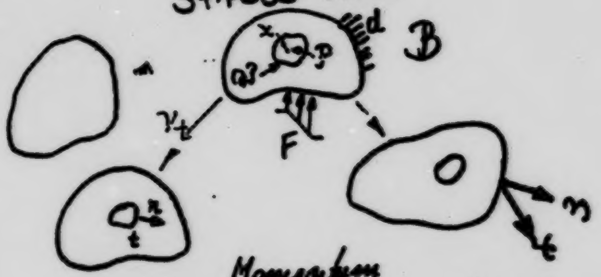

Momentum

$$\forall_t \forall_{P\subset B} \frac{d}{dt}\int_{\chi_t(P)} \rho v\, dV = \int_{\chi_t(P)} \rho b\, dV + \int_{\chi_t(\partial P)} t\, dS$$

Traction vector $\rightarrow t = \underset{\uparrow}{\tau} \cdot n \leftarrow$ normal vector to surface

Stress tensor

$$\forall_t \forall_{x\in B}\left(\frac{\partial v}{\partial t} + ((\nabla v))v\right) = \rho\dot{v} = \rho b \overbrace{\frac{\partial \tau_{11}}{\partial x_1} + \frac{\partial \tau_{21}}{\partial x_2} + \frac{\partial \tau_{31}}{\partial x_3}}^{+\operatorname{div}\tau}$$

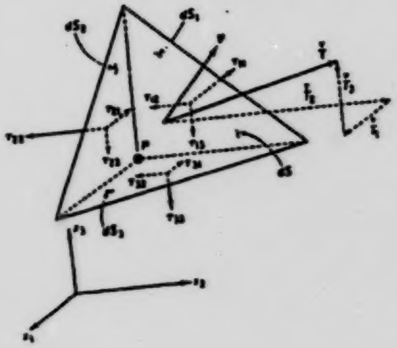

In static equilibrium $\dot{v}=0$.
If there are no body forces, $b=0$, then

$$\forall_t \forall_{P\subset B} \int_{\chi_t(\partial P)} t\, dS = 0$$

$t \rightarrow n\sigma \leftarrow$ stress tensor

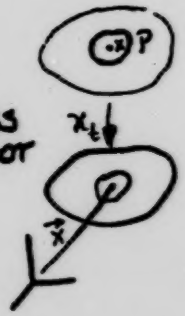

Moment of Momentum

$$\forall_t \forall_{P\subset B} \int_{\chi_t(\partial P)} \vec{x} \wedge t\, dS = 0$$

Exterior multiplication
$\vec{x}\otimes t - t\otimes\vec{x}$

Residual Stress – Stress State that results in the body if all external effects are removed

$\sin^2\psi$ - technique

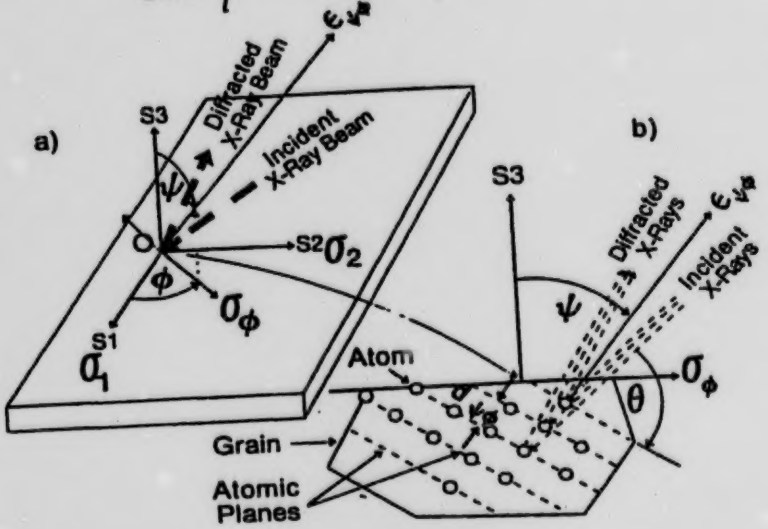

a)
b)
S3
S2
S1
Diffracted X-Ray Beam
Incident X-Ray Beam
$\varepsilon_{\psi\phi}$
ψ
ϕ
σ_2
σ_ϕ
σ_1
Diffracted X-Rays
Incident X-Rays
Atom
θ
Grain
Atomic Planes

a) Diffraction of X-rays, b) Angular relations between measured strain, stress state, and X-rays in a grain.

$$\varepsilon_{\psi\phi} = \frac{d_{\psi\phi} - d_o}{d_o} = \frac{1+\nu}{E}\sigma_\phi \sin^2\psi - \frac{\nu}{E}(\sigma_1 + \sigma_2)$$

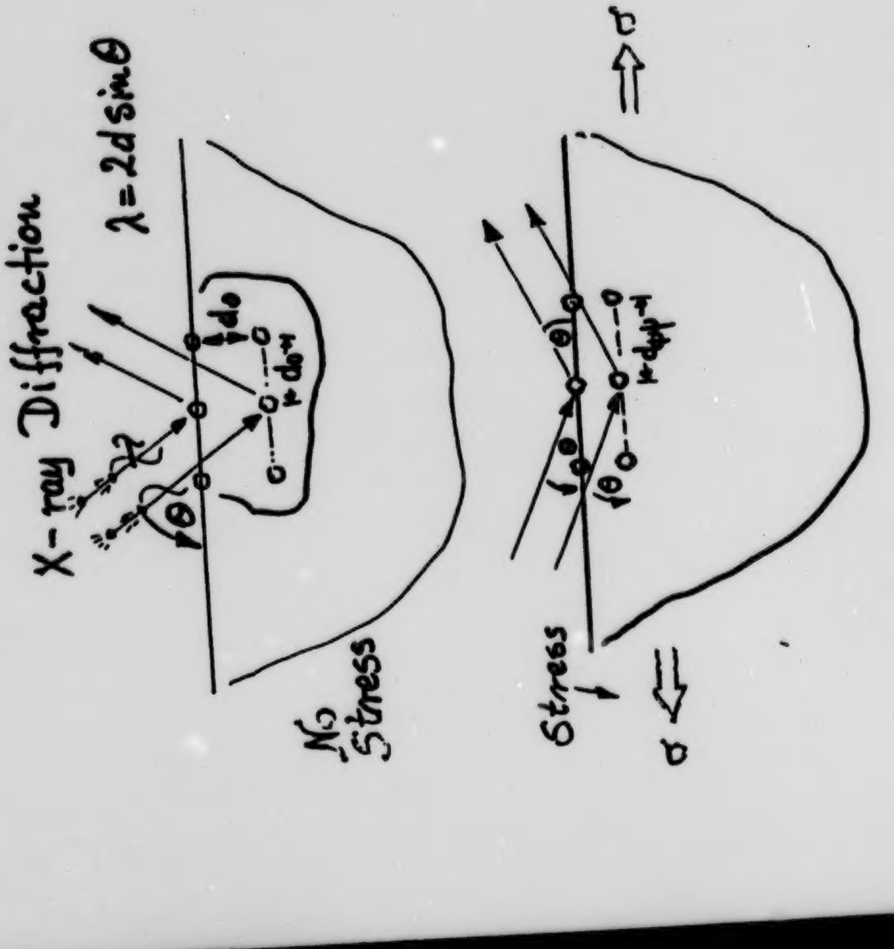

X-ray Diffraction
$\lambda = 2d\sin\theta$
λ
θ
d_o
No Stress
Stress
σ
σ
θ
$d_{\psi\phi}$

Magnetic Barkhausen Noise (MBN)

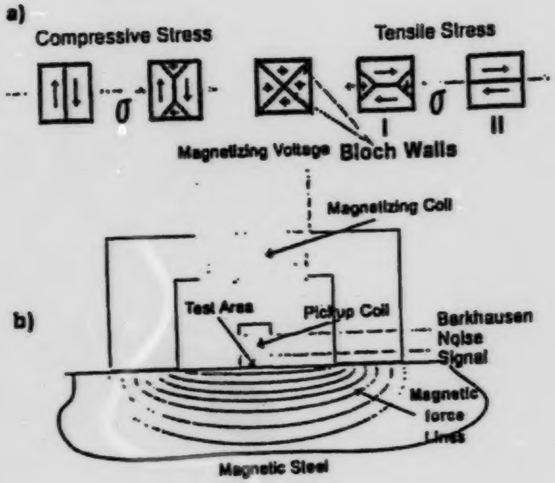
a)
Compressive Stress
Tensile Stress
σ
σ
I
II
Magnetizing Voltage
Bloch Walls
Magnetizing Coil
b)
Test Area
Pickup Coil
Barkhausen Noise Signal
Magnetic force Lines
Magnetic Steel

a) Effect of stress on displacement of magnetic domains along Bloch Walls, b) Setup to measure Magnetic Barkhausen Noise

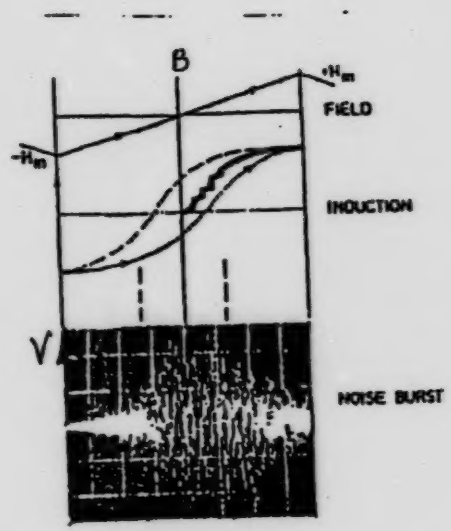

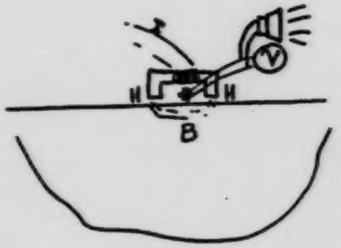

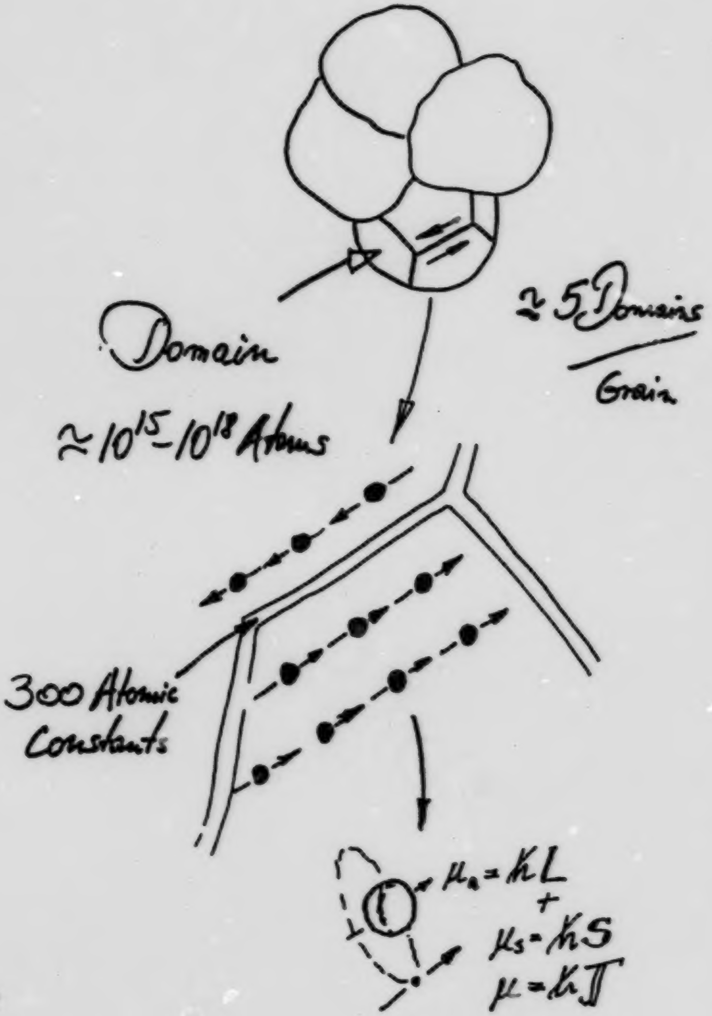
Domain
≈ 5 Domains / Grain
≈ 10^{15}–10^{18} Atoms
300 Atomic Constants
$\mu_a = kL$
+
$\mu_s = kS$
$\mu = kJ$

EMAT Stress Determination–
Surface Waves

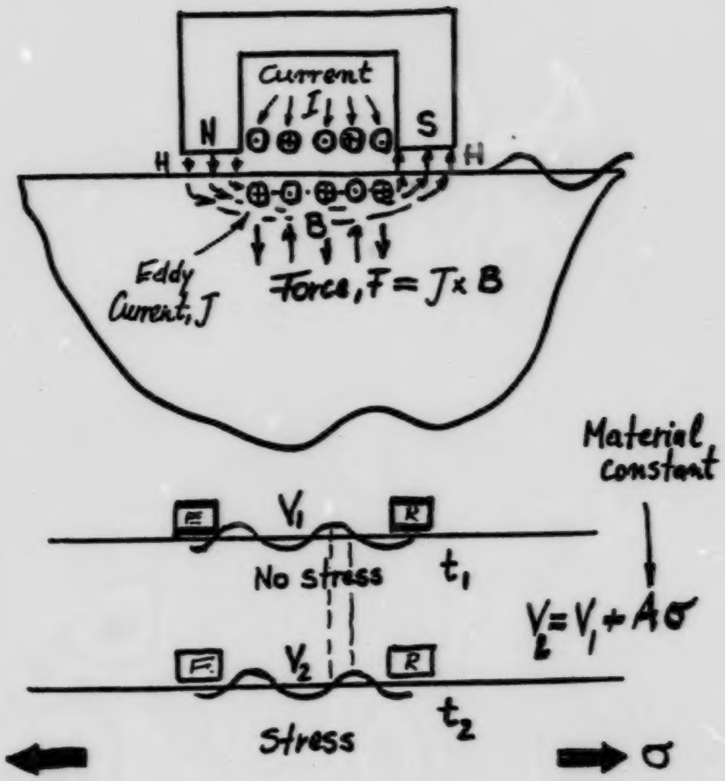
Current
I
N
S
H
H
B
Eddy Current, J
Force, F = J × B
Material constant
F
R
V_1
No stress
t_1
$V_2 = V_1 + A\sigma$
F
R
V_2
Stress
t_2
σ

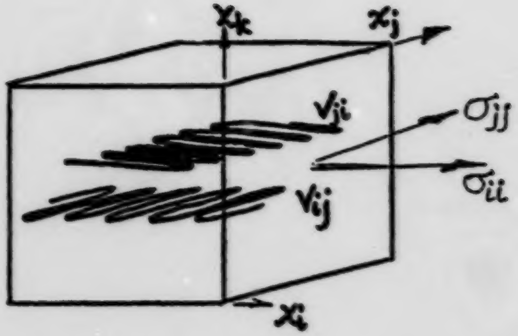
x_k
x_j
x_i
V_{ji}
V_{ij}
σ_{jj}
σ_{ii}

$$\sigma_{ii} - \sigma_{jj} = 2 C_{ij} C_{ij} \left(\frac{V_{ij} - V_{ji}}{V^{0}_{ij}} \right)$$

Hole Drilling Method

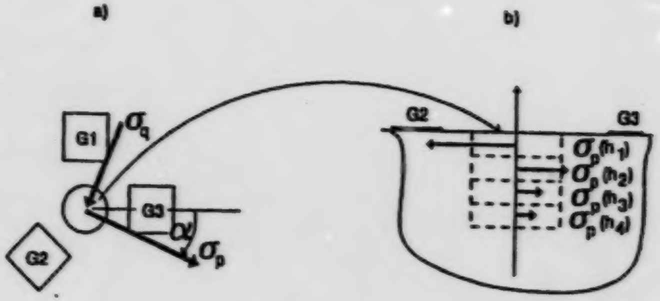
a)
b)
G1
G2
G3
σ_q
σ_p
α
G2
G3
$\sigma_p(h_1)$
$\sigma_p(h_2)$
$\sigma_p(h_3)$
$\sigma_p(h_4)$

a) Orientation of principal stresses with respect to rosette gauges, b) Residual stress distribution at four depths below the surface

Cutting and Sectioning

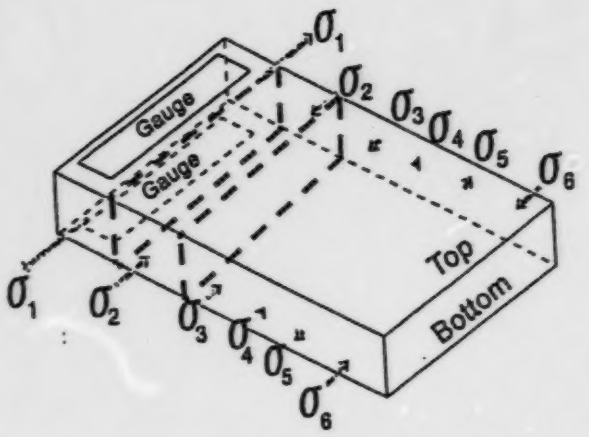
σ_1
σ_2
σ_3
σ_4
σ_5
σ_6
Gauge
Gauge
Top
Bottom

Layout of two blocks to be cut from the specimen with residual stresses.The top and bottom gauges are mounted on one block.

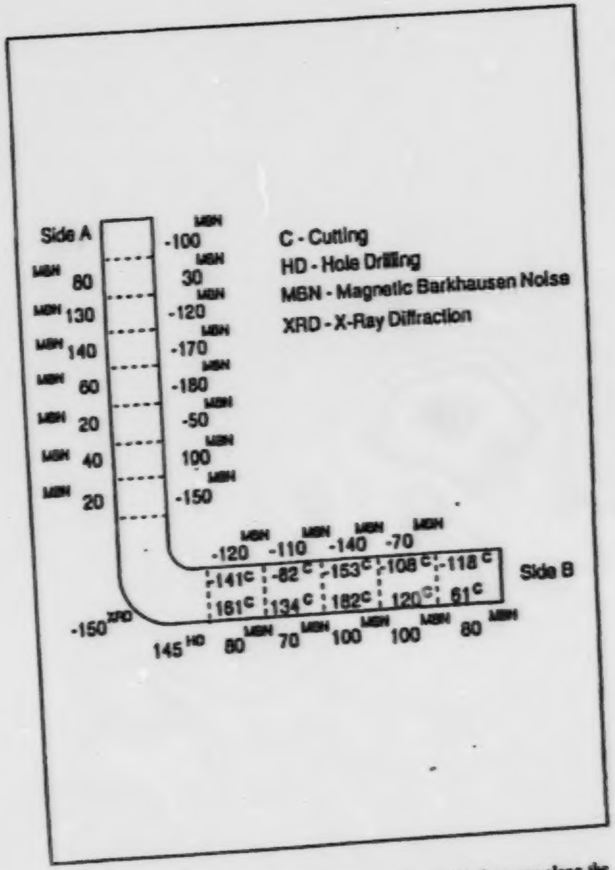
Side A
Side B
C - Cutting
HD - Hole Drilling
MBN - Magnetic Barkhausen Noise
XRD - X-Ray Diffraction
MBN 80
MBN 130
MBN 140
MBN 60
MBN 20
MBN 40
MBN 20
-100 MBN
30 MBN
-120 MBN
-170 MBN
-180 MBN
-50 MBN
100 MBN
-150 MBN
-120 MBN
-110 MBN
-140 MBN
-70 MBN
-141C
-82C
-153C
-108C
-118C
161C
134C
182C
120C
61C
-150 XRD
145 HD
80 MBN
70 MBN
100 MBN
100 MBN
80 MBN

Magnitude of the longitudinal components of surface residual stresses along the transverse direction in the specimen BA-109-21; all measurements in MPa.

#587241 ㊳

Measurement of Residual Stress, Plasticity and Fatigue in 350 WT Steels by Neutron Diffraction

T.M. Holden and J.H. Fox, Chalk River, ON, Canada K0J 1J0
and J. Pang and T.E. Mason, Physics Dept., Univ. of Toronto, Toronto, ON, Canada M5S 1A7

ABSTRACT

Neutron diffraction measurements have been carried out on 350 WT steel following cyclic loading to investigate the sensitivity of diffraction to fatigue loading. The first series of experiments showed that the measured line-broadening and residual strain correlated well with the degree of plastic deformation in the samples. The second series of experiments were designed to avoid plastic deformation during fatigue loading. Neither the strain nor the line-broadening were found to be correlated with fatigue parameters. A third set of experiments was designed to measure the strain response to applied stress below and above the yield point during tensile testing. The results have a bearing on the interpretation of any diffraction measurements of residual stress on engineering components.

1. Introduction

Portable diffraction techniques could provide an attractive non-destructive method of assessing the history of plastic deformation and the fatigue life of naval vessels by monitoring the residual strain or the diffraction linewidth at a sensitive location on the ship. The studies of 350 WT steel for the frigate program summarized in this paper were initiated by J.Porter to examine this possibility using the methods of neutron diffraction to measure the residual strain and linewidth. Neutron diffraction is analagous to X-ray diffraction, except that neutrons can penetrate 40 mm of steel whereas X-rays only penetrate the first few µm. This means that neutron diffraction is a probe of the whole volume of a sample and can be used to measure strain, texture and linewidth at depth, whereas X-rays from a conventional source give surface stresses, texture and linewidth.

Neutron diffraction has found increasing use over the past decade for solving industrial problems using the facilities at the NRU reactor, Chalk River operated by AECL. Since April 1st 1997 the neutron scattering program has become part of the Steacie Institute of Molecular Sciences of the National Research Council of Canada (NRCC) and is no longer part of AECL. As a result of this we have a wider mandate to serve Canadian industry with the resources of the NRCC behind us as well as preserving our contacts with expertise at Chalk River.

In this paper we summarise first the results of linewidth measurements on 350 WT steels, which showed a strong sensitivity to plastic deformation [1,2] This could have masked a dependence of width and residual stress on the fatigue parameters stress, S, and number of cycles, N, in high cycle fatigue. A second set of experiments [3] were designed to test the sensitivity to S and N in the absence of plastic deformation. We also report preliminary results of tensile test experiments on 350 WT steel at stresses below and above the yield point. These give the strain response of different crystallographic orientations of grains to the applied stress under conditions of plastic deformation. The results have a bearing on any diffraction stress measurements. They also provide test data for constitutive models of the material where the macroscopic properties of an element in a finite element array are calculated from the elastic and plastic behaviour of its constituent grains.

2. Experiments

2.1 Samples

2.1.1 Fatigue at High Maximum Stresses

The samples for the first series of experiments were cut from 350WT plate and fatigue-tested by Fleet Technology Ltd. The material exhibited an (upper) yield point of 480 MPa and an ultimate tensile strength of 546 MPa. Eleven standard hour-glass samples were fatigue-tested at stress ranges between 420 and 498 MPa with a stress ratio of 0.05. Nine of the eleven samples were tested to failure. It was noted that the diameters of the samples were reduced with respect to the pre-fatigue diameters indicating that plastic deformation had occurred. In addition to these samples a further five samples were studied whose fatigue history was not provided to us, and an unfatigued reference sample. Three of these had reduced diameters and had therefore been plastically deformed.

2.1.2 Fatigue at Low Maximum Stresses

The samples for the second series of experiments [3] were cut from a different plate of 350WT steel provided by Fleet Technology Ltd. The flow curve was measured at Chalk River and was characteristic of a carbon steel with a lower yield point of 425 MPa, an upper yield point of 470 MPa and an ultimate tensile strength of 519 MPa. The design of the second experiment required that there should be no plastic deformation to mask the fatigue effects so a symmetrical stress range was chosen with maximum values well below the yield point. With the aid of the "Atlas of Fatigue" [4] it was estimated that the stress ranges given in Table 1 would lead to the postulated number of cycles to failure. Measurements were made at 25%, 50%, 75% and 100% of these numbers of cycles in five samples together with a standard reference sample.

Table 1

Stress Range (MPa)	% of fracture strength	# of cycles
±235	45	10^6
±245	47	10^5
±255	49	5.10^4
±275	53	10^4
±295	57	10^3

2.2 Neutron Diffraction

The experiments were carried out on spectrometers at the NRU reactor at Chalk River employing neutrons of wavelength near 2Å reflected from the (331) planes of silicon and germanium monochromators. The incident and diffracted beams were highly collimated and gave instrumental linewidths of 0.26° and 0.22° for the first and second experiments respectively. To obtain high precision in the measured strains and linewidths, the maximum intensity in the peak was several thousand counts and the time to accumulate each peak was about eight hours. The samples were mounted vertically on a sample changer and the diffraction response studied was perpendicular to the direction of stress applied during the fatiguing of the samples. The peak position, 2θ, the integrated intensity and the linewidth, Δ_m, were obtained by fitting a Gaussian peak plus a sloping background to the data of counts versus angle. In a diffraction experiment, the spread of wavelengths and the finite collimation contribute to an instrumental linewidth, Δ_I .The instrumental linewidth was determined from the linewidth of the reference sample. The intrinsic linewidth due to plasticity or fatigue is found by subtracting Δ_I from Δ_m in quadrature as follows,

$$\Delta^2=\Delta^2_m-\Delta^2_I \qquad (1)$$

The lattice spacing is found from the angle of diffraction, 2θ ,with the aid of Bragg's law knowing the wavelength, λ, as follows,

$$\lambda=2d\sin(\theta) \qquad (2)$$

The strain is calculated with respect to the reference lattice spacing d_{ref} as follows,

$$\varepsilon=(d-d_{ref})/d_{ref} \qquad (3)$$

The precision of a typical linewidth measurement is about ±0.004° and the precision of the intrinsic linewidth is about ±0.015°. The precision of a strain measurement, taking into account the uncertainty in both the sample and the reference is about $\pm 0.8.10^{-4}$.

2.3 Results

2.3.1 Fatigue at High Maximum Stresses

For the samples which had broken under fatigue testing the diameters decreased towards the surface of the sample, so that the plastic deformation increased as the fracture surface was approached. Measurements of linewidth and residual strain were made as a function of distance from the fracture surface and it was found that the linewidth increased as the break was approached[1]. Measurements were also made on the six unbroken samples at the mid-height of the sample and 5mm above and below the mid-height. The intrinsic linewidth and the residual strains for all these samples are plotted against the plastic deformation deduced from the diametral reduction in Figs. 1 and 2. The intrinsic widths for all samples and positions fall on a single master curve when plotted against plastic deformation. A similar master curve is observed for the compressive residual strains, although there is more scatter. It was concluded from this series of experiments that the width was a good indicator of plasticity, but that the dependence on plasticity would mask any dependence on fatigue parameters.

2.3.2 Fatigue at Low Maximum Stresses

The differences between the linewidth in the fatigued samples and the reference sample for the measurements at 25%, 50%, 75% and 100% of the nominal fatigue life are shown in Fig. 3. Note that the absolute differences are plotted rather than the differences in quadrature. This is because the widths are scattered about the reference value and are as likely to be positive as negative. Within the experimental uncertainty we have observed no change in the diffraction linewidth. Likewise, to within the experimental uncertainty there was no fatigue-induced residual strain. There was no change of sample diameter and therefore no plastic deformation.

2.3.3 Tensile Test Experiments

Standard dogbone samples were cut from the second plate, see section 2.1.2, and mounted in an automated Universal Testing Machine installed on a spectrometer at the NRU reactor, Chalk River. Measurements were made on three samples oriented so that the strains were measured along the plate transverse direction (TD), the plate rolling direction (RD) and the rolling plane- normal direction (RPN).In each case the applied stress was applied along the rolling direction. An extensometer was mounted on the sample to measure the total strain in the direction of the applied stress. The UTM was operated in a constant stress mode. At each stress the (002),(112),(220) and (222) diffraction peaks were measured and the lattice spacing ,width, and peak intensity obtained. The initial lattice spacing for each reflection was obtained by extrapolation of the initial elastic response to zero stress. Measurements were made below the yield point to obtain the diffraction elastic constants and above the yield point to a maximum stress of 475 MPa to observe the development of the intergranular strains. Figure 5 shows the axial strain response parallel to the stress direction for the (220) and (002) peaks. For the (220) case there is little departure from the linear elastic behaviour even above the yield point. However, for the (002) case there is a strong departure from the linear response above the yield point and upon unloading to zero stress there is a sizable residual tensile strain. For the (112) reflection essentially no residual strain is observed and for the (222) reflection a tensile strain is recorded. These effects are not macroscopic strains but are intergranular or Type 2 strains on the scale of the grain size. They originate in the different plastic and elastic response of grains of different crystallographic orientations to an applied stress which exceeds the yield point. The sum of all these grain stresses in a given direction would be expected to balance to zero and the observation of some positive and some negative strains indicates that this is the case qualitatively.

The response perpendicular to the applied stress has also been obtained after cycling to 475 MPa and in this case the (220) strain is compressive, $(-3.5\pm1).10^{-4}$, while the (002) transverse strain is still tensile, $(3\pm1).10^{-4}$. Recall that the strain response perpendicular to the fatigue axis in the first series of experiments, Fig.2,was also compressive so that the two very different experiments are in agreement. The intergranular residual strains in the direction of the applied stress in the unloaded state observed for all four reflections are plotted in Fig. 6 as a function of the plastic strain. Use is made in Fig. 6 of two intermediate cycles of stress versus strain not shown in Fig.4. The results clearly show that (112) exhibits the smallest intergranular strain, that (220) grains show a slightly tensile effect, (222) grains show a compressive effect and (002) grains show a strong tensile effect. When measurements are made of an engineering component, the measured strain is the sum of Type 1, macrostrains and Type 2, intergranular strains and there is no non-destructive way of distinguishing them. If this measured strain is used with the other orthogonal components, together with the appropriate diffraction elastic constants, the calculated stresses will not be the macrostresses of interest to the engineer but a combination of macrostresses and microstresses. It is important to use reflections which are least sensitive to intergranular strains or to correct the data for the intergranular part. This work forms part of the Doctoral thesis of J.W.L. Pang at the University of Toronto.

4. Discussion

The physical manifestation of fatigue damage is the appearance of slip-bands on the surface of a sample which has been highly polished. Since, in high-cycle fatigue, the applied stress never exceeds the yield point local stress-risers have to be present to generate localized plastic deformation. This, in turn, generates localized slip-bands, particularly near the sample surface. However the depth of the slip-bands is only of order 10μm. Neutron diffraction probes the whole volume of a sample, by virtue of the high penetration of the neutron . On the basis of the fraction of the total volume represented by a continuous 10μm surface region, about 1% at most, neutron diffraction is insensitive to surface-localized deformation. On the other hand, X-rays are sensitive to the surface layers because of their 2-3μm penetration. However, one still has to locate the slip-band region. Previously X-rays have been used to detect fatigue damage under special conditions. The perfection of crystal alignment is destroyed by fatigue, and this appears as an increase in the mosaic spread of the sub-grains making up a single grain. Holden [5] looked inside a fatigue crack, where slip-bands are sure to be present, with an X-ray beam of order the size of the grains and observed the development of misalignment of the sub-grain structure. Regular powder diffraction from a polycrystalline sample does not give the required result since many grains are sampled, which are nearly randomly oriented and any further sub-grain misorientation is essentially masked.

5. Acknowledgements

We wish to acknowledge the help of R. R. Hosbons in arranging for the fatigue tests and for his advice on the microstructural effects of fatigue. A.P. Clarke played an important role in distinguishing between the effects of plasticity and fatigue in the first series of experiments. J. Porter initiated this work and provided strong support for it.

6. References

[1] A .P. Clarke, T. M. Holden and J. H. Fox, Available AECL report, ANDI-100, Sept. 1995.

[2] A.P.Clarke, T.M.Holden, J.F. Porter and R. Yee, Proc. Of the 2nd Canadian Forces/CRAD Meeting on Naval Applications of Materials Technology, 1995 May 2-4..

[3] T. M. Holden and J.H. Fox, Available AECL report, ANDI-108, March 1997.

[4] H. E. Boyer, "Atlas of Fatigue", (A. S. M. :Metals Park, Ohio) 1986, p28.

[5] J. Holden, Phil. Mag. 61, 547, 1961.

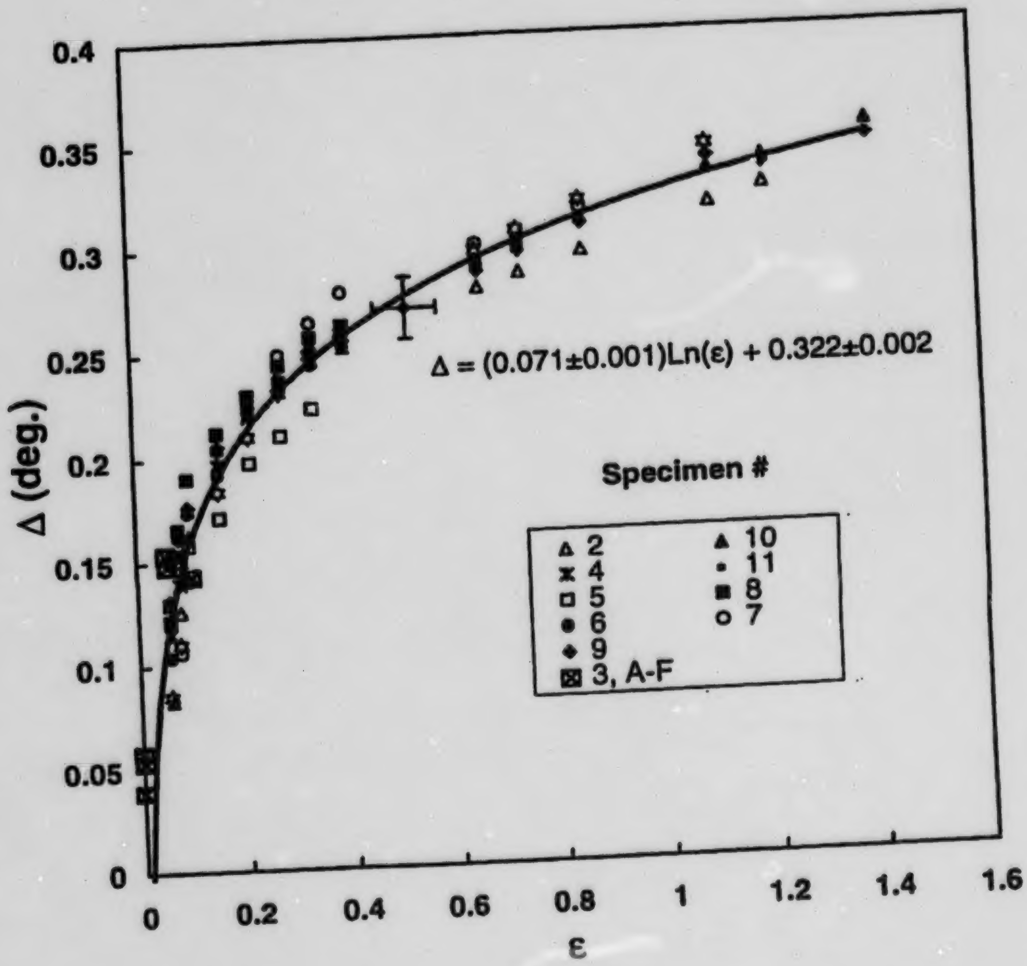

Fig. 1 Intrinsic linewidth versus plastic deformation for samples of 350WT steels fatigued at stresses close to and exceeding the yield point.

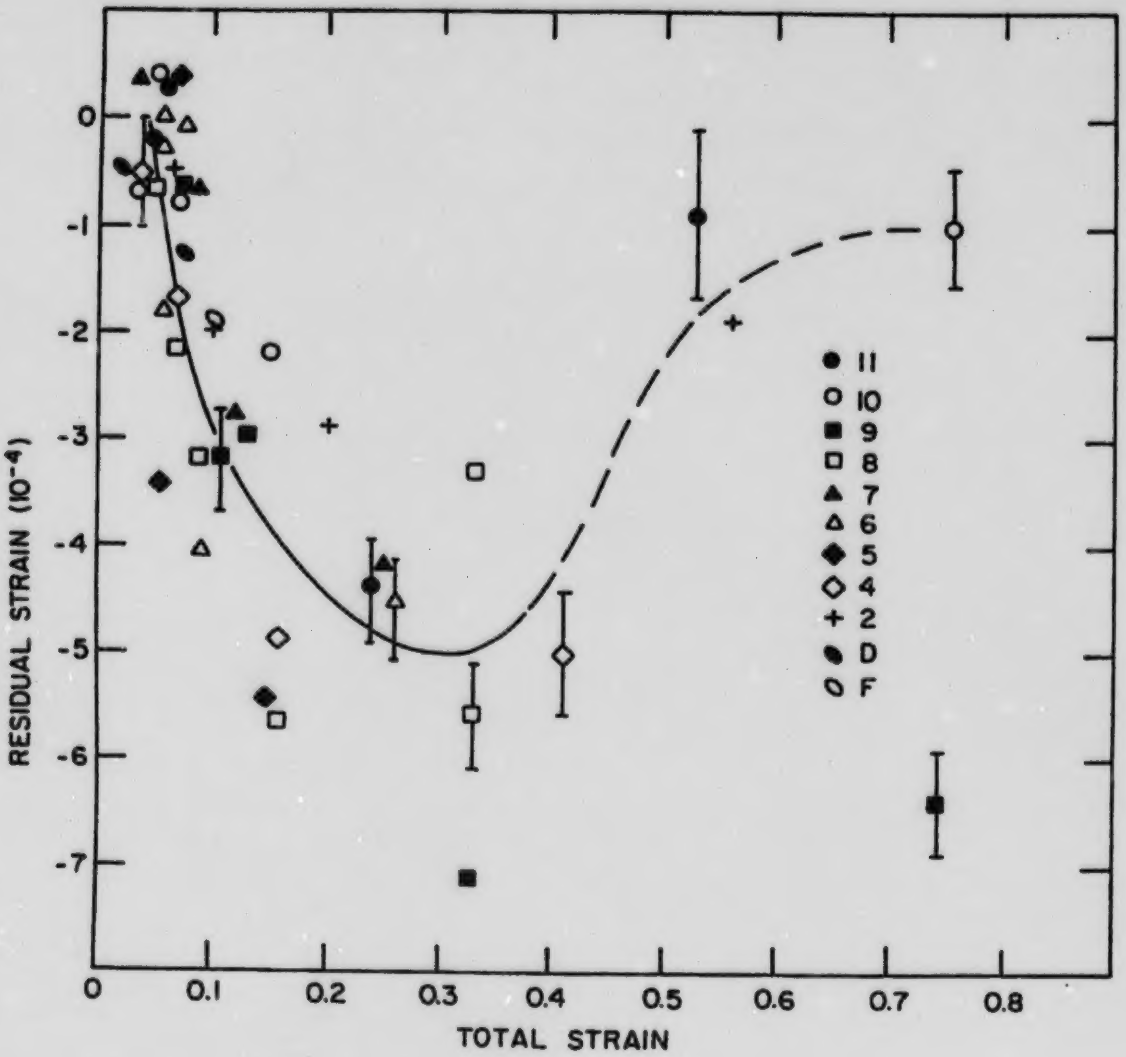

Fig.2 Residual strain versus plastic deformation for samples of 350WT steels fatigued at stresses close to and exceeding the yield point.

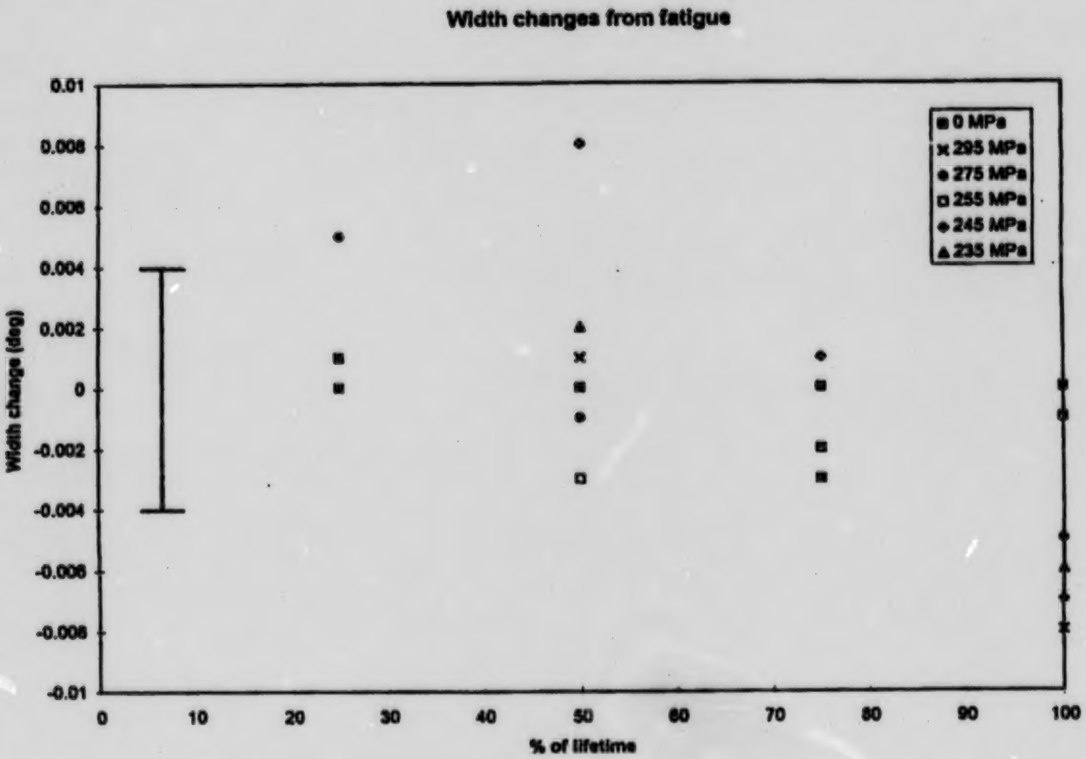

Fig. 3 Differences between linewidths of 350WT samples and a reference sample after fatiguing with no plastic deformation.

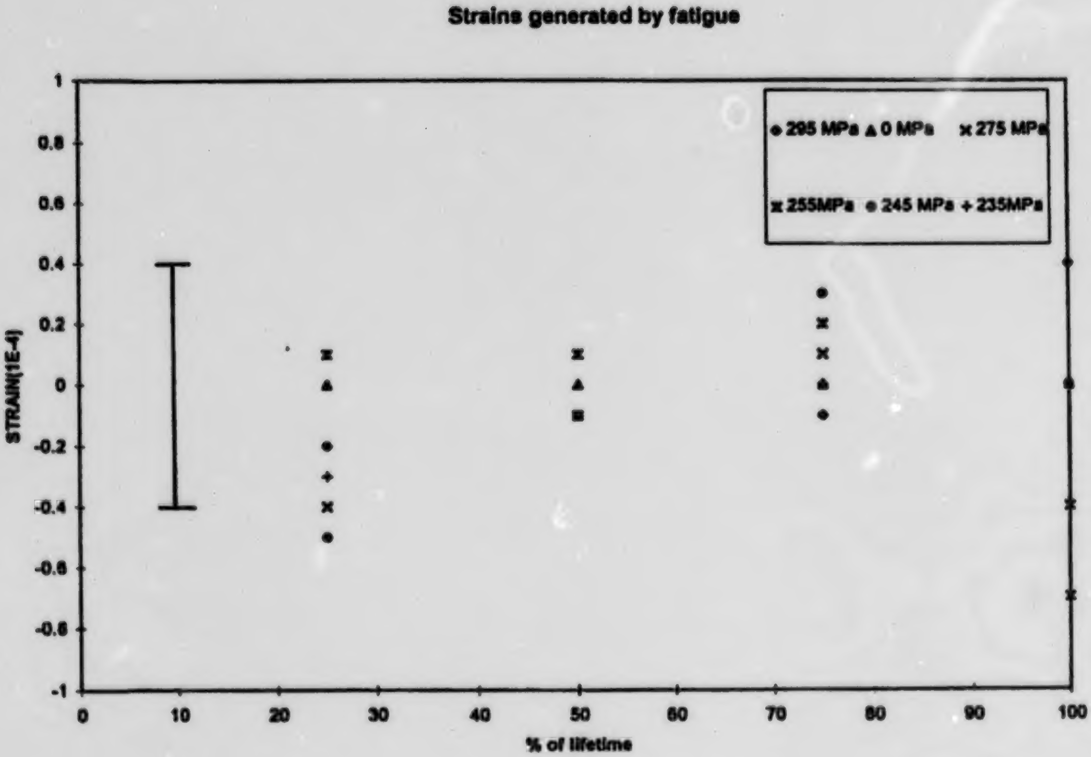

Fig. 4 Residual strains in 350WT samples with respect to a reference sample after fatiguing with no plastic deformation.

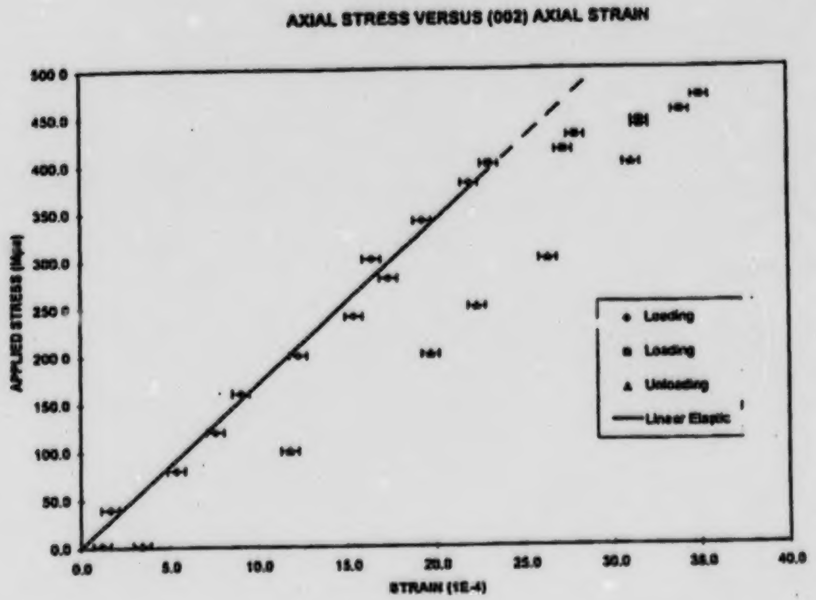
AXIAL STRESS VERSUS (002) AXIAL STRAIN

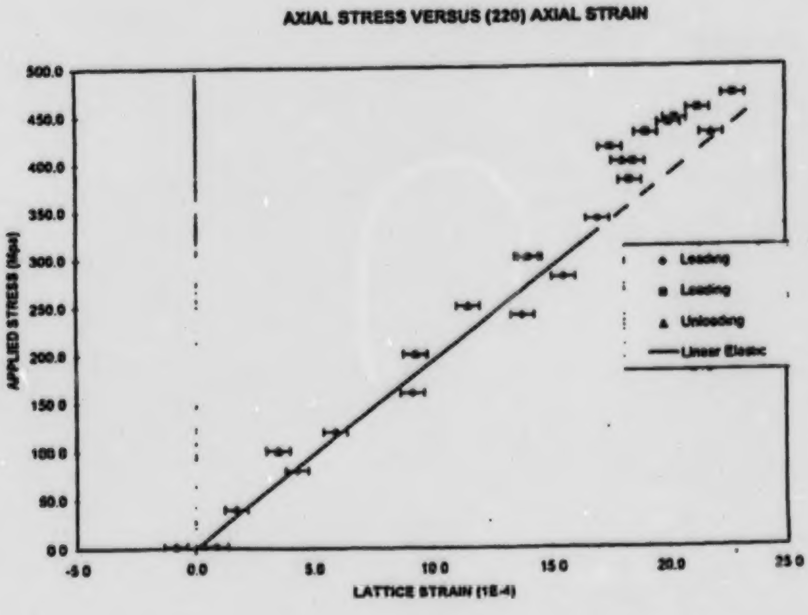
AXIAL STRESS VERSUS (220) AXIAL STRAIN

Fig. 5 Applied stress versus lattice strain for (220) and (002) grains in 350WT tensile test samples. The strain component measured is parallel to the stress axis.

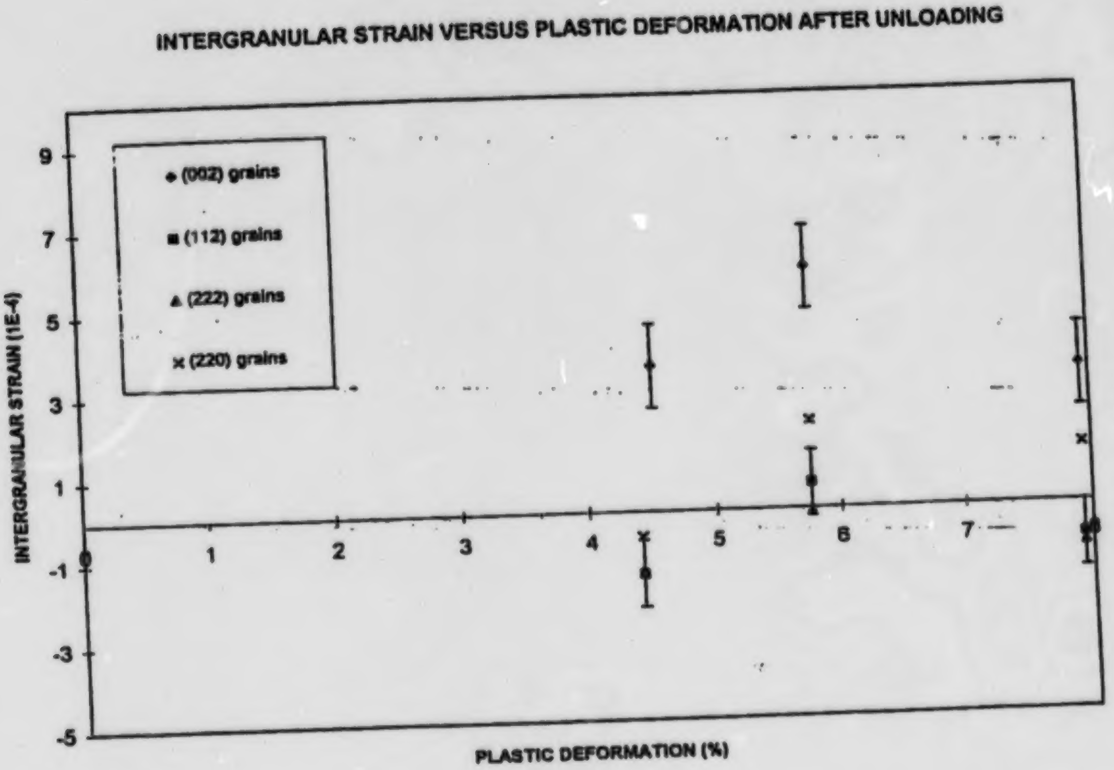

Fig. 6 Intergranular residual strain in 350 WT samples in the direction parallel to the stress axis as a function of plastic deformation.

#507242 (39)

An Overview of Some Current Research on Welding Residual Stresses and Distortion in the U.S. Navy

by

J.M. Blackburn
Naval Surface Warfare Center
West Bethesda, MD

M. Kirk, P.C. Conrardy, Michelaris, A,
DeBiccari, & Zheli Feng
Edison Welding Institute
Columbus, OH

P. Brand
University of Maryland
College Park, MD
Guest Researcher at NIST

H. Prask & R. Fields
National Institute of Standards and Technology
Gaithersburg, MD

R. Hendricks
Virginia Polytechnic Institute
Blacksburg, VA

M. Kleinowski, M. Tims, P. Kain,
L. Knipple, & D. Moyer
Concurrent Technologies Corp
Johnstown, PA

T. Zacharia
Oak Ridge National Laboratory
Oak Ridge, TN

Y.Y. Zhu
ANSYS, Inc
Houston, TX

J. Cohen & John Almer
Northwestern University,
Chicago, IL

R. Winholtz
University of Missouri
Columbia, MO

presented by Paul Holsberg
Naval Surface Warfare Center, West Bethesda, Maryland

ABSTRACT

This paper describes some of the current U.S. Navy efforts geared toward managing residual stresses and distortion during weld fabrication. These efforts include model development, model verification, thermo-mechanical and thermo-physical property development, the generation of residual stress measurement data using x-ray and neutron diffraction techniques, the analysis of the effects of residual stresses on fatigue and stress corrosion cracking, and the use of weld residual stresses to achieve desired shapes in part manufacturing.

Due to the complexities involved in weld residual stress development, significant emphasis has been placed on modeling. The importance of experimental data for model development and validation has been emphasized. It was shown that there were some differences between FE models and experimental results, but in general both were in good agreement. However, it was also shown that residual stress development is highly dependent upon the details of the fabrication process and the material properties and characteristics. Little difference between thermo-mechanically coupled and uncoupled FE results were demonstrated, but additional work is necessary since the work presented here did not include phase transformation effects or varying material properties representative of remelted or reheated material.

Careful experimental techniques for measuring residual stresses must be employed to obtain reliable neutron diffraction and x-ray diffraction results for comparing to model analysis. It was shown that welding creates a wide variation in material properties, and can therefore significantly affect measurement results. This was attributed to dilution and thermal cycling that occurs during welding. It was also shown that when analyzing x-ray diffraction results, it is important to realize that the technique is a surface analysis method and can therefore be influenced by surface conditions. Grinding stresses played an overwhelming role in masking the surface residual stresses developed by welding. However, the grinding stresses were able to be subtracted from the overall stress state to determine the surface stresses due to welding only. A comparison of surface residual stresses and bulk, through thickness stresses indicated that the surface stress state is not representative of the internal stress state.

The application of an empirical model to the distortion of stiffened thin section panels provided useful information relative to the options available for mitigating distortion. It was shown that simply reducing heat input was not feasible,

but intermittent welding and thermal tensioning could provide the desired reduction in distortion. The data generated by this empirical model also suggested that the initial plate flatness could also provide some benefit regarding distortion mitigation.

In a study on the effects of residual stresses on fatigue, it was shown that residual stresses play an important role in determining fatigue properties of materials. It was also shown that there was no difference in the fatigue crack growth rate of specimens containing residual stresses and those that did not. This was because the crack tip stress field appeared to obliterate the existing residual stresses out to about 1mm ahead of the tip so that the growing crack is never subjected to these stresses. In another study, weldments were subjected to SCC conditions. This study showed no crack initiation and limited crack growth as a result of weld residual stresses. However, this study was inconclusive due to crack location discrepancies and the possible existence of compressive residual stresses in the crack tip areas.

Introduction

Weld Residual Stress Formation

The formation of weld residual stresses is quite complex. Residual stress development and distribution are dependent on nearly every variable associated with weld fabrication as well as the mechanical and thermo-physical properties of the materials involved. This is because these variables directly affect the two basic factors which determine residual stress development: differential contraction and volumetric phase changes. Some of the variables are listed below:

- *Material Thickness*
- *Joint Geometry*
- *Welding Process and Parameters*
- *Heat Input*
- *Restraint*
- *Bead Sequencing*
- *Preheat and Interpass Temperature*
- *Welding Position*

Although the qualitative effects of welding variables affecting residual stresses are understood independently, it is the complex interactions which pose the greatest difficulty in predicting the quantitative outcome for a given set of conditions. However, some advances have been made in this direction and are the topic this paper.

Cracking Concerns

For the most part, the existence of tensile residual stresses in welded structures is considered undesirable. The presence of residual stresses can lead to cracking which can ultimately result in structural failure. Some types of cracking which can occur due to the presence of residual stresses are listed below:

- *Solidification and Hot Cracking*
- *Hydrogen Cracking*
- *Stress Corrosion Cracking*
- *Fatigue Cracking*
- *Corrosion Fatigue Cracking*

Weld residual stresses can contribute to the initiation. propagation or acceleration of these cracking types. The ability to know or control any one of the conditions that contribute to the onset of cracking is a distinct advantage in controlling the outcome. Unfortunately, the precise level and distribution of residual stresses are seldom known.

Design Concerns

It is common practice in design, or fitness-for-service assessments to assume yield level residual stresses in the absence of actual measurements. It is also difficult to determine the distribution of stresses under any one set of conditions. This can lead to excessively conservative results. For example, a structural member may require a greater thickness due to the assumption of yield level residual stresses, when, in fact, less than yield level residual stresses are present. Therefore, the thicker design requirement results in a heavier structure. In some cases additional weight may come with no other sacrifice, but in the case of shipbuilding, additional weight means slower speeds, increased fuel consumption, and a decreased capacity for additional future equipment. It is therefore desirable to optimize design and fitness-for-service analyses by utilizing appropriate inputs relative to residual stresses and their distributions.

Distortion Concerns

The trend in both military and commercial shipbuilding is to increase the use of higher strength steels. This means that thinner sections can be utilized to achieve the same structural load carrying capacities while reducing structural weight, thereby increasing payload capacity, reducing fuel costs, and increasing speed.

The cost of lighter weight structures comes at a large cost in terms of distortion control. It has been estimated that distortion costs $3.4 million per ship. [1] This cost includes labor costs for flame straightening, and other down-stream effects associated with replacement of materials, interruption of other trades, and increased fitting time. Once the ship is underway, distortion can also reduce hydrodynamic performance, causing decreased speed and increased fuel consumption. Distortion is also detrimental to the buckling resistance, thus reducing the capabilities and load carrying capacity of a ship.

Prevention, Control and Correction of Weld Residual Stresses and Its Adverse Side Effects

There are several methods that have been used to deal with the adverse effects of weld residual stresses. The methods have been quite diverse but they can be defined by three basic categories. They are 1) preventive, 2) control, and 3) corrective measures. The term "preventive," as used here, means to minimize the development of weld residual stresses in order to reduce or eliminate adverse side effects (*e.g.* minimize fillet weld size to reduce the amount of shrinkage to the point of reduced distortion). The term "control," means to manage the effects of residual stresses to the point of a desirable outcome (*e.g.*. presetting a butt welded plate to achieve a flat plate at the completion of welding). "Corrective" means to reverse the outcome in order to minimized or reduce the adverse side effect.(*e.g.* flame straightening of thin section panels subsequent to welding to reduce distortion within fairness requirements). Some methods for dealing with the adverse side effects of residual stresses, which have been used in the past, or are being considered for use by the U.S. Navy are listed below in Table 1.

Table 1. Some methods for preventing, controlling, and correcting weld residual stresses and their adverse effects.

Preventive	**Control**	**Corrective**
Minimize Weld Size/Heat Input	Pre-bending or Presetting	Flame Straightening
Thermal Tensioning	Back-stepping/Wandering	Post-heating
High Speed Welding	Bead Sequencing	
Intermittent Welds	Increased Restraint	
Flatter Plate	Chilling	
Mechanical Tensioning		
Preheating		
Dimensional Accuracy Control		

The ideal solutions are methods that are preventive. These methods reduce the development of residual stresses and hence the propensity for adverse side effects. Other methods counteract the anticipated side effect but do not necessarily reduce or eliminate the propensity for residual stress development. Therefore, their effects can be temporary. For example, it has been the experience of the U.S. Navy that some thin section bulkheads require repeated flame straightening at various stages of assembly in order to meet unfairness requirements. This is probably due to the fact that the residual stresses are not being removed by flame straightening, but rather redistributed. This redistribution results in free plate edges which are wavy in nature. These wavy edges must then be forced into position for welding to the adjacent plate. At the completion of ship assembly and after several flame straightening events, the final structure must also be flame straightened to meet unfairness requirements. This process of fixturing, welding and flame straightening is a viscious cycle that only aggravates the overall residual stress situation. The ability to minimize residual stresses and distortion from the initial stages of fabrication would diminish the cumulative effects throughout the complete assembly.

Some Positive Aspects of Weld Residual Stresses

In most cases, the existence of residual stresses is considered to be detrimental. However, not all residual stresses have negative effects. The presence of compressive stresses can provide positive effects in terms of material performance. Since tensile stresses are necessary to initiate and propagate cracks, the existence of compressive stresses can eliminate this problem. But in order to produce compressive stresses, a balance of tensile stresses will also exist elsewhere. In order to use residual stresses as an advantage, it is necessary to distribute them properly. In the case where peening is used to avoid fatigue crack initiation, compressive stresses are imparted on the surface of the material through plastic deformation. The balance of tensile stresses exist below the surface where they will not have an effect on fatigue crack initiation, since fatigue cracks generally initiate at the surface. In terms of welding, controlling the distribution of residual stresses to achieve the desired distribution of stresses is extremely complex due to the many variables associated with the process.

Needs

There is a need to generate specific information relative to the benefits of techniques proposed to prevent, control, or correct residual stresses. Although the shipbuilding industry has taken some measures to control residual stresses, satisfaction has not been fully achieved Some shipbuilders have gone as far as redesigning and rebuilding fabrication lines. For the most part, the countermeasures against residual stresses and distortion have been activated within the framework of existing fabrication lines. However, shipbuilders have been justifiably reluctant to invest significant capital in new equipment without sufficient evidence that some benefit will be achieved.

The development and demonstration of methods for preventing, controlling or correcting residual stresses, requires the aid of computer models and experimental data due to the vast complexity of the problem. In addition to empirical data, modeling provides the ability to perform experimentation on a computer without actually performing the experiments. However, it is essential that models be validated over a large range of conditions with sufficient, well-controlled experiments. The use of modeling could lead to means of controlling residual stress formation by either eliminating them, or by managing them to achieve some benefits.

Objectives

- Develop further understanding of residual stress formation and their interactions with their effects.
- Develop a quantitative understanding of how to reduce the residual stresses and their effects.

Approach

The approach to reducing or controlling residual stresses and their effects, as a result of welding, involves gaining a full understanding of the synergistic effects of the variables. The qualitative effects of individual variables are somewhat understood. The quantitative, synergistic effects are not well defined. Considering all of the variables that can affect residual stress development, it would be a monumental task to sort the quantitative effects through experimentation. Therefore, emphasis has been placed on model development to aid in understanding the complex interaction of variables.

For modeling to be a reliable means of predicting residual stresses, it is essential to develop the pertinent thermo-mechanical and thermo-physical properties. As part of the Navy program, a database is being developed which is a compilation of thermo-mechanical and thermo-physical properties. Data is being gathered from various sources for inclusion in the databases. Thermo-mechanical data is also being developed, specifically high temperature strength properties.

It is also necessary to validate the models with experimentation to the extent that reasonable agreement with experiments has been achieved over a large range of conditions. Therefore, controlled experimentation has been conducted which represents somewhat simplistic conditions, such as a stationary GTA spot weld, to more complex conditions such as a moving GMA multipass weld.

An essential part of managing residual stresses also involves developing an understanding of the effects that these stresses have on material performance. Efforts are also being pursued to determine the effects of residual stresses on fatigue performance and stress corrosion cracking. In both cases, residual stresses were induced in test samples to evaluate material performance.

Currently, the problem demanding the most attention relative to weld residual stresses is distortion in welded thin section panels as a result of bulkhead fabrication. In order to provide solutions in a short time frame, a practical approach, based on engineering analyses, was taken rather than an approach based totally on a first principles model. A predictive methodology was developed, thermo-mechanical properties were developed in support of the predictive methodology, and proposed solutions were evaluated using the predictive methodology.

Description of Work and Results

Modeling and Validation of Residual Stress Distributions in and HSLA-100 Disk

The purpose of this work was to validate residual stress models currently under development at Oak Ridge National Laboratory (ORNL). The details of this work are presented in References [2] and [3]. The residual stress distribution in a GTA spot welded, 19 mm thick, HSLA-100 steel disk (welded at the Naval Surface Warfare Center) was simulated using thermo-mechanically uncoupled and semi-coupled finite element (FE) formulations at ORNL and measured using neutron diffraction techniques at the National Institute of Standards and Technology (NIST). The process details are given in Figure 1.

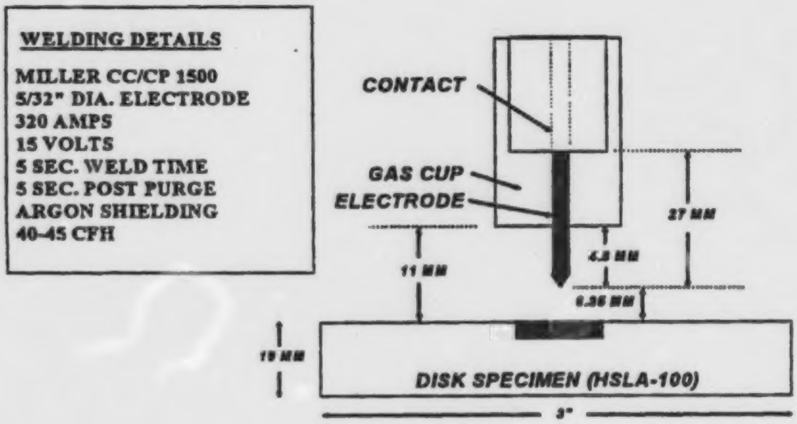
WELDING DETAILS
MILLER CC/CP 1500
5/32" DIA. ELECTRODE
320 AMPS
15 VOLTS
5 SEC. WELD TIME
5 SEC. POST PURGE
ARGON SHIELDING
40-45 CFH

Figure 1. Process details of GTAW stationary spot weld.

The uses of the GTAW process, the absence of filler metal, the stationary plasma, and the symmetrical heat flow represent a very simplistic condition for residual stress development and modeling. The formation of welding residual stresses in HSLA-100 steel is a thermo-mechanical - metallurgically coupled phenomenon. In order to model such a situation, it requires a thorough knowledge of the thermal, mechanical, and phase transformation phenomena and their interaction. In alloys such as austenitic stainless steels, which do not experience solid state phase transformations during welding, the metallurgical effects can be readily ignored or uncoupled from the thermo-mechanical aspects. As to the thermo-mechanical coupling, it is a common opinion that the coupling could be regarded as only a one-way process, that is, the mechanical responses of a weldment do not strongly influence its thermal behaviors during the course of welding. In this case, both a semi-coupled and uncoupled approaches were applied to the same weldment to compare to each other and to the actual neutron diffraction measurements. The purpose of the dual model approach was to determine whether the different FE formulations would result in any differences in predicting the residual stresses during welding. The microstructural changes in the HAZ and fusion zone were not included at this stage, in an attempt to provide the baseline information for on-going model development that will eventually include all the thermo-mechanical-metallurgical coupling effects.

In general, there was little difference between the results of the uncoupled and the semi-coupled models (Figure 2). There was also good agreement between either model and the neutron diffraction measurements in the far HAZ and the base metal. However, in the near HAZ and the fusion zone, predictions from both models are higher than those measured. The cause for these discrepancies can be complicated. Only the properties for the base metal were used in the model calculations. Any hardening, softening or phase transformation effects due to reheating were not considered. Even with this knowledge it is difficult to determine the reason for the differences. The hardening that occurred was due to the formation of untempered martensite. Therefore, the increase in strength would tend to increase the residual stress level. However, the phase transformation to martensite resulted in a volumetric expansion that partially diminishes the thermal contraction. This would tend to reduce the residual stress levels.

An unexpected factor was the occurrence of cracking in the fusion zone. Cracks ranging from 0.1 mm to 2 mm formed beneath the weld surface in the fusion zone. Obviously, the presence of cracks reduced the residual stress levels around the cracks. The presence of a crack was simulated in the model. The simulated crack was placed parallel to the axial direction, about 1 mm from the axial axis of the disk. It was 2 mm long, with the crack tip about 1.5 mm from the weld surface. As expected, the residual stress levels around the crack were significantly reduced (Figure 3). Surprisingly, the reduction was very localized. The effects of the introduced crack began to diminish at only 2.5 mm from the weld centerline, indicating that the presence of a crack in the fusion zone may not significantly change the residual stress levels in the base metal and far HAZ. This was consistent with the comparisons between the measurements and the modeling.

It was concluded in this study that there were some differences between the thermo-mechanically uncoupled and semi-coupled FE, but in general were in good agreement. Both predictions were in very good agreement far away from the fusion zone. Both predictions over-predicted the residual stresses in the fusion zone, probably due to the presence of cracking in the measured sample phase transformations and property changes not accounted for in the model. Preliminary FE analysis indicates that the effects of cracks on the relaxation of residual stresses are localized to the region around the cracks. Therefore, the residual stress predictions in the base metal and far HAZ were not greatly affected by the presence of the cracks.

Evolution of Residual Stresses in a Multi-pass HSLA-100 Weld

The purpose of this work was to describe the evolution of weld residual stresses as a function of each weld layer in a multi-pass, 19-mm thick, HSLA-100 steel plate. This was done to gain knowledge and information of how residual stresses evolve from weld pass to weld pass. Detailed information was maintained which allows models to accurately duplicate the conditions of the welding process. This work is described in detail in references [4] and [5]. This analysis was performed by NSWC and NIST. Neutron diffraction measurements and measurement development techniques were performed by NIST.

A weldment of HSLA-100 steel was prepared using the GMAW process using weld wire produced from a similar plate and using 98% Ar - 2% O shielding gas. Residual stress measurements were made using the neutron diffraction technique. Measurements were made subsequent to each weld layer in order to describe the evolution of residual stresses from layer to layer. Subsequent to completion of the weldment and measurements, 2mm cubes were removed from each measurement location in order to determine the stress-free lattice parameter, d_o. These values were then utilized to determine the stress values at each stress measurement location. The hydrostatic residual stress results are presented in Figures 4.

It was concluded that large stress gradients existed in both the weld metal and the baseplate. The initial deposition of a weld bead developed neutral stresses to compressive stresses. Subsequent deposition of weld beads resulted in the development of higher tension, to the point that high stress values near the biaxial yield strength were achieved, followed by relaxation with the deposition of additional weld beads. The baseplate developed high tensile stresses adjacent to the weld upon initial deposition of a weld bead, and continued to grow in tension with the deposition of subsequent weld beads. The baseplate also experienced some relaxation once very high tensile stresses were achieved. The tensile stresses in the baseplate proceeded to taper into compression at locations further from the weld(~11+ mm).

It was also concluded from this work that the unstressed lattice parameter, d_o, varies throughout the fabrication of the weld joint. It is therefore necessary to accommodate changing d_o values in the weld metal when calculating residual stress values from diffraction data, otherwise large errors can result in the calculated stress value. It was determined that d_o varied throughout the weld metal locations due to dilution and tempering. The d_o values were largest in the top weld passes. and tapered toward the baseplate values in the lower passes. The d_o value varied on the order of 0.001 Å. This variation was sufficient to cause an increase in the calculated residual stress value of 263 MPa.

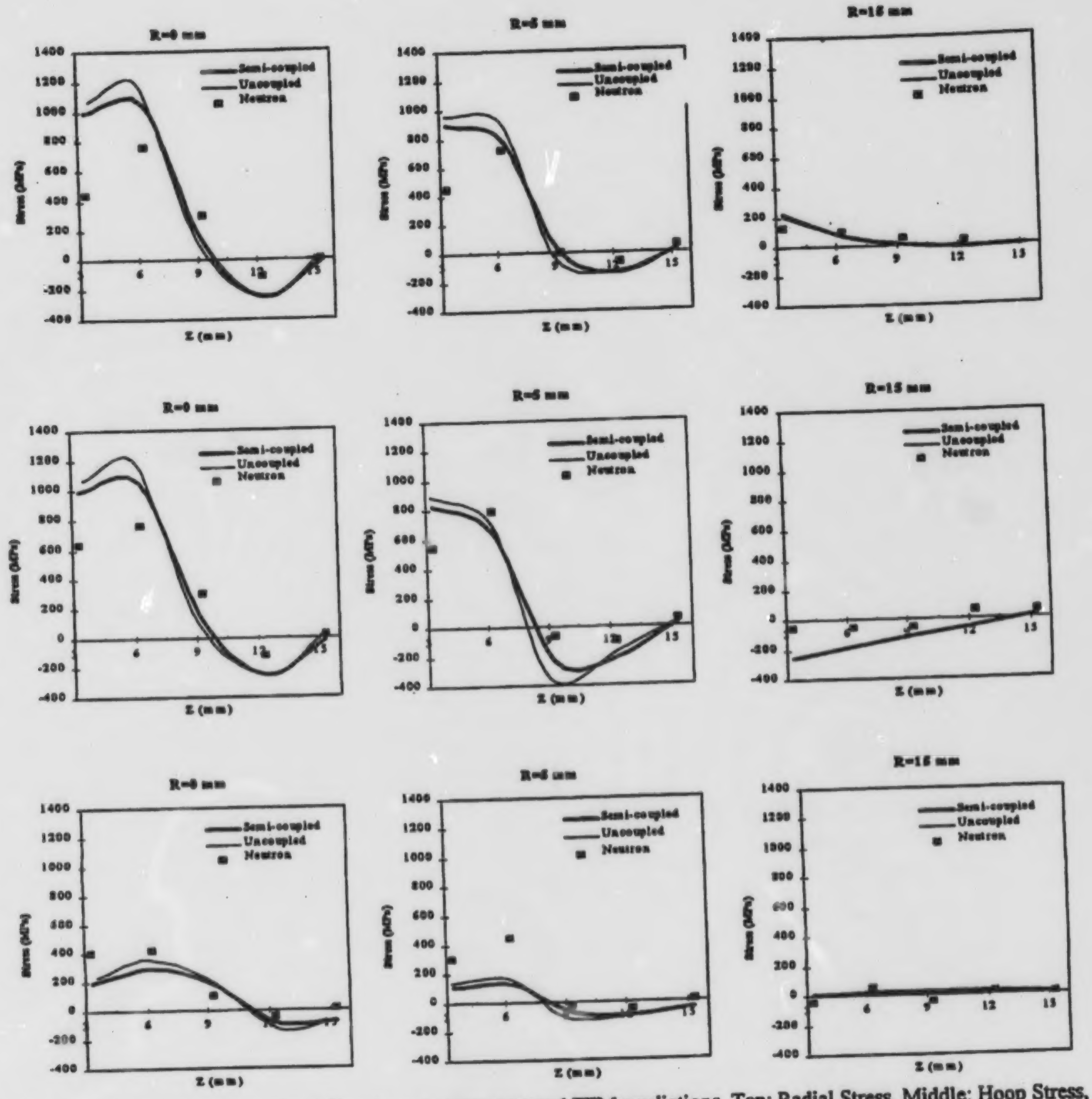

Figure 2. Comparison of neutron diffraction measurements and FEM predictions. Top: Radial Stress, Middle: Hoop Stress, and Bottom: Axial stress, Z = Distance in the normal direction, R = Distance in the radial direction.

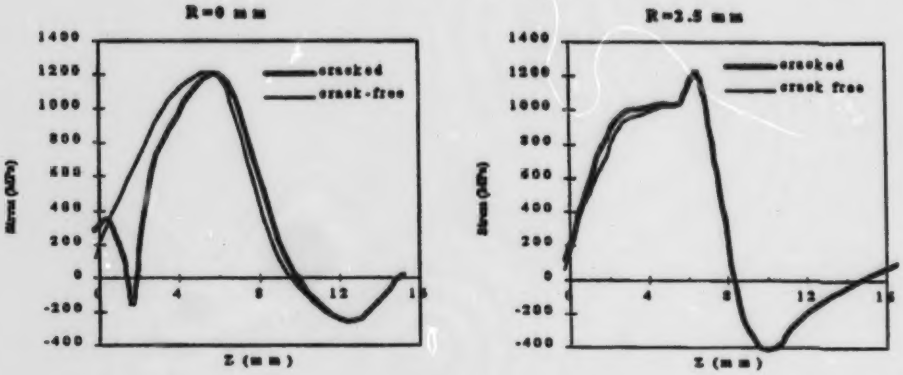

Figure 3. Effect of a single crack on the hoop residual stress distributions using the uncoupled model formulation at radial distances of 0 mm and 2.5 mm from the center of the disk..

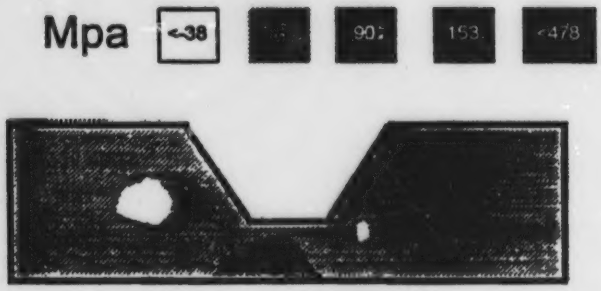

Prior to Welding

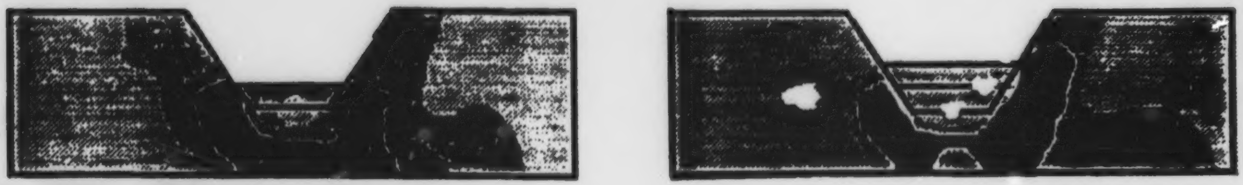

After Welding First Layer

After Welding Second Layer

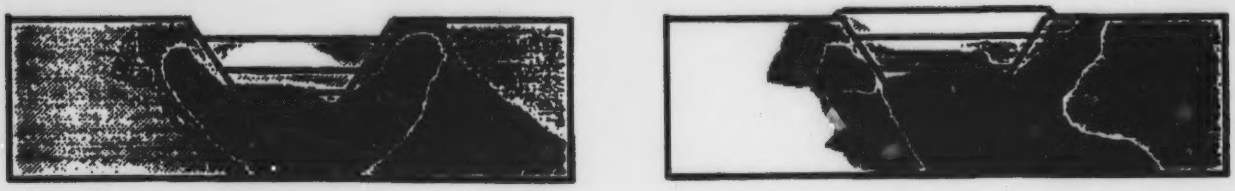

After Welding Third Layer

After Welding Fourth Layer

Figure 4. The evolution of the hydrostatic residual stresses.

Modeling of the Evolution of Residual Stresses in a Multi-pass HSLA-100 Weld

A weld solidification model has been developed by NCEMT in Johnstown, PA to aid in the optimization of high strength steels used in ship construction. This model contains the ability to predict residual stress distributions in addition to material properties. This model utilizes the ABAQUS finite-element code. The weld solidification is modeled using an uncoupled 2-D thermo-mechanical analysis with no account for fluid flow or magnetic effects. Individual bead-on-plate welds or multi-pass welds can be modeled using the element re-birth technique. Most of the modeling efforts have focused on GMA welding of high strength steel. To date, good agreement between model results and experimental data has been achieved with experimental data (residual stresses, microstructures, properties, and hardness). Results to date are reported in references [6] through [11].

The model described above has been used to simulate the evolution of residual stresses in a multipass HSLA-100 weld as described in the previous section. A comparison of the results is shown in Figure 5. The results were very similar in many respects. In both cases, large stress gradients existed in both the weld metal and the baseplate. The initial deposition of a weld bead developed neutral stresses to compressive stresses. Subsequent deposition of weld beads resulted in the development of higher tension in previous beads, followed by relaxation with the deposition of additional weld beads. The baseplate developed high tensile stresses adjacent to the weld upon initial deposition of a weld bead, and continued to grow in tension with the deposition of subsequent weld beads. The baseplate also experienced some relaxation once very high tensile stresses were achieved. The tensile stresses in the baseplate proceeded to taper into compression at locations further from the weld.

Some differences did exist. Primarily, the model predicted higher tensile results in the weld metal region and somewhat lower results at regions farther away in the baseplate. At this time, the specific reasons are not clear. However, one postulation is that the clamping forces employed to hold the plate in place were different in the experiment and the model. Since the clamping force was not measured in the experimental analysis, an arbitrary clamping pressure was provided in the model experiment. Although the clamping pressures were unable to be matched, a comparison of the angular distortion of each provides some insight, as shown in Figure 6. The amount of deflection in the actual weldment exceeded the deflection of the model prediction by a factor of 2. The fact that the amount of angular distortion was less in the model experiment, indicates that the clamping pressure may have been higher than the actual. Therefore, it is feasible that due to the increased amount of restraint in the model, higher residual stresses may have developed in the weld zone. The higher residual stresses in the weld zone may have led to more compressive stresses outside the weld zone in order to achieve a balance of forces. This issue will be addressed in future experimentation.

Effects of Grinding on the Surface Residual Stresses in HSLA-100 Steel Bead-on-Plate Weldments.

The initial intent of this project was to determine the effects of GMA welding variables such as preheat, current, voltage, heat input, and etc. on the resulting residual stresses as determined by x-ray diffraction techniques (at Virginia Polytechnic Institute (VPI)). However, it was determined that preparing the baseplate for welding by abrasive grinding had a significant effect on the resulting residual stresses. Initial results indicated that very low tensile stresses existed near the fusion zone and they increased in magnitude at increasing distances away from the fusion zone. Examples of this are shown in Figures 7. In this case, the bead-on-plate welds were deposited using two different preheating temperatures of 24°C and 204°C. In this and other cases it was noted that a maximum value of residual stress, near the yield strength of the material (~700 MPa) or greater, was frequently achieved within a few millimeters of the fusion zone. These residual stress patterns were unexpected and were not consistent with the traditional trends previously observed (i.e. high tensile residual stresses near the fusion boundary and tapering into compression at increasing distance). It was suspected that the grinding stresses, created during pre-weld base plate preparation, were affecting the results. Additional experimentation was performed to verify this.

The intent of additional tests was to eliminate pre-weld grinding stresses while also removing the plate production oxide scale. Additional plates were prepared by first machine grinding the plates to clean metal, followed by vacuum annealing at 650°C for up to 2 hours. Determination of the residual stresses using x-ray diffraction across the surface of the plate indicated that residual stresses due to grinding had been eliminated as a result of vacuum annealing. The average value of residual stresses indicated that the average stress value was -95 MPa ± 31 MPa. These values were consistent with values obtained using as-received plate material. The average stress value was achieved using an anneal time of 1 and 2 hours. The standard deviation was improved somewhat by annealing for 2 hours. It was concluded, at this point, that vacuum annealing reduced grinding stresses and prohibited the formation of scale.

After vacuum annealing, GMAW bead-on-plate welds were placed on the surface using preheating temperatures of 24°C and 204°C. Subsequent to welding, the surface residual stresses were determined using x-ray diffraction techniques at VPI. The results are plotted in Figures 8 and 9.

If the simplest case is assumed, that grinding stresses and welding stresses are linearly additive, then subtracting the stress-relieved data (welding stresses only) from the non-stress-relieved data (welding + grinding stresses) results in the residual stresses due to welding only. It is immediately apparent that grinding significantly changed the magnitude and even the sign of the surface residual stresses. The grinding stresses increased as the distance from the fusion zone increased. This is because the heat of welding provided a greater stress relief treatment in the higher temperature regions of the HAZ. Due to this heating effect, it was also seen in most cases that the data representing "welding stress only" and "welding + grinding" approach similar values at positions close to the fusion line. This indicates that the grinding residual stresses were reduced in this region. Using this technique it can be seen that the surface residual stresses due to welding were reduced as the preheat temperature increased from 24°C to 204°C.

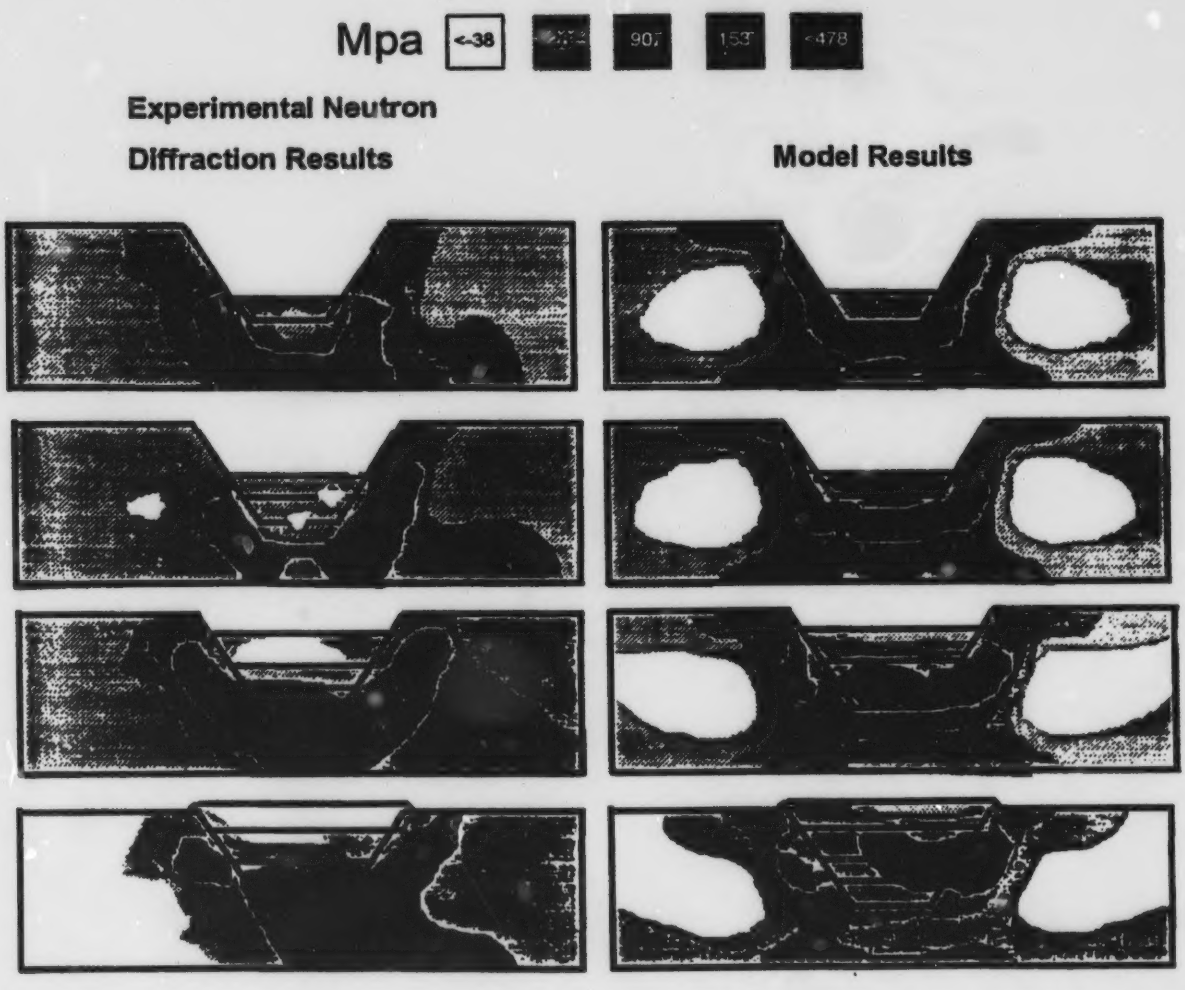

Figure 5. Comparison of the hydrostatic residual stresses as determined by neutron diffraction and predicted by a model.

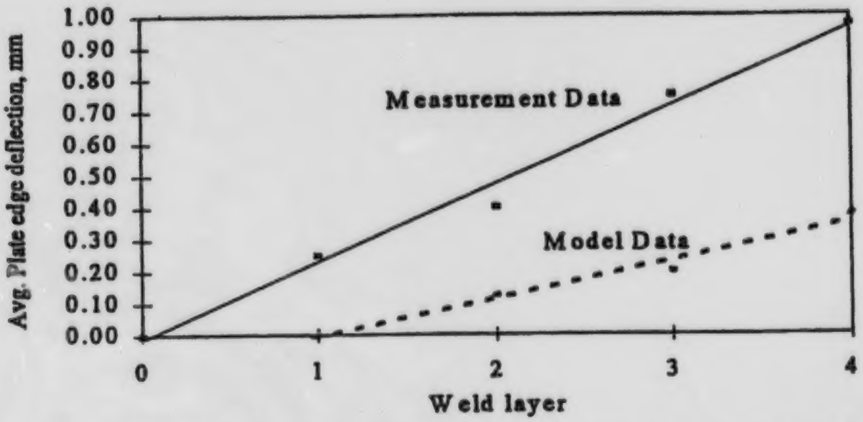

Figure 6. Comparison of the distortion that occurred in the actual welded plate and the model plate.

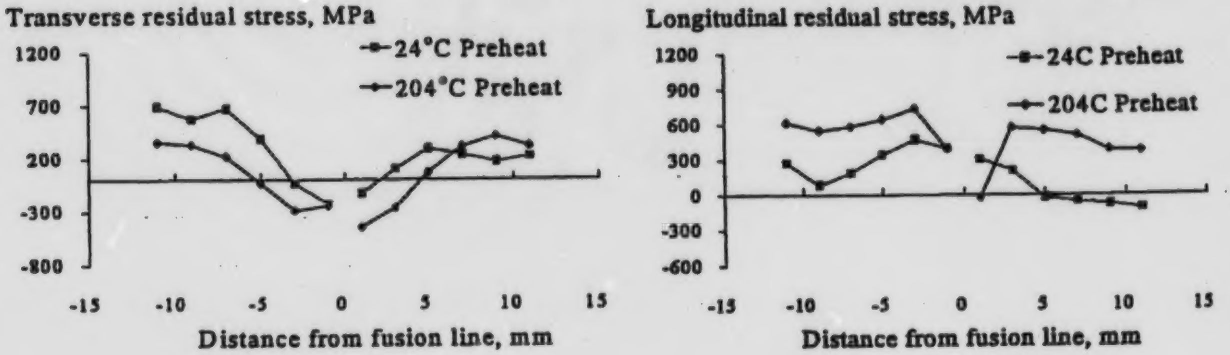

Figure 7. Transverse and longitudinal residual stress as a result of pre-weld grinding and welding.

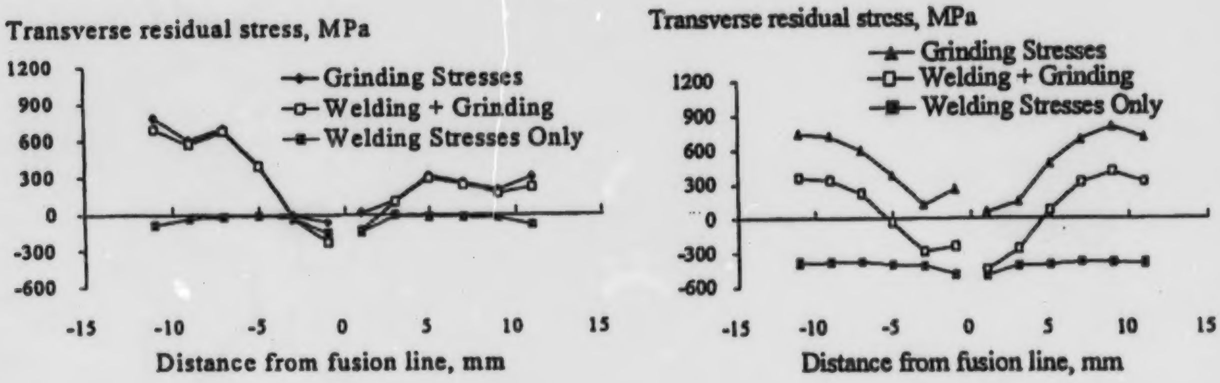

24°C Preheat

204°C Preheat

Figure 8. Separation of transverse residual grinding and welding stresses for 24°C and 204°C preheat.

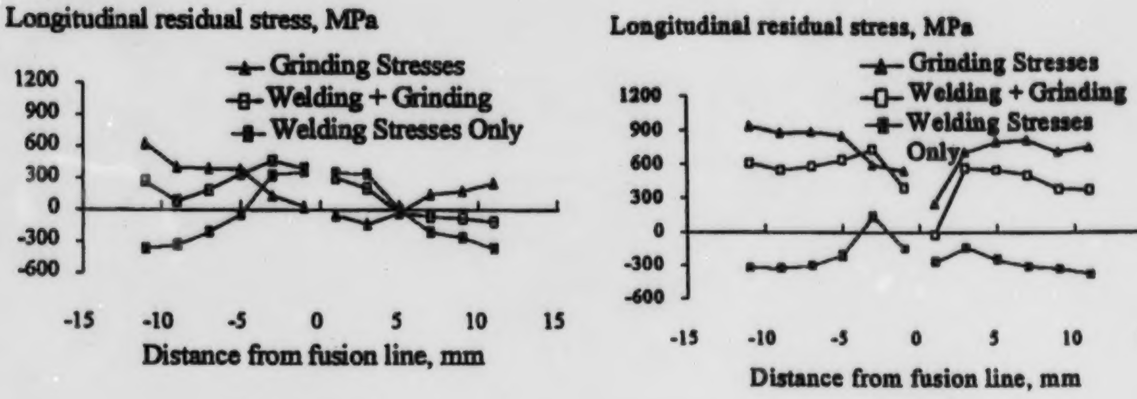

24°C Preheat

204°C Preheat

Figure 9. Separation of longitudinal residual grinding and welding stresses for 24°C and 204°C preheats.

In terms of model verification, it is important to isolate the residual stresses due to welding in order to accurately compare results from experimental x-ray analysis techniques to the model predictions. This approach is acceptable for the scientific study of residual stresses, but in actual shipbuilding or welding applications where pre-grinding is standard procedure, the final surface residual stress state will be very unlike what would be expected due to welding only.

It has also been shown that x-ray diffraction is a surface analysis technique and does not necessarily represent the bulk stress state. This is illustrated in Figure 10. A comparison of x-ray diffraction data and neutron diffraction data is made in Figure 10. The neutron diffraction data was extracted from the section above entitled "*Evolution of Residual Stresses in a Multi-pass HSLA-100 Weld*" This data represents the first weld pass placed in the multi-pass weld. The distances, regardless of the position within the thickness of the plate, were calculated to the center of the weld bead. It can be seen that the bulk stress state, represented by the neutron diffraction data, does not compare well with the surface stresses determined by x-ray diffraction.

It was concluded in this study that in order to isolate the development of surface residual stresses due to welding only, it is necessary to prepare the baseplate for welding with a means that will not itself induce residual stresses. However, surface stresses may be analyzed in the fusion boundary and the near HAZ even when pre-existing grinding stresses were present. Further details of this study can be found in references [12] and [13].

Ongoing work in this area includes the measurement of residual stresses associated with weld cracking tests such as the Welding Institute of Canada (WIC) weldability test using x-ray diffraction. This data will be used to characterize the residual stresses associated with various weldability tests.

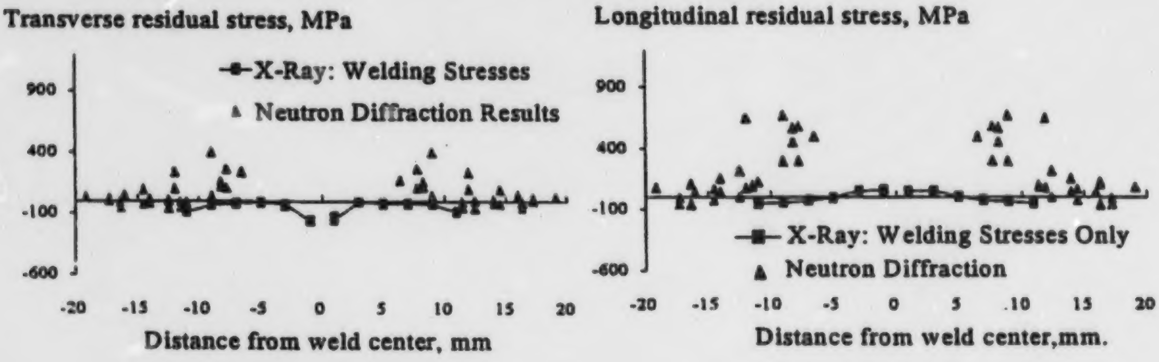

Figure 10. Comparison of neutron diffraction and x-ray diffraction results for the transverse and longitudinal residual stress component.

Prediction and Prevention of Distortion in Thin Section Panels

This work was performed by the Edison Welding Institute and it's partners in the Navy Joining Center (NJC). This was one of several tasks funded by NJC and managed by the Navy Mantech Program. This program was introduced to aid in the mitigation of distortion problems in *Arleigh Burke* Class destroyers (DDG-51). Support has also been provided by the DDG-51 program office and by the Naval Surface Warfare Center (NSWC).

Welding induced distortion both degrade the performance and increase the cost of the fabricated structure. While flame straightening is an effective method of reducing welding induced distortions to within fairness requirements, it is both cost and labor intensive. A better alternative would be to limit pro-actively and control distortion induced by welding as part of the fabrication process. Progress towards this goal is supported by a methodology that can predict the anticipated level of distortion in a fabricated structure from inputs of basic welding and design variables, such as that developed by Michaleris and DeBiccari [14]. The objective of this work was to determine likely candidates that may be employed to mitigate distortion in the fabrication of stiffened, thin-section panels. In doing so, the primary distortion modes were identified, a predictive methodology was developed, thermo-mechanical properties were developed in support of the predictive methodology, and potential solutions were evaluated using the predictive methodology. Details of this work are presented in reference [1].

In order to identify the distortion modes, multi-stiffener laboratory mock-ups having many features similar to production fabrication and design was adopted (e.g. material thickness and grade, stiffener size and spacing). The mock-up is illustrated in Figure 11. The plate was 4.76 mm thick AH-36 steel cut to a final dimension of 1.2 m x 1.2 m. The longitudinal stiffeners (102 mm x 102mm x 2.3 kg) were placed at a spacing of 68.6 cm on center. The transverse stiffeners (102 mm x 254 mm x 5.5 kg) were also placed at a spacing of 68.6 cm on center. Although transverse stiffeners are placed much further apart in actual production, this spacing permitted multiple stiffeners for this configuration. The typical fillet weld leg sizes for longitudinals were 3.2 mm to 4.8 mm, and for the transverse stiffeners, 4.8 mm. The FCAW process was used with a 1.32 mm dia. E71T-1 electrode and 100% CO_2 shielding gas. Out-of-plane distortion measurements were made using a dial indicator inserted into an array of vertical tubes situated beneath the plate of interest. Transient out-of-plane distortion measurements were also made using mechanical linear voltage displacement transducers (LVDT's). The motion of the plate surface during welding was determined by mounting the LVDT's under the mock-up and monitoring the change in their output with time.

The results of the distortion measurements due to welding the first and second longitudinal stiffeners are shown in Figure 12 for a 709 J/mm, 4.8 mm fillet weld mock-up. This sequence of figures illustrates how the out-of-plane distortion accumulated as a result of welding the longitudinal stiffeners. Welding of the longitudinal stiffeners produced buckling as evidenced by a characteristic S-shape. Buckling was also verified by the panel's stability in multiple configurations, which is a characteristic of buckling distortion only. By proper placement of force, the out-of-plane displacement was reversible. The panel popped suddenly as the mode shape switched sign. Welding of the transverse stiffeners removed much of the distortion due to the small transverse spacing. The spacing in actual production is typically much larger. Differential plots revealed the contribution of welding each stiffener to the total distortion. The longitudinals produced primarily buckling, while welding the transverse stiffeners produced angular distortion. It was therefore concluded that the dominant mode of distortion was buckling.

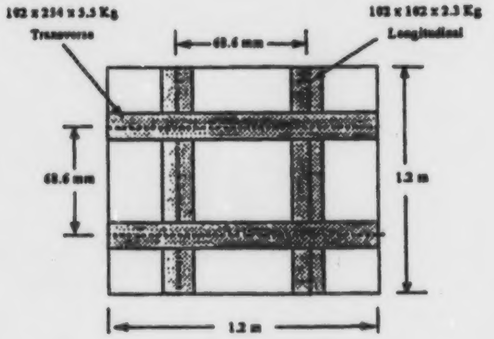

Figure 11. Laboratory stiffened panel mock-up.

Transient out-of-plane distortion measurements also showed the development of buckling distortion. Figure 13 shows typical traces from three transducers placed along one edge of the mock-up. The sudden change in these traces indicates buckling.

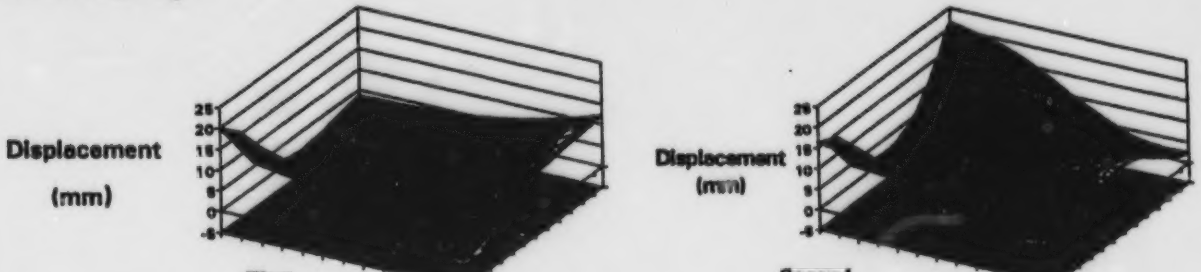

First
Longitudinal Welded

Second
Longitudinal Welded

Figure 12. Distortion after welding the first and second longitudinal (709 J/mm, 4.8 mm weld).

The compressive forces necessary to cause buckling are generated by the shrinkage which results upon the solidification of the weld metal. During cooling of the weld metal, the longitudinal shrinkage upon solidification of the weld metal is resisted by the cooler baseplate. In effect, the shrinkage of the weld metal applies a compressive force on the surrounding base plate in the longitudinal direction. When sufficient force is developed, buckling occurs.

The methodology developed by Michaleris and DeBiccari [14] for determining the occurrence of buckling in thin section panels was employed in this analysis. The predictive methodology consisted of two models. A two-dimensional model was used for weld process simulation. This model depended upon both welding parameters and on characteristics of the design local to the weld joint. The output of this model was the driving force for buckling, or *The Equivalent Applied Thermal Buckling Strain*,$\varepsilon_{\tau\text{-applied}}$. A three-dimensional elastic-plastic structural model was utilized to evaluate the stiffness of the structure, or the *Equivalent Resistance to Thermal Buckling*, ,$\varepsilon_{\tau\text{-resistance}}$. Assessment of buckling for a particular combination of design and welding variables was a simple comparison of the resistance to buckling and the driving force for buckling. In theory, if the driving force is greater than the resistance, the structure is expected to buckle. The ratio of the applied strain to the resistance strain was termed "Buckling Ratio". Hence the following equation.

$$\text{Buckling Ratio} = \varepsilon_{\tau\text{-applied}} / \varepsilon_{\tau\text{-resistance}}$$

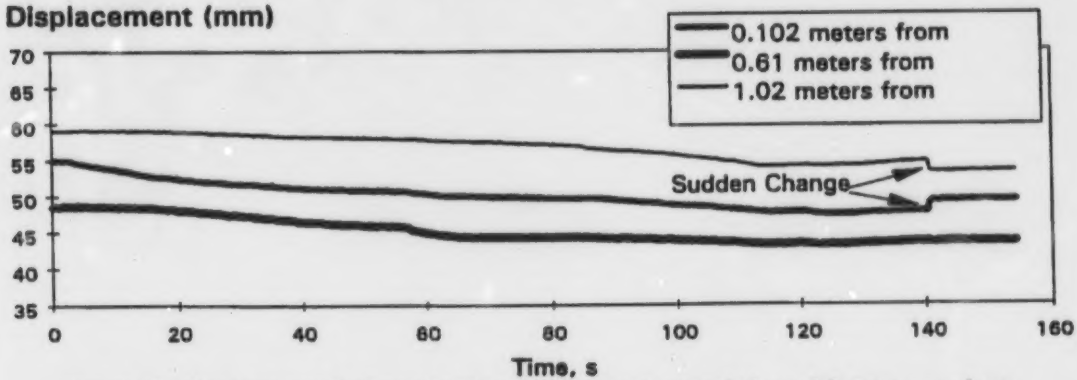

Figure 13. Transient out-of-plane distortion measurements recorded on a laboratory mock-up.

Upon comparing the buckling ratios, generated by the methodology, to the occurrence of buckling in a series of mock-ups, it was determined that the critical ratio required for buckling was a value of 0.75. In order to achieve this value in 4.8 mm plate it was necessary to reduce the welding heat input to 315 J/mm in order to avoid buckling distortion. An increase in the heat input to 354 J/mm was sufficient to cause buckling as demonstrated in Figure 14.

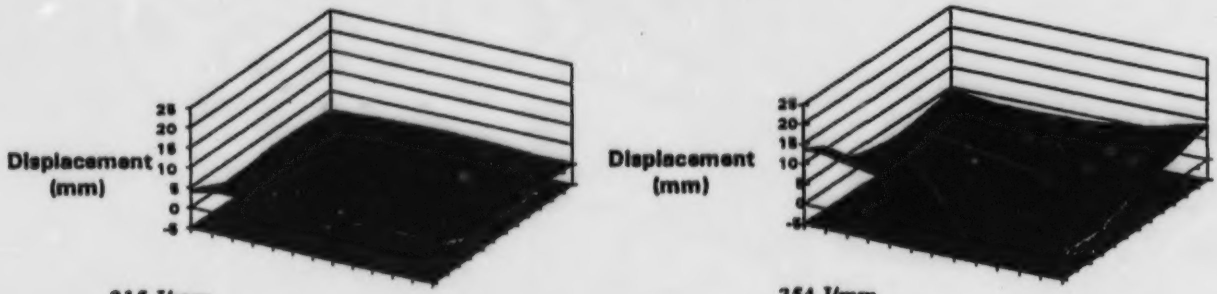

315 J/mm

354 J/mm

Figure 14. Measured out-of-plane distortion after the first longitudinal stiffener was welded for 315 and 354 J/mm welds.

This methodology was then applied to a 4.76 mm -thick, 6.1 m - long by 2.6 m - wide stiffened, shipyard production panel. This panel contained 3 longitudinal and 3 transverse stiffeners. The results are shown in Figure 15. It can be seen in this case that a heat input of about 200 J/mm is required due to the reduced stiffness of the larger geometry. This heat input will not produce the design minimum fillet weld size using the flux core arc welding process. A shipyard mock-up of this configuration was also prepared and welded at a heat input of 354 J/mm. The result was that buckling still occurred. It was concluded in this study that buckling distortion cannot be eliminated from the current design by better control of the welding practice even if the fit-up between the shell plating and the longitudinal stiffeners can be improved to a zero-gap condition.

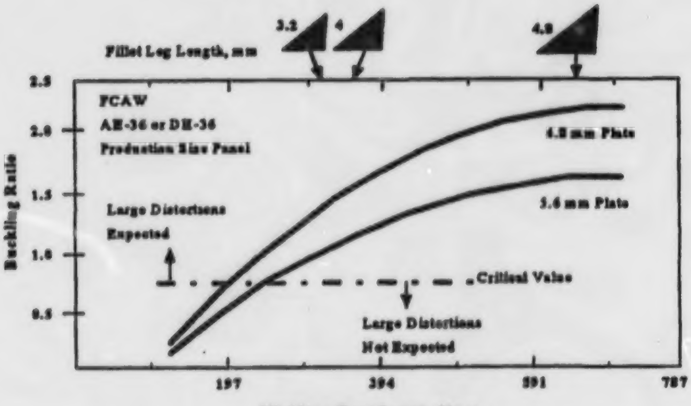

Figure 15. Results of buckling predictions for shipyard size panels.

Although heat input control or fit-up cannot eliminate buckling distortion, some other alternatives are currently being investigated. They are 1) the use of intermittent fillet welds, 2) the use of flatter initial base plate, and 3) thermal tensioning. Although the use of intermittent fillet welds is not permitted with the current design due to fatigue, corrosion, and shock resistance concerns, the initial results are promising, as illustrated in Figure 16. Two panels were fabricated using continuous fillet welds at low heat input and one at a relatively high heat input. It can be seen in Figure 16 that welding with intermittent fillet welds can dramatically reduce the buckling distortion even when the intermittent welds are much higher heat input.

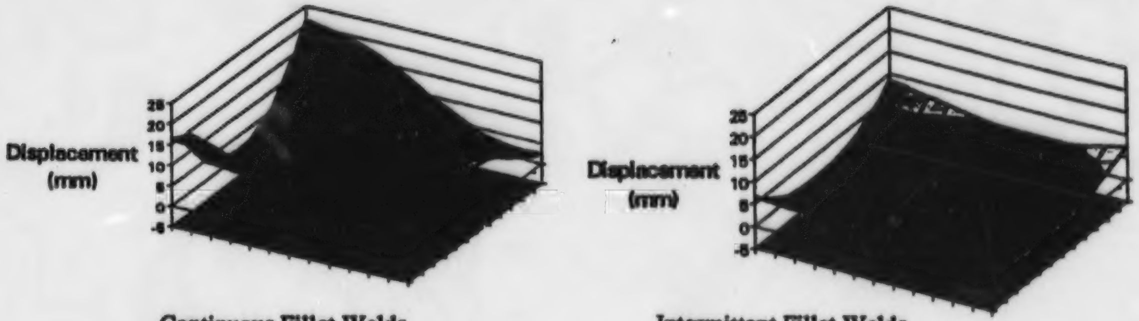

Continuous Fillet Welds

Intermittant Fillet Welds

Figure 16. Out of plane distortion measurements after welding two longitudinal stiffeners for continuous (709 J/mm) and intermittent fillet welds (1574 J/mm).

The idea of using flatter initial plate to control the final overall distortion has been debated for several years. However, Figure 17 indicates that some benefit may be realized. Using the methodology described above, the effect of initial plate fairness on final distortion was investigated. The initial unfairness was varied from 0.05 mm to 4.8 mm at the mid-span of the plate. The curves indicate that for each initial unfairness state, the displacement increases at a fairly low rate with applied load, and at a given load the rate increases dramatically. The greater degree of initial unfairness, the lower the required load at which the relationship between load and displacement accelerates. Not only do these curves indicate that flatter initial plate is beneficial, but that current distortion mitigation techniques may be more effective if flatter initial plate is utilized.

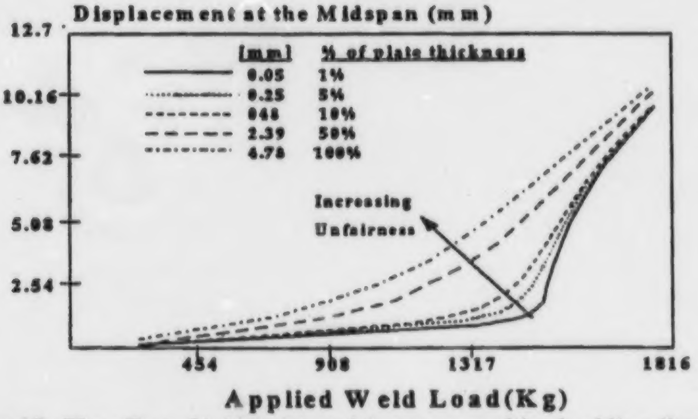

Figure 17. The effect of initial plate unfairness on resulting buckling distortion.

Thermal tensioning is a technique by which the compressive forces developed during welding are anticipated and counteracted by applying a tensile load to the weld joint prior to and during welding by imposing a preset temperature gradient through the use of heating and cooling elements. Cooling is applied beneath the plate along the length of the weld joint while heating is applied on both sides of the weld joint along the length of the weld joint. In order to be effective, the proper thermal gradient must be determined. The predictive methodology, discussed above, was utilized to determine thermal tensioning conditions which will result in elimination of buckling. These conditions were duplicated on actual panels to test the validity of the model. Figure 18. displays the results. It can be seen that for a weld heat input of 709 J/mm, which previously caused buckling ,that buckling distortion was eliminated with only angular distortion remaining. It was also shown that the maximum residual stresses were reduced from 349 MPa to 140 MPa. Angular distortion can be eliminated by applying an elastic pre-bending before and during welding.

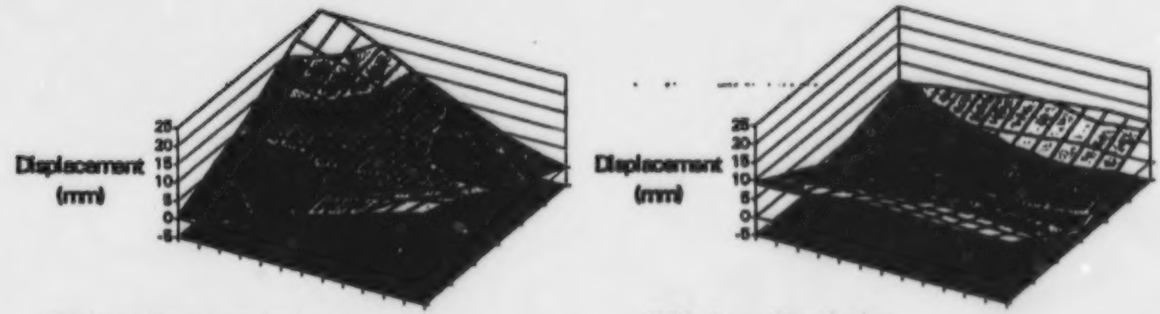

Without thermal tensioning

With thermal tensioning

Figure 18. Comparison of out of plane distortion with and without thermal tensioning as a result of welding one longitudinal stiffener at 630 J/mm.

The sensitivity of this predictive methodology was evaluated by analyzing the effect of variations in the material yield strength. The variation of yield strength with temperature used for the weld process simulations employed a room temperature yield strength of 356 MPa, the specified minimum for the material. However, the actual plates used in this investigation have measured room temperature properties ranging up to 524 Mpa. The study of the effect of these differences was motivated by the fact that most procured materials exceed the specified minimum tensile requirement. In this study, the variation of strength was allowed to increase by 30%. Since the formation of residual stresses and distortion are highly dependent upon high temperature tensile properties, high temperature tensile data was developed at NSWC as shown in Figure 19. It was also anticipated that some variations in these properties exist as well. Therefore, increases in the temperature range of 600°C to 700°C of up to 30% were also analyzed. It was demonstrated that changes in the applied strain as a result of these variations ranged from -0.2% to 4% difference from the baseline values. It was concluded that these variations need not be accounted for in the assessment for the propensity for buckling.

Upon reviewing the closed form solutions to the structural Eigenvalue analysis, it was concluded that the critical buckling load should scale with the square of the plate thickness. Upon comparing the analysis outputs with the scaled values for plate thickness, it was determined that the scaled values were within 5.8% of the analysis output. Thus, values of the structural resistance strain calculated for one thickness were found to be scaleable to predict results for other thicknesses over a limited range.

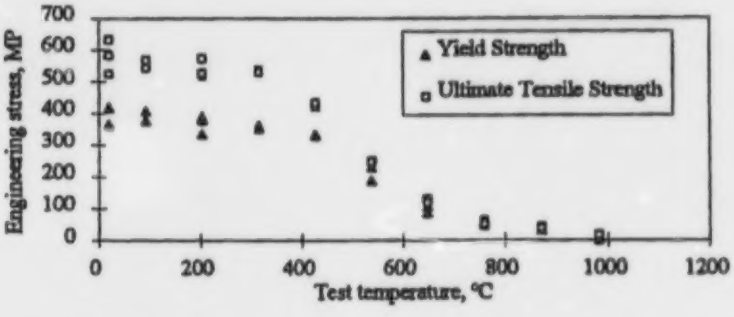

Figure 19. High temperature property data for AH-36 steel.

Development of Thermo-Physical and Thermo-Mechanical Property Data

The availability of thermo-physical and thermo-mechanical property data is essential for appropriate model performance. This data is not readily available or does not exist. This data is either developed on a case by case basis, or is extrapolated from information on similar materials. Even when best engineering judgment is used, extrapolation can lead to gross errors in the model due to the sensitivity of the output to the accuracy of the input parameters, and the cumulative effects of small errors. The direct use of experimental data for the materials of interest is often the most desirable when it is available.

Currently, there are three programs being performed at the National Center for Excellence in Metalworking Technology (NCEMT) in Johnstown, Pa. which include the development and collection of thermo-mechanical and thermo-physical property data. They are entitled "*Thermo-physical Properties in Metalworking Processes*", "*Thermo-mechanical Processing Initiative*", and ""*Atlas of Formability*". The following sections describe each of these programs. Although these programs are not specifically related to welding, it is recognized that the data is also applicable to any high temperature metalworking process, including welding.

Thermo-Physical Properties in Metalworking Processes

The objective of this project is to provide reliable thermo-physical property data that can be used in the optimization of metalworking processes involved in the production of DoD weapons systems. The primary benefit will be realized by the DoD and their vendors attempting to model, simulate, control, and optimize metalworking processes. The data, when integrated in process simulation, will be an essential tool to the manufacturing engineer for the prediction and optimization of various metalworking processes. The data will exist as a computerized database that will be available to the DoD and their vendors. Currently, the electronic database is under development, surveys are being performed to determine the needs of the metalworking community, and efforts to evaluate process simulation sensitivity, sensitivities to thermo-physical properties, estimation of property data, and evaluation of needed phase diagrams have begun.

Thermo-Mechanical Processing Initiative

The objective of this project is to develop and demonstrate technologies that can be used to optimize thermo-mechanical processes. The project is focused on improving the technologies needed to enhance the production of components. These technologies include improved process and material simulation techniques to predict and control microstructure and defects during processing as well as the advanced measurement techniques needed to verify the results. Other technologies include development of the advanced experimental techniques to provide the detailed material property data required for accurate simulation. Although the thermo-mechanical property data is being developed for specific manufacturing processing of components, the data is also applicable to weld modeling.

Atlas of Formability

The objective of this project is to generate forming data needed to develop and optimize forming processes for weapon system components. These data include flow behavior under industrial processing conditions (a wide range of temperatures and strain rates) and resulting microstructural changes for more than 150 materials. The material flow data is critical for the successful application of advanced analytical tools or techniques such as finite element modeling. Mechanical properties under investigation include: stress-strain relations at elevated temperatures and various strain rates, workability, forming limits, and strain to fracture. Once again, this data will be useful in weld modeling also.

The Effect of Residual Stresses on Fatigue Performance.

The role of residual stresses on fatigue crack growth behavior is currently being studied at Northwestern University and the University of Missouri. The combined effort is investigating the role of micro- and macro- residual stresses on the initiation and propagation of fatigue cracks in multiphase metallic materials using x-ray microbeam diffraction and neutron diffraction techniques. Presently, the effects of pre-existing stresses on fatigue analysis results and crack propagation behavior has been analyzed using x-ray diffraction techniques. The x-ray beam used for stress measurements was 220 µm in diameter formed with a linearly tapered capillary. The capillary focuses the x-rays, provides good spatial resolution to capture stress gradients, and provides adequate intensities for diffraction experiments. The material under investigation is 1080 steel containing 14% spherical Fe_3C particles in a ferrite matrix. The intensity from the capillary allows for the measurement of stresses in both phases, wherein they can be separated into macro- and micro-stresses. For the following results however, data for the macro-stress is presented, which by definition are equal between phases, and therefore only the ferrite stress data is shown.

Triaxial measurements were made near the crack tip of a compact tension specimen using the Fe 211 reflection and tilting to 31 different ψϕ angles and solving the stress tensor by least squares. This removed the assumption of a negligible σ_{33} component (normal to the surface) over the ~30 μm x-ray penetration depth.

Figure 20 shows the triaxial stress components at the tip of a fatigue crack under increasing applied load. The crack (15.2 mm long) was grown by machining the 1080 steel into a compact tension specimen, which was notched with a jeweler's saw and fatiguing at 3 Hz, R=-0.1 and P=940kg. After growing the crack to 15.2 mm the sample was statically loaded by pushing against the crack faces with a set screw. The stresses were then measured at the crack tip with a 220 μm x-ray beam. Figure 20 provides information on (a) the triaxial nature of the stresses experienced by the crack tip during loading, and (b) the interaction of residual and loading stresses. At zero load (the residual state) all three components are compressive, a result of the extensive plasticity associated with the crack tip singularity. The σ_{33} component, though smallest in magnitude, is finite at the tip even under the "plane stress" conditions at the surface. As the load is increased, the stresses increase rather linearly, which suggests that the applied stresses superimpose on the residual stresses at the tip. The stresses remain compressive until about 13.5 Mpa-m$^{1/2}$ thus the crack tip experienced compression over ~30% of its loading cycle. Since the crack will only propagate under tensile load, this is clear evidence of crack-tip shielding due to residual stresses generated by the crack itself. The implication is that the initial compressive stress state must be taken into account to accurately characterize the material performance. Otherwise, an overestimation of the fatigue performance will result. It is also clear that the existence of residual stresses is directly additive to the applied loads.

Figure 21 illustrates how the stress field of a growing fatigue crack interacts with a pre-existing residual macro-stress field. The stresses were introduced into a 1080 steel specimen by plastically force-fitting a plug into an undersized hole (~2%), which resulted in the tangential profile shown prior to crack growth. The crack was grown as described above, and the stresses were again measured using the x-ray diffraction technique described above. The stresses were predominantly tensile, which should accelerate crack growth. However, there was little difference in growth rates between these and the control samples. The explanation for this lies in the stress field pattern that exists during crack growth. The crack tip stress field appeared to obliterate the existing residual stresses out to about 1mm ahead of the tip so that the growing crack is never subjected to these stresses. Ahead of the tip-affected region the residual stresses are similar to the pre-crack values, which suggests that fatigue did not result in appreciable stress fading. In fact, the stresses are actually higher after fatigue. Thus it was the generated crack-tip stress field, rather than the fading of existing residual stresses, that led to the insensitivity of growth to pre-existing stresses. Future work is planned to evaluate the resulting stress fields in the presence of residual stresses of higher magnitude. Other work related to this topic can be found in reference [15].

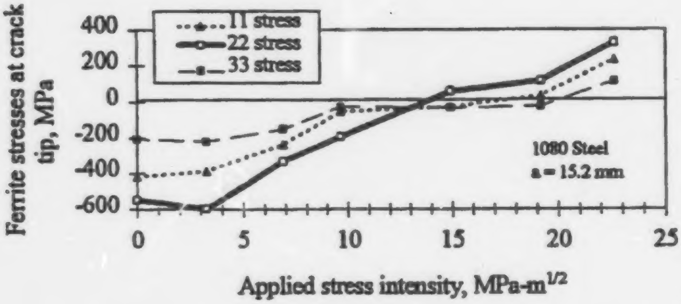

Figure 20. Triaxial ferrite stresses at fatigue crack tip under applied tensile load.

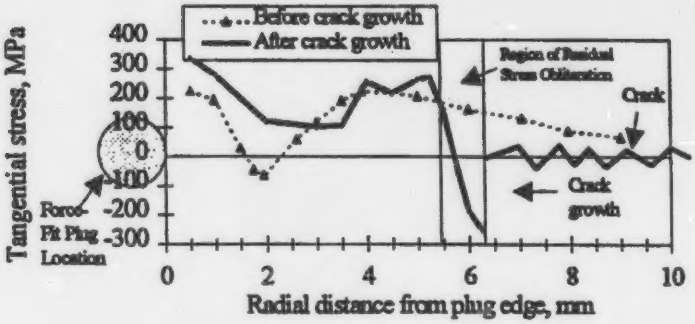

Figure 21. Tangential stresses in residual macrostress sample before and after crack growth.

The Effect of Weld Residual Stresses on Stress Corrosion Cracking (SCC)

The effect of weld residual stresses on stress corrosion cracking initiation and growth in HY-130 steel was investigated by NSWC using the trough weld test. The objective was to determine if weld residual stresses alone are sufficient to initiate or propagate SCC. Eighty four trough welds were prepared in 51 mm plate and subjected to seawater and impressed currents at -1.0 and -0.8 volts for up to three years. The trough weld test is a highly restrained, simulated repair weld which is shaped like a trough and is approximately 22 cm long by 38 mm deep by 63.5 mm wide. Seventy of the welds were produced using GMAW only. The remaining welds were prepared using GMAW and SMAW. The majority of the trough was filled using GMAW with the final 2 layers being SMAW. After welding, the welds were machined flush with the surface of the plate and inspected for cracks using magnetic particle inspection (MT) and ultrasonic inspection (UT). It was determined that the GMA weld metal did not contain any measurable cracks and all welds capped with SMAW contained several transverse indications ranging up to about 9.5 mm in surface or near surface length and about 1.6 mm in depth. Upon exposure to the corrosive conditions described above, it was determined that no cracks were initiated in the GMA weld metal. It was also concluded that pre-existing cracks in the SMAW welds did not grow significantly. Subsequent measurement of surface residual stresses using neutron diffraction data indicated that a significant amount of compressive residual stresses existed at the surface. Therefore, initiation or growth of cracks due to SCC would not be expected. However, there was some evidence that crack growth may have occurred, and in two instances cracks appeared to have grown significantly to 9.5 mm in depth. But due to discrepancies in crack location data, and early closure of the program, it was determined that there was insufficient data to verify actual crack growth and to therefore attribute crack growth to the presence of the residual stress field.

Summary

This paper describes some of the current U.S. Navy efforts geared toward managing residual stresses and distortion during weld fabrication. These efforts include model development, model verification, thermo-mechanical and thermo-physical property development, the generation of residual stress measurement data using x-ray and neutron diffraction techniques, the analysis of the effects of residual stresses on fatigue and stress corrosion cracking, and the use of weld residual stresses to achieve desired shapes in part manufacturing.

Due to the complexities involved in weld residual stress development, significant emphasis has been placed on modeling. The importance of experimental data for model development and validation has been emphasized. Although in their initial stages, programs have been initiated which are geared toward developing data bases to house thermo-mechanical and thermo-physical properties specifically for modeling purposes. In the past, data such as this has been developed in order to determine performance directly related to service conditions of materials. Therefore, there is a lack of data for many materials at conditions not typically encountered in service. In time, as these databases grow, modeling will continue to be enhanced.

Some of the capabilities of the current existing models were demonstrated. It was shown that there were some differences between FE models and experimental results, but in general were in good agreement. However, it was also shown that residual stress development is highly dependent upon the details of the fabrication process and the material properties and characteristics. Little difference between thermo-mechanically coupled and uncoupled FE results were demonstrated, but additional work is necessary since the work presented here did not include phase transformation effects or varying material properties representative of remelted or reheated material. Preliminary results indicated that the presence of cracking results in a reduction in the residual stress magnitude, but the effect was localized and therefore had no effect on the residual stresses far away from the crack location. Analysis also indicated that the amount of restraint that exists during welding affects the resulting stress magnitude and distribution, contributing to some differences between model analysis and measurement results.

It was demonstrated that careful experimental techniques for measuring residual stresses must be employed to obtain reliable neutron diffraction and x-ray diffraction results for comparing to model analysis. It was shown that welding creates a wide variation in material properties, and can therefore significantly affect measurement results. The reasons for this were attributed to dilution and thermal cycling that occurs during welding.

It was also shown that when analyzing x-ray diffraction results, it is important to realize that the technique is a surface analysis method and can therefore be influenced by surface condition. Grinding stresses played an overwhelming role in masking the surface residual stresses developed by welding. However, the grinding stresses were able to be subtracted from the overall stress state to determine the surface stresses due to welding only. A comparison of surface residual stresses and bulk, through thickness stresses indicated that the surface stress state is not representative of the internal stress state. It is therefore necessary to carefully plan experimental techniques and procedures that will be appropriate for the validation of model results.

It was shown how the iterative interaction between the development of empirical relationships and modeling can be beneficial in providing valuable information toward understanding and solving problems related to weld residual stresses. The application of an empirical model to the distortion of stiffened thin section panels provided useful information relative to the options available for mitigating distortion. It was shown that simply reducing heat input was not a feasible, but intermittent welding and thermal tensioning could provide the desired reduction in distortion. The data generated by this empirical model also suggested that the initial plate flatness could also provide some benefit regarding distortion mitigation.

Efforts were also described which focused on the effects of residual stresses on fatigue cracking and stress corrosion cracking. In a study on the effect of residual stresses on stress corrosion cracking, it was determined that there was insufficient data to reach a logical conclusion. In the study on the effects of residual stresses on fatigue, it was shown that residual stresses play an important role in determining fatigue properties of materials. It was concluded that if compressive residual stresses are not accounted for in fatigue specimens, that significant errors can result, overestimating the fatigue performance of a material. It was also shown that there was no difference in the fatigue crack growth rate of specimens containing residual stresses and those that did not. This was because the crack tip stress field appeared to obliterate the existing residual stresses out to about 1mm ahead of the tip so that the growing crack is never subjected to these stresses. Ahead of the tip-affected region the residual stresses were similar to the pre-crack values, which suggests that fatigue did not result in appreciable stress fading. In fact, the stresses were actually higher after fatigue. Thus it was the generated crack-tip stress field, rather than the fading of existing residual stresses, that led to the insensitivity of growth to pre-existing stresses.

Acknowledgments

This work was funded by the Office of Naval Research (ONR), in support of the Exploratory Development and Manufacturing Science and Technology Programs. The particular efforts of G. Yoder (ONR), S. Linder (ONR) and B. Cole (Naval Sea Systems Command, PMS400D) are greatly appreciated. Without their vision, the advancements in the area of weld residual stresses and distortion would not be possible.

References

1. Kirk, M, C. Conrardy, A. DeBiccari and P. Michaleris, "Prediction and Prevention of Excessive Unfairness in *ARLEIGH BURKE* (DDG-51) Class Deckhouse Fabrication," Welding and Weld Automation in Shipbuilding, A proceding of the Symposium sponsored by the Structural Materials Division of TMS held in Cleveland OH, Oct. 29-Nov. 2, 1995, Edited by R. DeNale, TMS Warrendale, PA, pp. 67-84, April,1996.

2. Brand, P.C., H.J. Prask, J. Blackburn, R. Fields, T.M. Proctor, "Possible Standard Specimens for Neutron Diffraction Residual Stress Measurements," Proceedings of the 1994 Fall Meeting of the Materials Research Society, Nov. 28 - Dec. 2, 1994.

3. Feng, Z., Y.Y Zhu, T. Zacharia, R.J. Fields, P.C. Brand, H. J. Prask and J. M. Blackburn, "Modeling and Validation of Residual Stress Distributions in an HSLA-100 Disk," Recent Trends in Welding Research, 1995, Gatlinburg, TN

4. Prask, H., R. Fields, P. Brand, J. Blackburn, "Evolution of Residual Stresses Around a V-Notch Weldment," Proceedings of the 4th International Conference on Residual Stress, Society for Experimental Mechanics, Inc., June 8-10, 1994.

5. Blackburn, J.M., P.C. Brand, H.J. Prask, R.J. Fields, "The Importance of the Unstressed Lattice Spacing in the Determination of Weld Residual Stresses Using Neutron Diffraction," Welding and Weld Automation in Shipbuilding, A proceding of the Symposium sponsored by the Structural Materials Division of TMS held in Cleveland OH, Oct. 29-Nov. 2, 1995, Edited by R. DeNale, TMS Warrendale, PA, pp. 47-66, April, 1996.

6. Das, S., D.K. Moyer, M.L. Tims, G.K. Upadhya, and, *"Modeling Heat Transfer, Microstructure Development, Transfomation Plasticity, and Residual Stresses in GMA Multi-Pass Butt Welds,"* International Conference Proceedings on Modeling and Control of Joining Processes, Orlando FL, Dec. 8-10, 1993

7. Das, S., G.K. Upadhya, U. Chandra, M.J.Kleinosky, and M.L. Tims, "Finite Element Modeling of a Single-Pass GMA Weldment," *Modeling of Casting, Welding and Advanced Solidification Processes VI,"* Ed. T.S. Piwonka, V. Coller, and L. Knigerman, The Minerals, Metals & Materials Society, 1993.

8. Jo, J., M.J. Kleinosky, C.R. Hubbard, X.L. Wang, and S. Spooner, "Evaluation of Thermal Stress Relief of HY-100 Weld Plate Using Neutron Diffraction," to be submitted to *Welding Journal*.

9. Jo, J., G. Caudill, and R. Santos, "Nondestructive Evaluation of Navy Structural Components Using Barkhausen Noise Analysis," *Navy Engineering Journal, pp 71-75* (Nov. 1994).

10. Jo. J., X.L. Wang, M.J. Kleinosky, C.R. Hubbard, and S. Spooner, "Evaluation of Stress Relief Treatments Using Diffraction," *International Conference on Residual Stresses*, Baltimore, MD, June 8-10, 1994.

11. Jo.J., S. Parthasarathi, V. Ramnarayan, R.E. Swanson, and J. Parnell, "Residual Stress Formation in Titanium Matrix Composites and Tooling During Consolidation Processing," *Residual Stresses in Composites: Measurement, Modeling and Effect on Thermomechanical Properties*, TMS, Feb. 1993.

12. Cunningham, D.R., H.D. Allison, R.W. Hendricks and J.M. Blackburn, "Effects of Pre-Grinding on the Residual Stresses Generated in HSLA-100 Steel Bead-on-Plate Weldments," Submitted to the Welding Journal, 1995.

13. Cunningham, D.R., "Determination of Residual Stresses in HSLA-100 Steel Weldments as a Function of Welding Parameters Using X-Ray Diffraction," Master of Science Thesis at Virginia Polytechnic Institute and State University, Blacksburg, VA, May 1994.

14. Michaleris, P., and A. DeBiccari, "A Predictive Technique for Buckling Analysis of Thin Section Panels Dueto Welding," Submitted for Presentation at the 1996 SNAME Ship Production Technical Symposium, San Diego, CA, 1996

15. J.Almer, J.Cohen, W.Kirk and A.Winholtz "An Analysis of Macro- and Microstresses Around a Fatigue Crack Tip" To be published in Vol.39 of *Advances in X-ray Analysis.*

#507243 ㊵

Modeling the Initiation and Propagation of Fatigue Cracks In Welded Steel Structures

by

S.B. Lambert[1], G. Glinka[1], and R.D. Yee[2]

[1]Department of Mechanical Engineering, University of Waterloo
[2]Fleet Technology Limited, Kanata, Ontario

ABSTRACT

In recent years, classification societies and naval design authorities have introduced explicit fatigue design criteria for welded structural details in merchant and naval ships. These criteria, which are largely based on well-established fatigue design procedures for welded joints in bridges and offshore structures are intended to ensure that there is a low probability of fatigue failures occurring during the design life of a ship, where failure is generally considered to be the initiation of a through-thickness crack several inches long. However, premature fatigue cracking as a result of fabrication or design errors can still occur. Furthermore, some fatigue cracking can still be expected in properly designed and fabricated ships. Therefore, quantitative techniques for predicting the residual life and residual strength of cracked structural welded details are needed to develop safe but cost-effective inspection schedules at the design stage. These techniques could also be used to optimize the scheduling of repairs for cracks found in service, to assess whether the operation of existing ships can be extended beyond their original design lives, and to assess the relative effects of environment and detail configuration on fatigue performance.

Fatigue cracking in welded details is a complex process that usually involves the initiation of multiple cracks along a weld toe in a pseudo-random manner, and the growth and coalescence of these cracks. Over the past decade, researchers at the University of Waterloo have developed probabilistic models for predicting the initiation and propagation of fatigue cracks in welded marine structures, including notch strain models for fatigue crack initiation and linear elastic fracture mechanics analysis for fatigue crack propagation. These models have been verified against experimental data on the initiation and propagation of fatigue cracks in large scale welded details.

This paper discusses the analytical basis of the models including the strain energy density approach to notch strain analysis, the weight function method for the efficient calculation of crack tip stress intensity factors, algorithms for simulating the coalescence of multiple cracks, and probabilistic methods to account for the variability of local weld geometry and material properties. In addition, developments currently underway to account for three-dimensional stress distributions and load shedding effects in ship structures are presented.

Outline

- Fatigue in Naval Structures
- Fatigue Modeling
  - Initiation
  - Propagation
  - Simulations
- T-Plate Example
  - Geometry and Loading
  - Input Data
  - Results

Fatigue in Naval Structures

- Fatigue Loading
  - *wave loading* - longitudinal and transverse bending, torsion
  - *fluctuating hydrostatic pressure* - tank walls, cargo holds
  - *machinery and hull vibration*
- Corrosive Environment
  - *seawater, sour crude oil*
  - *corrosion fatigue, localized thinning*

Fatigue in Naval Structures (con't)

- Welded Connections
  - hatch corners, bulkhead intersections, end connections
  - stress concentrations, residual stresses, weld defects, redundant load paths
- Fatigue Analyses
  - damage tolerant design
  - scheduling of inspections
  - fabrication or design errors

Fatigue Modeling

- Initiation
  - strain-life analysis
  - notch analysis
- Propagation
  - crack growth data
  - stress intensity factor calculations
  - crack shape development
- Simulations
  - initiation and propagation
  - Monte Carlo Techniques
  - input data

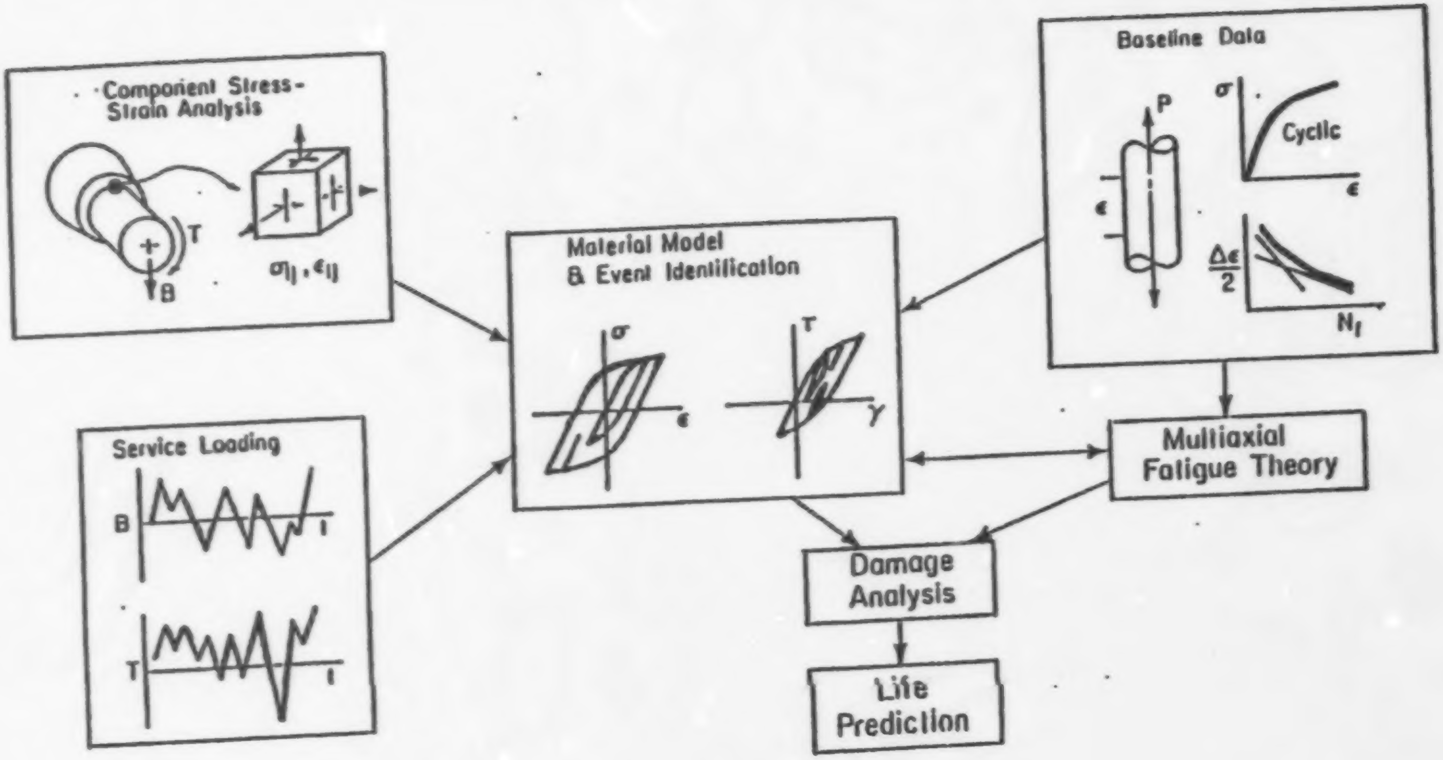

Component Stress-Strain Analysis
T
B
$\sigma_{ij}, \epsilon_{ij}$
Service Loading
B
t
T
t
Material Model & Event Identification
σ
ϵ
τ
γ
Baseline Data
P
ϵ
σ
Cyclic
ϵ
$\frac{\Delta\epsilon}{2}$
N_f
Multiaxial Fatigue Theory
Damage Analysis
Life Prediction

Schematic of Component Fatigue Analysis by the Local Stress-Strain Approach

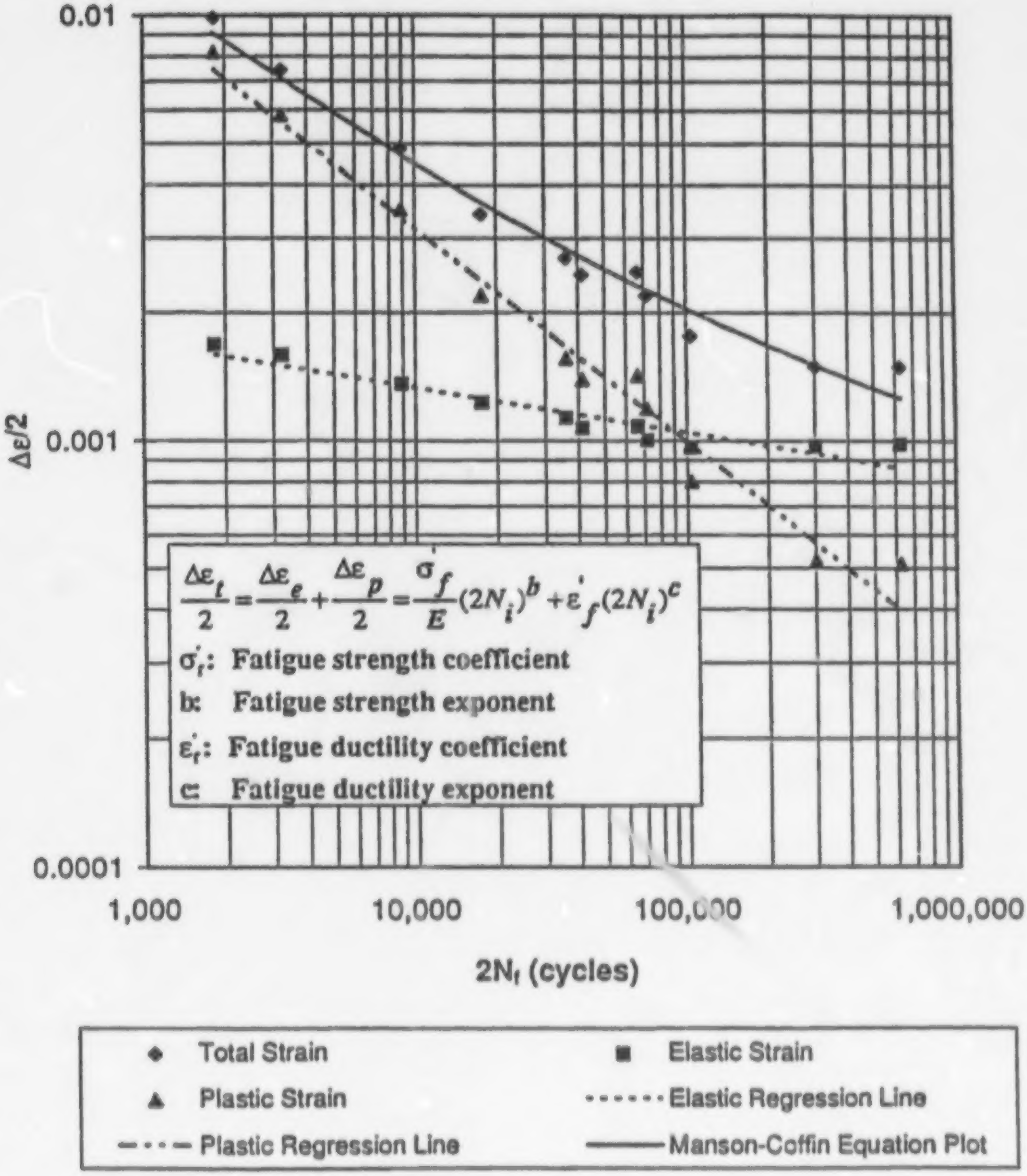
0.01
0.001
0.0001
$\Delta\varepsilon/2$
1,000
10,000
100,000
1,000,000
$2N_f$ (cycles)
$\frac{\Delta\varepsilon_t}{2}=\frac{\Delta\varepsilon_e}{2}+\frac{\Delta\varepsilon_p}{2}=\frac{\sigma'_f}{E}(2N_i)^b+\varepsilon'_f(2N_i)^c$
σ'_f: Fatigue strength coefficient
b: Fatigue strength exponent
ε'_f: Fatigue ductility coefficient
c: Fatigue ductility exponent
◆ Total Strain
■ Elastic Strain
▲ Plastic Strain
- - - - - - Elastic Regression Line
— · · · — Plastic Regression Line
——— Manson-Coffin Equation Plot

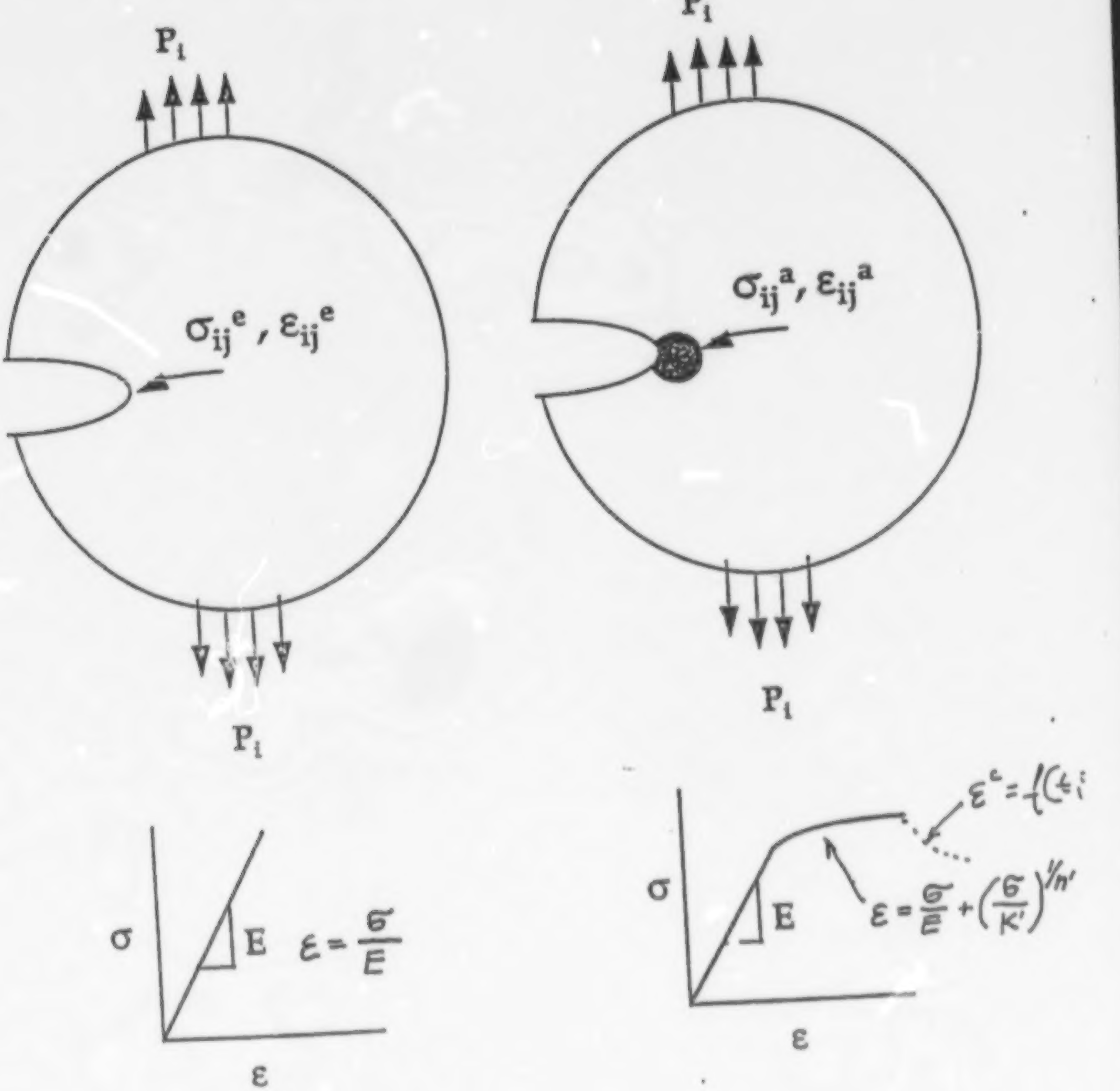
P_i
$\sigma_{ij}^e, \varepsilon_{ij}^e$
P_i
σ
E
$\varepsilon = \frac{\sigma}{E}$
ε
P_i
$\sigma_{ij}^a, \varepsilon_{ij}^a$
P_i
$\varepsilon^c = f(t;$
σ
E
$\varepsilon = \frac{\sigma}{E} + \left(\frac{\sigma}{K'}\right)^{1/n'}$
ε

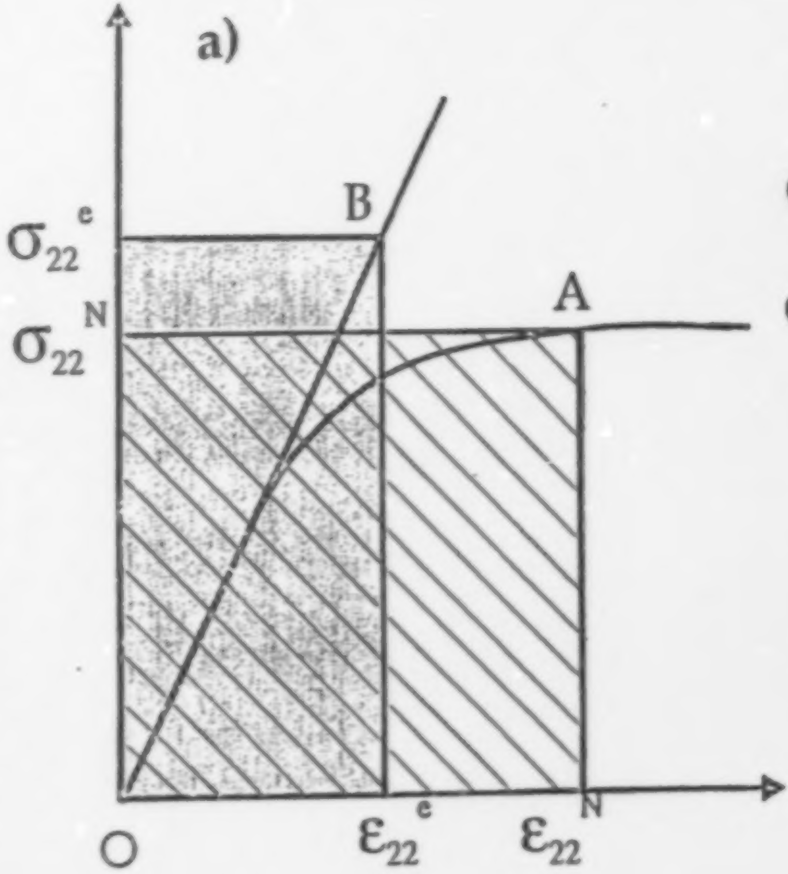

$$\sigma_{22}^{e}\varepsilon_{22}^{e}=\sigma_{22}^{N}\varepsilon_{22}^{N}$$

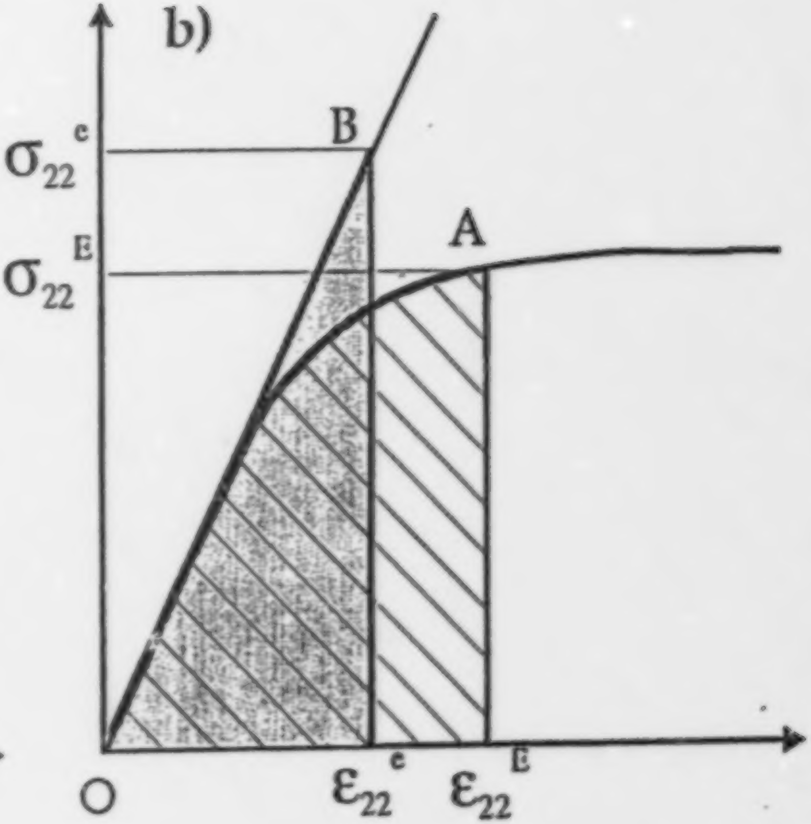

$$\frac{1}{2}\sigma_{22}^{e}\varepsilon_{22}^{e}=\int_{0}^{\varepsilon^{e}}\sigma_{22}^{E}\,d\varepsilon_{22}^{E}$$

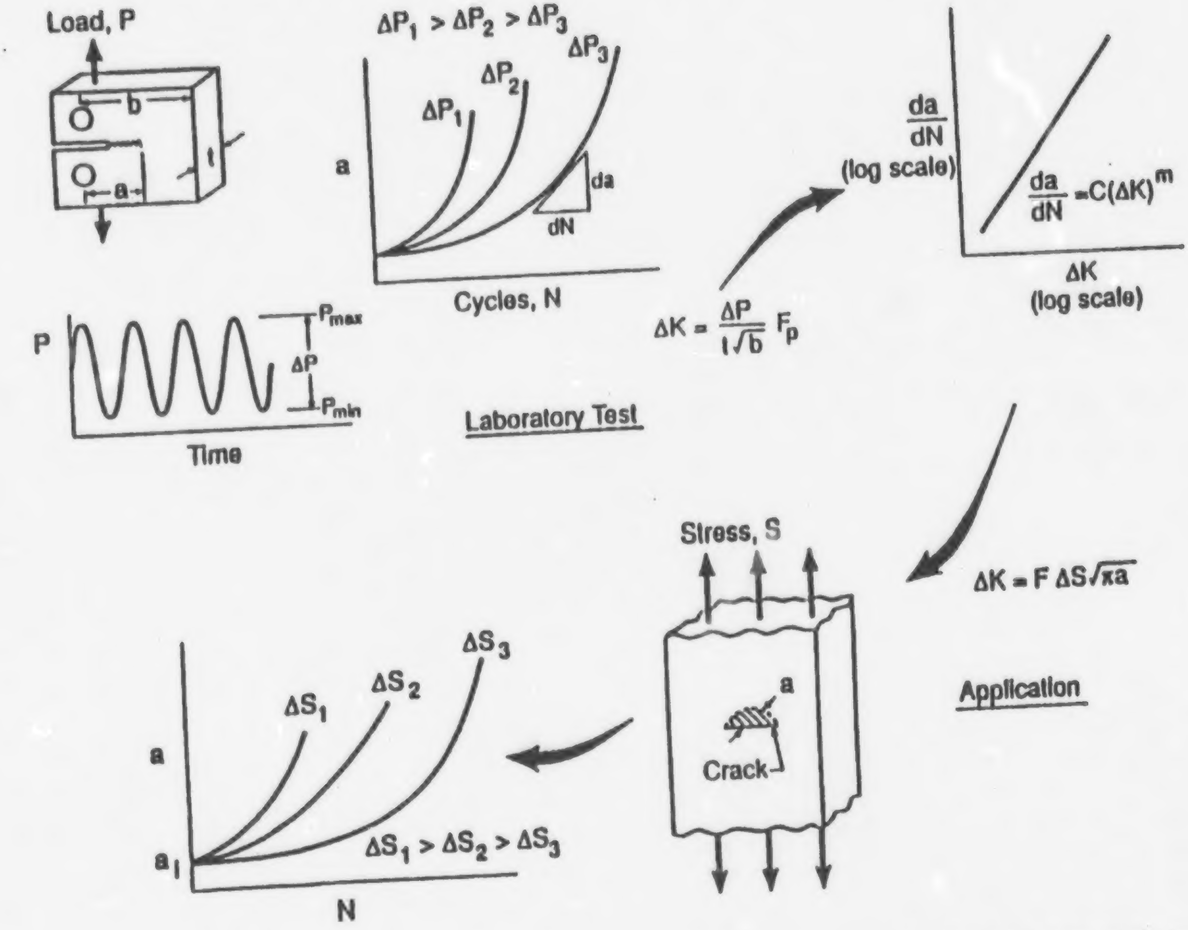
Load, P
b
t
a
P
Time
P_{max}
ΔP
P_{min}
$\Delta P_1 > \Delta P_2 > \Delta P_3$
ΔP_1
ΔP_2
ΔP_3
a
da
dN
Cycles, N
Laboratory Test
$\Delta K = \frac{\Delta P}{t\sqrt{b}} F_p$
$\frac{da}{dN}$ (log scale)
$\frac{da}{dN} = C(\Delta K)^m$
ΔK (log scale)
$\Delta K = F \Delta S\sqrt{\pi a}$
Application
Stress, S
a
Crack
ΔS_1
ΔS_2
ΔS_3
a
a_i
$\Delta S_1 > \Delta S_2 > \Delta S_3$
N

Steps in obtaining da/dN vs. ΔK data and using it for an engineering application.

Crack Propagation

- Stress Intensity Factor (K) Calculations

$$K = Y\sigma\sqrt{\pi a}$$

  - – Y - geometry correction factor
  - – σ - nominal (remote) stress
  - – a - crack depth
- handbooks, finite element methods, weight functions

Weight Functions: *m(x, a)*

$$K = \int_0^a m(x,a)\sigma(x)dx$$

$\sigma(x)$ - uncracked stress distribution on the prospective crack plane

Example: through crack in an infinite plate

$$m_A(x,a) = \frac{1}{\sqrt{\pi a}}\sqrt{\frac{a+x}{a-x}}$$

Weight Functions for semi-elliptic cracks in a flat plate:

$$m_A(x,a) = \frac{2}{\sqrt{2\pi(a-x)}}\left[1 + M_{1A}\left(1-\frac{x}{a}\right)^{1/2} + M_{2A}\left(1-\frac{x}{a}\right) + M_{3A}\left(1-\frac{x}{a}\right)^{3/2}\right]$$

at the deepest point, *A*, and

$$m_B(x,a) = \frac{2}{\sqrt{\pi x}}\left[1 + M_{1B}\left(\frac{x}{a}\right)^{1/2} + M_{2B}\left(\frac{x}{a}\right) + M_{3B}\left(\frac{x}{a}\right)^{3/2}\right]$$

at the surface point, *B*.

See Wang and Lambert, *Engineering Fracture Mechanics*, Vol. 51, No. 4, pp. 517-532, 1995.

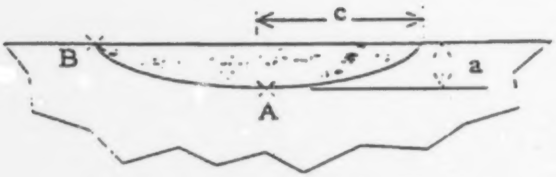

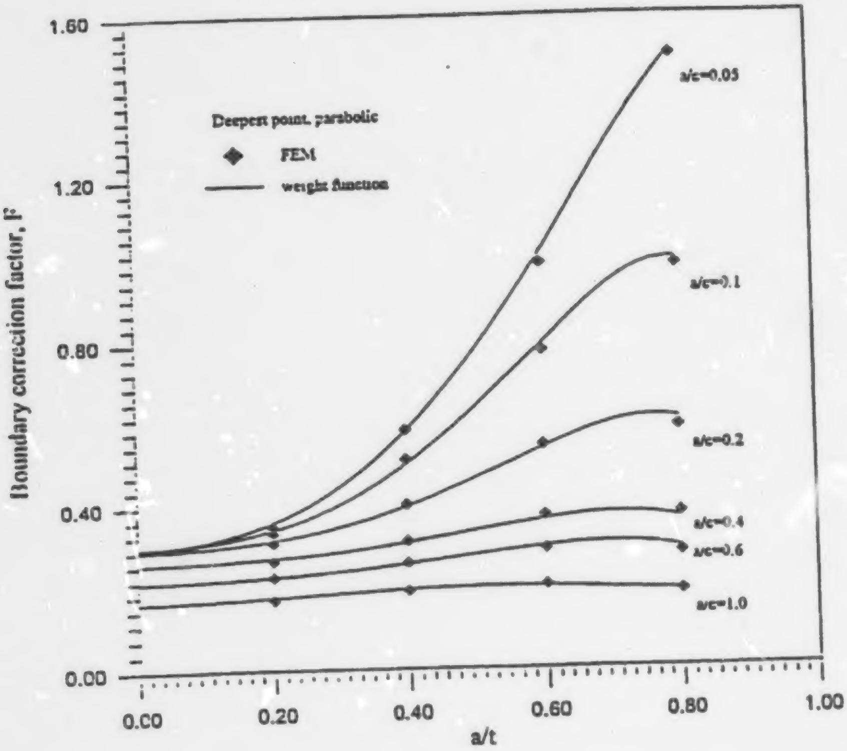
1.60
1.20
0.80
0.40
0.00
Boundary correction factor, F
Deepest point, parabolic
◆ FEM
—— weight function
a/c=0.05
a/c=0.1
a/c=0.2
a/c=0.4
a/c=0.6
a/c=1.0
0.00
0.20
0.40
0.60
0.80
1.00
a/t

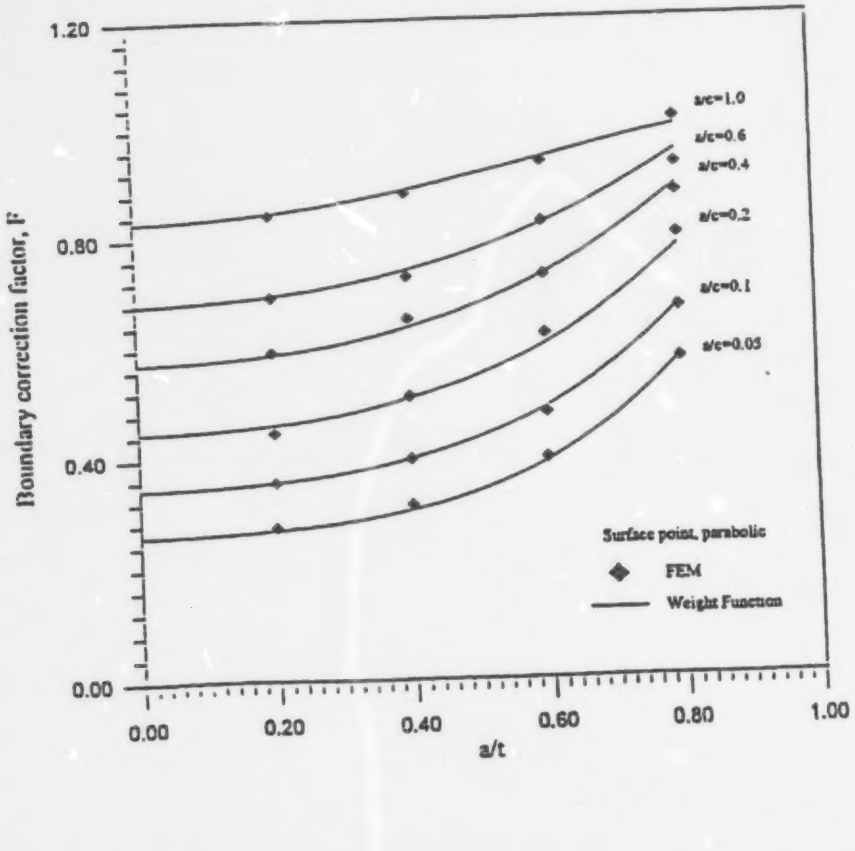
1.20
0.80
0.40
0.00
Boundary correction factor, F
a/c=1.0
a/c=0.6
a/c=0.4
a/c=0.2
a/c=0.1
a/c=0.05
Surface point, parabolic
◆ FEM
—— Weight Function
0.00
0.20
0.40
0.60
0.80
1.00
a/t

Crack shape development assumptions should be based on physical observations.

Example: T-plate welded joint:
Edge crack is the most conservative (shortest predicted life).

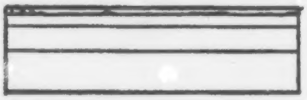

Single surface crack with 'natural' development is the least conservative.

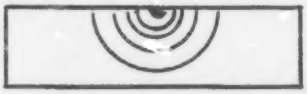

Single surface crack with a prescribed aspect ratio (forcing function) based on physical observations is more accurate.

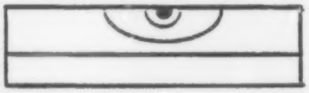

Multiple surface crack with simple coalescence rules is most accurate.

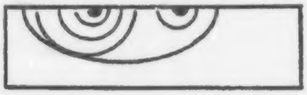

Example: T-Plate Welded Joint

See: R.L. Lecsek, R. Yee, S.B. Lambert and D.J. Burns, “A Probabilistic Model for Initiation and Propagation of Surface Cracks in Welded Joints”, *Fatigue & Fracture of Engineering Materials and Structures*, Vol. 18, No. 7/8. pp. 821-831, 1995.

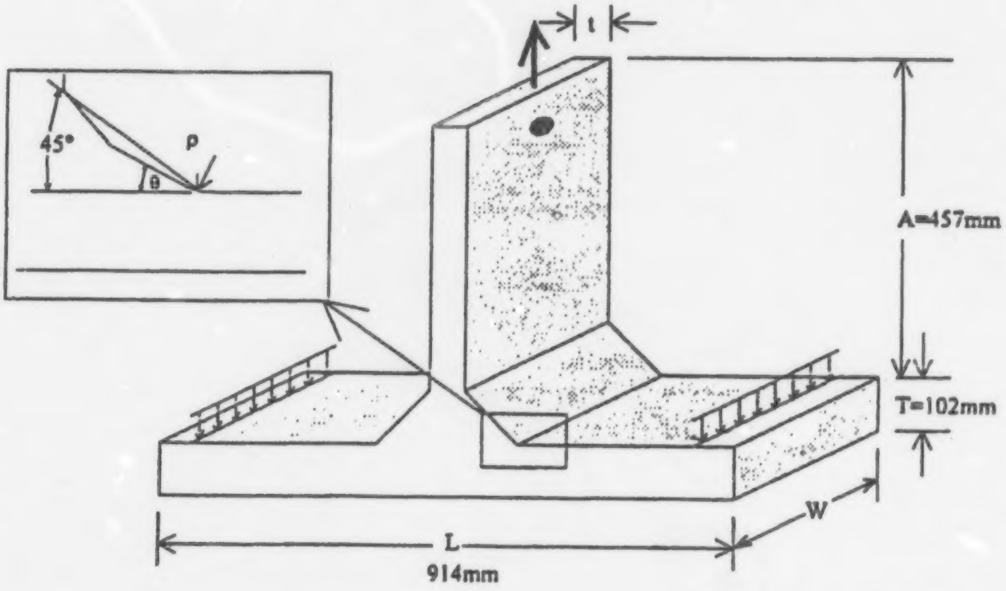
45°
ρ
θ
t
A=457mm
T=102mm
W
L
914mm

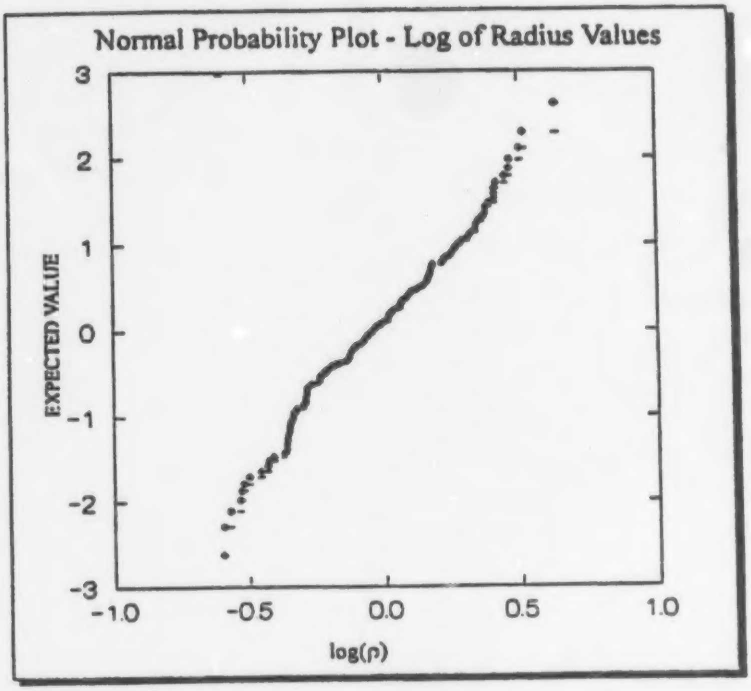
Normal Probability Plot - Log of Radius Values
EXPECTED VALUE
3
2
1
0
-1
-2
-3
-1.0
-0.5
0.0
0.5
1.0
log(ρ)

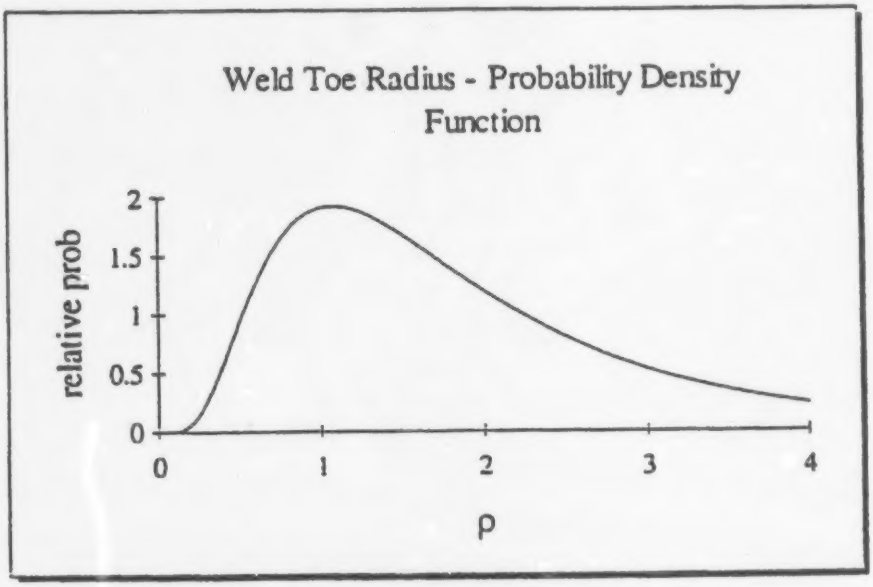
Weld Toe Radius - Probability Density Function
relative prob
2
1.5
1
0.5
0
0
1
2
3
4
ρ

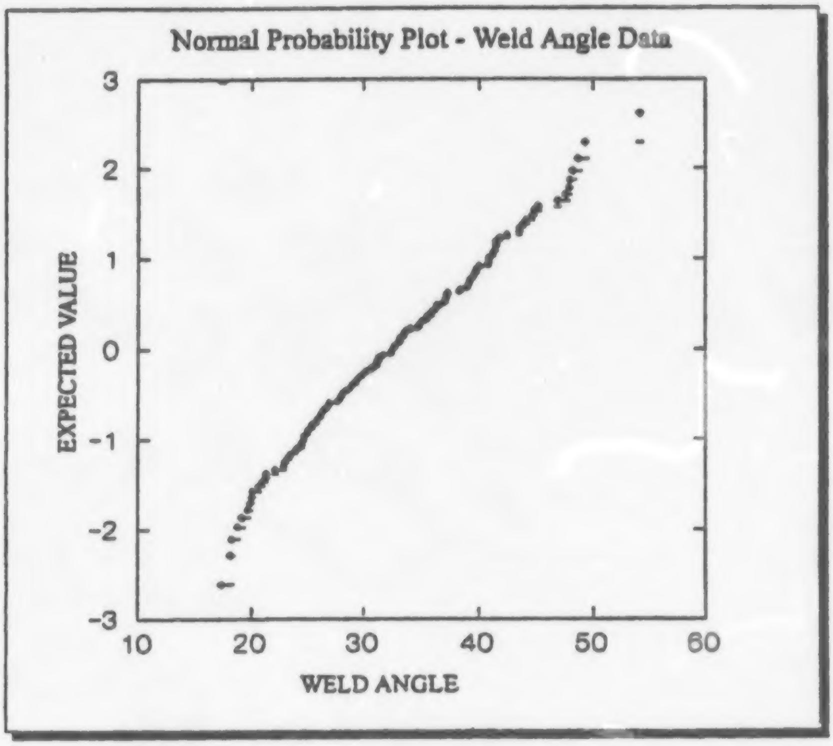
Normal Probability Plot - Weld Angle Data
EXPECTED VALUE
3
2
1
0
-1
-2
-3
10
20
30
40
50
60
WELD ANGLE

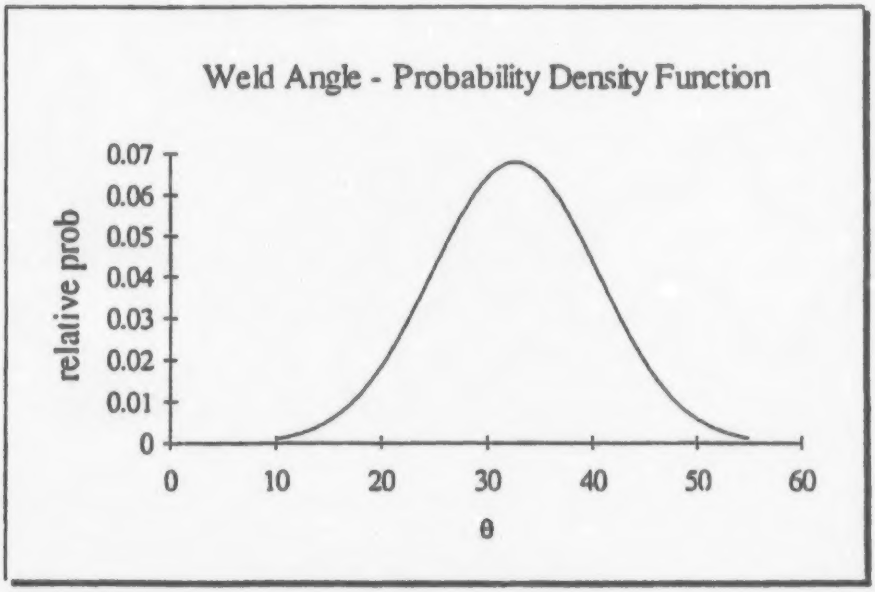
Weld Angle - Probability Density Function
relative prob
0.07
0.06
0.05
0.04
0.03
0.02
0.01
0
0
10
20
30
40
50
60
θ

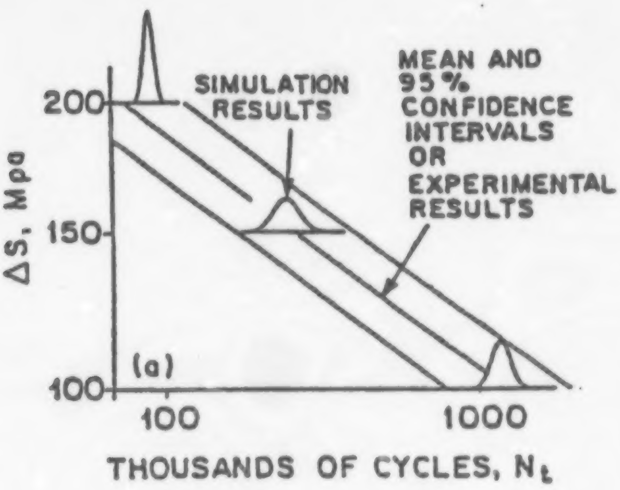
SIMULATION RESULTS
MEAN AND 95% CONFIDENCE INTERVALS OR EXPERIMENTAL RESULTS
ΔS, Mpa
200
150
100
(a)
100
1000
THOUSANDS OF CYCLES, N_t

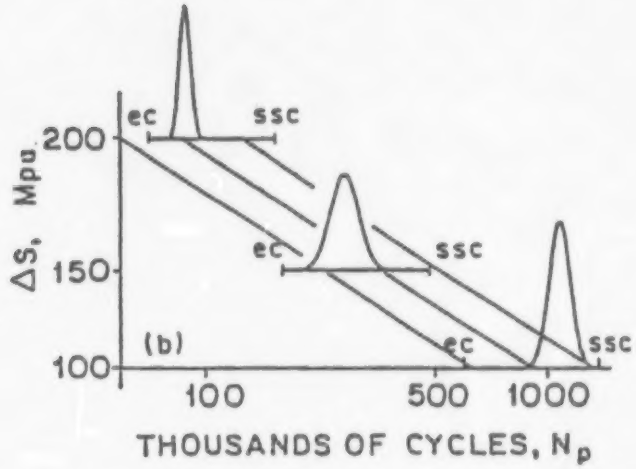
ec
ssc
ec
ssc
ec
ssc
ΔS, Mpa
200
150
100
(b)
100
500
1000
THOUSANDS OF CYCLES, N_p

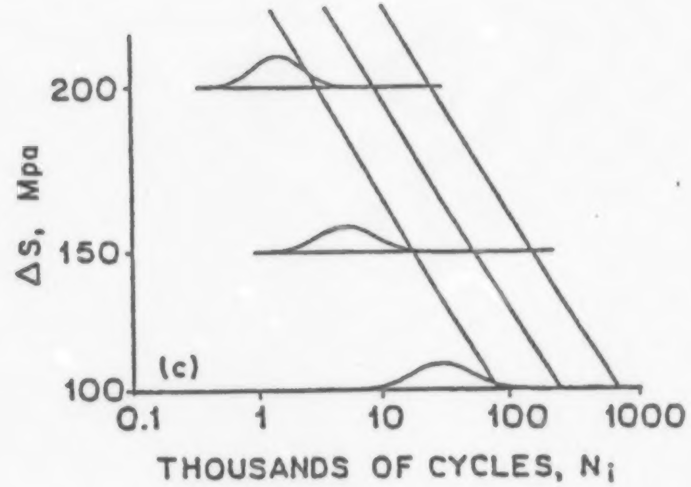
ΔS, Mpa
200
150
100
(c)
0.1
1
10
100
1000
THOUSANDS OF CYCLES, N_i

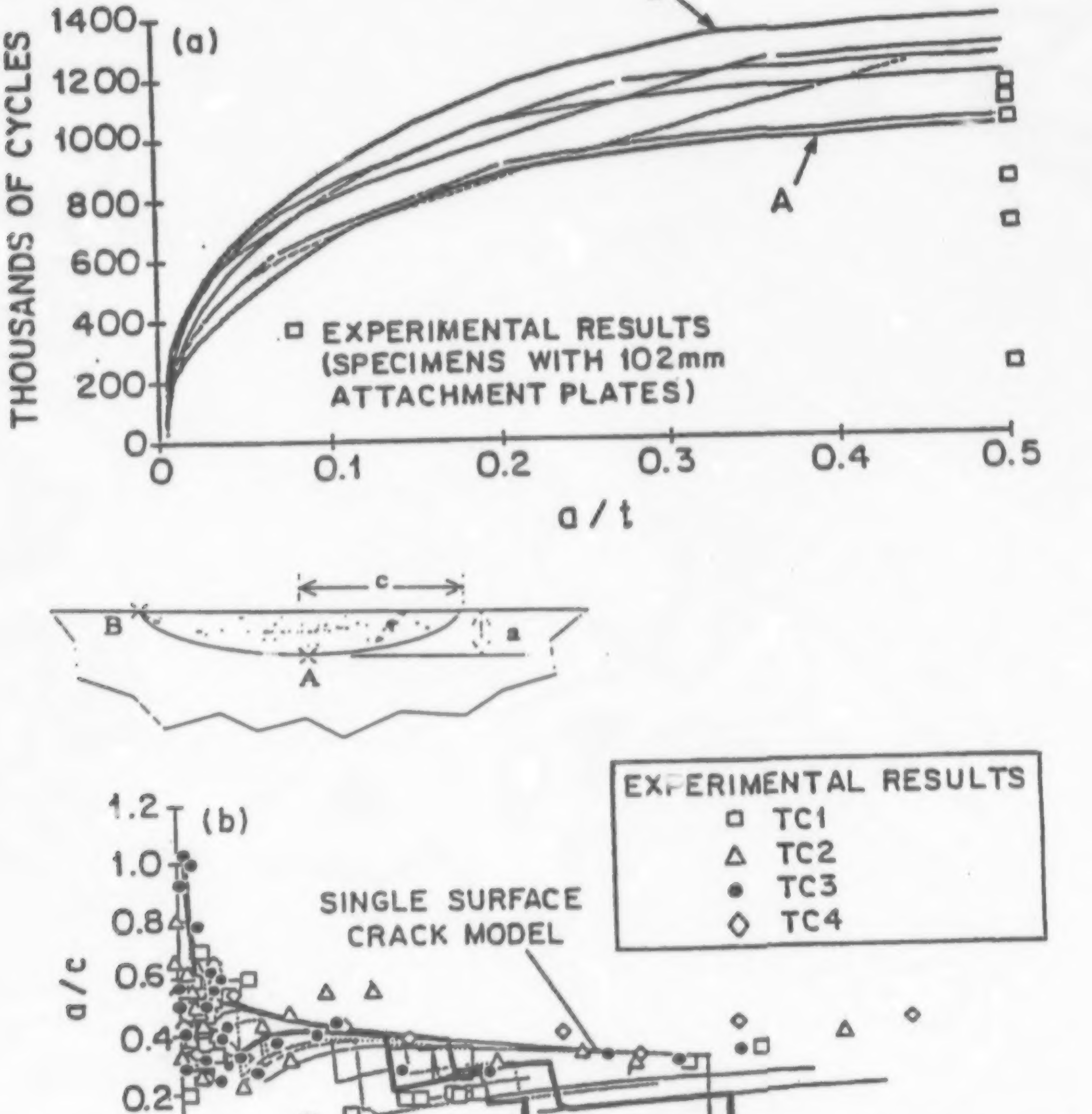
(a)
THOUSANDS OF CYCLES
0
200
400
600
800
1000
1200
1400
B
A
EXPERIMENTAL RESULTS (SPECIMENS WITH 102mm ATTACHMENT PLATES)
0
0.1
0.2
0.3
0.4
0.5
a / t
c
B
a
A
EXPERIMENTAL RESULTS
□ TC1
△ TC2
● TC3
◇ TC4
(b)
a/c
0
0.2
0.4
0.6
0.8
1.0
1.2
SINGLE SURFACE CRACK MODEL
0
0.1
A
0.2
0.3
B
0.4
0.5
a/t

#507244 (*)

An Overview of the CRAD Major Development Project Improved Ship Structures Maintenance Management (ISSMM)

by

LCdr. Steve Gibson
National Defence Headquarters, Ottawa, ON K1A OK2

John Porter and Neil Pegg
Defence Research Establishment Atlantic, P.O. Box 1012
Dartmouth, NS B2Y 3Z7

ABSTRACT

The Improved Ship Structural Maintenance Management (ISSMM) CRAD major project is being developed to provide a tool to assess the effect of various types of damage and degradation on the structural integrity of the Halifax Class patrol frigates. The structural assessment is being done primarily by finite element analysis using a top-down approach of global modeling of the complete hull structure with fine mesh models of specific areas of interest. The calculation of stress in structural details is required for the assessment of strength, endurance (fatigue) and stability limit states. In many cases the change in structural integrity due to the damage will be assessed by comparing results of the same analyses for the damaged and undamaged structure.

A prerequisite for the successful application of advanced numerical or analytical structural analysis methods is access to relevant and comprehensive material property data. Unfortunately, for the material systems employed during the construction of the HALIFAX Class Frigate, more commonly known as the Canadian Patrol Frigate (CPF), there is limited property data available. In addition to the development of analysis methods, structural tests and trials at sea, a significant element of the work is to develop a suitable materials property database, necessary for the implementation of the advanced numerical analysis systems that will be developed during the project.

#507245 (42)

Fatigue Crack Growth of Naval Platform Materials Under Spectrum Loading

by

John F. Porter
Defence Research Establishment Atlantic, P.O. Box 1012
Dartmouth, Nova Scotia, B2Y 3Z7

Richard Yee
Fleet Technology Limited, 311 Legget Drive
Kanata, Ontario, K2K 1Z8

Mike Chernuka
Martec Limited, 1888 Brunswick Street
Halifax, Nova Scotia, B3J 3J8

ABSTRACT

As part of the Defence Research Establishment Atlantic's continuing research efforts to quantify fatigue crack growth mechanisms in Canadian naval platform steels and weldments, the challenges associated with the prediction of fatigue crack growth under variable amplitude cyclic loading have been addressed, both experimentally and numerically. A number of unwelded A517 Grade F steel standard middle tension specimens have been fabricated and subjected to variable amplitude cyclic loading in accordance with the ASTM Standard E647. Realistic stress-time histories (incorporating pseudo-random stress ranges), which reflect representative long range statistical distributions of stresses in naval platform materials have been defined and employed in the experimental program. During the application of these cyclic stress-time histories to the precracked samples, their influence on crack extension has been continuously monitored. The results of these experiments have been compared with predictions based on current empirical fracture mechanics crack growth methodologies. The LIFE3D three dimensional finite element based fatigue analysis software package, which simulates the propagation of both surface and through-thickness cracks in solid bodies has been modified to incorporate variable amplitude loading conditions. In addition, crack retardation and crack closure models have been included in the software. The package has been employed to numerically simulate the crack growth of the A517 center cracked specimens, employing pseudo-random, hi-lo, lo-hi and root-mean-square representations of the afore-mentioned stress-time histories for comparison with the experimental crack growth results. The results of these studies to date will be presented, focusing on deficiencies in current available crack growth predictive methodologies, as applied to realistic loading conditions on naval platforms.

587246   43

A Summary of Experimental Strain Measurements on Canadian Patrol Frigates

by

John F. Porter
Defence Research Establishment Atlantic, PO Box 1012
Dartmouth, Nova Scotia, B2Y 3Z7

Rod Kennett
Naval Engineering Test Establishment, 9410 Wanklyn Drive
LaSalle, Quebec, H8R 1Z2

Bruce Paterson and Richard Yee
Fleet Technology Limited, 311 Legget Drive
Kanata, Ontario, K2K 1Z8

ABSTRACT

In ongoing efforts by Defence Research Establishment Atlantic to assess the suitability of current fatigue crack initiation and propagation methodologies to naval platforms, a number of experimental trials have been conducted on highly stressed regions on several Canadian Patrol Frigates (CPF). In collaboration with the Naval Engineering Testing Establishment, these experimental investigations have focused on quantifying dockside residential strain states via the recently developed miniature x-ray diffractometer (MXRD) and the applied cyclic strain states due to various ship operations, in the regions of interest. The results of these trials have been employed in advanced fatigue assessments (employing the current Canadian DND fatigue design guidelines (SSCP23), local strain analysis methods and linear elastic fracture mechanics methods) to make predictions of fatigue crack initiation and propagation lives for the weldments of interest. This presentation is intended to review the progress to date and to outline future testing requirements.

#567247 (44)

Research and Development Activities Within the CRAD Aircraft Structures and Materials Program

by

Ken McRae, Major B.J. Miller and Capt. B.A. Lepine

ABSTRACT

Following the closure of DREP, all research and development activity in the area of aircraft structures and materials has been conducted under the auspices of the Air Vehicles Research Detachment (AVRD) which has co-located with the National Research Council's Institute for Aerospace Research. This presentation will describe the scope of the R&D activities that have been performed or sponsored by AVRD since its inception in April 1995. Due to time limitations, it will not be possible to describe in complete detail each of the activities currently under way, however, brief descriptions of several projects will be described. It will be the intent to illustrate air-related activities in the context of general materials science with the potential for future collaboration between the marine and air materials programs within CRAD.

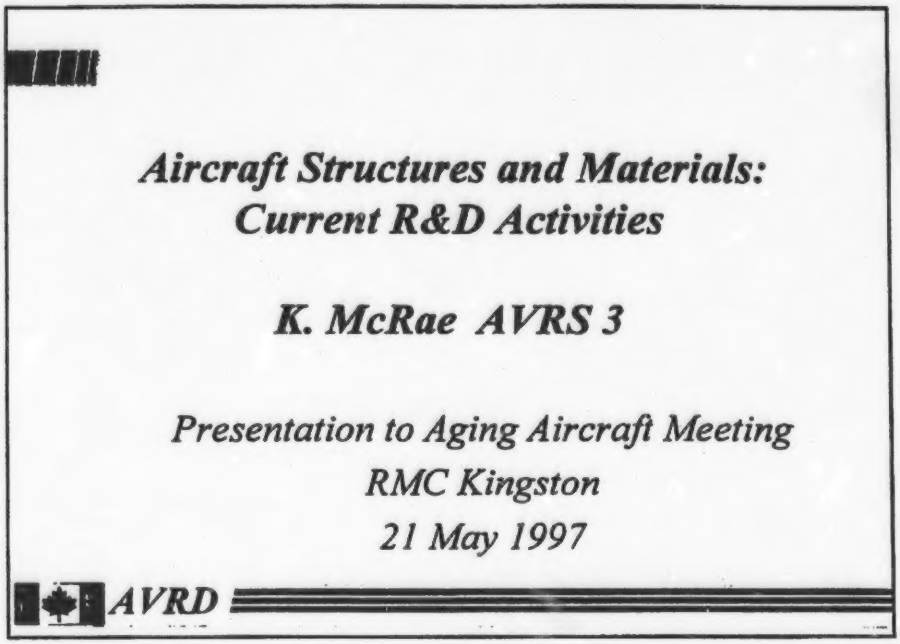

Aircraft Structures and Materials: Current R&D Activities

K. McRae AVRS 3

Presentation to Aging Aircraft Meeting
RMC Kingston
21 May 1997

AVRD

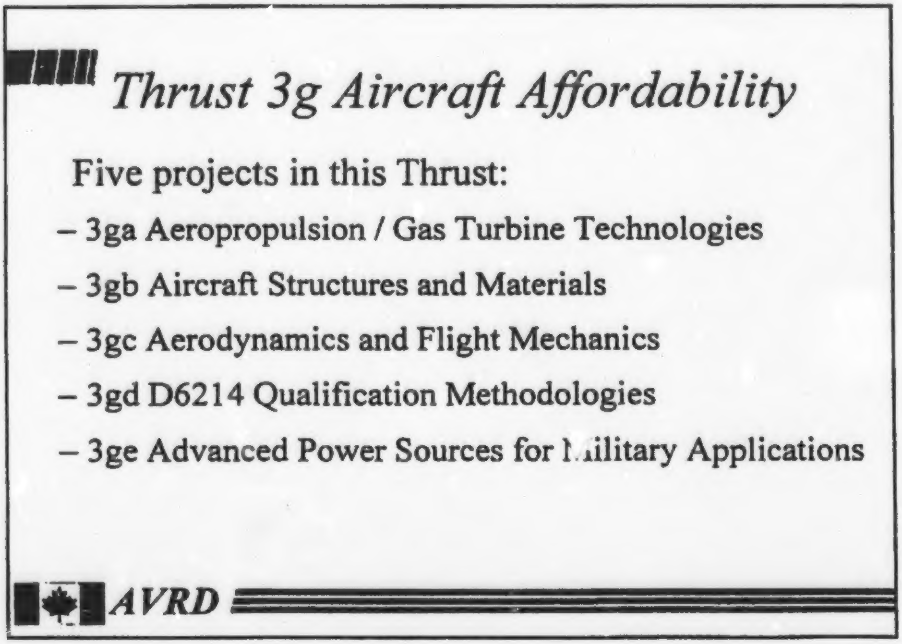

Thrust 3g Aircraft Affordability

Five projects in this Thrust:

- 3ga Aeropropulsion / Gas Turbine Technologies
- 3gb Aircraft Structures and Materials
- 3gc Aerodynamics and Flight Mechanics
- 3gd D6214 Qualification Methodologies
- 3ge Advanced Power Sources for Military Applications

AVRD

3GB Project Overview

- Total value $1.5M in FY 97/98
  - 7 Work Units - 40% research and 60% development
- Program delivery through:
  - NRC/IAR collaborations
    - » equivalent funding from NRC
    - » approx. 60 researchers/technologists
  - In-house research activities
  - External
    - » RMC, QETE, ATESS, Canadian industry/universities

AVRD

NRC Structures and Materials

NRC Aerospace Structures and Materials Collaborative Research (3GB12)

- Multiple site damage / corrosion
- D-Sight development & pillowing stresses
- Bonded repair technology
- NDT Data fusion
- Edge-of-light scanner for flaw detection

AVRD

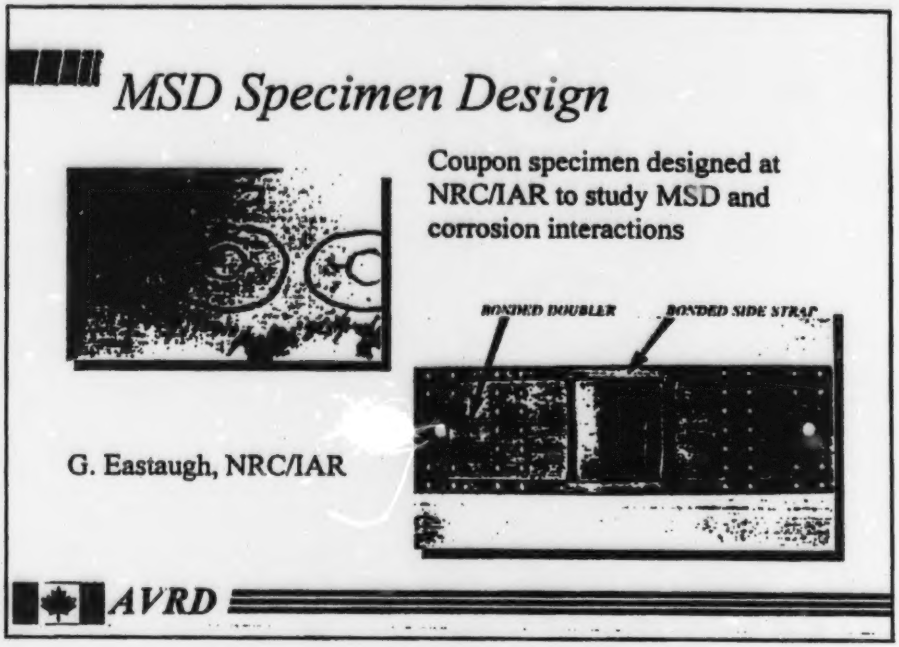

MSD Specimen Design

Coupon specimen designed at NRC/IAR to study MSD and corrosion interactions

BONDED DOUBLER
BONDED SIDE STRAP

G. Eastaugh, NRC/IAR

AVRD

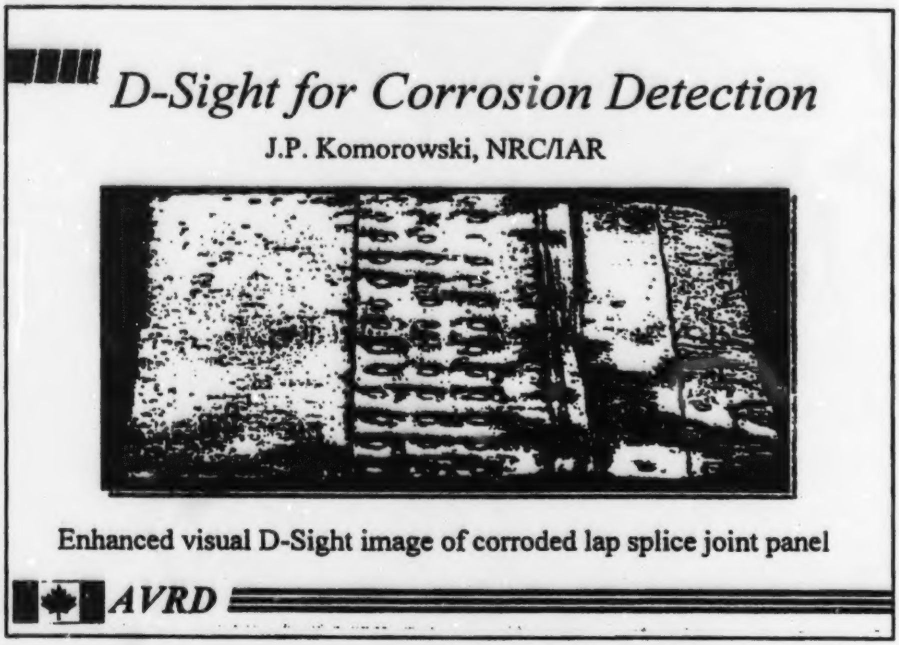

D-Sight for Corrosion Detection

J.P. Komorowski, NRC/IAR

Enhanced visual D-Sight image of corroded lap splice joint panel

AVRD

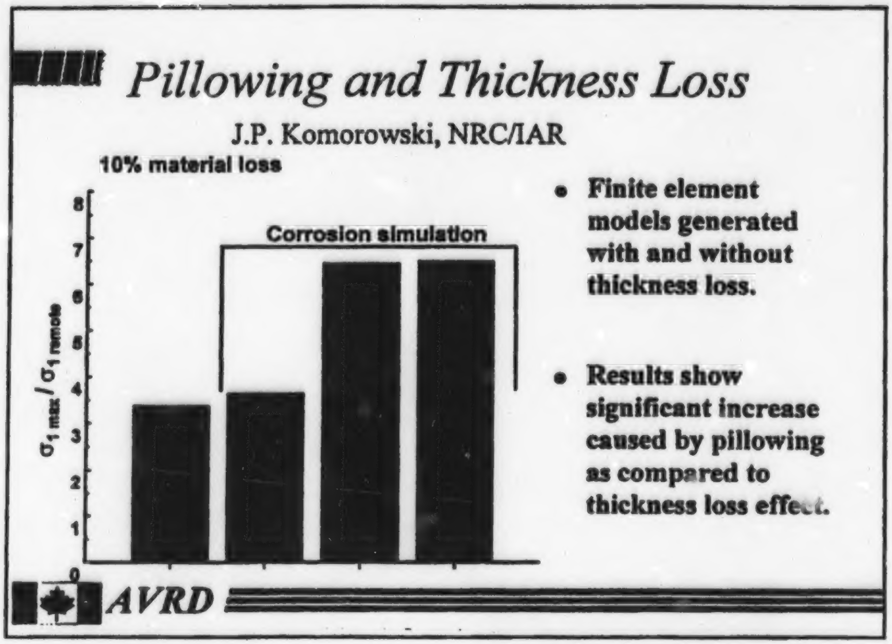

Pillowing and Thickness Loss

J.P. Komorowski, NRC/IAR

- Finite element models generated with and without thickness loss.
- Results show significant increase caused by pillowing as compared to thickness loss effect.

AVRD

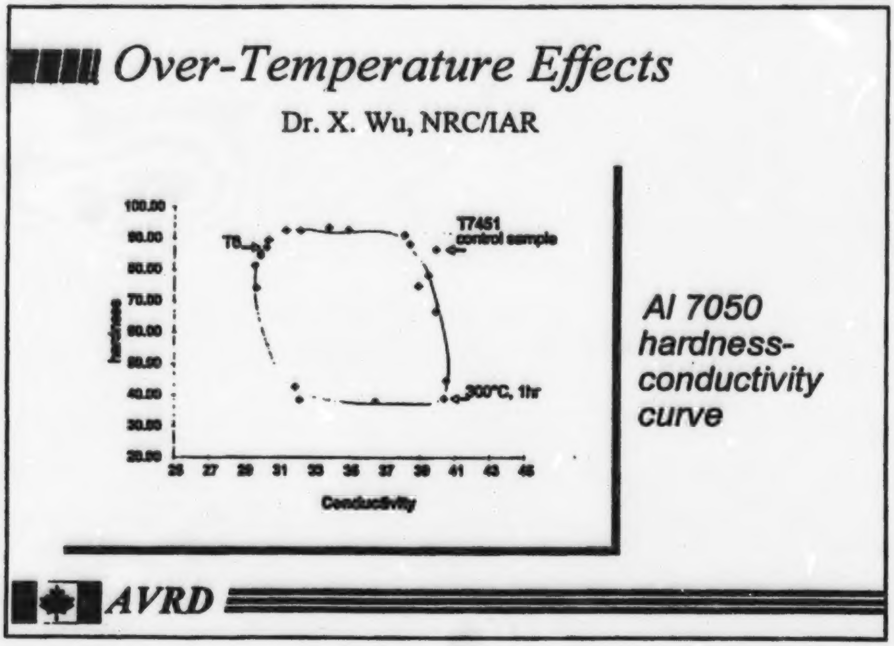

Over-Temperature Effects

Dr. X. Wu, NRC/IAR

Al 7050 hardness-conductivity curve

AVRD

Composite Patch Repairs

D. Raizenne, NRC/IAR

- Composite materials to enhance/repair thick section aluminum structure.
- Develop 3-D patch shapes.
- Develop simple and cost effective application.
- Composite patches could be classified as:
    - fatigue life enhancement, and/or
    - primary structure.
- F-18 Y470.5 bulkhead X-19 location identified.

AVRD

Multimode NDI

D. Forsyth, NRC/IAR

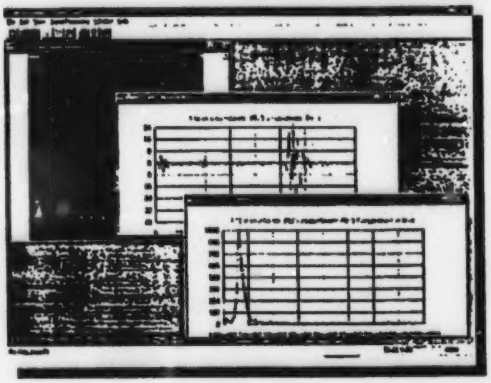

OBJECTIVE: apply advanced signal/image processing and AI techniques to combine information from multiple NDI sources

AVRD

Edge of Light enhanced optical NDI technique

D. Forsyth, NRC/IAR

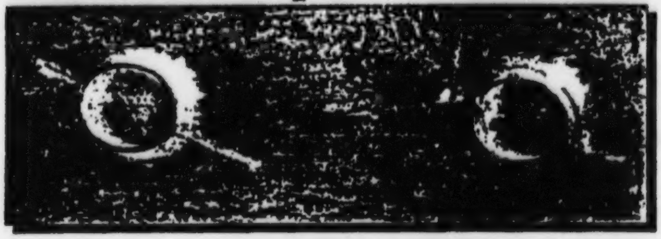

Crack Detection

Detection of Cold-working

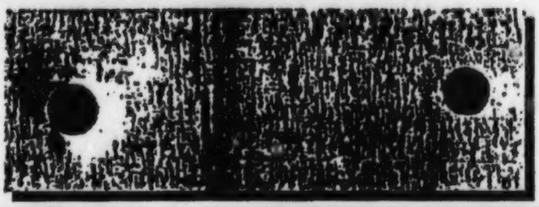

Corrosion Prevention

Corrosion Monitoring and Prevention Techniques (3GB21)

- Corrosion surveillance
- Relationship between environment and damage
- Environmental sensors
- KBS Corrosion System

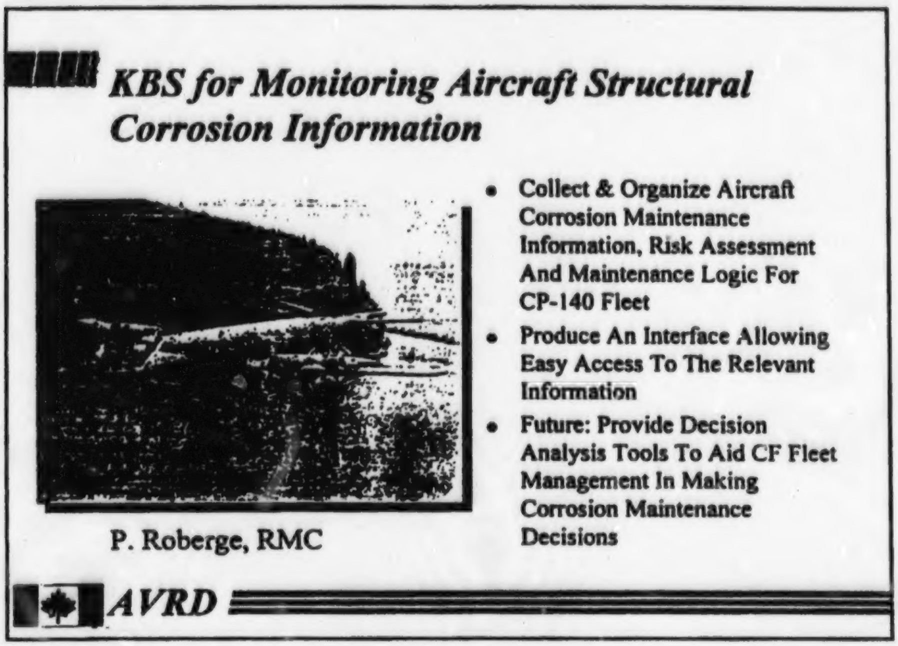

KBS for Monitoring Aircraft Structural Corrosion Information

- Collect & Organize Aircraft Corrosion Maintenance Information, Risk Assessment And Maintenance Logic For CP-140 Fleet
- Produce An Interface Allowing Easy Access To The Relevant Information
- Future: Provide Decision Analysis Tools To Aid CF Fleet Management In Making Corrosion Maintenance Decisions

P. Roberge, RMC

AVRD

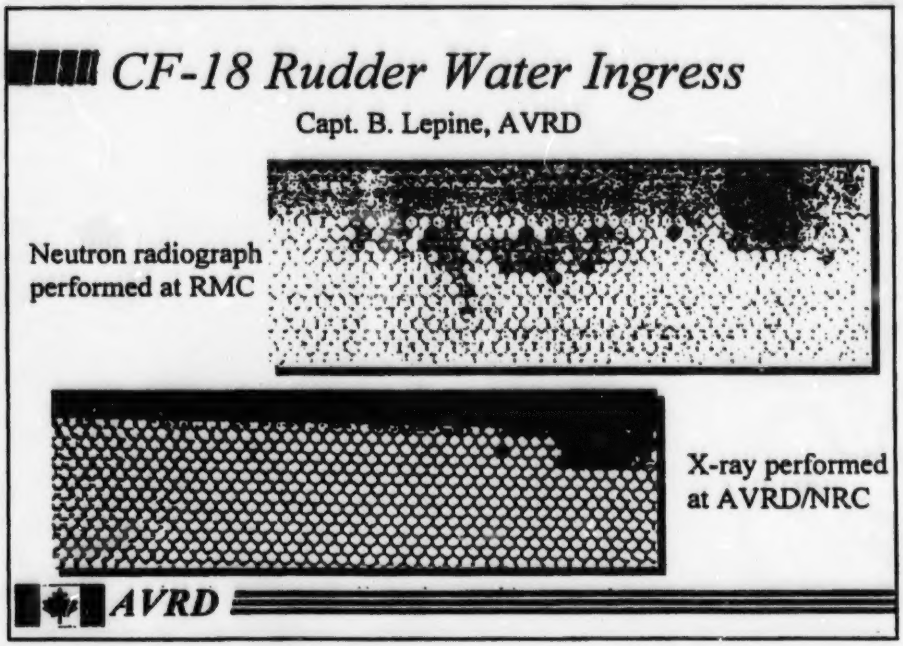

CF-18 Rudder Water Ingress

Capt. B. Lepine, AVRD

Neutron radiograph performed at RMC

X-ray performed at AVRD/NRC

AVRD

Advanced Materials Research

Advanced Structural Materials Concepts Development (3GB37)

- Alloy substitution for improved corrosion
- Advanced composites research
- Retrogression Reaging of 7075-T6 Alloys
- Ceramics, CMC's and intermetallics
- Adhesives research
- Thermal barrier / erosion coatings

AVRD

RRA of 7075-T6 Aluminum

R.T. Holt, NRC/IAR

CC-130 Hercules

Sloping longeron alloy enhancement for improved corrosion resistance

AVRD

Adhesives Research at RMC

R. Underhill, RMC

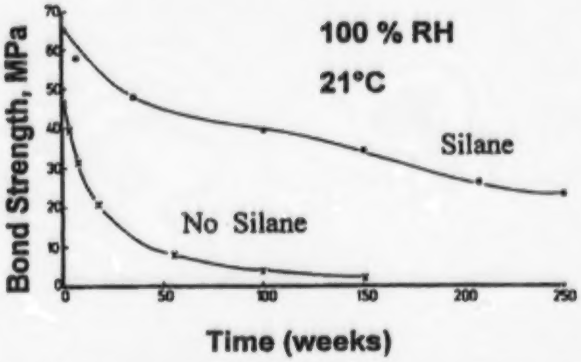

Thermal Barrier Coatings for Gas Turbine Applications

Capt. K. Jaansalu, AVRD

Photos courtesy of Orenda Engines

NDE Research

Structural Integrity Verification Research (3GB49)

- Detection of hidden corrosion
- Detection of cracks under installed fasteners
- Flight control surface water ingress
- Advanced inspection techniques

Delivered through NRC, AVRD, RMC and Tektrend

AVRD

Cracks Under Installed Fasteners

- Oblique incidence ultrasonics
- High frequency
- Optimally focussed

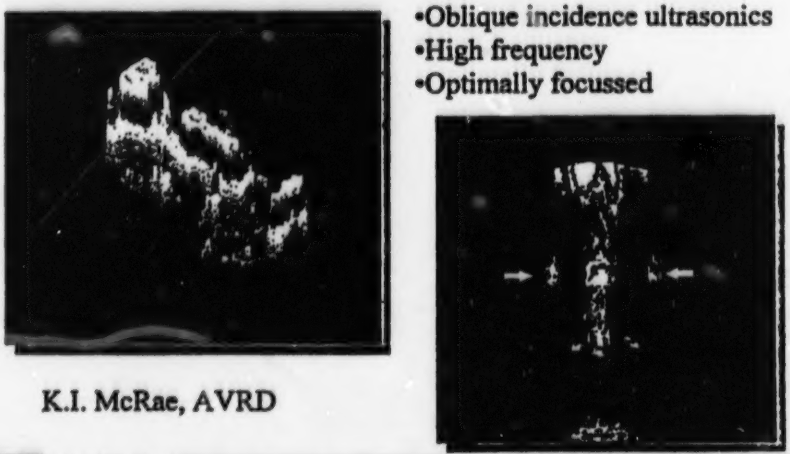

K.I. McRae, AVRD

AVRD

Fastener installed - no cracks detected

Detection of Hidden Corrosion

Capt. B. Lepine, AVRD

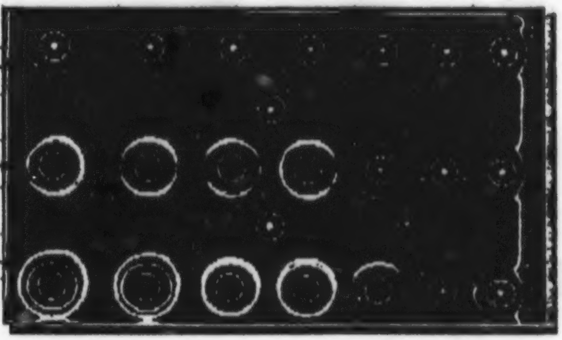

Shallow (6 mils)

Medium (28 mils)

and deep (72 mils) corrosion indication around fastener

Air-Coupled Ultrasonics

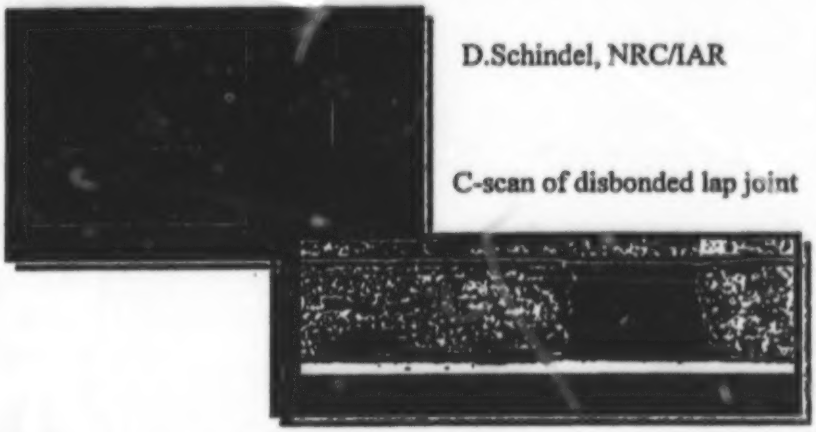

D.Schindel, NRC/IAR

C-scan of disbonded lap joint

Fatigue Related Development

Aircraft Structural Fatigue Technologies (3GB51)

- Material characterization
- Fracture mechanics
- MSD development projects
- Shot peening and cold working effects

Biaxial / Bypass Bearing Stresses

C. Poon, NRC/IAR and CAE

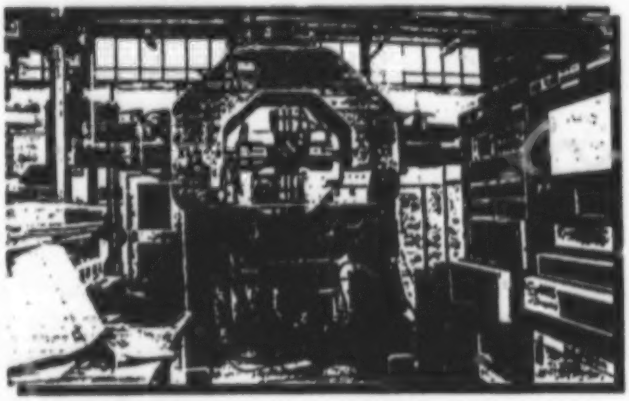

AVRD

Probabilistics

Probabilistic Applications to Aircraft Structural Integrity (3GB52)

- Structural Life Analysis
- Probabilistic Fracture Mechanics
- Probability of Detection
- Corrosion Severity Assessment

AVRD

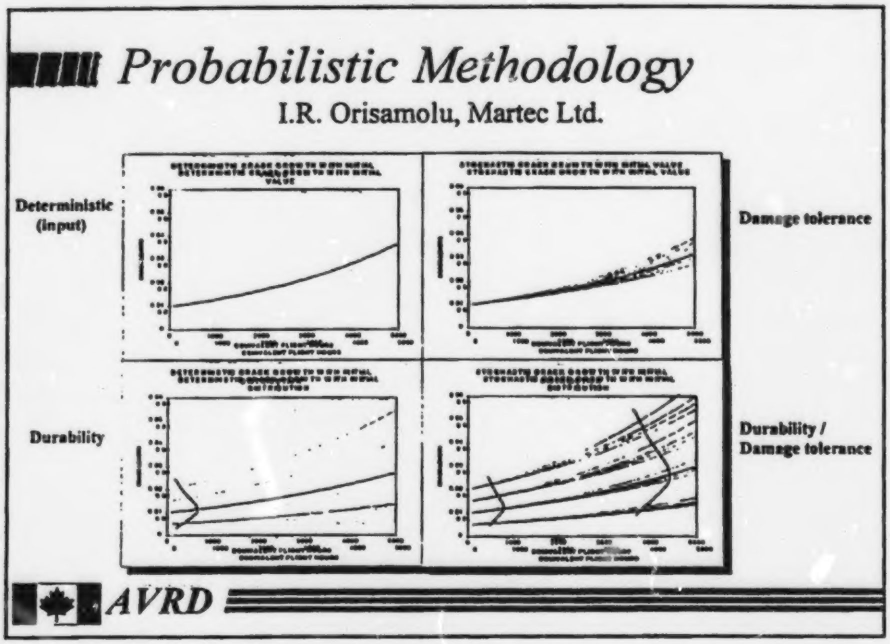

Probabilistic Methodology

I.R. Orisamolu, Martec Ltd.

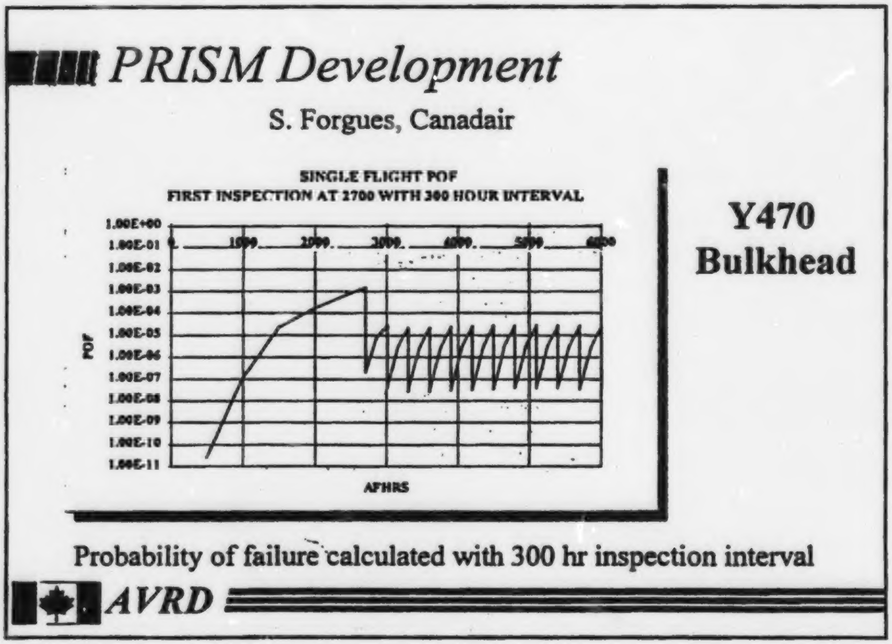

PRISM Development

S. Forgues, Canadair

Y470 Bulkhead

Probability of failure calculated with 300 hr inspection interval

Structural Integrity Development

Advanced Structural Integrity Concepts Development (3GB53)

- CF-18 active buffet suppression
- Information management
- Finite element studies
- General ASIP development

AVRD

CF-18 Active Buffet Suppression

D. Zimcik, NRC/IAR

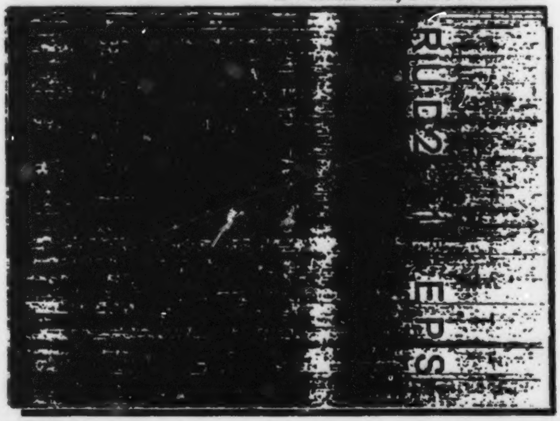

Active suppression of twin-tail buffet caused by vortex extending from LEX

AVRD

Hans Bakuwel
Ministry of Defence
Royal Netherlands Navy
Ship Research and Development Division
Postbus 20702
2500ES s-Gravenhage
The Netherlands

Dr. M.N. Bassim
Dept. of Mechanical Engineering
University of Manitoba
105 Administration Building
Winnipeg, Manitoba R3T 5V6
204 474-8524
fax 204 275-7507
bassim@cc.umanitoba.ca

Dr Philip Bates
Royal Military College of Canada
Department of Chemistry and Chemical Engr.
PO Box 1000, STN Forces
Kingston, Ontario K7K 7B4
613 541 6000 ext 6609
fax 542 9489
bates-p@rmc.ca

John Alexander Bell
Naval Staff
Headquarters New Zealand Defence Force
Private Bag
Wellington
New Zealand
64 4 496 0329
fax 64 4 496 0311

Harold Benner
Lanark Coating Services Ltd.
130 Industrial Ave.
Carleton Place
Ontario K7C 3T2
613 257 2792
fax 613 257 7808

Craig Bennett
Dept of Physics
Acadia University
Wolfville N.S. B0P 1X0
902 542 2200 x 1150
fax 902 542 1454
cbennett@dragon.acadiau.ca

Alain Berry
Groupe d'Acoustique
Département de Génie Mécanique
Université de Sherbrooke
2500 blvd Université
Sherbrooke Quebec J1K 2R1
berry@gme.usherb.ca

Dr. Prakash Bhartia
Director General
Defence Research Establishment Atlantic
P.O.Box 1012
Dartmouth, Nova Scotia B2Y 3Z7

Mr. John Bird
DNA & FP/NA115
Ash 1-0-N42-b
MOD Abbey Wood #95
PO Box 702
BRISTOL
BS12 7DU
United Kingdom
0117 9135050
fax 01179135943

Dr. Carman Bright
Deputy/Director General
Defence Research Establishment Atlantic
P.O.Box 1012
Dartmouth, Nova Scotia B2Y 3Z7

Dr. M.K. Chernuka
Martec Ltd. Suite 400
1888 Brunswick St.
Halifax, Nova Scotia B3F 3F8
(902) 425 5101

Mr Ron Chisholm
Engr Dept/NAO/Senior Hull Inspector HF31.3
Fleet Maintenance Facility Cape Scott
FMO Halifax, N.S. B3K 2X0
902 427 0550 3885
fax 427-4527

Mr. Patrick Charles Conor
Defence Operational Technology Support Est.
Private Bag 32901, Devonport
Aukland, New Zealand
64 9 445 5827
fax 64 9 445 5890
conor@dse.govt.nz

Mr. G. Corbett
National Defence Headquarters DMCS 3-6
101 Colonel Bye Dr
Ottawa Ont K1A 0K2

Terry Culliton
Saint John Shipbuilding Ltd.
15 Willett Ave.
P.O.Box 5250
St John, New Brunswick E2L 5C9
506 648 2226 fax 648 3522

Darrell Davis
Combat Systems Engr Dept
Fleet Maintenance Facility Cape Scott
PO Box Stn Forces 99000
Halifax, N.S. B3K 5X5
427 0550 ext 44551
fax 427 4527

Dr Virginia DeGiorgi
Code 6382
Naval Research Laboratory
4555 Overlook Ave. SW
Washington, D.C.
USA 20375-5000
(202) 767-9027
fax 404-7176
virginia@walkinghorse.nrl.navy.mil

Commodore Faulkner
Chief of Staff
Maritime Command Headquarters
P.O. Box 99000 Stn Forces
Halifax, Nova Scotia B3K 5X5

Dr. Terry Foster
Head/Dockyard Lab(E)
Esquimalt Defence Research Detachment
P.O. Box 17000 Stn Forces
Victoria, British Columbia V9A 7N2
250 363 2849
fax 250 363 2856
Terry.Foster@edrd.dnd.ca

Gene L. Franke
Naval Surface Warfare Center
Carderock Division Code 615
9500 MacArthur Blvd.
West Bethesda, MD 20817-5700
USA
301-227-5571
fax 301 227 5576
franke@metals.dt.navy.mil

John Galsworthy
Structural Materials Center
Room G8 Building P161
Defence Research Agency
Holton Heath
Poole, Dorset, BH16 6JU
United Kingdom
01252 392611
fax 01252 392533

Mr Stéphane Garneau DMSS 2-4-4
National Defence Headquarters
101 Colonel By Drive
Ottawa, Ontario K1A 0K2
613 994 8646
fax 994 8873

Steve Gibson DMSS 2
National Defence Headquarters
101 Colonel By Drive
Ottawa, Ontario K1A 0K2

Mr Jim Gianetto
Metals Technology Labs
Energy Mines and Resources Canada
555 Booth St.
Ottawa, Ontario K1A 0G1

Professor G Glinka
Department of Mechanical Engineering
University of Waterloo
Waterloo Ontario
N2L 3G1
519 888 1211 ext 3339
fax 888 6197
gggreg@konec.uwaterloo.ca

Dr Ross Graham
Defence Research Establishment Atlantic
P.O.Box 1012
Dartmouth, Nova Scotia B2Y 3Z7

Mr Xavier Guyot
Naval Engineering Test Establishment
9401 Wanklyn St.
LaSalle, QC H8R 1Z2
514 366 4310 x 318
fax 514 365 0262
guyotx@nete.dnd.ca

Dr. Bob Hay/Mr. R. Bergeron/
Dr. Emmanuel Bisse
Tektrend International Inc.
2113A St. Regis Boulevard
Dollard des Ormeaux QC H9B 2M9
(514) 421 1417
fax 421 1487

Dr John Hiltz
Dockyard Laboratory (A)
Defence Research Establishment Atlantic
P.O. Box 99000 Stn Forces
Halifax, Nova Scotia B3K 5X5
(902) 427-0550 Ext 3425
fax (902) 427-3435
hiltz@drea.dnd.ca

Dr. T. Holden
Atomic Energy of Canada Ltd.
Chalk River Nuclear Laboratories
Chalk River, Ontario N0R 1L0
(613) 584-3311

Dr. Roger S. Hollingshead
Dockyard Laboratory (A)
Defence Research Establishment Atlantic
P.O. Box 99000 Stn Forces
Halifax, Nova Scotia B3K 5X5
(902) 427-0550 Ext 3421
fax (902) 427-3435
hollingshead@drea.dnd.ca

Mr. Paul Holsberg
Naval Surface Warfare Center
Carderock Division
9500 MacArthur Blvd.
Welding and NDE Branch, Code 610
West Bethesda, MD 20817-5700
(301) 227-4401
fax 301-227-5576

LCdr Ken Holt DMSS 2-3
National Defence Headquarters
101 Colonel Bye Dr
Ottawa Ont K1A 0K2

Dr. Trisha Huber
Dockyard Lab(E)
Esquimalt Defence Research Detachment
PO Box 17000 STN FORCES
Victoria, British Columbia V9A 7N2
250 363 2887
fax 363 2887
huber@edrd.dnd.ca

Dr. S.Hutton
Department of Mechanical Engineering
University of British Columbia
2324 Main Mall
Vancouver, British Coumbia, V6T 1W5

Dr Calvin Hyatt
Dockyard Laboratory (A)
Defence Research Establishment Atlantic
P.O. Box 99000 Stn Forces
Halifax, Nova Scotia B3K 5X5
(902) 427-0550 Ext 3433
fax (902) 427-3435
hyatt@drea.dnd.ca

Dr. R.L. Jones
Structural Materials Center
Defence Research Agency
Farnborough, Hampshire, GU14 6TD
United Kingdom
011 44 1252 392125

Mr Ken KarisAllen
Facts Engineering
P.O.Box 20039
Halifax, Nova Scotia B3R 2K9

Rodney Kennett
Naval Engineering Test Establishment
9401 Wanklyn
LaSalle P.Q.
H8R 1Z2
514 366 4310 ext 407
fax 365 0262
kennettr@nete.dnd.ca

Donald Kerr
Halifax Shipyard Ltd.
3099 Barrington Street North
PO Box 9110
Halifax N.S. B3K 5M7
506 632-4756
fax 506 632 5917
donald_kerr@miti.nb.ca

Georges J. Kipouros
Dalhousie University Polytechnic
Dept. of Mining and Metallurgical Engineering
P.O.Box 1000
Halifax, Nova Scotia B3J 2X4
(902) 420 7847
fax (902) 425 1037
kipourgj@tuns.ca

David Knight
Naval Surface Warfare Center
Carderock Division
Welding and NDE Branch, Code 610
West Bethesda, MD 20817-5700

Dr T.S. Koko
Martec Ltd
1888 Brunswick Street, Suite 400
Halifax, N.S. B3J 3J8
902 425 5101
fax 4211923
koko@asa.ca

Gaetan Labbe
Liburdi Engineering Ltd
400 Highway 6 North
Dundas, Ontario
L9H 7K4
905 689 0734
fax 689 0739
liburdi@compuserve.com

Professor Steve Lambert
Department of Mechanical Engineering
University of Waterloo
Waterloo Ontario
N2L 3G1
519 888 4728
fax 888 6197
steve@uwaterloo.ca

Derek Lenard
Dockyard Lab(E)
Esquimalt Defence Research Detachment
P.O. Box 17000 Stn Forces
Victoria, British Columbia V9A 7N2

Douglas MacDonald
In NovaCorp
101 Research Dr
PO Box 790
Dartmouth, Nova Scotia B2Y 3Z7
902 424 8670-190
fax 424-4679
dmacdonald@innovacorp.ns.ca

Mr Scott MacIntyre
In NovaCorp
101 Research Dr
PO Box 790
Dartmouth, Nova Scotia B2Y 3Z7
902 424 8670-185 fax 424-4679
SMacintyre@innovacorp.ns.ca

Mr Ken MacKay
Martec Ltd. Suite 400
1888 Brunswick St.
Halifax, Nova Scotia B3F 3F8

Terri Ann Marsico
Applied Research Laboratory
The Pennsylvania State University
P.O. Box 30
165 Applied Science Building
State College
University Park PA 16804
tam14@psu.edu

Paul Martin
Dockyard Lab(E)
Esquimalt Defence Research Detachment
P.O. Box 17000 Stn Forces
Victoria, British Columbia V9A 7N2
martin@edrd.dnd.ca

Dr. James R. Matthews
Dockyard Laboratory (A)
Defence Research Establishment Atlantic
P.O. Box 99000 Stn Forces
Halifax, Nova Scotia B3K 5X5
(902) 427-0550 Ext 3444
fax (902) 427-3435
matthews@drea.dnd.ca

Ken McRae AVRS
National Defence Headquarters
190 O'Connor St.
Ottawa Ontario
K1A 0K2

Dr. Richard Morchat
Dockyard Laboratory (A)
Defence Research Establishment Atlantic
P.O. Box 99000 Stn Forces
Halifax, Nova Scotia B3K 5X5
(902) 427-0550 Ext 3434
fax (902) 427-3435
morchat@drea.dnd.ca

Dr Jack Morrison
Dockyard Lab(E)
Esquimalt Defence Research Detachment
P.O. Box 17000 Stn Forces
Victoria, British Columbia V9A 7N2

Mr. Dat Nguyen
J.O.Bernt and Associates Limited
3375 Laird Road, Unit 3
Mississauga,Ontario,Canada
L5L 5R7

Mr Corby Nicholson
Materials Technology Centre
311 Legget Drive
Kanata, Ontario K2K 1Z8

Warren C.E. Nethercote DSAM
National Defence Headquarters
190 O'Connor St.
Ottawa Ontario
K1A 0K2
613 992 7695
613 996 5177
warren.nethercote@crad.dnd.ca

Lt Cdr Doug O'Reilly D200
NEU(A)
FMF Cape Scott
P.O. Box 99000 Stn Forces
Halifax, Nova Scotia B3K 5X5
(902) 427-0550 ext 3858

Ms Sue Pecman DMSS 2
National Defence Headquarters
101 Colonel By Drive
Ottawa, Ontario K1A 0K2

Mr. N.G. Pegg
Defence Research Establishment Atlantic
P.O.Box 1012
Dartmouth, Nova Scotia B2Y 3Z7

Gigi Pelletier/ Gerry Piercey
Dockyard Laboratory (A)
Defence Research Establishment Atlantic
P.O. Box 99000 Stn Forces
Halifax, Nova Scotia B3K 5X5

Mr. John Porter
Dockyard Laboratory (A)
Defence Research Establishment Atlantic
P.O. Box 99000 Stn Forces
Halifax, Nova Scotia B3K 5X5
(902) 427-0550 Ext 3423
fax (902) 427-3435
porter@drea.dnd.ca

Jon Preston
Esquimalt Defence Research Detachment
P.O. Box 17000 Stn Forces
Victoria, British Columbia V9A 7N2
250 363 2892
fax 363 2856
preston@edrd.dnd.ca

Nick Pussegoda
Materials Technology Centre
311 Legget Drive
Kanata, Ontario K2K 1Z8
(613) 592-2830

P.R. Roberge
Department of Chemistry and Chemical Engineering
Royal Military College of Canada
Kingston, Ontario K7K 5L0
(613) 541 6000 ext 6485
fax 542 9489
roberge@rmc.ca

Dr George Roy
CANMET/MTL
568 Booth St.
Ottawa, Ontario K1A 0G1
613 992 0328
fax 613 992 8735
groy@emr1.emr.ca

David Ryan
Combat Systems Engr Dept
Fleet Maintenance Facility Cape Scott
PO Box Stn Forces 99000
Halifax, N.S. B3K 5X5
427 0550 ext 4840
fax 427 4527

Lt. Heather Skaarup
Defence Research Establishment Atlantic
P.O.Box 1012
Dartmouth, Nova Scotia B2Y 3Z7

Glen Shippam
FMF CAPE BRETON
Engineering Division (NA)
P.O. Box 17000 Stn Forces
Victoria, British Columbia V9A 7N2
250 363 5873
fax 250 363 2941

Mike Sim
DECCNA CP1-5-17
Department of Defence
Canberra ACT 2600   Australia
61 6 266 2862
fax 61 6 266 4580

Shawn Smedmor
Saint John Shipbuilding Ltd.
PO Box 970
430 Bayside Dr.
Saint John, N.B. E2L 4E5
506 648 2935
fax 506 648 2980

Dr Jeff Szabo
Dockyard Laboratory (A)
Defence Research Establishment Atlantic
P.O. Box 99000 Stn Forces
Halifax, Nova Scotia   B3K 5X5
(902) 427-0550 Ext 3427
fax (902) 427-3435
szabo@drea.dnd.ca

John Tanner
Ameron International- Devoe Marine Coatings
8 Dunmore Rd.
Baltimore, Md 21228
410 788 0431
fax 788 2129

Hugh Templin
Combat Systems Engr Dept
Fleet Maintenance Facility Cape Scott
PO Box Stn Forces 99000
Halifax, N.S. B3K 5X5
427 0550 ext 4529
fax 427 4527

Dr Bob Thomson
MHL Management Corp.
Suite 103   68 Robertson Rd
Nepean   Ontario K2H 8P5
613 596 6001
fax 613 596 6882
71762.1535@compuserve.com

Robert L Tollett
Liburdi Engineering Ltd
400 Highway 6 North
Dundas, Ontario, L9H 7K4
905 689 0734
fax 689 0739
liburdi@compuserve.com

Dr. J.C. Thornley
Research and Productivity Council
921 College Hill Road
Fredericton N.B. E3B 6Z9
506 452 1378
fax 506 452 1395
cthornle.rpc.unb.ca

M. Tullmin
Department of Chemistry and Chemical Engr.
Royal Military College of Canada
Kingston, Ontario K7K 7B4
613 541 6000 ext 6523
fax 542 9489
tullmin-m@rmc.ca

Mr Cees Van Sevenhoven
Ministry of Defence
Royal Netherlands Navy
Naval Design Department
van der Burchlaan 31
Head of Section: Materials and Corrosion
Postbus 20702
2500 ES The Hague
The Netherlands
31 703162708/2728
fax 31 703162751

Mr. Dwight Veinot
Dockyard Laboratory (A)
Defence Research Establishment Atlantic
P.O. Box 99000 Stn Forces
Halifax, Nova Scotia   B3K 5X5

Dr Hugh Williamson
Acoustic and Vibration Unit
School of Aerospace and Mechanical Engineering
Australian Defence Force Academy
Canberra Act 2600 Australia
61-6-268-8262   61-6-268-8276 fax
h-williamson@adfa.oz.au

Dr. Kam L. Yan/S. Aouadi
Cametoid Advanced Technologies Inc.
1451 Hopkins St
Whitby Ontario L1N 2C2
ph 905 666 3400
fax 905 666 3413
coatings@cametoid.com

Richard Yee
Materials Technology Centre
311 Legget Drive
Kanata, Ontario   K2K 1Z8

13. ABSTRACT (a brief and factual summary of the document. It may also appear elsewhere in the body of the document itself. It is highly desirable that the abstract of classified documents be unclassified. Each paragraph of the abstract shall begin with an indication of the security classification of the information in the paragraph (unless the document itself is unclassified) represented as (S), (C), (R), or (U). It is not necessary to include here abstracts in both official languages unless the text is bilingual).

This was the seventh naval materials CF/CRAD meeting. These meetings have been held every two years since 1985. The first four meetings were devoted to fabrication and inspection of submarine pressure hulls with sessions on welding, inspection and fracture. The last three have expanded to include all aspects of naval materials.

The purpose of these meetings has been to bring together industrial research contractors, university contractors, defence scientists, and NDHQ design authorities from the naval materials technology area and invited scientists and engineers from other countries to share advances in naval materials technology in a conference like setting. In 1997 the meeting was held in conjunction with the Inter Naval Corrosion Conference.

The combined program includes welding and laser surface modification, fracture and fatigue, Non-Destructive Evaluation, firesafe materials, organic materials (polymers), vibration and damping materials, and of course, corrosion and coatings.

14. KEYWORDS, DESCRIPTORS or IDENTIFIERS (technically meaningful terms or short phrases that characterize a document and could be helpful in cataloguing the document. They should be selected so that no security classification is required. Identifiers, such as equipment model designation, trade name, military project code name, geographic location may also be included. If possible keywords should be selected from a published thesaurus, e.g. Thesaurus of Engineering and Scientific Terms (TEST) and that thesaurus-identified. If it not possible to select indexing terms which are Unclassified, the classification of each should be indicated as with the title).

naval materials
corrosion
coatings
welding
fracture
NDE
fatigue
laser surface modification
fire safe materials
organic materials
polymers
vibration materials
damping materials

UNCLASSIFIED
SECURITY CLASSIFICATION OF FORM
(highest classification of Title, Abstract, Keywords)

DOCUMENT CONTROL DATA

(Security classification of title, body of abstract and indexing annotation must be entered when the overall document is classified)

1. ORIGINATOR (the name and address of the organization preparing the document Organizations for whom the document was prepared, e.g. Establishment sponsoring a contractor's report, or tasking agency, are entered in section 8.)

Defence Research Establishment Atlantic
PO Box 1012
Dartmouth N.S. B2Y 3Z7

2. SECURITY CLASSIFICATION (overall security classification of the document including special warning terms if applicable).

Unclassified

3. TITLE (the complete document title as indicated on the title page. Its classification should be indicated by the appropriate abbreviation (S,C,R or U) in parentheses after the title).

Abstracts and Summaries of 3rd (7th) CF/CRAD Meeting on Naval Applications of Materials Technology and InterNaval Corrosion Conference

4. AUTHORS (Last name, first name, middle initial. If military, show rank, e.g. Doe, Maj. John E.)

Matthews, James R. (editor)

5. DATE OF PUBLICATION (month and year of publication of document)

October 1997

6a. NO OF PAGES (total containing information include Annexes, Appendices, etc).

approx 675

6b. NO. OF REFS (total cited in document)

more than 200

7. DESCRIPTIVE NOTES (the category of the document, e.g. technical report, technical note or memorandum. If appropriate, enter the type of report, e.g. interim, progress, summary, annual or final. Give the inclusive dates when a specific reporting period is covered).

Conference Proceedings (Special Report)

8. SPONSORING ACTIVITY (the name of the department project office or laboratory sponsoring the research and development. Include the address).

DREA

9a. PROJECT OR GRANT NO. (if appropriate, the applicable research and development project or grant number under which the document was written. Please specify whether project or grant).

1gh

9b. CONTRACT NO. (if appropriate, the applicable number under which the document was written).

10a ORIGINATOR'S DOCUMENT NUMBER (the official document number by which the document is identified by the originating activity. This number must be unique to this document).

DREA SR/97/002

10b OTHER DOCUMENT NOS. (Any other numbers which may be assigned this document either by the originator or by the sponsor).

11. DOCUMENT AVAILABILITY (any limitations on further dissemination of the document, other than those imposed by security classification)

(X) Unlimited distribution
( ) Distribution limited to defence departments and defence contractors; further distribution only as approved
( ) Distribution limited to defence departments and Canadian defence contractors; further distribution only as approved
( ) Distribution limited to government departments and agencies; further distribution only as approved
( ) Distribution limited to defence departments; further distribution only as approved
( ) Other (please specify):

12. DOCUMENT ANNOUNCEMENT (any limitation to the bibliographic announcement of this document. This will normally correspond to the Document Availability (11). However, where further distribution (beyond the audience specified in 11) is possible, a wider announcement audience may be selected).